DISSERTATION

Defence held on 15/09/2023 in Esch-sur-Alzette

to obtain the degree of

DOCTEUR DE L'UNIVERSITÉ DU LUXEMBOURG

EN CHIMIE

by

Antoine ADJAOUD
Born on 4th November 1996 in Argenteuil, (France)

DESIGN AND SYNTHESIS OF NEW LIGNIN-BASED BENZOXAZINE VITRIMERS

Dissertation defence committee

Dr Pierre Verge, Dissertation Supervisor
Lead Scientist, Luxembourg Institute of Science and Technology

Dr Susanne Siebentritt, Chairman
Professor, Université du Luxembourg

Dr Frédéric Vidal, Vice-Chairman
Professor, CY Cergy Paris Université

Dr Damien Montarnal, Reviewer
Research Fellow, Université Claude Bernard Lyon 1

Dr Nicolas Brosse, Reviewer
Professor, Université de Lorraine

"*Alors ça c'est très tordu, mais bougrement intelligent*"

François Pignon

ABSTRACT

The concept of circular economy has prompted the scientific community to explore innovative strategies for enhancing the sustainability of polymeric materials. One such approach involves utilizing lignin biopolymer, the primary source of earthbound phenolic precursors, to create bio-derived thermosets. However, like conventional thermosets, their permanent cross-linked network impedes their recyclability and reprocessability, resulting in significant waste for the environment.

To overcome this issue, researchers have developed a method to introduce reversible bonds into thermoset structures, to make possible their recyclability. These new polymers, known as vitrimers, rely on activable associative exchange reactions that bridge the gap between recyclable thermoplastics and permanent thermosets. In particular, benzoxazine-based thermosets offer significant potential for developing lignin-derived thermosets and vitrimers. Indeed benzoxazines contain tertiary amines, which are particularly useful for creating catalyst-free vitrimers relying on transesterification reactions. Benzoxazine functions could be added on the chemical structure of lignin, if it were not counting on its insufficient number of *ortho*-free phenols. Further investigations are thus needed to explore this route.

The objective of this thesis was to investigate if and how lignin could be modified to create vitrimers *via* the formation of benzoxazine rings. To address this research question, two main research axes were followed: (1) the development of an approach to promote the modification of lignin with benzoxazine groups and (2) the development of benzoxazine-based vitrimers. In (1), a sustainable approach was developed to enhance the functionality of lignin *via* its esterification with a phenolic acid. In (2), the evidence that benzoxazine-based vitrimers can be developed was given, highlighting a remarkable effect of neighbouring group participation of the tertiary amines groups on transesterification. The combination of the two approaches ultimately enable the production of catalyst-free lignin-derived benzoxazine vitrimers relying on transesterification exchanges.

This thesis is presented as a cumulative work consisting of a comprehensive literature review and five chapters, each corresponding to a publication addressing the research axes. The first section of the thesis provides an overview of thermosets derived from lignin and details the strategies to develop lignin-derived vitrimers. The second publication highlights the development of benzoxazine monomers from model lignin-derived phenolic compounds. In the third publication, the process of increasing the reactivity of soda lignin by esterification with a bio-based phenolic acid, phloretic acid, is established and optimized. The fourth and fifth publications demonstrate that benzoxazines can be used to design catalyst-free vitrimers relying on transesterification exchange reactions. Each work focuses on a bio-based synthon, either polyethylene glycol or isosorbide, derived from sugar cane and agricultural wheat straw waste, respectively. The final publication addresses the core research question of this thesis, by detailing the procedure for developing lignin-derived benzoxazines vitrimers. It also examines how adjusting the molecular structure of the precursors can enhance properties such as hydrophobicity and fire retardancy.

In summary, this thesis examined the potential of vitrimers derived from lignin as a promising avenue for the development of sustainable materials. It was successfully demonstrated that lignin can be converted into benzoxazine-based vitrimers, with remarkable thermal, mechanical, and vitrimer properties. These findings emphasize the significance of lignin as a valuable precursor for the creation of environmentally friendly materials with enhanced performances. This thesis provides a foundation for future advancements in lignin-derived vitrimer research, contributing to the progress of sustainable.

ACKNOWLEDGMENTS

I would like also to thank the University of Luxembourg (UL) for hosting me as a Ph.D. student and for the administrative management, the quality of transferable skills trainings, the Learning Centre, and the Food Lab (I don't forget you CY Cergy Paris University).

I wanted to express my sincere gratitude to the Luxembourg Institute of Science and Technology (LIST) and the Materials Research and Technology (MRT) department for giving me an opportunity to discover the wonderful world of science during my first internship experience and to become an actor of it during my Ph.D. The healthy working environment within the MRT department has been conducive to the sustainable development of fulfilled scientists.

I would like to express my gratitude to Dr. Pierre Verge for providing scientific knowledge, support, and guidance during the development of this research work. I would like to thank you Pierre for being an "*Outstanding Mentor*" (he received a FNR award for that) and for the trust and the liberty to thrive and learn. During these years, you have contributed to increasing my research competencies, progressing in my research career, and pursuing revolutionary research. My gratitude goes also to Dr. Laura Puchot for being always available for discussions and scientific advices that were great assets throughout this journey.

I would like to extend my appreciation to the members of the jury for accepting to review my work.

I also thank all the trainees (Ambre, Axelle, Nathan, Robin, Tina), former Ph.D. students (Acerina, Arnaud, Lilia, Sebastien, Youri), current Ph.D. students (Aymane-DJ Snake, Carlito, Célia, Channya, Daniil-Kremlin, Killian, Vladislav-Kremlin, et même toi Vincent #JusDeBoubou qui j'espère un jour trouveras le cadre), postdoc (Adrien, Carlos, Dhahabia, Joao, Sergei-Kremlin) and football teammates (Adriano, Bertrand, Elisa, Kamal, Kevin, Marco-porto, Marko, Tim, Victor, Vincent, Servane) for the nice moments we had in the past years. A very warm thanks to my Indian friends, Arpan and Rohan, who support me and believe in me throughout the four years of my Ph.D.

My sincere acknowledgment to LIST researchers for the fruitful scientific discussions (Alexander, Daniel, Reiner, Stephan) and non-scientific discussions (Alexander, Frédéric, Salim, Yao). I also want to mention the technical support provided by Alexander (one more time), Anès-Omega Swatch, Benoît de Longwy, Denis, Mohamed, Régis, and Sébastien Klein (le meilleur qui mériterai un paragraphe à part entière). Without your valuable help, my Ph.D. experience would not have been the same.

To all G4S guardians (watchmen of so many doors), with whom I deeply appreciate the (very) long conversations and spend precious moments (especially from 22h02 to 22h09 when you were pushing me outside LIST' building when the alarm rang), many thanks!

Finally, a very warm thank goes out to my amazing family who helped and encouraged me along the way. I am indebted to my parents Samia and Djillali who gave me the strength to become the person I am today. A special thanks to my dad's super-Kangoo that dropped me (overloaded with mum's food) at the train station in only a few seconds. I would like also to thank Amélie and Alexandre, my siblings who consider me a woodcutter, for trying to understand why I do research.

Last but not least, the best for the end, the icing on the cake or the indispensable fries with a kebab! I cannot express enough all my gratitude to you Farida and I am very grateful for your priceless support in all aspects of my life. I can write a second manuscript to explain the "symbiose" between us since the first week of the first year of our bachelor's degree (another reason why I will never forget Cergy). In addition to being a wonderful partner, you are also an excellent scientist and soon it will be your turn to produce a cumulative thesis. I hope I will be able to push you as far as you push me.

LIST OF SCIENTIFIC CONTRIBUTIONS

Published articles

- Trejo-Machin, A.; <u>Adjaoud, A.</u>; Puchot, L.; Dieden, R.; Verge, P.; Elucidating the thermal and polymerization behaviours of benzoxazines from lignin derivatives, *Eur. Polym. J.* **2020**, 124, 109468, https://doi.org/10.1016/j.eurpolymj.2019.109468.

- <u>Adjaoud, A.</u>; Dieden, R.; Verge, P.; Sustainable Esterification of a Soda Lignin with Phloretic Acid, *Polymers* **2021**, 13 (4), 637, https://doi.org/10.3390/polym13040637.

- <u>Adjaoud, A.</u>; Trejo-Machin, A.; Puchot, L.; Verge, P.; Polybenzoxazines: a sustainable platform for the design of fast responsive and catalyst-free vitrimers based on trans-esterification exchanges, *Polym. Chem.* **2021**, 12 (22), 3276-3289, https://doi.org/10.1039/d1py00324k.

- <u>Adjaoud, A.</u>; Puchot, L.; Verge, P.; High-Tg and Degradable Isosorbide-Based Polybenzoxazine Vitrimer, *ACS Sustain. Chem. Eng.* **2022,** 10 (1), 594-602, https://doi.org/10.1021/acssuschemeng.1c07093.

- <u>Adjaoud, A.</u>; Puchot, L.; Federico, C. E.; Das, R.; Verge, P.; Lignin-based benzoxazines: A tunable key-precursor for the design of hydrophobic coatings, fire resistant materials and catalyst-free vitrimers, *Chem. Eng. J.* **2023**, 453 (2), 139895, https://doi.org/10.1016/j.cej.2022.139895.

Articles in preparation

- <u>Adjaoud, A.</u>; Puchot, L.; Verge, P.; From lignin-derived thermosets to lignin-derived vitrimers: a roadmap.

- <u>Adjaoud, A.</u>; Marcolini, B.; Vaudemont, R.; Dieden, R.; Puchot, P.; Verge, P.; Direct evidence of catalyst-free transesterification in benzoxazine vitrimers.

Patents

- WO2021250024A1: BENZOXAZINE DERIVATIVES VITRIMERS (Dépôt n° LU101846 du 10/06/2020), Pierre VERGE, <u>Antoine ADJAOUD</u>, Acerina TREJO MACHIN, Laura PUCHOT.

- WO2022122735: BENZOXAZINE DERIVATIVES VITRIMERS (Dépôt n° LU102318 du 09/12/2020), Pierre VERGE, <u>Antoine ADJAOUD</u>, Acerina TREJO MACHIN, Laura PUCHOT.

- WO202212882: CATALYSTS FOR BENZOXAZINE (Dépôt n° LU102316 du 09/12/2020), Pierre VERGE, <u>Antoine ADJAOUD</u>, Laura PUCHOT.

- LU07842: HIGH-PERFORMANCE BENZOXAZINE DERIVATIVES VITRIMERS (Dépôt n° LU500714 du 07/10/2021), Pierre VERGE, <u>Antoine ADJAOUD</u>, Laura PUCHOT, Henri PERRIN, Daniel SCHMIDT.

- LU08435-A: DUAL CURABLE VITRIMERS (dépôt n° LU503197 du 16/12/2022), Pierre VERGE, Ambre MEYER, Antoine ADJAOUD, Laura PUCHOT, Alexander SHAPLOV, Joamin GONZALEZ GUTIERREZ.

- LU08435-B: DUAL CURABLE VITRIMERS (Dépôt n° LU503198 du 16/12/2022), Pierre VERGE, Antoine ADJAOUD, Laura PUCHOT, Alexander SHAPLOV, Joamin GONZALEZ GUTIERREZ.

- LU08436: VITRIMERS WITH WIDE PROCESSING WINDOW (Dépôt n° LU503199 du 16/12/2022), Pierre VERGE, Antoine ADJAOUD, Laura PUCHOT.

Oral communication

- 19th SAMPE Benelux Student Meeting, May 10th – 11th 2021, Geleen, The Netherlands (hosted online). *"A fully bio-based vitrimeric polybenzoxazine resin to elaborate fiber-reinforced self-healable and recyclable composites"*.

- 4th International Symposium on Polybenzoxazines (ISPBZ2021), May 31st – June 4th 2021, Bascharage, Luxembourg (hosted online). *"Polybenzoxazines: a sustainable platform for the design of fast responsive and catalyst-free vitrimers"*.

- 11th European Polymer Congress (EPF2022), June 26th – July 1st 2022, Prague, Czech Republic. *"Multi-purpose lignin-based benzoxazines: from hydrophobic coatings to catalyst-free vitrimers"*.

- 1st International Conference on Sustainable Chemical and Environmental Engineering (SUSTENG22), August 31st – September 4th, Rethymno, Greece. *"Multi-purpose lignin-based benzoxazines: from hydrophobic coatings to catalyst-free vitrimers"*.

- 31st International Conference on Polyphenols (ICP2023), July 3rd – 6th 2023, Nantes, France. *"Lignin-based benzoxazines: a versatile platform of functional and recyclable polyphenolic materials"*.

Poster presentation

- 9th IUPAC International Conference on Green Chemistry (ICGC2022), September 5th – 9th 2022, Athens, Greece. *"Lignin-based benzoxazines: a tunable key-precursor for various applications"*.

- European Polymer Conference on "Dynamic Polymer Networks" (EUPOC23), May 14th – 18th 2023, Bertinoro, Italy. *"Lignin-based benzoxazines: a sustainable platform for the design of catalyst-free vitrimers"*.

CONTENT

State-of-the-art

Research axis I: Design of lignin-based benzoxazines

Research axis II: Synthesis of benzoxazine-based vitrimers

Research axis I+ II: Design and synthesis of new lignin-based benzoxazine vitrimers

Annexes

GENERAL INTRODUCTION

In 2011, the UN Secretary-General urges governments during the 17th Conference of the Parties (COP17) to undertake long-term action towards transitioning to sustainable energy, emphasizing that the imminent threat of climate change necessitates moving away from a reliance on fossil fuels[1]. He emphasized that burning our way to prosperity is not a viable option and called for a new, sustainable path to achieve the desired future. Over a decade later, the debate is still ongoing, and the discovery of the "eighth continent" of plastic in the Pacific has heightened the focus on the problems stemming from the excessive production and consumption of plastic goods. Olefin and aromatic petrochemicals are essential building blocks for commodity plastics and represent a market size value of 585 billion USD in 2022 [2]. The past decades have clearly demonstrated the linear nature of the "*black gold*" economic flow, as evidenced by the steady increase in the value of Brent crude oil from 23.8 USD in 1990 to 93.5 USD in 2022 [3]. The inflation trend will grow in the coming years as the supply is limited by the depletion of petroleum resources and the demand is driven by the increasing worldwide population [4]. Apart from economic considerations which were once the dominating lever for major decisions, global awareness on the planet and human health propels the transition toward a sustainable economy. The biggest challenge of our generation relies on the reduction of greenhouse gas emissions. Despite a punctual decrease during the COVID pandemic, global carbon dioxide (CO_2) emissions increased steadily since the beginning of the 21st century to reach disturbing levels (39.7 Gt in 2021)[5]. Commodity plastics account for a large fraction of CO_2 emissions across their lifecycle, from their production to their consumption. Of even greater concern, mismanagement in their disposal and cost-effective recycling strategies generate long-term pollution, especially in marine environments [6]. The worrying consequences of the so-called "*white pollution*" prompt scientists to find sustainable strategies to protect the environment and human health. Following the Paris Agreement, the European Union (EU) set cross-cutting objectives to slow down global warming and attain climate neutrality by 2050. The "*Pathway to a Healthy Planet for All*" envisions the transition from a linear to a circular economy model [7]. Applied to commodity polymers, the historical "*take, make, dispose*" model pivots towards the modernistic "*reduce, reuse, and recycle*" philosophy[8, 9]. Concomitantly to economic considerations, the paradigm of polymers' circularity embraces interconnected pillars of sustainable development. Among them, the concept of "*safe and sustainable by design chemicals and materials*" supported by the European Green Deal foresee a circular polymer bio-economy[10].

The ubiquity of plants flourishing on the surface of Earth (~ 450 GtC) [11] inspired scientists to identify eco-friendly alternatives to depleted petroleum resources. Also known as lignocellulosic biomass (LCB), non-edible vegetal feedstocks such as wood trees, agricultural residues, and perennial grasses afford a fertile ground for exploitable organic matters. Essentially composed of earthbound polymers, LCB is a natural source of polysaccharides (cellulose, hemi-cellulose) and polyphenolic (lignin)

materials. Over the past century, various industrial technologies and biorefinery processes have been developed to lever LCB. If cellulose received considerable interest from the paper and food packaging industries, the heterogeneity of lignin biopolymer constitutes the main lock for industrial applications. Downstream and emerging *in-situ* strategies intend to convert lignin into functional precursors that can be subsequently integrated into the design of renewable polymers. However, even if these considerations afford for more sustainable sourcing of plastic, the issue pertaining to the end of life is generally overlooked or not adequately addressed at this stage.

The recycling of commodity plastics remains a societal challenge. In the classification of synthetic polymers, semi-crystalline thermoplastics differ from cross-linked thermosets stemming from their ability to be reshaped. However, both classes of polymers are generally not designed to be degraded or reprocessed being mostly incinerated or landfilled after their use (~80 % in 2015)[12]. One pioneering approach to address the lack of circularity in plastics focuses on labile bonds to anticipate and create a more favorable scenario for the end-of-life of the material. More recently, the incorporation of reversible covalent bonds in polymer networks to form covalent adaptable networks (CANs) has opened up possibilities for the recycling of non-reprocessable class of plastics. The elegant chemical structures implemented in these vitrimeric materials offer the potential to mitigate the adverse impacts of plastic pollution on the environment.

The purpose of the thesis was to apply both the sustainable-by-design and Green Chemistry principles to develop a new family of high-performance lignin-derived vitrimers; in other words, new bio-based and recyclable thermosets (Figure 1). The manuscript is a cumulative thesis, distributed between six chapters, starting with chapter one presenting an extensive review of lignin-derived materials. This chapter detailed the origin and extraction of the biopolymer to the prominent strategies deployed to develop bio-derived and functional polymers. This chapter also reviews the research works toward the design of lignin-derived recyclable polymers, focusing attention on the development of vitrimers.

Polybenzoxazine, an emerging class of phenolic resin, was selected as thermosetting matrix to apply these fundamental approaches. The experimental work focuses on two primary research axis: making benzoxazine greener through the exploration of lignin-derived benzoxazines and making benzoxazine smarter focusing on the advancement of benzoxazine-based vitrimers (each research axis covered in two chapters). These two research fields converge in the final chapter, showcasing the introduction of the first lignin-derived benzoxazine vitrimers.

The second chapter focuses on the design of renewable benzoxazines from lignin-based phenols. It addresses the investigation of the thermal behavior of lignin-based benzoxazines monomers synthesized from depolymerized model compounds. Five *ortho*-methoxy phenol with different *para*-substitutions were selected to understand the role played by the *para*-substituents on the thermal properties of benzoxazine monomers. This preliminary study is representative of what could happen in lignin where the great majority of phenolic units are *para*-substituted with non-reactive interunit linkages.

The third chapter details an innovative chemical pathway developed specifically to increase the reactivity of lignin toward the chemistry of benzoxazines. A design-of-experiment methodology was employed to evaluate the influence of the reaction time, the catalyst loading, and the ratio between reactive species on the increase of the *ortho*-free phenolic group content. The assessment of the structure, its solubility, and its thermal behavior are detailed.

The following chapter, the first of the second research field dedicated to the development of benzoxazine vitrimers, demonstrates the evidence that benzoxazines can be used to develop vitrimers relying on transesterification reactions. While the field related to vitrimers is generally covered by epoxy or polyurethane thermosetting materials, it is the first time that benzoxazines are sued to develop vitrimers. The chapter related the unique synthesis protocol especially developed to this aim, as well as the characterization of the thermal, thermo-mechanical, viscoelastic, and vitrimer properties.

The fifth chapter focuses on the degradability of a bio-based polybenzoxazine vitrimer relying on transesterification. The dynamic networks were synthesized from the combination of naturally occurring precursors to tailor the resin properties. Alongside the structural, thermo-mechanical, and dynamic characterizations, the chapter also explores the mechanical and chemical reprocessing ability of the polybenzoxazine vitrimers.

The manuscript ends with the sixth chapter, which describes a way to develop a series of lignin-derived benzoxazines with properties that are ranging from hydrophobic coatings, fire retardant materials, and vitrimers, depending on the selected amine-based precursors. The success of this accomplishment is entirely dependent on the knowledge generated in the first six chapters of this manuscript.
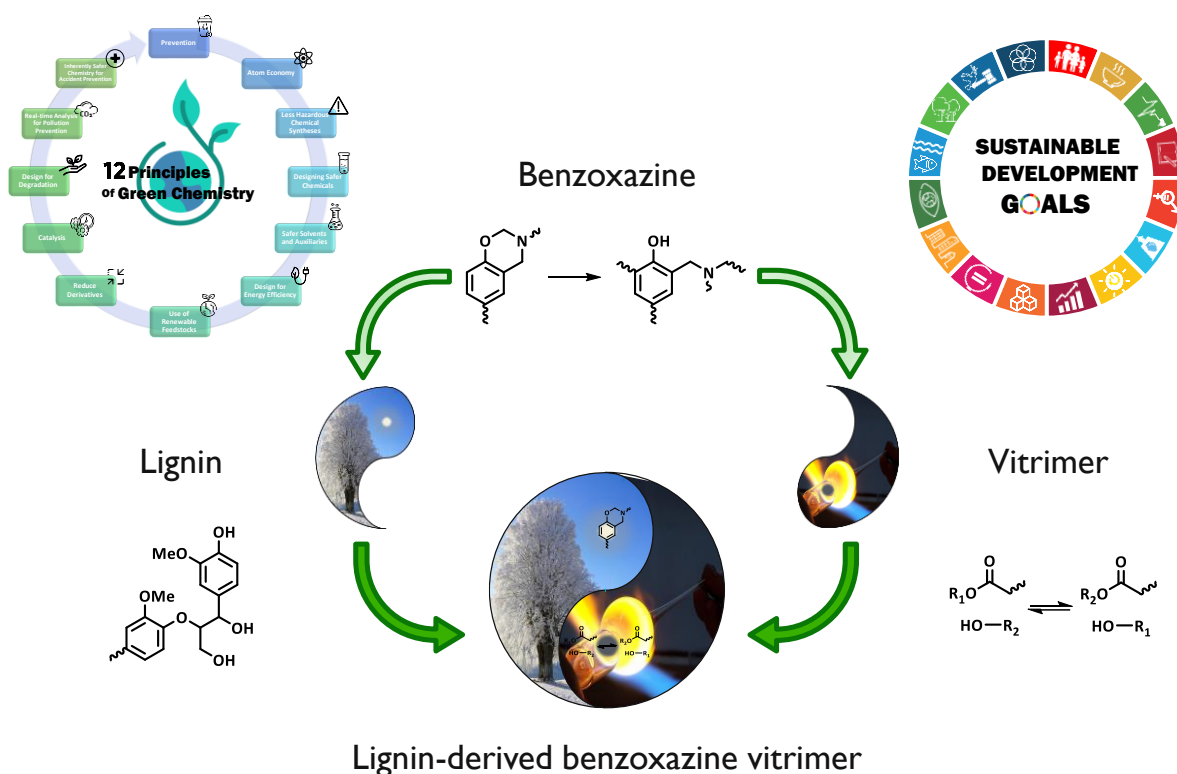

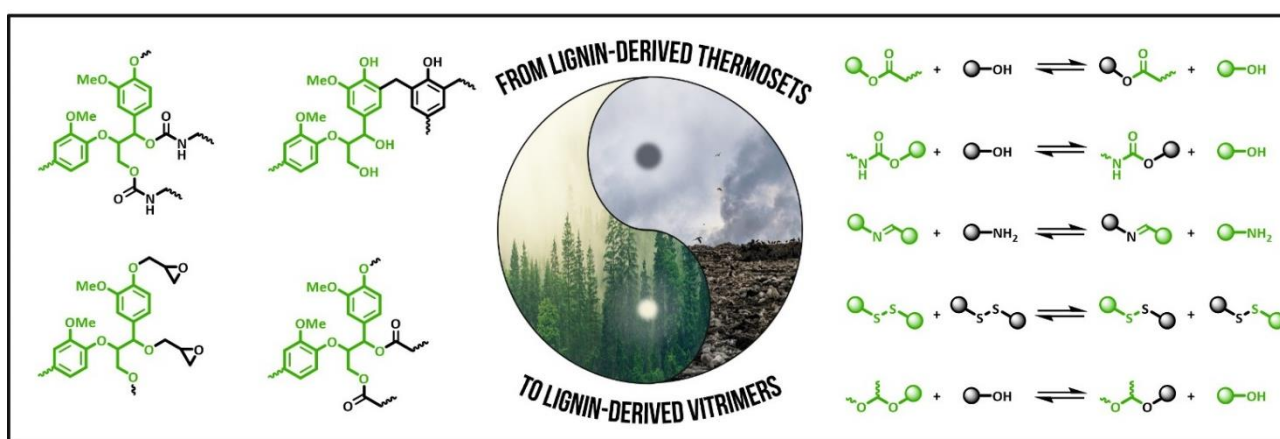**Figure 1** Research strategy to develop renewable and recyclable thermosets.

References

(1) Secretary-General, U. Spelling Out Priorities at 'Clean Industrial Revolution' Event in Durban. Department of Public Information: **2011**.

(2) https://www.grandviewresearch.com (accessed 28/06/2023).

(3) https://www.insee.fr/en/statistiques/serie/010002077#Tableau (accessed 29/06/2023).

(4) Sadigov, R. Rapid Growth of the World Population and Its Socioeconomic Results. The Scientific World Journal 2022, **2022**, 8110229. DOI: https://doi.org/10.1155/2022/8110229.

(5) Crippa, M.; Guizzardi, D.; Banja, M.; Solazzo, E.; Muntean, M.; Schaaf, E.; F, P.; Monforti-Ferrario, F.; Olivier, J. G. J.; Quadrelli, R.; et al. CO2 emissions of all world countries. Union, P. O. o. t. E., Ed.; Luxembourg, **2022**.

(6) Jambeck, J. R.; Geyer, R.; Wilcox, C.; Siegler, T. R.; Perryman, M.; Andrady, A.; Narayan, R.; Law, K. L. Plastic waste inputs from land into the ocean. Science **2015**, 347 (6223), 768-771. DOI: https://doi.org/10.1126/science.1260352.

(7) https://eur-lex.europa.eu/legal-content/EN/ALL/?uri=CELEX:52021DC0400 (accessed 30/06/2023).

(8) Collias, D. I.; James, M. I.; Layman, J. M. Introduction—Circular Economy of Polymers and Recycling Technologies. In Circular Economy of Polymers: Topics in Recycling Technologies, ACS Symposium Series, Vol. 1391; American Chemical Society, **2021**; pp 1-21.

(9) Korley, L. T. J.; Epps, T. H.; Helms, B. A.; Ryan, A. J. Toward polymer upcycling—adding value and tackling circularity. Science **2021**, 373 (6550), 66-69. DOI: https://doi.org/10.1126/science.abg4503.

(10) European, C.; Joint Research, C.; Caldeira, C.; Farcal, L.; Garmendia Aguirre, I.; Mancini, L.; Tosches, D.; Amelio, A.; Rasmussen, K.; Rauscher, H.; et al. Safe and sustainable by design chemicals and materials : framework for the definition of criteria and evaluation procedure for chemicals and materials; Publications Office of the European Union, **2022**. DOI: https://doi.org/10.2760/487955.

(11) Bar-On, Y. M.; Phillips, R.; Milo, R. The biomass distribution on Earth. Proceedings of the National Academy of Sciences **2018**, 115 (25), 6506-6511. DOI: https://doi.org/10.1073/pnas.1711842115.

(12) Ritchie, H.; Roser, M. Plastic Pollution. 2018. (accessed 15/06/2022).

State-of-the-art

Chapter one: "From-lignin-derived thermosets to lignin-derived vitrimers: a roadmap"

Naturally occurring in wood, agricultural residues, and perennial plants, lignin is the second largest source of renewable carbon produced on Earth. Despite its million tons scale production as industrial wastes or as biorefinery-valuable products, its irregular and complex structure limits its use. The state of the art mainly focuses on lignin-derived thermosets and vitrimers. Numerous chemistries have been utilized to develop lignin-based materials, extensively discussed in various review articles. Despite the commendable efforts of the authors in gathering, critiquing, and interpreting relevant research, the connection between lignin chemistry to develop thermosets and the potential to create vitrimers using these materials remained unexplored. The main objective of this state of the art is to bridge this gap as comprehensively as possible. The document starts by introducing the foundation of lignin background, (origin, structure, extraction, and refining), and describes the pathways explored to design synthetic polymers from technical, refined, or chemically modified lignin. The chapter concludes with a description of the performance of the few reported lignin-derived vitrimers thus far. To avoid redundancy with the introductions of published research papers constituting each chapter of this cumulative thesis, the state of the art of vitrimers and benzoxazine is intentionally not covered in this first chapter. However, a concise review is provided at the beginning of each research axis to establish the essential foundations necessary for understanding the rationale and conclusions of this research work.

Summary

List of figures

List of tables

List of abbreviations

LCB	Lignocellulosic Biomass
H	*para*-Hydroxyphenyl
G	Guaiacyl
S	Syringyl
T_g	Glass transition temperature
T_{onset}	Onset of thermal decomposition
$-OCH_3$	Methoxyl
$-OH$	Hydroxyl
$-C=O$	Carbonyl
$-COOH$	Carboxyl
NMR	Nuclear Magnetic Resonance
LCC	Lignin-Carbohydrate Complex
NaOH	Sodium Hydroxide
Na_2S	Sodium Sulfide
$-SH$	Thiol
SO_2	Sulfur Dioxide
M_n	Number Average Molecular Weight
M_w	Weight Average Molecular Weight
Đ	Dispersity
2G	Second-Generation
EHL	Enzymatic Hydrolysis Lignin
HTL	Hydrothermal Liquefaction
H_2SO_4	Sulphuric Acid
H_3PO_4	Phosphoric Acid
LHO	Lignin Hydrogenolysis Oil
Pd/C	Carbon-Supported Palladium
Pt/C	Carbon-Supported Platinum
Ru/C	Carbon-Supported Ruthenium
HCl	Hydrochloric Acid
H_2SO_4	Sulfuric Acid
PU	Polyurethanes
NCO	Isocyanate

Sn(oct)$_2$	Stannous Octoate
MDI	Methylene Diphenyl Diisocyanate
TDI	Toluene Diisocyanate
CMR	Carcinogenic Mutagenic Reprotoxic
NIPU	Non-Isocyanate Polyurethane
CO$_2$	Carbon Dioxide
RPUF	Rigid Polyurethane Foams
FPUF	Flexible Polyurethane Foams
DEG	Diethylene Glycol
PEG	Polyethylene Glycol
GC	Gel Content
ρ	Density
DES	Deep Eutectic Solvent
PPG	Polypropylene Glycol
LPUe	Lignin-derived Polyurethane Elastomer
THF	Tetrahydrofuran
VA	Vanillic Acid
HDI	Hexamethylene Diisocyanate
IPDI	Isophorone Diisocyanate
PO	Propylene Oxide
ECH	Epichlorohydrin
EC	Ethylene Carbonate
PC	Propylene Carbonate
PF	Phenol-Formaldehyde
LPF	Lignin-derived Phenol-Formaldehyde
ROP	Ring-Opening Polymerization
BPA	Bisphenol-A
BADGE	Bisphenol-A Diglycidyl Ether
PEGDGE	Polyethylene Glycol Diglycidyl Ether
EGDGE	Ethylene Glycol Diglycidyl Ether
GDGE	Glycerol Diglycidyl Ether
DETA	Diethylenetriamine
PE	Polyester

PVA	Polyvinyl Alcohol
FRP	Free Radical Polymerization
CRP	Controlled Radical Polymerization
LMA	Lauryl Methacrylate
THFMA	Tetrahydrofurfuryl Methacrylate
ATRP	Atom Transfer Radical Polymerization
BiBB	2-Bromoisobutyryl Bromide
NIPAM	N-Isopropylacrylamide
PEGMA	Polyethylene Glycol Methyl Ether Methacrylate
PS	Polystyrene
PMMA	Polymethyl Methacrylate
RAFT	Reversible Addition-Fragmentation Chain-Transfer
Am	Acrylamide
AA	Acrylic Acid
AIBN	Azobisisobutyronitrile
CTA	Chain Transfer Agent
PEO	Polyethylene Oxide
PLA	Polylactide
PCL	Polycaprolactone
$-N_3$	Azide
$-C{\equiv}C$	Alkyne
PEG-SH	Thiol-terminated Polyethylene Glycol
DA	Diels-Alder
CAN	Covalent Adaptable Network
DCB	Dynamic Covalent Bond
T_v	Topology Freezing Temperature
Ea	Activation Energy
τ^*	Relaxation Time
LPUe	Lignin Polyurethane Elastomer
PHU	Polyhydroxyurethane

1. Origin of lignin

1.1. Lignocellulosic biomass

Lignocellulosic biomass (LCB) is abundantly present across the Earth's surface and serves as an endless source of renewable feedstock. It comprises natural lignocelluloses found in both woody (*i.e.* hardwood, softwood) and non-woody plants (*i.e.* grasses, agricultural crops). LCB consists of three main building-blocks: cellulose, hemi-cellulose, and lignin. The distribution of polysaccharides (cellulose and hemi-cellulose) and polyphenols (lignin) within LCB can vary depending on factors such as the plant species and spacetime factors such as geographical location or seasonal period[1]. The carbohydrate content of lignocellulose primarily includes 25-50 wt.% of cellulose and 15-35 wt.% of hemi-cellulose[2]. Lignin constitutes the remaining portion (10-30 wt.%). Each component of LCB possesses distinct physicochemical properties and provides plant with a specific role[3]. Crystalline cellulose, arranged in bundled fibrils within wood cells, is a linear glucose polymer that provides structural reinforcement in plant cell walls. Hemi-cellulose, on the other hand, acts as an amorphous copolymer of various sugars and functions as a physical barrier against enzymatic degradation of cellulose[4]. Lignin, characterized by a heterogenous cross-linked network, forms complexes with cellulose *via* hydrogen bonding and covalent linking in the extracellular network of plant cell walls. The unique aromatic structure of lignin confers impermeability, structural integrity, and rigidity to the entire plant, while its phenolic moieties exhibit antimicrobial and antioxidant aptitudes to prevent degradation[5].

1.2. Structure of lignin

Native lignin, also known as protolignin, is bio-synthesized from the random polymerization of three aromatic alcohol precursors (monolignols): *para*-coumaryl, coniferyl, and sinapyl alcohols[6]. The structure of monolignols is constituted of a phenolic ring systematically *para*-substituted with propyl side chain (α,β, and γ), and frequently *ortho*-substituted with methoxyl groups (in C_3 or C_5 positions). In lignin, phenolic substructures resulting from the combination of phenylpropane units are referred to as *para*-hydroxyphenyl (H, methoxy-free), guaiacyl (G, monosubstituted), and syringyl (S, disubstituted) sub-units (Figure 1.a). The distribution of lignin and monolignols varies from the biomass feedstock. The highest content of lignin is found in softwood (20-30 %), followed by hardwood (16-22 %), agricultural crops and grasses (10-30 %)[2]. While the structure of coniferous tree-based softwood lignin is dominated by G units, deciduous tree-based hardwood lignin is composed of a mixture of G and S units (almost in equal proportion). Herbaceous lignin species contains all sub-units in addition to a minor amount of hydroxycinnamates[7].

The versatility of vegetal sources has presented challenges in the elucidation of the chemical structure of native lignin and lead to the development of various model (Freudenberg[8], Adler[9]). In the "*so-called*" phenylpropanoid pathway, enzyme-mediated dehydrogenation initiates the oxidation of monolignols into phenoxy-radicals with various resonance structures. The electrophilic benzyl carbon of the quinone methide intermediate undergoes nucleophilic addition forming a dimer and restoring the aromaticity of the benzene ring[10]. *In vivo* lignification process involves oligomer−oligomer or oligomer−monomer couplings to form a three-dimensional molecular architecture composed of phenolic substructures interrelated by ether (C–O) or carbon (C–C) bonds. The β–O–4' ether bond, which is the most prevalent interunit linkage, connects the β-carbon from the aliphatic side chain to a phenolic group from another sub-units (∼ 50 % regardless of the plant species). In addition to aryl (β–O–4', α–O–4') or diaryl (4–O–5') ether bonds, carbon bonds could also be formed to obtain phenylcoumaran (β–5'), 1,2-diaryl propane (β–1'), resinol (β-β'), and biphenyl (5–5') linkages, as illustrated in Figure 1.b. The heterogeneity and complexity of lignin arises from the diversity of possible interunit linkages. This complexity is further influenced by the source of lignin. For instance, hardwood typically exhibit a higher content of ether bonds due to its elevated content of substituted phenolic units (Figure 1.c)[1]. The variation of monolignols content in plant sources not only affects lignin structural characteristics, but also alter the processability (broad glass transition temperature: T_g= 100-160 °C)[4], the thermal stability (multi-stage thermal decomposition: T_{onset}= 150 °C)[11], and the solubility behavior (hydrophilicity controlled by the content of hydroxyl groups)[12] of lignin-based materials.

In summary, the biosynthesis of lignin results in a branched polymer composed of various functional groups including primary methoxyl (–OCH$_3$), phenolic and aliphatic hydroxyl (–OH) groups, and some carbonyl (–C=O) moieties at a lower extent[13]. Recent advances have been made in non-destructive spectroscopic techniques, leading a significant breakthrough in the understanding of lignin chemical structure[14]. The identification and quantification of the various hydroxyl and carboxyl functionalities of lignin have been significantly promoted by the phosphorous-31 nuclear magnetic resonance method (^{31}P NMR) developed by Argyropoulos and co-workers[15]. Irrespective of the plant source, aliphatic hydroxyl groups predominate over phenolic counterparts, and carboxylic moieties occur in smaller quantities ([COOH]= 0.02-0.33 mmol.g^{-1})[13].
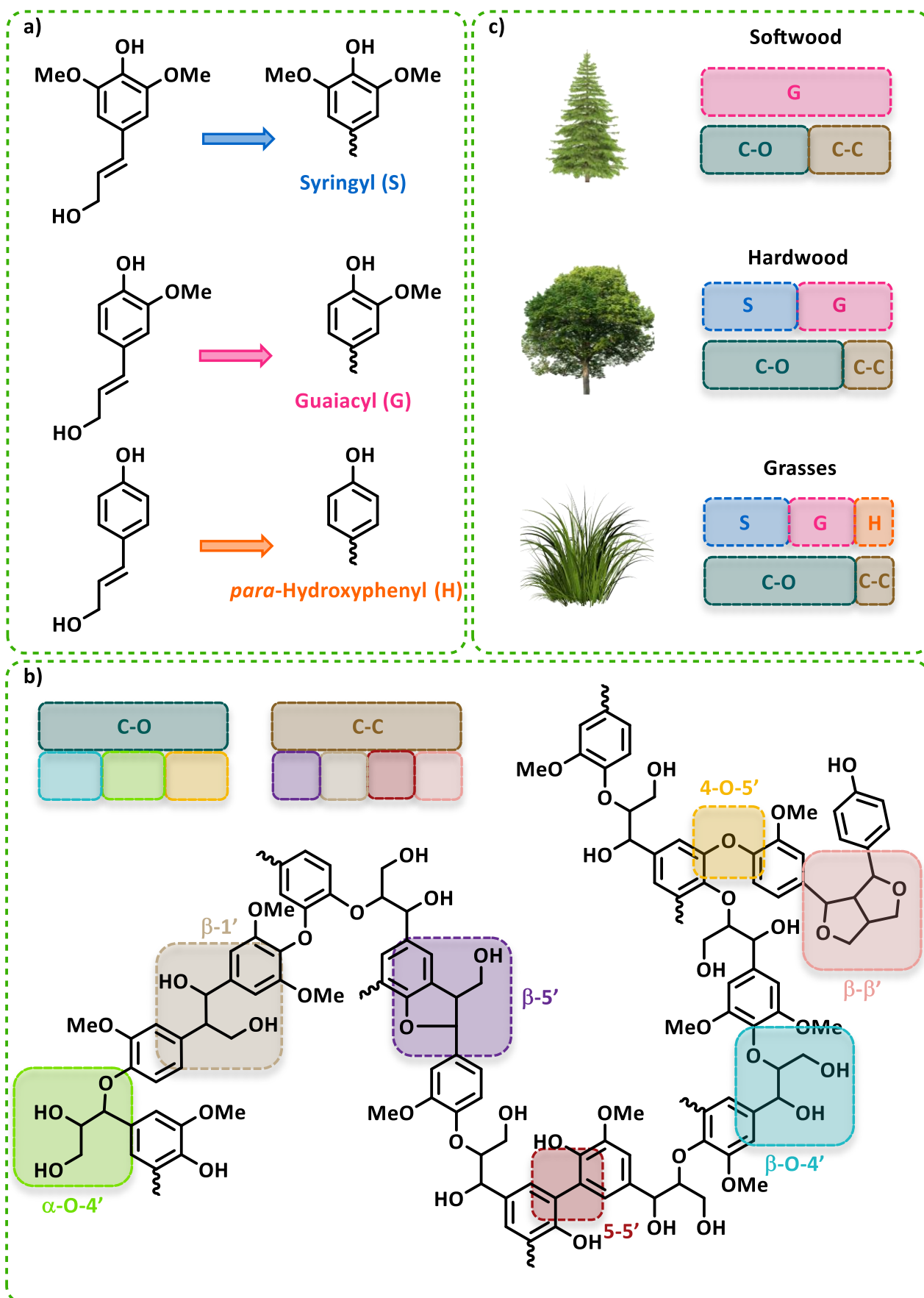
Figure 1 a) Chemical structure of monolignols and resulting phenolic substructures. b) Schematic structure of lignin and most occurrent ether (C-O) and carbon (C-C) interunit linkages. c) Distribution of phenolic substructures and interunit linkages in softwood[1], hardwood[1], and grasses[1]* (* occurrence of bonding motif adapted from [16]).

The valorization of LCB aims at unlocking its potential to serve as renewable feedstock for fuels, chemicals, and materials. The first upgrading stage relies in the isolation of targeted components naturally occurring in LCB. Various strategies have been developed to retrieve economically valuable precursors in high yield and purity[17]. The isolated lignins, generally referred as technical lignins, possess distinct physicochemical features depending on their botanical source and their separation technique[11]. Regardless of the process used, the structural difference between technical and native lignins originates from the cleavage of covalent links in lignin-carbohydrate complex (LCC) and from the chemical modifications occurring during the isolation process (typically depolymerization and condensation)[1]. Technical lignins can be classified according to various criteria such as the extent of structural modification from native lignin (significant or mild)[18], the extraction solvent (alkali, organic, ionic liquid, or deep eutectic solvents)[19], the scale of their extraction (industrial or analytical scale)[20], their solubility in the pulping media (dissolved or insoluble residue)[1, 21], their pre-treatment method (physical, chemical, physicochemical, or biological)[17, 22-24], or the presence of sulfur in their structure (sulfur or sulfur-free lignin)[11, 25-27]. In the context of this review, only the main isolation strategies for the industrial-scale production of technical lignins are provided below (Figure 2)[25, 28-31].

1.3.1. From the pulp and paper industry

The major production of technical lignins comes historically from the papermaking, leading to Kraft lignin and lignosulfonate. These well-established delignification technologies are primarily intended to extract insoluble cellulosic fibers, meanwhile, degraded lignin fragments are recovered as by-products.

1.3.1.1. Kraft lignin

The Kraft process plays a major role in the production of cellulose fibers in the pulp and papermaking industries. Kraft lignin (also known as alkali lignin) is recovered as a by-product of the thermal treatment of wood chips in a strong alkali mixture (white liquor) composed of sodium hydroxide (NaOH) and sodium sulfide (Na_2S)[10]. The fragmentation of native lignin is achieved from the cleavage of aryl ether-bonds (mainly β-O-4') by nucleophilic reactions with hydrosulfide ions that are also responsible for the incorporation of thiol groups (–HS) within lignin structure (< 3 wt.%, Scheme 1.a)[26]. Meanwhile, alkali-soluble fragments undergoes C_5-condensation reactions promoting lignin repolymerization through the formation of alkali-stable carbon-carbon linkages[1]. The resulting liquor pulp, more commonly known as black liquor, contains depolymerized lignin in various amounts depending on the operation time and the biomass source. After acidification and precipitation, the isolated Kraft lignin is hydrophobic and characterized by a polydisperse structure enriched in phenolic groups. The renewable organic materials produced in a pulp mill (tens of millions of tons annually[32]) are traditionally burned and used as primary energy sources to provide the energy required to recover the

pulping chemicals. Therefore, the amount of commercially available Kraft lignin accounts for a small fraction of the worldwide volume production of black liquor (~ 2% representing 265 kt in 2018)[33]. The bottleneck production of black liquor in pulp mills drives the scientific community to explore optimization[34] and valorization[35] routes for the conversion of lignin into value-added chemicals. Additionally, LignoBoost[TM] or LignoForce[TM] technologies emerge as efficient extraction strategies reducing operation costs and improving the yield and purity of Kraft lignin[36, 37].

1.3.1.2. Lignosulfonate

The sulfite process is the oldest sulfur-based pulping technique. It involves the treatment of woody biomass with a hot aqueous solution of sulfur dioxide (SO_2) and/or bi-sulfite salts (*e.g.* calcium, sodium, magnesium, or ammonium) under acidic conditions[38]. The deconstruction of lignin-cellulose bonds occurs through a series of aryl-ether bond cleavage, condensation, and sulfonation reactions catalyzed by sulfite (SO_3^{2-}) or bi-sulfite (HSO_3^-) ions[25]. The sulfonate groups linked to the α-carbon on the aliphatic side chains of phenylpropane units confer water-solubility, thereby promoting lignin hydrolysis while preventing its recondensation[1]. Lignin fragments are further isolated from the carbohydrates-rich liquor pulp by selective precipitation, chemical, filtration, or fermentation techniques[39]. The resulting lignin, better known as lignosulfonate, is an anionic polyelectrolyte containing sulfonate groups (4-8 wt.% sulfur content, Scheme 1.b) and characterized by a high molecular weight and a low purity. Although the pulp's volume production is lower compared to the Kraft process (< tens of millions tons annually[32]), lignosulfonate represents the largest commercially available technical lignin with a supply capacity of 1315 kt in 2018[33]. The preeminent solubility characteristic over almost the entire pH range allows for the valorization of lignosulfonates in a wide range of industrial applications[40].

1.3.2. From biorefinery processes

The substantial progresses in digital technologies propelled our generation into the era of digitalization of services, thereby reducing the demand for paper and the production of technical lignins from pulp mills[26]. At the same time, the concept of biorefinery raised considerable interest in leveraging all components of biomass feedstock[39]. Driven by the global awareness on sustainable production ("*zero-waste policy*"), biorefineries use sulfur-free processes and various biomass pretreatment to recover separately cellulose, hemi-cellulose, lignin, and targeted chemicals[41, 42]. The lignin produced from the lignocellulosic-ethanol fuel biorefinery falls in this category, and its production will significantly increase in the coming years in light of the new environmental regulations imposing the use of renewable energy sources (*e.g.* bio-ethanol)[32].

1.3.2.1. Soda lignin

The soda process is an industrial pulping technique well-suited for the treatment of non-wood botanic species such as annual plants and agricultural crops. In comparison to Kraft pulping, the soda delignification requires a lower amount of sodium hydroxide stemming from the easier impregnation of non-woody materials[43]. The biomass is treated under reduced pressure in a heated alkaline solution, sometimes in the presence of anthraquinone to stabilize carbohydrates and improve lignin dissolution[44]. Despite being subjected to chemical modifications during isolation (hydrolytic cleavage and condensation reactions), soda lignin containing *para*-hydroxyphenyl and carboxylic acid units is known to have a structure close to native lignin (Scheme 1.c)[14]. Technical soda lignins recovered *via* acid precipitation are characterized by lower macromolecular size compared to Kraft lignin or lignosulfonate (M_n= 800–3000, 1500-5000, and 15000-50000 g.mol^{-1}, respectively)[45]. The lowest production capacity of industrial soda lignin originates from the variability of the biomass feedstock that is strongly influenced by climate conditions[32]. Being less contaminated and sulfur-free, soda lignin is a prime candidate for subsequent chemical modifications and downstream catalytic processes. In this context, it is noteworthy to mention that sulfur species are considered as poison for metal catalysts, therefore hampering the catalytic conversion of Kraft lignin and lignosulfonate into value-added products.

1.3.2.2. Organosolv lignin

Some mature technologies such as Alcell[46] or Organocell[47] processes developed at the pilot scale have emerged as greener alternatives for the production of sulfur-free lignins. In this approach, a wide variety of low-boiling organic solvents (*e.g.* alcohol, organic acids, and their combination) are used to isolate individual streams of lignocellulosic biomass in high purity[48]. Organosolv pulping is efficient to selectively break carbohydrate-lignin bonds and stabilizing lignin structure. Organosolv lignins retrieved under acidic conditions contain a high proportion of oxidized units such as *para*-hydroxybenzoates or end-group Hibbert's ketone (Scheme 1.d)[14]. These oxidized species can improve their solubility in polar organic solvents and their compatibility with functional polymers. In addition to benefits from milder process conditions, organosolv lignins are less polydisperse and considered of highest purity due to lower waste accumulation[49]. However, high capital investments in the implemented technologies impede the large-scale production of technical organosolv lignin from the paper industry[50]. Recently, organosolv processes regained interest as environmentally-friendly pretreatment techniques in modern biorefineries, especially in second-generation biorefineries (2G) producing high value-added chemicals from non-edible feedstocks[20]. Advancements in developing environmentally friendly pulping solvents and enhancing their recovery efficiency hold great promise for the economic viability of closed-loop biorefineries[45]. As the papermaking industries decline, the growing prominence of biorefineries is expected to significantly boost the market share of sulfur-free organosolv lignin in the years to come.

Over the past decade, there have been a significant rise in the development of ethanol biorefineries and the pilot-scale production of enzymatic hydrolysis lignin (EHL) derived from the enzyme-mediated degradation processes of diverse cellulosic plants. Lignin acts as a physical barrier within lignocellulose, limiting the access to cellulose and its digestion by cellulase enzymes[51]. It results in lowering the production yield of bio-ethanol. To address this issue, most biorefineries include advanced pre-treatment technologies (*e.g.* steam explosion or dilute acids) to promote the hydrolysis of carbohydrates prior their enzymatic digestion into soluble oligo/monosaccharides[22, 52]. Even if the industrial production of highly-condensed EHL is straightforward[53], the low purity of isolated lignins correlated to the strong pre-treatment methods hampers their valorization into high-value added products[54]. Like the Kraft pulp, hydrolysis lignin is primarily used as a fuel source for energy recovery. However, additional purification methods (*e.g.* mild acid hydrolysis or organic solvent extraction) are employed to remove carbohydrate impurities (7-8 %[26]) and create new opportunities for the valorization in sustainable polymeric materials. In addition to bio-ethanol, the diversification of sugar derivatives retrieved from biorefineries contributes to the production of technical EHL.
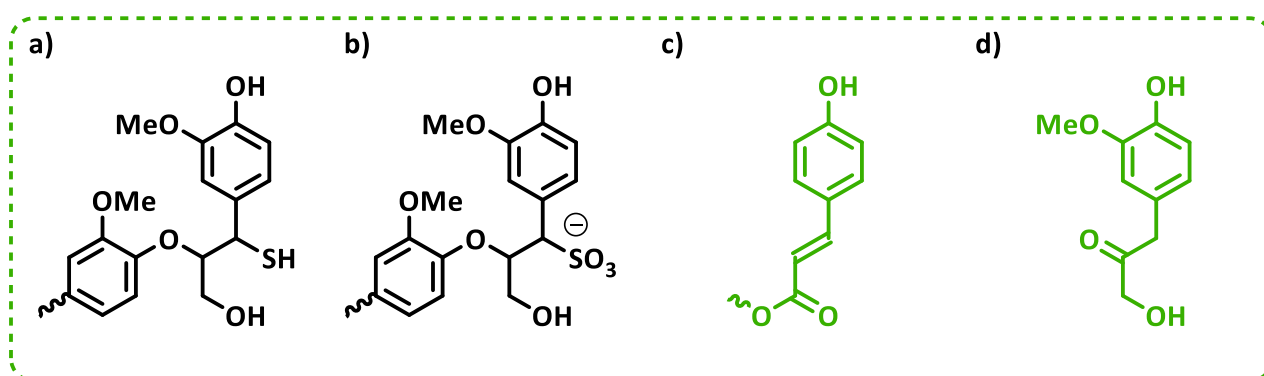
Scheme 1 Example of specific chemical structures find into technical lignins: a) thiol moieties in Kraft lignin, b) sulfonate groups in lignosulfonate, c) *para*-coumarates in soda lignin, and d) Hibbert's ketones in acid-catalyzed organosolv lignin[14].

1.4. Refining

Pulping and biorefinery processes intend to separate lignin from carbohydrates in order to recover dissolved or undissolved lignin macromolecules. Along with the cleavage of labile etherified linkages, the structure of native lignin is altered by the chemicals (functionality and concentration) and the extraction conditions (time, temperature, and pressure) employed during isolation. In most processes, *in-situ* generated unstable reactive species promote lignin repolymerization through the formation of carbon−carbon bonds. All these modifications intensify the structural heterogeneity of technical lignins and hinder their incorporation in the synthesis of sustainable polymeric materials. Upstream pre-treatments receive increasing interest to refine lignin macromolecules into low-molecular weight

components with tunable properties (Figure 2). Among these upgrading technologies, depolymerization and fractionation processes can be directly applied to technical lignins or integrated into the biorefinery unit, hence occurring during lignin isolation from biomass (early-stage catalytic conversion of lignin[16]).

1.4.1. Depolymerization

The process of depolymerization aims at converting lignin macromolecules into oligomers and monomers. The depolymerized products are produced in various amounts and compositions depending on the breakdown method and the plant feedstock[1]. Interestingly, the molecular weight and the functionality of the lignin oil can be tailored by varying to the experimental conditions. The topic of lignin breakdown has been covered by multiple reviews to harness lignin aromaticity for the production of bio-based chemicals as alternatives to petroleum-based feedstock[1, 13, 18, 21, 23, 28, 55-57]. The great variety of depolymerization techniques includes catalytic cracking and hydrolysis, reduction, or oxidation reactions[23], and can be classified as thermochemical and biological treatments[28, 57]. The depolymerization is generally conducted in a solvent at elevated temperature and pressure, and most often with catalysts (acid, base, or metal)[57]. While the reductive depolymerization of lignin macromolecules produces a mixture of aromatic compounds that can be incorporated into the synthesis of lignin-derived polymers, oxidation treatments convert lignin into fine chemicals. Among the wide range of depolymerization techniques, the following section will introduce the main deconstruction strategies employed to produce depolymerized lignin fragments of lower dispersity and higher reactivity.

1.4.1.1. Catalytic liquefaction

Hydrothermal liquefaction (HTL), also known as hydrolytic depolymerization[58], is a straightforward thermomechanical method producing a mixture of phenolic derivatives in the form of a crude oil[59, 60]. Subcritical or near-critical water is used as reaction medium under controlled temperature and pressure conditions (T= 150-350 °C, P= 0.5–25 MPa)[61] to deconstruct lignocellulose or technical lignins in short times (few minutes to few hours). When it comes to the structural modifications ensuing catalytic liquefaction, the cleavage of the alkyl-aryl ether linkages contributes to simultaneously increasing lignin reactivity, reducing its heterogeneity, and producing low-molecular-weight fragments enriched in phenolic groups. Catalysts are generally added to the aqueous solution to prevent recondensation reactions and recover depolymerized adducts in high yield[60]. In some examples, acid catalysts such as sulphuric acid (H_2SO_4) or phosphoric acid (H_3PO_4) have been used to produce a bio-oil from hydrolysis lignin[62] or waste biomass feedstock[63], respectively. Being cheap and convenient for large scale utilization, sodium hydroxide (NaOH) has been extensively studied as an alkaline catalyst promoting lignin depolymerization[62-64]. In this context, it is worth highlighting the predominant role of the catalyst loading in the deconstruction process, with almost no depolymerization observed at low content of alkaline catalyst (< 10 wt.% NaOH)[64]. Another way to improve lignin depolymerization relies on the use of organic co-solvents which are also known to prevent the formation of char residue[58].

Hydrogenolysis, also known as hydropyrolysis[1], hydrogenation[21], hydroprocessing[13, 56], hydrocracking[58], or reductive catalytic fractionation[65]; is a reductive depolymerization technique that operates in the presence of an organic solvent, a catalyst, and hydrogen. In the context of lignin-derived materials, relatively mild hydro-processing conditions are applied to deconstruct lignin into a liquid mixture of oligomeric and monomeric (methoxy)phenols (T= 130-390°C, P= 10-100 bar)[56]. The lignin hydrogenolysis oil (LHO) is obtained through a series of reduction reactions and cleavage of carbon and interunit linkages[1]. The choice of catalyst is motivated by various attributes such as low activity toward ring hydrogenation or resistance toward deactivation in sulfur-containing lignins[1]. If acid/base catalysts have shown effectiveness in depolymerizing lignin, heterogeneous metal catalysts such as carbon-supported palladium, platinum, or ruthenium (Pd/C, Pt/C, and Ru/C, respectively) offers higher selectivity toward the production of specific chemicals[66]. In a similar approach, nickel-based catalyst systems are alternatives well-suited to industrial developments as they can replace expensive noble catalysts[57]. Catalytic hydrogenolysis also benefits from the radical scavenging activity of the hydrogen source that contributes to suppressing char formation. Additionally, *in situ* generated hydrogen produced *via* the thermal decomposition of active hydrogen-donating solvents (typically formic acid[67]) emerged as a substitute to gaseous hydrogen that is currently supplied externally from fossil fuels[68].

1.4.2. Fractionation

The broad molecular weight distribution of technical lignins arises from the structural modifications ensuing biomass fractionation. One promising approach to attain a more uniform feedstock relies on downstream lignin fractionation[19, 69-71]. Membrane or solvent-mediated fractionation intend to refine polydisperse lignin into high-quality fractions with tuneable and reproductible physico-chemical properties. The subdivided lignin fractions benefits from narrow dispersion and higher functionality well-suited for the synthesis of polymeric materials. In recent years, solvent fractionation processes such as organic solvent and pH-dependent techniques generated interest due to their efficiency and ease of implementation (Figure 2)[71].

Organic solvents show promise in the fractionation of biomass to retrieve low-molecular weight lignins (*c.f.* 1.3.2.2). When applied to technical lignins, solvent fractionation processes take advantage of the partial solubility of lignin into organic solvents to separate less-disperse lignin fractions in high-purity. The selection of solvent is based on its Hansen solubility parameters [70], especially with a high hydrogen bonding contribution to facilitate lignin dissolution[72]. Lignin can be dissolved in a single or a mixture of solvents (*e.g.* methanol, (*iso*)-propanol, *tert*-butanol, acetone, methyl ethyl ketone, ethyl acetate), and this strategy can be applied stepwise to retrieve various fractions of lignins. The soluble-lignin fractions are recovered after solvent evaporation[72, 73] or by sequential precipitation using an

antisolvent, typically water[74] or hexane[75, 76]. The lignin fractions retrieved after successive extraction are characterized by different molecular weights (high molecular weight fractions collected from solvents with high hydrogen bonding capacity[73]) and structural compositions (phenolic-rich lignin from low molecular weight fractions[76]).

1.4.2.2. pH-dependent precipitation

The gradient acid precipitation is a practical method to reduce lignin heterogeneity by isolating lignin fractions at different pH value[28]. Based on the same concept as the precipitation from the black liquor, colloidal lignin macromolecules dispersed under alkaline conditions tend to coagulate when subjected to protonation. After the controlled addition of an acid (*e.g.* HCl[77-79], H_2SO_4[77, 80]) to the alkaline solution, the precipitated lignin fraction is separated from the supernatant by centrifugation. The sequential decrease of the pH (from pH~12 to pH~1) generates lignin fractions of different molecular weight distribution, with generally lower molecular weight fractions retrieved at lower pH values. Even if the extent of structural degradation is reduced during the fractionation process[79], the composition of the lignin fraction depends on the nature of the acid employed for the precipitation[77].
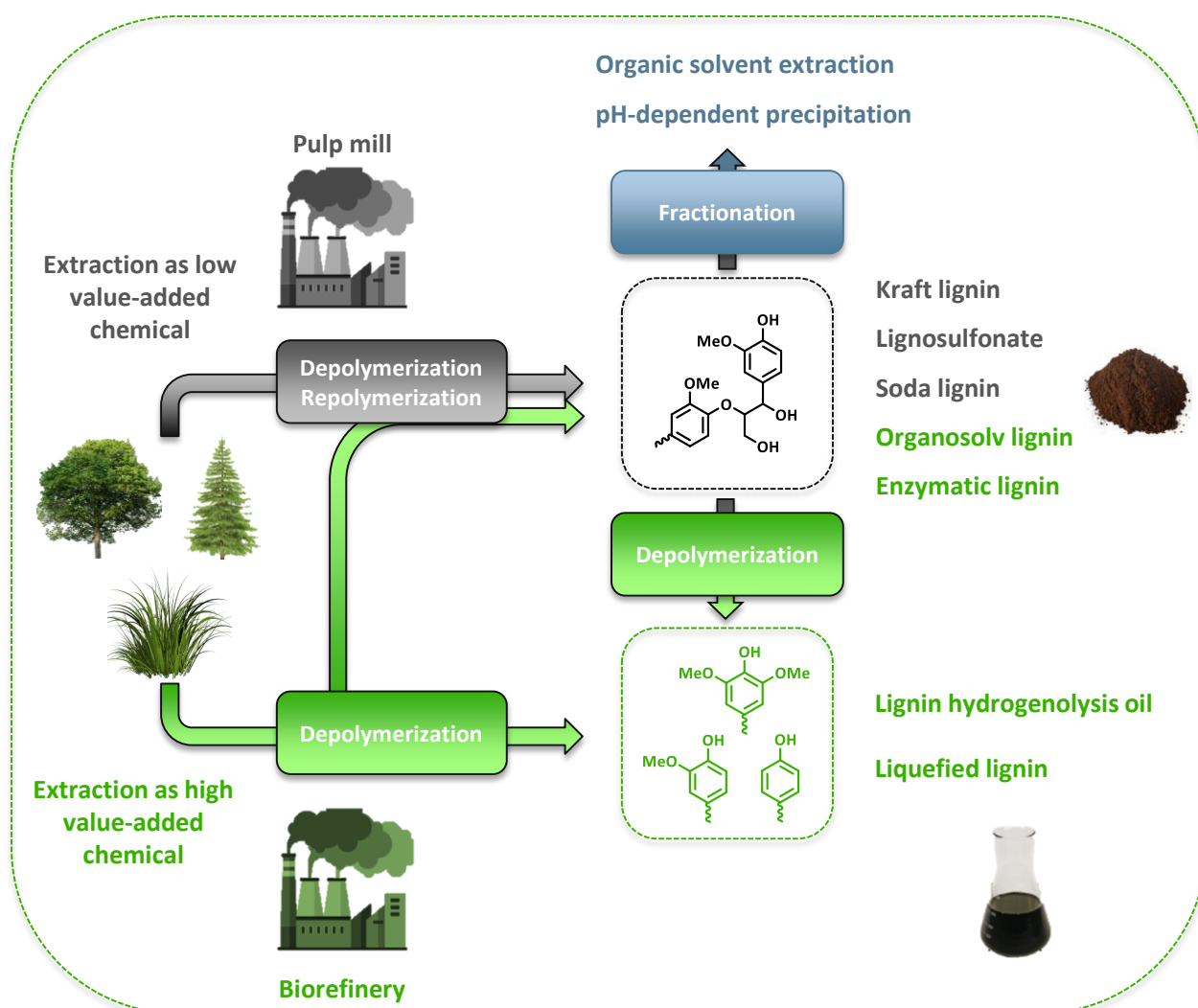
Figure 2 Summary of the strategies used to recover technical and refined lignins.

2. Lignin-derived thermosets

The increasing demand from downstream markets has led to the mass production of polymeric materials such as polyurethanes, polyesters, phenolic, and epoxy resins (Figure 3)[81]. However, the depletion of fossil resources poses a significant economic threat for these materials, and the growing awareness of sustainable development is driving the scientific community to reduce reliance on petrochemicals. To address current and future environmental challenges, the emerging biomass refining technologies presents a promising opportunity for a lignocellulose-to-materials valorization chain. The use of lignin bio-polymer provides a renewable alternative to fossil-based components and can serve as an inexpensive and renewable macromolecular scaffold in bio-derived polymers. Although technical lignins have structural differences based on the plant source and isolation process, they possess multifunctional reactive sites that are well-suited for a variety of cross-linking reactions. However, the heterogeneous architecture of lignin poses some limitations on the design of regular polymers with advanced properties, even though lignin can provide hardness and thermal resistance to bio-derived materials. Refining and functionalization strategies aid in increasing the solubility, reactivity, and selectivity of lignin macromolecules, thereby improving better incorporation in a cross-linked network. The following paragraphs will illustrate the different strategies implemented to design various class of lignin-derived thermosets from technical, refined, and chemically modified lignins. A selection of the most prominent strategies is gathered in a summary table for each class of thermosets.
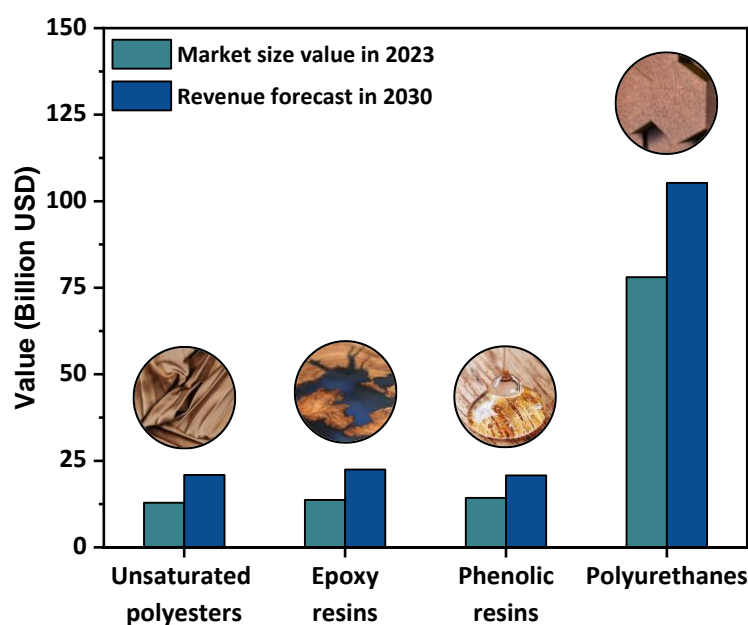
Figure 3 Current and forecast market size value of thermosetting materials.

2.1. Lignin-derived polyurethanes

Polyurethanes (PU) are versatile polymeric materials that can be designed to produce thermoplastics, thermosets and elastomers to cover a wide range of applications. The production of insulating materials for the construction market dominates the worldwide manufacture of PU thermosets[27]. While flexible and rigid PU foams play a crucial role in applications where thermal insulation is essential to reduce energy requirements, PU resins are more used in applications such as adhesives and coatings[82].

Typical PU chemistry involves the polycondensation reaction of polyols (–OH) and polyisocyanate (–NCO) to form a cross-linked network composed of urethane bonds (carbamate, –NHCOO–). Segmented PU backbone can be synthesized from soft macrodiol segments (telechelic polyethers and polyesters) and rigid chain extenders (low molecular weight diols or diamines) with various structure and functionalities depending on the raw materials[83]. Although vegetable oils have emerged as effective alternatives to petroleum-based polyols, the use of edible biomass raises ethical concerns. Lignin has been investigated as renewable and low-cost macropolyol for PU synthesis (Scheme 2)[84-86]. Comprehensive reviews have identified the tremendous impact of lignin on PU materials, such as strengthening mechanical performance, enhancing thermal stability, and increasing biodegradability, among other benefits[59, 87-90]. Although lignin is often reported as a filler[91, 92], it can also be covalently incorporated into the PU network by reacting with a stoichiometric excess of diisocyanate[93], most often in the presence of a tin-based catalyst (typically stannous octoate, Sn(oct)$_2$). However, the highly-condensed network of lignin hampers the complete conversion of –OH groups, necessitating refining and functionalization pathways to increase lignin reactivity toward urethanization. It is worth noting that aromatic methylene diphenyl diisocyanate (MDI) and toluene diisocyanate (TDI) are commonly used –NCO precursors, despite being classified as carcinogenic, mutagenic, and reprotoxic chemicals (CMR). However, alternative and more sustainable approaches to designing lignin-derived non-isocyanate polyurethane (NIPU) have emerged.
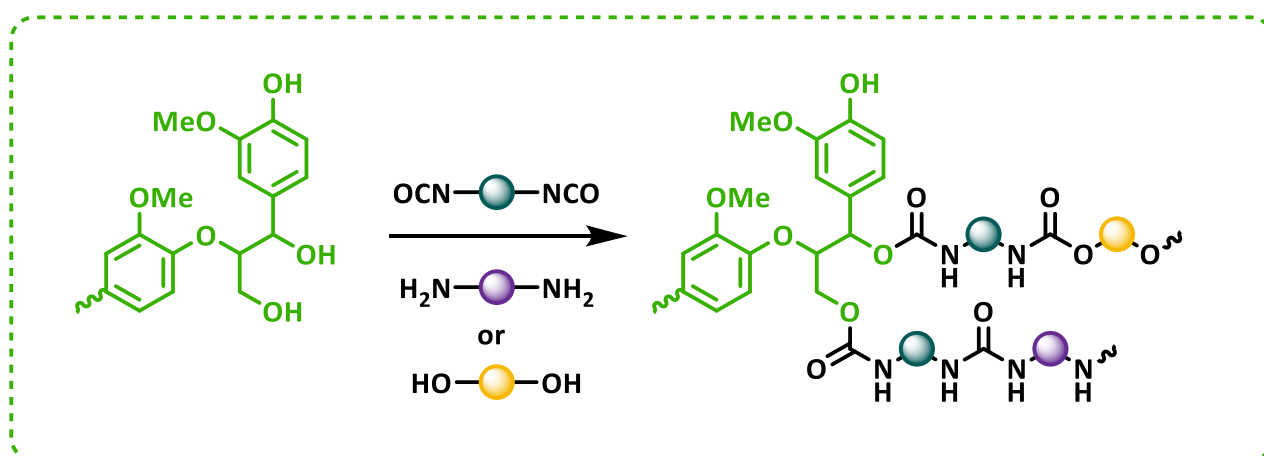
Scheme 2 Proposed scheme for the synthesis of lignin-derived polyurethane.

2.1.1. Polyurethanes from technical lignins

Polyurethane foams and resins have been a key player in the global polymer market since the last century[82]. The foaming process involves a cross-linking reaction between polyol and polyisocyanate precursors, along with the use of other chemicals such as co-crosslinking, blowing, catalysts, and surfactant agents. The cellular structure can be formed either by the vaporization of a physical blowing agent during exothermic urethanization or by the reaction of a chemical blowing agent that releases carbon dioxide (CO_2) and amine through the decomposition of *in-situ* generated carbamic acid. The mechanical characteristics of PU foams, from rigid to flexible, are governed by the ratio between hard and soft segments, while the precursors' reactivity and blowing agent control the cellular morphology.

Lignin-derived rigid PU foams (RPUF) are characterized by a closed-cell morphology and rigidity imparted by highly-crosslinked lignin[88]. Pan and Sandlers conducted a study to investigate the effects of gradually replacing a commercial polyether triol (Voranol[TM] 270) with lignins extracted from mixed hardwood (Figure 4.a)[94]. The resulting chemically cross-linked foam prepared from ethanol-organosolv lignin and polymeric MDI (pMDI) exhibited a high gel content level (GC= 93%) and superior mechanical properties (25 mol.% polyol substitution, ρ= 105 kg.m^{-3}, $\sigma_{compressive}$= 0.31 MPa). A similar trend was observed when partially replacing diethylene glycol (DEG) or polyethylene glycol (PEG) with softwood Kraft lignin[95] and corncob alkaline lignin[96], respectively. In both cases, the addition of wood particles[95] or pulp fibers[96] reinforced the performance of the lignin-derived RPUF. The combination of synthetic and natural oil-based polyol also helped to offset the rigidity of lignin segments[97-100]. Hayati *et al.* developed a temperature-mediated mixing process to improve the dispersion of Kraft lignin in a polyol mixture composed of commercially available sucrose/glycerine-initiated polyether (Voranol[TM] RH 360) and glycerol[99]. At a lignin content of 5 wt.% and with a slight excess of isocyanate, the enhanced disaggregation of lignin microparticles contributed to superior compressive strength and thermal insulation (ρ= 39 kg.m^{-3}, $\sigma_{compressive}$= 0.2 MPa, K~ 0.025 W.m^{-1}.K^{-1}). In a similar manner, efficient dispersion methodologies in commercial aromatic polyester polyol/glycerol mixtures[101] or ternary deep eutectic solvent (DES)[102] proved to be effective in enhancing the properties of lignin-derived RPUF.

Flexible PU foams (FPUF), characterized by an open-cell morphology and a low density, have been widely used as cushioning materials. Lignin-derived FPUF are segmented copolymers composed of hard lignin blocks and soft chain extenders[83], and are generally characterized by a lower cross-linking density originating from lower extent of isocyanate precursors in the PU network. A comparative study has identified low –OH content, low-T_g, and high solubility in the co-polyol as predominant features affecting the foam flexibility (Figure 4.b)[103].

For resin applications, the inherent rigidity of the lignin aromatic backbone can result in the formation of brittle materials[93, 104]. To address this, one approach involves controlling the hard-to-soft segment ratio by adjusting co-polyol chain length, lignin content, and ratio of reactive functions (generally NCO:OH <

1)[105]. For instance, mixing lignin with rubbery cross-linker such as castor oil[106, 107] or PEG[108, 109] has been shown to facilitate the formation of PU materials with low cross-link density, which can improve their flexibility and toughness. In another approach, synthetic polyol can be turned into isocyanate precursor *via* isocyanation[110, 111]. Bonini *et al.* demonstrated that isocyanate prepolymers such as polymeric 1,4-butanediol end-capped with TDI facilitated the formation of PU network in steam-exploded lignin[110]. Lang *et al.* extended the length of the polyol using PEG end-capped with TDI to prepare lignin-derived PU films from various plant sources, resulting in a low cross-linking density material composed of 40 wt.% of lignin and properties such as E= 21 MPa and T_g= -45 °C [111].

Meanwhile various technical lignins could replace synthetic polyol in PU networks[111, 112], their intrinsic heterogeneity often limits the substitution rate. Moreover, the direct incorporation of lignin in PU synthesis poses processability issues and can lead to brittleness in resins and to the formation of irregular cells in foams.

2.1.2. Polyurethanes from refined lignins

Technical lignins are characterized by a broad dispersity impeding their valorization for polymeric materials with reproducible properties. Various depolymerization and fractionation strategies endeavour to selectively refine lignin macromolecules in low-molecular weight fractions.

2.1.2.1. Depolymerization

The depolymerization of lignin is a promising strategy to achieve a higher substitution rate of synthetic polyol in lignin-derived polymers. The hydrothermal liquefaction operates at high temperature and pressure under alkaline conditions[113] and sometimes in the presence of co-solvents such as iso-propanol[114] or ethanol[115]. For example, depolymerized Kraft lignin (M_w= 1700 g.mol^{-1}) was incorporated in the synthesis of RPUF to partially replace polypropylene glycol (PPG) or sucrose polyol (50 wt.% substitution, $\sigma_{compressive}$= 0.22-0.37 MPa, K= 32-38 mW.m^{-1}.K^{-1})[113]. The depolymerization strategy also aims to advance the production of self-supporting and shape-controllable lignin-derived PU resins. Li *et al.* recovered lignin fragments with higher functionality and lower molecular weight through alkaline depolymerization (M_n= 600 g.mol^{-1}, [OH]= 9.2 mmol.g^{-1})[116]. This refined lignin efficiently cross-links with PPG-TDI soft domains, yielding homogeneous lignin-derived PU elastomer (LPUe). The enhanced thermomechanical properties of the LPUe, as the amount of lignin increases, originate from to the abundant number of hydrogen bonds formed between the urethane bonds and residual –OH moieties (40 wt.% lignin, E= 0.18 MPa, ε= 1394 %, T_g= 8 °C).

Hydrothermal liquefaction has shown effectiveness in converting biomass or technical lignins into low-molecular weight polyol well-adapted for incorporation in PU network[117]. In presence of polyhydric alcohols, the solvolytic liquefaction promotes lignin dissolution and fragmentation through a series of

condensation reactions[59]. Liquefaction solvents such as DEG[118], crude glycerol[119], PEG alone[120] or in mixture with glycerol[121-127], form a polyol mixture with lignin adducts. Hu et Li followed a sequential two-step liquefaction pathway using crude glycerol samples as liquefaction solvent to refine corn stovers[119]. After successive acid and base-catalyzed liquefaction, functional polyols react with pMDI to form rigid and semi-rigid PU foam with promising properties ($\sigma_{compressive}$= 0.22-024 MPa, K= 32.2-38.9 mW.m^{-1}.K^{-1}). In another example, the dispersibility of alkaline corncob lignin was improved through acid-catalyzed liquefaction in a PEG$_{400}$/glycerol polyol mixture[121]. The lignin-based polyols were recovered in a short time and high yield under microwave irradiations (t= 5-30 min, Y> 97%, M_n= 460-480 g.mol^{-1}, [OH]= 8.2-8.6 mmol.g^{-1}) and incorporated effectively into lignin-derived RPUF. This microwave-assisted pathway also showed its worth in lignin-derived FPUF[122]. Soft chain extenders with reduced T_g and low hydroxyl content such as PPG or castor oil were added to the mixture, imparting mobility in the network. When extended to a technical soda lignin (Protobind^{TM} 1000)[123], the resulting PU foam displayed an improved compression force value with densities ranging from 70-145 kg.m^{-3}.

In another approach, a lignin hydrogenolysis oil was recovered from the biorefinery process of apple wood using ruthenium supported over silicon carbide (Ru/SiC) as chemoselective depolymerization catalyst[128]. The residue replaced up to 50 wt.% of commercial polyether polyol in water and flame resistant RPUF (Figure 4.c). Vendamme and colleagues comprehensively investigated the reactivity of the various –OH groups toward urethanization with aliphatic and aromatic isocyanate precursors[129]. The LHO retrieved from the metal-catalyzed depolymerization of softwood Kraft lignin is characterized by a low molecular weight and a high functionality (M_n = 401 g.mol^{-1}, [OH]= 8.19 mmol.g^{-1}). They found that aromatic isocyanate cured faster, especially with the aliphatic –OH groups.

In summary, the liquefaction of lignin is a common method to generate processable, functional, and low molecular weight lignin fractions that can be effectively incorporated into lignin-derived PU network, from flame-retardant[118, 124] and oil- absorbent foams[125-127], to elastomeric materials[120].

2.1.2.2. Fractionation

For a long time, solvent fractionation has been used to refine lignin for its incorporation within the PU network[104]. For instance, solvent extraction and gradient precipitation processes intent to narrow lignin heterogeneity and retrieve polyols with desirable properties.

Lignin fractionation from various organic solvents, such as acetone[130-133], 1,4-butanediol[134], dichloromethane[135], ether[104, 136], ethyl acetate[133], methyl-ethyl ketone[137], methanol[104, 132, 133, 135], tetrahydrofuran (THF)[130, 138, 139], methyl-THF[140], or a mixture of them[135, 141, 142] is a commonly employed method to recover well-defined lignin fractions. These fractions are characterized by their physicochemical features, which determine their performance in lignin-derived PU materials[130]. Griffini and colleagues converted vanillic acid (VA), a phenolic acid produced through the oxidative

depolymerization of lignin, into a VA-NCO precursor through a series of chemical reactions including dimerization (1,4-dibromobutane), acyl azide conversion (sodium azide), and thermal treatment (Curtius rearrangement). This precursor was then reacted with the acetone-soluble fraction of a hardwood organosolv lignin (M_n= 1490 g.mol^{-1}, [OH]= 5.58 g.mol^{-1}) to produce lignin-derived PU coatings with hydrophobic and adhesive properties (80 wt.% lignin, θ_{H2O}= 89.7 °, $\sigma_{adhesive,}$= 1.21 MPa). Researchers showed that a sequential precipitation pathway was effective in refining softwood Kraft lignin into low-, medium-, and high-molecular-weight fractions using a mild solvent system (room temperature, acetone-methanol-hexane co-solvent system, M_w= 1322-65521 g.mol^{-1})[141]. The resulting lignin-derived PU resins had mechanical characteristics that were strongly influenced by the combined effects of hard lignin segments and soft secondary polyols, which provided stiffness and ductility (43-60 wt.% lignin, E_Y= 611-961 MPa). Later the same research group tailored the properties of lignin-derived PU by adjusting pretreatment reaction conditions[139] or molecular interactions with secondary polyols[142].

Even if less reported, solvent fractionation proved nevertheless to be an effective way to refine lignocellulosic biomass[136] or technical lignin[133] into processable polyol in view of preparing PU foam (Figure 4.d). For example, the ether-soluble (monomers/dimers) and insoluble (oligomers) fractions of LHO retrieved from Pinus radiata wood were incorporated in the design of RPUF to replace up to 50 wt.% of sorbitol polyether polyol[136]. In another study, sequential fractionation pathway reduced the heterogeneity of technical lignin with dispersity values ranging from Đ= 4.44 for alkaline lignin to Đ= 1.67-2.92 for the refined fractions[133]. Further reacted with aliphatic hexamethylene diisocyanate (HDI) and PEG$_{2000}$ as secondary polyol, highly resilient PU foam were produced (30 wt.% substitution, elastic recovery after 20 compression cycle > 95%).

Klein *et al.* have successfully incorporated a higher amount of Kraft lignin, obtained from gradient acid preparation, into flexible PU film under mild polymerization conditions with a stoichiometric excess of MDI (70 wt.% lignin)[143]. In a similar approach, Cao *et al.* explored the gradient acid precipitation of corn stover black liquor to unveil the structure-to-property relationship in lignin-derived RPUF[144]. The lignin fraction recovered at pH 5 exhibited higher –OH content and molecular weight ([OH]= 7.52 mmol.g^{-1}, M_n= 1830 g.mol^{-1}). Statistical analysis showed that these features play paramount roles in the properties of RPUF. After surface functionalization with pMDI, the RPUF showed a lower density and higher compressive strength (50 wt.% polyol substitution, ρ= 42 kg.m^{-3}, $\sigma_{compressive}$= 0.39 MPa).

Solvent fractionation is a commonly employed method to recover well-defined lignin fractions, which can then be functionalized and incorporated into PU resins to enhance their mechanical[132], anticorrosive[138], and adhesive properties[130, 140]. The mechanical properties of the resulting lignin-derived PU resins are strongly influenced by the synergetic effects of hard lignin segments and soft secondary polyols. These advancements in solvent fractionation are leading to advancements in lignin-derived PU materials competitive with commercial polymeric products[137].

2.1.3. Polyurethanes from chemically modified lignins

2.1.3.1. Isocyanation

A series of chemical modifications have been implemented to increase the processability and the reactivity of lignin towards urethane bond formation. Isocyanation is a process that aims to functionalize technical or refined lignins and convert them into isocyanate precursors[144-149]. When using MDI, aliphatic –OH groups show nearly quantitative conversion towards isocyanation. Researchers have also identified a hierarchy of reactivity between phenolic moieties, where less hindered H units are the most reactive[150]. As a result, pre-polymerization with diisocyanate precursors yields partially cross-linked lignin with unbonded isocyanate reactive groups. Zieglowski and colleagues reacted Kraft lignin (UPM Biopiva[TM] 100) with MDI, TDI, or HDI, to form a series of lignin-based isocyanate prepolymer with 56, 100 and 66 % free isocyanate content, respectively[146]. Aliphatic isophorone diisocyanate (IPDI) can be also used to partly functionalized softwood Kraft lignin before foaming (Figure 4.e)[147]. Partial replacement of non-edible castor oil with functionalized lignin led to a higher open cell content and enhanced flexibility (10 wt.% polyol substitution, 39 % resilience). When mixed with phosphorus-containing polyols, the flame-retardant property of the foam was improved by the high-melt viscosity of the degraded product, which prevented melt-dripping[148]. Additionally, the unreacted isocyanate groups can act as covalent bridges with –OH-terminated polymers to form sustainable PU copolymers[149].

2.1.3.2. Esterification

The partial esterification of lignin –OH groups with acetic anhydride appears as an effective strategy to control lignin reactivity toward isocyanate precursors[151, 152]. Gouveia and colleagues converted 45 and 62 % of the aromatic and aliphatic –OH groups of Kraft lignin into acetyl moieties, thereby improving its solubility and thermal stability[152]. This strategy enables higher incorporation of the ester-capped polyol into PU resin with lignin content ranging from 30.9 to 49.5 %. Another approach reported by Averous *et al.* involves the synthesis of star-like polyol composed of soft linear chains connected to a rigid lignin core[153]. The flexible polyol block was obtained *via* successive esterification of hardwood organosolv lignin –OH groups using oleic chloride, epoxidation of arm chain-double bonds with peracetic acid, and oxirane ring-opening. When reacted with prepolymers of MDI, all lignin-derived PU architectures exhibit elastomeric characteristics (T_g= -6 to -42 °C, ε= 181–360 %, E_Y= 0.2–2.8 MPa).

2.1.3.3. Hydroxyalkylation

2.1.3.3.1 Propylene oxide

The oxypropylation pathway is particularly of interest since it reduces steric hindrance and increases the reactivity of lignin –OH groups[154-158]. Under alkaline conditions, lignin aliphatic and aromatic –OH functionalities initiate the ring opening of cyclic ethers, mainly propylene oxide (PO),

resulting in oxypropylated lignins[113, 154-165]. These processable polyols are liquid mixtures composed of low molecular weight PO oligomers and lignin-*g*-extended ether chains with a terminal –OH group (Scheme 3.a). The functionality of these polyols is controlled by the lignin/PO stoichiometry[155]. Li and Ragauskas investigated the replacement of sucrose and glycerol polyols with an oxypropylated lignin derived from softwood Kraft lignin[159]. The PU foam synthesized solely from the oxypropylated lignin had better mechanical properties due to the higher cross-linking density in the PU network (ρ= 30 kg.m^{-3}, $\sigma_{compressive}$= 0.14 MPa). This approach was further extended to ethanol-organosolv lignin harvested from pine wood chips and the reinforcement with cellulose nanowhiskers results in a foam with higher compressive strength (ρ= 62 kg.m^{-3}, $\sigma_{compressive}$= 0.52 MPa)[160].

Refining and oxypropylation techniques have been found to produce high-performance lignin-derived PU foam[113, 161]. Mahmood *et al.* used liquefied and oxypropylated Kraft lignin (M_w= 3600 g.mol^{-1}, [OH]= 350 mg$_{KOH}$.g^{-1}) as a single polyol feedstock to design lignin-derived RPUF with superior compression strength and thermal conductivity (ρ= 55 kg.m^{-3}, $\sigma_{compressive,20\%}$= 0.58 MPa, K= 29 mW.m^{-1}.K^{-1})[113]. In another study, Li *et al.* fractionated corn stovers into functional and low molecular weight lignin using an ethanol/water solvent mixture (M_n= 1175 g.mol^{-1}, [OH]= 6.07 mmol.g^{-1})[161]. After oxypropylation, the functionalized lignin was incorporated in the manufacture of lignin-derived RPUF (ρ= 85 kg.m^{-3}, $\sigma_{compressive}$= 0.83 MPa, K= 37 mW.m^{-1}.K^{-1}). Qiu and coworkers followed an alternative pathway for the oxypropylation of a softwood alkaline lignin to produce homogeneous and resilient lignin-derived FPUF (Figure 4.f)[166]. Linear PEG$_{2000}$ chains were grafted onto lignin *via* successive ring-opening of epichlorohydrin (ECH) and etherification with lignin aromatic –OH groups, converted into aliphatic units in the lignin-based polyol ([OH]$_{ali}$= 1.31 mmol.g^{-1}). In this study, soft chain extenders provided by PEG$_{2000}$ or by lignin-*g*-PEG$_{2000}$ conferred high interfacial compatibility and elasticity to the PU foam (50 wt.% polyol substitution, ρ= 201 kg.m^{-3}, $\sigma_{compressive}$= 0.27 MPa, 94% elastic recovery).

In summary, oxypropylation proved to be effective to produce lignin-derived PU foam with improved biodegradability[156, 157], rigidity[162-164], and thermo-responsive[165] aptitudes.

2.1.3.3.2   Carbonate

Recently, cyclocarbonate derivatives have been explored to replace PO due to its toxic classification[167, 168]. Etherification using high-boiling point cyclocarbonate is conducted under mild-basic conditions, with the mechanism depending on the reactivity of the hydroxyl groups involved. Meanwhile aliphatic –OH groups formed carbonate bonds upon reaction with ethylene carbonate[167] (EC) or its derivatives[168], the ring-opening of cyclocarbonate with aromatic –OH groups generates a mixture of polycarbonate and polyether linkages through the nucleophilic attack on alkylene carbon and *in-situ* decarboxylation (Scheme 3.b). As a result, nearly quantitative conversion is reached under short time to

form a lignin-based polyol mixture with increased content of aliphatic –OH groups. Duval and colleagues upscaled the non-toxic hydroxyalkylation of organosolv lignin using triethylene glycol or PEG as co-solvent (Figure 4.g)[169]. The series of lignin-based polyols exhibit tunable hydroxyl content (I_{OH}= 300-700 mg$_{KOH}$.g^{-1}) suited for a wide range of targeted applications. Researchers applied this environmentally-friendly protocol for the hydroxyalkylation of softwood Kraft lignin (Indulin® AT)[170]. With optimized lignin loading in PEG$_{400}$ co-solvent (50 wt.%), the ensuing lignin-derived RPUF emphasized the potential of EC for a clean hydroxyalkylation process (ρ= 58 kg.m^{-3}, $\sigma_{compressive}$= 0.14 MPa). Similarly, propylene carbonate (PC) was used as hydroxyalkylation reagent to produce lignin-derived PU adhesive[171] or foam[172].
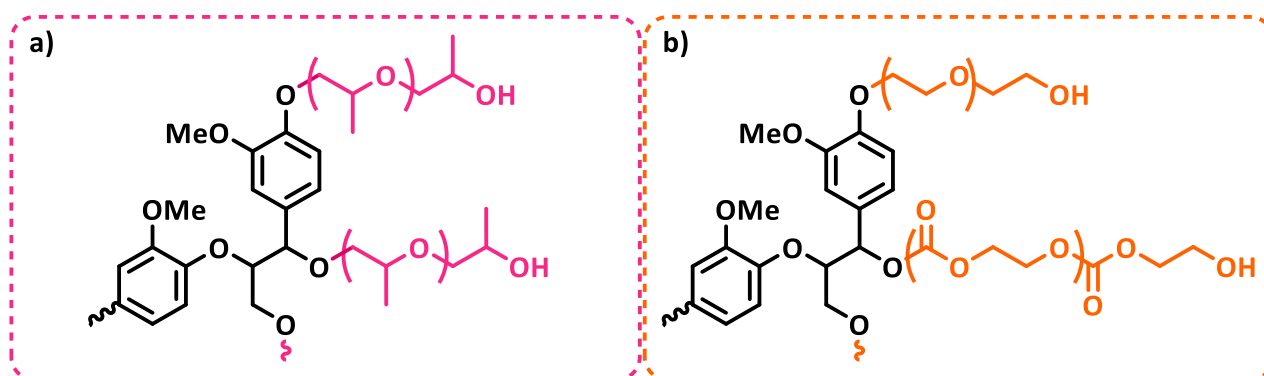
Scheme 3 Structure of oxyalkylated lignin prepared from a) propylene oxide or b) cyclocarbonate.

2.1.4. Non-isocyanate polyurethane (NIPU)

In recent years, there has been a shift towards developing safer alternative to isocyanate for the development of non-isocyanate polyurethane (NIPU)[173, 174]. Lignin-derived NIPU can be synthesized through the step-growth reaction between a carbonate (polycondensation) [175-177] or a cyclocarbonate (polyaddition)[178-183] and an amine (Scheme 4). Various methods have been developed to attach carbonate moieties onto lignin, such as the chemical fixation of CO_2 onto epoxidized lignin[178, 179, 181], etherification by glycerol carbonate ring-opening, followed by cyclocarbonation through ring-closing transesterification of dimethyl carbonate (Scheme 5)[180, 182, 183], or direct carbonation with dimethyl carbonate[175, 176]. In the pioneering work of Lee *et al.*, 3-aminopropyltriethoxysilane was used to initiate to the ring-opening of carbonated soybean oil[177]. The resulting urethane monomer was then cross-linked with Kraft lignin through silanization of aromatic –OH groups. Salanti *et al.* successfully prepared lignin-derived NIPU from cyclocarbonated soda lignin (hard segments), cyclocarbonated PEG (soft segments), and 1,12-diaminododecane (chain extender)[178]. Cyclocarbonated lignin was used as cross-linker in lignin-derived NIPU resins in various applications, including bio-adhesive[176], anti-bacterial coatings[179], and hybrid NIPU/epoxy composite[181]. To create high-performing lignin-derived NIPU foam, Sternberg and Pilla developed a non-toxic process involving the polyaddition of softwood Kraft lignin bearing cyclocarbonated moieties and dimer diamine (Priamine™ 1074) in a 1:1 ratio[182]. The resulting foam had

a density of 337 kg.m^{-3} and compressive strength of 0.17 MPa (Figure 4.h). The authors also investigated the chemical recycling of this bio-based foam through successive hydrolysis and glycolysis pathways[183]. Alternatively, Meng *et al.* introduced a new method to produce lignin-derived NIPU, where an aminated lignin was employed as a hard segment to cross-link a carbonate terminated prepolymer[184]. All these isocyanate-free modifications emerged as a promising approach to enhance the flexibility and adhesion performance of lignin-derived PU materials.
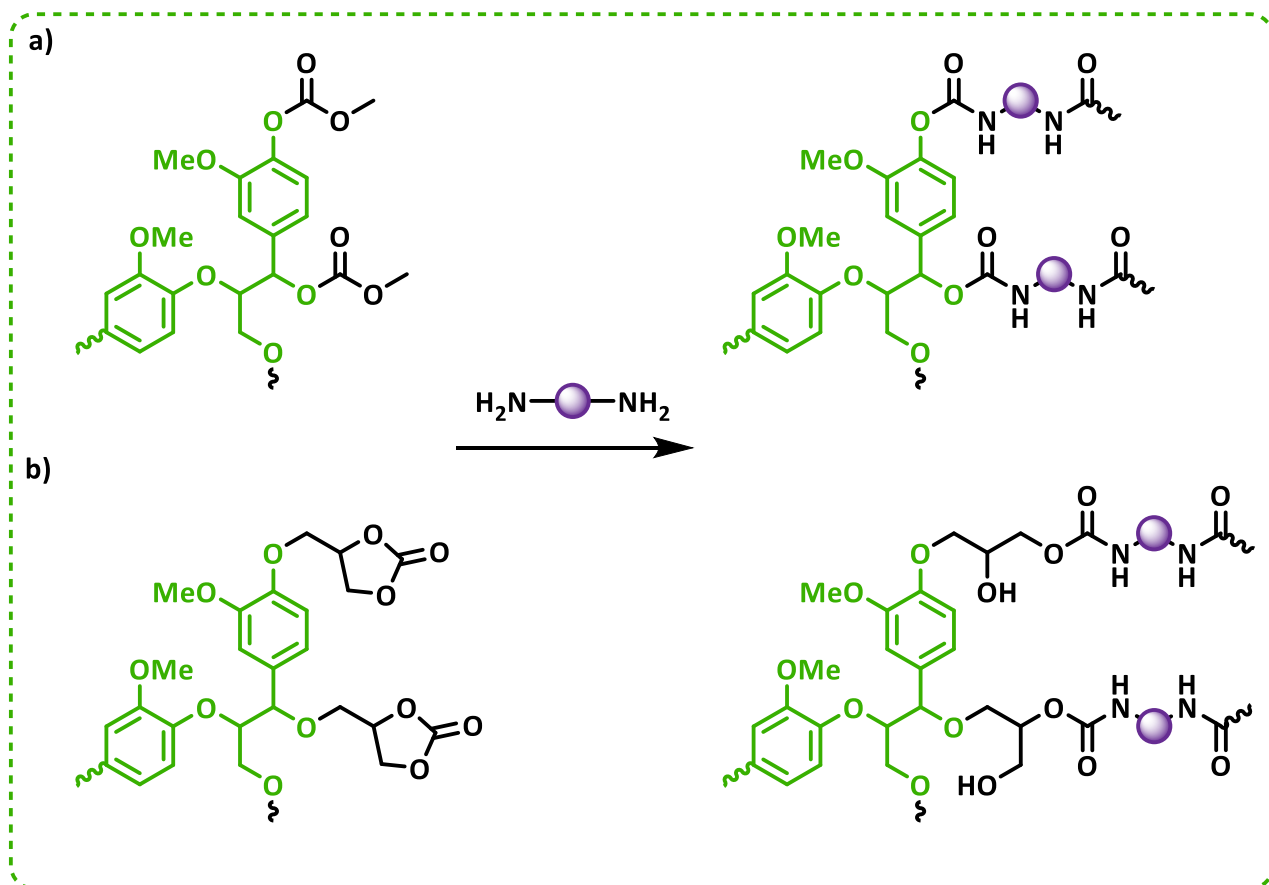
Scheme 4 Proposed scheme for the synthesis of non-isocyanate lignin-derived polyurethane by a) polycondensation or b) polyaddition.
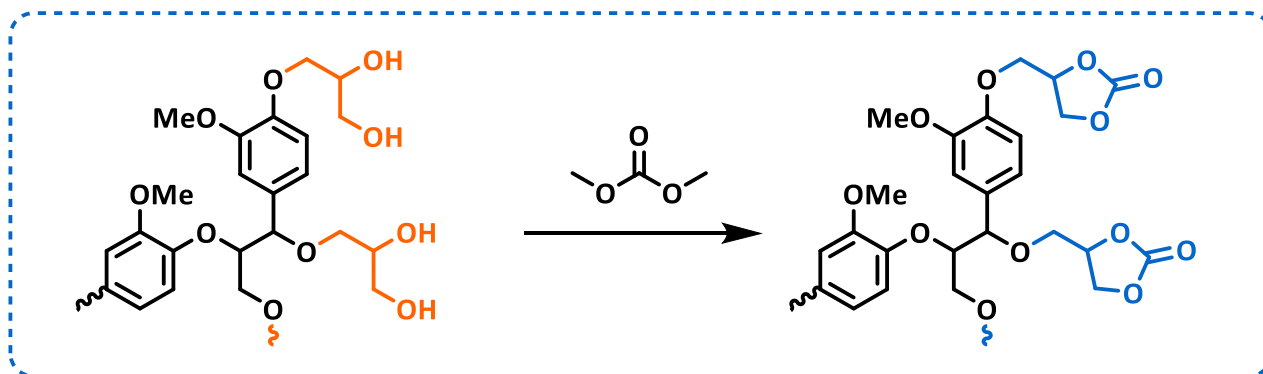
Scheme 5 Structure of cyclocarbonated lignin synthesized from oxyalkylated lignin (glycerol carbonate) and ethylene carbonate.
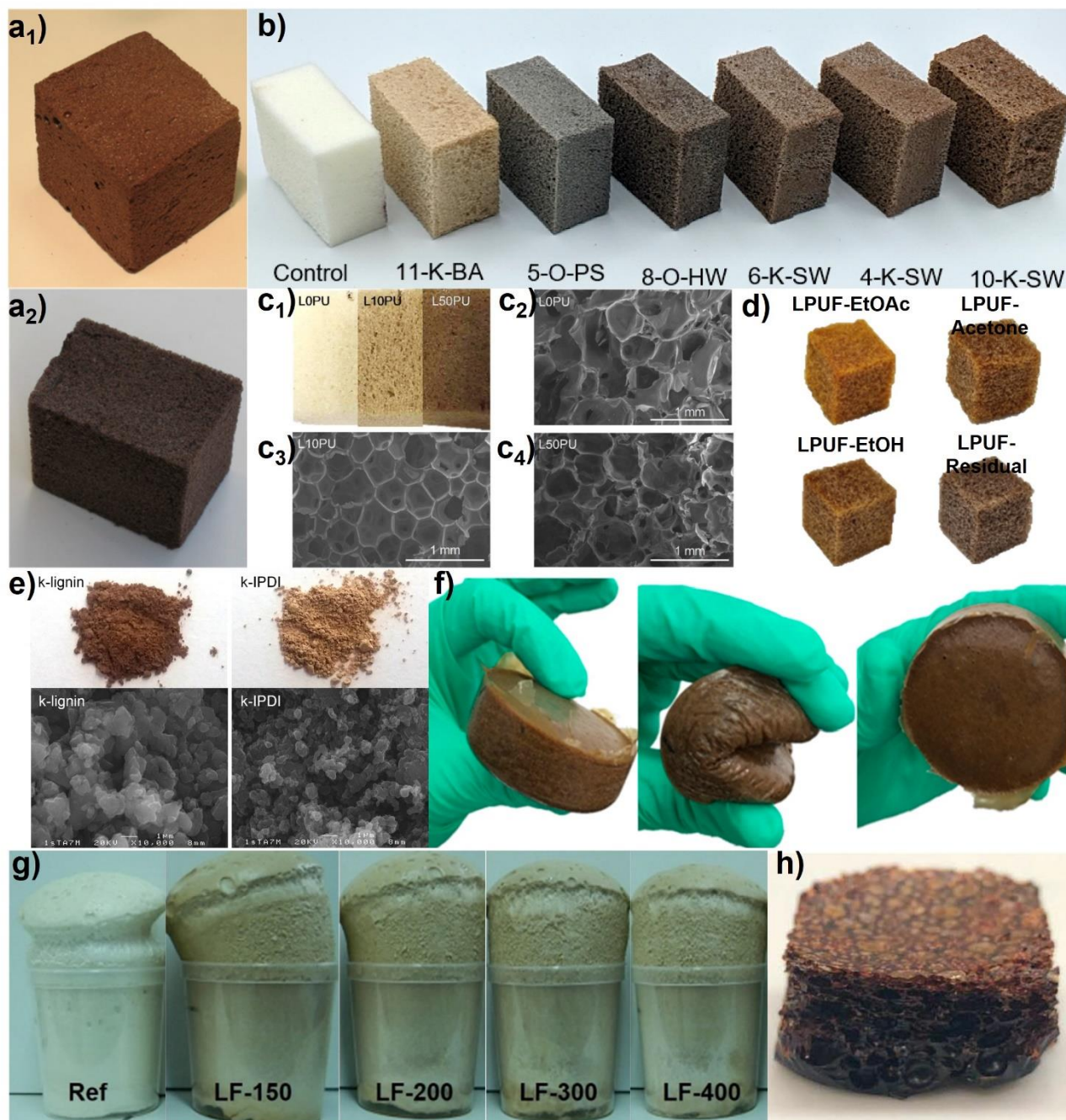
Figure 4 Examples of lignin-derived polyurethane foams.

(a-d) Rigid and (e-h) flexible lignin- PU foams. a) Photographs of RPUF containing (1) hardwood ethanol organosolv lignin or (2) hardwood kraft lignin (adapted from [94]). b) Photographs of FPUF prepared from various type of lignin (adapted from [103]). c) (1) Photographs RPUF prepared from LHO. SEM micrographs of RPUF containing (2) 0 %, (3) 10 %, and (4) 50 % of LHO (adapted from [128]). d) Photographs of LPUF prepared from different fractions of alkaline lignin (adapted from [133]). e) Photographs and SEM micrographs of unmodified and surface functionalized Kraft lignin (IPDI)(adapted from [147]). f) Photographs of resilient FPUF prepared from oxypropylated alkali lignin before, under, and after compression (adapted from [166]). g) Photographs of RPUF prepared from carbonate-hydroxyalkylated lignin (adapted from [169]). h) Photograph of NIPU foam prepared from Kraft lignin (adapted from [182]).

Table 1 Examples of PU foam synthesized from technical, refined, or chemically modified lignin.

Lignin source	* Foaming agents	** Manufacture process	LPUF characteristic (control characteristic)	Ref.
Hardwood organosolv-ethanol lignin	BA: H_2O SA: Tegostab® BF 2370 CA: Kosmos® 29 PO: [a] Voranol™	*Unmodified*: HEL 23 % HEL / [b] pMDI [1.1]	[1] ρ= 105 (118) kg.m^{-3} [2] σ_{comp}= 0.31 (0.51) MPa [3] K= n.c.	94
Kraft lignin (LignoForce™)	BA: Acetone/ H_2O SA: Silicone oil CA: [c] Mixture PO: [d] PPG$_{400}$	*Depolymerized:* Hydrothermal in NaOH (DKL50) 50 % DKL / [e] pMDI [1.1]	[4] ρ= 105 (56) kg.m^{-3} [5] σ_{comp}= 0.23 (0.11) MPa K= 38 (40) mW.m^{-1}.K^{-1}	113
Wheat straw soda lignin (Protobind™ 1000)	BA: H_2O SA: Silicone oil CA: [f] Mixture PO: [g] PPG triol	*Depolymerized:* Liquefaction in [h] GY/PEG$_{400}$ (PPG-D) 50 % LL / [i] pMDI [< 1]	[6] ρ= 80 (n.c.) kg.m^{-3} σ_{comp}= n.c. K= n.c.	123
Corn straw bagasse alkali lignin	BA: Teda-A33 / H_2O SA: Silicon oil CA: Stannous octoate PO: [j] Polyether 4110 A	*Fractionated/ Isocyanated* : gradient acid precipitation/ pre-polymer pMDI (SFL5.0) 50 % SFL5.0 / [k] pMDI [n.c.]	[7] ρ= 42 (45) kg.m^{-3} [8] σ_{comp}= 0.39 (0.18) MPa [9] K= 39 (38) mW.m^{-1}.K^{-1}	144
Corn stover organosolv lignin	BA: H_2O SA: Silicone oil CA: [l] Mixture PO: [m] Polyether ([n] BD)	*Fractionated/ Oxypropylated:* 15 % EtOH:H_2O (v:v)/ PO (B-RPF15= OFOL) 100 % OFOL / [k] pMDI [1.05]	[10] ρ= 85 (131) kg.m^{-3} [11] σ_{comp}= 0.83 (0.72) MPa K= 37 (47) mW.m^{-1}.K^{-1}	161
Softwood Kraft lignin (Indulin® AT)	BA: H_2O SA: Silicone oil CA: [o] DBTDL PO: n.c.	*Hydroxyalkylated carbonate*: [p] EC:PEG$_{400}$ mixt. (50:50 v:v) (OKL) 100 % OKL / [q] pMDI [1.2]	[12] ρ= 57 kg.m^{-3} [13] σ_{comp}= 0.14 MPa K= n.c.	170
Softwood Kraft lignin (BioChoice™)	BA: [r] PMHS SA: n.c. CA: n.c. PO: n.c.	*Non-isocyanate PU*: Hydroxyalkylation [s] GC/ Cyclocarbonation [t] DMC (CC) 100 % CC/ [u] DD [1]	ρ= 337 kg.m^{-3} [14] σ_{comp}= 0.17 MPa K= n.c.	182

* Foaming agents: BA= blowing agent, SA= surfactant, CA= catalyst, PO= commercial polyol (co-crosslinking agent).

** Nomenclature: percentage of polyol substitution by unmodified, refined, or modified lignin/ isocyanate (or amine for NIPU) source, and molar ratio hydroxyl (or amine for NIPU): isocyanate (or cyclocarbonate for NIPU).

[a] Voranol™ 270 [OH]= 4.3 mmol.g^{-1}, [b] PAPI 27™ [NCO]= 7.5 mmol.g^{-1}, [c] tri-ethanolamine, triethylene diamine, and dibutyltin dilaurate, [d] polypropylene glycol M$_n$= 400 g.mol^{-1}, [e] 31.2% –NCO content, [f] DABCO33LV gelling catalyst and DABCOBL11 blowing catalyst, [g] Polypropylene glycol triol, [h]

Glycerol/ Polyethylene glycol M_n= 400 g.mol^{-1}, [i] ISO 116/ 125.7 % –NCO content, [j] [OH]= 450 mg$_{KOH}$.g^{-1}, [k] pMDI 200, [l] stannous octoate and triethylenediamine, [m] polyether polyol (polyether 4110), [n] 1,4-butanediol, [o] dibutyltin dilaurate, [p] ethylene carbonate and polyethylene glycol M_n= 400 g.mol^{-1}, [q] [NCO]= 7.61 mmol.g^{-1}, [r] poly(methylhydrosiloxane), [s] glycerol carbonate, [t] dimethyl carbonate, [u] dimer diamine Priamine^{TM} 1074 [NH$_2$]= 209 mg$_{KOH}$.g^{-1}.

[1] Apparent density, [2] compressive strength measured according to ASTM D-1621 standard, [3] thermal conductivity, [4] measured according to ASTM D-1622-03 standard, [5] compression strength at 20 % deformation measured according to ASTM D-1621-00 standard, [6] Apparent density of PU foam prepared in free expansion, [7] measured according to GB/T 6343–2009 standard, [8] measured according to GB/T 8813–2008 standard, [9] measured according to GB/T 10294–2008 standard, [10] measured according GB/T 6343-95 standard, [11] compressive strength at 10 % deformation measured according GB/T 8813-2008 standard, [12] measured according to ASTM D-1622-08 standard, [13] measured according to ASTM D-1621-10 standard, [14] compressive strength at 10 % deformation.

Table 2 Examples of PU resins synthesized from technical, refined, or chemically modified lignin.

Lignin source	* Manufacture process	GC (%)	Resin characteristic	Application	Ref.
Wheat straw soda lignin (Protobind™ 1000)	*Unmodified*: WSSL 40 wt.%/ [a] PPGTDI (60 wt.%) [0.31]	n.c.	[1] E= 21 MPa [2] SH= 74 [3] T_g= -45 °C	Elastomer	111
n.c.	*Depolymerized*: NaOH (600-LPUe 40 wt.%)/ PPGTDI (60 wt.%) [0.14]	n.c.	[4] E_Y= 176 MPa [5] ε= 1394 % T_g= 8 °C	Elastomer	116
Hardwood organosolv lignin	*Fractionated*: Acetone (COL, 80 wt.%)/ [b] VA-NCO (20 wt.%) [0.17]	98	[6] $\sigma_{adhesive}$= 1.21 MPa [7] θ_{H2O}= 89.2 ° T_g= 163 °C	Adhesive/ hydrophobic coating	130
Hardwood organosolv lignin	*Esterified*: Lignin-fatty acid based polyol (LOAP, 89 wt.%)/ [c] PPGMDI (11 wt.%) [0.20]	n.c.	E_Y= 1.6 MPa ε= 173 % T_g= -7 °C	Elastomer	153
Softwood Sodium lignosulfonate (Vixilex SD)	*Oxypropylated*: [d] PO (LS-oxy, 10 wt.%)/ [e] CO (15 wt.%)/ [f] pMDI (75 wt.%) [1.20]	n.c.	[8] E_{flex}= 1.0 GPa [9] ε_{flex}= 4.5 % [10] T_α= 60 °C	Composite	158
Harwood Kraft lignin	*Hydroxyalkylated carbonate*: [g] PC (HKL_PC, 30 wt.%)/ [h] CO (23 wt.%)/ [i] pMDI (47 wt.%) [1.20]	n.c.	[11] $\sigma_{adhesive}$= 3.40 MPa E_Y= 48.9 MPa ε= 33 %	Adhesive	171
Wheat straw soda lignin (Protobind™ 1000)	*Non-isocyanate PU*: [j] Cyclocarbonation (Lign$_{CC}$, 29.9 wt.%)/ [k] PEGCC / [l] DAD [1.00]	n.c.	T_g= -15.7 °C	Elastomer	181

* Nomenclature: unmodified, refined, or modified lignin/ second polyol/ isocyanate (or amine for NILPU) source, and molar ratio isocyanate: hydroxyl (or amine: cyclocarbonate for NILPU).

[a] Tolylene 2,4-di-isocyanate terminated poly(propylene glycol) (M_n= 2300 g.mol^{-1}), [b] Vanillic acid based α,ω-diisocyanate, [c] Methylene 4,4-di-isocyanate terminated poly(propylene glycol) (M_n= 425 g.mol^{-1}), [d] Propylene oxide, [e] Castor oil [OH]= 155 mg$_{KOH}$.g^{-1}, [f] Desmodur® 44V20L/ 31.3 % –NCO content, [g] Propylene carbonate, [h] Castor oil [OH]= 159 mg$_{KOH}$.g^{-1}, [i] 32.9 % –NCO content, [j] cyclocarbonated lignin (M_n~ 2400 g.mol^{-1}, [CC]= 1.35 mmol.g^{-1}), [k] cyclocarbonated polyethylene glycol (M_n~ 2400 g.mol^{-1}), [l] 1,12-diaminododecane.

[1] Storage modulus (complex G), [2] Shore hardness value (type A), [3] Glass transition temperature (DSC), [4] Young modulus, [5] Elongation at break, [6] Dry adhesive strenght wood, [7] Static contact angle with an ultrapure water drop, [8] Flexural strenght (three points system), [9] Flexural deformation, [10] α-relaxation temperature, [11] Single-lap shear test between two wood plates.

2.2. Lignin-derived phenolic resins

Phenolic resin, a commonly used wood adhesive in the construction industry, has piqued the interest of diverse stakeholders due to its exceptional characteristics. This resin is synthesized *via* the step-growth polymerization of phenol and formaldehyde used at different proportions to control the degree of cross-linking[185]. When there is an excess of formaldehyde over phenol, a thermoset-like resin (resole) is formed, while an excess of phenol leads to a thermoplastic-like resin (novolac). However, the scarcity and increasing cost of petroleum-based phenol retrieved from the cumene hydroperoxide process have prompted the exploration of alternative bio-based sources. Polyphenolic lignin, which is abundant on Earth, is a prime candidate for substituting synthetic phenol in the production of bio-based phenol-formaldehyde (PF) resins[186-188]. Although extensive research studies have been conducted on incorporating lignin into PF resin[189-191], the chemical heterogeneity of lignin remains a significant challenge, as it impedes its large-scale inclusion in PF resin without compromising the curing process (gelation and viscosity), mechanical stability, and adhesion performance. In most of the reported cases, the content of lignin does not exceed 50 wt.% phenol replacement independently of its origin or its extraction process[192-204].

In conventional PF resins, formaldehyde substitutes phenolic *ortho-* and *para-*positions due to an electron-donating effect. However, in the case of lignin, formaldehyde substitutes only *ortho-*free positions to form a hydroxymethyl group, which is then polymerized with aromatic rings through a methylene bridge (Scheme 6). Lignin mainly consists of methoxylated phenolic units (G and S), and refining and functionalization strategies aim to enhance its reactivity toward formaldehyde, and increase the percentage of lignin replacement in some cases. Recent studies also aim to make lignin-derived PF (LPF) resins more environmentally friendly and safer by replacing formaldehyde, which is classified as a carcinogen for humans[205].
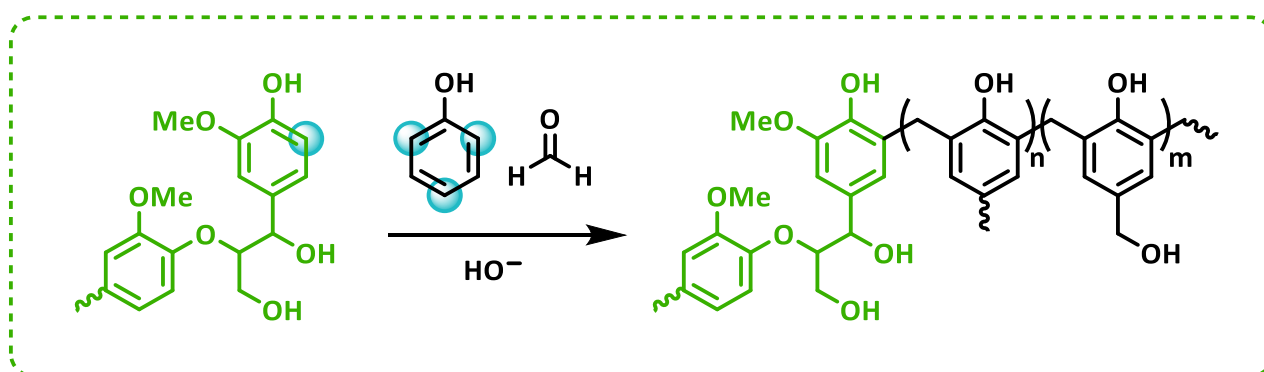
Scheme 6 Proposed scheme for the synthesis of lignin-derived phenolic resin (reactive sites highlighted in blue).

2.2.1. Phenolic resins from technical lignins

The development of lignin-based adhesives has gained attention as a promising strategy to reduce the use of phenol and other harmful chemicals in the wood industry. The elucidation of the structure-to-property relationship of lignins extracted from different LCB through various isolation process has been essential to understanding the reactivity of phenolic active sites in adhesive performance[206-209]. Researchers have found that lignin with abundant phenolic groups, narrow molecular weight distribution, and unsubstituted aromatic positions are the most suitable features for polymerization in wood adhesives[206]. Among various technical lignins, Kraft and soda-anthraquinone pulps display higher reactivity toward formaldehyde condensation and the higher total phenolic content of Kraft lignin can improve the adhesive performance ($[OH]_{phe} \sim 4$ g.mol^{-1})[207]. Furthermore, organosolv pulping has been shown to be effective in substituting synthetic phenol in LPF resins by utilizing low-molecular-weight lignin fractions enriched in *ortho*-free phenolic active sites (Figure 5.a)[208, 209].

2.2.2. Phenolic resins from refined lignins

2.2.2.1. Depolymerization

By employing different depolymerization strategies, researchers have successfully developed lignin-based adhesives with tailored properties, such as superior bonding strength and low formaldehyde emissions, while achieving high levels of phenol substitution. The alkaline-catalyzed HTL is known to narrow lignin heterogeneity, increase the content of active sites (up to 48 wt.% in lignosulfonate[210]), and accelerate curing kinetics[211]. Yan *et al.* retrieved lignin fragments from the depolymerization of corn stalk in hot-compressed water (T= 260 °C, t= 10-30 min)[212]. They then partially substituted synthetic phenol with liquefied lignin, which exhibited a dry adhesive strength of 1.19 MPa with 60 wt.% phenol substitution. In an eco-friendly and cost-effective depolymerization strategy, Li *et al.* used aqueous NaOH/urea mixture to cleave β-O-4' ether bridges in alkali lignin under mild conditions (T= − 16 °C, t= 24 h), and form phenylpropane trimers with active protons in higher amounts [213]. LPF resins containing 50 % of this depolymerized lignin met the standard for exterior-grade plywood panels.

Hydrogenolysis proved also to be effective in refining lignin into functional and low molecular-weight fragments in view of producing LPF resins (Figure 5.b)[214, 215]. Cheng *et al.* reported the nickel-catalyzed hydrogenolysis to convert an organosolv lignin into low-molecular-weight fragments ($M_n \sim$ 200-600 g.mol^{-1})[214]. The depolymerized lignin incorporates LPF resins characterized by a superior adhesive strength and reduced free formaldehyde content (75 wt.% phenol substitution, $\sigma^*_{adhesive} > 1.5$ MPa in dry and wet conditions, FA$_{free}$= 0.7 %).

Solvent fractionation is a useful approach for managing the functionality and distribution of the molecular weight of specific lignin fraction [71]. With a potential to be sourced renewably, acetone[131, 216], ethyl acetate[217], and various alcohol[218] were selected as extraction solvent for the one-step fractionation of lignin in view of producing LPF resins. Arefmanesh *et al.* investigated acetone fractionation in the design of phenolic resins consisting entirely of lignin[131]. The acetone soluble fraction of softwood Kraft lignin, characterized by a narrower dispersity and a higher total phenolic content (Đ= 2.1, $[OH]_{phe}$= 3.86 mmol.g^{-1}), displayed superior adhesive strength compared to the lab formulated PF resin ($\sigma^{*}_{adhesive,dry}$= 4.4 and 3.4 MPa, respectively). In comparison to the direct incorporation of Kraft lignin, the superior bonding performance of LPF adhesives prepared from the ethyl acetate soluble fractions originates from higher solubility and miscibility in the resin (Figure 5.c)[217]. Recently, Wang *et al.* employed sequential fractionation of hardwood Kraft lignin at the refluxing temperature of organic solvents (*iso*-propanol, ethanol, methanol) to obtain homogeneous and functional lignin fractions with a narrow distribution and a tunable phenolic content (Đ= 1.1-1.3, $[OH]_{phe}$= 3.01-3.82 mmol.g^{-1})[218]. LPF resins with customized wet bonding strength and low formaldehyde emissions were supplied after phenolation reactivity enhancement and formaldehyde polymerization, (Figure 5.d, $\sigma_{adhesive,wet}$= 1.00-2.16 MPa, $FA_{emissions}$< 0.4 mg.L^{-1}). Kalami *et al.* used a patented methodology[219] to isolate low-molecular-weight phenolic oligomers (M_n= 552 g.mol^{-1}) from a lignin bio-residue obtained after the conversion of agricultural biomass into ethanol[220]. The isolated lignin retrieved after acid precipitation was further reacted with formaldehyde in 100 % lignin-derived plywood adhesive ($\sigma^{*}_{adhesive,wet}$= 2.6 MPa, FA_{free}= 7.1 %).

In summary, fractionation through solvent extraction or acid precipitation appears as an effective refining strategy to achieve complete substitution of synthetic phenol in lignin-derived PF resins.

2.2.3. *Phenolic resins from chemically modified lignins*

For a considerable period of time, researchers have explored chemical modifications like hydroxymethylation, phenolation, and demethylation to increase the reactivity of lignin toward formaldehyde[221, 222].

Also known as Lederer-Manasse hydroxyalkylation, the base-catalyzed addition of formaldehyde on the aromatic C_5 positions of G and H units introduce hydroxymethyl to form lignin pre-polymer (Scheme 7.a)[223-225]. Taverna and colleagues identified the content of formaldehyde, the pH, and the temperature as reaction parameters affecting the activation of various technical lignin by hydroxymethymation[226]. Even though this method may not increase the degree of phenolic reactive sites[227], methylolated lignin can substitute up to 50 wt.% of synthetic phenol in LPF resins[228] ($\sigma_{adhesive,wet}$= 1.16 MPa, FA_{free}= 0.17 %).

In the phenolation pathway, the *ortho-* and *para*-positions of synthetic phenol react with the aliphatic –OH groups of lignin under acidic[229-233] or alkaline[234-236] conditions (Scheme 7.b). The acid-catalyzed phenolation process involves the β-elimination of the γ-hydroxymethyl group in the β-O-4' interunit linkage, resulting in phenolated lignin containing a higher content of phenolic active sites and lower molecular weight fractions stemming from side-chain cleavage[229]. In the presence of oxalic acid, the addition of phenol on the *ortho*-position of lignosulfonate predominates over the *para*-addition adduct[230]. Podschun *et al.* optimized the acid-catalyzed phenolation of an organosolv lignin to reach a maximum phenolation level of 1.8 phenols per lignin C_9 unit[231], representing a total amount of reactive sites of 9.0 mmol.g^{-1}. The degree of phenolation correlates to the content of aliphatic –OH groups[232] and can result in LPF resins with enhanced internal bond strength (40 wt.% phenol substitution, $\sigma^*_{adhesive,dry}= 0.67$ MPa)[233].

Yang *et al.* investigated the base-catalyzed phenolation of technical lignins obtained from different biorefinery processes, resulting in a significant increase in degree of *ortho*-free active sites compared to unmodified lignins (from 0.99-1.72 to 2.20-3.14 mmol.g^{-1}, respectively)[234]. By optimizing the phenolation of a steam-exploded lignin, LPF resins containing up to 70 wt.% of phenolated lignin can be produced ($\sigma_{adhesive,wet}= 0.72$-1.15 MPa)[235].

2.2.3.3.   Demethylation

Through the nucleophilic addition of demethylation catalysts such as enzymes[237], alkyl halides[238], halogen acids[239] or salts[240-242], the aromatic methoxy groups of lignin backbone turn into reactive catechol moieties (Scheme 7.c). Li and colleagues optimized the sulfur-mediated demethylation process of lignin under mild conditions[240, 241]. With a content of –OMe groups decreasing from 1.93 to 1.09 mmol.g^{-1}, LPF resins produced from demethylated lignin exhibit fast curing speed and superior adhesive performance (50 % phenol substitution, $\sigma^*_{adhesive,wet}= 1.07$ MPa, $F_{emission}= 0.22$ mg.L^{-1}).
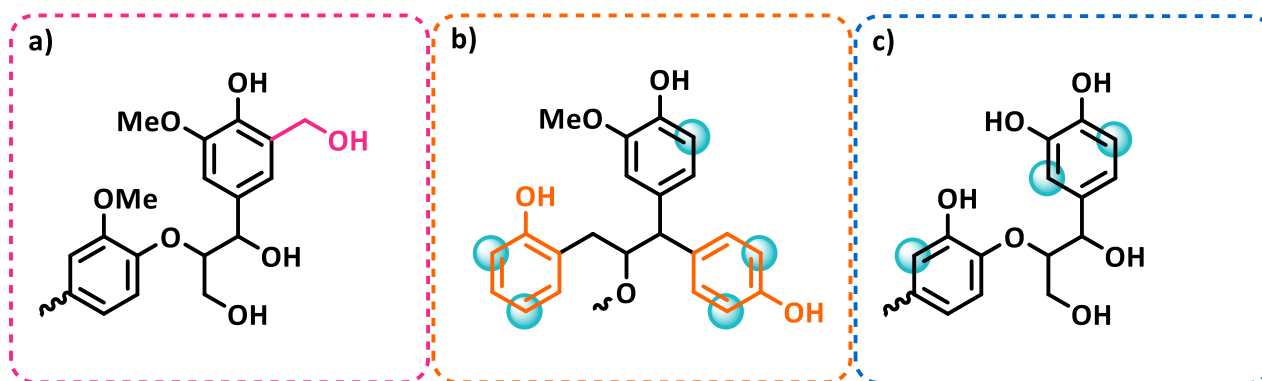
Scheme 7 Structure of a) hydroxymethylated, b) phenolated, and c) demethylated lignin.

2.2.4. Formaldehyde-free phenolic resins

2.2.4.1.   Glyoxal

Lignin is chemically heterogeneous, which makes it difficult to achieve complete addition of carcinogenic, mutagenic, and reprotoxic formaldehyde in PF resins. International standard specifications therefore restrict formaldehyde emissions to a certain level depending on the application, and sustainable alternatives are being developed to make lignin-derived phenolic resins safer and more environmentally friendly. In this regard, Mansouri *et al.* have demonstrated the potential of using glyoxal, the simplest non-volatile dialdehyde, as a substitute for formaldehyde in wood panel adhesive (Scheme 8.a)[243-245]. Preliminary results indicate sufficient reactivity between lignin and glyoxal for this purpose. Similarly to the pre-activation step with formaldehyde, glyoxalation could also enhance the reactivity of lignin in phenolic resin[29]. Brosse and coworkers have investigated the use of glyoxalated tannin and steam-exploded lignin as a sustainable alternative to formaldehyde-based phenolic resins[246]. They found that an equimassic mixture of glyoxalated lignin and tannin exhibited a higher maximum modulus of elasticity ($MOE_{max} \sim$ 6 GPa) compared to other mixtures. In another study, Hussin and colleagues have produced a series of lignin-phenol glyoxal resins using organosolv pulp from oil palm fronds (OLPG)[247], as well as lignin pulp extracted from kenaf core (SLPG)[248] or coconut husk (KLPG)[249] through Kraft and soda processes, respectively. OLPG resins show higher viscosity and shorter gel time due to the higher loading of glyoxalated lignin when formulated with synthetic phenol (50 wt.% phenol substitution, η= 1000 cP, gel time= 60 s)[247]. Meanwhile, the lignin recovered from the soda process has functional polyols that benefits the development of SLPG resins with strong mechanical properties (30 wt.% phenol substitution, σ= 72 MPa, ε= 34.4 %)[248]. Siahkamari *et al.* evaluated the gradual substitution of formaldehyde with glyoxal for interior-grade plywood adhesive and found that the alkalinity decreased concurrently with the increased viscosity as formaldehyde was replaced with glyoxal (100 % glyoxal, 2.4 % alkalinity, η= 60 cP) [250]. Finally, the optimized lignin-glyoxal resin exhibits similar adhesive properties to the all-lignin-based resin prepared with formaldehyde (Figure 5.e, $\sigma^*_{adhesive,dry}$= 3.9 and 4.0 MPa, respectively).

2.2.4.2.   Furfural derivatives

Furfuryl alcohol and 5-hydroxymethyl furfural, obtained from the catalytic dehydration of glucose, have demonstrated effectiveness in cross-linking lignin to produce various lignin-derived thermosets[251], bio-composites[252], or ion-exchange resins (Figure 5.f)[253]. Furfural, a monofunctional furan-based aldehyde, reacts at the *ortho*-free positions of lignin to produce phenolic resins (Scheme 8.b)[254]. Introduced as a cross-linking agent in LPF resin prepared from phenolated Kraft lignin, furfural showed similar adhesion properties compared to the commercial PF resin (15 wt.% furfural, $\sigma^*_{adhesive,wet} \sim$ 1.3 MPa). Dongre *et al.* designed a lignin-furfural based adhesive from an unpurified lignin recovered from sugar maple by acid hydrolysis of hot-water extract[255]. The adhesive was prepared under acidic conditions

and exhibited comparable mechanical properties to the control PF resin reinforced with glass fibers (16 % furfural, E= 3.9 and 3.5 GPa, respectively).
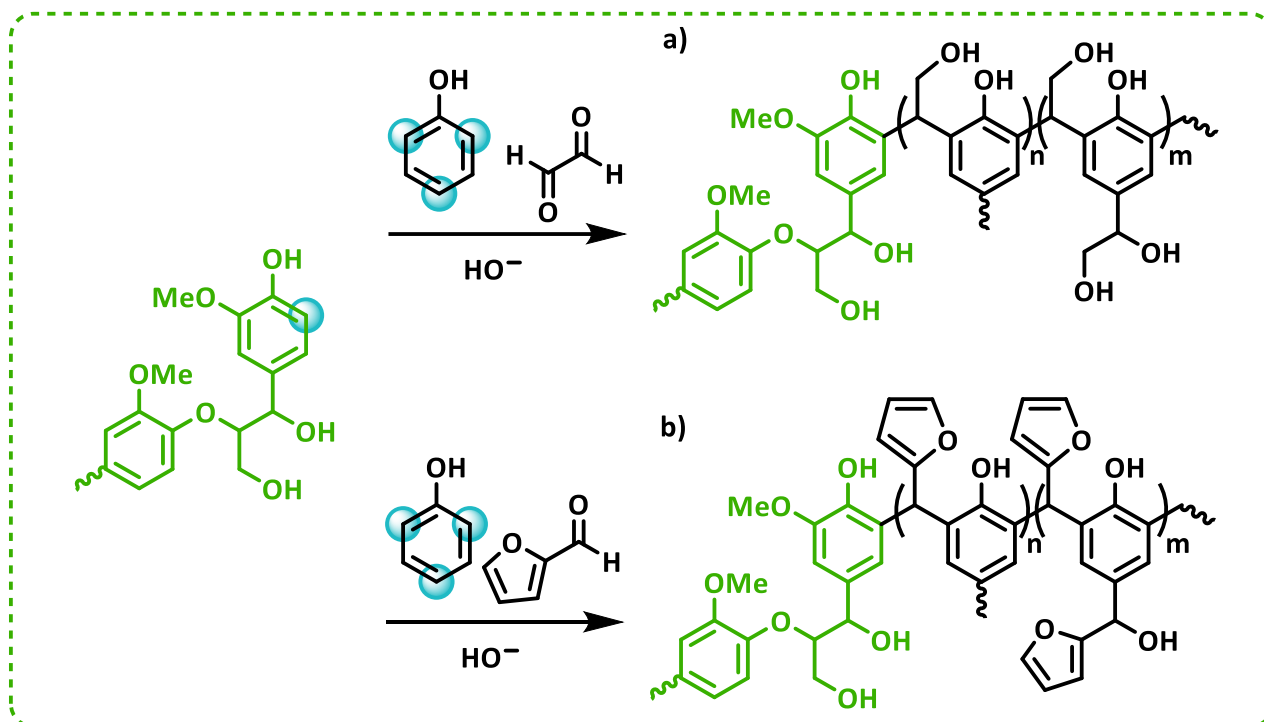
Scheme 8 Proposed scheme for the synthesis of formaldehyde-free lignin-derived phenolic resin using a) glyoxal or b) furfural as aldehyde source.
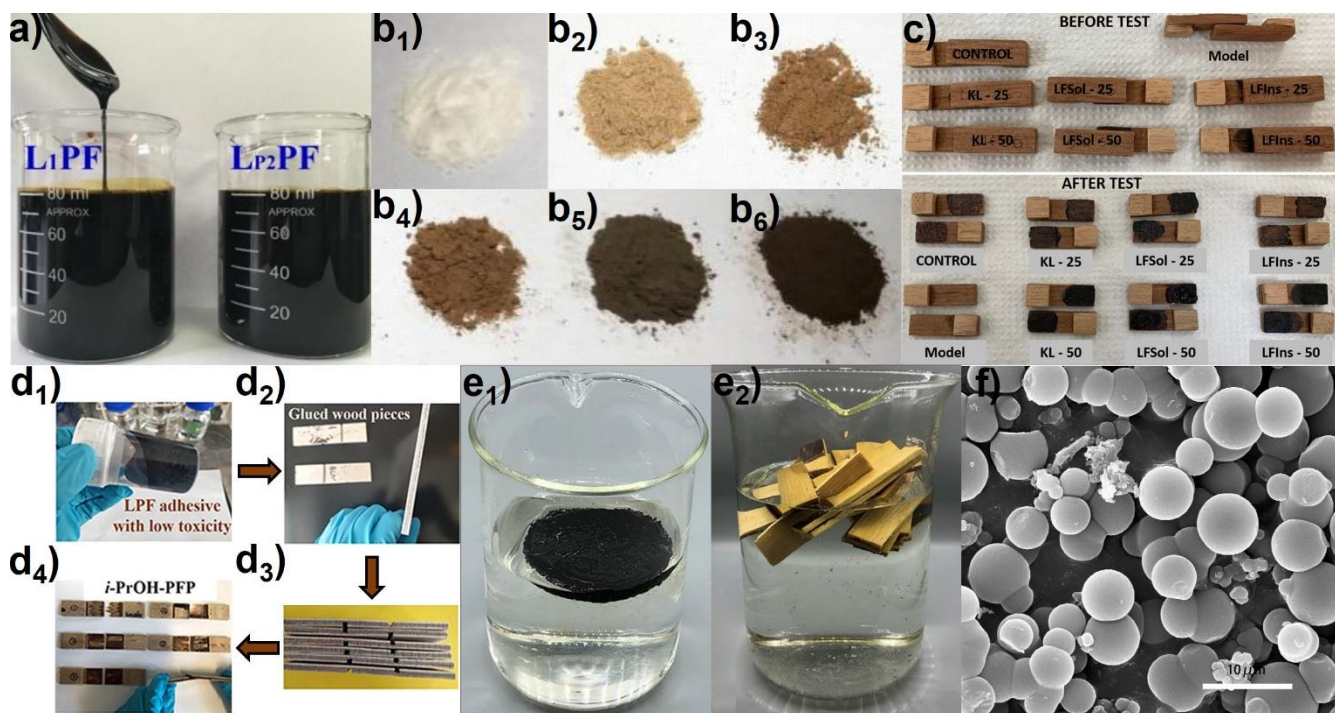
Figure 5 Examples of lignin-derived phenolic resins.

a) Photographs of LPF resins prepared from technical lignins obtained from an acidic and an alkaline organosolv pulping of bamboo (adapted from [208]). b) Photographs of PF resins prepared containing (1) 0 %, (2) 20 %, (3) 30 %, (4) 40%, and (5) 50 % of depolymerized lignin oil, and (6) technical lignin (adapted from [215]). c) Photographs of glued birch veneers specimens using the control PF resin and LPF resins prepared from technical and fractionnated Kraft lignin (adapted from [217]). d) Plywood manufacture process and workflow test using LPF adhesive prepared from fractionated and phenolated alkaline lignin. Photographs of (1) LPF adhesive, (2) glued wood pieces, (3) specimens after boiling−drying−boiling pretreatment, and (4) wood failure performance (adapted from [218]). e) Photographs of lignin-glyoxal adhesive during (1) water resistance test and (2) single-lap plywood detached after the boiled water test (adapted from [250]). f) SEM micrographs of lignin-based material prepared from the condensation of lignosulfonate and in-situ generated hydroxymethylfurfural (adapted from [253]).

Table 3 Examples of phenolic resins synthesized from technical, refined, or chemically modified lignin.

Lignin source	* Manufacture process	LPF characteristic (control characteristic)	Application	Ref.
Bamboo organosolv lignin	*Unmodified*: 50% L/ [a] FA (n.a.)	[1] $\sigma_{adhesive, wet}$ = 0.94 (1.53) MPa [2] FA_{em} = 0.36 (0.25) mg.L^{-1}	Plywood adhesive (poplar veneers)	132
Technical corn stalk lignin	*Depolymerized*: hot-compressed water (DLPF) 60% DLPF/ FA (1:1.8)	[3] $\sigma_{adhesive,dry}$ = 1.19 (0.92) MPa [4] FA_{free} = 0.23 (0.05) %	Plywood adhesive (poplar veneers)	212
Softwood Kraft lignin	*Fractionated*: acetone soluble lignin (AS-L) 100% AS-L/ FA (1:2)	[5] $\sigma^{*}_{adhesive,dry}$ = 4.4 (3.4) MPa [6] FA_{free} = 1.3 (0.3) %	Plywood adhesive (poplar veneers)	131
Corn stalk steam-exploded alkali lignin	*Hydroxymethylated*: 37% FA, NaOH 5M (L) 30% L/ FA (1:1.6)	[7] $\sigma_{adhesive,wet}$ = 0.92 (1.41) MPa [8] FA_{free} = 0.17 (0.24) %	Plywood adhesive (poplar veneers)	228
Beech organosolv lignin	*Phenolated*: phenol, [b] H$_2$SO$_4$ conc. (pOL) 40% pOL/ FA (1.5:1)	[9] $\sigma^{*}_{adhesive,dry}$ = 3.8 (6.8) MPa [10] FA_{em} = 0.26 (0.92) mg.$_{100}$g^{-1}	Particleboard adhesive (veneer strips)	233
Acidified alkali lignin	*Demethylated*: NaOH, [c] Na$_2$SO$_3$, (DLPF-Y1) 50% DLPF-Y1/ FA (1:2.2)	[5] $\sigma^{*}_{adhesive,dry}$ = 1.07 (1.24) MPa [11] FA_{em} = 0.22 (0.42) mg.L^{-1}	Plywood adhesive (eucalyptus veneers)	241
Biorefinery corn stover lignin	*Formaldehyde-free*: opt. lignin-glyoxal (OLG) 100% OLG/ [d] GA (1:2)	[12] $\sigma^{*}_{adhesive,dry}$ = 3.9 (4.6) MPa [6] FA_{free} = 0 (0.22) %	Plywood adhesive (Douglas fir veneers)	250

* Nomenclature: percentage of synthetic phenol substitution by unmodified, refined or modified lignin/ aldehyde source, and molar ratio phenol: aldehyde.

[a] formaldehyde, [b] sulfuric acid, [c] sodium sulfite, [d] glyoxal.

[1] Bonding strenght measured according to GB/T 17657-2013 standard, [2] Formaldehyde emission measured according to Chinese National Standard GB/T 9846-2004.3.standard, [3] Tensile strenght measured according to GB/T 17657-1999 standard, [4] Free formaldehyde content determined according to hydroxylamine hydrochloride standard method, [5] Lap shear strength measured according to ASTM D906-98 A standard, [6] Hydroxylamine hydrochloride standard method (European Standard DIN EN ISO, 9397, 1995), [7] GB/T 14732-2006 standard, [8] Hydroxylamine hydrochloride standard method (Chinese National Standard ISO 9397:1995), [9] European Standard EN 319-1993, [10] European Standard EN 120-1992 (mg per 100 g of oven dry board), [11] Formaldehyde emissions measured according to the acetylacetone standard method, [12] Lap shear strenght measured according to ASTM D5868-01 standard.

2.3. Lignin-derived epoxy resins

Epoxy resins are widely used in the production of thermoset composites due to their exceptional chemical, mechanical, and thermal resistance[256]. The ring-opening polymerization (ROP) of oxirane cyclic ethers is initiated by the heteroatomic or carbon nucleophile precursors under the influence of an external stimulus[257]. Curing agent, more commonly known as hardeners (multifunctional amines, acids, anhydrides, alcohols, phenols, or thiols), are combined with epoxide precursors to tailor the properties of thermosets. Epoxide groups are commonly grafted onto bisphenol-A (BPA) through the O-glycidilation with epichlohydrin (ECH)[258]. Upon curing, the aromatic structure of bisphenol-A diglycidyl ether (BADGE) confers significant rigidity to the cross-linked epoxy network. One of the challenges in enhancing the sustainability of epoxy resins is finding non-toxic and bio-based alternatives to carcinogenic and petroleum-based BPA. In this regard, lignin biopolymer holds potential to replace BPA[65, 259].

2.3.1. Epoxy resins from technical lignins

The incorporation of lignin into epoxy resins resulted in a cross-linked network upon thermal curing[260-262]. Among the various functionalities supported by lignin macromolecules, carboxyl and unsubstituted aromatic –OH groups promote the ROP of epoxy groups[263]. These functionalities reacts mainly with the less substituted carbon of oxirane rings through S_N2 nucleophilic additions. As result, technical lignins can be incorporated as hardener in the design of epoxy resin from polyethylene glycol diglycidyl ether (PEGDGE, M_n= 526 g.mol^{-1})[264]. Most often sterically hindered by –OMe groups or condensed structures, the reduced reactivity of phenolic units hampers the potential of technical lignins to be used as epoxy hardener.

2.3.2. Epoxy resins from refined lignins

Depolymerization intents to increase the availability of lignin –OH groups toward the ring-opening of oxirane rings. For example, the higher reactivity of depolymerized lignosulfonate (M_n= 400 g.mol^{-1}) as co-hardener in a commercial epoxy resin is reflected by the lower activation energy and curing temperatures[265]. Fractionation also provides low molecular-weight fragments that can cross-link epoxidized PEG (Figure 6.a)[266], glycerol[267], vegetable oils[268], or resorcinol[269]. Asada *et al.* used the acetone soluble fraction of lignin retrieved from waste Moso bamboo to cure a commercial BADGE resin[270]. In comparison to a control aliphatic polyamine, the fractionated lignin provides superior thermal resistance to the epoxy resin ($T_{d5\%}$= 298 and 327 °C, respectively). However, the direct incorporation of technical[31, 262] or fractionated[267] lignin as reactive fillers in epoxy matrix faces reactivity and compatibility issues, making derivatization a preferred method to develop lignin-derived epoxy resins.

### 2.3.3. Epoxy resins from chemically modified lignins

2.3.3.1. Amination

To address microscopic and thermo-mechanical immiscibility above a certain lignin loading, one approach is to convert lignin into a bio-based hardener. Various methods have been developed to derivatize lignin with primary and secondary amines, such as the Mannich condensation of technical[271-273] or epoxidized lignin[274] (Scheme 9.a), or the ring-opening of epoxidized lignin with an excess of diamine[275, 276] (Scheme 9.b). Some studies recommended phenolation pre-treatment to selectively functionalize the free *ortho*-positions of softwood Kraft lignin under Mannich conditions[271]. The molecular flexibility of aminated lignin afforded a controlled tailoring of resin properties, as identified by Ott *et al.*, who showed that aminated lignin chains play a paramount role in the mechanical properties of lignin-derived epoxy resins (Figure 6.b)[272]. Partial substitution of commercial hardener with aminated lignin resulted in homogenous epoxy films characterized by improved thermal stability (40 wt.% substitution of isophorone diamine)[276]. Alternatively, Nikafshar *et al.* followed a three-step pathway to design an amine hardener from softwood Kraft lignin *via* successive demethylation, tosylation, and metal-catalyzed amination[277]. The aminated lignin was cross-linked with BADGE to produce uniform lignin-derived epoxy resins (T_g= 158 °C, σ= 87 MPa, ε= 3.23 %).

2.3.3.2. Esterification

The ring-opening of cyclic anhydrides generates active hydrogen species that promote cross-linking into epoxy resins[257, 278-285]. Hatakeyama and colleagues were the first to convert alcoholysis lignin[278, 279] or sodium lignosulfonate[280] into anhydride hardener (Scheme 9.c). Succinic anhydride reacts with lignin –OH groups by esterification to generate a mixture of polyacids containing lignin-derived poly(ester-carboxylic acid), sometimes with ethylene glycol[278, 279] or glycerol[280] as a reactive diluent,. After reacting with ethylene glycol or glycerol diglycidyl ether (EGDGE[279] and GDGE[280], respectively), lignin acts as a hard segment in the copolymer. Later, Jin and colleagues comprehensively evidenced the synergistic effect of rigid lignosulfonate and flexible EG segments on enhancing the thermal, mechanical, and shape-memory performance of BADGE-type epoxy resin[281]. Researchers have also taken advantage of the high solubility of partially depolymerized Kraft lignin[282] or organosolv lignin[283] to conduct the esterification with succinic anhydride. When used as polycarboxylic acid curing agent in commercially available epoxy resins (DER353[282] or DER332[283]), the addition of co-curing agent[282] or an increasing amount of carboxylated lignin[283] strengthened the thermo-mechanical properties of lignin-derived epoxy resins (Figure 6.c). Liu *et al.* suggested that the toughening effect of carboxylated lignin in epoxy monophasic networks originates from a balance of segmental confinement, reduced cross-linking density, and increased free volume[284]. Recently, Ma and colleagues opted for the glycidol-mediated hydroxyalkylation of EHL to increase the rate of carboxylation through esterification with maleic anhydride[285]. The multi-

carboxylated lignin was later combined with epoxidized soybean oil and citric acid to yield degradable lignin-derived epoxy resins with superior performance (E_Y= 60.2 MPa, σ= 10.1 MPa, ε= 55.1 %).
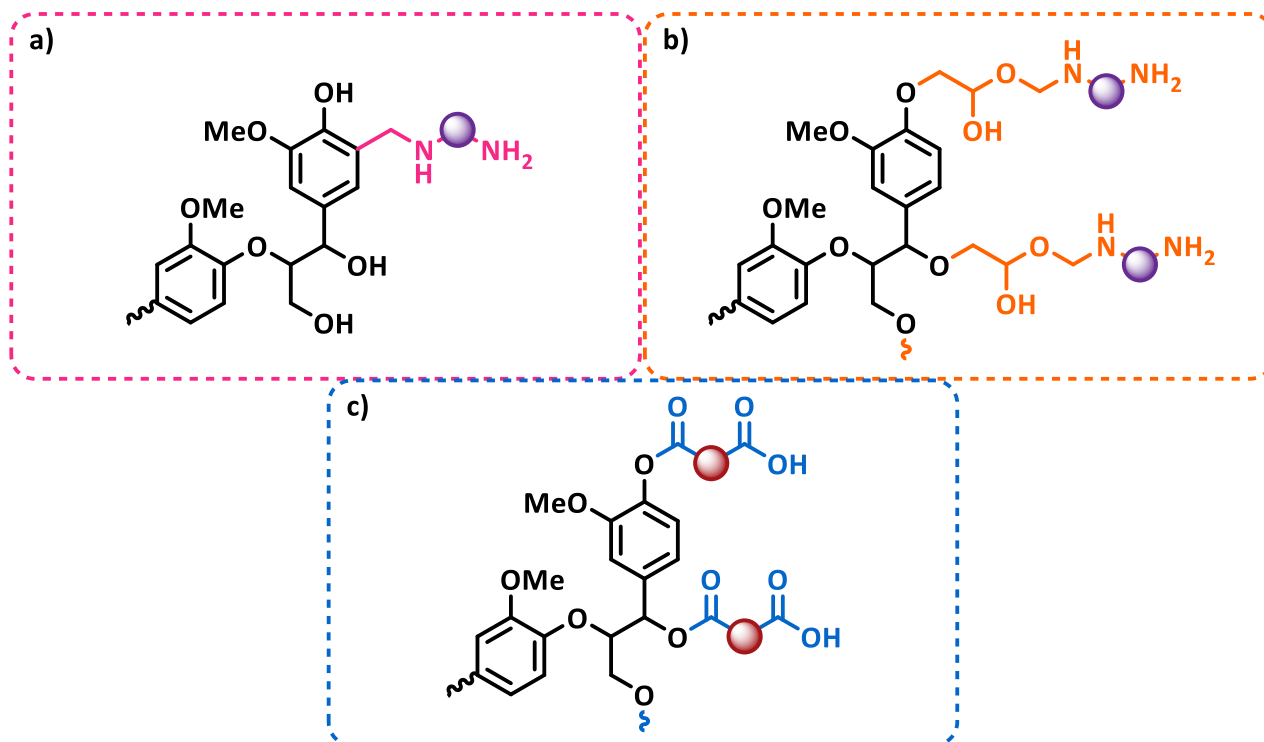
Scheme 9 Structure of lignin hardener in epoxy resins. Aminated lignin designed from a) Mannich condensation or b) ring-opening of oxirane groups with a diamine. Carboxylated lignin designed from c) esterification with anhydride.

2.3.3.3.   Glycidilation

2.3.3.3.1   From technical lignins

The O-glycidilation process (also known as epoxidation) have been widely studied to reduce the use petroleum-based BADGE by converting lignin into an epoxy precursor[286-317]. This chemical modification suitable for a wide range of lignin[318] involves the nucleophilic attack of lignin –OH groups on ECH under alkaline conditions to introduce a substantial amount of oxirane ring onto the surface of lignin (Scheme 10). The biphasic phase transfer catalyst system (BPTC) with quaternary ammonium (tetrabutylammonium bromide[287, 288, 293, 294, 304, 311]) enhances the glycidilation of more lignin –OH groups. Substituting a portion of BADGE with epoxidized lignin shows promise for improving the mechanical properties of lignin-derived epoxy resins (33 wt.% lignin content, E_Y= 1.9 GPa, ε= 1.7 %, T_α= 159 °C) (Scheme 10)[287]. Nikafshar *et al.* investigated the glycidilation of a series of thirteen unmodified lignins[288]. Regardless the content of –OH groups, low molecular weight oligomers from corn stover organosolv and hardwood Kraft lignins demonstrate higher reactivity toward epoxidation ([OH]= 3.24 and 6.09 mmol.g^{-1}, M_n= 1900 and 1400 g.mol^{-1}, 12.53 and 11.98 % epoxy content, respectively).
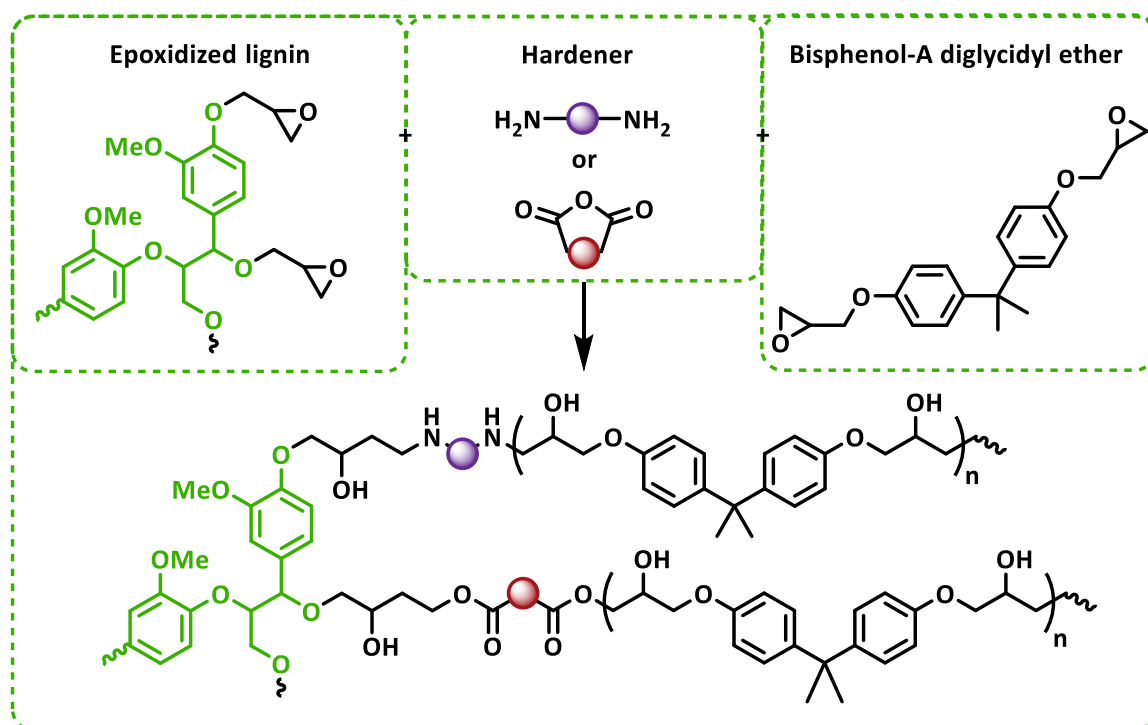
Scheme 10 Proposed scheme for the synthesis of lignin-derived epoxy copolymers.

To enhance the sustainability of epoxy resins, epoxidized lignin macromolecules are being explored to completely substitutes petroleum-based epoxide precursors (Scheme 11). Nakamura and colleagues have demonstrated successful incorporation of lignins obtained from steam-exploded plants in epoxy resins[289-291]. The epoxidized lignins display comparable epoxy resin yield to the control epoxy precursor (63.4-70 %). These epoxidized lignin were able to cure with their unmodified parent to produce solder-dip resistant epoxy resins with high lignin content (86.1-88.2 %)[290].
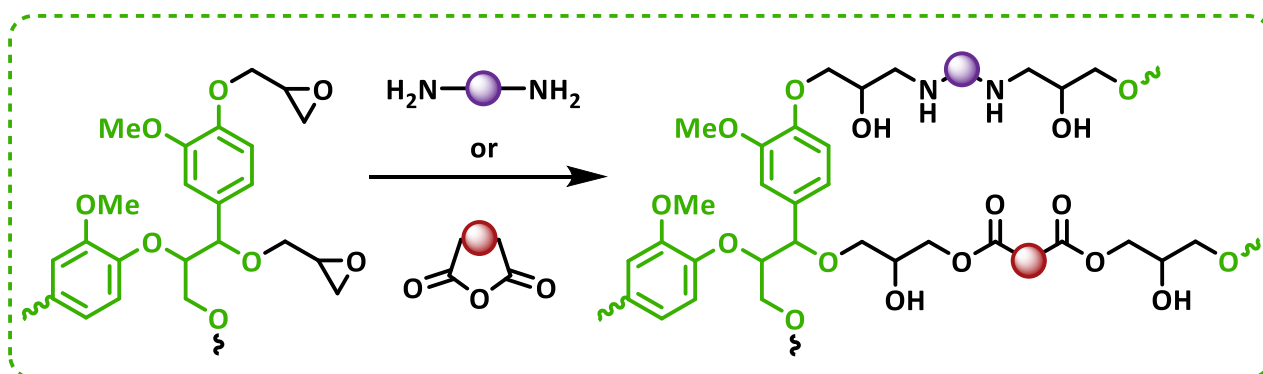
Scheme 11 Proposed scheme for the synthesis of lignin-derived epoxy resins.

2.3.3.3.2   From refined lignins

2.3.3.3.2.1.   Depolymerization

Lignin can be refined through various reductive depolymerization methods to enhance the degree of glycidilation. Ferdosian *et al.* have demonstrated the reductive depolymerization of organosolv lignin

using ruthenium-based catalyst to design lignin-derived epoxy copolymers [292-296]. An optimization study has revealed that the temperature and the molar ratio between depolymerized lignin and NaOH as key factors in maximizing the yield of glycidilation[293]. Kraft lignin, which contains a higher content of –OH groups, has been found to promote glycidilation and the curing process with aliphatic and aromatic amine hardeners (E_a= 69.3 and 42.5 kJ.mol^{-1}, respectively)[294].

Torr and coworkers have investigated the palladium-catalyzed hydrogenolysis of softwood[297, 298] and hardwood[299] biomass to produce a solvent-soluble lignin oil. The mild hydrogenolysis process selectively cleaves etherified interunit linkage generating a mixture of phenolic compounds ($[OH]_{phe}$= 4.11 g.mol^{-1})[297]. This process can be extended to the pilot scale, enabling the retrieval of depolymerized lignin fragments *in-situ* fractionated from ethyl acetate (M_n= 282-341 g.mol^{-1})[298]. After derivatization, the refined lignin with high epoxy equivalent weight (EEW_{LHEP}= 359 g.eq^{-1}) reacts with diethylenetriamine (DETA) hardener and commercial epoxy prepolymer to form lignin-derived epoxy copolymer that exhibit superior mechanical properties as compared to the control resin ($E_{FLEX} \geqslant$ 3.7 GPa, $\sigma_{FLEX} \geqslant$ 126 MPa). The depolymerization is also adaptable for native Eucalyptus hardwood (M_n= 240-275 g.mol^{-1}, [OH]= 4.11-4.77 g.mol^{-1}) and the best-performing copolymers contain 33 wt.% of epoxidized lignin in replacement of synthetic BADGE (Figure 6.d, E_{FLEX}= 3.5 GPa, σ_{FLEX}=139 MPa)[299].

The reductive depolymerization have also shown effectiveness to completely substitute commercial epoxy precursors. Liu *et al.* obtained lignin oligomers from the palladium-catalyzed depolymerization of hardwood alkali lignin (M_n= 836-1725 g.mol^{-1}, [OH]= 4.56-5.44 mmol.g^{-1})[300], which subsequently epoxidized and cured with methyltetrahydrophthalic anhydride to produce rigid lignin-derived epoxy resin (T_g= 78-104 °C, E'= 7-22 MPa, σ= 47-60 MPa). To overcome the brittleness of these lignin-based materials, the authors also suggested adding cardanol glycidyl ether in the blend as a reactive diluent and plasticizer. In another study, Xin *et al.* used Raney nickel catalyst to depolymerize enzymolysis lignin with the aim to improve the viscoelastic performance of asphalt using a flexible curing agent from the Diels−Alder adduct of methyl esters of allosteric acid and maleic anhydride[301].

In an innovative solvolysis pathway, Kaiho *et al.* refined lignin fragments from Eucalyptus wood meals through acid-catalyzed depolymerization[302]. They selectively cleave the predominant β'–O–4 bond producing low molecular weight fragments bearing acetal structures. These fragments can be subjected to trans-acetalization or intramolecular annulation, imparting flexibility and rigidity into epoxidized lignin (EEW= 376 and 352 g.eq^{-1}, respectively).

2.3.3.3.2.2. *Fractionation*

Solvent fractionation is typically performed under mild conditions and can enhance the solubility and the reactivity of lignin fractions towards glycidilation[303]. Jablonskis *et al.* suggested performing the

fractionation step after glycidilation to produce Kraft lignin-derived epoxy copolymers[304]. Thus, the acetone-soluble fraction of epoxidized lignin (EEW= 309-439 g.eq^{-1}) successfully incorporates a commercial epoxy resin as reactive and mechanical filler. Substituting 10 wt.% of the epoxy resin with this fraction results in materials with superior mechanical properties, including a Young modulus of 3.4 GPa, strain at break of 4.9 % and stress at break of 66.2 MPa.

To further customize the thermo-mechanical properties of lignin-derived epoxy resins, Gioia *et al.* fractionated softwood Kraft lignin through a sequential solvent fractionation approach[305]. The resulting glycidylated lignin fractions (2.7-3.9 mmol.g^{-1} oxirane content) were cross-linked with a polyetheramine to create a homogeneous thermoset (Figure 6.e). While the soft diamine segments provided flexibility to the molecular network ($T_g \sim$ -50 °C), the mechanical performance of this series of bio-based materials was mainly influenced by the higher molecular weight lignin fractions (E_Y= 6-100 MPa, σ= 1.2-50 MPa, ε= 44-47 %). In a different study, the authors investigated the contribution of lignin structural characteristics on the mechanical properties of lignin-derived thermosets[306]. The authors observed that while the flexible fractions enriched in methoxy units improve the mechanical flexibility of the network, the condensed aromatic structure of softwood Kraft lignin decreases the molecular mobility in the cross-linked network.

Van Aelst *et al.* developed a method to fractionate softwood lignin into different molecular weights and functionalities using successive reductive catalytic fractionation and sequential solvent/anti-solvent precipitation (M_n= 445-1146 g.mol^{-1}, [OH]= 3.56-4.37 mmol.g^{-1})[307]. Silau *et al.* recently reported a similar work, with the sequential solvent fractionation and depolymerization of softwood Kraft lignin (M_n= 570-1170 g.mol^{-1}, [OH]= 6.87-7.84 mmol.g^{-1})[308]. These oils were then subjected to glycidilation and finally cured with a fatty acid that results in lignin-derived epoxy networks with adjustable mechanical performance (E_Y= 0.9-1.4 GPa).

2.3.3.3.3 *From chemically modified lignins*

Various functionalization strategies, such as phenolation[309-311], demethylation[311], and hydroxymethylation[311-313] have been explored to increase the reactivity of technical lignins towards glycidilation. Zhang *et al.* compared these methods to develop chemical grouting materials from wheat straw organosolv lignin[311]. They found that hydroxymethylation produced the most reactive precursors, while phenolated-epoxidized lignin had better miscibility with BADGE-type epoxy resin. The base-catalyzed hydroxymethylation of lignin was found to favor the formation of oxirane moieties upon glycidilation (3.3% epoxy index in the solid resin)[312]. Zhao *et al.* optimized a multistep pathway comprising self-assembly of solid nanoparticles and liquefaction[313]. They found that substituting 25 wt.% polyol with lignin produced composites with good mechanical properties (E_Y= 1.5-2.8 GPa, ε= 12.3-19.3 %, σ= 16.5-44.8 MPa).

Abu-Omar and colleagues developed multistep pre-functionalization pathways to design renewable lignin-derived epoxy resin[314, 315]. In the formaldehyde-containing approach, demethylated organosolv lignin undergoes successive one-pot phenolation/ oligomerization with deprotected dihydroeugenol and formaldehyde, glycidilation with ECH, and polymerization with DETA. As a result, the incorporated novolac polyphenol exhibits superior mechanical performance (E'= 1.3 GPa). In the formaldehyde-free approach, successive phenolation with catechol and condensation with salicyl alcohol aim to simultaneously functionalize organosolv lignin with hydroxymethyl group and reactive phenolic units[315]. Up to 19 wt.% of lignin incorporates the epoxy network containing 69 wt.% renewable content (E'= 1.8 GPa). For both approaches, the lignin-incorporated polyphenols and epoxy show enhanced uniformity compared to the blended networks (Figure 6.f). Later, synthetic phenol was employed during the phenolation process to increase the cross-linking density in the lignin-incorporated polyphenol epoxy network[316, 317].

In an alternative pathway, Vásquez-Garay *et al.* proposed a chemoenzymatic catalyzed-epoxidation method to substitute petroleum-based ECH[319]. In this method, allylated lignin reacts under mild reaction conditions with caprylic acid in the presence of a bio-catalyst (immobilized Candida antarctica lipase B) to convert up to 90 % of lignin –OH groups into oxirane counterparts.

From an application point of view, lignin-derived epoxy copolymers profitably sprang into the design of renewable adhesive (Figure 6.g)[320-323], coating (Figure 6.h)[324-327], and flame-retardant materials (Figure 6.i)[328-331].
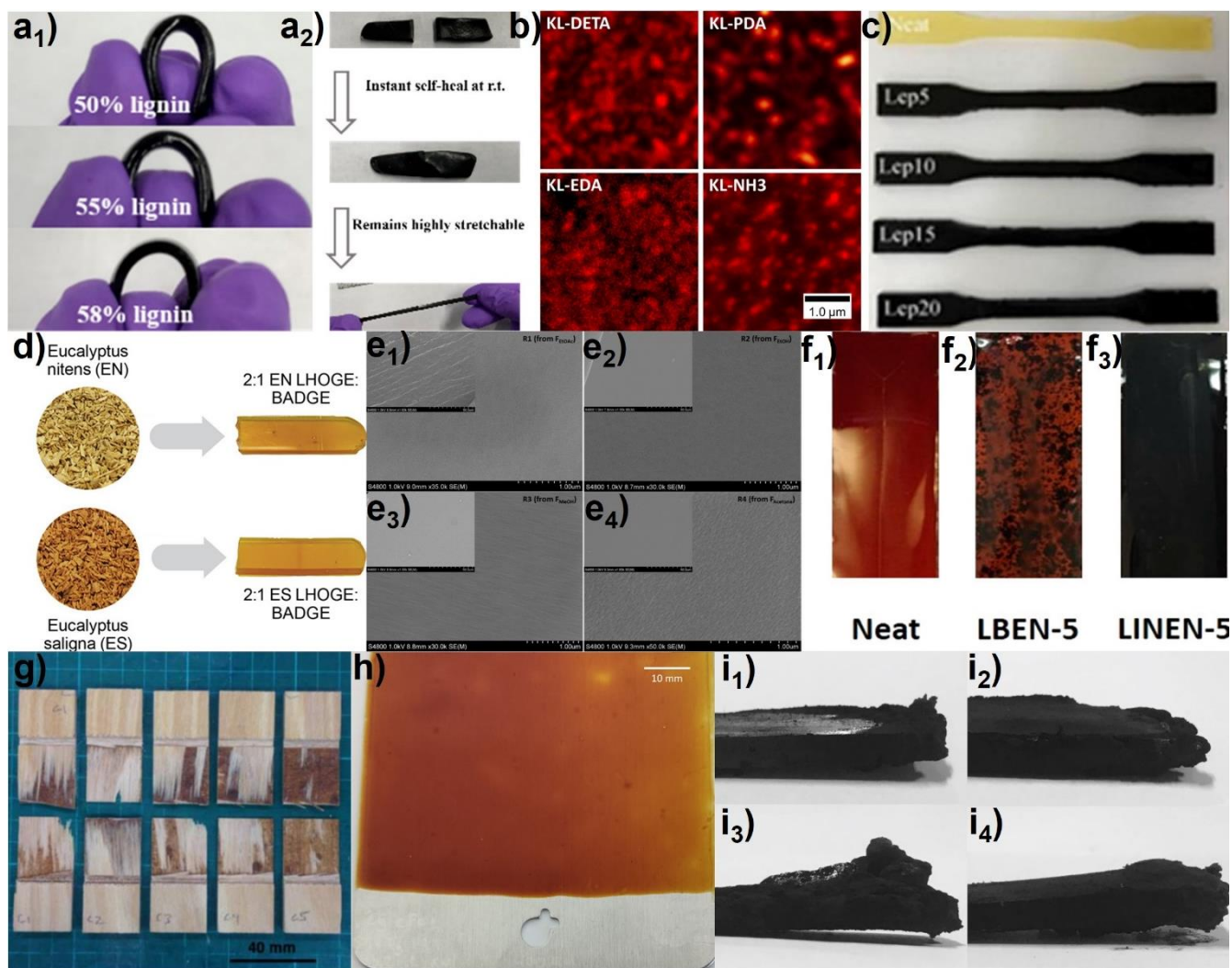
Figure 6 Examples of lignin-derived epoxy resins.

a) Photographs of epoxy resins prepared from fractionated lignin and diglycidyl ether PEG (1) materials and (2) self-healing aptitude (adapted from [266]). b) Confocal laser scanning microscopy (CLSM) images of composites prepared from different aminated lignins (adapted from [272]). c) Photographs of lignin-derived epoxy resins prepared from carboxylated lignin and commercial BADGE (adapted from [283]). d) Photographs of epoxy composites produced from depolymerized lignin retrieved from Eucalyptus hardwood (adapted from [299]). e) SEM images of epoxy resins produced from the (1) ethyl acetate-, (2) ethanol-, (3) methanol-, (4) acetone-soluble fractions of lignin (adapted from [305]). f) Images of (1) neat epoxy resin and lignin-derived epoxy resins with (2) blended or (3) incorporated novolac polyphenol (adapted from [314]). g) Photographs of wood failures in plywood test samples (birch hardwood) using a lignin-derived epoxy adhesive (adapted from [320]). h) Photographs of cured lignin-derived epoxy coating on aluminum panel (adapted from [327]). i) Photographs after UL-94 testing of (1) neat epoxy resin and lignin-derived epoxy composites containing 10 wt.% of (2) phenolated lignin, (3) Mannich adduct of phenolated lignin and piperazine/DOPO intermediate, and (4) Atherton−Todd adduct with DOPO (adapted from [328]).

Table 4 Examples of epoxy resins synthesized from glycidylated lignin.

| Lignin source	* Manufacture process	GC (%)	Resin characteristic	Application	Ref.
Steam-exploded bamboo organosolv lignin	*Unmodified*: [a] GL (73 wt.%)/ Lignin (–OH) (27 wt.%) [1.0]	n.c.	[1] σ_{flex}= 61 MPa [2] CR_{800}= 38.5 % [3] $T_{d5\%}$= 260.5 °C	Resin for electric-al/tronic industries	289
Hardwood alkali lignin	*Depolymerized*: [b] GL (69 wt.%)/ [c] MeTHPA (–COOH) (31 wt.%) [1.18]	99	[4] E'= 22 MPa [5] σ= 60 MPa [6] T_g= 128 °C	Lignin-derived rigid thermoset	300
Softwood Kraft lignin	*Fractionated:* [d] Ace-GL (42 wt.%)/ [e] JD-2000 (–NH) (58 wt.%) [2.0]	n.c.	[7] E_Y= 0.1 GPa σ= 5 MPa T_g= -52 °C	Lignin-derived flexible thermoset	305
Hardwood Kraft lignin	*Fractionated:* [f] EtOAc-GL (64 wt.%)/ [g] JD-400 (–NH) (36 wt.%) [1.0]	n.c.	E_Y= 1.4 GPa σ= 59 MPa T_g= 73 °C	Lignin-derived rigid thermoset	306
Softwood Kraft lignin (UPM BioPiva™ 395)	*Fractionated & Depolymerized:* [h] GL (82 wt.%)/ [i] TOFACA (–COOH) (18 wt.%) [1.0]	n.c.	E_Y= 1.4 GPa σ= n.c. (low) T_g= 80 °C	Lignin-derived rigid thermoset	308
Organosolv lignin	*Formaldehyde-free phenolated:* [j] PL-GL (89 wt.%)/ [k] DETA (–NH₂) (11 wt.%) [1.0]	n.c.	[8] E'= 1.8 GPa $T_{d5\%}$= 213 °C [9] T_{α}= 106 °C	Lignin-derived rigid thermoset	315
Softwood Kraft lignin	[l] *Demethylation & phenolation*: DL-PL-GL (53 wt.%)/ [m] MNA (–COOH) (47 wt.%) [1.0]	n.c.	E'= 2.7 GPa $T_{d5\%}$= 267 °C T_{α}= 147 °C	Lignin-derived rigid thermoset	317

* Nomenclature: epoxide precursor from unmodified, refined, or modified glycidylated lignin/ curing agent (reactive function)/ molar ratio oxirane ring: hardener reactive function.

[a] Glycidylated lignin, [b] Mild hydrogenolysis over Raney nickel catalyst (DL4, M_n= 1725 g.mol⁻¹, [OH]= 4.56 mmol.g⁻¹), [c] Methyltetrahydrophthalic anhydride in presence of N,N-dimethylbenzylamine initiator, [d] Acetone-soluble fraction (M_n= 2700 g.mol⁻¹, [OH]= 6.40 mmol.g⁻¹), [e] Poly(propylene oxide) diamine Jeffamine® D-2000, [f] Ethyl acetate fraction (EF₁, M_n= 700 g.mol⁻¹, [OH]= 5.10 mmol.g⁻¹), [g] Poly(propylene oxide) diamine Jeffamine® D-400, [h] Acetone-soluble fraction depolymerized via palladium-catalyzed hydrogenolysis (F4-LDO, M_n= 1070 g.mol⁻¹, [OH]= 7.14 mmol.g⁻¹), [i] Ancamide® 3030 in presence of tris-2,4,6-(dimethylaminomethyl)phenol accelerator, [j] GL synthesized from incorporated polyphenol composed of 40 wt.% phenolated lignin and 60 wt.% salicyl alcohol (EN-PL₄₀SA₆₀), [k] Diethylenetriamine, [l] GL synthesized from formaldehyde and incorporated polyphenol composed of 20 wt.% demethylated lignin and 80 wt.% phenol (DPLINP), [m] Methyl nadic anhydride in presence of 2-ethylimidazole initiator.

[1] Flexural strenght, [2] Char yield, [3] Temperature of 5% thermal decomposition, [4] Storage modulus, [5] Tensile strenght, [6] Glass transition temperature, [7] Young modulus, [8] Storage modulus, [9] α-relaxation temperature.

2.4. Lignin-derived polyesters

Polyesters (PE) are widely used, with applications ranging from synthetic fibers in the textile industry[332] to reinforcing materials in tire cord[333]. Ester linkages are formed by the equilibrium reaction between a carboxylic acid and a hydroxyl group, releasing water as a by-product. Acid chlorides and acid anhydrides are commonly used to initiate the nearly quantitative esterification. Lignin, with its abundant hydroxyl groups, provides a sustainable platform for esterification. Acetylation has traditionally been used to improve the solubility of lignin in organic solvents, facilitating the characterization of its solubility parameters[334] and structure[335]. Lignin-derived PE materials are produced by polycondensation reactions between a multi-functional esterification reagent and lignin macropolyol, either alone (Scheme 12) or in combination with commercial polyol (Scheme 13).
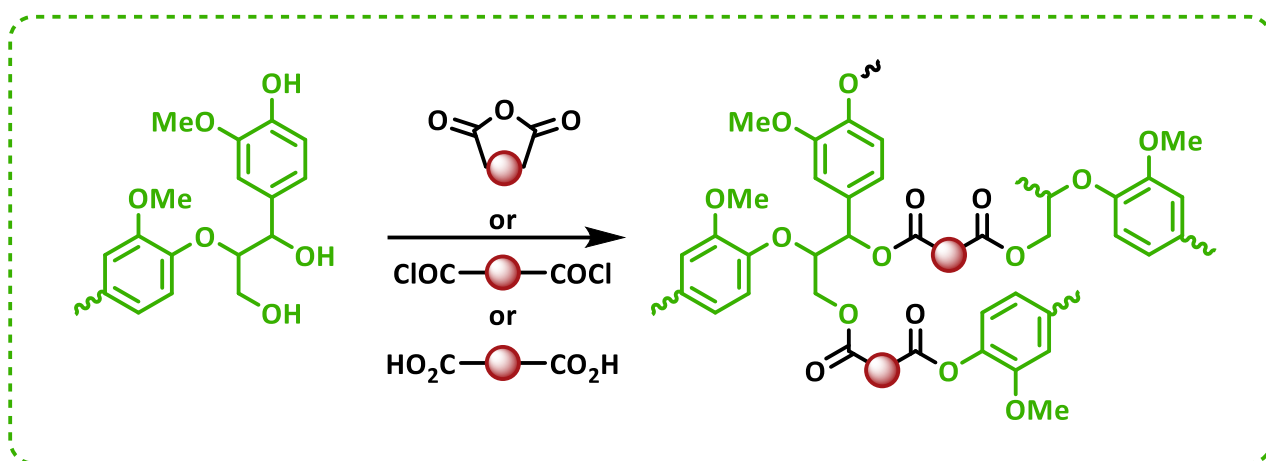
Scheme 12 Proposed scheme for the synthesis of lignin-derived polyesters.
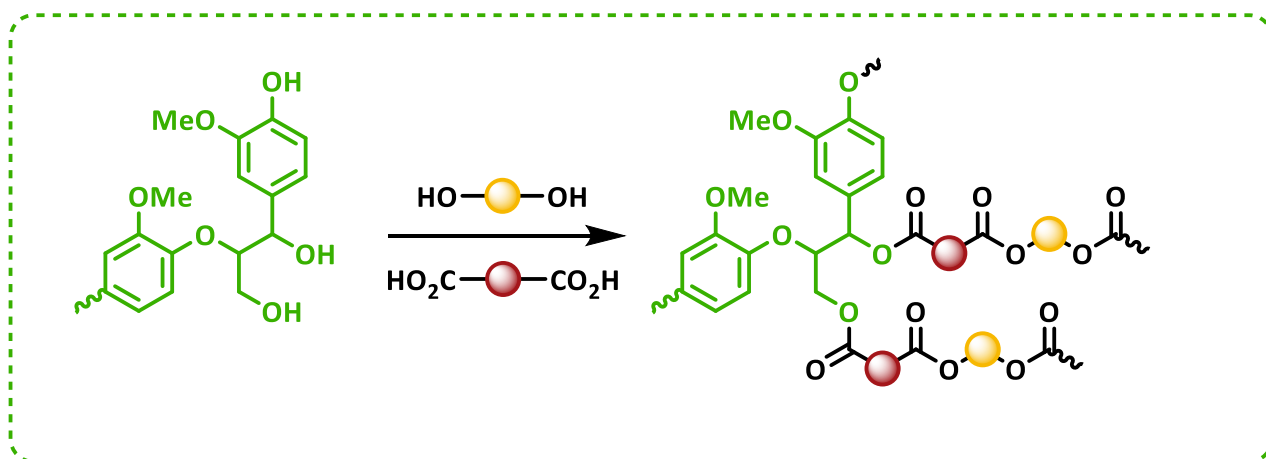
Scheme 13 Proposed scheme for the synthesis of lignin-derived polyester copolymers.

2.4.1. Polyesters from technical lignins

One strategy for developing lignin-derived PE involves using multifunctional carboxylic acids as covalent bridge between lignin macromolecules and alcohol-containing precursors (Scheme 13)[336-339]. For example, the melt polycondensation between EHL, short diols, and sebacic acid, a naturally occurring dicarboxylic acid, provides liquid polyester polyol used as toughening agent in epoxy resins[336]. Different amount of maleic acid were used to cross-link amorphous alkali lignin and semi-crystalline polyvinyl alcohol (PVA, Figure 7.a)[337]. The resulting esterified PVA-lignin resin exhibits superior mechanical properties (E_Y= 2.4 GPa) and adhesive strength (failure strength= 6.8 MPa) when optimal curing temperature (T= 180 °C) and maleic acid content (40 wt.%) were used. In another study, Larrañeta and colleagues selected poly(methyl vinyl ether-co-maleic acid) as polyacid precursor to cross-link lignin with PEG under micro-wave radiations in the view of preparing antimicrobial hydrogel with high lignin content (24-40 wt.%)[338].

Citric acid, a trifunctional organic acid naturally found in juicy fruits, has emerged as a key component in recent strategies for manufacturing lignin-derived PE copolymers[340-343]. Xu *et al.* developed a series of lignin-derived PE with tailored properties in a one-pot process that combined citric acid, Kraft lignin, and PEG_{400}[340]. At constant cross-linker loading, a higher content of lignin relative to the PEG_{400} reactive diluent led to rigid thermoset resin with almost 100 % gel content, high glass transition temperature ($73 < T_\alpha < 102$ °C), and remarkable tensile strength ($14 < \sigma < 34$ MPa). These materials also exhibited shape memory performance due to their design with soft segment (Figure 7.b). Kim and colleagues developed a series of lignin-derived PE copolymers using PVA as a substitute[342]. The homogenous blend of citric acid, PVA, and alkali lignin (≈ 25 wt.%) was thermally treated at 180 °C to produce self-supported films. The optimal citric acid feed ratio of 30 wt.% improved the mechanical and adhesive properties of the lignin-derived PE. This bio-based blend was further reacted and impregnated into nanocellulose long fiber mats to form an all-green fiber-reinforced polymer composites[341].

An alternative method to design PE from technical lignin involves self-polymerization with multi-functional acid halides[344-348], carboxylic acids[349], or anhydride[350] (Scheme 12). Similar to fatty acid chloride[351, 352], esterification with dicarboxylic acid chloride, such as sebacoyl chloride[346-348], confers lignin with a thermoplastic-like behavior (Figure 7.c), and numerous examples of this approach are reported in the literature. Itaconic acid, a naturally occurring dicarboxylic acid, was used to form a PE from EHL and 1,12-dodecanediol with shape-memory performance[349]. Di Francesco and co-workers followed a pre-activation strategy by reacting adipic acid with isoprenyl acetate to form an anhydride mixture with a high degree of functionality (Figure 7.d)[350]. The mixed anhydride mixture is partially esterified with softwood Kraft lignin to produce a homogenous pourable pre-polymer. Upon thermal curing, the resulting lignin-derived poly-adipates are cross-linked thermoset with a high lignin content (60 wt.%) and a high gel content (GC 97%).

2.4.2. Polyesters from refined lignins

The fractionation of technical lignins found to be efficient in developing lignin-derived PE network[353-356]. McDonald and colleagues synthesized tribranched carboxylic acid pre-polymer by the melt condensation of adipic acid with triethanolamine, which was later condensed with fractionated soda lignin to obtain flexible thermosets with high gel content (94%) and single glass transition ($T_g \sim$ 8 °C)[353]. Later this strategy was extended to the methanol-soluble fraction of various technical lignins to develop lignin-co(polyester-amines) with shape-memory effect[354]. In another study, Scarica *et al.* esterified a fractionated softwood Kraft lignin with succinic anhydride, which resulted in covalently-bonded ester linkages and free-carboxylic acid functional groups[355]. These functional groups subsequently underwent self-polyesterification at high temperature, resulting in lignin-derived PE coatings with scratch resistance (Figure 7.e) and remarkable adhesive strength on different substrates, especially on wood ($\sigma_{adhesive,wet} >$ 9 MPa). The sustainability of lignin-derived PE copolymers was extended by Xu *et al.* through a microwave-assisted extraction/degradation strategy[356]. A softwood Kraft lignin was fractionated in ethanol under microwave irradiations before cross-linking with PEG_{400} and citric acid. Composed of lower molecular weight lignin fractions ($M_n \sim$ 1000 g.mol^{-1}), bio-based polyester resins were degraded and recycled into a new thermoset (Figure 7.f).

2.4.3. Polyesters from chemically modified lignins

2.4.3.1. Esterification

The esterification derivatization relies on two main strategies to tune the reactivity of technical lignins toward subsequent condensation. In one study, Chung *et al.* introduced acetic acid as a capping agent to control the degree of cross-linking of lignin-derived PE[357]. By adjusting the ratio between difunctional succinic acid and acetic acid, esters of softwood Kraft lignin were developed with activated and deactivated reaction sites, respectively. Copolymerization with PEG of different chain lengths further demonstrated the correlation between the degree of cross-linking and thermal properties of the resulting materials with thermoplastic-like behaviours. In another study, the same group converted the aliphatic –OH groups of dealkaline lignin into carboxylic acid through the Steglich esterification with sebacic acid[358]. The resulting polyacid was further condensed with hydroxyl-terminated poly(ethylene brassylate), a castor-oil based biodegradable polyester, to form graft-polymer with modified lignin content ranging from 20 to 50 wt.% and Young modulus up to 0.4 GPa (Figure 7.g).

2.4.3.2. Hydroxyalkylation

The reactivity of methanol-insoluble Kraft lignin towards esterification can be increased by oxypropylation, which promote cross-linking of fractionated lignin macromolecules with sebacic acid[359]. However, phenolic units demonstrate lower reactivity toward esterification due to steric hindrance and

strong hydrogen bonding. To address this challenge, Liu *et al.* have developed an optimized strategy to convert 95% of phenolic units into hydroxyalkyl ethers which results in lignin derivatives with uniform chemical functionalities[360]. This green strategy involves reacting softwood Kraft lignin with ethylene carbonate under alkaline conditions to obtain a higher yield of propionate ester for the hydroxyalkylated lignin compared to technical lignin (90 vs 70%, respectively). Downward precipitation is then used to retrieve lignin fractions with tailored characteritsics[361].
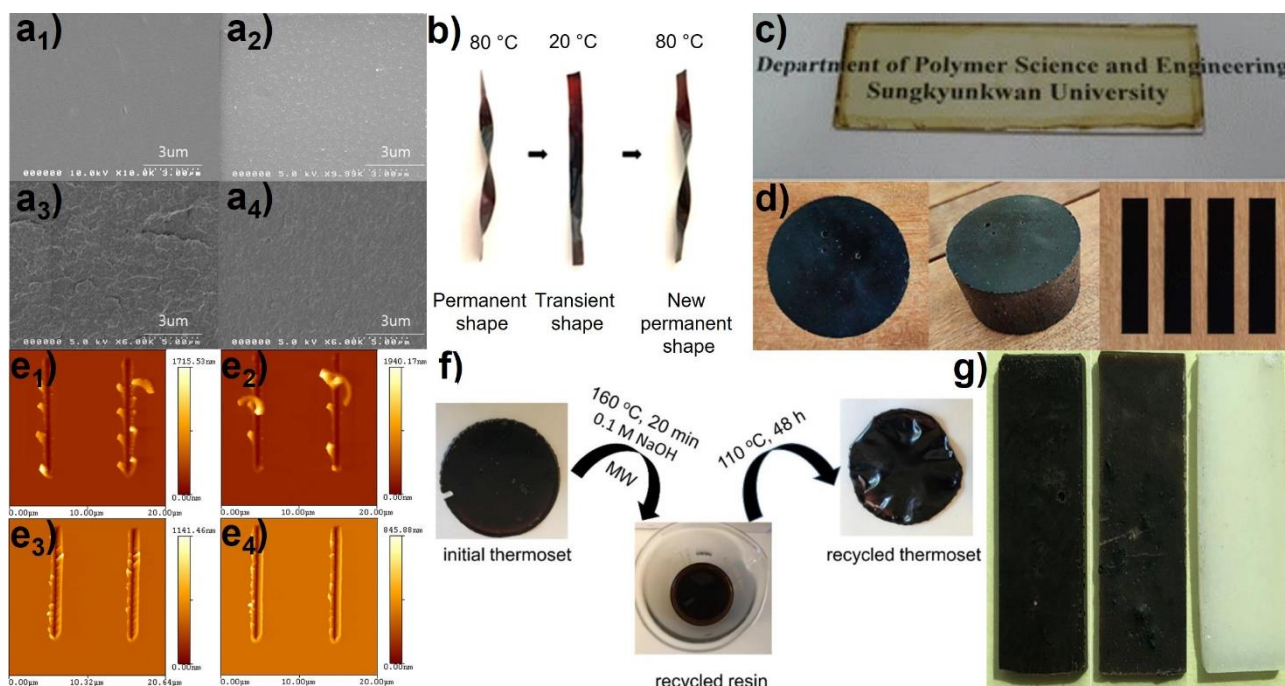

Figure 7 Examples of lignin-derived polyesters.

a) Surface (1-2) and cross-sectional (3-4) scanning electron microscopy (SEM) micrographs of (1-3) pristine lignin-PVA resin and (2-4) esterified lignin-PVA resin cross-linked with 40 wt.% maleic acid (adapted from [337]), b) Images of shape-memory performance of polyester prepared from softwood Kraft lignin, PEG$_{400}$, and citric acid (adapted from [340]), c) Image of lignin-sebacoyl copolyester thin film on a glass substrate (adapted from [347]), d) Images of Kraft lignin poly-adipate samples: disc, cylinder, and bars from left to right (adapted from [350]). e) AFM height images of scratched PE coatings prepared from Kraft lignin and succinic anhydride (1-2) self-crosslinked (3-4) cross-linked with an external curing agent. Recorded at two different nanoscratch rates: (1-3) 0.1 μm.s^{-1}; (2-4) 10 μm.s^{-1} (adapted from [355]). f) Images of microwave-assisted recycling of polyester prepared from softwood Kraft lignin, PEG$_{400}$, and citric acid (adapted from [356]). g) Photographs of lignin-*g*-PEB, blended esterified lignin and PEB, and PEB homopolymer from left to right (adapted from [358]).

**Table 5** Examples of polyesters synthesized from technical, refined, or chemically modified lignin.

Lignin source	Manufacture process	GC (%)	Resin characteristic	Application	Ref.
Alkali lignin	*Unmodified:* Lignin (30 wt.%)/ Maleic acid (30 wt.%)/ [a] PVA (40 wt.%)	n.a.	[1] E_Y= 2.4 GPa [2] σ= 48.5 MPa [3] ε= 2.7 %	Natural fiber reinforced composite	337
Softwood Kraft lignin	*Unmodified:* Lignin (40 wt.%)/ Citric acid (40 wt.%)/ PEG_{400} (20 wt.%)	99.9	[4] G_{25}= 2.0 GPa σ= 34 MPa [5] T_α= 102 °C	Shape-memory polymer	340
Alkali lignin	*Unmodified:* Lignin (25 wt.%)/ Citric acid (45 wt.%)/ PVA (30 wt.%)	n.a.	E_Y= 6.5 GPa σ= 185 MPa ε= 9.9 %	Natural fiber reinforced composite	342
Softwood Kraft lignin (LignoBoost®)	*Unmodified:* Lignin (60 wt.%)/ Adipic acid (11 wt.%)/ [b] IPA (29 wt.%)	97	E_Y= 1400 MPa σ= 15 MPa ε= 10 %	Lignin-derived rigid thermoset	350
Wheat straw soda lignin (Protobind™ 1000)	*Fractionated*: [c] MeOH-Lignin (40 wt.%)/ Adipic acid (36 wt.%)/ [d] TEA (24 wt.%)	94	E_Y= 189 MPa σ= 34 MPa [6] $T_{g,E''}$ = 8 °C	Lignin-derived flexible thermoset	353
Softwood Kraft lignin (Indulin® AT)	*Fractionated*: [e] THF-Lignin (83 wt.%)/ Succinic Anhydride (17 wt.%)	n.a.	[7] $T_{d5\%}$= 174 °C [8] θ_{H20}= 90 ° T_g= 138 °C	Coatings and adhesives	355
Softwood Kraft lignin	*Esterified*: [f] EL (50 wt.%)/ [g] PEG_{2000} (50 wt.%)	n.a.	[9] T_m= 55 °C [10] T_c= 68 % [11] T_g= -5 °C	Lignin-derived thermoplastic	357

[a] Polyvinyl alcohol, [b] Isoprenyl acetate, [c] Methanol-soluble fraction, [d] Triethanolamine, [e] Tetrahydrofuran-soluble fraction, [f] Lignin capped with 27% acetyl groups and 63% succinic ester, [g] Polyethylene glycol (M_n= 2000 g.mol^{-1}).

[1] Young modulus, [2] Tensile strenght, [3] Strain at break, [4] Storage modulus at 25.0 °C, [5] α-relaxation temperature, [6] Glass transition (loss modulus), [7] Temperature of 5% thermal decomposition, [8] Static contact angle with a water drop, [9] Melting temperature, [10] Crystallinity index, [11] Glass transition (DSC).

2.5. Lignin-derived copolymers via grafting strategies

Lignin can be used as macroinitiators to create three-dimensional networks by linking each macromolecules with linear chains. Two main synthetic routes are considered for creating lignin-derived copolymers: the "*grafting-from*" and the "*grafting-to*" (Scheme 14)[4, 362] approaches. In the "*grafting-from*" method, technical or derivatized lignin macromolecules are used for initiating and growing monomer units using free or controlled radical polymerization (FRP and CRP) of vinylic monomers, or to trigger the ROP of cyclic monomers. The "*grafting-to*" approach involves the reaction between lignin and the terminal groups of telechelic polymers through efficient coupling processes.
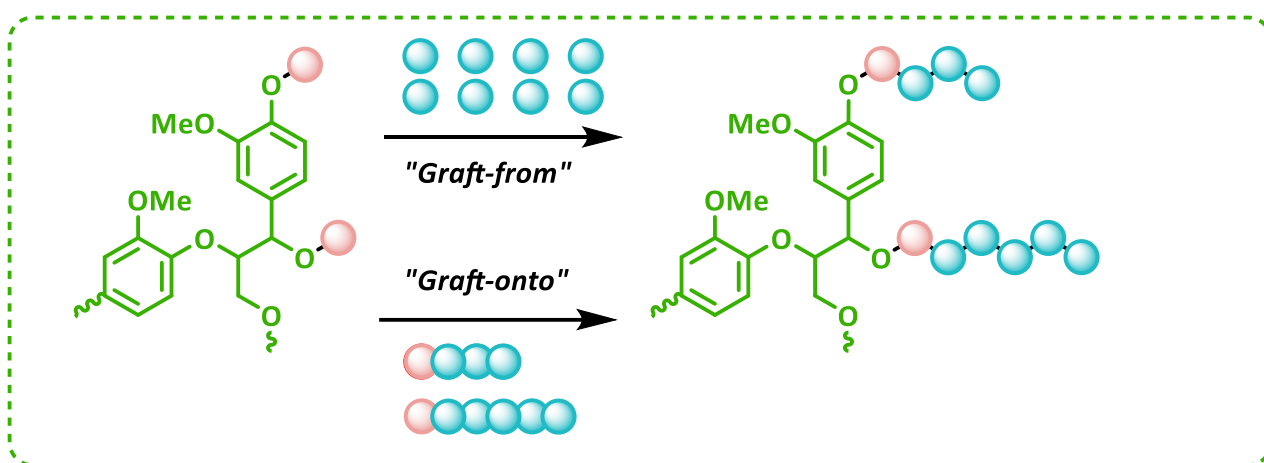
Scheme 14 Proposed scheme for the synthesis of lignin-derived copolymers based on "*grafting-from*" and "*grafting-onto*" strategies.

2.5.1. "Graft-from" lignin-derived copolymer

2.5.1.1. Radical polymerization

2.5.1.1.1 Free radical polymerization (FRP)

FRP method has been successful used to functionalize lignin with various vinylic monomers including acrylonitrile[363], dimer acid[364], styrene[365], itaconic acid[366, 367], acrylic [368-370] or methacrylic[371] acid, methyl methacrylate [372-374], acrylamide[375-377], and its derivative[378, 379]. For instance, Sun *et al.* chemically grafted renewable lauryl and tetrahydrofurfuryl methacrylate (LMA and THFMA, respectively) onto alkali lignin recovered from the corncob biorefinery using sodium chloride- hydrogen peroxide as free-radical polymerization initiator[380]. The resulting lignin-*g*-P(LMA-co-THFMA) copolymer was used to toughen commercial PLA matrix. In another approach, lignin has been converted into a methacrylate precursor through esterification with methacrylic anhydride[381, 382] or imidazole-derived 2-hydroxyethyl methacrylate (HEMA-Im)[383] (Scheme 15.a). Chmely and colleagues 3D printed this lignin with an UV curing agent and commercial acrylate precursors to yield films with 15 wt.% methracylated lignin (Figure 8.a)[382]. The content of renewable materials was further increased in lignin-*g*-HEMA containing up to 40 wt.% of methracylated lignin to manufacture tunable hydrogels[383].

CRP can be used to adjust the length of polymer chains. In this regard, atom transfer radical polymerization (ATRP) has gained considerable interest as the experimental conditions needed to conduct it are mild enough to be compatible with lignin. Lignin-based ATRP-macroinitiators are usually synthesized from its esterification with 2-bromoisobutyryl bromide (BiBB) (Scheme 15.b)[384-396].

In 2010, Kadla and colleagues pioneered the copolymerization of lignin with N-isopropylacrylamide (NIPAM) using the ATRP technique[384]. By selective grafting onto hardwood Kraft lignin, controlled molecular weights of lignin-*g*-PNIPAM were obtained with a high degree of polymerization (DP$_{NIPAM}$ > 40) and low dispersity (1.01 < Đ < 3.01). In a more environmentally friendly approach, the authors substituted copper-based catalyst with various enzymes to immobilize PNIPAM chains onto lignin core[385]. Later, the same research group used the ATRP technique to electrospun softwood Kraft lignin nanofibers to design a series of thermo- and ionic-responsive lignin-g-PNIPAM[397]. In fact, lignin-*g*-PNIPAM exhibits a thermoresponsive phase transition from a hydrophilic to a hydrophobic structure similar to the threshold lower critical solution temperature of PNIPAM homopolymer (LCST= 32 °C). Moreover, the ATRP method offers a promising approach to design thermoresponsive materials by grafting lignin with polyethylene glycol methyl ether methacrylate (PEGMA)[387] or N-vinyl caprolactam[388] using metal-free[387] or low catalyst loading[388] conditions.

Hilburg *et al.* prepared "one-component" hybrid nanocomposites from controlled fractions of lignin-derived copolymer grafted with polystyrene (lignin-*g*-PS) or polymethyl methacrylate (lignin-*g*-PMMA) [398]. The graft-copolymers show enhanced compatibility with the grafted thermoplastics compared to their analogous binary lignin/polymer blends (up to 22 wt.% lignin). By controlling the feed ratio between lignin macroinitiator and MMA monomer, lignin-*g*-PMMA copolymers with adjustable mechanical properties (E$_Y$= 1.5-1.7 GPa)[389] and glass transition (T$_g$= 101-131 °C)[390] can be prepared. Subsequently blended with PCL, nanofibrous lignin-*g*-PMMA/PCL composites prepared by electrospinning match typical requirements for biomedical applications[390]. In a similar approach, Cho *et al.* used lignin-*g*-PMMA to increase the thermal stability and UV-protection of a commercial PLA matrix without reducing its mechanical properties[391]. Tang *et al.* applied ARTP strategy to graft rosin-derived monomers onto lignin[394]. By using a methacrylate precursor, the high glass transition of the technical lignin (T$_g$ ≈ 95 °C) was preserved to design hydrophobic lignin-*g*-rosin films (θ$_{H2O}$≈ 90 °, Figure 8.b).

Apart from thermoresponsive and composites materials, lignin-graft copolymers synthesized *via* the ATRP route find applications in various other areas[392, 393]. For instance, other studies have reported the ATRP-mediated copolymerization of lignin with a combination of PEGMA/glycidyl methacrylate, or solely with 2-4-benzoyl-3-hydroxyphenyl acrylate, produces sustainable solid polymer electrolytes[395] and lignin-derived materials with improved UV absorption capacity[396], respectively.

Reversible addition-fragmentation chain-transfer (RAFT) is another living polymerization technique that benefits from the predictable and the controllable molecular weight of growing polymer chains. Washburn, Gupta, and co-workers developed a series of lignin-*g*-polyacrylamide following the RAFT pathway[399-401]. Kraft lignin was activated from acyl chloride xanthate to yield a macroinitiator assimilated to a RAFT transfer agent (Scheme 15.c). Further reacted with acrylamide (Am) or acrylic acid (AA) in presence of azobisisobutyronitrile initiator (AIBN), lignin-*g*-PAm/PAA contain hydrophilic and hydrophobic domains effective for surfactant applications[399]. While random copolymerization resulted in a nanogel, lignin-*g*-PAm copolymers synthesized from the RAFT technique are characterized by an organized architecture at the root of dispersant performance[400]. Additionally, lignin-*g*-PAm were designed for the long-term stabilization of water/ cyclohexane Pickering emulsions (Figure 8.c)[401].

Various methods have been explored to transform lignin into a chain transfer agent (CTA) including esterification with carboxylic acid derivatives[402, 403]. Using the lignin-macroinitiator, a series of soy-based vinyl monomers were grafted with high conversion yields (74-94 %) to produce thermally stable and solvent-soluble copolymers[403]. In another study, organosolv lignin was first converted into alkyne-bromine precursor through esterification with BiBB and subsequently converted into a CTA[404]. After copolymerization with n-butyl acrylate and 1-vinylimidazole, the lignin-derived material exhibits adhesive and self-healing aptitudes.

It is worth mentioning that the potential to develop lignin-derived materials with high cross-link density from radical polymerization techniques is limited by the inherent radical-scavenger activity of aromatic –OH groups[405]. To prevent the radical inhibitory effect, Qu *et al.* functionalized the –OH groups of pyrolytic lignin with methacryloyl and acetyl chlorides[406]. Acetylation eliminated the radical-scavenging effect of residual hydroxyl groups and the partially methracrylated lignin was then subjected to self-polymerization under RAFT conditions.
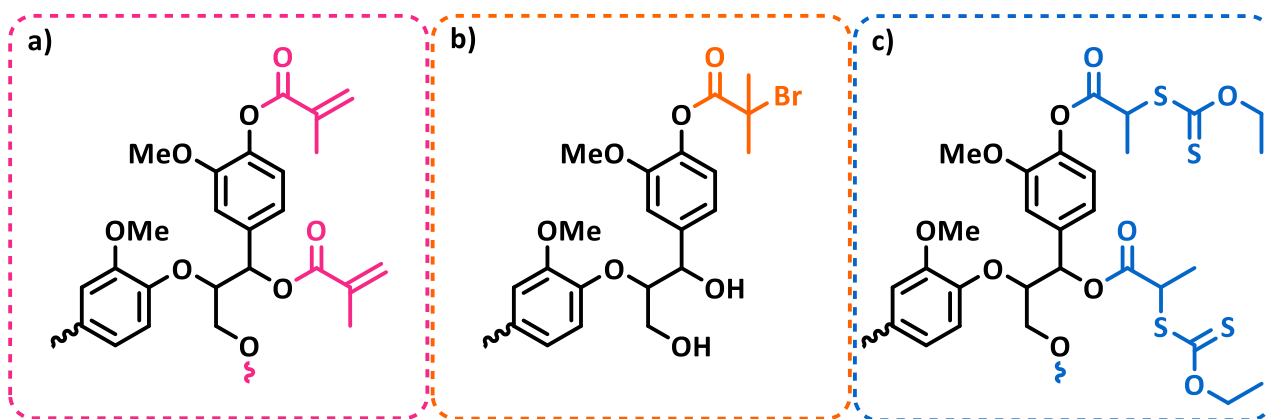
Scheme 15 Structure of lignin-macroinitiator for a) free-radical polymerization (methacrylic anhydride), b) atom transfer radical polymerization (2-bromoisobutyryl bromide), and c) reversible addition-fragmentation chain-transfer (acyl chloride xanthate).

2.5.1.2. Ring-opening polymerization (ROP)

ROP is a chain-growth polymerization strategy well fitted for the control of (co)polymers architecture[407]. Star-like polymer chains arise from the ring-opening of cyclic monomers on lignin terminal reactive centers. The oxyanionic ROP of ethylene oxide (EO) has been widely reported as an effective pathway to enhance the processability of lignin polyol, especially for lignin-derived PU. For another purpose, lignin-*g*-PEO can be employed as a bio-based surfactant for the emulsion polymerization of styrene[408]. If a few studies reports the ROP of oxazoline[409, 410], lignin-derived copolymers synthesized from ROP mainly focuses on polylactide (lignin-*g*-PLA, **Scheme 16.a**)[411-417] and poly(ε-caprolactone) (lignin-*g*-PCL, **Scheme 16.b**)[418-424], or the mixture of both polymers[425-427].

2.5.1.2.1 Lactide

Lactide (LA) is a cyclic ester existing in three different stereoisomeric forms, and its ROP leads to the formation of polylactide (PLA)[428]. Technical lignins have been traditionally used as functional fillers to enhance the properties of PLA while reducing production costs[429]. However, the poor interactions between lignin and PLA prompted researchers to find alternatives such as chemical modifications or graft copolymerization strategies. Chung *et al.* selected an unsulfonated Kraft lignin (Indulin® AT) as a macroinitiator to polymerize lactide[411]. Although the melting of PLA is still observed at low content of lignin (1-10 wt.%), the single glass transition detected at higher lignin content (20-50 wt.%) translates the lack of crystal structure in lignin-*g*-PLA ($DP_{PLA}< 14$). The copolymer obtained through this solvent-less and metal-free approach shows enhanced dispersibility and toughening effect when blended with PLA (**Figure 8.d**). Similarly, Ren *et al.* explored a selective alkylation pretreatment step to facilitate the grafting of PLA chains[412]. In this study, the aromatic and carboxylic –OH groups of alkaline lignin were selectively alkylated with 1-bromododecane. As a result, only unreacted aliphatic –OH groups from dodecylated lignin participate in the ROP of LA. The molecular weight of PLA chains grafted onto lignin ranges from 28200 to 1382 Da for a lignin content ranging from 1 to 20 wt.%, respectively (Đ ⩽ 1.41). Besides enhancing biocompatibility with PLA, the use of lignin-*g*-PLA as a functional filler has shown potential in promoting several desired properties including improved crystallization[413], or increased UV-resistance[414, 430], antioxydant activity[414, 415, 431], and recycling[416, 417] aptitudes.

2.5.1.2.2 Lactone

Lignin has been traditionally employed as a macroinitiator to initiate the ROP of ε-caprolactone monomer to form polycaprolactone (PCL)[418]. Starting from various technical lignins refined into well-defined fractions, Ragauskas and colleagues identified aliphatic –OH groups to preferentially initiate the ROP of CL[421, 422]. As a result, hydroxymethylated lignin containing higher amount of aliphatic –OH groups promote the formation of the starlike copolymer[423]. Laurichesse and Avérous elucidated the

structure-to-property relationship of a series of lignin-*g*-PCL[419]. ε-Caprolactone was used as reactive solvent for the organotin-catalyzed ROP. Meanwhile brittle materials were obtained for a monomer: macroinitiator feed ratio ranging from 10 to 100, the threshold ratio [CL]:[–OH]= 5 lead to flexible amorphous materials (T_g= -30 to -40 °C). However, a high lignin content prevents the crystallization and the diffusion of PCL chains[420]. Liu *et al.* followed this "*graft-from*" strategy for the solvent-free organo-catalyzed ROP of CL using bio-butanol lignin, a co-product of butanol biorefinery production, as macroinitiator[424]. In this study, lignin-*g*-PCL coatings exhibit good surface dispersibility and improved UV absorption capability (Figure 8.e). Additionally, lignin –OH groups can also be used to initiate the ROP β-butyrolactone[432, 433].

2.5.1.2.3 Lactide-co-lactone

Lactide and lactone can also be copolymerized using lignin as a macroinitiator[425]. The resulting lignin-*g*-P(CL-co-LLA) exhibits a rubber-like behavior that originates from the physically cross-linked structure of PCLLA. Further polymerized onto the inner rubbery block, outer segments of D-lactide induced stereocomplexation and interfacial compatibilization between lignin-*g*-P(CL-co-LLA) and external PLLA matrix. Following a similar pathway, electrospun[426] or melt-processed[427] lignin-*g*-P(CL-co-LLA) reinforced the antioxidant activity of PCL[426] and the heat resistance of PLA[427], respectively.
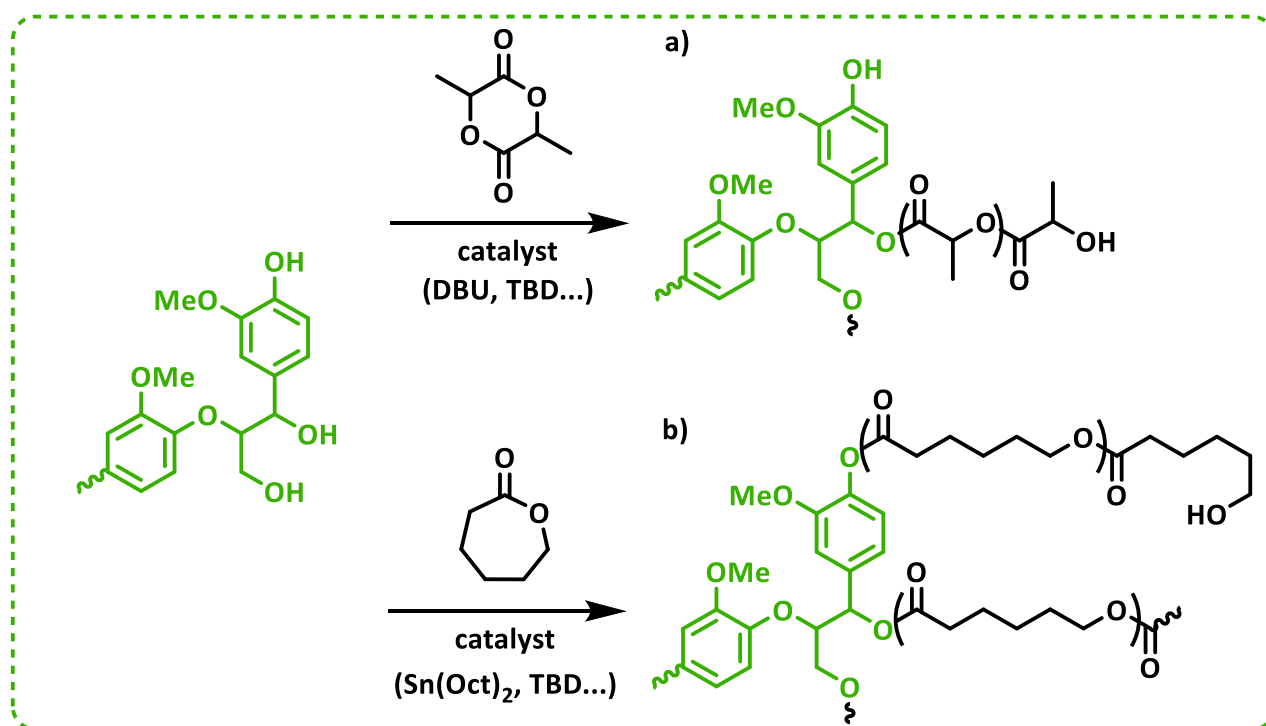
Scheme 16 Proposed scheme for the synthesis of lignin-derived copolymers based on "*graft-from*" ring-opening polymerization of a) lactide and b) caprolactone starting from lignin macroinitiator.

2.5.2. "Graft-onto" lignin-derived copolymer

The "*graft-onto*" approach offers greater versatility in extending the use of polymer chains covalently bonded onto lignin macromolecules. In contrast, the "*graft-from*" strategy is limited by the functionality of the monomeric units (e.g. vinylic or heterocyclic monomers). The "*graft-onto*" approach covers a wide range of telechelic polymers that can be grafted onto lignin through multiple coupling reactions.

2.5.2.1. Nucleophilic substitution of halogen precursors

Various strategies have been used to convert synthetic polymeric chains into telechelic alkyl[434, 435] or acyl chloride[436] precursors. Lin *et al.* synthesized an amphiphilic copolymer from Kraft lignin and a chloride-terminated PEG prepared from the Lewis-acid catalyzed ROP of ECH[434]. PEG end-capped with chloride group were chemically grafted onto the aromatic –OH groups of Kraft lignin through base-catalyzed etherification, improving its dispersibility. In another approach, researchers synthesized a high-efficiency lignin-grafted cationic polyacrylamide flocculant using EHL, acrylamide, and acryloyloxyethyltrimethyl ammonium chloride[435]. They used a "*grafting-onto*" method to graft the linear pre-polymer of cationic polyacrylamide terminated with chlorine onto EHL (77.9 - 99.9 % grafting yield). Chile *et al.* investigated the synthesis of lignin-*g*-PLA copolymers *via* different routes[436]. The topology of the products is affected by the initial lignin concentration, with low lignin loading generating cyclic PLAs and higher lignin loadings forming star-shaped lignin-*g*-PLA copolymers. By coupling lignin with acyl chloride terminated-PLA, the "*graft-onto*" approach gave highest lignin incorporation in the copolymer (up to 21 wt.%).

2.5.2.2. Radical coupling

ATRP has been shown to be effective for grafting PEGMA onto lignin macroinitiator to manufacture thermoresponsive[387], mechanoresponsive[437], and antioxidant copolymers[438]. Additionally, Yuan and colleagues reported the radical coupling of well-defined polyacrylamide and polybutyl acrylate macromolecules onto Kraft lignin[439, 440] using a ternary catalytic system of horseradish peroxidase /acetylacetone/ hydrogen peroxide to initiate, both RAFT polymerization of vinylic precursors and lignin oxidation. In another study, softwood Kraft lignin and poly(3-hydroxybutyrate-co-3-hydroxyvalerate) were co-polymerized using dicumyl peroxide as initiator, forming a biopolymer alloy with strong interfacial adhesion[441].

2.5.2.3. Click reactions

2.5.2.3.1 Azide-alkyne Huisgen cycloaddition

Barner-Kowollik *et al.* have outlined the fundamental principles of successful "click" reaction, which includes modularity, chemoselectivity, and orthogonalility[442]. The Huisgen cycloaddition, which produces a triazole group by the reaction between an azide ($-N_3$) and an alkyne ($-C{\equiv}C$) is exemplified on

Scheme 17.a. In 2015, Tang and coworkers introduced "click" chemistry into lignin-derived thermoset[443]. Alkyne and azide moieties were incorporated onto lignin –OH groups by alkylation with propargyl and esterification with 4-bromobutryl chloride followed by nucleophilic substitution with sodium azide, respectively. These functional lignins were clicked together under metal-free conditions using azide-functionalized PEG, or alkyl functionalized PCL or PLA, forming a series of graft copolymers. This approach proved to be effective in grafting lignin with 5-acetylaminopentyl acrylate or soybean oil to produce self-healing materials[444] and thermoset elastomers[445], respectively. In a novel approach, Jang *et al.* used softwood Kraft lining as a renewable material to develop thermoset foams[446]. The researchers synthesized multifunctional lignin macromonomers with azide and alkyne groups and turned them into thin films using hot pressing. The films were then cross-linked through a thermal reaction without the need for copper-based catalysts, resulting in all-lignin-based thermoset foams with a high gel fraction, randomly distributed pores, and flame resistance aptitude (Figure 8.f).

2.5.2.3.2   Michael addition

2.5.2.3.2.1.   Thiol-ene

Thiol-Michael additions induced by heat or light are also considered to be "click" reactions[447]. Johansson and colleagues used thiol-ene chemistry to develop a series of lignin-derived thermosets (Scheme 17.b)[448-450]. A refined Kraft lignin was selectively modified through allylation of aromatic –OH groups[448]. The lignin was then cross-linked by thermal-activation using a trifunctional thiol cross-linker led to a homogenous and translucid thermoset (Figure 8.g). This approach was extended to five fractionated lignins to study the structure-to-property relationship in this series of copolymers ($E'_{-50°C}$ = 1.9-5.9 GPa)[449]. By adjusting the degree of functionality of the thiol-based cross-linker lignin-derived thermosets (composed of 67 wt.% of lignin), with similar morphology and tunable properties could be obtained (T_α = 120-157 °C)[450]. Additionally, the thiol-ene "click" reaction between allylated lignin and 2-mercaptoethanol allowed for the design of bio-based polyols that could be subsequently condensed with a –NCO precursor to produce LPU anti-corrosive coating[451].

Liu and Chung demonstrated that softwood Kraft lignin could be clicked onto thiol-terminated PEG (PEG-SH) using visible- or sun-light triggered thiol−ene reaction with high efficiency (~ 95 %)[452]. Similarly, Yang *et al.* used UV-light irradiation to carry out the thiol-ene reaction between esterified lignin and PEG-SH for drug delivery systems[453]. Another alternative approach involved the use of allyl bromide to convert the phenolic–OH groups of lignin into ene-precursor, subsequently irradiated with cysteine for metal-ion adsorbent applications[454].

In an early study, propargylated lignin was reacted with 1,2,4-triazole-3-thiol using photochemically-triggered thiol-yne click to produce lignin-based absorbent[455]. More recently, Bernaets and colleagues developed lignin-derived thermosets *via* thiol-yne "click" chemistry between propargylated lignin and an excess of tetrafunctional thiol-based cross-linker (Scheme 17.c)[456, 457]. Post-curing treatment *via* Claisen rearrangement strengthens the network density (gel content 100 %, T_g= 56 °C, $T_{d5\%}$= 296 °C) and the addition of propargylated reactive diluent resulted in lignin-derived thermosets with superior adhesive performance ($\sigma_{adhesive}$= 2.3-2.5 GPa)[456]. Fractionated lignins were also used as a scaffold for the tandem UV-initiated thiol-yne "click" reaction/Claisen rearrangement to develop anti-corrosive coatings with high lignin content (46-61 wt.%)[457].

2.5.2.3.3   Diels-Alder cycloaddition

The Diels-Alder (DA) "click" reaction is a versatile tool to create various macromolecular architectures for different applications[458]. Lignin-derived copolymers based on the furan-maleimide DA reaction were first proposed by Duval *et al.* (Scheme 17.d)[459]. Similarly, Habibi and co-workers used a similar pathway to develop a series of lignin-derived thermosets based on thiol-maleimide and DA "click" reactions[460, 461]. In this method, a technical soda lignin was esterified with chlorinated 11-maleimidoundecylenic acid in solvent/catalyst-free conditions to introduce maleimide moieties onto the lignin structure[460]. The maleimide-functionalized lignin was further reacted with multifunctional thiol-based cross-linkers *via* the thiol-ene "click" polymerization to design thermosets (T_α= 19-59 °C). Later, the same thiol-based cross-linkers were reacted with furfuryl glycidyl ether[461]. The polyfunctional furan linkers were then reacted with maleimide-functionalized lignin by DA cycloaddition in a short time. The dissociative retro-DA reaction was used to demonstrate the ability of the resulting thermoset to be recycled.
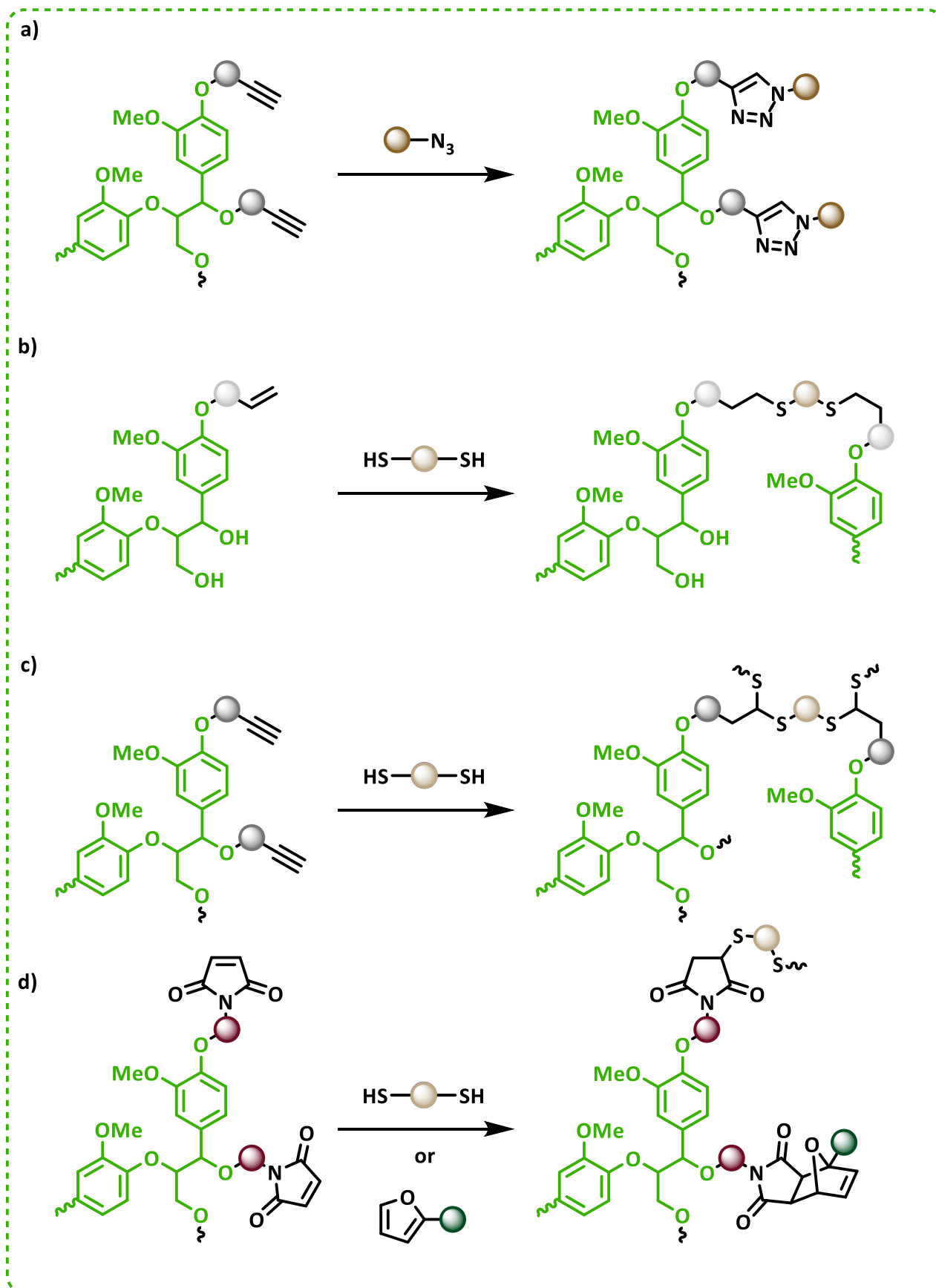
Scheme 17 Proposed scheme for the synthesis of lignin-derived copolymers based on "*graft-onto*" strategy. a) azide-alkyne Huisgen cycloaddition, b) thiol-ene based Michael addition, c) thiol–yne based Michael addition, d) thiol-maleimide based Michael addition or furan-maleimide Diels-Alder reaction.
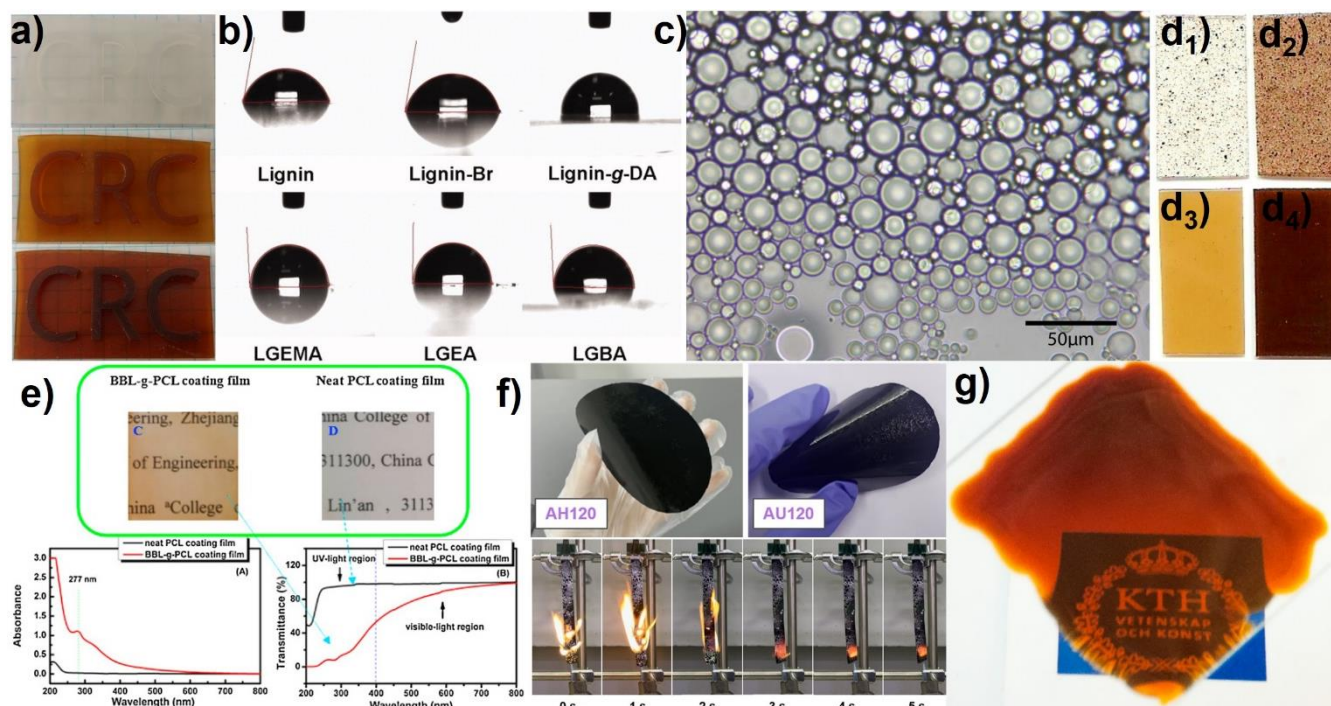
Figure 8 Example of lignin-derived copolymer preprared via "*graft-from*" and "*graft-onto*" strategies.

a) Photographs of 3D prints containing 0 to 10% methracylated lignin prepared via FRP (adapted from [382]). b) Static contact angle images of water droplets on lignin-*g*-rosin copolymer prepared *via* ATRP (adapted from [394]). c) Emulsion droplets water/cyclohexane stabilized by lignin-*g*-PAm prepared *via* RAFT (adapted from [401]). d) Photographs of PLA−lignin composites from (1-2) unmodified lignin or (3-4) lignin-*g*-PLA copolymer prepared *via* ROP. The lignin contents for (1-3) and (2-4) are 0.9−1.0 and 4.4−4.8 wt %, respectively (adapted from [411]). e) UV-absorption capacity of lignin-*g*-PCL coating films prepared via ROP (adapted from [424]). f) Photographs of lignin-g-copolymer films prepared via azide-alkyne cyclo-addition and flame-retardant application after oxidation (adapted from [446]). g) Photographs of lignin-g-copolymer cured thermoset prepared via thiol-ene reaction (adapted from [448]). h) Photographs of self-healing capability of lignin-*g*-copolymer preprared via Diels-Alder reaction (adapted from [461]).

Table 6 Examples of lignin-derived copolymers prepared *via* "*graft-from*" and "*graft-onto*" strategy.

Lignin source	Manufacture process	GC (%)	Resin characteristic	Application	Ref.
Acidified wheat straw alkali lignin	*Graft-from* (FRP) Lignin (~ 5 wt.%) [a] LMA/ [b] THFMA (~ 24/71 wt.%)	n.a.	[1] E= 239 MPa [2] ε= 14.1 % [3] T_g= 30 °C	Composite PLA	[380]
Acidified alkali lignin	*Graft-from* (ATRP) [c] Lignin-Br (~ 22.1 %) / [d] MMA Condition: PMDETA, CuBr	n.a.	E= 56 MPa ε= 23 % [4] $T_{g,E''}$= 77 °C	Composite Thermoplastic	[398]
Technical soda lignin (Protobind™ 1000)	*Graft-from* (ROP-PCL) Lignin (43 wt.%)/ [e] CL Conditions: SnOct$_2$	n.a.	E= 25 MPa ε= 33.0 % T_g= -45 °C	Lignin-derived thermoset	[419]
Technical softwood Kraft lignin (Amallin™)	*Graf-onto* ("Click" azide-alkyne) [f] Lignin-(N$_3$) (20 wt.%) [g] Lignin-(–C≡C) (80 wt.%)	99	E= 4.3 MPa ε= 1.4 % [5] $T_{d10\%}$= 258 °C	All-lignin thermoset foam	[446]
Softwood Kraft lignin (LignoBoost®)	*Graf-onto* ("Click" thiol-ene) [h] TMP 3P3 (–SH) (43 wt.%) [i] Lignin-(–CH=CH$_2$) (57 wt.%)	n.a.	[6] T_d> 250 °C [7] E'= 5.9 GPa [8] $T_α$= 94 °C	Lignin-derived thermoset	[449]
Technical soda lignin (Protobind™ 1000)	*Graf-onto* ("Click" thiol-yne) [j] PETMP (–SH) (48 wt.%) [k] Lignin: [l] P4MS (39:13 wt.%)	100	$T_{d5\%}$= 276 °C T_g= 45 °C	Renewable adhesive resin	[456]
Technical soda lignin (Protobind™ 1000)	*Graf-onto* ("Click" Diels-Alder) [m] TMP 3P3-furan (36 wt.%) [n] Lignin-maleimide (64 wt.%)	n.a.	E= 4.5 MPa ε= 101.4 % $T_α$= 23 °C	Self-healable thermoset	[461]

[a] lauryl methacrylate, [b] tetrahydrofurfuryl methacrylate, [c] lignin esterified with ethyl 2-bromoisobutyrate (lignin content determined by NMR), [d] methyl methacrylate, [e] ε-caprolactone, [f] lignin-azide synthesized from epoxy ring-opening of glycidylated phenolated lignin with NaN$_3$, [g] propargylated lignin synthesized from epoxy ring-opening of glycidylated phenolated lignin with 5-hexynoic acid,), [h] trimethylolpropane tris(3-mercaptopropionate) (1 eq. of thiol per allyl moiety), [i] allylated lignin synthesized from allyl chloride (acetone fraction), [j] propargylated lignin synthesized from propargyl bromide, [k] 4-methylsyringyl propargyl ether reactive diluent, [l] pentaerythritol tetrakis(3-mercaptopropionate) (2 eq. of thiol per propargyl moiety), [m] furan linker synthesized from pentaerythritol tetrakis(3-mercaptopropionate) and furfuryl glycidyl ether, [n] maleimido functionalized lignin synthesized from 11-maleimidoundecanoyl chloride.

[1] Young/tensile modulus, [2] strain at break, [3] glass transition temperature (DSC), [4] glass transition temperature (peak in the loss modulus), [5] temperature of 10% thermal decomposition, [6] onset of thermal decomposition, [7] storage modulus at -50 °C, [8] α-relaxation temperature.
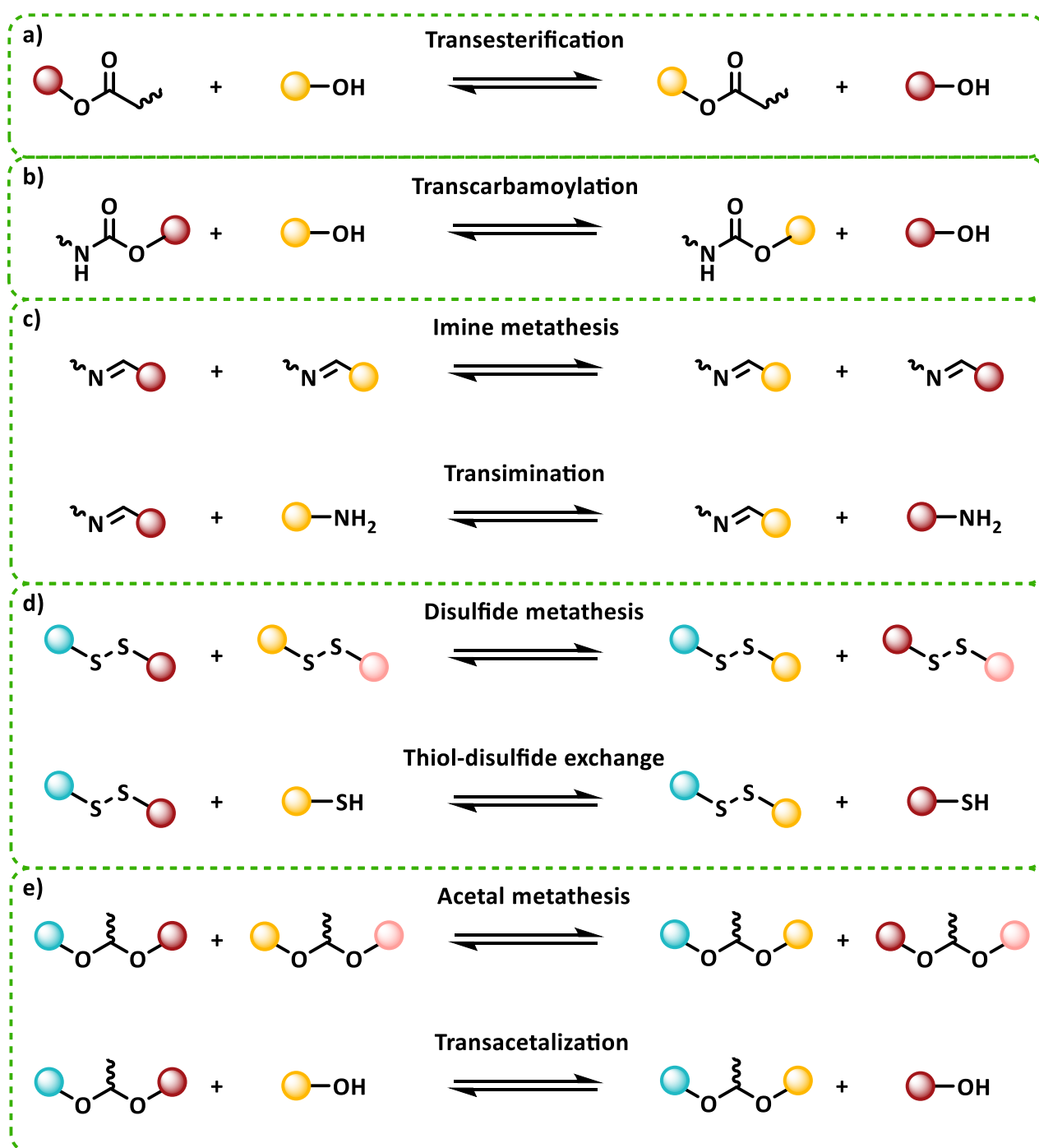
3. Lignin-derived vitrimers

3.1. Introduction to vitrimers

Thermosets are polymeric systems composed of a permanently and covalently cross-linked structure, that enables high solvent resistance and superior thermo-mechanical properties. However, it also impedes their recyclability, as they do not melt or can be depolymerized, in contrast to thermoplastics. To tackle this issue, dynamic bonds can be introduced into their structure, opening up opportunities of recycling like mechanical reprocessing. Covalent adaptable networks (CANs) are polymer networks composed of permanent and dynamic covalent bonds (DCBs)[462, 463]. From the standpoint of chemistry, a distinction is made about the mechanisms governing the reversibility of DCBs. CANs operating under dissociative exchanges are characterized by successive bond breaking and reformation altering the cross-link density of the network over time (elimination-addition). Diels-Alder (DA) reversible reactions fall into this category. DA bonds tend to depolymerize in a temperature range around 120 °C, and can reform when the material is cooled at room temperature. On the other hand, associative CANs retain their network integrity, the DCBs being described as able to reform following an addition-elimination mechanism. From a mechanistic perspective, the viscosity of associative and dissociative CANs correlates to the rate of exchange of the DCB[464]. Unlike the abrupt drop in thermoplastics' viscosity observed above their melting temperatures, the viscosity of CANs gradually decreases upon heating. Inspired by the gradual fluidity and the permanent connectivity of inorganic silica materials upon vitrification, associative CANs have been termed "*vitrimers*" by Leibler and colleagues[465-467]. In addition to the usual T_g of thermosets, vitrimers exhibit a topology freezing temperature (T_v) corresponding to the transition from a viscoelastic solid to a viscoelastic liquid[468]. Below T_v, vitrimers behave like a classical thermoset with a cross-linked network composed of dormant DCBs. Above T_v, the topological rearrangements induced by activated DCBs endow vitrimeric materials with a macroscopic flow at the root of their reshaping and their reprocessability aptitudes. This unique rheological behavior is commonly evaluated through the ability of the dynamic network to relax stress in response to a strain deformation[465]. The activation energy (Ea) of the reversible exchange is calculated from the temperature-dependent stress-relaxation experiments from which relaxation times are determined (τ^*, time for the vitrimeric material to recover 1/e of the original relaxation modulus) and fitted using an Arrhenius model.

While some vitrimers require the addition of catalysts to reach the thermodynamic equilibrium of the DCB on a reasonable time scale, internal catalysis and neighboring group participation theory afford alternatives to the aging or leaching issues regularly associated with external catalysts[469, 470]. Since their discovery[465], various exchangeable bonds have been investigated to develop vitrimers[471-474]. This includes transesterification[465], transcarbonation[475], transcarbamoylation[476], transamination of vinylogous urethane[477], transalkylation[478], olefin metathesis[479], acetal exchange[480], imine exchange[481], dioxaborolane metathesis[482], disulfide exchange[483], siloxane exchange[484], among others.

3.2. Dynamic covalent bonds in lignin-derived vitrimers

Increasing research efforts have been done to combine the concept of vitrimers with bio-derived polymers[474]. The high cross-linking density of lignin ensures dimensional stability in thermoset networks and facilitates the development of thermally and creep-resistant materials. However, processability and vitrimerization issues may impede their manufacture and prohibit their segmental mobility. One challenge in designing vitrimer-like materials from highly cross-linked lignin is to find a good balance between the ratio of permanent and dynamic cross-links. In this section is reviewed the current status of introducing DCBs into lignin-derived thermosets (Scheme 18).

Scheme 18 Dynamic covalent reactions inmplemented in lignin-derived vitrimers.

3.2.1. Transesterification

Implemented in pioneering work of Montarnal *et al.*[465], the dynamic transesterification involves a reaction between an ester and a hydroxyl group that results in the formation of new ester and hydroxyl moieties (Scheme 18.a). The reversible exchange is thermally activated, and usually conducted in the presence of a catalyst that activates ester bonds. Transesterification-based vitrimers benefit from a versatile design. Most of the research works on the synthesis of lignin-derived vitrimers focus on the cross-linking of epoxy resins with carboxylic acid curing agents[485-491]. Two main chemical pathways have been explored to conduct the opening of epoxy rings.

In a first approach, lignin is converted into a polycarboxylic acid hardener by oxidative treatment[485, 487] or esterification with a cyclic anhydride[486]. Zhang *et al.* pioneered the design of lignin-derived vitrimers starting from an ozonated Kraft lignin cured with a difunctional epoxy derived from sebacic acid[485]. Ozonolysis was employed to improve the number of carboxylic moieties of polyphenolic lignins ([COOH]= 2.30 mmol.g^{-1}). In the presence of zinc acetylacetonate catalyst (10 mol.%), heat-induced transesterification exchanges enable the manufacture of thermally repairable adhesives (Figure 8.a). Later, the ozonation treatment has been integrated within the LignoForce^{TM} process for the valorization of Kraft lignin into bio-derived vitrimer[487]. In another study, Zhang *et al.* reacted the –OH groups of Kraft lignin with cyclic anhydride to generate a polycarboxylic acid cross-linker, subsequently cured with PEGDE to form an epoxy-vitrimer network[486]. By increasing the content of carboxylated lignin from 47 to 63 wt.%, the thermomechanical properties were improved while the dynamic behavior was preserved (T$_g$= 37-76°C, $\tau^*_{200°C}$= 720-920 s). The addition of EG was found to promote topological rearrangements and self-healing capability (92% damage repairability in 15 minutes at 190 °C).

In the second approach, lignin-derived epoxy vitrimers were prepared from glycidylated lignin, followed by a curing step in the presence of polyfunctional carboxylic acid[488-490]. Xue *et al.* investigated the gradual substitution of DGEBA with glycidylated lignin (GEL) to develop zinc-catalyzed vitrimers[488]. Increasing the content of GEL is suitable to develop a cross-linked network with robust mechanical performance (33 wt.% GEL, E= 2.0 GPa). However, stress relaxation experiments evidenced the detrimental impact of the high number of permanent bonds on the segmental mobility of the dynamic network. To identify the prominent structural parameters regulating the performance of lignin-derived epoxy vitrimers, Tang *et al.* refined EHL through solvent fractionation[489]. The various lignin fractions were converted into glycidyl ether and subsequently cured with sebacic acid to develop reprocessable materials with tuneable properties. Characterized by a lower molecular weight and higher amount of non-condensed phenolic units (M$_n$= 1402 g.mol^{-1}, [OH]$_{phenol}$=3.34 mmol.g^{-1}), the epoxy vitrimer prepared from the ethanol-soluble fraction presents the higher self-repairing and reprocessing efficiency. If trans-esterification is usually triggered by heat, the conjugated structure of lignin is also amenable to photo-thermal transformations offering reduced energy consumption in comparison to hot-press treatment[490].

Du *et al.* combined the two above-mentioned approaches and cross-linked a glycidylated lignin with carboxylated lignin (maleic anhydride) in the presence of PEG$_{400}$ spacer[491]. As an excess of −OH groups activates ester bonds through hydrogen bonding, the network was able to behave as a catalyst-free vitrimer with lignin content up of 73 wt.% (Figure 9.b). [492]. Apart from epoxy networks, various lignin-derived thermosets can also be designed with dynamic features driven by transesterification. For example, Johnson *et al.* explored a "*graft-onto*" strategy to design reprocessable thermosets from the thiol-ene "*click*" reaction of partially methracrylated dealkaline lignin with PEG-dithiol moieties[493].

In summary, transesterification exchanges promote rapid topological rearrangements endowing lignin-derived vitrimers with self-healing, reshaping, and reprocessability aptitudes. Being synthesized from readily available building-blocks and compatible with various classes of polymers, transesterifications-based vitrimers stand as ideal candidate for industrial development.

3.2.2. *Transcarbamoylation*

Urethane linkages are known to dissociate into their precursors (−OH and −NCO) when reacted with hydroxyl groups at high temperatures, and to reform upon cooling[494]. Although transcarbamoylation equilibrium proceeds likely through a dissociative mechanism, an associative mechanism is observed under typical reprocessing conditions (< 200 °C) in the presence of a suitable catalyst (Scheme 18.b). The profuse number of −OH groups in lignin is favorable to designing transcarbamoylation-based vitrimer. In the literature, ethanol-fractionated alkali lignin[495] or technical[496, 497], nano-sized[498], and depolymerized EHL[499] were employed as polyol to bring hydroxyl functionalities into lignin-derived PU networks.

The first report of transcarbamoylation exchange in lignin-derived PU used a partially depolymerized lignin (DEL, M_n= 1200 g.mol^{-1}) to cross-link HDI-end capped polytetramethylene ether glycol[499]. The base-catalyzed liquefaction process improves the reactivity of lignin macromolecules toward isocyanation and its interfacial compatibility in the PU elastomer matrix (LPUe). In the presence of dibutyltin dilaurate catalyst, thermally-induced transcarbamoylation enables reprocessability with a high rate of Young's modulus retention after two recycling processes (retention> 85 % for LPUe containing up to 4-17 wt.% of DEL). In a follow-up work, the same group introduces photothermal-responsive triazole functionalities in LPUe to form a dual-crosslink network composed of dynamic non-covalent bonds (hydrogen and Zn^{2+}-coordination bonds) and DCBs (carbamates)[495]. The coordination bonds endow the lignin-derived PU networks with fast light-induced healing capabilities under NIR stimulation and promote close-looped chemical recyclability[497]. To reduce the consumption of catalysts, Ma and colleagues increased the content of pendant aliphatic −OH groups by tuning the initial ratio of isocyanate/ hydroxyl (NCO/OH<1)[496]. As evidenced by stress-relaxation experiments, the excess of unreacted −OH groups promote catalyst-free transcarbamoylation in the lignin-derived PU network.

Illustrated in Figure 8.c, a robust and dynamic cross-linked network was manufactured with extrusion-mediated reprocessing and shape-memory capabilities (50 wt.% PEG_{2000} polyol substitution, NCO/OH= 0.8, GC> 95%, Ea= 106 kJ.mol^{-1}).

In addition to being synthesized from safer chemicals, hydroxyurethane bonds in NIPU networks promote the associative mechanism in transcarbamoylation exchange[500-502]. Zhao *et al.* developed a straightforward and environmentally friendly pathway for the ring-opening of polyfunctional cyclic carbonate with dimer fatty amine and EHL[502]. The homogenous distribution of −OH groups within the NIPU network induces hydrogen-bonding between lignin macromolecules and polyhydroxyurethane (PHU) matrix improving the interfacial compatibility. The cross-linking density of PHU materials increased concomitantly with lignin content, thereby reducing the elasticity of the material (from 0 to 50 wt.% EHL, T_g= -3 to 4 °C, Y= 2 to 43 MPa). As reported in Figure 8.d, the resulting elastomers can be mechanically reprocessed *via* catalyst-free transcarbamoylation reactions (120 °C) or chemically recycled *via* reversible cyclic carbonate aminolysis (*n*-butylamine).

The highly condensed structure of lignin brings a significant amount of permanent and thermally-resistant cross-link in the vitrimer network. One of the challenges in the synthesis of transcarbamoylation-based vitrimers is to avoid an overlap of the thermo-mechanical transitions and the depolymerization temperature of urethane bonds. Therefore, it is considered in most of the research works treating of transcarbamoylation-based lignin-derived vitrimers to incorporate soft segments into the structure of lignin with the aim to avoid this overlap while promoting elastomeric features.

3.2.3. Imine exchange

Schiff base contains imine bonds that are formed following the condensation reaction of a primary amine with an aldehyde or a ketone. Imine bonds can reshuffle under catalyst-free associative exchanges, either by imine metathesis or transimination reactions (Scheme 18.c). The former refers to the exchange reactions between two imine units while the latter corresponds to the reversible aminolysis of imine bonds. Generally triggered by heat, imine exchanges are also sensitive to water and pH. Indeed, imine bonds are prone to hydrolysis in a reversible dissociative pathway. Under typical service conditions, hydrolysis slightly affects the integrity of the cross-linked network and offers water-assisted malleability at ambient temperature[481]. The main strategy to incorporate imine bonds in lignin consists in its conversion into a polyaldehyde precursor, either by chemical functionalization[503] or by oxidation treatment[504]. Gao *et al.* exploited a "*grafting-from*" strategy to design star-like copolymers made up of a lignin core decorated with aldehyde side-chains[503]. An esterified lignin bearing dithiobenzoate moieties (2.64 mmol.g^{-1}) was used as a chain transfer agent for the RAFT polymerization of vanillin and lauryl methacrylate. The copolymer was then polymerized with diamines of various chain lengths to form an

antifungal polyimine adhesive with reprocessing and self-healing capabilities. In another approach, the oxidative treatment of organosolv lignin with Dess–Martin periodinane allows converting −OH groups into ketones and aldehydes (5.31 mmol.g^{-1})[504]. The oxidized lignin was then reacted at room temperature with an excess of a dimer diamine (Priamine^{TM} 1071) to form a lignin-derived polyimine network with thermo-mechanical properties that can be tuned by adjusting the stoichiometric ratio between aldehyde and amine (E= 6-117 MPa, $T_{d5\%}$= 298-323 °C). The lignin-derived vitrimer could be reprocessed at 170 °C with well-preserved mechanical strength (Figure 8.e).

If the hydrolysis of imine bonds opens up potential chemical recycling pathway, it also impedes their use in any type of applications where the materials would be exposed to humidity. By designing lignin-derived polyimine vitrimer, this drawback could be tackled thanks to its prominent hydrophobicity.

3.2.4. Disulfide exchange

The dynamic nature of sulfur bonds has been widely investigated to develop reprocessable materials. Many research works have focused the topic of their investigation onto the understanding of the mechanisms governing the dynamicity of disulfide exchanges (Scheme 18.d). Triggered by heat or UV-light, the associative disulfide metathesis between two disulfide bonds is deemed the most common mechanism, but reversible thiol-disulfide exchange could be also occur when dangling −SH moieties or a nucleophilic catalyst are employed. In the case of lignin-based disulfide vitrimer, and as in any other disulfide-based vitrimers, the disulfide bond is not generated through cross-linking reactions. It must be incorporated into using precursors that contains the disulfide bond. Bis(4-aminophenyl) disulfide or bis(2-hydroxyethyl) disulfide have been used to introduce dynamic disulfide bonds into lignin-derived polyurea[505] or PUe[506], respectively. For the former system, depolymerized EHL was reacted with formaldehyde and long-chain polyetheramine (Jeffamine® D-2000) through Mannich condensation. Combined with the amine-containing disulfide, the amine-functionalized lignin was used to cross-link an isocyanate-terminated prepolymer. The dynamic reactions in the polyurea network can be activated at relatively low temperatures with fast stress relaxation observed at 50 °C (τ^{*} < 5 min). The disulfide exchange endows lignin-derived polyurea adhesive with reusable ability and can be self-healed in a short time (Figure 8.f).

In response to the fast reshuffling of disulfide bonds that may limit their applicability at service temperature, the highly-crosslinked structure of lignin may favor the synthesis of highT_g materials. The rate of dynamic bonds can be adjusted to finely tuned the dynamicity of disulfide exchanges while ensuring dimensional stability over a wider temperature range.

3.2.5. Acetal exchange

The reversible reaction between two acetals, namely acetal metathesis, emerged recently as a promising DCB for vitrimeric materials (Scheme 18.e). Moreno *et al.* developed a one-pot strategy for the design of an acetal network by the thermally accelerated alcohol–vinyl ether "*click*" addition between poly(ethylene glycol) divinyl ether and softwood Kraft lignin[507]. The thermo-mechanical properties of the cross-linked network was tuned according to the lignin content (from 28 to 50 wt.%) with glass transition ranging from 109 to 121 °C and Young modulus from 0.01 to 2.1 GPa, respectively (Figure 8.g). The stress relaxation behavior was following an Arrhenius-like temperature dependence, which is characteristic of vitrimers. The linear correlation between the calculated activation energy and lignin content (E_a= 204 to 77 kJ.mol^{-1} from 37 to 50 wt.%) suggests that the mechanism of exchange is promoted by lignin' −OH groups. Model molecules were designed to reveal that transacetalization reactions associated with the reversible alcoholysis of acetal were occurring. Therefore, the dynamicity of acetal networks is driven both by the catalyst-free acetal metathesis and transacetalization exchanges. The lignin-derived vitrimer was used as a recoverable adhesive capable to preserve adhesion performance after reprocessing (93%) and to resist to an aggressive environment such as concentrated saline water.

To prevent the degradability of acetal motif in hot-water[480], the hydrophobic nature of lignin confers water-resistance well-suited for improving the robustness of the dynamic acetal network.
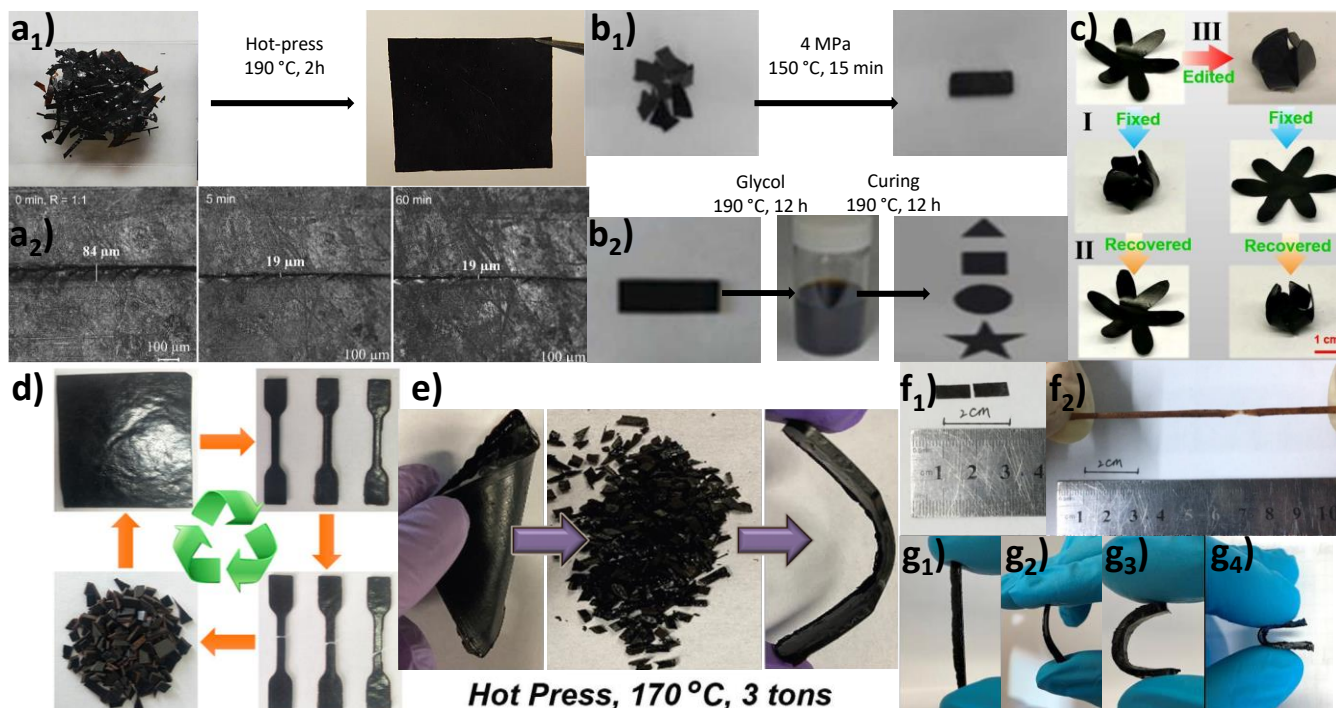
Figure 9 Examples of lignin-derived vitrimers.

a) Transesterification-based epoxy vitrimer prepared from ozonated Kraft lignin. (1) Photographs of mechanical reprocessing through hot-press treatment and (2) micrographs of thermally-induced self-healing in pressure-free conditions (adapted from [485]), b) Photographs of recycling performance of epoxy vitrimer relying on catalyst-free transesterification Recycling tests:(1) Mechanical reprocessing and (2) chemical recycling (adapted from [491]), c) Photographs of tunable shape memory responses induced by catalyst-free transcarbamoylation in lignin-derived PU network (adapted from [496]), d) Photographs of reprocessing in transcarbamoylation-based LPHU vitrimer (adapted from [502]), e) Photographs of reprocessable lignin-derived polyimine vitrimer (adapted from [504]), f) Photographs of fast self-healing performance of lignin-derived polyurea adhesives containing disulfide bonds. (1) Fracture surfaces and (2) stretched elastomer after 2 minutes healing (adapted from [505]), g) Photographs of the bending ability of transacetalization-based vitrimers prepared from the "*click*" addition of poly(ethylene glycol) divinyl ether (PVD) and softwood Kraft lignin (SKL). PDV-SKL ratio (1) 1:1, (2) 1:0.8, (3) 1:0.6 and (4) 1:0.4 (adapted from [507]).

Table 7 Examples of lignin-derived vitrimers synthesized from different dynamic covalent bonds.

Lignin source	Manufacture process	GC (%)	Resin characteristic	Vitrimer characteristic	Ref.
Technical enzymatic hydrolysis lignin	*Transesterification (epoxy)* [a] GEL (18 wt.%)/ [b] DGEBA (42 wt.%)/ [c] DEA (35 wt.%) Catalyst: [d] Zn(acac)$_2$ (4 wt.%)	83	[1] E_Y= 0.5 GPa [2] σ= 23 MPa [3] T_α= 41 °C	[4] E_a= n.a. [5] $\tau^*_{160°C}$= 1570 s [6] $RR_{\sigma,2}$= 96 %	488
Technical enzymatic hydrolysis lignin	*Transesterification (epoxy)* [a] EP-EL (33 wt.%)/ [e] CA-EL (33 wt.%)/ [f] PEG$_{400}$ (33 wt.%) Catalyst: ∅	n.a.	T_α= 121 °C σ= 48 MPa [7] $T_{d5\%}$= 277 °C	E_a= 18 kJ.mol^{-1} $\tau^*_{220°C}$= ~ 1000 s RR= n.a.	491
Technical enzymatic hydrolysis lignin	*Transcarbamoylation (PU)* [g] DEL (17 wt.%)/ [h] PTMEG (67 wt.%)/ [i] HDI (16 wt.%) Catalyst: [j] DBTDL (< 1 wt.%)	94	E_Y= 0.02 GPa σ= 39 MPa $T_{d5\%}$= 301 °C	E_a= n.a. $\tau^*_{160°C}$= < 300 s $RR_{Ey,2}$= 86 %	499
Technical enzymatic hydrolysis lignin	*Transcarbamoylation (NIPU)* EHL (30 wt.%)/ [k] BCC (25 wt.%)/ [l] DDA (45 wt.%) Catalyst: ∅	n.a.	E_Y= 0.01 GPa σ= 8 MPa [8] T_g= 2 °C	E_a= n.a. τ^*= n.a. $RR_{Ey,4}$= 90 %	502
Organosolv lignin	*Imine exchange (polyimine)* [m] OL (22 wt.%)/ [n] DDA (78 wt.%) Catalyst: ∅	n.a.	E_Y= 0.12 GPa σ= 3 MPa $T_{d5\%}$= 298 °C	E_a= n.a. τ^*= n.a. $RR_{Ey,1}$= 100 %	504
Technical enzymatic hydrolysis lignin	*Disulfide exchange (PU)* [o] LC (7 wt.%)/ [p] D2000 (66 wt.%)/ [q] SS (8 wt.%)/ [r] IPDI (18 wt.%) Catalyst: ∅	n.a.	σ= 0.8 MPa T_g= -58 °C $T_{d5\%}$= 278 °C	E_a= n.a. $\tau^*_{50°C}$= < 150 s [9] $RR_{\sigma,1}$= 78 %	505
Softwood Kraft lignin (UPM BioPiva™ 100)	*Acetal exchange (polyacetal)* SKL (50 wt.%)/ [s] PDV (50 wt.%) Catalyst: ∅	98	E_Y= 2.1 GPa σ= 51 MPa T_g= 121 °C	E_a= 77 kJ.mol^{-1} $\tau^*_{180°C}$= 77s $RR_{Ey,2}$= 88 %	507

[a] Glycidilated lignin, [b] Diglycidyl ether bisphenol A, [c] Dodecanedioic acid, [d] Zinc acetylacetonate, [e] Lignin carboxylated with maleic anhydride, [f] Polyethylene glycol (M$_n$= 400 g.mol^{-1}), [g] Partially depolymerized lignin, [h] Polytetramethylene ether glycol (PTMEG$_{2000}$), [i] Hexamethylene diisocyanate, [j] Dibutyltin dilaurate, [k] Bis(6-membered cyclic carbonate), [l] Dimer diamine (Priamine™ 1074), [m] Lignin oxidized with Dess–Martin Periodinane, [n] Priamine™ 1071, [o] Polyetheramine-grafted lignin, [p] Polyetheramine (Jeffamine® D-2000), [q] Bis(4-aminophenyl)disulfide, [r] Isophorone diisocyanate, [s] PEG divinyl ether.

[1] Young modulus, [2] Tensile strenght, [3] α-relaxation temperature, [4] Activation energy, [5] Relaxation time, [6] Retention ratio of the tensile strenght after two reprocessing, [7] Temperature of 5% thermal decomposition, [8] Glass transition (DSC), [9] Retention ratio of the tensile strenght after 1h self-healing.

3.3. Other potential dynamic exchanges to design lignin-derived vitrimers

Some DCBs, such as radical-mediated olefin metathesis, are not compatible with lignin as a building block due to the inherent radical scavenging activity of lignin that impede the dynamic exchange. However, several other chemistries have not yet been investigated while they could be considered to develop lignin-based DCBs. Scheme 19 gathers a non-exhaustive selection of dynamic covalent linkages that have not been introduced, to date, in the design of reprocessable lignin-derived materials, and these mechanisms are discussed in the following bullet points:

➢ Transcarbonation proceeds through the metal-catalyzed exchange between a carbonate and an alcohol (Scheme 19.a). Various strategies have been developed to incorporate carbonate moieties onto the structure of lignin, especially for the synthesis of lignin-derived NIPU (Scheme 4 and Scheme 5). The structure of lignin is ideally suited to develop vitrimers relying on transcarbonation. The abundant number of hydroxyl groups on lignin could be used to trigger the ROP of cyclocarbonate, resulting in lignin-derived materials composed of carbonate and –OH groups able to exchange through transcarbonation.

➢ Vinylogous urethanes are DCBs obtained from the condensation of acetoacetates and amines. The reversible nucleophile addition of primary amines and vinylogous urethanes is called transamination (Scheme 19.b) . Lignin can be either converted into a polyacetoacetate through the acetoacetylation of its hydroxyl groups (generally by transesterification of *tert*-butyl acetoacetate) or into a polyamine through Mannich condensation. The cross-linking of amine- and acetoacetate-derived precursors (the latter introduced in slightly off-stoichiometric conditions) leads to a dynamic network composed of free amines and vinylogous urethane bonds.

➢ Boronic ester units are known to exchange either *via* dioxaborolane metathesis between two boronic esters moieties or *via* transesterification involving hydroxyl groups (Scheme 19.c). The dynamic network containing cyclic boronic ester bonds is generally synthesized from the cyclization of a polyol with diboronic acid in anhydrous conditions. The prominent β-O-4' interunit linkage in lignin structure contains a 1,3-diol motif suited for conversion in a 6-membered boronic ester ring. It is assumed that hydrophobic lignin could protect boronic ester from the water-assisted dissociation into parent diol and boronic acid.

➢ While siloxane or silyl ether bonds can rearrange through a metathesis mechanism, an excess of –OH groups promote associative silyl ether-hydroxyl exchange (Scheme 19.d). The cross-linking of lignin with siloxane-based precursors leads to thermosetting materials with flame-

retardant[508] or degradability[509] aptitudes. Lignin provides robustness to siloxane-based materials that usually exhibit elastomeric features. The investigation of the dynamicity of silyl ether bonds in lignin-derived vitrimers could extend their applicability to reprocessable thermosets. As well, siloxane exchanges occurs at high temperature (typically around 180 -220 °C)[510], and could be highly suitable for the design of high-T_g vitrimers, in concomitance with the structure of lignin.
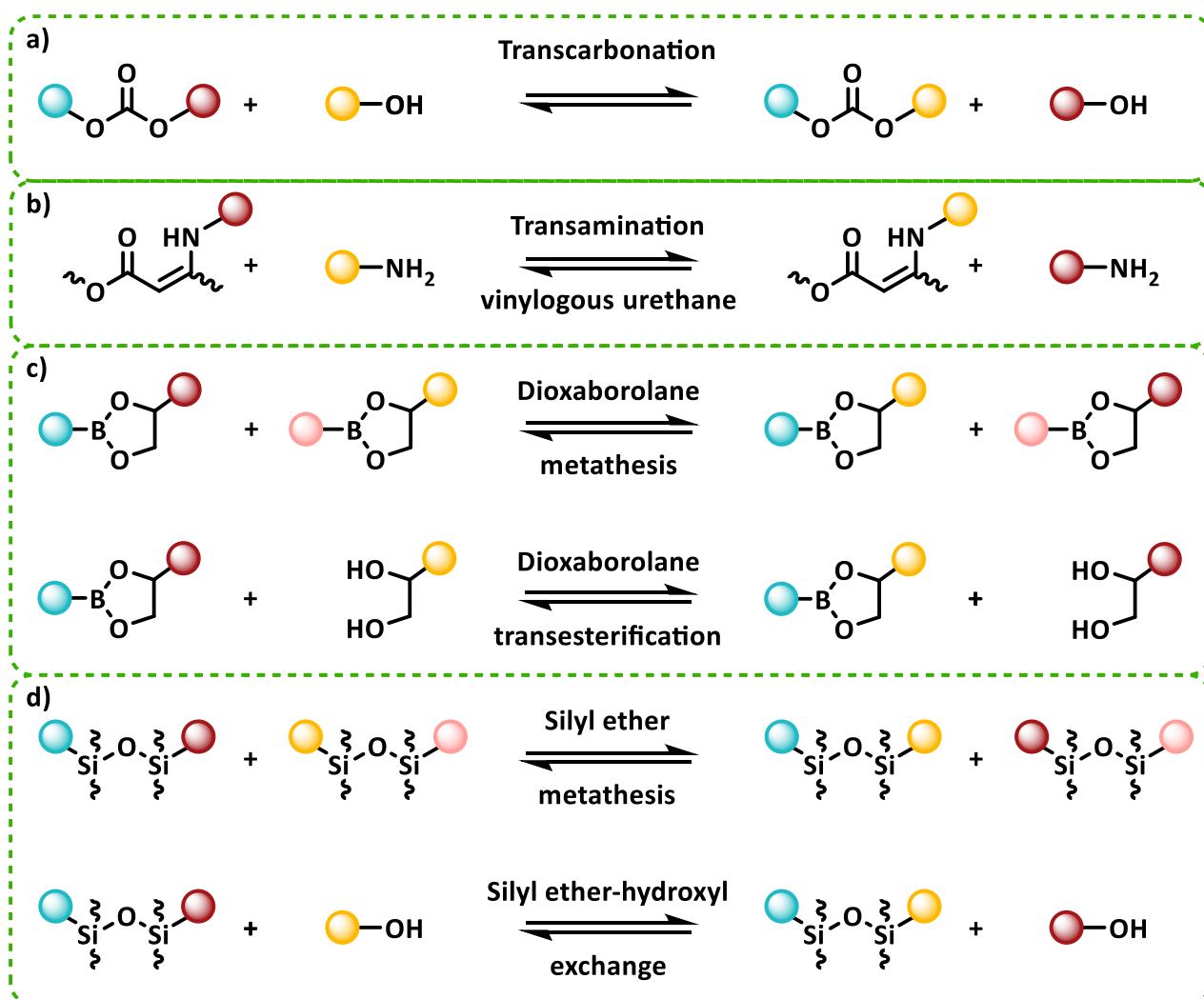
Scheme 19 Non exhaustive selection of dynamic covalent bonds not explored for the design of lignin-derived vitrimers.

4. References

(1) Azadi, P.; Inderwildi, O. R.; Farnood, R.; King, D. A. Liquid fuels, hydrogen and chemicals from lignin: A critical review. *Renewable and Sustainable Energy Reviews* **2013**, *21*, 506-523. DOI: https://doi.org/10.1016/j.rser.2012.12.022.

(2) Isikgor, F. H.; Becer, C. R. Lignocellulosic biomass: a sustainable platform for the production of bio-based chemicals and polymers. *Polymer Chemistry* **2015**, *6* (25), 4497-4559. DOI: http://dx.doi.org/10.1039/C5PY00263J.

(3) Li, T.; Takkellapati, S. The current and emerging sources of technical lignins and their applications. *Biofuels, Bioproducts and Biorefining* **2018**, *12* (5), 756-787. DOI: https://doi.org/10.1002/bbb.1913.

(4) Bass, G. F.; Epps, T. H. Recent developments towards performance-enhancing lignin-based polymers. *Polymer Chemistry* **2021**, *12* (29), 4130-4158. DOI: http://dx.doi.org/10.1039/D1PY00694K.

(5) Biosynthesis of Lignin. In *Lignin and Lignans as Renewable Raw Materials*, 2015; pp 75-112.

(6) Gellerstedt, G.; Henriksson, G. Chapter 9 - Lignins: Major Sources, Structure and Properties. In *Monomers, Polymers and Composites from Renewable Resources*, Belgacem, M. N., Gandini, A. Eds.; Elsevier, 2008; pp 201-224.

(7) Ponnusamy, V. K.; Nguyen, D. D.; Dharmaraja, J.; Shobana, S.; Banu, J. R.; Saratale, R. G.; Chang, S. W.; Kumar, G. A review on lignin structure, pretreatments, fermentation reactions and biorefinery potential. *Bioresource Technology* **2019**, *271*, 462-472. DOI: https://doi.org/10.1016/j.biortech.2018.09.070.

(8) Freudenberg, K. Lignin: Its Constitution and Formation from p-Hydroxycinnamyl Alcohol. *Science* **1965**, *148* (3670), 595-600. DOI: https://doi.org/10.1126/science.148.3670.595.

(9) Adler, E. Lignin chemistry—past, present and future. *Wood Science and Technology* **1977**, *11* (3), 169-218. DOI: https://doi.org/10.1007/BF00365615.

(10) Chakar, F. S.; Ragauskas, A. J. Review of current and future softwood kraft lignin process chemistry. *Industrial Crops and Products* **2004**, *20* (2), 131-141. DOI: https://doi.org/10.1016/j.indcrop.2004.04.016.

(11) Laurichesse, S.; Avérous, L. Chemical modification of lignins: Towards biobased polymers. *Progress in Polymer Science* **2014**, *39* (7), 1266-1290. DOI: https://doi.org/10.1016/j.progpolymsci.2013.11.004.

(12) Yoo, C. G.; Ragauskas, A. J. Opportunities and Challenges of Lignin Utilization. In *Lignin Utilization Strategies: From Processing to Applications*, ACS Symposium Series, Vol. 1377; American Chemical Society, 2021; pp 1-12.

(13) Li, C.; Zhao, X.; Wang, A.; Huber, G. W.; Zhang, T. Catalytic Transformation of Lignin for the Production of Chemicals and Fuels. *Chemical Reviews* **2015**, *115* (21), 11559-11624. DOI: https://doi.org/10.1021/acs.chemrev.5b00155.

(14) Constant, S.; Wienk, H. L. J.; Frissen, A. E.; Peinder, P. d.; Boelens, R.; van Es, D. S.; Grisel, R. J. H.; Weckhuysen, B. M.; Huijgen, W. J. J.; Gosselink, R. J. A.; et al. New insights into the structure and composition of technical lignins: a comparative characterisation study. *Green Chemistry* **2016**, *18* (9), 2651-2665. DOI: http://dx.doi.org/10.1039/C5GC03043A.

(15) Granata, A.; Argyropoulos, D. S. 2-Chloro-4,4,5,5-tetramethyl-1,3,2-dioxaphospholane, a Reagent for the Accurate Determination of the Uncondensed and Condensed Phenolic Moieties in Lignins. *Journal of Agricultural and Food Chemistry* **1995**, *43* (6), 1538-1544. DOI: https://doi.org/10.1021/jf00054a023.

(16) Rinaldi, R.; Jastrzebski, R.; Clough, M. T.; Ralph, J.; Kennema, M.; Bruijnincx, P. C. A.; Weckhuysen, B. M. Paving the Way for Lignin Valorisation: Recent Advances in Bioengineering, Biorefining and Catalysis. *Angewandte Chemie International Edition* **2016**, *55* (29), 8164-8215. DOI: https://doi.org/10.1002/anie.201510351.

(17) Wang, H.; Pu, Y.; Ragauskas, A.; Yang, B. From lignin to valuable products–strategies, challenges, and prospects. *Bioresource Technology* **2019**, *271*, 449-461. DOI: https://doi.org/10.1016/j.biortech.2018.09.072.

(18) Sun, Z.; Fridrich, B.; de Santi, A.; Elangovan, S.; Barta, K. Bright Side of Lignin Depolymerization: Toward New Platform Chemicals. *Chemical Reviews* **2018**, *118* (2), 614-678. DOI: https://doi.org/10.1021/acs.chemrev.7b00588.

(19) Xu, J.; Li, C.; Dai, L.; Xu, C.; Zhong, Y.; Yu, F.; Si, C. Biomass Fractionation and Lignin Fractionation towards Lignin Valorization. *ChemSusChem* **2020**, *13* (17), 4284-4295. DOI: https://doi.org/10.1002/cssc.202001491.

(20) Duval, A.; Lawoko, M. A review on lignin-based polymeric, micro- and nano-structured materials. *Reactive and Functional Polymers* **2014**, *85*, 78-96. DOI: https://doi.org/10.1016/j.reactfunctpolym.2014.09.017.

(21) Pandey, M. P.; Kim, C. S. Lignin Depolymerization and Conversion: A Review of Thermochemical Methods. *Chemical Engineering & Technology* **2011**, *34* (1), 29-41. DOI: https://doi.org/10.1002/ceat.201000270.

(22) Sun, Y.; Cheng, J. Hydrolysis of lignocellulosic materials for ethanol production: a review. *Bioresource Technology* **2002**, *83* (1), 1-11. DOI: https://doi.org/10.1016/S0960-8524(01)00212-7.

(23) Zakzeski, J.; Bruijnincx, P. C. A.; Jongerius, A. L.; Weckhuysen, B. M. The Catalytic Valorization of Lignin for the Production of Renewable Chemicals. *Chemical Reviews* **2010**, *110* (6), 3552-3599. DOI: https://doi.org/10.1021/cr900354u.

(24) Baruah, J.; Nath, B. K.; Sharma, R.; Kumar, S.; Deka, R. C.; Baruah, D. C.; Kalita, E. Recent Trends in the Pretreatment of Lignocellulosic Biomass for Value-Added Products. *Frontiers in Energy Research* **2018**, *6*, Review. DOI: https://doi.org/10.3389/fenrg.2018.00141.

(25) Zevallos Torres, L. A.; Lorenci Woiciechowski, A.; de Andrade Tanobe, V. O.; Karp, S. G.; Guimarães Lorenci, L. C.; Faulds, C.; Soccol, C. R. Lignin as a potential source of high-added value compounds: A review. *Journal of Cleaner Production* **2020**, *263*, 121499. DOI: https://doi.org/10.1016/j.jclepro.2020.121499.

(26) Bajwa, D. S.; Pourhashem, G.; Ullah, A. H.; Bajwa, S. G. A concise review of current lignin production, applications, products and their environmental impact. *Industrial Crops and Products* **2019**, *139*, 111526. DOI: https://doi.org/10.1016/j.indcrop.2019.111526.

(27) Jędrzejczak, P.; Collins, M. N.; Jesionowski, T.; Klapiszewski, Ł. The role of lignin and lignin-based materials in sustainable construction – A comprehensive review. *International Journal of Biological Macromolecules* **2021**, *187*, 624-650. DOI: https://doi.org/10.1016/j.ijbiomac.2021.07.125.

(28) Margarida Martins, M.; Carvalheiro, F.; Gírio, F. An overview of lignin pathways of valorization: from isolation to refining and conversion into value-added products. *Biomass Conversion and Biorefinery* **2022**. DOI: https://doi.org/10.1007/s13399-022-02701-z.

(29) Van Nieuwenhove, I.; Renders, T.; Lauwaert, J.; De Roo, T.; De Clercq, J.; Verberckmoes, A. Biobased Resins Using Lignin and Glyoxal. *ACS Sustainable Chemistry & Engineering* **2020**, *8* (51), 18789-18809. DOI: https://doi.org/10.1021/acssuschemeng.0c07227.

(30) Tardy, B. L.; Lizundia, E.; Guizani, C.; Hakkarainen, M.; Sipponen, M. H. Prospects for the integration of lignin materials into the circular economy. *Materials Today* **2023**. DOI: https://doi.org/10.1016/j.mattod.2023.04.001.

(31) Ridho, M. R.; Agustiany, E. A.; Rahmi Dn, M.; Madyaratri, E. W.; Ghozali, M.; Restu, W. K.; Falah, F.; Rahandi Lubis, M. A.; Syamani, F. A.; Nurhamiyah, Y.; et al. Lignin as Green Filler in Polymer Composites: Development Methods, Characteristics, and Potential Applications. *Advances in Materials Science and Engineering* **2022**, *2022*, 1363481. DOI: https://doi.org/10.1155/2022/1363481.

(32) Tribot, A.; Amer, G.; Abdou Alio, M.; de Baynast, H.; Delattre, C.; Pons, A.; Mathias, J.-D.; Callois, J.-M.; Vial, C.; Michaud, P.; et al. Wood-lignin: Supply, extraction processes and use as bio-based material. *European Polymer Journal* **2019**, *112*, 228-240. DOI: https://doi.org/10.1016/j.eurpolymj.2019.01.007.

(33) Dessbesell, L.; Paleologou, M.; Leitch, M.; Pulkki, R.; Xu, C. Global lignin supply overview and kraft lignin potential as an alternative for petroleum-based polymers. *Renewable and Sustainable Energy Reviews* **2020**, *123*, 109768. DOI: https://doi.org/10.1016/j.rser.2020.109768.

(34) Axelsson, E.; Olsson, M. R.; Berntsson, T. Increased capacity in kraft pulp mills: Lignin separation and reduced steam demand compared with recovery boiler upgrade. *Nordic Pulp & Paper Research Journal* **2006**, *21* (4), 485-492. DOI: https://doi.org/10.3183/npprj-2006-21-04-p485-492.

(35) Di Francesco, D.; Dahlstrand, C.; Löfstedt, J.; Orebom, A.; Verendel, J.; Carrick, C.; Håkansson, Å.; Eriksson, S.; Rådberg, H.; Wallmo, H.; et al. Debottlenecking a Pulp Mill by Producing Biofuels from Black Liquor in Three Steps. *ChemSusChem* **2021**, *14* (11), 2414-2425. DOI: https://doi.org/10.1002/cssc.202100496.

(36) Kouisni, L.; Gagné, A.; Maki, K.; Holt-Hindle, P.; Paleologou, M. LignoForce System for the Recovery of Lignin from Black Liquor: Feedstock Options, Odor Profile, and Product Characterization. *ACS Sustainable Chemistry & Engineering* **2016**, *4* (10), 5152-5159. DOI: https://doi.org/10.1021/acssuschemeng.6b00907.

(37) Tomani, P. The lignoboost process. *Cellulose Chemistry and Technology* **2010**, *44*.

(38) Lora, J. Chapter 10 - Industrial Commercial Lignins: Sources, Properties and Applications. In *Monomers, Polymers and Composites from Renewable Resources*, Belgacem, M. N., Gandini, A. Eds.; Elsevier, 2008; pp 225-241.

(39) Strassberger, Z.; Tanase, S.; Rothenberg, G. The pros and cons of lignin valorisation in an integrated biorefinery. *RSC Advances* **2014**, *4* (48), 25310-25318. DOI: http://dx.doi.org/10.1039/C4RA04747H.

(40) Vishtal, A.; Kraslawski, A. Challenges in industrial applications of technical lignins. *BioResources* **2011**, *6*, 3547-3568. DOI: https://dx.doi.org/10.15376/biores.6.3.3547-3568.

(41) CHRISTOPHER, L. P. Integrated Forest Biorefineries: Current State and Development Potential. In *Integrated Forest Biorefineries*, Christopher, L. Ed.; The Royal Society of Chemistry, 2012; p 0.

(42) Ferreira, J. A.; Taherzadeh, M. J. Improving the economy of lignocellulose-based biorefineries with organosolv pretreatment. *Bioresource Technology* **2020**, *299*, 122695. DOI: https://doi.org/10.1016/j.biortech.2019.122695.

(43) Doherty, W. O. S.; Mousavioun, P.; Fellows, C. M. Value-adding to cellulosic ethanol: Lignin polymers. *Industrial Crops and Products* **2011**, *33* (2), 259-276. DOI: https://doi.org/10.1016/j.indcrop.2010.10.022.

(44) Suota, M.; Kochepka, D.; Moura, M.; Pirih, C.; Matos, M.; Magalhães, W.; Pereira Ramos, L. Lignin Functionalization Strategies and the Potential Applications of Its Derivatives - A Review. *BioResources* **2021**, *16*, 6471-6511. DOI: https://dx.doi.org/10.15376/biores.16.3.Suota.

(45) Wang, Y.-Y.; Meng, X.; Pu, Y.; J. Ragauskas, A. Recent Advances in the Application of Functionalized Lignin in Value-Added Polymeric Materials. In *Polymers*, 2020; Vol. 12.

(46) Pye, E. K. The Alcell process: a proven alternative to kraft pulping. In *Pulping Conference:[proceedings](USA)*, 1990.

(47) Lindner, A.; Wegener, G. Characterization of lignins from organosolv pulping according to the organocell process PART 1. Elemental analysis, nonlignin portions and functional groups. *Journal of Wood Chemistry and Technology* **1988**, *8* (3), 323-340. DOI: https://doi.org/10.1080/02773818808070688.

(48) Wei Kit Chin, D.; Lim, S.; Pang, Y. L.; Lam, M. K. Fundamental review of organosolv pretreatment and its challenges in emerging consolidated bioprocessing. *Biofuels, Bioproducts and Biorefining* **2020**, *14* (4), 808-829. DOI: https://doi.org/10.1002/bbb.2096.

(49) Nitsos, C.; Rova, U.; Christakopoulos, P. Organosolv Fractionation of Softwood Biomass for Biofuel and Biorefinery Applications. In *Energies*, 2018; Vol. 11.

(50) Smolarski, N. High-value opportunities for lignin: unlocking its potential. *Frost & Sullivan* **2012**, *1*, 1-15.

(51) Huang, C.; Jiang, X.; Shen, X.; Hu, J.; Tang, W.; Wu, X.; Ragauskas, A.; Jameel, H.; Meng, X.; Yong, Q. Lignin-enzyme interaction: A roadblock for efficient enzymatic hydrolysis of lignocellulosics. *Renewable and Sustainable Energy Reviews* **2022**, *154*, 111822. DOI: https://doi.org/10.1016/j.rser.2021.111822.

(52) Hamelinck, C. N.; Hooijdonk, G. v.; Faaij, A. P. C. Ethanol from lignocellulosic biomass: techno-economic performance in short-, middle- and long-term. *Biomass and Bioenergy* **2005**, *28* (4), 384-410. DOI: https://doi.org/10.1016/j.biombioe.2004.09.002.

(53) Nakagame, S.; Chandra, R. P.; Kadla, J. F.; Saddler, J. N. The isolation, characterization and effect of lignin isolated from steam pretreated Douglas-fir on the enzymatic hydrolysis of cellulose. *Bioresource Technology* **2011**, *102* (6), 4507-4517. DOI: https://doi.org/10.1016/j.biortech.2010.12.082.

(54) Yuan, Y.; Jiang, B.; Chen, H.; Wu, W.; Wu, S.; Jin, Y.; Xiao, H. Recent advances in understanding the effects of lignin structural characteristics on enzymatic hydrolysis. *Biotechnology for Biofuels* **2021**, *14* (1), 205. DOI: https://doi.org/10.1186/s13068-021-02054-1.

(55) Wang, H.; Tucker, M.; Ji, Y. Recent Development in Chemical Depolymerization of Lignin: A Review. *Journal of Applied Chemistry* **2013**, *2013*, 838645. DOI: https://doi.org/10.1155/2013/838645.

(56) Schutyser, W.; Renders, T.; Van den Bosch, S.; Koelewijn, S. F.; Beckham, G. T.; Sels, B. F. Chemicals from lignin: an interplay of lignocellulose fractionation, depolymerisation, and upgrading. *Chemical Society Reviews* **2018**, *47* (3), 852-908. DOI: http://dx.doi.org/10.1039/C7CS00566K.

(57) Chio, C.; Sain, M.; Qin, W. Lignin utilization: A review of lignin depolymerization from various aspects. *Renewable and Sustainable Energy Reviews* **2019**, *107*, 232-249. DOI: https://doi.org/10.1016/j.rser.2019.03.008.

(58) Xu, C.; Ferdosian, F. Degradation of Lignin by Depolymerization. In *Conversion of Lignin into Bio-Based Chemicals and Materials*, Xu, C., Ferdosian, F. Eds.; Springer Berlin Heidelberg, 2017; pp 35-54.

(59) Ma, X.; Chen, J.; Zhu, J.; Yan, N. Lignin-Based Polyurethane: Recent Advances and Future Perspectives. *Macromolecular Rapid Communications* **2021**, *42* (3), 2000492. DOI: https://doi.org/10.1002/marc.202000492.

(60) Lawoko, M.; Samec, J. S. M. Kraft lignin valorization: Biofuels and thermoset materials in focus. *Current Opinion in Green and Sustainable Chemistry* **2023**, *40*, 100738. DOI: https://doi.org/10.1016/j.cogsc.2022.100738.

(61) Cao, Y.; Chen, S. S.; Zhang, S.; Ok, Y. S.; Matsagar, B. M.; Wu, K. C. W.; Tsang, D. C. W. Advances in lignin valorization towards bio-based chemicals and fuels: Lignin biorefinery. *Bioresource Technology* **2019**, *291*, 121878. DOI: https://doi.org/10.1016/j.biortech.2019.121878.

(62) Mahmood, N.; Yuan, Z.; Schmidt, J.; Xu, C. Hydrolytic depolymerization of hydrolysis lignin: Effects of catalysts and solvents. *Bioresource Technology* **2015**, *190*, 416-419. DOI: https://doi.org/10.1016/j.biortech.2015.04.074.

(63) Posmanik, R.; Martinez, C. M.; Cantero-Tubilla, B.; Cantero, D. A.; Sills, D. L.; Cocero, M. J.; Tester, J. W. Acid and Alkali Catalyzed Hydrothermal Liquefaction of Dairy Manure Digestate and Food Waste. *ACS Sustainable Chemistry & Engineering* **2018**, *6* (2), 2724-2732. DOI: https://doi.org/10.1021/acssuschemeng.7b04359.

(64) Yuan, Z.; Cheng, S.; Leitch, M.; Xu, C. Hydrolytic degradation of alkaline lignin in hot-compressed water and ethanol. *Bioresource Technology* **2010**, *101* (23), 9308-9313. DOI: https://doi.org/10.1016/j.biortech.2010.06.140.

(65) Pappa, C.; Feghali, E.; Vanbroekhoven, K.; Triantafyllidis, K. S. Recent advances in epoxy resins and composites derived from lignin and related bio-oils. *Current Opinion in Green and Sustainable Chemistry* **2022**, *38*, 100687. DOI: https://doi.org/10.1016/j.cogsc.2022.100687.

(66) Cheng, C.; Shen, D.; Gu, S.; Luo, K. H. State-of-the-art catalytic hydrogenolysis of lignin for the production of aromatic chemicals. *Catalysis Science & Technology* **2018**, *8* (24), 6275-6296. DOI: http://dx.doi.org/10.1039/C8CY00845K.

(67) Huang, S.; Mahmood, N.; Tymchyshyn, M.; Yuan, Z.; Xu, C. Reductive de-polymerization of kraft lignin for chemicals and fuels using formic acid as an in-situ hydrogen source. *Bioresource Technology* **2014**, *171*, 95-102. DOI: https://doi.org/10.1016/j.biortech.2014.08.045.

(68) Galkin, M. V.; Samec, J. S. M. Lignin Valorization through Catalytic Lignocellulose Fractionation: A Fundamental Platform for the Future Biorefinery. *ChemSusChem* **2016**, *9* (13), 1544-1558. DOI: https://doi.org/10.1002/cssc.201600237.

(69) Gigli, M.; Crestini, C. Fractionation of industrial lignins: opportunities and challenges. *Green Chemistry* **2020**, *22* (15), 4722-4746. DOI: http://dx.doi.org/10.1039/D0GC01606C.

(70) Sadeghifar, H.; Ragauskas, A. Perspective on Technical Lignin Fractionation. *ACS Sustainable Chemistry & Engineering* **2020**, *8* (22), 8086-8101. DOI: https://doi.org/10.1021/acssuschemeng.0c01348.

(71) Pang, T.; Wang, G.; Sun, H.; Sui, W.; Si, C. Lignin fractionation: Effective strategy to reduce molecule weight dependent heterogeneity for upgraded lignin valorization. *Industrial Crops and Products* **2021**, *165*, 113442. DOI: https://doi.org/10.1016/j.indcrop.2021.113442.

(72) Duval, A.; Vilaplana, F.; Crestini, C.; Lawoko, M. Solvent screening for the fractionation of industrial kraft lignin. *Holzforschung* **2016**, *70* (1), 11-20. DOI: https://doi.org/10.1515/hf-2014-0346.

(73) Passoni, V.; Scarica, C.; Levi, M.; Turri, S.; Griffini, G. Fractionation of Industrial Softwood Kraft Lignin: Solvent Selection as a Tool for Tailored Material Properties. *ACS Sustainable Chemistry & Engineering* **2016**, *4* (4), 2232-2242. DOI: https://doi.org/10.1021/acssuschemeng.5b01722.

(74) Domínguez-Robles, J.; Tamminen, T.; Liitiä, T.; Peresin, M. S.; Rodríguez, A.; Jääskeläinen, A.-S. Aqueous acetone fractionation of kraft, organosolv and soda lignins. *International Journal of Biological Macromolecules* **2018**, *106*, 979-987. DOI: https://doi.org/10.1016/j.ijbiomac.2017.08.102.

(75) Cui, C.; Sun, R.; Argyropoulos, D. S. Fractional Precipitation of Softwood Kraft Lignin: Isolation of Narrow Fractions Common to a Variety of Lignins. *ACS Sustainable Chemistry & Engineering* **2014**, *2* (4), 959-968. DOI: https://doi.org/10.1021/sc400545d.

(76) Wang, Y.-Y.; Li, M.; Wyman, C. E.; Cai, C. M.; Ragauskas, A. J. Fast Fractionation of Technical Lignins by Organic Cosolvents. *ACS Sustainable Chemistry & Engineering* **2018**, *6* (5), 6064-6072. DOI: https://doi.org/10.1021/acssuschemeng.7b04546.

(77) Santos, P. S. B. d.; Erdocia, X.; Gatto, D. A.; Labidi, J. Characterisation of Kraft lignin separated by gradient acid precipitation. *Industrial Crops and Products* **2014**, *55*, 149-154. DOI: https://doi.org/10.1016/j.indcrop.2014.01.023.

(78) Lourençon, T. V.; Hansel, F. A.; da Silva, T. A.; Ramos, L. P.; de Muniz, G. I. B.; Magalhães, W. L. E. Hardwood and softwood kraft lignins fractionation by simple sequential acid precipitation. *Separation and Purification Technology* **2015**, *154*, 82-88. DOI: https://doi.org/10.1016/j.seppur.2015.09.015.

(79) Chen, W.-J.; Zhao, B.-C.; Cao, X.-F.; Yuan, T.-Q.; Shi, Q.; Wang, S.-F.; Sun, R.-C. Structural Features of Alkaline Dioxane Lignin and Residual Lignin from Eucalyptus grandis × E. urophylla. *Journal of Agricultural and Food Chemistry* **2019**, *67* (3), 968-974. DOI: https://doi.org/10.1021/acs.jafc.8b05760.

(80) Alekhina, M.; Ershova, O.; Ebert, A.; Heikkinen, S.; Sixta, H. Softwood kraft lignin for value-added applications: Fractionation and structural characterization. *Industrial Crops and Products* **2015**, *66*, 220-228. DOI: https://doi.org/10.1016/j.indcrop.2014.12.021.

(81) https://www.grandviewresearch.com/. (accessed 2023 03/04).

(82) Sonnenschein, M. *Polyurethanes: Science, Technology, Markets, and Trends*; 2014. DOI: https://doi.org/10.1002/9781118901274.

(83) Yilgör, I.; Yilgör, E.; Wilkes, G. L. Critical parameters in designing segmented polyurethanes and their effect on morphology and properties: A comprehensive review. *Polymer* **2015**, *58*, A1-A36. DOI: https://doi.org/10.1016/j.polymer.2014.12.014.

(84) Glasser, W. G.; Hsu, O. H. H.; Reed, D. L.; Forte, R. C.; Wu, L. C. F. Lignin-Derived polyols, Polyisocyanates, and Polyurethanes. In *Urethane Chemistry and Applications*, ACS Symposium Series, Vol. 172; AMERICAN CHEMICAL SOCIETY, 1981; pp 311-338.

(85) Hsu, O. H. H.; Glasser, W. G. Polyurethane foams from carboxylated lignins. *Applied polymer symposia* **1975**, (28), 297-307.

(86) Hsu, O. H. H. Polyurethane adhesives and coatings from modified lignin. *Wood science* **1976**, 97-103.

(87) Silva, E. A. B. d.; Zabkova, M.; Araújo, J. D.; Cateto, C. A.; Barreiro, M. F.; Belgacem, M. N.; Rodrigues, A. E. An integrated process to produce vanillin and lignin-based polyurethanes from Kraft lignin. *Chemical Engineering Research and Design* **2009**, *87* (9), 1276-1292. DOI: https://doi.org/10.1016/j.cherd.2009.05.008.

(88) Mahmood, N.; Yuan, Z.; Schmidt, J.; Xu, C. Depolymerization of lignins and their applications for the preparation of polyols and rigid polyurethane foams: A review. *Renewable and Sustainable Energy Reviews* **2016**, *60*, 317-329. DOI: https://doi.org/10.1016/j.rser.2016.01.037.

(89) Alinejad, M.; Henry, C.; Nikafshar, S.; Gondaliya, A.; Bagheri, S.; Chen, N.; Singh, S. K.; Hodge, D. B.; Nejad, M. Lignin-Based Polyurethanes: Opportunities for Bio-Based Foams, Elastomers, Coatings and Adhesives. *Polymers* **2019**, *11* (7), 1202. DOI: https://doi.org/10.3390/polym11071202.

(90) Li, H.; Liang, Y.; Li, P.; He, C. Conversion of biomass lignin to high-value polyurethane: A review. *Journal of Bioresources and Bioproducts* **2020**, *5* (3), 163-179. DOI: https://doi.org/10.1016/j.jobab.2020.07.002.

(91) Santos, O. S. H.; Coelho da Silva, M.; Silva, V. R.; Mussel, W. N.; Yoshida, M. I. Polyurethane foam impregnated with lignin as a filler for the removal of crude oil from contaminated water. *Journal of Hazardous Materials* **2017**, *324*, 406-413. DOI: https://doi.org/10.1016/j.jhazmat.2016.11.004.

(92) Feldman, D.; Lacasse, M. A. Polymer–filler interaction in polyurethane kraft lignin polyblends. *Journal of Applied Polymer Science* **1994**, *51* (4), 701-709. DOI: https://doi.org/10.1002/app.1994.070510416.

(93) Saraf, V. P.; Glasser, W. G. Engineering plastics from lignin. III. Structure property relationships in solution cast polyurethane films. *Journal of Applied Polymer Science* **1984**, *29* (5), 1831-1841. DOI: https://doi.org/10.1002/app.1984.070290534.

(94) Pan, X.; Saddler, J. N. Effect of replacing polyol by organosolv and kraft lignin on the property and structure of rigid polyurethane foam. *Biotechnology for Biofuels* **2013**, *6* (1), 12. DOI: https://doi.org/10.1186/1754-6834-6-12.

(95) Luo, S.; Gao, L.; Guo, W. Effect of incorporation of lignin as bio-polyol on the performance of rigid lightweight wood–polyurethane composite foams. *Journal of Wood Science* **2020**, *66* (1), 23. DOI: https://doi.org/10.1186/s10086-020-01872-5.

(96) Xue, B.-L.; Wen, J.-L.; Sun, R.-C. Lignin-Based Rigid Polyurethane Foam Reinforced with Pulp Fiber: Synthesis and Characterization. *ACS Sustainable Chemistry & Engineering* **2014**, *2* (6), 1474-1480. DOI: https://doi.org/10.1021/sc5001226.

(97) Tanaka, R.; Hirose, S.; Hatakeyama, H. Preparation and characterization of polyurethane foams using a palm oil-based polyol. *Bioresource Technology* **2008**, *99* (9), 3810-3816. DOI: https://doi.org/10.1016/j.biortech.2007.07.007.

(98) Luo, X.; Mohanty, A.; Misra, M. Lignin as a reactive reinforcing filler for water-blown rigid biofoam composites from soy oil-based polyurethane. *Industrial Crops and Products* **2013**, *47*, 13-19. DOI: https://doi.org/10.1016/j.indcrop.2013.01.040.

(99) Hayati, A. N.; Evans, D. A. C.; Laycock, B.; Martin, D. J.; Annamalai, P. K. A simple methodology for improving the performance and sustainability of rigid polyurethane foam by incorporating industrial lignin. *Industrial Crops and Products* **2018**, *117*, 149-158. DOI: https://doi.org/10.1016/j.indcrop.2018.03.006.

(100) Fang, Z.; Qiu, C.; Ji, D.; Yang, Z.; Zhu, N.; Meng, J.; Hu, X.; Guo, K. Development of High-Performance Biodegradable Rigid Polyurethane Foams Using Full Modified Soy-Based Polyols. *Journal of Agricultural and Food Chemistry* **2019**, *67* (8), 2220-2226. DOI: https://doi.org/10.1021/acs.jafc.8b05342.

(101) Haridevan, H.; McLaggan, M. S.; Evans, D. A. C.; Martin, D. J.; Seaby, T.; Zhang, Z.; Annamalai, P. K. Dispersion Methodology for Technical Lignin into Polyester Polyol for High-Performance Polyurethane Insulation Foam. *ACS Applied Polymer Materials* **2021**, *3* (7), 3528-3537. DOI: https://doi.org/10.1021/acsapm.1c00430.

(102) Xue, B.; Yang, Y.; Tang, R.; Xue, D.; Sun, Y.; Li, X. Efficient dissolution of lignin in novel ternary deep eutectic solvents and its application in polyurethane. *International Journal of Biological Macromolecules* **2020**, *164*, 480-488. DOI: https://doi.org/10.1016/j.ijbiomac.2020.07.153.

(103) Gondaliya, A.; Nejad, M. Lignin as a Partial Polyol Replacement in Polyurethane Flexible Foam. *Molecules* **2021**, *26* (8), 2302. DOI: https://doi.org/10.3390/molecules26082302.

(104) Vanderlaan, M. N.; Thring, R. W. Polyurethanes from Alcell® lignin fractions obtained by sequential solvent extraction. *Biomass and Bioenergy* **1998**, *14* (5), 525-531. DOI: https://doi.org/10.1016/S0961-9534(97)10058-7.

(105) Wadekar, M.; Eevers, W.; Vendamme, R. Influencing the properties of LigninPU films by changing copolyol chain length, lignin content and NCO/OH mol ratio. *Industrial Crops and Products* **2019**, *141*, 111655. DOI: https://doi.org/10.1016/j.indcrop.2019.111655.

(106) Tavares, L.; Stilhano Vilas Boas, C.; Ravanhani Schleder, G.; Nacas, A.; Rosa, D.; Santos, D. Bio-based polyurethane prepared from Kraft lignin and modified castor oil. *eXPRESS Polymer Letters* **2016**, *10*, 927-940. DOI: https://doi.org/10.3144/expresspolymlett.2016.86.

(107) Cassales, A.; Ramos, L. A.; Frollini, E. Synthesis of bio-based polyurethanes from Kraft lignin and castor oil with simultaneous film formation. *International Journal of Biological Macromolecules* **2020**, *145*, 28-41. DOI: https://doi.org/10.1016/j.ijbiomac.2019.12.173.

(108) Avelino, F.; Almeida, S.; Duarte, E.; Sousa, J.; Mazzetto, S.; Filho, M. Thermal and mechanical properties of coconut shell lignin-based polyurethanes synthesized by solvent-free polymerization. *Journal of Materials Science* **2018**, *53*. DOI: https://doi.org/10.1007/s10853-017-1562-z.

(109) Chen, X.; Li, Z.; Zhang, L.; Wang, H.; Qiu, C.; Fan, X.; Sun, S. Preparation of a novel lignin-based film with high solid content and its physicochemical characteristics. *Industrial Crops and Products* **2021**, *164*, 113396. DOI: https://doi.org/10.1016/j.indcrop.2021.113396.

(110) Bonini, C.; D'Auria, M.; Emanuele, L.; Ferri, R.; Pucciariello, R.; Sabia, A. R. Polyurethanes and polyesters from lignin. *Journal of Applied Polymer Science* **2005**, *98* (3), 1451-1456. DOI: https://doi.org/10.1002/app.22277.

(111) Lang, J. M.; Shrestha, U. M.; Dadmun, M. The Effect of Plant Source on the Properties of Lignin-Based Polyurethanes. *Frontiers in Energy Research* **2018**, *6*, Original Research. DOI: https://doi.org/10.3389/fenrg.2018.00004.

(112) Henry, C.; Gondaliya, A.; Thies, M.; Nejad, M. Studying the Suitability of Nineteen Lignins as Partial Polyol Replacement in Rigid Polyurethane/Polyisocyanurate Foam. *Molecules* **2022**, *27* (8), 2535. DOI: https://doi.org/10.3390/molecules27082535.

(113) Mahmood, N.; Yuan, Z.; Schmidt, J.; Xu, C. Preparation of bio-based rigid polyurethane foam using hydrolytically depolymerized Kraft lignin via direct replacement or oxypropylation. *European Polymer Journal* **2015**, *68*, 1-9. DOI: https://doi.org/10.1016/j.eurpolymj.2015.04.030.

(114) Xue, B.-L.; Huang, P.-L.; Sun, Y.-C.; Li, X.-P.; Sun, R.-C. Hydrolytic depolymerization of corncob lignin in the view of a bio-based rigid polyurethane foam synthesis. *RSC Advances* **2017**, *7* (10), 6123-6130. DOI: http://dx.doi.org/10.1039/C6RA26318F.

(115) Mahmood, N.; Yuan, Z.; Schmidt, J.; Tymchyshyn, M.; Xu, C. Hydrolytic liquefaction of hydrolysis lignin for the preparation of bio-based rigid polyurethane foam. *Green Chemistry* **2016**, *18* (8), 2385-2398. DOI: http://dx.doi.org/10.1039/C5GC02876K.

(116) Li, H.; Sun, J.-T.; Wang, C.; Liu, S.; Yuan, D.; Zhou, X.; Tan, J.; Stubbs, L.; He, C. High Modulus, Strength, and Toughness Polyurethane Elastomer Based on Unmodified Lignin. *ACS Sustainable Chemistry & Engineering* **2017**, *5* (9), 7942-7949. DOI: https://doi.org/10.1021/acssuschemeng.7b01481.

(117) Hu, S.; Luo, X.; Li, Y. Polyols and Polyurethanes from the Liquefaction of Lignocellulosic Biomass. *ChemSusChem* **2014**, *7* (1), 66-72. DOI: https://doi.org/10.1002/cssc.201300760.

(118) Lu, W.; Li, Q.; Zhang, Y.; Yu, H.; Hirose, S.; Hatakeyama, H.; Matsumoto, Y.; Jin, Z. Lignosulfonate/APP IFR and its flame retardancy in lignosulfonate-based rigid polyurethane foams. *Journal of Wood Science* **2018**, *64* (3), 287-293. DOI: https://doi.org/10.1007/s10086-018-1701-4.

(119) Hu, S.; Li, Y. Two-step sequential liquefaction of lignocellulosic biomass by crude glycerol for the production of polyols and polyurethane foams. *Bioresource Technology* **2014**, *161*, 410-415. DOI: https://doi.org/10.1016/j.biortech.2014.03.072.

(120) Huang, J.; Wang, H.; Liu, W.; Huang, J.; Yang, D.; Qiu, X.; Zhao, L.; Hu, F.; Feng, Y. Solvent-free synthesis of high-performance polyurethane elastomer based on low-molecular-weight alkali lignin. *International Journal of Biological Macromolecules* **2023**, *225*, 1505-1516. DOI: https://doi.org/10.1016/j.ijbiomac.2022.11.207.

(121) Xue, B.-L.; Wen, J.-L.; Sun, R.-C. Producing Lignin-Based Polyols through Microwave-Assisted Liquefaction for Rigid Polyurethane Foam Production. *Materials* **2015**, *8* (2), 586-599. DOI: https://doi.org/10.3390/ma8020586.

(122) Cinelli, P.; Anguillesi, I.; Lazzeri, A. Green synthesis of flexible polyurethane foams from liquefied lignin. *European Polymer Journal* **2013**, *49* (6), 1174-1184. DOI: https://doi.org/10.1016/j.eurpolymj.2013.04.005.

(123) Bernardini, J.; Cinelli, P.; Anguillesi, I.; Coltelli, M.-B.; Lazzeri, A. Flexible polyurethane foams green production employing lignin or oxypropylated lignin. *European Polymer Journal* **2015**, *64*, 147-156. DOI: https://doi.org/10.1016/j.eurpolymj.2014.11.039.

(124) Zhu, H.; Peng, Z.; Chen, Y.; Li, G.; Wang, L.; Tang, Y.; Pang, R.; Khan, Z. U. H.; Wan, P. Preparation and characterization of flame retardant polyurethane foams containing phosphorus–nitrogen-functionalized lignin. *RSC Advances* **2014**, *4* (98), 55271-55279. DOI: http://dx.doi.org/10.1039/C4RA08429B.

(125) Oribayo, O.; Feng, X.; Rempel, G. L.; Pan, Q. Synthesis of lignin-based polyurethane/graphene oxide foam and its application as an absorbent for oil spill clean-ups and recovery. *Chemical Engineering Journal* **2017**, *323*, 191-202. DOI: https://doi.org/10.1016/j.cej.2017.04.054.

(126) Mohammadpour, R.; Mir Mohamad Sadeghi, G. Effect of Liquefied Lignin Content on Synthesis of Bio-based Polyurethane Foam for Oil Adsorption Application. *Journal of Polymers and the Environment* **2020**, *28* (3), 892-905. DOI: https://doi.org/10.1007/s10924-019-01650-5.

(127) Ma, X.; Zhang, C.; Gnanasekar, P.; Xiao, P.; Luo, Q.; Li, S.; Qin, D.; Chen, T.; Chen, J.; Zhu, J.; et al. Mechanically robust, solar-driven, and degradable lignin-based polyurethane adsorbent for efficient crude oil spill remediation. *Chemical Engineering Journal* **2021**, *415*, 128956. DOI: https://doi.org/10.1016/j.cej.2021.128956.

(128) Huang, Y.; Duan, Y.; Qiu, S.; Wang, M.; Ju, C.; Cao, H.; Fang, Y.; Tan, T. Lignin-first biorefinery: a reusable catalyst for lignin depolymerization and application of lignin oil to jet fuel aromatics and polyurethane feedstock. *Sustainable Energy & Fuels* **2018**, *2* (3), 637-647. DOI: http://dx.doi.org/10.1039/C7SE00535K.

(129) Rubens, M.; Wesemael, M. V.; Feghali, E.; Lufungula, L. L.; Blockhuys, F.; Vanbroekhoven, K.; Eevers, W.; Vendamme, R. Exploring the reactivity of aliphatic and phenolic hydroxyl groups in lignin hydrogenolysis oil towards urethane bond formation. *Industrial Crops and Products* **2022**, *180*, 114703. DOI: https://doi.org/10.1016/j.indcrop.2022.114703.

(130) de Haro, J. C.; Allegretti, C.; Smit, A. T.; Turri, S.; D'Arrigo, P.; Griffini, G. Biobased Polyurethane Coatings with High Biomass Content: Tailored Properties by Lignin Selection. *ACS Sustainable Chemistry & Engineering* **2019**, *7* (13), 11700-11711. DOI: https://doi.org/10.1021/acssuschemeng.9b01873.

(131) Arefmanesh, M.; Nikafshar, S.; Master, E. R.; Nejad, M. From acetone fractionation to lignin-based phenolic and polyurethane resins. *Industrial Crops and Products* **2022**, *178*, 114604. DOI: https://doi.org/10.1016/j.indcrop.2022.114604.

(132) Handika, S. O.; Lubis, M. A.; Sari, R. K.; Laksana, R. P.; Antov, P.; Savov, V.; Gajtanska, M.; Iswanto, A. H. Enhancing Thermal and Mechanical Properties of Ramie Fiber via Impregnation by Lignin-Based Polyurethane Resin. *Materials* **2021**, *14* (22). DOI: https://doi.org/10.3390/ma14226850.

(133) Guo, W.; Sun, S.; Wang, P.; Chen, H.; Zheng, J.; Lin, X.; Qin, Y.; Qiu, X. Successive organic solvent fractionation and homogenization of technical lignin for polyurethane foam with high mechanical performance. *International Journal of Biological Macromolecules* **2022**, *221*, 913-922. DOI: https://doi.org/10.1016/j.ijbiomac.2022.09.074.

(134) Jia, Z.; Lu, C.; Zhou, P.; Wang, L. Preparation and characterization of high boiling solvent lignin-based polyurethane film with lignin as the only hydroxyl group provider. *RSC Advances* **2015**, *5* (66), 53949-53955. DOI: http://dx.doi.org/10.1039/C5RA09477A.

(135) Arshanitsa, A.; Krumina, L.; Telysheva, G.; Dizhbite, T. Exploring the application potential of incompletely soluble organosolv lignin as a macromonomer for polyurethane synthesis. *Industrial Crops and Products* **2016**, *92*, 1-12. DOI: https://doi.org/10.1016/j.indcrop.2016.07.050.

(136) Quinsaat, J. E. Q.; Feghali, E.; van de Pas, D. J.; Vendamme, R.; Torr, K. M. Preparation of Mechanically Robust Bio-Based Polyurethane Foams Using Depolymerized Native Lignin. *ACS Applied Polymer Materials* **2021**, *3* (11), 5845-5856. DOI: https://doi.org/10.1021/acsapm.1c01081.

(137) Vendamme, R.; Behaghel de Bueren, J.; Gracia-Vitoria, J.; Isnard, F.; Mulunda, M. M.; Ortiz, P.; Wadekar, M.; Vanbroekhoven, K.; Wegmann, C.; Buser, R.; et al. Aldehyde-Assisted Lignocellulose Fractionation Provides Unique Lignin Oligomers for the Design of Tunable Polyurethane Bioresins. *Biomacromolecules* **2020**, *21* (10), 4135-4148. DOI: https://doi.org/10.1021/acs.biomac.0c00927.

(138) Carlos de Haro, J.; Magagnin, L.; Turri, S.; Griffini, G. Lignin-Based Anticorrosion Coatings for the Protection of Aluminum Surfaces. *ACS Sustainable Chemistry & Engineering* **2019**, *7* (6), 6213-6222. DOI: https://doi.org/10.1021/acssuschemeng.8b06568.

(139) Wang, Y.-Y.; Sengupta, P.; Scheidemantle, B.; Pu, Y.; Wyman, C. E.; Cai, C. M.; Ragauskas, A. J. Effects of CELF Pretreatment Severity on Lignin Structure and the Lignin-Based Polyurethane Properties. *Frontiers in Energy Research* **2020**, *8*, Original Research. DOI: https://doi.org/10.3389/fenrg.2020.00149.

(140) Griffini, G.; Passoni, V.; Suriano, R.; Levi, M.; Turri, S. Polyurethane Coatings Based on Chemically Unmodified Fractionated Lignin. *ACS Sustainable Chemistry & Engineering* **2015**, *3* (6), 1145-1154. DOI: https://doi.org/10.1021/acssuschemeng.5b00073.

(141) Wang, Y.-Y.; Wyman, C. E.; Cai, C. M.; Ragauskas, A. J. Lignin-Based Polyurethanes from Unmodified Kraft Lignin Fractionated by Sequential Precipitation. *ACS Applied Polymer Materials* **2019**, *1* (7), 1672-1679. DOI: https://doi.org/10.1021/acsapm.9b00228.

(142) Wang, Y.-Y.; Scheidemantle, B.; Wyman, C. E.; Cai, C. M.; Ragauskas, A. J. Polyurethanes Based on Unmodified and Refined Technical Lignins: Correlation between Molecular Structure and Material Properties. *Biomacromolecules* **2021**, *22* (5), 2129-2136. DOI: https://doi.org/10.1021/acs.biomac.1c00223.

(143) Klein, S. E.; Rumpf, J.; Kusch, P.; Albach, R.; Rehahn, M.; Witzleben, S.; Schulze, M. Unmodified kraft lignin isolated at room temperature from aqueous solution for preparation of highly flexible transparent polyurethane coatings. *RSC Advances* **2018**, *8* (71), 40765-40777. DOI: http://dx.doi.org/10.1039/C8RA08579J.

(144) Cao, H.; Liu, R.; Li, B.; Wu, Y.; Wang, K.; Yang, Y.; Li, A.; Zhuang, Y.; Cai, D.; Qin, P. Biobased rigid polyurethane foam using gradient acid precipitated lignin from the black liquor: Revealing the relationship

between lignin structural features and polyurethane performances. *Industrial Crops and Products* **2022**, *177*, 114480. DOI: https://doi.org/10.1016/j.indcrop.2021.114480.

(145) Zhang, X.; Jeremic, D.; Kim, Y.; Street, J.; Shmulsky, R. Effects of Surface Functionalization of Lignin on Synthesis and Properties of Rigid Bio-Based Polyurethanes Foams. *Polymers* **2018**, *10* (7), 706. DOI: https://doi.org/10.3390/polym10070706.

(146) Zieglowski, M.; Trosien, S.; Rohrer, J.; Mehlhase, S.; Weber, S.; Bartels, K.; Siegert, G.; Trellenkamp, T.; Albe, K.; Biesalski, M. Reactivity of Isocyanate-Functionalized Lignins: A Key Factor for the Preparation of Lignin-Based Polyurethanes. *Frontiers in Chemistry* **2019**, *7*, Original Research. DOI: https://doi.org/10.3389/fchem.2019.00562.

(147) Gómez-Fernández, S.; Ugarte, L.; Calvo-Correas, T.; Peña-Rodríguez, C.; Corcuera, M. A.; Eceiza, A. Properties of flexible polyurethane foams containing isocyanate functionalized kraft lignin. *Industrial Crops and Products* **2017**, *100*, 51-64. DOI: https://doi.org/10.1016/j.indcrop.2017.02.005.

(148) Gómez-Fernández, S.; Günther, M.; Schartel, B.; Corcuera, M. A.; Eceiza, A. Impact of the combined use of layered double hydroxides, lignin and phosphorous polyol on the fire behavior of flexible polyurethane foams. *Industrial Crops and Products* **2018**, *125*, 346-359. DOI: https://doi.org/10.1016/j.indcrop.2018.09.018.

(149) Zhang, Y.; Liao, J.; Fang, X.; Bai, F.; Qiao, K.; Wang, L. Renewable High-Performance Polyurethane Bioplastics Derived from Lignin–Poly(ε-caprolactone). *ACS Sustainable Chemistry & Engineering* **2017**, *5* (5), 4276-4284. DOI: https://doi.org/10.1021/acssuschemeng.7b00288.

(150) Antonino, L. D.; Gouveia, J. R.; de Sousa Júnior, R. R.; Garcia, G. E. S.; Gobbo, L. C.; Tavares, L. B.; dos Santos, D. J. Reactivity of Aliphatic and Phenolic Hydroxyl Groups in Kraft Lignin towards 4,4' MDI. *Molecules* **2021**, *26* (8), 2131. DOI: https://doi.org/10.3390/molecules26082131.

(151) Jeong, H.; Park, J.; Kim, S.; Lee, J.; Ahn, N.; Roh, H.-g. Preparation and characterization of thermoplastic polyurethanes using partially acetylated kraft lignin. *Fibers and Polymers* **2013**, *14* (7), 1082-1093. DOI: https://doi.org/10.1007/s12221-013-1082-7.

(152) Gouveia, J. R.; de Sousa Júnior, R. R.; Ribeiro, A. O.; Saraiva, S. A.; dos Santos, D. J. Effect of soft segment molecular weight and NCO:OH ratio on thermomechanical properties of lignin-based thermoplastic polyurethane adhesive. *European Polymer Journal* **2020**, *131*, 109690. DOI: https://doi.org/10.1016/j.eurpolymj.2020.109690.

(153) Laurichesse, S.; Huillet, C.; Avérous, L. Original polyols based on organosolv lignin and fatty acids: new bio-based building blocks for segmented polyurethane synthesis. *Green Chemistry* **2014**, *16* (8), 3958-3970. DOI: http://dx.doi.org/10.1039/C4GC00596A.

(154) Nadji, H.; Bruzzèse, C.; Belgacem, M. N.; Benaboura, A.; Gandini, A. Oxypropylation of Lignins and Preparation of Rigid Polyurethane Foams from the Ensuing Polyols. *Macromolecular Materials and Engineering* **2005**, *290* (10), 1009-1016. DOI: https://doi.org/10.1002/mame.200500200.

(155) Cateto, C. A.; Barreiro, M. F.; Rodrigues, A. E.; Belgacem, M. N. Optimization Study of Lignin Oxypropylation in View of the Preparation of Polyurethane Rigid Foams. *Industrial & Engineering Chemistry Research* **2009**, *48* (5), 2583-2589. DOI: https://doi.org/10.1021/ie801251r.

(156) Amaral, J. S.; Sepúlveda, M.; Cateto, C. A.; Fernandes, I. P.; Rodrigues, A. E.; Belgacem, M. N.; Barreiro, M. F. Fungal degradation of lignin-based rigid polyurethane foams. *Polymer Degradation and Stability* **2012**, *97* (10), 2069-2076. DOI: https://doi.org/10.1016/j.polymdegradstab.2012.03.037.

(157) Cateto, C. A.; Barreiro, M. F.; Ottati, C.; Lopretti, M.; Rodrigues, A. E.; Belgacem, M. N. Lignin-based rigid polyurethane foams with improved biodegradation. *Journal of Cellular Plastics* **2013**, *50* (1), 81-95. DOI: https://doi.org/10.1177/0021955X13504774.

(158) Oliveira, F. d.; Ramires, E. C.; Frollini, E.; Belgacem, M. N. Lignopolyurethanic materials based on oxypropylated sodium lignosulfonate and castor oil blends. *Industrial Crops and Products* **2015**, *72*, 77-86. DOI: https://doi.org/10.1016/j.indcrop.2015.01.023.

(159) Li, Y.; Ragauskas, A. J. Kraft Lignin-Based Rigid Polyurethane Foam. *Journal of Wood Chemistry and Technology* **2012**, *32* (3), 210-224. DOI: https://doi.org/10.1080/02773813.2011.652795.

(160) Li, Y.; Ragauskas, A. J. Ethanol organosolv lignin-based rigid polyurethane foam reinforced with cellulose nanowhiskers. *RSC Advances* **2012**, *2* (8), 3347-3351. DOI: http://dx.doi.org/10.1039/C2RA00646D.

(161) Li, B.; Zhou, M.; Huo, W.; Cai, D.; Qin, P.; Cao, H.; Tan, T. Fractionation and oxypropylation of corn-stover lignin for the production of biobased rigid polyurethane foam. *Industrial Crops and Products* **2020**, *143*, 111887. DOI: https://doi.org/10.1016/j.indcrop.2019.111887.

(162) Kurańska, M.; Pinto, J. A.; Salach, K.; Barreiro, M. F.; Prociak, A. Synthesis of thermal insulating polyurethane foams from lignin and rapeseed based polyols: A comparative study. *Industrial Crops and Products* **2020**, *143*, 111882. DOI: https://doi.org/10.1016/j.indcrop.2019.111882.

(163) Saffar, T.; Bouafif, H.; Braghiroli, F. L.; Magdouli, S.; Langlois, A.; Koubaa, A. Production of Bio-based Polyol from Oxypropylated Pyrolytic Lignin for Rigid Polyurethane Foam Application. *Waste and Biomass Valorization* **2020**, *11* (11), 6411-6427. DOI: https://doi.org/10.1007/s12649-019-00876-7.

(164) Wu, M.; Peng, J.-J.; Dong, Y.-M.; Pang, J.-H.; Zhang, X.-M. Preparation of rigid polyurethane foam from lignopolyol obtained through mild oxypropylation. *RSC Advances* **2022**, *12* (34), 21736-21741. DOI: http://dx.doi.org/10.1039/D2RA02895F.

(165) Liu, L.-Y.; Karaaslan, M. A.; Hua, Q.; Cho, M.; Chen, S.; Renneckar, S. Thermo-Responsive Shape-Memory Polyurethane Foams from Renewable Lignin Resources with Tunable Structures–Properties and Enhanced Temperature Resistance. *Industrial & Engineering Chemistry Research* **2021**, *60* (32), 11882-11892. DOI: https://doi.org/10.1021/acs.iecr.1c01717.

(166) Wang, S.; Liu, W.; Yang, D.; Qiu, X. Highly Resilient Lignin-Containing Polyurethane Foam. *Industrial & Engineering Chemistry Research* **2019**, *58* (1), 496-504. DOI: https://doi.org/10.1021/acs.iecr.8b05072.

(167) Kühnel, I.; Saake, B.; Lehnen, R. Oxyalkylation of lignin with propylene carbonate: Influence of reaction parameters on the ensuing bio-based polyols. *Industrial Crops and Products* **2017**, *101*, 75-83. DOI: https://doi.org/10.1016/j.indcrop.2017.03.002.

(168) Duval, A.; Avérous, L. Cyclic Carbonates as Safe and Versatile Etherifying Reagents for the Functionalization of Lignins and Tannins. *ACS Sustainable Chemistry & Engineering* **2017**, *5* (8), 7334-7343. DOI: https://doi.org/10.1021/acssuschemeng.7b01502.

(169) Duval, A.; Vidal, D.; Sarbu, A.; René, W.; Avérous, L. Scalable single-step synthesis of lignin-based liquid polyols with ethylene carbonate for polyurethane foams. *Materials Today Chemistry* **2022**, *24*, 100793. DOI: https://doi.org/10.1016/j.mtchem.2022.100793.

(170) Zhang, X.; Kim, Y.; Elsayed, I.; Taylor, M.; Eberhardt, T. L.; Hassan, E. I. B.; Shmulsky, R. Rigid polyurethane foams containing lignin oxyalkylated with ethylene carbonate and polyethylene glycol. *Industrial Crops and Products* **2019**, *141*, 111797. DOI: https://doi.org/10.1016/j.indcrop.2019.111797.

(171) Antonino, L. D.; Garcia, G. E. S.; Gouveia, J. R.; Santos, A. N. B.; da Silva Bisneto, M. P.; dos Santos, D. J. Polyurethane adhesives from castor oil and modified lignin via reaction with propylene carbonate. *Journal of Applied Polymer Science* **2022**, *139* (27), e52477. DOI: https://doi.org/10.1002/app.52477.

(172) Vieira, F. R.; Gama, N. V.; Barros-Timmons, A.; Evtuguin, D. V.; Pinto, P. C. O. R. Development of Rigid Polyurethane Foams Based on Kraft Lignin Polyol Obtained by Oxyalkylation Using Propylene Carbonate. *ChemEngineering* **2022**, *6* (6), 95. DOI: https://doi.org/10.3390/chemengineering6060095.

(173) Delebecq, E.; Pascault, J.-P.; Boutevin, B.; Ganachaud, F. On the Versatility of Urethane/Urea Bonds: Reversibility, Blocked Isocyanate, and Non-isocyanate Polyurethane. *Chemical Reviews* **2013**, *113* (1), 80-118. DOI: https://doi.org/10.1021/cr300195n.

(174) Maisonneuve, L.; Lamarzelle, O.; Rix, E.; Grau, E.; Cramail, H. Isocyanate-Free Routes to Polyurethanes and Poly(hydroxy Urethane)s. *Chemical Reviews* **2015**, *115* (22), 12407-12439. DOI: https://doi.org/10.1021/acs.chemrev.5b00355.

(175) Santiago-Medina, F. J.; Basso, M. C.; Pizzi, A.; Delmotte, L. Polyurethanes from Kraft Lignin without Using Isocyanates. *Journal of Renewable Materials* **2018**, *6* (4), 413--425.

(176) Arias, A.; Entrena-Barbero, E.; Feijoo, G.; Moreira, M. T. Sustainable non-isocyanate polyurethanes bio-adhesives for engineered wood panels are revealed as promising candidates to move from formaldehyde-based alternatives. *Journal of Environmental Chemical Engineering* **2022**, *10* (1), 107053. DOI: https://doi.org/10.1016/j.jece.2021.107053.

(177) Lee, A.; Deng, Y. Green polyurethane from lignin and soybean oil through non-isocyanate reactions. *European Polymer Journal* **2015**, *63*, 67-73. DOI: https://doi.org/10.1016/j.eurpolymj.2014.11.023.

(178) Salanti, A.; Zoia, L.; Mauri, M.; Orlandi, M. Utilization of cyclocarbonated lignin as a bio-based cross-linker for the preparation of poly(hydroxy urethane)s. *RSC Advances* **2017**, *7* (40), 25054-25065. DOI: http://dx.doi.org/10.1039/C7RA03416D.

(179) Yang, Y.; Cao, H.; Liu, R.; Wang, Y.; Zhu, M.; Su, C.; Lv, X.; Zhao, J.; Qin, P.; Cai, D. Fabrication of ultraviolet resistant and anti-bacterial non-isocyanate polyurethanes using the oligomers from the reductive catalytic fractionated lignin oil. *Industrial Crops and Products* **2023**, *193*, 116213. DOI: https://doi.org/10.1016/j.indcrop.2022.116213.

(180) Mimini, V.; Amer, H.; Hettegger, H.; Bacher, M.; Gebauer, I.; Bischof, R.; Fackler, K.; Potthast, A.; Rosenau, T. Lignosulfonate-based polyurethane materials via cyclic carbonates: preparation and characterization. *Holzforschung* **2020**, *74* (2), 203-211. DOI: https://doi.org/10.1515/hf-2018-0298.

(181) Quinsaat, J. E. Q.; Feghali, E.; van de Pas, D. J.; Vendamme, R.; Torr, K. M. Preparation of Biobased Nonisocyanate Polyurethane/Epoxy Thermoset Materials Using Depolymerized Native Lignin. *Biomacromolecules* **2022**, *23* (11), 4562-4573. DOI: https://doi.org/10.1021/acs.biomac.2c00706.

(182) Sternberg, J.; Pilla, S. Materials for the biorefinery: high bio-content, shape memory Kraft lignin-derived non-isocyanate polyurethane foams using a non-toxic protocol. *Green Chemistry* **2020**, *22* (20), 6922-6935. DOI: http://dx.doi.org/10.1039/D0GC01659D.

(183) Sternberg, J.; Pilla, S. Chemical recycling of a lignin-based non-isocyanate polyurethane foam. *Nature Sustainability* **2023**. DOI: https://doi.org/10.1038/s41893-022-01022-3.

(184) Meng, X.; Zhang, S.; Scheidemantle, B.; Wang, Y.-y.; Pu, Y.; Wyman, C. E.; Cai, C. M.; Ragauskas, A. J. Preparation and characterization of aminated co-solvent enhanced lignocellulosic fractionation lignin as a renewable building block for the synthesis of non-isocyanate polyurethanes. *Industrial Crops and Products* **2022**, *178*, 114579. DOI: https://doi.org/10.1016/j.indcrop.2022.114579.

(185) Pilato, L. Resin Chemistry. In *Phenolic Resins: A Century of Progress*, Pilato, L. Ed.; Springer Berlin Heidelberg, 2010; pp 41-91.

(186) Olivares, M.; Guzmán, J. A.; Natho, A.; Saavedra, A. Kraft lignin utilization in adhesives. *Wood Science and Technology* **1988**, *22* (2), 157-165. DOI: https://doi.org/10.1007/BF00355851.

(187) Vázquez, G.; Antorrena, G.; González, J.; Mayor, J. Lignin-phenol-formaldehyde adhesives for exterior grade plywoods. *Bioresource Technology* **1995**, *51* (2), 187-192. DOI: https://doi.org/10.1016/0960-8524(94)00120-P.

(188) Danielson, B.; Simonson, R. Kraft lignin in phenol formaldehyde resin. Part 1. Partial replacement of phenol by kraft lignin in phenol formaldehyde adhesives for plywood. *Journal of Adhesion Science and Technology* **1998**, *12* (9), 923-939. DOI: https://doi.org/10.1163/156856198X00542.

(189) Gao, Z.; Lang, X.; Chen, S.; Zhao, C. Mini-Review on the Synthesis of Lignin-Based Phenolic Resin. *Energy & Fuels* **2021**, *35* (22), 18385-18395. DOI: https://doi.org/10.1021/acs.energyfuels.1c03177.

(190) Gong, X.; Meng, Y.; Lu, J.; Tao, Y.; Cheng, Y.; Wang, H. A Review on Lignin-Based Phenolic Resin Adhesive. *Macromolecular Chemistry and Physics* **2022**, *223* (4), 2100434. DOI: https://doi.org/10.1002/macp.202100434.

(191) Li, W.; Sun, H.; Wang, G.; Sui, W.; Dai, L.; Si, C. Lignin as a green and multifunctional alternative to phenol for resin synthesis. *Green Chemistry* **2023**, *25* (6), 2241-2261. DOI: http://dx.doi.org/10.1039/D2GC04319J.

(192) Çetin, N. S.; Özmen, N. Use of organosolv lignin in phenol–formaldehyde resins for particleboard production: I. Organosolv lignin modified resins. *International Journal of Adhesion and Adhesives* **2002**, *22* (6), 477-480. DOI: https://doi.org/10.1016/S0143-7496(02)00058-1.

(193) Khan, M. A.; Ashraf, S. M.; Malhotra, V. P. Development and characterization of a wood adhesive using bagasse lignin. *International Journal of Adhesion and Adhesives* **2004**, *24* (6), 485-493. DOI: https://doi.org/10.1016/j.ijadhadh.2004.01.003.

(194) Tejado, A.; Peña, C.; Labidi, J.; Echeverria, J. M.; Mondragon, I. Physico-chemical characterization of lignins from different sources for use in phenol–formaldehyde resin synthesis. *Bioresource Technology* **2007**, *98* (8), 1655-1663. DOI: https://doi.org/10.1016/j.biortech.2006.05.042.

(195) Jin, Y.; Cheng, X.; Zheng, Z. Preparation and characterization of phenol–formaldehyde adhesives modified with enzymatic hydrolysis lignin. *Bioresource Technology* **2010**, *101* (6), 2046-2048. DOI: https://doi.org/10.1016/j.biortech.2009.09.085.

(196) Moubarik, A.; Grimi, N.; Boussetta, N.; Pizzi, A. Isolation and characterization of lignin from Moroccan sugar cane bagasse: Production of lignin–phenol-formaldehyde wood adhesive. *Industrial Crops and Products* **2013**, *45*, 296-302. DOI: https://doi.org/10.1016/j.indcrop.2012.12.040.

(197) Zhang, W.; Ma, Y.; Wang, C.; Li, S.; Zhang, M.; Chu, F. Preparation and properties of lignin–phenol–formaldehyde resins based on different biorefinery residues of agricultural biomass. *Industrial Crops and Products* **2013**, *43*, 326-333. DOI: https://doi.org/10.1016/j.indcrop.2012.07.037.

(198) Zhang, W.; Ma, Y.; Xu, Y.; Wang, C.; Chu, F. Lignocellulosic ethanol residue-based lignin–phenol–formaldehyde resin adhesive. *International Journal of Adhesion and Adhesives* **2013**, *40*, 11-18. DOI: https://doi.org/10.1016/j.ijadhadh.2012.08.004.

(199) Yang, S.; Zhang, Y.; Yuan, T.-Q.; Sun, R.-C. Lignin–phenol–formaldehyde resin adhesives prepared with biorefinery technical lignins. *Journal of Applied Polymer Science* **2015**, *132* (36). DOI: https://doi.org/10.1002/app.42493.

(200) Ghorbani, M.; Liebner, F.; Van Herwijnen, H.; Pfungen, L.; Krahofer, M.; Budjav, E.; Konnerth, J. Lignin Phenol Formaldehyde Resoles: The Impact of Lignin Type on Adhesive Properties. *Bioresources* **2016**, *11*, 6727-6741. DOI: https://doi.org/10.15376/biores.11.3.6727-6741.

(201) Stücker, A.; Schütt, F.; Saake, B.; Lehnen, R. Lignins from enzymatic hydrolysis and alkaline extraction of steam refined poplar wood: Utilization in lignin-phenol-formaldehyde resins. *Industrial Crops and Products* **2016**, *85*, 300-308. DOI: https://doi.org/10.1016/j.indcrop.2016.02.062.

(202) Kalami, S.; Chen, N.; Borazjani, H.; Nejad, M. Comparative analysis of different lignins as phenol replacement in phenolic adhesive formulations. *Industrial Crops and Products* **2018**, *125*, 520-528. DOI: https://doi.org/10.1016/j.indcrop.2018.09.037.

(203) Bansode, A.; Barde, M.; Asafu-Adjaye, O.; Patil, V.; Hinkle, J.; Via, B. K.; Adhikari, S.; Adamczyk, A. J.; Farag, R.; Elder, T.; et al. Synthesis of Biobased Novolac Phenol–Formaldehyde Wood Adhesives from Biorefinery-Derived Lignocellulosic Biomass. *ACS Sustainable Chemistry & Engineering* **2021**, *9* (33), 10990-11002. DOI: https://doi.org/10.1021/acssuschemeng.1c01916.

(204) Mennani, M.; Ait Benhamou, A.; Kasbaji, M.; Boussetta, A.; Ablouh, E.-H.; Kassab, Z.; El Achaby, M.; Boussetta, N.; Grimi, N.; Moubarik, A. Insights on the physico-chemical properties of alkali lignins from different agro-industrial residues and their use in phenol-formaldehyde wood adhesive formulation. *International Journal of Biological Macromolecules* **2022**, *221*, 149-162. DOI: https://doi.org/10.1016/j.ijbiomac.2022.08.191.

(205) Protano, C.; Buomprisco, G.; Cammalleri, V.; Pocino, R. N.; Marotta, D.; Simonazzi, S.; Cardoni, F.; Petyx, M.; Iavicoli, S.; Vitali, M. The Carcinogenic Effects of Formaldehyde Occupational Exposure: A Systematic Review. *Cancers* **2022**, *14* (1), 165. DOI: https://doi.org/10.3390/cancers14010165.

(206) Mansouri, N.-E. E.; Salvadó, J. Structural characterization of technical lignins for the production of adhesives: Application to lignosulfonate, kraft, soda-anthraquinone, organosolv and ethanol process lignins. *Industrial Crops and Products* **2006**, *24* (1), 8-16. DOI: https://doi.org/10.1016/j.indcrop.2005.10.002.

(207) Mohamad Ibrahim, M. N.; Zakaria, N.; Sipaut, C. S.; Sulaiman, O.; Hashim, R. Chemical and thermal properties of lignins from oil palm biomass as a substitute for phenol in a phenol formaldehyde resin production. *Carbohydrate Polymers* **2011**, *86* (1), 112-119. DOI: https://doi.org/10.1016/j.carbpol.2011.04.018.

(208) Pang, B.; Yang, S.; Fang, W.; Yuan, T.-Q.; Argyropoulos, D. S.; Sun, R.-C. Structure-property relationships for technical lignins for the production of lignin-phenol-formaldehyde resins. *Industrial Crops and Products* **2017**, *108*, 316-326. DOI: https://doi.org/10.1016/j.indcrop.2017.07.009.

(209) Wang, M.; Leitch, M.; Xu, C. Synthesis of phenol–formaldehyde resol resins using organosolv pine lignins. *European Polymer Journal* **2009**, *45* (12), 3380-3388. DOI: https://doi.org/10.1016/j.eurpolymj.2009.10.003.

(210) El Mansouri, N.-E.; Farriol, X.; Salvadó, J. Structural modification and characterization of lignosulfonate by a reaction in an alkaline medium for its incorporation into phenolic resins. *Journal of Applied Polymer Science* **2006**, *102* (4), 3286-3292. DOI: https://doi.org/10.1002/app.24744.

(211) Siddiqui, H.; Mahmood, N.; Yuan, Z.; Crapulli, F.; Dessbesell, L.; Rizkalla, A.; Ray, A.; Xu, C. Sustainable Bio-Based Phenol-Formaldehyde Resoles Using Hydrolytically Depolymerized Kraft Lignin. *Molecules* **2017**, *22* (11), 1850. DOI: https://doi.org/10.3390/molecules22111850.

(212) Yan, L.; Cui, Y.; Gou, G.; Wang, Q.; Jiang, M.; Zhang, S.; Hui, D.; Gou, J.; Zhou, Z. Liquefaction of lignin in hot-compressed water to phenolic feedstock for the synthesis of phenol-formaldehyde resins. *Composites Part B: Engineering* **2017**, *112*, 8-14. DOI: https://doi.org/10.1016/j.compositesb.2016.10.094.

(213) Li, J.; Zhang, J.; Zhang, S.; Gao, Q.; Li, J.; Zhang, W. Alkali lignin depolymerization under eco-friendly and cost-effective NaOH/urea aqueous solution for fast curing bio-based phenolic resin. *Industrial Crops and Products* **2018**, *120*, 25-33. DOI: https://doi.org/10.1016/j.indcrop.2018.04.027.

(214) Cheng, S.; Yuan, Z.; Leitch, M.; Anderson, M.; Xu, C. Highly efficient de-polymerization of organosolv lignin using a catalytic hydrothermal process and production of phenolic resins/adhesives with the depolymerized lignin as a substitute for phenol at a high substitution ratio. *Industrial Crops and Products* **2013**, *44*, 315-322. DOI: https://doi.org/10.1016/j.indcrop.2012.10.033.

(215) Chen, S.; Xin, Y.; Zhao, C. Multispectroscopic Analysis in the Synthesis of Lignin-Based Biophenolic Resins. *ACS Sustainable Chemistry & Engineering* **2021**, *9* (46), 15653-15660. DOI: https://doi.org/10.1021/acssuschemeng.1c06135.

(216) Wibowo, E. S.; Park, B.-D. The role of acetone-fractionated Kraft lignin molecular structure on surface adhesion to formaldehyde-based resins. *International Journal of Biological Macromolecules* **2023**, *225*, 1449-1461. DOI: https://doi.org/10.1016/j.ijbiomac.2022.11.202.

(217) Rodrigues, J. S.; de Freitas, A. d. S. M.; Maciel, C. C.; Mendes, S. F.; Diment, D.; Balakshin, M.; Botaro, V. R. Selection of kraft lignin fractions as a partial substitute for phenol in synthesis of phenolic resins: Structure-property correlation. *Industrial Crops and Products* **2023**, *191*, 115948. DOI: https://doi.org/10.1016/j.indcrop.2022.115948.

(218) Wang, L.; Lagerquist, L.; Zhang, Y.; Koppolu, R.; Tirri, T.; Sulaeva, I.; Schoultz, S. v.; Vähäsalo, L.; Pranovich, A.; Rosenau, T.; et al. Tailored Thermosetting Wood Adhesive Based on Well-Defined Hardwood Lignin Fractions.

ACS Sustainable Chemistry & Engineering **2020**, *8* (35), 13517-13526. DOI: https://doi.org/10.1021/acssuschemeng.0c05408.

(219) Abächerli, A.; Doppenberg, F. Method for preparing alkaline solutions containing aromatic polymers 2001.

(220) Kalami, S.; Arefmanesh, M.; Master, E.; Nejad, M. Replacing 100% of phenol in phenolic adhesive formulations with lignin. *Journal of Applied Polymer Science* **2017**, *134* (30), 45124. DOI: https://doi.org/10.1002/app.45124.

(221) Vázquez, G.; González, J.; Freire, S.; Antorrena, G. Effect of chemical modification of lignin on the gluebond performance of lignin-phenolic resins. *Bioresource Technology* **1997**, *60* (3), 191-198. DOI: https://doi.org/10.1016/S0960-8524(97)00030-8.

(222) Hu, L.; Pan, H.; Zhou, Y.; Zhang, M. Methods to improve lignin's reactivity as a phenol substitute and as replacement for other phenolic compounds: A brief review. *Bioresources* **2011**, *6*. DOI: https://doi.org/10.15376/biores.6.3.3515-3525.

(223) Benar, P.; Gonçalves, A. R.; Mandelli, D.; Schuchardt, U. Eucalyptus organosolv lignins: study of the hydroxymethylation and use in resols. *Bioresource Technology* **1999**, *68* (1), 11-16. DOI: https://doi.org/10.1016/S0960-8524(98)00076-5.

(224) Paiva, J. M. F.; Frollini, E. Sugarcane bagasse reinforced phenolic and lignophenolic composites. *Journal of Applied Polymer Science* **2002**, *83* (4), 880-888. DOI: https://doi.org/10.1002/app.10085.

(225) Alonso, M. V.; Oliet, M.; Rodríguez, F.; Astarloa, G.; Echeverría, J. M. Use of a methylolated softwood ammonium lignosulfonate as partial substitute of phenol in resol resins manufacture. *Journal of Applied Polymer Science* **2004**, *94* (2), 643-650. DOI: https://doi.org/10.1002/app.20887.

(226) Taverna, M. E.; Felissia, F.; Area, M. C.; Estenoz, D. A.; Nicolau, V. V. Hydroxymethylation of technical lignins from South American sources with potential use in phenolic resins. *Journal of Applied Polymer Science* **2019**, *136* (26), 47712. DOI: https://doi.org/10.1002/app.47712.

(227) Stücker, A.; Podschun, J.; Heitmann, M.; Lehnen, R. Organosolv lignin in Phenol-Formaldehyde resins - effect of molecular weight and lignin methylolation. In *Towards forest products and processes with lower environmental impact : 5th International Conference on Environmentally Compatible Forest Products*, Editions University Fernando Pessoa, 2014; pp 251-261.

(228) Wang, G.; Chen, H. Carbohydrate elimination of alkaline-extracted lignin liquor by steam explosion and its methylolation for substitution of phenolic adhesive. *Industrial Crops and Products* **2014**, *53*, 93-101. DOI: https://doi.org/10.1016/j.indcrop.2013.12.020.

(229) Jiang, X.; Liu, J.; Du, X.; Hu, Z.; Chang, H.-m.; Jameel, H. Phenolation to Improve Lignin Reactivity toward Thermosets Application. *ACS Sustainable Chemistry & Engineering* **2018**, *6* (4), 5504-5512. DOI: https://doi.org/10.1021/acssuschemeng.8b00369.

(230) Alonso, M. V.; Oliet, M.; Rodríguez, F.; García, J.; Gilarranz, M. A.; Rodríguez, J. J. Modification of ammonium lignosulfonate by phenolation for use in phenolic resins. *Bioresource Technology* **2005**, *96* (9), 1013-1018. DOI: https://doi.org/10.1016/j.biortech.2004.09.009.

(231) Podschun, J.; Saake, B.; Lehnen, R. Reactivity enhancement of organosolv lignin by phenolation for improved bio-based thermosets. *European Polymer Journal* **2015**, *67*, 1-11. DOI: https://doi.org/10.1016/j.eurpolymj.2015.03.029.

(232) Podschun, J.; Stücker, A.; Saake, B.; Lehnen, R. Structure–Function Relationships in the Phenolation of Lignins from Different Sources. *ACS Sustainable Chemistry & Engineering* **2015**, *3* (10), 2526-2532. DOI: 10.1021/acssuschemeng.5b00705.

(233) Podschun, J.; Stücker, A.; Buchholz, R. I.; Heitmann, M.; Schreiber, A.; Saake, B.; Lehnen, R. Phenolated Lignins as Reactive Precursors in Wood Veneer and Particleboard Adhesion. *Industrial & Engineering Chemistry Research* **2016**, *55* (18), 5231-5237. DOI: https://doi.org/10.1021/acs.iecr.6b00594.

(234) Yang, S.; Wen, J.-L.; Yuan, T.-Q.; Sun, R.-C. Characterization and phenolation of biorefinery technical lignins for lignin–phenol–formaldehyde resin adhesive synthesis. *RSC Advances* **2014**, *4* (101), 57996-58004. DOI: http://dx.doi.org/10.1039/C4RA09595B.

(235) Zhao, M.; Jing, J.; Zhu, Y.; Yang, X.; Wang, X.; Wang, Z. Preparation and performance of lignin–phenol–formaldehyde adhesives. *International Journal of Adhesion and Adhesives* **2016**, *64*, 163-167. DOI: https://doi.org/10.1016/j.ijadhadh.2015.10.010.

(236) Qiao, W.; Li, S.; Guo, G.; Han, S.; Ren, S.; Ma, Y. Synthesis and characterization of phenol-formaldehyde resin using enzymatic hydrolysis lignin. *Journal of Industrial and Engineering Chemistry* **2015**, *21*, 1417-1422. DOI: https://doi.org/10.1016/j.jiec.2014.06.016.

(237) Venkatesagowda, B.; Dekker, R. F. H. Enzymatic demethylation of Kraft lignin for lignin-based phenol-formaldehyde resin applications. *Biomass Conversion and Biorefinery* **2020**, *10* (2), 203-225. DOI: https://doi.org/10.1007/s13399-019-00407-3.

(238) Song, Y.; Wang, Z.; Yan, N.; Zhang, R.; Li, J. Demethylation of Wheat Straw Alkali Lignin for Application in Phenol Formaldehyde Adhesives. *Polymers* **2016**, *8* (6), 209. DOI: https://doi.org/10.3390/polym8060209.

(239) Wang, H.; Eberhardt, T. L.; Wang, C.; Gao, S.; Pan, H. Demethylation of Alkali Lignin with Halogen Acids and Its Application to Phenolic Resins. *Polymers* **2019**, *11* (11), 1771. DOI: https://doi.org/10.3390/polym11111771.

(240) Li, J.; Wang, W.; Zhang, S.; Gao, Q.; Zhang, W.; Li, J. Preparation and characterization of lignin demethylated at atmospheric pressure and its application in fast curing biobased phenolic resins. *RSC Advances* **2016**, *6* (71), 67435-67443. DOI: http://dx.doi.org/10.1039/C6RA11966B.

(241) Li, J.; Zhang, J.; Zhang, S.; Gao, Q.; Li, J.; Zhang, W. Fast Curing Bio-Based Phenolic Resins via Lignin Demethylated under Mild Reaction Condition. *Polymers* **2017**, *9* (9), 428. DOI: https://doi.org/10.3390/polym9090428.

(242) Liu, Q.; Xu, Y.; Kong, F.; Ren, H.; Zhai, H. Synthesis of phenolic resins by substituting phenol with modified spruce kraft lignin. *Wood Science and Technology* **2022**, *56* (5), 1527-1549. DOI: https://doi.org/10.1007/s00226-022-01408-8.

(243) Mansouri, N.-E. E.; Pizzi, A.; Salvado, J. Lignin-based polycondensation resins for wood adhesives. *Journal of Applied Polymer Science* **2007**, *103* (3), 1690-1699. DOI: https://doi.org/10.1002/app.25098.

(244) El Mansouri, N.-e.; Pizzi, A.; Salvadó, J. Lignin-based wood panel adhesives without formaldehyde. *Holz als Roh- und Werkstoff* **2007**, *65* (1), 65-70. DOI: https://doi.org/10.1007/s00107-006-0130-z.

(245) Mansouri, H. R.; Navarrete, P.; Pizzi, A.; Tapin-Lingua, S.; Benjelloun-Mlayah, B.; Pasch, H.; Rigolet, S. Synthetic-resin-free wood panel adhesives from mixed low molecular mass lignin and tannin. *European Journal of Wood and Wood Products* **2011**, *69* (2), 221-229. DOI: https://doi.org/10.1007/s00107-010-0423-0.

(246) He, Q.; Ziegler-Devin, I.; Chrusciel, L.; Obame, S. N.; Hong, L.; Lu, X.; Brosse, N. Lignin-First Integrated Steam Explosion Process for Green Wood Adhesive Application. *ACS Sustainable Chemistry & Engineering* **2020**, *8* (13), 5380-5392. DOI: https://doi.org/10.1021/acssuschemeng.0c01065.

(247) Hazwan Hussin, M.; Samad, N. A.; Latif, N. H. A.; Rozuli, N. A.; Yusoff, S. B.; Gambier, F.; Brosse, N. Production of oil palm (Elaeis guineensis) fronds lignin-derived non-toxic aldehyde for eco-friendly wood adhesive. *International Journal of Biological Macromolecules* **2018**, *113*, 1266-1272. DOI: https://doi.org/10.1016/j.ijbiomac.2018.03.048.

(248) Hazwan Hussin, M.; Aziz, A. A.; Iqbal, A.; Ibrahim, M. N. M.; Latif, N. H. A. Development and characterization novel bio-adhesive for wood using kenaf core (Hibiscus cannabinus) lignin and glyoxal. *International Journal of Biological Macromolecules* **2019**, *122*, 713-722. DOI: https://doi.org/10.1016/j.ijbiomac.2018.11.009.

(249) Aziz, N. A.; Latip, A. F. A.; Peng, L. C.; Latif, N. H. A.; Brosse, N.; Hashim, R.; Hussin, M. H. Reinforced lignin-phenol-glyoxal (LPG) wood adhesives from coconut husk. *International Journal of Biological Macromolecules* **2019**, *141*, 185-196. DOI: https://doi.org/10.1016/j.ijbiomac.2019.08.255.

(250) Siahkamari, M.; Emmanuel, S.; Hodge, D. B.; Nejad, M. Lignin-Glyoxal: A Fully Biobased Formaldehyde-Free Wood Adhesive for Interior Engineered Wood Products. *ACS Sustainable Chemistry & Engineering* **2022**, *10* (11), 3430-3441. DOI: https://doi.org/10.1021/acssuschemeng.1c06843.

(251) Guigo, N.; Mija, A.; Vincent, L.; Sbirrazzuoli, N. Eco-friendly composite resins based on renewable biomass resources: Polyfurfuryl alcohol/lignin thermosets. *European Polymer Journal* **2010**, *46* (5), 1016-1023. DOI: https://doi.org/10.1016/j.eurpolymj.2010.02.010.

(252) Zhang, Y.; Yuan, Z.; Mahmood, N.; Huang, S.; Xu, C. Sustainable bio-phenol-hydroxymethylfurfural resins using phenolated de-polymerized hydrolysis lignin and their application in bio-composites. *Industrial Crops and Products* **2016**, *79*, 84-90. DOI: https://doi.org/10.1016/j.indcrop.2015.10.048.

(253) Liang, F.-B.; Song, Y.-L.; Huang, C.-P.; Li, Y.-X.; Chen, B.-H. Synthesis of Novel Lignin-Based Ion-Exchange Resin and Its Utilization in Heavy Metals Removal. *Industrial & Engineering Chemistry Research* **2013**, *52* (3), 1267-1274. DOI: https://doi.org/10.1021/ie301863e.

(254) Zhang, Y.; Li, N.; Chen, Z.; Ding, C.; Zheng, Q.; Xu, J.; Meng, Q. Synthesis of High-Water-Resistance Lignin-Phenol Resin Adhesive with Furfural as a Crosslinking Agent. *Polymers* **2020**, *12* (12), 2805. DOI: https://doi.org/10.3390/polym12122805.

(255) Dongre, P.; Driscoll, M.; Amidon, T.; Bujanovic, B. Lignin-Furfural Based Adhesives. *Energies* **2015**, *8* (8), 7897-7914. DOI: https://doi.org/10.3390/en8087897.

(256) Dornbusch, M.; Christ, U.; Rasing, R.; GmbH, V. N.; KG, C. *Epoxy Resins: Fundamentals and Applications*; Vincentz Network, 2016.

(257) Vidil, T.; Tournilhac, F.; Musso, S.; Robisson, A.; Leibler, L. Control of reactions and network structures of epoxy thermosets. *Progress in Polymer Science* **2016**, *62*, 126-179. DOI: https://doi.org/10.1016/j.progpolymsci.2016.06.003.

(258) Wan, J.; Zhao, J.; Zhang, X.; Fan, H.; Zhang, J.; Hu, D.; Jin, P.; Wang, D.-Y. Epoxy thermosets and materials derived from bio-based monomeric phenols: Transformations and performances. *Progress in Polymer Science* **2020**, *108*, 101287. DOI: https://doi.org/10.1016/j.progpolymsci.2020.101287.

(259) Lu, X.; Gu, X. A review on lignin-based epoxy resins: Lignin effects on their synthesis and properties. *International Journal of Biological Macromolecules* **2023**, *229*, 778-790. DOI: https://doi.org/10.1016/j.ijbiomac.2022.12.322.

(260) Feldman, D.; Banu, D.; Natansohn, A.; Wang, J. Structure–properties relations of thermally cured epoxy–lignin polyblends. *Journal of Applied Polymer Science* **1991**, *42* (6), 1537-1550. DOI: https://doi.org/10.1002/app.1991.070420607.

(261) Feldman, D.; Banu, D.; Luchian, C.; Wang, J. Epoxy–lignin polyblends: Correlation between polymer interaction and curing temperature. *Journal of Applied Polymer Science* **1991**, *42* (5), 1307-1318. DOI: https://doi.org/10.1002/app.1991.070420514.

(262) Simionescu, C. I.; Rusan, V.; Macoveanu, M. M.; Cazacu, G.; Lipsa, R.; Vasile, C.; Stoleriu, A.; Ioanid, A. Lignin/epoxy composites. *Composites Science and Technology* **1993**, *48* (1), 317-323. DOI: https://doi.org/10.1016/0266-3538(93)90149-B.

(263) Wu, L. C. F.; Glasser, W. G. Engineering plastics from lignin. I. Synthesis of hydroxypropyl lignin. *Journal of Applied Polymer Science* **1984**, *29* (4), 1111-1123. DOI: https://doi.org/10.1002/app.1984.070290408.

(264) Delmas, G.-H.; Benjelloun-Mlayah, B.; Bigot, Y. L.; Delmas, M. Biolignin™ based epoxy resins. *Journal of Applied Polymer Science* **2013**, *127* (3), 1863-1872. DOI: https://doi.org/10.1002/app.37921.

(265) Zhang, Z.; Li, J.; Zhang, Y.; Jin, Z. Kinetics of partially depolymerized lignin as co-curing agent for epoxy resin. *International Journal of Biological Macromolecules* **2020**, *150*, 786-792. DOI: https://doi.org/10.1016/j.ijbiomac.2020.02.059.

(266) Cui, M.; Nguyen, N. A.; Bonnesen, P. V.; Uhrig, D.; Keum, J. K.; Naskar, A. K. Rigid Oligomer from Lignin in Designing of Tough, Self-Healing Elastomers. *ACS Macro Letters* **2018**, *7* (11), 1328-1332. DOI: https://doi.org/10.1021/acsmacrolett.8b00600.

(267) Engelmann, G.; Ganster, J. Bio-based epoxy resins with low molecular weight kraft lignin and pyrogallol. *Holzforschung* **2014**, *68* (4), 435-446. DOI: https://doi.org/10.1515/hf-2013-0023.

(268) Ortiz, P.; Vendamme, R.; Eevers, W. Fully Biobased Epoxy Resins from Fatty Acids and Lignin. *Molecules* **2020**, *25* (5), 1158. DOI: https://doi.org/10.3390/molecules25051158.

(269) Dinu, R.; Cantarutti, C.; Mija, A. Design of Sustainable Materials by Cross-linking a Biobased Epoxide with Keratin and Lignin. *ACS Sustainable Chemistry & Engineering* **2020**, *8* (17), 6844-6852. DOI: https://doi.org/10.1021/acssuschemeng.0c01759.

(270) Asada, C.; Honjo, K.; Nakamura, Y. Utilization of Steam-Treated and Milling-Treated Lignin from Moso Bamboo as Curing Agent of Epoxy Resin. *Waste and Biomass Valorization* **2021**, *12* (11), 6261-6272. DOI: https://doi.org/10.1007/s12649-021-01444-8.

(271) Du, X.; Li, J.; Lindström, M. E. Modification of industrial softwood kraft lignin using Mannich reaction with and without phenolation pretreatment. *Industrial Crops and Products* **2014**, *52*, 729-735. DOI: https://doi.org/10.1016/j.indcrop.2013.11.035.

(272) Ott, M. W.; Dietz, C.; Trosien, S.; Mehlhase, S.; Bitsch, M. J.; Nau, M.; Meckel, T.; Geissler, A.; Siegert, G.; Huong, J.; et al. Co-curing of epoxy resins with aminated lignins: insights into the role of lignin homo crosslinking during lignin amination on the elastic properties. *Holzforschung* **2021**, *75* (4), 390-398. DOI: https://doi.org/10.1515/hf-2020-0060.

(273) Mendis, G. P.; Hua, I.; Youngblood, J. P.; Howarter, J. A. Enhanced dispersion of lignin in epoxy composites through hydration and mannich functionalization. *Journal of Applied Polymer Science* **2015**, *132* (1). DOI: https://doi.org/10.1002/app.41263.

(274) Liu, X.; Zhu, H.; Qin, C.; Zhou, J.; Zhao, J.; Wang, S. Adsorption of Heavy Metal Ion from Aqueous Single Metal Solution by Aminated Epoxy-Lignin. *BioResources* **2013**, *8*. DOI: https://doi.org/10.15376/biores.8.2.2257-2269.

(275) Pan, H.; Sun, G.; Zhao, T. Synthesis and characterization of aminated lignin. *International Journal of Biological Macromolecules* **2013**, *59*, 221-226. DOI: https://doi.org/10.1016/j.ijbiomac.2013.04.049.

(276) Pan, H.; Sun, G.; Zhao, T.; Wang, G. Thermal properties of epoxy resins crosslinked by an aminated lignin. *Polymer Engineering & Science* **2015**, *55* (4), 924-932. DOI: https://doi.org/10.1002/pen.23960.

(277) Nikafshar, S.; Zabihi, O.; Moradi, Y.; Ahmadi, M.; Amiri, S.; Naebe, M. Catalyzed Synthesis and Characterization of a Novel Lignin-Based Curing Agent for the Curing of High-Performance Epoxy Resin. *Polymers* **2017**, *9* (7), 266. DOI: https://doi.org/10.3390/polym9070266.

(278) Hirose, S.; Hatakeyama, T.; Hatakeyama, H. Glass transition and thermal decomposition of epoxy resins from the carboxylic acid system consisting of ester-carboxylic acid derivatives of alcoholysis lignin and ethylene glycol with various dicarboxylic acids. *Thermochimica Acta* **2005**, *431* (1), 76-80. DOI: https://doi.org/10.1016/j.tca.2005.01.043.

(279) Hirose, S.; Hatakeyama, T.; Hatakeyama, H. Synthesis and thermal properties of epoxy resins from ester-carboxylic acid derivative of alcoholysis lignin. *Macromolecular Symposia* **2003**, *197* (1), 157-170. DOI: https://doi.org/10.1002/masy.200350715.

(280) Ismail, T. N. M. T.; Hassan, H. A.; Hirose, S.; Taguchi, Y.; Hatakeyama, T.; Hatakeyama, H. Synthesis and thermal properties of ester-type crosslinked epoxy resins derived from lignosulfonate and glycerol. *Polymer International* **2010**, *59* (2), 181-186. DOI: https://doi.org/10.1002/pi.2705.

(281) Li, J.; Zhang, Z.; Zhang, Y.; Sun, F.; Wang, D.; Wang, H.; Jin, Z. Synergistic effect of lignin and ethylene glycol crosslinked epoxy resin on enhancing thermal, mechanical and shape memory performance. *International Journal of Biological Macromolecules* **2021**, *192*, 516-524. DOI: https://doi.org/10.1016/j.ijbiomac.2021.10.035.

(282) Qin, J.; Woloctt, M.; Zhang, J. Use of Polycarboxylic Acid Derived from Partially Depolymerized Lignin As a Curing Agent for Epoxy Application. *ACS Sustainable Chemistry & Engineering* **2014**, *2* (2), 188-193. DOI: https://doi.org/10.1021/sc400227v.

(283) Zhang, Y.; Wang, H.; Eberhardt, T. L.; Gu, Q.; Pan, H. Preparation of carboxylated lignin-based epoxy resin with excellent mechanical properties. *European Polymer Journal* **2021**, *150*, 110389. DOI: https://doi.org/10.1016/j.eurpolymj.2021.110389.

(284) Liu, W.; Zhou, R.; Goh, H. L. S.; Huang, S.; Lu, X. From Waste to Functional Additive: Toughening Epoxy Resin with Lignin. *ACS Applied Materials & Interfaces* **2014**, *6* (8), 5810-5817. DOI: https://doi.org/10.1021/am500642n.

(285) Zhou, S.; Huang, K.; Xu, X.; Wang, B.; Zhang, W.; Su, Y.; Hu, K.; Zhang, C.; Zhu, J.; Weng, G.; et al. Rigid-and-Flexible, Degradable, Fully Biobased Thermosets from Lignin and Soybean Oil: Synthesis and Properties. *ACS Sustainable Chemistry & Engineering* **2023**, *11* (8), 3466-3473. DOI: https://doi.org/10.1021/acssuschemeng.2c06990.

(286) Nieh, W. L.-S.; Glasser, W. G. Lignin Epoxide. In *Lignin*, ACS Symposium Series, Vol. 397; American Chemical Society, 1989; pp 506-514.

(287) Over, L. C.; Grau, E.; Grelier, S.; Meier, M. A. R.; Cramail, H. Synthesis and Characterization of Epoxy Thermosetting Polymers from Glycidylated Organosolv Lignin and Bisphenol A. *Macromolecular Chemistry and Physics* **2017**, *218* (4), 1600411. DOI: https://doi.org/10.1002/macp.201600411.

(288) Nikafshar, S.; Wang, J.; Dunne, K.; Sangthonganotai, P.; Nejad, M. Choosing the Right Lignin to Fully Replace Bisphenol A in Epoxy Resin Formulation. *ChemSusChem* **2021**, *14* (4), 1184-1195. DOI: https://doi.org/10.1002/cssc.202002729.

(289) Sasaki, C.; Wanaka, M.; Takagi, H.; Tamura, S.; Asada, C.; Nakamura, Y. Evaluation of epoxy resins synthesized from steam-exploded bamboo lignin. *Industrial Crops and Products* **2013**, *43*, 757-761. DOI: https://doi.org/10.1016/j.indcrop.2012.08.018.

(290) Asada, C.; Basnet, S.; Otsuka, M.; Sasaki, C.; Nakamura, Y. Epoxy resin synthesis using low molecular weight lignin separated from various lignocellulosic materials. *International Journal of Biological Macromolecules* **2015**, *74*, 413-419. DOI: https://doi.org/10.1016/j.ijbiomac.2014.12.039.

(291) Asada, C.; Fujii, M.; Suzuki, A.; Nakamura, Y. Cured epoxy resin synthesized using acetone-soluble lignin and ligno-p-cresol obtained from steam-exploded wheat straw. *Biomass Conversion and Biorefinery* **2021**. DOI: https://doi.org/10.1007/s13399-021-02032-5.

(292) Ferdosian, F.; Yuan, Z.; Anderson, M.; Xu, C. Chemically Modified Lignin through Epoxidation and its Thermal Properties. *journal of Science & Technology for Forest Products and Processes* **2012**, *2*, 11-15.

(293) Ferdosian, F.; Yuan, Z.; Anderson, M.; Xu, C. Synthesis of lignin-based epoxy resins: optimization of reaction parameters using response surface methodology. *RSC Advances* **2014**, *4* (60), 31745-31753. DOI: http://dx.doi.org/10.1039/C4RA03978E.

(294) Ferdosian, F.; Yuan, Z.; Anderson, M.; Xu, C. Sustainable lignin-based epoxy resins cured with aromatic and aliphatic amine curing agents: Curing kinetics and thermal properties. *Thermochimica Acta* **2015**, *618*, 48-55. DOI: https://doi.org/10.1016/j.tca.2015.09.012.

(295) Ferdosian, F.; Yuan, Z.; Anderson, M.; Xu, C. C. Thermal performance and thermal decomposition kinetics of lignin-based epoxy resins. *Journal of Analytical and Applied Pyrolysis* **2016**, *119*, 124-132. DOI: https://doi.org/10.1016/j.jaap.2016.03.009.

(296) Ferdosian, F.; Zhang, Y.; Yuan, Z.; Anderson, M.; Xu, C. Curing kinetics and mechanical properties of bio-based epoxy composites comprising lignin-based epoxy resins. *European Polymer Journal* **2016**, *82*, 153-165. DOI: https://doi.org/10.1016/j.eurpolymj.2016.07.014.

(297) van de Pas, D. J.; Torr, K. M. Biobased Epoxy Resins from Deconstructed Native Softwood Lignin. *Biomacromolecules* **2017**, *18* (8), 2640-2648. DOI: https://doi.org/10.1021/acs.biomac.7b00767.

(298) Feghali, E.; van de Pas, D. J.; Torr, K. M. Toward Bio-Based Epoxy Thermoset Polymers from Depolymerized Native Lignins Produced at the Pilot Scale. *Biomacromolecules* **2020**, *21* (4), 1548-1559. DOI: https://doi.org/10.1021/acs.biomac.0c00108.

(299) Feghali, E.; van de Pas, D. J.; Parrott, A. J.; Torr, K. M. Biobased Epoxy Thermoset Polymers from Depolymerized Native Hardwood Lignin. *ACS Macro Letters* **2020**, *9* (8), 1155-1160. DOI: https://doi.org/10.1021/acsmacrolett.0c00424.

(300) Liu, G.; Jin, C.; Huo, S.; Kong, Z.; Chu, F. Preparation and properties of novel bio-based epoxy resin thermosets from lignin oligomers and cardanol. *International Journal of Biological Macromolecules* **2021**, *193*, 1400-1408. DOI: https://doi.org/10.1016/j.ijbiomac.2021.10.203.

(301) Xin, J.; Li, M.; Li, R.; Wolcott, M. P.; Zhang, J. Green Epoxy Resin System Based on Lignin and Tung Oil and Its Application in Epoxy Asphalt. *ACS Sustainable Chemistry & Engineering* **2016**, *4* (5), 2754-2761. DOI: https://doi.org/10.1021/acssuschemeng.6b00256.

(302) Kaiho, A.; Mazzarella, D.; Satake, M.; Kogo, M.; Sakai, R.; Watanabe, T. Construction of the di(trimethylolpropane) cross linkage and the phenylnaphthalene structure coupled with selective β-O-4 bond cleavage for synthesizing lignin-based epoxy resins with a controlled glass transition temperature. *Green Chemistry* **2016**, *18* (24), 6526-6535. DOI: http://dx.doi.org/10.1039/C6GC02211A.

(303) Hofmann, K.; Glasser, W. G. Engineering Plastics from Lignin. 21.1Synthesis and Properties of Epoxidized Lignin-Poly (Propylene Oxide) Copolymers. *Journal of Wood Chemistry and Technology* **1993**, *13* (1), 73-95. DOI: https://doi.org/10.1080/02773819308020508.

(304) Jablonskis, A.; Arshanitsa, A.; Arnautov, A.; Telysheva, G.; Evtuguin, D. Evaluation of Ligno Boost™ softwood kraft lignin epoxidation as an approach for its application in cured epoxy resins. *Industrial Crops and Products* **2018**, *112*, 225-235. DOI: https://doi.org/10.1016/j.indcrop.2017.12.003.

(305) Gioia, C.; Lo Re, G.; Lawoko, M.; Berglund, L. Tunable Thermosetting Epoxies Based on Fractionated and Well-Characterized Lignins. *Journal of the American Chemical Society* **2018**, *140* (11), 4054-4061. DOI: https://doi.org/10.1021/jacs.7b13620.

(306) Gioia, C.; Colonna, M.; Tagami, A.; Medina, L.; Sevastyanova, O.; Berglund, L. A.; Lawoko, M. Lignin-Based Epoxy Resins: Unravelling the Relationship between Structure and Material Properties. *Biomacromolecules* **2020**, *21* (5), 1920-1928. DOI: https://doi.org/10.1021/acs.biomac.0c00057.

(307) Van Aelst, K.; Van Sinay, E.; Vangeel, T.; Zhang, Y.; Renders, T.; Van den Bosch, S.; Van Aelst, J.; Sels, B. F. Low molecular weight and highly functional RCF lignin products as a full bisphenol a replacer in bio-based epoxy resins. *Chemical Communications* **2021**, *57* (46), 5642-5645. DOI: http://dx.doi.org/10.1039/D1CC02263F.

(308) Silau, H.; Melas, A.; Dam-Johansen, K.; Wu, H.; Daugaard, A. E.; Høj, M. Solvent Fractionation and Depolymerization Provide Liquid Lignin Fractions Exploited as Bio-based Aromatic Building Blocks in Epoxies. *ACS Sustainable Chemistry & Engineering* **2023**, *11* (4), 1591-1597. DOI: https://doi.org/10.1021/acssuschemeng.2c06668.

(309) Zhao, B.; Chen, G.; Liu, Y.; Hu, K.; Wu, R. Synthesis of lignin base epoxy resin and its characterization. *Journal of Materials Science Letters* **2001**, *20* (9), 859-862. DOI: https://doi.org/10.1023/A:1010975132530.

(310) Sun, G.; Sun, H.; Liu, Y.; Zhao, B.; Zhu, N.; Hu, K. Comparative study on the curing kinetics and mechanism of a lignin-based-epoxy/anhydride resin system. *Polymer* **2007**, *48* (1), 330-337. DOI: https://doi.org/10.1016/j.polymer.2006.10.047.

(311) Zhang, Y.; Pang, H.; Wei, D.; Li, J.; Li, S.; Lin, X.; Wang, F.; Liao, B. Preparation and characterization of chemical grouting derived from lignin epoxy resin. *European Polymer Journal* **2019**, *118*, 290-305. DOI: https://doi.org/10.1016/j.eurpolymj.2019.05.003.

(312) Mansouri, N.-e. E.; Yuan, Q.; Huang, F. Synthesis and characterization of kraft lignin-based epoxy resins. *BioResources* **2011**. DOI: https://dx.doi.org/10.15376/biores.6.3.2492-2503.

(313) Zhao, X.; Zhang, Z.; Pang, J.; Su, L. Study on the preparation of epoxy resin materials from nano-lignin polyols. *Industrial Crops and Products* **2022**, *185*, 115158. DOI: https://doi.org/10.1016/j.indcrop.2022.115158.

(314) Zhao, S.; Abu-Omar, M. M. Synthesis of Renewable Thermoset Polymers through Successive Lignin Modification Using Lignin-Derived Phenols. *ACS Sustainable Chemistry & Engineering* **2017**, *5* (6), 5059-5066. DOI: https://doi.org/10.1021/acssuschemeng.7b00440.

(315) Zhao, S.; Huang, X.; Whelton, A. J.; Abu-Omar, M. M. Formaldehyde-Free Method for Incorporating Lignin into Epoxy Thermosets. *ACS Sustainable Chemistry & Engineering* **2018**, *6* (8), 10628-10636. DOI: https://doi.org/10.1021/acssuschemeng.8b01962.

(316) Zhen, X.; Li, H.; Xu, Z.; Wang, Q.; Zhu, S.; Wang, Z.; Yuan, Z. Facile synthesis of lignin-based epoxy resins with excellent thermal-mechanical performance. *International Journal of Biological Macromolecules* **2021**, *182*, 276-285. DOI: https://doi.org/10.1016/j.ijbiomac.2021.03.203.

(317) Zhen, X.; Li, H.; Xu, Z.; Wang, Q.; Xu, J.; Zhu, S.; Wang, Z.; Yuan, Z. Demethylation, phenolation, and depolymerization of lignin for the synthesis of lignin-based epoxy resin via a one-pot strategy. *Industrial Crops and Products* **2021**, *173*, 114135. DOI: https://doi.org/10.1016/j.indcrop.2021.114135.

(318) Zhang, Y.; Stepanova, S.; Van Aelst, K.; Sels, B. F. Consider lignin's hydroxyl groups content and type, its molecular weight and content when converting it into epoxy resin. *Current Opinion in Green and Sustainable Chemistry* **2023**, *40*, 100750. DOI: https://doi.org/10.1016/j.cogsc.2022.100750.

(319) Vásquez-Garay, F.; Teixeira Mendonça, R.; Peretti, S. W. Chemoenzymatic lignin valorization: Production of epoxidized pre-polymers using Candida antarctica lipase B. *Enzyme and Microbial Technology* **2018**, *112*, 6-13. DOI: https://doi.org/10.1016/j.enzmictec.2018.01.007.

(320) Li, R. J.; Gutierrez, J.; Chung, Y.-L.; Frank, C. W.; Billington, S. L.; Sattely, E. S. A lignin-epoxy resin derived from biomass as an alternative to formaldehyde-based wood adhesives. *Green Chemistry* **2018**, *20* (7), 1459-1466. DOI: http://dx.doi.org/10.1039/C7GC03026F.

(321) Gouveia, J. R.; Garcia, G. E. S.; Antonino, L. D.; Tavares, L. B.; dos Santos, D. J. Epoxidation of Kraft Lignin as a Tool for Improving the Mechanical Properties of Epoxy Adhesive. *Molecules* **2020**, *25* (11), 2513. DOI: https://doi.org/10.3390/molecules25112513.

(322) Chen, S.; Chen, H.; Yang, S.; Fan, D. Developing an antifungal and high-strength soy protein-based adhesive modified by lignin-based polymer. *Industrial Crops and Products* **2021**, *170*, 113795. DOI: https://doi.org/10.1016/j.indcrop.2021.113795.

(323) Wang, W.; Li, Y.; Zhang, H.; Chen, T.; Sun, G.; Han, Y.; Li, J. Double-Interpenetrating-Network Lignin-based Epoxy Resin Adhesives for Resistance to Extreme Environment. *Biomacromolecules* **2022**, *23* (3), 779-788. DOI: https://doi.org/10.1021/acs.biomac.1c01204.

(324) Yan, R.; Yang, D.; Zhang, N.; Zhao, Q.; Liu, B.; Xiang, W.; Sun, Z.; Xu, R.; Zhang, M.; Hu, W. Performance of UV curable lignin based epoxy acrylate coatings. *Progress in Organic Coatings* **2018**, *116*, 83-89. DOI: https://doi.org/10.1016/j.porgcoat.2017.11.011.

(325) Yan, R.; Liu, Y.; Liu, B.; Zhang, Y.; Zhao, Q.; Sun, Z.; Hu, W.; Zhang, N. Improved performance of dual-cured organosolv lignin-based epoxy acrylate coatings. *Composites Communications* **2018**, *10*, 52-56. DOI: https://doi.org/10.1016/j.coco.2018.04.006.

(326) Wang, X.; Leng, W.; Nayanathara, R. M. O.; Caldona, E. B.; Liu, L.; Chen, L.; Advincula, R. C.; Zhang, Z.; Zhang, X. Anticorrosive epoxy coatings from direct epoxidation of bioethanol fractionated lignin. *International Journal of Biological Macromolecules* **2022**, *221*, 268-277. DOI: https://doi.org/10.1016/j.ijbiomac.2022.08.177.

(327) Silau, H.; Garcia, A. G.; Woodley, J. M.; Dam-Johansen, K.; Daugaard, A. E. Bio-Based Epoxy Binders from Lignin Derivatized with Epoxidized Rapeseed Fatty Acids in Bimodal Coating Systems. *ACS Applied Polymer Materials* **2022**, *4* (1), 444-451. DOI: https://doi.org/10.1021/acsapm.1c01351.

(328) Dai, P.; Liang, M.; Ma, X.; Luo, Y.; He, M.; Gu, X.; Gu, Q.; Hussain, I.; Luo, Z. Highly Efficient, Environmentally Friendly Lignin-Based Flame Retardant Used in Epoxy Resin. *ACS Omega* **2020**, *5* (49), 32084-32093. DOI: https://doi.org/10.1021/acsomega.0c05146.

(329) Liang, D.; Zhu, X.; Dai, P.; Lu, X.; Guo, H.; Que, H.; Wang, D.; He, T.; Xu, C.; Robin, H. M.; et al. Preparation of a novel lignin-based flame retardant for epoxy resin. *Materials Chemistry and Physics* **2021**, *259*, 124101. DOI: https://doi.org/10.1016/j.matchemphys.2020.124101.

(330) Lu, X.; Guo, H.; Que, H.; Wang, D.; Liang, D.; He, T.; Robin, H. M.; Xu, C.; Zhang, X.; Gu, X. Pyrolysis mechanism and kinetics of high-performance modified lignin-based epoxy resins. *Journal of Analytical and Applied Pyrolysis* **2021**, *154*, 105013. DOI: https://doi.org/10.1016/j.jaap.2020.105013.

(331) Lu, X.; Yu, M.; Wang, D.; Xiu, P.; Xu, C.; Lee, A. F.; Gu, X. Flame-retardant effect of a functional DOPO-based compound on lignin-based epoxy resins. *Materials Today Chemistry* **2021**, *22*, 100562. DOI: https://doi.org/10.1016/j.mtchem.2021.100562.

(332) Palacios-Mateo, C.; van der Meer, Y.; Seide, G. Analysis of the polyester clothing value chain to identify key intervention points for sustainability. *Environmental Sciences Europe* **2021**, *33* (1), 2. DOI: https://doi.org/10.1186/s12302-020-00447-x.

(333) Thomas, J.; Patil, R. The Road to Sustainable Tire Materials: Current State-of-the-Art and Future Prospectives. *Environmental Science & Technology* **2023**, *57* (6), 2209-2216. DOI: https://doi.org/10.1021/acs.est.2c07642.

(334) Thielemans, W.; Wool, R. P. Lignin Esters for Use in Unsaturated Thermosets: Lignin Modification and Solubility Modeling. *Biomacromolecules* **2005**, *6* (4), 1895-1905. DOI: https://doi.org/10.1021/bm0500345.

(335) Månsson, P. Quantitative Determination of Phenolic and Total Hydroxyl Groups in Lignins. **1983**, *37* (3), 143-146. DOI: https://doi.org/10.1515/hfsg.1983.37.3.143.

(336) Shang, X.; Xue, L.; Zhang, Y. Toughness Improvement of Epoxy Composites Using a Kind of Environment-Friendly Bio-Based Polyester Polyol. *Journal of Polymers and the Environment* **2022**, *30* (10), 4492-4499. DOI: https://doi.org/10.1007/s10924-022-02470-w.

(337) Ko, H.-U.; Kim, J. W.; Kim, H. C.; Zhai, L.; Kim, J. Esterified PVA-lignin resin by maleic acid applicable for natural fiber reinforced composites. *Journal of Applied Polymer Science* **2020**, *137* (26), 48836, https://doi.org/10.1002/app.48836. DOI: https://doi.org/10.1002/app.48836 (acccessed 2023/02/17).

(338) Larrañeta, E.; Imízcoz, M.; Toh, J. X.; Irwin, N. J.; Ripolin, A.; Perminova, A.; Domínguez-Robles, J.; Rodríguez, A.; Donnelly, R. F. Synthesis and Characterization of Lignin Hydrogels for Potential Applications as Drug Eluting Antimicrobial Coatings for Medical Materials. *ACS Sustainable Chemistry & Engineering* **2018**, *6* (7), 9037-9046. DOI: https://doi.org/10.1021/acssuschemeng.8b01371.

(339) Young, E. L.; McDonald, A. G. Preparation and Characterization of Biobased Lignin-Co-Polyester/Amide Thermoplastics. *Molecules* **2021**, *26* (9), 2437. DOI: https://doi.org/10.3390/molecules26092437.

(340) Xu, Y.; Odelius, K.; Hakkarainen, M. One-Pot Synthesis of Lignin Thermosets Exhibiting Widely Tunable Mechanical Properties and Shape Memory Behavior. *ACS Sustainable Chemistry & Engineering* **2019**, *7* (15), 13456-13463. DOI: https://doi.org/10.1021/acssuschemeng.9b02921.

(341) Panicker, P. S.; Agumba, D. O.; Kim, J. High-Strength, Multifunctional, and Long Nanocellulose Hybrid Fibers Coated with Esterified Poly(vinyl alcohol)–Citric Acid–Lignin Resin. *ACS Sustainable Chemistry & Engineering* **2022**, *10* (30), 10024-10033. DOI: https://doi.org/10.1021/acssuschemeng.2c02785.

(342) Agumba, D. O.; Kumar, B.; Latif, M.; Panicker, P. S.; Pham, H. D.; Kim, H. C.; Kim, J. High-performance Esterified-Poly (vinyl alcohol)-Citric acid-Lignin resin and its application to Wet-spun nanocellulose Filament-Reinforced polymer composite. *Composites Part A: Applied Science and Manufacturing* **2022**, *153*, 106735. DOI: https://doi.org/10.1016/j.compositesa.2021.106735.

(343) Agumba, D. O.; Panicker, P. S.; Pham, D. H.; Kim, J. Advanced Green Thermoset Resin Tailored for Nanocellulose-Based Filament-Reinforced Polymer Composite and Sustainable Development. *Advanced Sustainable Systems* **2022**, *6* (12), 2200369. DOI: https://doi.org/10.1002/adsu.202200369.

(344) Guo, Z.-X.; Gandini, A. Polyesters from lignin—2. The copolyesterification of kraft lignin and polyethylene glycols with dicarboxylic acid chlorides. *European Polymer Journal* **1991**, *27* (11), 1177-1180. DOI: https://doi.org/10.1016/0014-3057(91)90053-Q.

(345) Guo, Z.-X.; Gandini, A.; Pla, F. Polyesters from lignin. 1. The reaction of kraft lignin with dicarboxylic acid chlorides. *Polymer International* **1992**, *27* (1), 17-22. DOI: https://doi.org/10.1002/pi.4990270104.

(346) Thanh Binh, N. T.; Luong, N. D.; Kim, D. O.; Lee, S. H.; Kim, B. J.; Lee, Y. S.; Nam, J.-D. Synthesis of Lignin-Based Thermoplastic Copolyester Using Kraft Lignin as a Macromonomer. *Composite Interfaces* **2009**, *16* (7-9), 923-935. DOI: https://doi.org/10.1163/092764409X12477479344485.

(347) Luong, N. D.; Binh, N. T. T.; Duong, L. D.; Kim, D. O.; Kim, D.-S.; Lee, S. H.; Kim, B. J.; Lee, Y. S.; Nam, J.-D. An eco-friendly and efficient route of lignin extraction from black liquor and a lignin-based copolyester synthesis. *Polymer Bulletin* **2012**, *68* (3), 879-890. DOI: https://doi.org/10.1007/s00289-011-0658-x.

(348) Kang, Y.; Chen, Z.; Wang, B.; Yang, Y. Synthesis and mechanical properties of thermoplastic films from lignin, sebacic acid and poly(ethylene glycol). *Industrial Crops and Products* **2014**, *56*, 105-112. DOI: https://doi.org/10.1016/j.indcrop.2014.02.027.

(349) Jin, X.; Li, X.; Liu, X.; Du, L.; Su, L.; Ma, Y.; Ren, S. Simple lignin-based, light-driven shape memory polymers with excellent mechanical properties and wide range of glass transition temperatures. *International Journal of Biological Macromolecules* **2023**, *228*, 528-536. DOI: https://doi.org/10.1016/j.ijbiomac.2022.12.098.

(350) Di Francesco, D.; Rigo, D.; Reddy Baddigam, K.; Mathew, A. P.; Hedin, N.; Selva, M.; Samec, J. S. M. A New Family of Renewable Thermosets: Kraft Lignin Poly-adipates. *ChemSusChem* **2022**, *15* (11), e202200326. DOI: https://doi.org/10.1002/cssc.202200326.

(351) Gordobil, O.; Robles, E.; Egüés, I.; Labidi, J. Lignin-ester derivatives as novel thermoplastic materials. *RSC Advances* **2016**, *6* (90), 86909-86917. DOI: http://dx.doi.org/10.1039/C6RA20238A.

(352) Wang, H.-M.; Wang, B.; Yuan, T.-Q.; Zheng, L.; Shi, Q.; Wang, S.-F.; Song, G.-Y.; Sun, R.-C. Tunable, UV-shielding and biodegradable composites based on well-characterized lignins and poly(butylene adipate-co-terephthalate). *Green Chemistry* **2020**, *22* (24), 8623-8632. DOI: http://dx.doi.org/10.1039/D0GC03284K.

(353) Sivasankarapillai, G.; McDonald, A. G. Synthesis and properties of lignin-highly branched poly (ester-amine) polymeric systems. *Biomass and Bioenergy* **2011**, *35* (2), 919-931. DOI: https://doi.org/10.1016/j.biombioe.2010.11.002.

(354) Li, H.; Sivasankarapillai, G.; McDonald, A. G. Lignin valorization by forming toughened thermally stimulated shape memory copolymeric elastomers: Evaluation of different fractionated industrial lignins. *Journal of Applied Polymer Science* **2015**, *132* (5). DOI: https://doi.org/10.1002/app.41389.

(355) Scarica, C.; Suriano, R.; Levi, M.; Turri, S.; Griffini, G. Lignin Functionalized with Succinic Anhydride as Building Block for Biobased Thermosetting Polyester Coatings. *ACS Sustainable Chemistry & Engineering* **2018**, *6* (3), 3392-3401. DOI: https://doi.org/10.1021/acssuschemeng.7b03583.

(356) Xu, Y.; Odelius, K.; Hakkarainen, M. Recyclable and Flexible Polyester Thermosets Derived from Microwave-Processed Lignin. *ACS Applied Polymer Materials* **2020**, *2* (5), 1917-1924. DOI: https://doi.org/10.1021/acsapm.0c00130.

(357) Kim, S.; Chung, H. Convenient Cross-Linking Control of Lignin-Based Polymers Influencing Structure–Property Relationships. *ACS Sustainable Chemistry & Engineering* **2023**, *11* (5), 1709-1719. DOI: https://doi.org/10.1021/acssuschemeng.2c05651.

(358) Kim, S.; Chung, H. Synthesis and Characterization of Lignin-graft-poly(ethylene brassylate): a Biomass-Based Polyester with High Mechanical Properties. *ACS Sustainable Chemistry & Engineering* **2021**, *9* (44), 14766-14776. DOI: https://doi.org/10.1021/acssuschemeng.1c04334.

(359) Lee, Y.; Park, C.-H.; Lee, E. Y. Chemical Modification of Methanol-Insoluble Kraft Lignin Using Oxypropylation Under Mild Conditions for the Preparation of Bio-Polyester. *Journal of Wood Chemistry and Technology* **2017**, *37* (5), 334-342. DOI: https://doi.org/10.1080/02773813.2017.1303512.

(360) Liu, L.-Y.; Cho, M.; Sathitsuksanoh, N.; Chowdhury, S.; Renneckar, S. Uniform Chemical Functionality of Technical Lignin Using Ethylene Carbonate for Hydroxyethylation and Subsequent Greener Esterification. *ACS Sustainable Chemistry & Engineering* **2018**, *6* (9), 12251-12260. DOI: https://doi.org/10.1021/acssuschemeng.8b02649.

(361) Liu, L.-Y.; Chen, S.; Ji, L.; Jang, S.-K.; Renneckar, S. One-pot route to convert technical lignin into versatile lignin esters for tailored bioplastics and sustainable materials. *Green Chemistry* **2021**, *23* (12), 4567-4579. DOI: http://dx.doi.org/10.1039/D1GC01033F.

(362) Ganewatta, M. S.; Lokupitiya, H. N.; Tang, C. Lignin Biopolymers in the Age of Controlled Polymerization. *Polymers* **2019**, *11* (7), 1176. DOI: https://doi.org/10.3390/polym11071176.

(363) Liu, P.; Zhang, N.; Yi, Y.; Gibril, M. E.; Wang, S.; Kong, F. Effect of lignin-based monomer on controlling the molecular weight and physical properties of the polyacrylonitrile/lignin copolymer. *International Journal of Biological Macromolecules* **2020**, *164*, 2312-2322. DOI: https://doi.org/10.1016/j.ijbiomac.2020.08.119.

(364) Fang, R.; Cheng, X. S.; Lin, W. S. Preparation and application of dimer acid/lignin graft copolymer. *BioResources* **2011**, *6*, 2874-2884. DOI: https://dx.doi.org/10.15376/biores.6.3.2874-2884.

(365) Ghavidel, N.; Fatehi, P. Synergistic effect of lignin incorporation into polystyrene for producing sustainable superadsorbent. *RSC Advances* **2019**, *9* (31), 17639-17652. DOI: http://dx.doi.org/10.1039/C9RA02526J.

(366) Liang, L.; Ibrahim, M. N. M. Preparation of Lignin Graft Copolymer as a Fluid Loss Additive for Water-based Mud. 2013.

(367) Ghosh, T.; Elo, T.; Parihar, V. S.; Maiti, P.; Layek, R. Poly (itaconic acid) functionalized lignin/polyvinyl acetate composite resin with improved sustainability and wood adhesion strength. *Industrial Crops and Products* **2022**, *187*, 115299. DOI: https://doi.org/10.1016/j.indcrop.2022.115299.

(368) Mohamad Ibrahim, M. N.; Ahmed-Haras, M. R.; Sipaut, C. S.; Aboul-Enein, H. Y.; Mohamed, A. A. Preparation and characterization of a newly water soluble lignin graft copolymer from oil palm lignocellulosic waste. *Carbohydrate Polymers* **2010**, *80* (4), 1102-1110. DOI: https://doi.org/10.1016/j.carbpol.2010.01.030.

(369) Wang, X.; Li, X.; Peng, L.; Han, S.; Hao, C.; Jiang, C.; Wang, H.; Fan, X. Effective removal of heavy metals from water using porous lignin-based adsorbents. *Chemosphere* **2021**, *279*, 130504. DOI: https://doi.org/10.1016/j.chemosphere.2021.130504.

(370) Hua, Q.; Liu, L.-Y.; Cho, M.; Karaaslan, M. A.; Zhang, H.; Kim, C. S.; Renneckar, S. Functional Lignin Building Blocks: Reactive Vinyl Esters with Acrylic Acid. *Biomacromolecules* **2023**, *24* (2), 592-603. DOI: https://doi.org/10.1021/acs.biomac.2c00806.

(371) Gan, M.; Pan, J.; Zhang, Y.; Dai, X.; Yin, Y.; Qu, Q.; Yan, Y. Molecularly imprinted polymers derived from lignin-based Pickering emulsions and their selectively adsorption of lambda-cyhalothrin. *Chemical Engineering Journal* **2014**, *257*, 317-327. DOI: https://doi.org/10.1016/j.cej.2014.06.110.

(372) Liu, X.; Wang, J.; Li, S.; Zhuang, X.; Xu, Y.; Wang, C.; Chu, F. Preparation and properties of UV-absorbent lignin graft copolymer films from lignocellulosic butanol residue. *Industrial Crops and Products* **2014**, *52*, 633-641. DOI: https://doi.org/10.1016/j.indcrop.2013.11.036.

(373) Yang, W.; Rallini, M.; Wang, D.-Y.; Gao, D.; Dominici, F.; Torre, L.; Kenny, J. M.; Puglia, D. Role of lignin nanoparticles in UV resistance, thermal and mechanical performance of PMMA nanocomposites prepared by a combined free-radical graft polymerization/masterbatch procedure. *Composites Part A: Applied Science and Manufacturing* **2018**, *107*, 61-69. DOI: https://doi.org/10.1016/j.compositesa.2017.12.030.

(374) Goliszek, M.; Podkościelna, B.; Sevastyanova, O.; Fila, K.; Chabros, A.; Pączkowski, P. Investigation of accelerated aging of lignin-containing polymer materials. *International Journal of Biological Macromolecules* **2019**, *123*, 910-922. DOI: https://doi.org/10.1016/j.ijbiomac.2018.11.141.

(375) Mai, C.; Milstein, O.; Hüttermann, A. Chemoenzymatical grafting of acrylamide onto lignin. *Journal of Biotechnology* **2000**, *79* (2), 173-183. DOI: https://doi.org/10.1016/S0168-1656(00)00230-3.

(376) Hasan, A.; Fatehi, P. Stability of kaolin dispersion in the presence of lignin-acrylamide polymer. *Applied Clay Science* **2018**, *158*, 72-82. DOI: https://doi.org/10.1016/j.clay.2018.02.048.

(377) Migliore, N.; Zijlstra, D. S.; Van Kooten, T. G.; Deuss, P. J.; Raffa, P. Amphiphilic Copolymers Derived from Butanosolv Lignin and Acrylamide: Synthesis, Properties in Water Solution, and Potential Applications. *ACS Applied Polymer Materials* **2020**, *2* (12), 5705-5715. DOI: https://doi.org/10.1021/acsapm.0c01006.

(378) Ma, Y.; Lv, L.; Guo, Y.; Fu, Y.; Shao, Q.; Wu, T.; Guo, S.; Sun, K.; Guo, X.; Wujcik, E. K.; et al. Porous lignin based poly (acrylic acid)/organo-montmorillonite nanocomposites: Swelling behaviors and rapid removal of Pb (II) ions. *Polymer* **2017**, *128*, 12-23. DOI: https://doi.org/10.1016/j.polymer.2017.09.009.

(379) Zerpa, A.; Pakzad, L.; Fatehi, P. Hardwood Kraft Lignin-Based Hydrogels: Production and Performance. *ACS Omega* **2018**, *3* (7), 8233-8242. DOI: https://doi.org/10.1021/acsomega.8b01176.

(380) Sun, Y.; Ma, Z.; Xu, X.; Liu, X.; Liu, L.; Huang, G.; Liu, L.; Wang, H.; Song, P. Grafting Lignin with Bioderived Polyacrylates for Low-Cost, Ductile, and Fully Biobased Poly(lactic acid) Composites. *ACS Sustainable Chemistry & Engineering* **2020**, *8* (5), 2267-2276. DOI: https://doi.org/10.1021/acssuschemeng.9b06593.

(381) Hajirahimkhan, S.; Xu, C. C.; Ragogna, P. J. Ultraviolet Curable Coatings of Modified Lignin. *ACS Sustainable Chemistry & Engineering* **2018**, *6* (11), 14685-14694. DOI: https://doi.org/10.1021/acssuschemeng.8b03252.

(382) Sutton, J. T.; Rajan, K.; Harper, D. P.; Chmely, S. C. Lignin-Containing Photoactive Resins for 3D Printing by Stereolithography. *ACS Applied Materials & Interfaces* **2018**, *10* (42), 36456-36463. DOI: https://doi.org/10.1021/acsami.8b13031.

(383) Rajan, K.; Mann, J. K.; English, E.; Harper, D. P.; Carrier, D. J.; Rials, T. G.; Labbé, N.; Chmely, S. C. Sustainable Hydrogels Based on Lignin-Methacrylate Copolymers with Enhanced Water Retention and Tunable Material Properties. *Biomacromolecules* **2018**, *19* (7), 2665-2672. DOI: https://doi.org/10.1021/acs.biomac.8b00282.

(384) Kim, Y. S.; Kadla, J. F. Preparation of a Thermoresponsive Lignin-Based Biomaterial through Atom Transfer Radical Polymerization. *Biomacromolecules* **2010**, *11* (4), 981-988. DOI: https://doi.org/10.1021/bm901455p.

(385) Gao, G.; Karaaslan, M. A.; Kadla, J. F.; Ko, F. Enzymatic synthesis of ionic responsive lignin nanofibres through surface poly(N-isopropylacrylamide) immobilization. *Green Chemistry* **2014**, *16* (8), 3890-3898. DOI: http://dx.doi.org/10.1039/C4GC00757C.

(386) Dai, L.; Li, Y.; Kong, F.; Liu, K.; Si, C.; Ni, Y. Lignin-Based Nanoparticles Stabilized Pickering Emulsion for Stability Improvement and Thermal-Controlled Release of trans-Resveratrol. *ACS Sustainable Chemistry & Engineering* **2019**, *7* (15), 13497-13504. DOI: https://doi.org/10.1021/acssuschemeng.9b02966.

(387) Zaborniak, I.; Macior, A.; Chmielarz, P.; Caceres Najarro, M.; Iruthayaraj, J. Lignin-based thermoresponsive macromolecules via vitamin-induced metal-free ATRP. *Polymer* **2021**, *219*, 123537. DOI: https://doi.org/10.1016/j.polymer.2021.123537.

(388) Liu, R.; Ding, T.; Deng, P.; Yan, X.; Xiong, F.; Chen, J.; Wu, Z. Preparation of LCST regulable DES-lignin-g-PNVCL thermo-responsive polymer by ARGET-ATRP. *International Journal of Biological Macromolecules* **2022**, *194*, 358-365. DOI: https://doi.org/10.1016/j.ijbiomac.2021.11.077.

(389) Huang, W.; Wu, M.; Liu, W.; Hua, Z.; Wang, Z.; Zhou, L. Value-adding of organosolv lignin: Designing mechanically robust UV-resistant polymeric glass via ARGET ATRP. *Applied Surface Science* **2019**, *475*, 302-311. DOI: https://doi.org/10.1016/j.apsusc.2018.12.266.

(390) Kai, D.; Jiang, S.; Low, Z. W.; Loh, X. J. Engineering highly stretchable lignin-based electrospun nanofibers for potential biomedical applications. *Journal of Materials Chemistry B* **2015**, *3* (30), 6194-6204. DOI: http://dx.doi.org/10.1039/C5TB00765H.

(391) Cho, Y.-M.; Kim, J.-H.; Choi, J.-H.; Kim, J.-C.; Cho, S.-M.; Park, S.-W.; Kwak, H. W.; Choi, I.-G. Physicochemical characteristics of lignin-g-PMMA/PLA blend via atom transfer radical polymerization depending on the structural difference of organosolv lignin. *International Journal of Biological Macromolecules* **2023**, *226*, 279-290. DOI: https://doi.org/10.1016/j.ijbiomac.2022.11.316.

(392) Qian, Y.; Zhang, Q.; Qiu, X.; Zhu, S. CO2-responsive diethylaminoethyl-modified lignin nanoparticles and their application as surfactants for CO2/N2-switchable Pickering emulsions. *Green Chemistry* **2014**, *16* (12), 4963-4968. DOI: http://dx.doi.org/10.1039/C4GC01242A.

(393) Liu, X.; Yin, H.; Zhang, Z.; Diao, B.; Li, J. Functionalization of lignin through ATRP grafting of poly(2-dimethylaminoethyl methacrylate) for gene delivery. *Colloids and Surfaces B: Biointerfaces* **2015**, *125*, 230-237. DOI: https://doi.org/10.1016/j.colsurfb.2014.11.018.

(394) Wang, J.; Yao, K.; Korich, A. L.; Li, S.; Ma, S.; Ploehn, H. J.; Iovine, P. M.; Wang, C.; Chu, F.; Tang, C. Combining renewable gum rosin and lignin: Towards hydrophobic polymer composites by controlled polymerization. *Journal of Polymer Science Part A: Polymer Chemistry* **2011**, *49* (17), 3728-3738. DOI: https://doi.org/10.1002/pola.24809.

(395) Jeong, D.; Shim, J.; Shin, H.; Lee, J.-C. Sustainable Lignin-Derived Cross-Linked Graft Polymers as Electrolyte and Binder Materials for Lithium Metal Batteries. *ChemSusChem* **2020**, *13* (10), 2642-2649. DOI: https://doi.org/10.1002/cssc.201903466.

(396) Wu, Y.; Qian, Y.; Zhang, A.; Lou, H.; Yang, D.; Qiu, X. Light Color Dihydroxybenzophenone Grafted Lignin with High UVA/UVB Absorbance Ratio for Efficient and Safe Natural Sunscreen. *Industrial & Engineering Chemistry Research* **2020**, *59* (39), 17057-17068. DOI: https://doi.org/10.1021/acs.iecr.9b06970.

(397) Gao, G.; Dallmeyer, J. I.; Kadla, J. F. Synthesis of Lignin Nanofibers with Ionic-Responsive Shells: Water-Expandable Lignin-Based Nanofibrous Mats. *Biomacromolecules* **2012**, *13* (11), 3602-3610. DOI: https://doi.org/10.1021/bm301039f.

(398) Hilburg, S. L.; Elder, A. N.; Chung, H.; Ferebee, R. L.; Bockstaller, M. R.; Washburn, N. R. A universal route towards thermoplastic lignin composites with improved mechanical properties. *Polymer* **2014**, *55* (4), 995-1003. DOI: https://doi.org/10.1016/j.polymer.2013.12.070.

(399) Gupta, C.; Washburn, N. R. Polymer-Grafted Lignin Surfactants Prepared via Reversible Addition–Fragmentation Chain-Transfer Polymerization. *Langmuir* **2014**, *30* (31), 9303-9312. DOI: https://doi.org/10.1021/la501696y.

(400) Gupta, C.; Sverdlove, M. J.; Washburn, N. R. Molecular architecture requirements for polymer-grafted lignin superplasticizers. *Soft Matter* **2015**, *11* (13), 2691-2699. DOI: http://dx.doi.org/10.1039/C4SM02675F.

(401) Silmore, K. S.; Gupta, C.; Washburn, N. R. Tunable Pickering emulsions with polymer-grafted lignin nanoparticles (PGLNs). *Journal of Colloid and Interface Science* **2016**, *466*, 91-100. DOI: https://doi.org/10.1016/j.jcis.2015.11.042.

(402) Liu, Z.; Lu, X.; Xie, J.; Feng, B.; Han, Q. Synthesis of a novel tunable lignin-based star copolymer and its flocculation performance in the treatment of kaolin suspension. *Separation and Purification Technology* **2019**, *210*, 355-363. DOI: https://doi.org/10.1016/j.seppur.2018.08.025.

(403) Xu, Y.; Yuan, L.; Wang, Z.; Wilbon, P. A.; Wang, C.; Chu, F.; Tang, C. Lignin and soy oil-derived polymeric biocomposites by "grafting from" RAFT polymerization. *Green Chemistry* **2016**, *18* (18), 4974-4981. DOI: http://dx.doi.org/10.1039/C6GC00859C.

(404) Wang, W.; Wang, F.; Zhang, C.; Tang, J.; Zeng, X.; Wan, X. Versatile value-added application of hyperbranched lignin derivatives: Water-resistance adhesive, UV protection coating, self-healing and skin-adhesive sensing. *Chemical Engineering Journal* **2021**, *404*, 126358. DOI: https://doi.org/10.1016/j.cej.2020.126358.

(405) Dizhbite, T.; Telysheva, G.; Jurkjane, V.; Viesturs, U. Characterization of the radical scavenging activity of lignins—natural antioxidants. *Bioresource Technology* **2004**, *95* (3), 309-317. DOI: https://doi.org/10.1016/j.biortech.2004.02.024.

(406) Qu, W.; Huang, Y.; Luo, Y.; Kalluru, S.; Cochran, E.; Forrester, M.; Bai, X. Controlled Radical Polymerization of Crude Lignin Bio-oil Containing Multihydroxyl Molecules for Methacrylate Polymers and the Potential Applications. *ACS Sustainable Chemistry & Engineering* **2019**, *7* (9), 9050-9060. DOI: https://doi.org/10.1021/acssuschemeng.9b01597.

(407) Nuyken, O.; Pask, S. D. Ring-Opening Polymerization—An Introductory Review. *Polymers* **2013**, *5* (2), 361-403. DOI: https://doi.org/10.3390/polym5020361.

(408) Schmidt, B. V. K. J.; Molinari, V.; Esposito, D.; Tauer, K.; Antonietti, M. Lignin-based polymeric surfactants for emulsion polymerization. *Polymer* **2017**, *112*, 418-426. DOI: https://doi.org/10.1016/j.polymer.2017.02.036.

(409) Nemoto, T.; Konishi, G.-i.; Tojo, Y.; An, Y. C.; Funaoka, M. Functionalization of lignin: Synthesis of lignophenol-graft-poly(2-ethyl-2-oxazoline) and its application to polymer blends with commodity polymers. *Journal of Applied Polymer Science* **2012**, *123* (5), 2636-2642. DOI: https://doi.org/10.1002/app.34623.

(410) Mahata, D.; Jana, M.; Jana, A.; Mukherjee, A.; Mondal, N.; Saha, T.; Sen, S.; Nando, G. B.; Mukhopadhyay, C. K.; Chakraborty, R.; et al. Lignin-graft-Polyoxazoline Conjugated Triazole a Novel Anti-Infective Ointment to Control Persistent Inflammation. *Scientific Reports* **2017**, *7* (1), 46412. DOI: https://doi.org/10.1038/srep46412.

(411) Chung, Y.-L.; Olsson, J. V.; Li, R. J.; Frank, C. W.; Waymouth, R. M.; Billington, S. L.; Sattely, E. S. A Renewable Lignin–Lactide Copolymer and Application in Biobased Composites. *ACS Sustainable Chemistry & Engineering* **2013**, *1* (10), 1231-1238. DOI: https://doi.org/10.1021/sc4000835.

(412) Ren, W.; Pan, X.; Wang, G.; Cheng, W.; Liu, Y. Dodecylated lignin-g-PLA for effective toughening of PLA. *Green Chemistry* **2016**, *18* (18), 5008-5014. DOI: http://dx.doi.org/10.1039/C6GC01341D.

(413) Liu, R.; Dai, L.; Hu, L.-Q.; Zhou, W.-Q.; Si, C.-L. Fabrication of high-performance poly(l-lactic acid)/lignin-graft-poly(d-lactic acid) stereocomplex films. *Materials Science and Engineering: C* **2017**, *80*, 397-403. DOI: https://doi.org/10.1016/j.msec.2017.06.006.

(414) Boarino, A.; Schreier, A.; Leterrier, Y.; Klok, H.-A. Uniformly Dispersed Poly(lactic acid)-Grafted Lignin Nanoparticles Enhance Antioxidant Activity and UV-Barrier Properties of Poly(lactic acid) Packaging Films. *ACS Applied Polymer Materials* **2022**, *4* (7), 4808-4817. DOI: https://doi.org/10.1021/acsapm.2c00420.

(415) Kai, D.; Ren, W.; Tian, L.; Chee, P. L.; Liu, Y.; Ramakrishna, S.; Loh, X. J. Engineering Poly(lactide)–Lignin Nanofibers with Antioxidant Activity for Biomedical Application. *ACS Sustainable Chemistry & Engineering* **2016**, *4* (10), 5268-5276. DOI: https://doi.org/10.1021/acssuschemeng.6b00478.

(416) Dai, L.; Liu, R.; Si, C. A novel functional lignin-based filler for pyrolysis and feedstock recycling of poly(l-lactide). *Green Chemistry* **2018**, *20* (8), 1777-1783. DOI: http://dx.doi.org/10.1039/C7GC03863A.

(417) Dai, L.; Cao, Q.; Wang, K.; Han, S.; Si, C.; Liu, D.; Liu, Y. High efficient recovery of L-lactide with lignin-based filler by thermal degradation. *Industrial Crops and Products* **2020**, *143*, 111954. DOI: https://doi.org/10.1016/j.indcrop.2019.111954.

(418) de Oliveira, W.; Glasser, W. G. Multiphase materials with lignin. 11. Starlike copolymers with caprolactone. *Macromolecules* **1994**, *27* (1), 5-11. DOI: https://doi.org/10.1021/ma00079a002.

(419) Laurichesse, S.; Avérous, L. Synthesis, thermal properties, rheological and mechanical behaviors of lignins-grafted-poly(ε-caprolactone). *Polymer* **2013**, *54* (15), 3882-3890. DOI: https://doi.org/10.1016/j.polymer.2013.05.054.

(420) Pérez–Camargo, R. A.; Saenz, G.; Laurichesse, S.; Casas, M. T.; Puiggalí, J.; Avérous, L.; Müller, A. J. Nucleation, Crystallization, and Thermal Fractionation of Poly (ε-Caprolactone)-Grafted-Lignin: Effects of Grafted Chains Length and Lignin Content. *Journal of Polymer Science Part B: Polymer Physics* **2015**, *53* (24), 1736-1750. DOI: https://doi.org/10.1002/polb.23897.

(421) Li, M.; Pu, Y.; Chen, F.; Ragauskas, A. J. Synthesis and Characterization of Lignin-grafted-poly(ε-caprolactone) from Different Biomass Sources. *New Biotechnology* **2021**, *60*, 189-199. DOI: https://doi.org/10.1016/j.nbt.2020.10.005.

(422) Xie, D.; Pu, Y.; Meng, X.; Bryant, N. D.; Zhang, K.; Wang, W.; Ragauskas, A. J.; Li, M. Effect of the Lignin Structure on the Physicochemical Properties of Lignin-Grafted-Poly(ε-caprolactone) and Its Application for Water/Oil Separation. *ACS Sustainable Chemistry & Engineering* **2022**, *10* (50), 16882-16895. DOI: https://doi.org/10.1021/acssuschemeng.2c05495.

(423) Abdollahi, M.; Bairami Habashi, R.; Mohsenpour, M. Poly(ε-caprolactone) chains grafted from lignin, hydroxymethylated lignin and silica/lignin hybrid macroinitiators: Synthesis and characterization of lignin- based thermoplastic copolymers. *Industrial Crops and Products* **2019**, *130*, 547-557. DOI: https://doi.org/10.1016/j.indcrop.2019.01.012.

(424) Liu, X.; Zong, E.; Jiang, J.; Fu, S.; Wang, J.; Xu, B.; Li, W.; Lin, X.; Xu, Y.; Wang, C.; et al. Preparation and characterization of Lignin-graft-poly (ε-caprolactone) copolymers based on lignocellulosic butanol residue. *International Journal of Biological Macromolecules* **2015**, *81*, 521-529. DOI: https://doi.org/10.1016/j.ijbiomac.2015.08.046.

(425) Sun, Y.; Yang, L.; Lu, X.; He, C. Biodegradable and renewable poly(lactide)–lignin composites: synthesis, interface and toughening mechanism. *Journal of Materials Chemistry A* **2015**, *3* (7), 3699-3709. DOI: http://dx.doi.org/10.1039/C4TA05991C.

(426) Kai, D.; Zhang, K.; Jiang, L.; Wong, H. Z.; Li, Z.; Zhang, Z.; Loh, X. J. Sustainable and Antioxidant Lignin–Polyester Copolymers and Nanofibers for Potential Healthcare Applications. *ACS Sustainable Chemistry & Engineering* **2017**, *5* (7), 6016-6025. DOI: https://doi.org/10.1021/acssuschemeng.7b00850.

(427) Yang, W.; Zhu, Y.; He, Y.; Xiao, L.; Xu, P.; Puglia, D.; Ma, P. Preparation of toughened poly(lactic acid)-poly(ε-caprolactone)-lignin nanocomposites with good heat- and UV-resistance. *Industrial Crops and Products* **2022**, *183*, 114965. DOI: https://doi.org/10.1016/j.indcrop.2022.114965.

(428) Madhavan Nampoothiri, K.; Nair, N. R.; John, R. P. An overview of the recent developments in polylactide (PLA) research. *Bioresource Technology* **2010**, *101* (22), 8493-8501. DOI: https://doi.org/10.1016/j.biortech.2010.05.092.

(429) Zhou, S.-J.; Wang, H.-M.; Xiong, S.-J.; Sun, J.-M.; Wang, Y.-Y.; Yu, S.; Sun, Z.; Wen, J.-L.; Yuan, T.-Q. Technical Lignin Valorization in Biodegradable Polyester-Based Plastics (BPPs). *ACS Sustainable Chemistry & Engineering* **2021**, *9* (36), 12017-12042. DOI: https://doi.org/10.1021/acssuschemeng.1c03705.

(430) Park, S. Y.; Kim, J.-Y.; Youn, H. J.; Choi, J. W. Utilization of lignin fractions in UV resistant lignin-PLA biocomposites via lignin-lactide grafting. *International Journal of Biological Macromolecules* **2019**, *138*, 1029-1034. DOI: https://doi.org/10.1016/j.ijbiomac.2019.07.157.

(431) Yang, W.; Weng, Y.; Puglia, D.; Qi, G.; Dong, W.; Kenny, J. M.; Ma, P. Poly(lactic acid)/lignin films with enhanced toughness and anti-oxidation performance for active food packaging. *International Journal of Biological Macromolecules* **2020**, *144*, 102-110. DOI: https://doi.org/10.1016/j.ijbiomac.2019.12.085.

(432) Kai, D.; Chong, H. M.; Chow, L. P.; Jiang, L.; Lin, Q.; Zhang, K.; Zhang, H.; Zhang, Z.; Loh, X. J. Strong and biocompatible lignin /poly (3-hydroxybutyrate) composite nanofibers. *Composites Science and Technology* **2018**, *158*, 26-33. DOI: https://doi.org/10.1016/j.compscitech.2018.01.046.

(433) Kai, D.; Zhang, K.; Liow, S. S.; Loh, X. J. New Dual Functional PHB-Grafted Lignin Copolymer: Synthesis, Mechanical Properties, and Biocompatibility Studies. *ACS Applied Bio Materials* **2019**, *2* (1), 127-134. DOI: https://doi.org/10.1021/acsabm.8b00445.

(434) Lin, X.; Zhou, M.; Wang, S.; Lou, H.; Yang, D.; Qiu, X. Synthesis, Structure, and Dispersion Property of a Novel Lignin-Based Polyoxyethylene Ether from Kraft Lignin and Poly(ethylene glycol). *ACS Sustainable Chemistry & Engineering* **2014**, *2* (7), 1902-1909. DOI: https://doi.org/10.1021/sc500241g.

(435) Chen, N.; Liu, W.; Huang, J.; Qiu, X. Preparation of octopus-like lignin-grafted cationic polyacrylamide flocculant and its application for water flocculation. *International Journal of Biological Macromolecules* **2020**, *146*, 9-17. DOI: https://doi.org/10.1016/j.ijbiomac.2019.12.245.

(436) Chile, L.-E.; Kaser, S. J.; Hatzikiriakos, S. G.; Mehrkhodavandi, P. Synthesis and Thermorheological Analysis of Biobased Lignin-graft-poly(lactide) Copolymers and Their Blends. *ACS Sustainable Chemistry & Engineering* **2018**, *6* (2), 1650-1661. DOI: https://doi.org/10.1021/acssuschemeng.7b02866.

(437) Kai, D.; Low, Z. W.; Liow, S. S.; Abdul Karim, A.; Ye, H.; Jin, G.; Li, K.; Loh, X. J. Development of Lignin Supramolecular Hydrogels with Mechanically Responsive and Self-Healing Properties. *ACS Sustainable Chemistry & Engineering* **2015**, *3* (9), 2160-2169. DOI: https://doi.org/10.1021/acssuschemeng.5b00405.

(438) Kai, D.; Chua, Y. K.; Jiang, L.; Owh, C.; Chan, S. Y.; Loh, X. J. Dual functional anti-oxidant and SPF enhancing lignin-based copolymers as additives for personal and healthcare products. *RSC Advances* **2016**, *6* (89), 86420-86427. DOI: http://dx.doi.org/10.1039/C6RA21433A.

(439) Bao, X.; Yu, Y.; Wang, Q.; Wang, P.; Yuan, J. "Graft to" Modification of Lignin by the Combination of Enzyme-Initiated Reversible Addition–Fragmentation Chain Transfer and Grafting. *ACS Sustainable Chemistry & Engineering* **2019**, *7* (15), 12973-12980. DOI: https://doi.org/10.1021/acssuschemeng.9b02028.

(440) Bao, X.; Fan, X.; Yu, Y.; Wang, Q.; Wang, P.; Yuan, J. Graft modification of lignin-based cellulose via enzyme-initiated reversible addition-fragmentation chain transfer (RAFT) polymerization and free-radical coupling. *International Journal of Biological Macromolecules* **2020**, *144*, 267-278. DOI: https://doi.org/10.1016/j.ijbiomac.2019.12.078.

(441) Luo, S.; Cao, J.; McDonald, A. G. Interfacial Improvements in a Green Biopolymer Alloy of Poly(3-hydroxybutyrate-co-3-hydroxyvalerate) and Lignin via in Situ Reactive Extrusion. *ACS Sustainable Chemistry & Engineering* **2016**, *4* (6), 3465-3476. DOI: https://doi.org/10.1021/acssuschemeng.6b00495.

(442) Barner-Kowollik, C.; Du Prez, F. E.; Espeel, P.; Hawker, C. J.; Junkers, T.; Schlaad, H.; Van Camp, W. "Clicking" Polymers or Just Efficient Linking: What Is the Difference? *Angewandte Chemie International Edition* **2011**, *50* (1), 60-62. DOI: https://doi.org/10.1002/anie.201003707.

(443) Han, Y.; Yuan, L.; Li, G.; Huang, L.; Qin, T.; Chu, F.; Tang, C. Renewable polymers from lignin via copper-free thermal click chemistry. *Polymer* **2016**, *83*, 92-100. DOI: https://doi.org/10.1016/j.polymer.2015.12.010.

(444) Liu, H.; Chung, H. Self-Healing Properties of Lignin-Containing Nanocomposite: Synthesis of Lignin-graft-poly(5-acetylaminopentyl acrylate) via RAFT and Click Chemistry. *Macromolecules* **2016**, *49* (19), 7246-7256. DOI: https://doi.org/10.1021/acs.macromol.6b01028.

(445) Yuan, L.; Zhang, Y.; Wang, Z.; Han, Y.; Tang, C. Plant Oil and Lignin-Derived Elastomers via Thermal Azide–Alkyne Cycloaddition Click Chemistry. *ACS Sustainable Chemistry & Engineering* **2019**, *7* (2), 2593-2601. DOI: https://doi.org/10.1021/acssuschemeng.8b05617.

(446) Jang, M.; Shin, H. Y.; Jang, D.; Jo, S. M.; Kim, S.; Kim, S.-S. All-Lignin-Based Thermoset Foams via Azide–Alkyne Cycloaddition and Their Fire Resistance after Oxidation. *ACS Applied Polymer Materials* **2022**, *4* (4), 2712-2723. DOI: https://doi.org/10.1021/acsapm.2c00034.

(447) Nair, D. P.; Podgórski, M.; Chatani, S.; Gong, T.; Xi, W.; Fenoli, C. R.; Bowman, C. N. The Thiol-Michael Addition Click Reaction: A Powerful and Widely Used Tool in Materials Chemistry. *Chemistry of Materials* **2014**, *26* (1), 724-744. DOI: https://doi.org/10.1021/cm402180t.

(448) Jawerth, M.; Johansson, M.; Lundmark, S.; Gioia, C.; Lawoko, M. Renewable Thiol–Ene Thermosets Based on Refined and Selectively Allylated Industrial Lignin. *ACS Sustainable Chemistry & Engineering* **2017**, *5* (11), 10918-10925. DOI: https://doi.org/10.1021/acssuschemeng.7b02822.

(449) Jawerth, M. E.; Brett, C. J.; Terrier, C.; Larsson, P. T.; Lawoko, M.; Roth, S. V.; Lundmark, S.; Johansson, M. Mechanical and Morphological Properties of Lignin-Based Thermosets. *ACS Applied Polymer Materials* **2020**, *2* (2), 668-676. DOI: https://doi.org/10.1021/acsapm.9b01007.

(450) Ribca, I.; Jawerth, M. E.; Brett, C. J.; Lawoko, M.; Schwartzkopf, M.; Chumakov, A.; Roth, S. V.; Johansson, M. Exploring the Effects of Different Cross-Linkers on Lignin-Based Thermoset Properties and Morphologies. *ACS Sustainable Chemistry & Engineering* **2021**, *9* (4), 1692-1702. DOI: https://doi.org/10.1021/acssuschemeng.0c07580.

(451) Cao, Y.; Liu, Z.; Zheng, B.; Ou, R.; Fan, Q.; Li, L.; Guo, C.; Liu, T.; Wang, Q. Synthesis of lignin-based polyols via thiol-ene chemistry for high-performance polyurethane anticorrosive coating. *Composites Part B: Engineering* **2020**, *200*, 108295. DOI: https://doi.org/10.1016/j.compositesb.2020.108295.

(452) Liu, H.; Chung, H. Visible-Light Induced Thiol–Ene Reaction on Natural Lignin. *ACS Sustainable Chemistry & Engineering* **2017**, *5* (10), 9160-9168. DOI: https://doi.org/10.1021/acssuschemeng.7b02065.

(453) Yang, Z.; Zhou, Z.; Li, Y.; Zhu, L.; Chen, J.; Cheng, J.; Su, J.; Zhuang, Z.; Ning, Z.; Yu, Q.; et al. Assessing the Potential of New Lignin-Based pH-Responsive Nanoparticles as Drug Carriers for Cancer Treatment. *ACS Sustainable Chemistry & Engineering* **2022**, *10* (32), 10590-10603. DOI: https://doi.org/10.1021/acssuschemeng.2c02209.

(454) Jin, C.; Zhang, X.; Xin, J.; Liu, G.; Chen, J.; Wu, G.; Liu, T.; Zhang, J.; Kong, Z. Thiol–Ene Synthesis of Cysteine-Functionalized Lignin for the Enhanced Adsorption of Cu(II) and Pb(II). *Industrial & Engineering Chemistry Research* **2018**, *57* (23), 7872-7880. DOI: https://doi.org/10.1021/acs.iecr.8b00823.

(455) Jin, C.; Zhang, X.; Xin, J.; Liu, G.; Wu, G.; Kong, Z.; Zhang, J. Clickable Synthesis of 1,2,4-Triazole Modified Lignin-Based Adsorbent for the Selective Removal of Cd(II). *ACS Sustainable Chemistry & Engineering* **2017**, *5* (5), 4086-4093. DOI: https://doi.org/10.1021/acssuschemeng.7b00072.

(456) Jedrzejczyk, M. A.; Kouris, P. D.; Boot, M. D.; Hensen, E. J. M.; Bernaerts, K. V. Renewable Thiol–yne "Click" Networks Based on Propargylated Lignin for Adhesive Resin Applications. *ACS Applied Polymer Materials* **2022**, *4* (4), 2544-2552. DOI: https://doi.org/10.1021/acsapm.1c01853.

(457) Jedrzejczyk, M. A.; Madelat, N.; Wouters, B.; Smeets, H.; Wolters, M.; Stepanova, S. A.; Vangeel, T.; Van Aelst, K.; Van den Bosch, S.; Van Aelst, J.; et al. Preparation of Renewable Thiol-Yne "Click" Networks Based on Fractionated Lignin for Anticorrosive Protective Film Applications. *Macromolecular Chemistry and Physics* **2022**, *223* (13), 2100461. DOI: https://doi.org/10.1002/macp.202100461.

(458) Tasdelen, M. A. Diels–Alder "click" reactions: recent applications in polymer and material science. *Polymer Chemistry* **2011**, *2* (10), 2133-2145. DOI: http://dx.doi.org/10.1039/C1PY00041A.

(459) Duval, A.; Lange, H.; Lawoko, M.; Crestini, C. Reversible crosslinking of lignin via the furan–maleimide Diels–Alder reaction. *Green Chemistry* **2015**, *17* (11), 4991-5000. DOI: http://dx.doi.org/10.1039/C5GC01319D.

(460) Buono, P.; Duval, A.; Averous, L.; Habibi, Y. Lignin-Based Materials Through Thiol–Maleimide "Click" Polymerization. *ChemSusChem* **2017**, *10* (5), 984-992. DOI: https://doi.org/10.1002/cssc.201601738.

(461) Buono, P.; Duval, A.; Averous, L.; Habibi, Y. Thermally healable and remendable lignin-based materials through Diels – Alder click polymerization. *Polymer* **2017**, *133*, 78-88. DOI: https://doi.org/10.1016/j.polymer.2017.11.022.

(462) Kloxin, C. J.; Bowman, C. N. Covalent adaptable networks: smart, reconfigurable and responsive network systems. *Chemical Society Reviews* **2013**, *42* (17), 7161-7173. DOI: http://dx.doi.org/10.1039/C3CS60046G.

(463) Zou, W.; Dong, J.; Luo, Y.; Zhao, Q.; Xie, T. Dynamic Covalent Polymer Networks: from Old Chemistry to Modern Day Innovations. *Advanced Materials* **2017**, *29* (14), 1606100. DOI: https://doi.org/10.1002/adma.201606100.

(464) Elling, B. R.; Dichtel, W. R. Reprocessable Cross-Linked Polymer Networks: Are Associative Exchange Mechanisms Desirable? *ACS Central Science* **2020**, *6* (9), 1488-1496. DOI: https://doi.org/10.1021/acscentsci.0c00567.

(465) Montarnal, D.; Capelot, M.; Tournilhac, F.; Leibler, L. Silica-Like Malleable Materials from Permanent Organic Networks. *Science* **2011**, *334* (6058), 965-968. DOI: https://www.science.org/doi/abs/10.1126/science.1212648.

(466) Capelot, M.; Montarnal, D.; Tournilhac, F.; Leibler, L. Metal-Catalyzed Transesterification for Healing and Assembling of Thermosets. *Journal of the American Chemical Society* **2012**, *134* (18), 7664-7667. DOI: https://doi.org/10.1021/ja302894k.

(467) Capelot, M.; Unterlass, M. M.; Tournilhac, F.; Leibler, L. Catalytic Control of the Vitrimer Glass Transition. *ACS Macro Letters* **2012**, *1* (7), 789-792. DOI: https://doi.org/10.1021/mz300239f.

(468) Denissen, W.; Winne, J. M.; Du Prez, F. E. Vitrimers: permanent organic networks with glass-like fluidity. *Chemical Science* **2016**, *7* (1), 30-38. DOI: http://dx.doi.org/10.1039/C5SC02223A.

(469) Cuminet, F.; Caillol, S.; Dantras, É.; Leclerc, É.; Ladmiral, V. Neighboring Group Participation and Internal Catalysis Effects on Exchangeable Covalent Bonds: Application to the Thriving Field of Vitrimer Chemistry. *Macromolecules* **2021**, *54* (9), 3927-3961. DOI: https://doi.org/10.1021/acs.macromol.0c02706.

(470) Van Lijsebetten, F.; Holloway, J. O.; Winne, J. M.; Du Prez, F. E. Internal catalysis for dynamic covalent chemistry applications and polymer science. *Chemical Society Reviews* **2020**, *49* (23), 8425-8438. DOI: http://dx.doi.org/10.1039/D0CS00452A.

(471) Fortman, D. J.; Brutman, J. P.; De Hoe, G. X.; Snyder, R. L.; Dichtel, W. R.; Hillmyer, M. A. Approaches to Sustainable and Continually Recyclable Cross-Linked Polymers. *ACS Sustainable Chemistry & Engineering* **2018**, *6* (9), 11145-11159. DOI: https://doi.org/10.1021/acssuschemeng.8b02355.

(472) Van Zee, N. J.; Nicolaÿ, R. Vitrimers: Permanently crosslinked polymers with dynamic network topology. *Progress in Polymer Science* **2020**, *104*, 101233. DOI: https://doi.org/10.1016/j.progpolymsci.2020.101233.

(473) Zheng, N.; Xu, Y.; Zhao, Q.; Xie, T. Dynamic Covalent Polymer Networks: A Molecular Platform for Designing Functions beyond Chemical Recycling and Self-Healing. *Chemical Reviews* **2021**, *121* (3), 1716-1745. DOI: https://doi.org/10.1021/acs.chemrev.0c00938.

(474) Lucherelli, M. A.; Duval, A.; Avérous, L. Biobased vitrimers: Towards sustainable and adaptable performing polymer materials. *Progress in Polymer Science* **2022**, *127*, 101515. DOI: https://doi.org/10.1016/j.progpolymsci.2022.101515.

(475) Snyder, R. L.; Fortman, D. J.; De Hoe, G. X.; Hillmyer, M. A.; Dichtel, W. R. Reprocessable Acid-Degradable Polycarbonate Vitrimers. *Macromolecules* **2018**, *51* (2), 389-397. DOI: https://doi.org/10.1021/acs.macromol.7b02299.

(476) Fortman, D. J.; Brutman, J. P.; Cramer, C. J.; Hillmyer, M. A.; Dichtel, W. R. Mechanically Activated, Catalyst-Free Polyhydroxyurethane Vitrimers. *Journal of the American Chemical Society* **2015**, *137* (44), 14019-14022. DOI: https://doi.org/10.1021/jacs.5b08084.

(477) Denissen, W.; Rivero, G.; Nicolaÿ, R.; Leibler, L.; Winne, J. M.; Du Prez, F. E. Vinylogous Urethane Vitrimers. *Advanced Functional Materials* **2015**, *25* (16), 2451-2457. DOI: https://doi.org/10.1002/adfm.201404553.

(478) Hendriks, B.; Waelkens, J.; Winne, J. M.; Du Prez, F. E. Poly(thioether) Vitrimers via Transalkylation of Trialkylsulfonium Salts. *ACS Macro Letters* **2017**, *6* (9), 930-934. DOI: https://doi.org/10.1021/acsmacrolett.7b00494.

(479) Lu, Y.-X.; Guan, Z. Olefin Metathesis for Effective Polymer Healing via Dynamic Exchange of Strong Carbon–Carbon Double Bonds. *Journal of the American Chemical Society* **2012**, *134* (34), 14226-14231. DOI: https://doi.org/10.1021/ja306287s.

(480) Li, Q.; Ma, S.; Wang, S.; Yuan, W.; Xu, X.; Wang, B.; Huang, K.; Zhu, J. Facile catalyst-free synthesis, exchanging, and hydrolysis of an acetal motif for dynamic covalent networks. *Journal of Materials Chemistry A* **2019**, *7* (30), 18039-18049. DOI: http://dx.doi.org/10.1039/C9TA04073K.

(481) Taynton, P.; Yu, K.; Shoemaker, R. K.; Jin, Y.; Qi, H. J.; Zhang, W. Heat- or Water-Driven Malleability in a Highly Recyclable Covalent Network Polymer. *Advanced Materials* **2014**, *26* (23), 3938-3942. DOI: https://doi.org/10.1002/adma.201400317.

(482) Röttger, M.; Domenech, T.; van der Weegen, R.; Breuillac, A.; Nicolaÿ, R.; Leibler, L. High-performance vitrimers from commodity thermoplastics through dioxaborolane metathesis. *Science* **2017**, *356* (6333), 62-65. DOI: https://doi.org/10.1126/science.aah5281.

(483) Rekondo, A.; Martin, R.; Ruiz de Luzuriaga, A.; Cabañero, G.; Grande, H. J.; Odriozola, I. Catalyst-free room-temperature self-healing elastomers based on aromatic disulfide metathesis. *Materials Horizons* **2014**, *1* (2), 237-240. DOI: http://dx.doi.org/10.1039/C3MH00061C.

(484) Zheng, P.; McCarthy, T. J. A Surprise from 1954: Siloxane Equilibration Is a Simple, Robust, and Obvious Polymer Self-Healing Mechanism. *Journal of the American Chemical Society* **2012**, *134* (4), 2024-2027. DOI: https://doi.org/10.1021/ja2113257.

(485) Zhang, S.; Liu, T.; Hao, C.; Wang, L.; Han, J.; Liu, H.; Zhang, J. Preparation of a lignin-based vitrimer material and its potential use for recoverable adhesives. *Green Chemistry* **2018**, *20* (13), 2995-3000. DOI: http://dx.doi.org/10.1039/C8GC01299G.

(486) Hao, C.; Liu, T.; Zhang, S.; Brown, L.; Li, R.; Xin, J.; Zhong, T.; Jiang, L.; Zhang, J. A High-Lignin-Content, Removable, and Glycol-Assisted Repairable Coating Based on Dynamic Covalent Bonds. *ChemSusChem* **2019**, *12* (5), 1049-1058. DOI: https://doi.org/10.1002/cssc.201802615.

(487) More, A.; Elder, T.; Pajer, N.; Argyropoulos, D. S.; Jiang, Z. Novel and Integrated Process for the Valorization of Kraft Lignin to Produce Lignin-Containing Vitrimers. *ACS Omega* **2023**, *8* (1), 1097-1108. DOI: https://doi.org/10.1021/acsomega.2c06445.

(488) Xue, B.; Tang, R.; Xue, D.; Guan, Y.; Sun, Y.; Zhao, W.; Tan, J.; Li, X. Sustainable alternative for bisphenol A epoxy resin high-performance and recyclable lignin-based epoxy vitrimers. *Industrial Crops and Products* **2021**, *168*, 113583. DOI: https://doi.org/10.1016/j.indcrop.2021.113583.

(489) Tang, R.; Xue, B.; Tan, J.; Guan, Y.; Wen, J.; Li, X.; Zhao, W. Regulating Lignin-Based Epoxy Vitrimer Performance by Fine-Tuning the Lignin Structure. *ACS Applied Polymer Materials* **2022**, *4* (2), 1117-1125. DOI: https://doi.org/10.1021/acsapm.1c01541.

(490) Zheng, Y.; Liu, T.; He, H.; Lv, Z.; Xu, J.; Ding, D.; Dai, L.; Huang, Z.; Si, C. Lignin-based epoxy composite vitrimers with light-controlled remoldability. *Advanced Composites and Hybrid Materials* **2023**, *6* (1), 53. DOI: https://doi.org/10.1007/s42114-023-00633-4.

(491) Du, L.; Jin, X.; Qian, G.; Yang, W.; Su, L.; Ma, Y.; Ren, S.; Li, S. Lignin-based vitrimer for circulation in plastics, coatings, and adhesives with tough mechanical properties, catalyst-free and good chemical solvent resistance. *Industrial Crops and Products* **2022**, *187*, 115439. DOI: https://doi.org/10.1016/j.indcrop.2022.115439.

(492) Han, J.; Liu, T.; Hao, C.; Zhang, S.; Guo, B.; Zhang, J. A Catalyst-Free Epoxy Vitrimer System Based on Multifunctional Hyperbranched Polymer. *Macromolecules* **2018**, *51* (17), 6789-6799. DOI: https://doi.org/10.1021/acs.macromol.8b01424.

(493) Johnson, R. M.; Cortés-Guzmán, K. P.; Perera, S. D.; Parikh, A. R.; Ganesh, V.; Voit, W. E.; Smaldone, R. A. Lignin-based covalent adaptable network resins for digital light projection 3D printing. *Journal of Polymer Science* **2023**, *n/a* (n/a). DOI: https://doi.org/10.1002/pol.20230026.

(494) Bakkali-Hassani, C.; Berne, D.; Ladmiral, V.; Caillol, S. Transcarbamoylation in Polyurethanes: Underestimated Exchange Reactions? *Macromolecules* **2022**, *55* (18), 7974-7991. DOI: https://doi.org/10.1021/acs.macromol.2c01184.

(495) Wang, H.; Huang, J.; Liu, W.; Huang, J.; Yang, D.; Qiu, X.; Zhang, J. Tough and Fast Light-Controlled Healable Lignin-Containing Polyurethane Elastomers. *Macromolecules* **2022**, *55* (19), 8629-8641. DOI: https://doi.org/10.1021/acs.macromol.2c01401.

(496) Ma, X.; Li, S.; Wang, F.; Wu, J.; Chao, Y.; Chen, X.; Chen, P.; Zhu, J.; Yan, N.; Chen, J. Catalyst-Free Synthesis of Covalent Adaptable Network (CAN) Polyurethanes from Lignin with Editable Shape Memory Properties. *ChemSusChem* **2023**, *16* (5), e202202071. DOI: https://doi.org/10.1002/cssc.202202071.

(497) Ma, X.; Wang, X.; Zhao, H.; Xu, X.; Cui, M.; Stott, N. E.; Chen, P.; Zhu, J.; Yan, N.; Chen, J. High-Performance, Light-Stimulation Healable, and Closed-Loop Recyclable Lignin-Based Covalent Adaptable Networks. *Small* **2023**, *n/a* (n/a), 2303215. DOI: https://doi.org/10.1002/smll.202303215.

(498) Qi, G.; Yang, W.; Puglia, D.; Wang, H.; Xu, P.; Dong, W.; Zheng, T.; Ma, P. Hydrophobic, UV resistant and dielectric polyurethane-nanolignin composites with good reprocessability. *Materials & Design* **2020**, *196*, 109150. DOI: https://doi.org/10.1016/j.matdes.2020.109150.

(499) Liu, W.; Fang, C.; Wang, S.; Huang, J.; Qiu, X. High-Performance Lignin-Containing Polyurethane Elastomers with Dynamic Covalent Polymer Networks. *Macromolecules* **2019**, *52* (17), 6474-6484. DOI: https://doi.org/10.1021/acs.macromol.9b01413.

(500) Xue, D.; Xue, B.; Tang, R.; Shen, C.; Li, X.; Zhao, W. Synthesis of Reprocessable Lignin-based Non-isocyanate Poly(imine-hydroxyurethane)s Networks. *Paper and Biomaterials* **2021**, *6* (1), 11-21. DOI: https://doi.org/10.12103/j.issn.2096-2355.2021.01.002.

(501) Shen, C.; Xue, B.; Xue, D.; Tang, R.; Zhao, W.; Li, X. Synthesis of Lignin-based Non-isocyanate Poly(imine-hydroxyurethane)s Networks. Part Ⅱ: Self-healing, Reprocessing, and Degradation. *Paper and Biomaterials* **2021**, *6* (3), 1-9. DOI: https://doi.org/10.1213/j.issn.2096-2355.2021.03.001.

(502) Zhao, W.; Liang, Z.; Feng, Z.; Xue, B.; Xiong, C.; Duan, C.; Ni, Y. New Kind of Lignin/Polyhydroxyurethane Composite: Green Synthesis, Smart Properties, Promising Applications, and Good Reprocessability and

Recyclability. *ACS Applied Materials & Interfaces* **2021**, *13* (24), 28938-28948. DOI: https://doi.org/10.1021/acsami.1c06822.

(503) Gao, S.; Cheng, Z.; Zhou, X.; Liu, Y.; Wang, J.; Wang, C.; Chu, F.; Xu, F.; Zhang, D. Fabrication of lignin based renewable dynamic networks and its applications as self-healing, antifungal and conductive adhesives. *Chemical Engineering Journal* **2020**, *394*, 124896. DOI: https://doi.org/10.1016/j.cej.2020.124896.

(504) Buzoglu Kurnaz, L.; Bension, Y.; Tang, C. Facile Catalyst-Free Approach toward Fully Biobased Reprocessable Lignin Thermosets. *Macromolecular Chemistry and Physics* **2023**, *224* (3), 2200303. DOI: https://doi.org/10.1002/macp.202200303.

(505) Liu, W.; Fang, C.; Chen, F.; Qiu, X. Strong, Reusable, and Self-Healing Lignin-Containing Polyurea Adhesives. *ChemSusChem* **2020**, *13* (17), 4691-4701. DOI: https://doi.org/10.1002/cssc.202001602.

(506) Sun, N.; Wang, Z.; Ma, X.; Zhang, K.; Wang, Z.; Guo, Z.; Chen, Y.; Sun, L.; Lu, W.; Liu, Y.; et al. Preparation and characterization of lignin-containing self-healing polyurethane elastomers with hydrogen and disulfide bonds. *Industrial Crops and Products* **2021**, *174*, 114178. DOI: https://doi.org/10.1016/j.indcrop.2021.114178.

(507) Moreno, A.; Morsali, M.; Sipponen, M. H. Catalyst-Free Synthesis of Lignin Vitrimers with Tunable Mechanical Properties: Circular Polymers and Recoverable Adhesives. *ACS Applied Materials & Interfaces* **2021**, *13* (48), 57952-57961. DOI: https://doi.org/10.1021/acsami.1c17412.

(508) Zhang, J.; Fleury, E.; Chen, Y.; Brook, M. A. Flame retardant lignin-based silicone composites. *RSC Advances* **2015**, *5* (126), 103907-103914. DOI: http://dx.doi.org/10.1039/C5RA24093J.

(509) Zhang, W.; Wang, B.; Xu, X.; Feng, H.; Hu, K.; Su, Y.; Zhou, S.; Zhu, J.; Weng, G.; Ma, S. Green and facile method for valorization of lignin to high-performance degradable thermosets. *Green Chemistry* **2022**, *24* (24), 9659-9667. DOI: http://dx.doi.org/10.1039/D2GC03302J.

(510) Debsharma, T.; Amfilochiou, V.; Wróblewska, A. A.; De Baere, I.; Van Paepegem, W.; Du Prez, F. E. Fast Dynamic Siloxane Exchange Mechanism for Reshapable Vitrimer Composites. *Journal of the American Chemical Society* **2022**, *144* (27), 12280-12289. DOI: https://doi.org/10.1021/jacs.2c03518.

Research axis I

Design of lignin-based benzoxazines

Polybenzoxazines are an emerging class of mono-component phenolic resin synthesized from the Mannich-like condensation of a phenol, an amine (aliphatic or aromatic), and a methylene donor (generally formaldehyde) (Scheme 1). This one-pot hetero-cyclization approach fuses a benzene ring with a 1,3-oxazine motif consisting of a 6-membered ring of four carbons, one oxygen, and one nitrogen atom. The thermal ring-opening polymerization (ROP) of benzoxazine monomers generates high-performance thermosetting resins well-suited for advanced applications. The self-catalyzed polymerization of mono- or multifunctional benzoxazine monomers leads to the formation of linear polymer chains or three-dimensional cross-linked networks, respectively. Polybenzoxazines show promise in numerous industries owing to their outstanding solvent resistance and thermo-mechanical stability, among other assets. This wide range of properties makes them promising alternatives to conventional phenolic or epoxy resins.
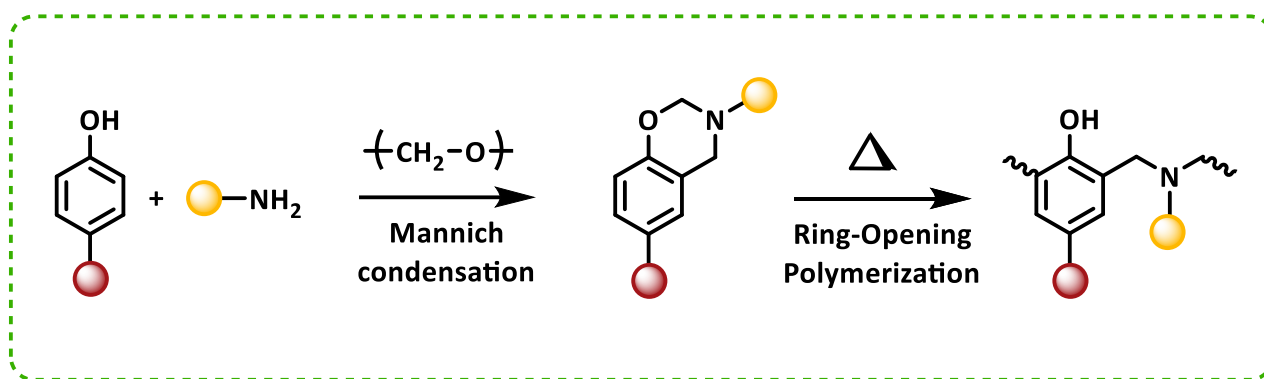
Scheme 1 Synthesis of benzoxazine monomers from Mannich-like ring-closure and benzoxazine materials from ring-opening polymerization of benzoxazine monomers.

The ability to tailor the properties of benzoxazine resins originates from the design flexibility of their chemical structures. If a wide range of commercially available precursors can be used for their synthesis, polybenzoxazines are traditionally produced from fossil fuel-based chemicals such as bisphenol-A (phenol derivative) and aniline (amine derivative). In addition to the depletion of petroleum resources, the disposal of the materials issued from them contributes to the pollution of terrestrial and marine environments.

In recent years, the sustainability of polybenzoxazines has been greatly enhanced driven by the necessity to minimize the dependence on fossil fuels. The design of environmentally friendly materials encompasses the use of bio-derived precursors that benefit from greater availability and reduced environmental footprint compared to petroleum-derived counterparts. Numerous studies have been conducted to explore the rich variety of natural resources to develop renewable benzoxazines. Among them, a wide range of bio-based amines and bio-based phenols derived from biomass waste streams (typically agricultural residues) have been investigated. The following chapters aim to delve into the design and the process-optimization of renewable benzoxazines from bio-based phenols that originate from lignocellulosic biomass.

Chapter two: "Elucidating the thermal and polymerization behaviours of benzoxazines from lignin derivatives"

In response to growing global awareness, lignin biopolymer has gathered significant attention as an environmentally friendly substitute for feedstocks derived from petroleum. Over the past decades, progresses in the oxidative conversion of lignin macromolecules into depolymerized fragments has paved the way toward the design of bio-phenol precursors. The commercial availability of lignin-derived monomers leverage the sustainability of benzoxazine monomers. Among the lignin-derived bio-phenols, vanillin, vanillic acid, methyl vanillate, eugenol, and guaiacol, are *ortho*-methoxy substituted phenolic precursors characterized by different *para*-substitutions (aldehyde, carboxylic acid, methyl ester, allyl, and hydrogen, respectively). In chapter two, the solventless synthesis of monofunctional benzoxazine monomers from the abovementioned bio-sourced phenols is described. The following study elucidates the role of *para*-substitution on the curing and thermal properties of renewable benzoxazine monomers. The participation of *para*-substitution in the formation of a three-dimensional network has a significant impact on the ring-opening polymerization (ROP) of benzoxazine. Furthermore, the thermal stability of lignin-based benzoxazines is closely related to their ability to establish hydrogen bonding.
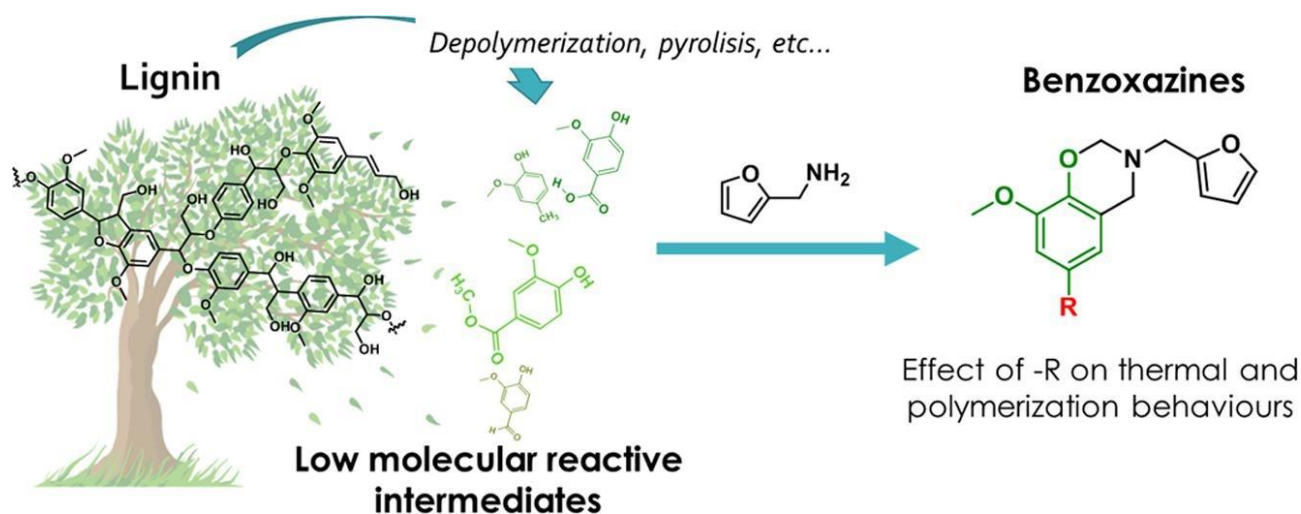
Contribution: I participated to the chemical synthesis of all model molecules and their characterization by different techniques (NMR, FTIR, DSC, TGA). Furthermore, I co-authored the manuscript and contributed to the original draft, correction, and revision.

ELSEVIER

Elucidating the thermal and polymerization behaviours of benzoxazines from lignin derivatives

Acerina Trejo-Machin[a,b,1], Antoine Adjaoud[a,b,1], Laura Puchot[a], Reiner Dieden[a], Pierre Verge[a,*]

[a] *Luxembourg Institute of Science and Technology, Materials Research and Technology Department, 5 Avenue des Hauts-Fourneaux, L-4362 Esch-sur-Alzette, Luxembourg*
[b] *University of Luxembourg, 2, Avenue de l'Université, L-4365 Esch-sur-Alzette, Luxembourg*

ABSTRACT

Due to their abundance, biophenols are widely targeted for the design of polybenzoxazines. Among them, *ortho*-methoxy substituted phenolic compounds are an attractive source of inspiration, abundantly issued from polyphenol depolymerisation. In most of the cases, they are substituted in the *para*-position with a group affecting the thermal properties of benzoxazine. This paper challenged to elucidate the role of the *p*-substituents found in lignin-occurring phenolic compounds, by studying the properties of purified monomers prepared from a solvent-free condensation of furfurylamine and model molecules: vanillin (V-fa), vanillic acid (VA-fa), guaiacol (G-fa), methyl vanillate (MV-fa) and creosol (Cr-fa). G-fa and V-fa were able to form 3D networks, the first one due to its unsubstituted *para*-position, and the second one due to the involvement of the –CHO group during the polymerization. Interestingly, these two substituents were providing a substantial stability to the monomers upon heating. On the contrary, Cr-fa and MV-fa, which were respectively dimerizing and oligomerizing, underwent substantially degradation during their curing.

1. Introduction

A rich variety of readily available phenolic and polyphenolic compounds considered for the synthesis of monomers or polymers can be found in nature. The major sources of bio-based phenolic compounds are stemming from plants or wastes generated by industries such as agriculture and paper [1]. In particular, the chemical structure of lignin suggests that it may be a good source of valuable chemicals when broken into smaller molecular units. For instance, lignin pyrolysis leads to mixtures of phenolic compounds containing major quantities of guaiacol, creosol, vanillin and their derivatives [2].

Many of these phenolic compounds exhibit suitable chemical features to be a potent feedstock for the design of renewable benzoxazine (BZ) monomers [3]. Polybenzoxazines (PBZ) are a type of phenolic thermosetting resin obtained by the thermal polymerization of benzoxazine monomers. They have outstanding and competitive properties [4–5] such as high thermal stability [6], high char yield [7], high glass transition temperature [8], near-zero shrinkage upon polymerization [9], low water absorption [10] and excellent electrical and mechanical properties [11]. The most attractive asset of these materials is the exceptional versatility of the design of their chemical structure making possible the use of a wide range of bio-sources for their synthesis. In

particular, the use of bio-phenols has been extensively reported in the literature in the last years [2,12–16], and specific roles of *p*-substituents have been highlighted (Table 1). For instance, the aldehyde group (–CHO) in the *p*-position of vanillin is known to affect the BZ ring opening polymerization (ROP) through its decarboxylation upon heating [17–18]. As well, a catalytic effect is observed on various *p*-hydroxycinnamic acid based BZ, for instance *p*-coumaric, ferulic and phloretic acids [19].

Previous studies reported by Ishida et al. [25] and Sebatián and Marquet et al. [26] examined the effect of *para*-, *meta*- and *ortho*-substituents on the thermal properties of mono-functional BZ. The two research teams focused on a wide range of electronic effects by varying the substituents of phenolic compounds to make the thermal behaviour of BZ predictable. However, most of the studied chemical groups cannot be found in natural phenolic compounds. Even if some trends may be extrapolated, no clear conclusions can be drawn.

The current work aims at providing additional knowledge on the potential use of by-products from lignin depolymerisation for the conception of benzoxazine. To this aim, *ortho*-methoxy substituted model candidates, all potentially derived from lignin pyrolysis, were selected to prepare novel fully bio-based BZ monomers: creosol (Cr), methyl vanillate (MV) and vanillic acid (VA). BZ from vanillin (V) and guaiacol

Table 1
Thermal characteristics of lignin sourced phenolic-based benzoxazine monomers.

Abbreviation	Group in *para*	Group in *ortho*	Tm[a] (°C)	Tp[b] (°C)	Y[c] (%)	Refs
V-a	−CHO	−OCH₃	83	231	55	[20]
V-fa	−CHO	−OCH₃	125	205	65	[17]
G-fa	−H	−OCH₃	97	240	56	[21]
FA-a	−CH=CHCOOH	−OCH₃	121	130	34	[19]
Eu-fa	−CH₂CH=CH₂	−OCH₃	74	222	54	[22]
VG-fa	−CH=CH₂	−OCH₃	97	235	35	[23]
FAM-a	−CH=CHCOOCH₃	−OCH₃	166	203	45	[19]
CA-a	−CH=CHCOOH	−H	117	137	30	[19]
PA-a	CH₂CH₂COOH	−H	122	212	43	[19]
CAM-a	−CH=CHCOOCH₃	−H	109	216	43	[19]
PAM-a	−CH₂HCOOCH₃	−H	156	197	43	[19]
pHBA-a	−COOH	−H	–	165	42	[24]

Vanillin-aniline (V-a), Vanillin-furfurylamine (V-fa), Guaiacol-furfurylamine (G-fa), Ferulic acid-aniline (FA-a), Eugenol-furfurylamine (Eu-fa), Vinyl Guaiacol-furfurylamine (VG-fa), Methylated ferulic acid-aniline (FAM-fa), Coumaric acid-aniline (CA-a), Methylated Phloretic acid (PAM-a), Methylated Coumaric acid-aniline (CAM-a), Phloretic acid (PA-a), p-hydroxybenzoic acid (pHBA-a). [a] Melting temperature; [b] Polymerization temperature; [c] Char yield at 800 °C.

(G) were also studied for the sake of comparison. We decided to use furfurylamine as the design of bio-based benzoxazine reported in the literature by other authors is, in almost all the cases, dealing with the use of this bio-amine. The chemical structure of each benzoxazine is reported in Chart 1.

2. Experimental part

2.1. Materials

Vanillin (99%), guaiacol (99%), vanillic acid (97%), methyl vanillate (99%), creosol (98%), paraformaldehyde (95%), furfurylamine (99%), and the solvents used for the synthesis or the purification of the benzoxazine monomers, were purchased from Sigma-Aldrich and used as received.

2.2. General synthesis of benzoxazine monomers

Benzoxazine monomers were synthesized by reacting furfurylamine with paraformaldehyde and different bio-based phenolic compounds, in stoichiometric ratio 1/2/1, respectively. The reactions were carried out without solvent at 85 °C for 24 h, except for the VA-fa monomer for which chloroform was used as a solvent (Scheme 1).

Guaiacol-furfurylamine (G-fa). 2.44 g of furfurylamine (25 mmol), 1.50 g of paraformaldehyde (50 mmol) and 3.12 g of guaiacol (25 mmol) were reacted for 24 h at 85 °C. The reaction crude was

solubilized in chloroform and purified by 3 liquid–liquid extractions with a 2 N NaOH solution and 3 with distilled water. The organic layer was dried over sodium sulphate and the solvent evaporate off. The final product (white powder) was recovered by recrystallization in ethyl acetate/hexane (3:1) and dried at 60 °C for 12 h under vacuum and freeze-dried. Reaction yield after purification is 25%.

1H NMR (DMSO-d_6, 600 MHz, 298 K) δ (ppm) = (assignment, multiplicity (coupling constant), attribution, experimental integration, theoretical integration). δ = 3.73 (O−CH₃, s, [5], exp 3.03H, th 3.00H); 3.82 (N−CH₂, s, [6], integration reference th 2.00H); 3.90 (N−CH₂−Ar, s, [2], exp 1.99H, th 2.00H); 4.82 (N−CH₂−O, s, [1], exp 1.95H, th 2.00H); 6.31 (−CH*=C−O−, s, [7], exp 0.89H, th 1.00H); 6.42 (−CH=CH*−CH−, s, [8], exp 0.96H, th 1.00H); 6.58 (H–Ar, d (J = 6.8 Hz), [3], exp 0.91H, th 1.00H); 6.80 (H-Ar, m, [4,10], exp 1.97H, th 2.00H); 7.61 (-O-CH=, s, [9], exp 0.83H, th 1.00H).

13C NMR (DMSO-d_6, 600 MHz, 298 K) δ (ppm) = 48.0 [j], 49.1 [b], 55.9 [i], 81.9 [a], 109.1 [l], 110.6 [f], 110.7 [m], 119.8 [d], 120.3 [e], 120.7 [c], 143.1 [n], 143.6 [h], 147.9 [g], 152.3 [k].

FTIR (cm^{-1}): 1582 (stretching of furan ring), 1482 (stretching of tetrasubstituted benzene ring), 1220 (C-O-C asymmetric stretching), 917 (benzoxazine related mode).

Creosol-furfurylamine (Cr-fa). 2.41 g of furfurylamine (25 mmol), 1.51 g of paraformaldehyde (50 mmol) and 3.45 g of creosol (25 mmol) were reacted for 24 h at 85 °C. The reaction crude was solubilized in chloroform and purified by 3 liquid-liquid extractions with a 2 N NaOH solution and 3 with distilled water. The organic layer was dried over sodium sulphate and the solvent evaporate off. The final product (white powder) was recovered after three successive recrystallizations in ethyl acetate/hexane (3:1) and dried at 60 °C for 12 h under vacuum and freeze-dried. Reaction yield after purification is 45.5%.

1H NMR (DMSO-d_6, 600 MHz, 298 K) δ (ppm) = (assignment, multiplicity (coupling constant), attribution, experimental integration, theoretical integration). δ = 2.19 (Ar-CH₃, s, [10], exp 3.07H, th 3.00H); 3.72 (O-CH₃, s, [5], exp 3.04H, th 3.00H); 3.81 (N-CH₂, s, [6], integration reference 2.00H); 3.84 (N-CH₂-Ar, s, [2], exp 2.03H, th 2.00H); 4.77 (N-CH₂-O, s, [1], exp 2.00H, th 2.00H); 6.31 (−CH*=-C−O−, d (J = 3.02 Hz), [7], exp 0.96H, th 1.00H); 6.38 (H−Ar, s, [3], exp 0.99H, th 1.00H); 6.42 (−CH=CH*−CH−, q (J = 1.83 Hz), [8], exp 0.96H, th 1.00H); 6.63 (H-Ar, s, [4], exp 1.00, th 1.00H); 7.61 (−O−CH=, s, [9], exp 0.91H, th 1.00H).

13C NMR (DMSO-d_6, 600 MHz, 298 K) δ (ppm) = 21.2 [o], 47.9 [j], 49.1 [b], 55.8 [i], 81.8 [a], 109.1 [l], 110.9 [m], 111.5 [f], 119.8 [f], 120.2 [c], 129.2 [e], 141.2 [h], 143.1 [n], 147.6 [g], 152.3 [k].

FTIR (cm^{-1}): 1593 (stretching of furan ring), 1496 (stretching of tetrasubstituted benzene ring), 1221 (C-O-C asymmetric stretching), 922 (benzoxazine related mode).

Vanillin-furfurylamine (V-fa). 2.43 g of furfurylamine (25 mmol), 1.50 g of paraformaldehyde (50 mmol) and 3.80 g of vanillin (25 mmol) were reacted for 24 h at 85 °C. The reaction crude was solubilized in chloroform and purified by 3 liquid-liquid extractions with a 2 N NaOH
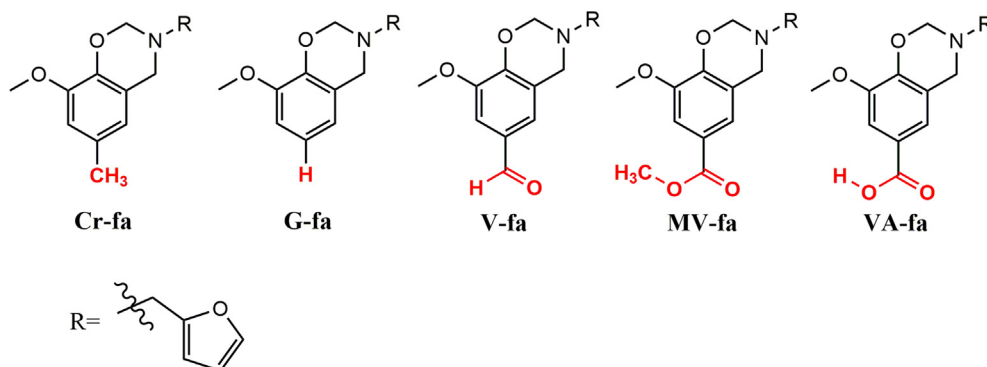
Chart 1. Chemical structures of the synthesized benzoxazine monomers.

R = -H, -CH₃, -CHO, -COOCH₃, -COOH

* for -COOH synthesis in CHCl$_3$
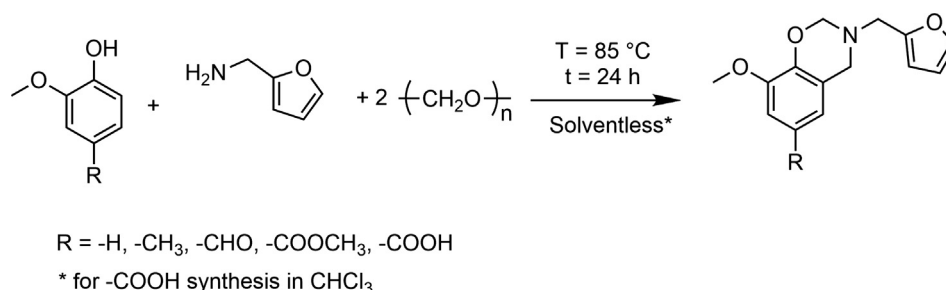
Scheme 1. Synthetic route for the bio-based benzoxazine monomers.

solution and 3 with distilled water. The organic layer was dried over sodium sulphate and the solvent evaporated. The final product (white powder) was recovered after three successive recrystallizations in ethyl acetate/pentane (3:1) and dried at 60 °C for 12 h under vacuum and freeze-dried. Reaction yield after purification is 22%.

^{1}H NMR (DMSO-d_6, 600 MHz, 298 K) δ (ppm) = (assignment, multiplicity (coupling constant), attribution, experimental integration, theoretical integration). δ = 3.83 (O−CH$_3$, s, [5], exp 2.91H, th 3.00H); 3.84 (N-CH$_2$, s, [6], integration reference 2.00H); 4.01 (N-CH$_2$-Ar, s, [2], exp 1.94H, th 2.00H); 4.98 (N−CH$_2$−O, s, [1], exp 1.94H, th 2.00H); 6.33 (−CH*=C−O−, d (J = 2.93 Hz), [7], exp 0.91H, th 1.00H); 6.42 (−CH=CH*−CH−, q (J = 1.84 Hz), [8], exp 0.87H, th 1.00H); 7.28 (H−Ar, s, [4], exp 0.90, th 2.00H); 7.29 (H−Ar, s, [3], exp 0.95, th 2.00H); 7.62 (−O−CH=, s, [9], exp 0.81H, th 1.00H); 9.79 (−(C=O)−H, s, [10], exp 0.88H, th 1.00H).

^{13}C NMR (DMSO-d_6, 600 MHz, 298 K) δ (ppm) = 47.9 [j], 48.6 [b], 56.0 [i], 83.0 [a], 109.0 [f], 109.9 [l], 110.9 [m], 120.6 [c], 124.6 [d], 129.0 [e], 143.3 [n], 148.5 [g], 149.4 [h], 151.9 [k], 191.8 [o].

FTIR (cm^{-1}): 1684 (C=O stretching), 1578 (stretching of furan ring), 1488 (stretching of tetrasubstituted benzene ring), 1226 (C−O−C asymmetric stretching), 901 (benzoxazine related mode).

Methyl vanillate-furfurylamine (MV-fa). 2.44 g of furfurylamine (25 mmol), 1.50 g of paraformaldehyde (50 mmol) and 4.55 g of methyl vanillate (25 mmol) were reacted for 24 h at 85 °C. The reaction crude was solubilized in chloroform and purified by 3 liquid-liquid extractions with a 2 N NaOH solution and 3 with distilled water. The organic layer was dried over sodium sulphate and the solvent evaporated. The final product (white powder) was recovered after three successive recrystallizations in ethyl acetate/hexane (3:1) and dried at 60 °C for 12 h under vacuum and freeze-dried. Reaction yield after purification is 46%.

^{1}H NMR (DMSO-d_6, 600 MHz, 298 K) δ (ppm) = (assignment, multiplicity (coupling constant), attribution, experimental integration, theoretical integration) δ = 3.81 (O−CH$_3$, s, [5,10], exp 5.90H, th 6.00H); 3.82 (N−CH$_2$, s, [6], integration reference 2.00H); 3.97 (N−CH$_2$-Ar, s, [2], exp 2.00H, th 2.00H); 4.94 (N−CH$_2$−O, s, [1], exp 2.11H, th 2.00H); 6.33 (−CH*=C−O−, d (J = 2.80 Hz), [7], exp 0.97H, th 1.00H); 6.42 (−CH=CH*−CH−, q (J = 1.87 Hz), [8], exp 0.96H, th 1.00H); 7.31 (H−Ar, s, [3,4], exp 1.96H th 2.00H); 7.62 (−O−CH=, s, [9], exp 0.91H, th 1.00H).

^{13}C NMR (DMSO-d_6, 600 MHz, 298 K) δ (ppm) = 47.9 [j], 48.8 [b], 52.3 [p], 56.0 [i], 82.7 [a], 109.3 [l], 110.6 [f], 110.9 [m], 120.4 [c], 121.3 [e], 122.1 [d], 143.2 [n], 147.7 [g], 148.1 [h], 152.0 [j], 166.5 [n].

FTIR (cm^{-1}): 1715 (C=O stretching), 1588 (stretching of furan ring), 1499 (stretching of tetrasubstituted benzene ring), 1219 (C-O-C asymmetric stretching), 914 (benzoxazine related mode).

Vanillic acid-furfurylamine (VA-fa). 2.43 g of furfurylamine (25 mmol), 1.50 g of paraformaldehyde (50 mmol) and 4.22 g of vanillic acid (25 mmol) were reacted in two steps (first step: paraformaldehyde and furfurylamine, second step: vanillic acid) for 24 h in CHCl$_3$ at 85 °C. After cooling the reaction solvent was evaporated and the final product (white powder) was recovered by three successive

recrystallizations from ethanol and dried at 60 °C for 12 h under vacuum and freeze-dried. Reaction yield after purification is 42%.

^{1}H NMR (DMSO-d_6, 600 MHz, 298 K) δ (ppm) = (assignment, multiplicity (coupling constant), attribution, experimental integration, theoretical integration). δ = 3.80 (O−CH$_3$, s, [5], exp 3.10H, th 3.00H); 3.82 (N−CH$_2$, s, [6], integration reference 2.00H); 3.97 (N-CH$_2$-Ar, s, [2], exp 2.00H, th 2.00H); 4.92 (N-CH$_2$-O, s, [1], exp 2.03H, th 2.00H); 6.33 (−CH*=C−O−, d (J = 2.83 Hz), [7], exp 0.98H, th 1.00H); 6.42 (−CH = CH*−CH−, q (J = 1.79 Hz), [8], exp 1.02H, th 1.00H); 7.28 (H−Ar, s, [3], exp 1.01H, th 1.00H); 7.32 (H−Ar, s, [4], exp 1.01H, th 1.00H); 7.62 (−O−CH=, s, [9], exp 0.96H, th 1.00H).

^{13}C NMR (DMSO-d_6, 600 MHz, 298 K) δ (ppm) = 47.9 [j], 48.8 [b], 55.9 [i], 82.6 [a], 109.3 [l], 110.8 [f], 110.9 [m], 120.1 [c], 122.2 [d], 122.5 [e], 143.2 [n], 147.6 [h], 147.7 [g], 152.0 [k], 167.6 [o].

FTIR (cm^{-1}): 2834 (O-H stretching), 1674 (C=O stretching), 1585 (stretching of furan ring), 1499 (stretching of tetrasubstituted benzene ring), 1224 (C-O-C asymmetric stretching), 894 (benzoxazine related mode).

2.3. Measurements

Nuclear magnetic resonance (NMR) spectra were recorded using an AVANCE III HD Bruker spectrometer operating at a proton frequency of 600 MHz and equipped with a 5 mm BBO-probe. For solution NMR, the samples were dissolved in either deuterated chloroform (CDCl$_3$) or deuterated dimethyl sulfoxide (DMSO-d_6). The spectra were referenced relative to tetramethylsilane (TMS). Assignments were performed using a combination of COSY, HSQC and HMBC spectra.

Solid-state NMR spectra have been recorded on a Bruker Avance III HD 600 MHz spectrometer equipped with a 4 mm standard bore H-X probe. ^{1}H NMR solid-state spectra were recorded with a onePulse sequence at a MAS frequency of 15 kHz, using a 90° pulse at 100 kHz. ^{13}C-CP/MAS spectra were recorded at a MAS frequency of 14 kHz using a 62.5 kHz 90° pulse and SPINAL64 dipolar decoupling [27] at 100 kHz. CP was applied a nutation frequency of 41.5 kHz using a 70–100% amplitude ramp [28] on ^{1}H centered on the first side-band at and a contact time of 3.5 ms. 64 or 128 transients were co-added with a recycle delay of 3 s. Chemical shifts were referenced using adamantane as an external reference for tetramethylsilane (TMS), setting the CH$_2$ signal to 38.48 ppm [29–30].

2D single-quantum double-quantum [1]H -^{1}H correlation MAS spectra were acquired using homonuclear wPMLG decoupling and post-C7 DQ-excitation and reconversion[31] using 7 basic post-C7 elements, and 16 oversampled data points with a z-filter delay of 1.5 ms and 128 accumulated transients per increment. wPMLG decoupling used m5mp shaped-pulses.

Fourier transform infrared spectroscopy (FTIR) was conducted on a Bruker TENSOR 27 (Ettlingen, Germany) in the attenuated total reflection (ATR) mode using a diamond crystal. The background and sample spectra were recorded at 4 cm^{-1} spectral resolution across the 4000–400 cm^{-1} range.

Differential Scanning Calorimetry (DSC) thermograms were recorded by means of a Netzsch DSC 204 F1 Phoenix apparatus operating

at inert atmosphere (nitrogen) with a linear heating ramp from 20 to 250 °C at 10 °C·min^{-1} rate for the analyses of the thermal behaviour of the monomers. DSC was used to measure the glass transition temperature (T$_g$) of polybenzoxazines after isothermal curing inside the DSC furnace. The measurement was performed applying a heating ramp from −50 to at least 50 °C above the T$_g$ of the sample, T$_g$ being defined as the middle point of the temperature interval when the baseline shift upon heating.

Rheo-kinetic measurements were performed using an Anton Paar Physica MCR 302 rheometer equipped with a CTD 450 temperature control device with a disposable aluminium plate-plate (diameter: 25 mm, measure gap: 0.35 mm) geometry. The polymerization measurements were recorded in the oscillation mode at an imposed 1% strain amplitude (γ) and a frequency (f) of 1 Hz. Heating ramps of 20 °C/min were applied to reach the temperatures of 170 °C and 190 °C. The sample deformation was ramped linearly from 1% to 0.2% to remain within the instrument's limitation and to maintain a linear viscoelastic behaviour as the moduli increase by several orders of magnitude upon curing. A gap of 0.5 mm was maintained during all the measurement.

A 1260 Infinity II gel permeation chromatograph (Agilent Technologies) was used to determine M$_n$, M$_w$ and M$_w$/M$_n$ ratio of polymer samples. The chromatograph was equipped with an integrated multi-detector composed of IR, UV, viscometer and light scattering. The separation was conducted using in series a PLgel guard column, PLgel 5 mm MIXED-D column, and PLgel 5 mm MIXED-C column (Agilent Technologies). The eluent was CHCl$_3$ and the flow rate was of 1.0 mL·min^{-1} at 40 °C. Polystyrene standards (Agilent Technologies, Mp = [162–364000] g/mol) were used to perform calibration.

Thermo-Gravimetric Analysis (TGA) was performed using a Netzsch TG 409 PC Luxx device operating under nitrogen flow. The evolution of the weight of the monomers was first recorded during curing: heating ramp (10 °C/min) from room temperature to 170 °C, 1 h at 170 °C, heating ramp (10 °C/min) from 170 °C to 190 °C, 30 min at 190 °C. Traditional thermogravimetrical analysis with a heating ramp of 10 °C/min up to 800 °C was performed on the resulting materials.

3. Results and discussion

3.1. Synthesis and molecular characterization

The benzoxazine monomers were all synthetized following the traditional Mannich condensation reaction between paraformaldehyde, furfurylamine and the selected p-substituted phenolic compounds (Scheme 1). It is noteworthy that the syntheses were all performed without solvent, except for VA-fa which required to be solubilized. To avoid any reaction between the carboxylic acid and the amine, VA-fa was synthetized by reacting first paraformaldehyde and furfurylamine, followed by the addition of vanillic acid once the iminium intermediate was formed. Significant attention was paid to the purity of the BZ monomers, which were all recrystallized three times in appropriate solvent mixtures.

The chemical structures of the benzoxazine monomers were determined by NMR. The ^{1}H NMR spectra of Cr-fa, VA-fa and MV-fa are displayed in Fig. 1. NMR spectra of G-fa and V-fa are given in the supporting information (Figs. S1 and S2) as they have been previously reported.[19,22] The detailed chemical shifts and integrations of each monomer are summarized in Table S1.

In all cases, the two characteristic singlet resonance signals corresponding to the −CH$_2$ protons of the oxazine ring (N−CH$_2$−Ar and N−CH$_2$−O) are found at δ = 4.77, 4.94 and 4.92 ppm for N−CH$_2$−O [1] protons and at δ = 3.84, 3.97 and 3.97 ppm for N−CH$_2$−Ar [2] protons, respectively for Cr−fa, MV−fa and VA−fa. The ratio of 1:1 between the experimental integrations of the methylene peaks further supports the formation of the oxazine rings. Finally, the signals corresponding to the aminomethyl group of furfurylamine (Table S1, rows 4,

9, 14, 19, 24) as well as the −OCH$_3$ group (Table S1, rows 3, 8, 13, 18, 23) are also clearly detected on the spectra.

It can be noted that a slight deviation of the resonances corresponding to the oxazine rings were observed, from 3.82 to 4.01 ppm for N-CH$_2$-Ar protons, and from 4.77 to 4.98 ppm for N-CH$_2$-O protons, caused by the electronic effects induced by the p-substituents[26].

In addition, experimental integrations are in close correlation with the theoretical values. The corresponding [13] C NMR spectra (Figs. S3–S7) support the chemical structures with the characteristic resonances of O-CH$_2$-N and Ar−CH$_2$−N observed around 82–83 ppm and 48–49 ppm, respectively.

It is worthy to note that the para-substituents were all preserved (Table S1, rows 5, 10, 15, 20, 25). The presence of the −COOH of VA−fa was confirmed by solid state ^{1}H NMR using CRAMPS (Fig. S8).

The molecular structure of each monomer was also confirmed by FTIR measurements (cf. Fig. 5 and Figs. S9–S12).

3.2. Structure-to-thermal properties relationship

The influence of the substituents was studied by DSC (Fig. 2), and melting (Tm) and polymerization temperatures (Tp) are all listed in Table 2. As previously reported, the electronic influence of the phenolic substituent group is affecting the DSC profile of the monomer [26,27].

Commonly, the melting behaviour of BZ monomer is influenced by the dipole-dipole interactions governed by the electron withdrawing effects of the substituents (Hammett substituent constant). The trend does not appear to be so clear in the case of the phenolic compounds tested here, compared to what was reported by the past [25–26], presumably due to the conformation of the molecules. The lowest melting temperatures (Tm) are obtained for G-fa (93 °C), which is unsubstituted and has a Hammett constant σ equal to 0, followed by the melting temperature of Cr-fa (96 °C) for which σ is equal to −0.17. The melting temperatures were increasing in the following order: G-fa (−H) = 93 °C, Cr−fa (−CH$_3$) = 96 °C, V-fa (−CHO) = 121 °C, MV-fa (−COOCH$_3$) = 129 °C and VA-fa (−COOH) = 188 °C. VA-fa exhibits the highest melting temperature (188 °C), far above the melting temperature of MV-fa (129 °C) due to more H-bonding. The existence of these H-bonds was assessed by solid state 2D SQ-DQ correlation NMR. In this experiment, only −COOH protons taking part in a hydrogen-bonded dimer structure can give rise to a −COOH auto-correlation signal in the ^{1}H SQ-DQ MAS spectrum. The ability of the VA-fa monomers to form dimers by H-bonding is evidenced by the presence of the correlation peak squared on the left bottom on the ^{1}H SQ-DQ MAS spectrum on Fig. 3.

The presence of electro-donating substituents like −CH$_3$ raised up the ring opening temperature of Cr-fa (Tp = 244 °C) compared to the non-substituted G-fa (Tp = 236 °C) and reducing the ability of the oxazine ring to open. On the contrary, the presence of electro-withdrawing substituents such as −COOCH$_3$, −CHO, or −COOH, promotes the ring opening by decreasing Tp from 236 °C (G-fa) to 223, 200 and 191 °C for MV-fa, V-fa and VA-fa respectively. The general trend of Tp is following the Hammett constants, excepting for V−fa and VA−fa due to the ability of the –CHO and −COOH functions to trigger the ROP as previously described [17,35–36]. The ROP activation energy of VA−fa is even quite high (172 kJ·mol^{-1} and 163 kJ·mol^{-1} from Kissinger and Ozawa methods, respectively) compared to what is generally reported for benzoxazines (around 110–120 kJ·mol^{-1})[37–39]. The high activation energy value for VA−fa is presumed to be affected by its high melting temperature, impeding its polymerization. In addition, it may be assumed that the −COOH undergoes a decarboxylation upon heating [19], which may contribute to the high activation energy of the monomer.

3.3. Curing profile and properties of polybenzoxazines

The polymerization mechanisms of each BZ were followed by
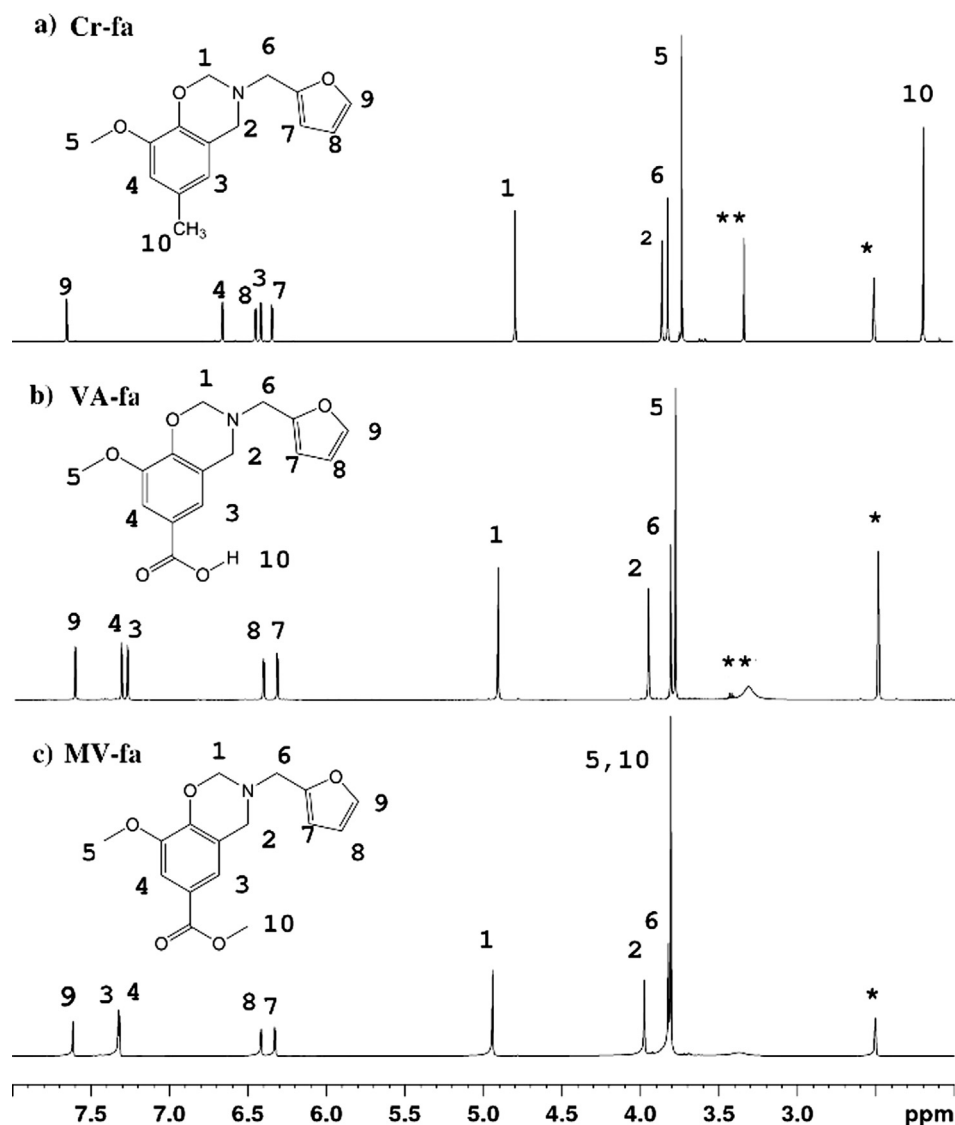
Fig. 1. ^{1}H NMR (in DMSO-d_6 (*)) of a) Cr-fa, b) VA-fa, c) MV-fa. (**water).
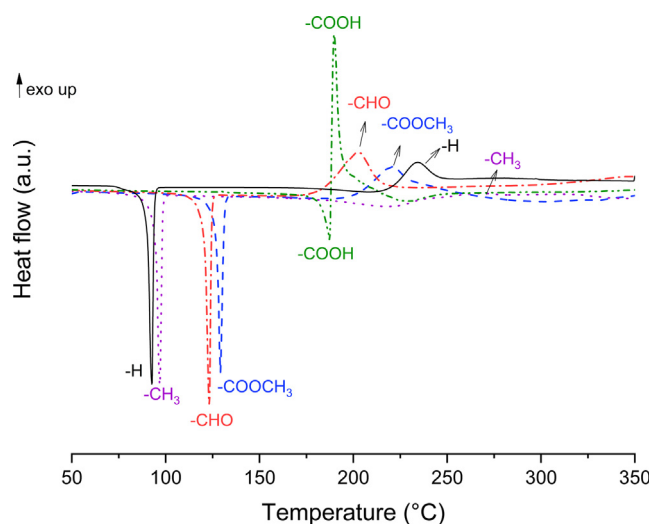
Fig. 2. DSC characterizations of the benzoxazine monomers synthesized from various phenolic compounds: −H═G−fa; −CH$_3$═Cr−fa; −CHO═V−fa; −COOCH$_3$═MV−fa; −COOH═VA-fa (N$_2$, 10 °C·min$^{−1}$).

rheological measurements, except for VA-fa, unable to cure as it is degrading and melting as the exact same temperature (TGA thermogram in Fig. S13) and polymerization (Tm = 188 °C, $T_{5\%}$ = 189 °C and Tp = 191 °C). All attempts led to a carbonized material. The curing curves of each sample are reported on Fig. 4, where two main behaviours are depicted. On one hand, V−fa and G−fa polymerize, their complex viscosity increasing after 22 min at 170 °C and after 10 min once the isothermal at 190 °C was reached, respectively. Their glass transition temperatures were measured by DSC after an isothermal cure of 1 h at 170 °C followed by 30 min at 190 °C (Table 3, column 2; Fig. S14).

On the other hand, MV-fa and Cr-fa remained in the liquid/molten state, with a complex viscosity around 200 mPa·s. The absence of a clear increase of the complex viscosity was a good indication that poly(Cr-fa) and poly(MV-fa) were not cross-linked, and thus solubilized in chloroform to be analysed by GPC. Their weight average molecular weight (M_w) was found to be equal to 417 g/mol and 6101 g/mol respectively (with a M_w/M_n ratio above a value of 4 in both cases), meaning Cr-fa was mainly dimerizing while MV-fa was forming a polymer of about 20 repetitive units.

Furthermore, the visco-elastic properties of each PBZ were monitored by rheological measurements (cf. SI Fig. S15). Poly(Cr-fa) and poly(MV-fa) exhibit a thermoplastic-like behaviour, switching from a

Table 2
Thermal properties of benzoxazine monomers synthesized from various phenolic compounds obtained from DSC.

Bz monomer (*para*-substituent)	σ_p[a]	T_m[b] (°C)	ΔH_m[c] (kJ·mol^{-1})	T_p[d] (°C)	ΔH_p[e] (kJ·mol^{-1})	Ea (Kissinger plot)[f] (kJ·mol^{-1})	Ea (Ozawa plot)[g] (kJ·mol^{-1})
Cr-fa (–CH$_3$)	− 0.17	96	–32.6	244	/	165	157
G-fa (-H)	0.00	93	− 30.5	236	11.9	124	118
V-fa (–CHO)	0.42	121	− 39.4	200	44.4	113	107
MV-fa (–COOCH$_3$)	0.45	129	− 38.1	223	28.2	121	115
VA-fa (–COOH)	0.45	188	− 8.2	191	33.5	172	163

[a] Hammett substituent constant in *para*-position [32].
[b] Maximum temperature of the melting endotherm by DSC (N$_2$, 10 °C·min^{-1}).
[c] Enthalpy of the endotherm by DSC (N$_2$, 10 °C·min^{-1}).
[d] Maximum temperature of the melting exotherm by DSC (N$_2$, 10 °C·min^{-1}).
[e] Enthalpy of the exotherm by DSC (N$_2$, 10 °C·min^{-1}).
[f] Activation energy (Ea) calculated from Kissinger plots [33].
[g] Activation energy (Ea) calculated from Ozawa plots [34].

solid to a molten state at a temperature of 70 °C for poly(Cr-fa) and 130 °C for poly(MV-fa). Their T_g was measured by DSC (Table 3, column 2) to be 55 °C and 93 °C respectively. The reasonably high T_g of poly(MV-fa) cannot be only explained by its M_w. Actually, according to the Flory-Fox equation, such a chemical structure cannot reach a T_g of 90 °C with a Mw below 20000 g/mol [40].

For a deeper understanding, poly(MV-fa) was characterized by NMR and the crosslinking process of MV-fa was followed by FTIR. The COSY NMR spectra of the MV-fa monomer and poly(MV-fa) were compared and are reported in SI (Fig. S16). The correlations between the three protons of the furfuryl part are clearly visible on the spectrum corresponding to the monomer. On the contrary, on the spectrum of poly (MV-fa), only furfuryl protons in the region between 5.9 and 6.5 ppm are visible and no correlation with lower field protons are detected. This indicates the participation of the furan ring in the polymerization

of the monomer. Additionally, the monomer was isothermally cured 1 h at 170 °C followed by 30 min at 190 °C and IR spectra were recorded at the end of each step (Fig. 5). The specific adsorption bands corresponding to the benzoxazine related mode at 914 cm^{-1} and C-O-C asymmetric stretching at 1219 cm^{-1} become broad and disappeared with the temperature increase, indicating the ring-opening polymerization of the BZ monomer. Similar observations are made for each PBZ (Figs. S9–S12). Furthermore, a broad absorption around 1600 cm^{-1} indicates that electrophilic aromatic substitutions occur on the furan ring. This demonstrates the involvement of this group in the polymerization mechanism of the studied BZ [41] in accordance with above mentioned NMR results. In addition to these phenomena, the absorption band at 1715 cm^{-1} of MV-fa is significantly decreasing and shifting to lower wavenumbers, reaching 1706 cm^{-1} when poly(MV-fa) is formed. Such a bathochromic shift is explained by the formation of H-
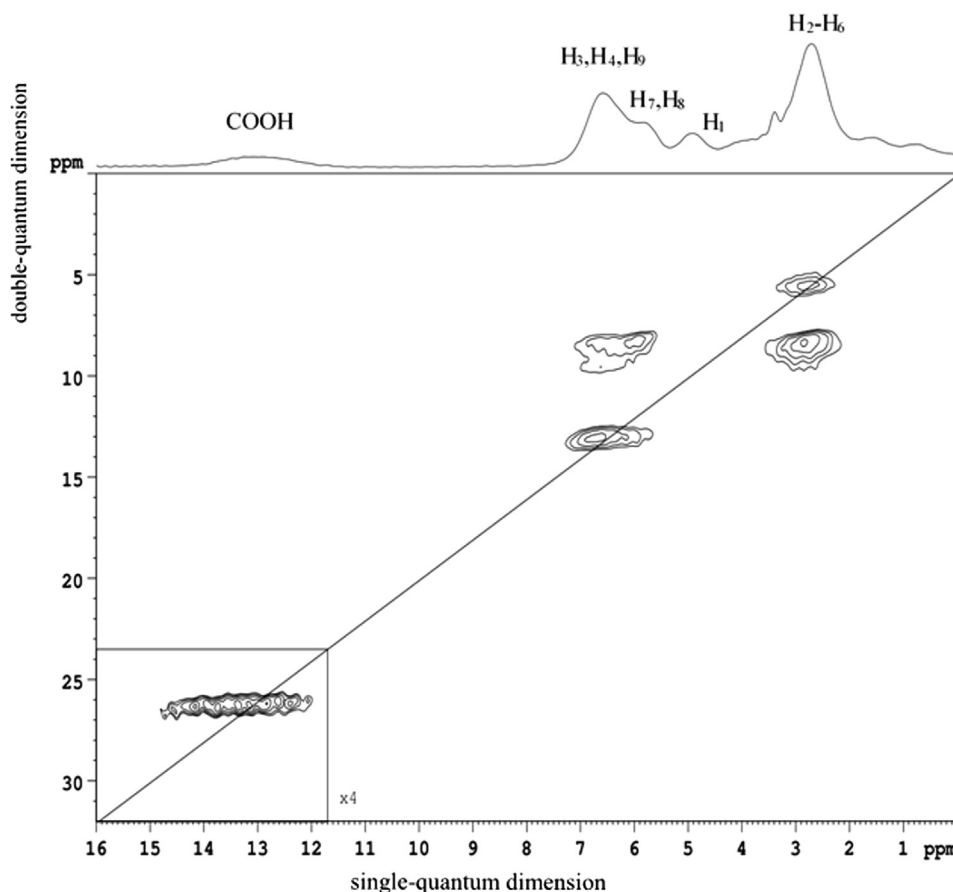
Fig. 3. Solid state ^{1}H double quantum spectroscopy of VA-fa monomer.
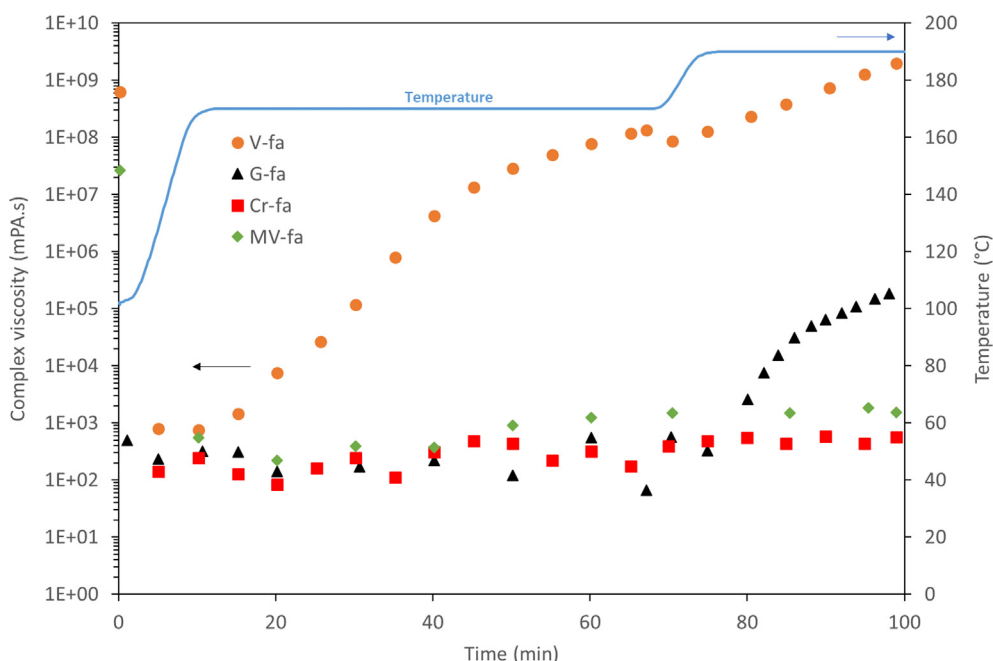
Fig. 4. Isothermal rheology monitoring of Cr-fa, G-fa, MV-fa and V-fa at 170 °C and 190 °C. Filled markers: storage moduli (G') and empty markers: loss moduli (G").
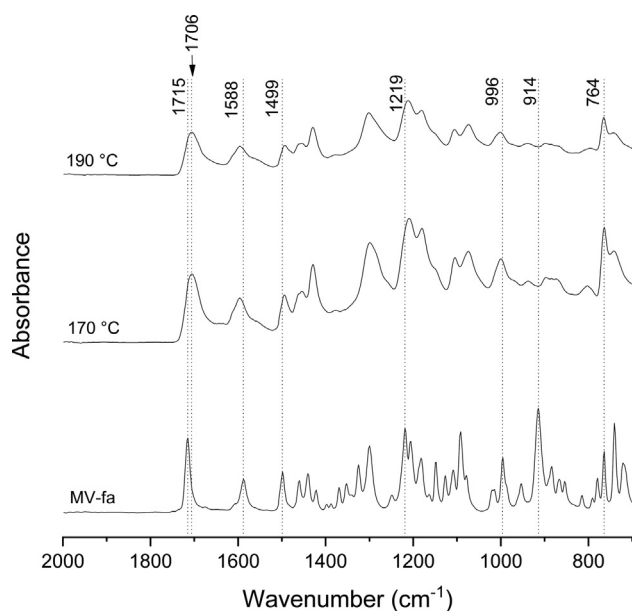
Fig. 5. FTIR characterization of the curing of MV-fa after 1 h at 170 °C and 30 min at 190 °C.

Table 3

Thermal properties of benzoxazine polymers synthesized from various phenolic compounds obtained from DSC and TGA.

Bz monomer (*para*-substituent)	T_g [a] (°C)	$T_{5\%}$ [b] (°C)	W_{lost} [c] (%)	Y^d (%)
Cr-fa ($-CH_3$)	55	190	56	7
G-fa (-H)	92	190	54	20
V-fa ($-CHO$)	173	190	13	55
MV-fa ($-COOCH_3$)	93	207	21	30

[a] Glass transition temperatures by DSC (N_2, 10 °C·min^{-1}).
[b] Temperature of 5% weight loss under an N_2 atmosphere by TGA.
[c] Weight loss during the curing 1 h at 170 °C and 20 min at 190 °C.
[d] Char yield at 800 °C calculated from the initial mass of monomer.

bonding in the materials, between the −OH of the phenolic group once the oxazine ring is opened, and the free doublets of −C=O[42]. These H-bonding are responsible for the high T_g observed for this material.

Finally, the evolution of the weight of BZ during curing was monitored by TGA (Fig. 6). In the cases of Cr−fa and G−fa, a significant weight loss is observed (respectively 56% and 54%), indicating a large part of the monomer is lost. For MV-fa and V-fa, the weight loss is lower, 21 and 13%, respectively. These results highlight the major role played by the *p*-substituents onto the thermal stability of the BZ upon curing.

The involvement of either the –COOCH$_3$ or –CHO group from MV-fa and V-fa may stabilize the polybenzoxazine structure, delaying the degradation of the polymer and the Schiff base formation. Meanwhile, the Schiff base may be less stabilized for Cr-fa and G-fa due to the lack of reactive sites, explaining the higher weight loss.

The thermal stability of the polybenzoxazine materials were analysed by TGA measurements. The $T_{5\%}$ values are reported in Table 3, column 3. The Cr-fa, G-fa and V-fa polybenzoxazines are stable up to 190 °C while MV-fa is stable until 207 °C. The char yield (Table 3, column 5), calculated here from the initial mass of monomer, are directly related to the polymerization mechanism and to the monomers weight loss during the curing process. Cr-fa and G-fa char's yield are very low (7 and 20%), while the highest char yield is reached for V-fa (55%).

Based on rheological, FTIR and TGA measurements, a tentative representation of the postulated chemical structures obtained after the ring opening process are depicted on Scheme 2.

G-fa and V-fa are both crosslinking to form a 3D network. In the case of G-fa, the availability of the *para*-position in addition to the involvement of the furan ring, allows the formation of the 3D network (Scheme 2, a). However, a significant weight loss is occurring during this process. For V-fa, the aldehyde group is involved in the formation of the cross-linked structure (Scheme 2, b), as Varma reported it by the past [18].

Cr-fa only dimerizes through the furan ring (Scheme 2, c). A large amount of monomer is also lost once the oxazine ring is opened, explaining its poor ability to polymerize.

Interestingly, MV-fa is able to polymerize through the furan ring up to a molecular weight of ca. 6000 g/mol in the conditions of curing
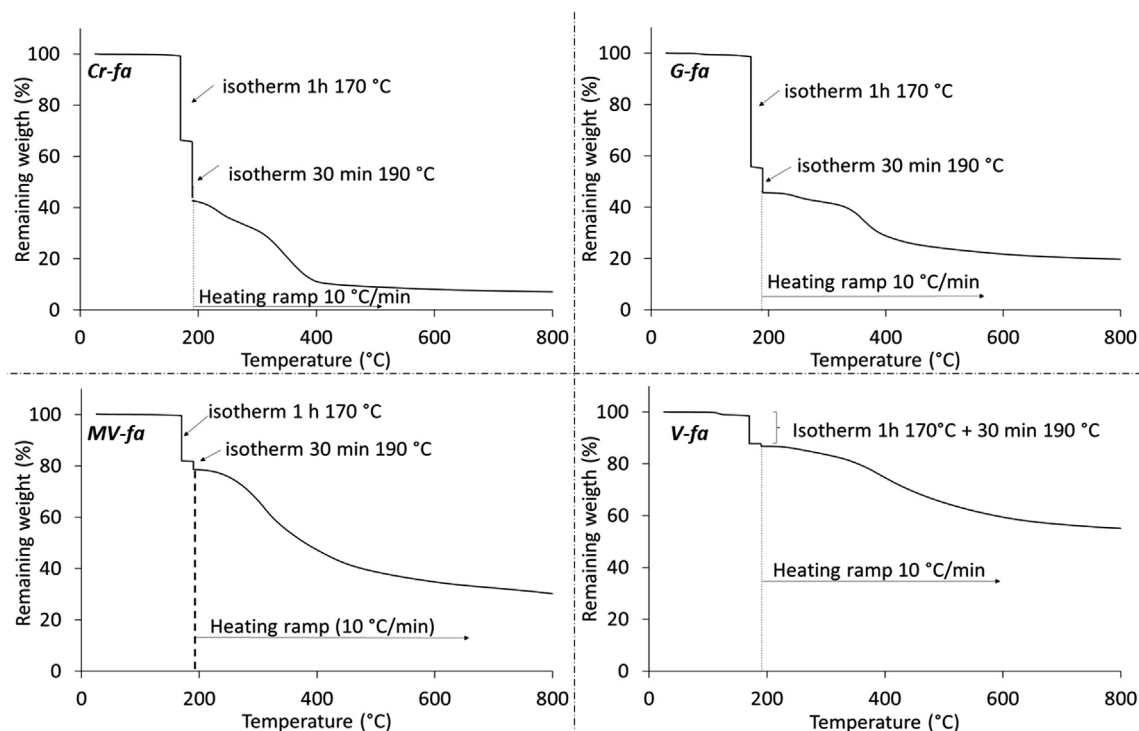
Fig. 6. TGA thermograms of Cr-fa, G-fa, MV-fa and V-fa during isothermal curing step followed by the analyses of resulting PBZ.

reported here. It leads to a thermoplastic-like material, with a T_g of 90 °C. The T_g is ensured by hydrogen bonding interactions (Scheme 2, d).

4. Conclusions

The chemical structure of lignin suggests it may be a good source of chemicals for the synthesis of benzoxazine when broken into smaller molecular units, as for instance guaiacol, creosol, vanillin, vanillic acid, etc.. This work provides an experimental review of the thermal

properties of benzoxazine monomers obtained from model phenolic compounds found in depolymerized lignin.

Para-substituted benzoxazines have been prepared from solvent-free condensation of furfurylamine with either vanillic acid (VA-fa), vanillin (V-fa), guaiacol (G-fa), methyl vanillate (MV-fa) or creosol (Cr-fa). Monomers of high purity were obtained by consecutive recrystallizations.

G-fa and V-fa are able to form 3D networks, the first one due to its unsubstituted *para*-position, the second one due to the involvement of the −CHO group during the polymerization process. Cr-fa just
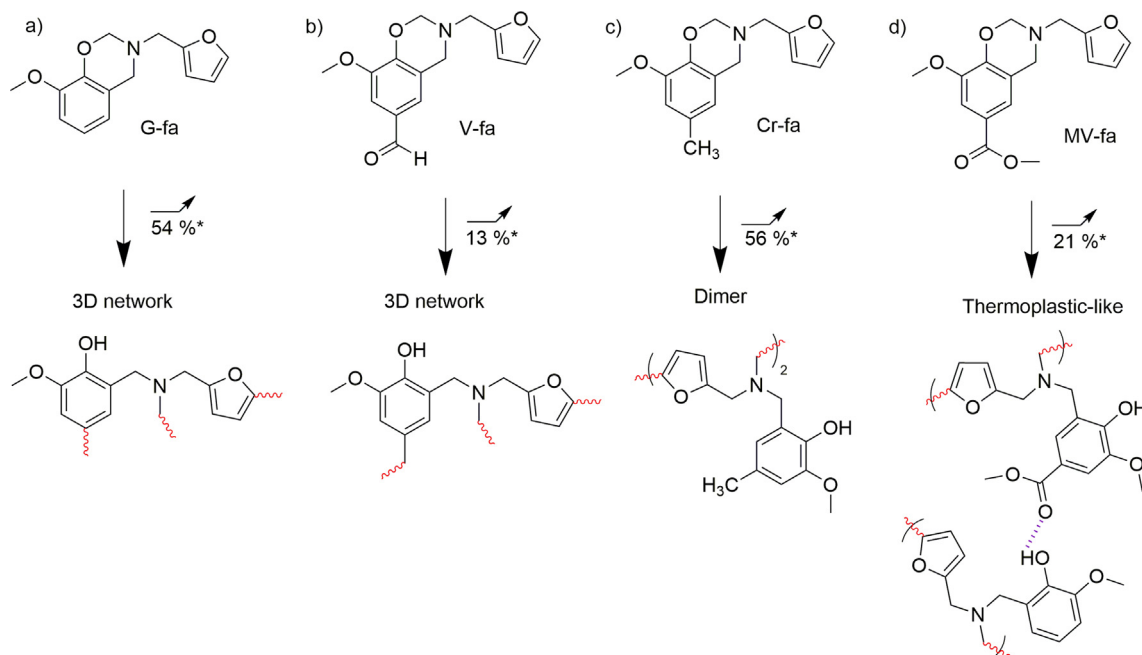
Scheme 2. Postulated chemical structures involved in the cross-linking mechanism a) 3D network from G-fa, b) 3D network from V-fa, c) Dimers from Cr-fa and d) Thermoplastic-like materials from MV-fa. The labelled numbers with * correspond to the percentage of weight loss during polymerization).

dimerizes, while MV-fa oligomerizes. For this last one, the ester interacts via H-bonds with the phenolic group of the opened oxazine ring.

TGA measurements reveals *p*-substituents highly influences the thermal stability of the monomers during their curing. A high rate of degradation is highlighted for Cr-fa and G-fa, while MV-fa and V-fa are more stable. *P*-substituents able to form either chemical or physical bonds during the cross-linking have a beneficial impact on the monomers thermal stability.

CRediT authorship contribution statement

Acerina Trejo-Machin: Validation, Investigation, Writing - original draft, Writing - review & editing. **Antoine Adjaoud:** Validation, Investigation, Writing - original draft, Writing - review & editing. **Laura Puchot:** Validation, Investigation, Writing - original draft, Writing - review & editing. **Reiner Dieden:** Validation, Investigation, Resources, Writing - original draft, Writing - review & editing. **Pierre Verge:** Conceptualization, Validation, Investigation, Resources, Writing - original draft, Writing - review & editing, Supervision, Project administration, Funding acquisition.

Declaration of Competing Interest

The authors declare that they have no known competing financial interests or personal relationships that could have appeared to influence the work reported in this paper.

Acknowledgements

Data availability

The data that support the findings of this study are available from the corresponding author, Pierre Verge, upon reasonable request.

Appendix A. Supplementary material

Supplementary data to this article can be found online at https://doi.org/10.1016/j.eurpolymj.2019.109468.

References

[1] N. Balasundram, K. Sundram, S. Samman, Phenolic compounds in plants and agri-industrial by-products: Antioxidant activity, occurrence, and potential uses, Food Chem. 99 (1) (2006) 191–203, https://doi.org/10.1016/j.foodchem.2005.07.042.

[2] C. Chio, M. Sain, W. Qin, Lignin utilization: A review of lignin depolymerization from various aspects, Renew. Sustain. Energy Rev. 107 (2019) 232–249, https://doi.org/10.1016/j.rser.2019.03.008.

[3] K. Chiou, H. Ishida, Incorporation of Natural Renewable Components and Waste Byproducts to Benzoxazine Based High Performance Materials, Curr. Org. Chem. 17 (9) (2013) 913–925.

[4] G. Lligadas, A. Tüzün, J.C. Ronda, M. Galià, V. Cádiz, Polybenzoxazines: new players in the bio-based polymer arena, Polym. Chem. 5 (23) (2014) 6636–6644, https://doi.org/10.1039/C4PY00914B.

[5] H. Ishida, P. Froimowicz, Advanced and Emerging Polybenzoxazine Science and Technology, in: H. Ishida, P. Froimowicz (Eds.), Advanced and Emerging Polybenzoxazine Science and Technology, Elsevier, Amsterdam, 2017, , https://doi.org/10.1016/B978-0-12-804170-3.09987-X.

[6] S. Ohashi, J. Kilbane, T. Heyl, H. Ishida, Synthesis and Characterization of Cyanate Ester Functional Benzoxazine and Its Polymer, Macromolecules 48 (23) (2015) 8412–8417, https://doi.org/10.1021/acs.macromol.5b02285.

[7] K. Zhang, J. Liu, S. Ohashi, X. Liu, Z. Han, H. Ishida, Synthesis of high thermal stability polybenzoxazoles via ortho-imide-functional benzoxazine monomers, J. Polym. Sci., Part A: Polym. Chem. 53 (11) (2015) 1330–1338, https://doi.org/10.1002/pola.27565.

[8] K. Zhang, J. Liu, H. Ishida, An ultrahigh performance cross-linked polybenzoxazole

[9] H. Ishida, H.Y. Low, A study on the volumetric expansion of benzoxazine-based phenolic resin, Macromolecules 30 (4) (1997) 1099–1106, https://doi.org/10.1021/ma960539a.

[10] H. Ishida, D.J. Allen, Physical and mechanical characterization of near-zero shrinkage polybenzoxazines, J. Polym. Sci., Part B: Polym. Phys. 34 (6) (1996) 1019–1030, https://doi.org/10.1002/(SICI)1099-0488(19960430)34:6<1019::AID-POLB1>3.0.CO;2-T.

[11] M.W. Wang, C.H. Lin, T.Y. Juang, Steric hindrance control synthesis of primary amine-containing benzoxazines and properties of the resulting poly(benzoxazine imide) thermosetting films, Macromolecules 46 (22) (2013) 8853–8863, https://doi.org/10.1021/ma401756d.

[12] P. Froimowicz, C.R. Arza, L. Han, H. Ishida, Smart, sustainable, and ecofriendly chemical design of fully bio-based thermally stable thermosets based on benzoxazine, Chemistry. ChemSusChem 9 (15) (2016) 1921–1928, https://doi.org/10.1002/cssc.201600577.

[13] L. Puchot, P. Verge, T. Fouquet, C. Vancaeyzeele, F. Vidal, Y. Habibi, Breaking the symmetry of dibenzoxazines: a paradigm to tailor the design of bio-based thermosets, Green Chem. 18 (11) (2016) 3346–3353, https://doi.org/10.1039/C5GC03102H.

[14] M.L. Salum, D. Iguchi, C.R. Arza, L. Han, H. Ishida, P. Froimowicz, Making benzoxazines greener: design, synthesis, and polymerization of a biobased benzoxazine fulfilling two principles of green chemistry, ACS Sustainable Chem. Eng. (2018), https://doi.org/10.1021/acssuschemeng.8b02641.

[15] L.R.V. Kotzebue, J.R. de Oliveira, J.B. da Silva, S.E. Mazzetto, H. Ishida, D. Lomonaco, Development of fully biobased high-performance bis-benzoxazine under environmentally friendly conditions, ACS Sustainable Chem. Eng. 6 (4) (2018) 5485–5494, https://doi.org/10.1021/acssuschemeng.8b00340.

[16] A. Trejo-Machin, P. Verge, L. Puchot, R. Quintana, Phloretic acid as an alternative to the phenolation of aliphatic hydroxyls for the elaboration of polybenzoxazine, Green Chem. 19 (21) (2017) 5065–5073, https://doi.org/10.1039/C7GC02348K.

[17] N.K. Sini, J. Bijwe, I.K. Varma, Renewable benzoxazine monomer from vanillin: synthesis, characterization, and studies on curing behavior, J. Polym. Sci., Part A: Polym. Chem. 52 (1) (2014) 7–11, https://doi.org/10.1002/pola.26981.

[18] N.K. Sini, J. Bijwe, I.K. Varma, Thermal behaviour of bis-benzoxazines derived from renewable feed stock 'vanillin', Polym. Degrad. Stab. 109 (2014) 270–277, https://doi.org/10.1016/j.polymdegradstab.2014.07.015.

[19] M. Comí, G. Lligadas, J.C. Ronda, M. Galià, V. Cádiz, Renewable benzoxazine monomers from "lignin-like" naturally occurring phenolic derivatives, J. Polym. Sci., Part A: Polym. Chem. 51 (22) (2013) 4894–4903, https://doi.org/10.1002/pola.26918.

[20] A. Van, K. Chiou, H. Ishida, Use of renewable resource vanillin for the preparation of benzoxazine resin and reactive monomeric surfactant containing oxazine ring, Polymer 55 (6) (2014) 1443–1451, https://doi.org/10.1016/j.polymer.2014.01.041.

[21] C. Wang, J. Sun, X. Liu, A. Sudo, T. Endo, Synthesis and copolymerization of fully bio-based benzoxazines from guaiacol, furfurylamine and stearylamine, Green Chem. 14 (10) (2012) 2799–2806, https://doi.org/10.1039/C2GC35796H.

[22] P. Thirukumaran, A. Shakila, S. Muthusamy, Synthesis and characterization of novel bio-based benzoxazines from eugenol, RSC Adv. 4 (16) (2014) 7959–7966, https://doi.org/10.1039/C3RA46582A.

[23] Y. Lou, Z. Zhao, Z. Chen, Z. Dai, F. Fu, Y. Zhang, L. Zhang, X. Liu, Processability improvement of a 4-vinylguaiacol derived benzoxazine using reactive diluents, Polymer 160 (2019) 316–324, https://doi.org/10.1016/j.polymer.2018.11.056.

[24] B. Lochab, I.K. Varma, J. Bijwe, Blends of benzoxazine monomers, J. Therm. Anal. Calorim. 111 (2) (2013) 1357–1364, https://doi.org/10.1007/s10973-012-2469-1.

[25] S. Ohashi, D. Iguchi, T.R. Heyl, P. Froimowicz, H. Ishida, Quantitative studies on the p-substituent effect of the phenolic component on the polymerization of benzoxazines, Polym. Chem. 9 (31) (2018) 4194–4204, https://doi.org/10.1039/C8PY00760H.

[26] A. Martos, R.M. Sebastián, J. Marquet, Studies on the ring-opening polymerization of benzoxazines: understanding the effect of the substituents, Eur. Polym. J. 108 (2018) 20–27, https://doi.org/10.1016/j.eurpolymj.2018.08.025.

[27] B. Fung, A. Khitrin, K. Ermolaev, An improved broadband decoupling sequence for liquid crystals and solids, J. Magn. Reson. 142 (1) (2000) 97–101.

[28] G. Metz, X.L. Wu, S.O. Smith, Ramped-amplitude cross polarization in magic-angle-spinning NMR, J. Magn. Reson., Ser A 110 (2) (1994) 219–227, https://doi.org/10.1006/jmra.1994.1208.

[29] S. Hayashi, K. Hayamizu, Chemical shift standards in high-resolution solid-state NMR (1) 13C, 29Si, and 1H nuclei, Bull. Chem. Soc. Jpn. 64 (2) (1991) 685–687.

[30] C.R. Morcombe, K.W. Zilm, Chemical shift referencing in MAS solid state NMR, J. Magn. Reson. 162 (2) (2003) 479–486.

[31] S.P. Brown, A. Lesage, B. Elena, L. Emsley, Probing proton − proton proximities in the solid state: high-resolution two-dimensional 1H − H double-quantum CRAMPS NMR spectroscopy, J. Am. Chem. Soc. 126 (41) (2004) 13230–13231, https://doi.org/10.1021/ja045461p.

[32] C. Hansch, A. Leo, R.W. Taft, A survey of Hammett substituent constants and resonance and field parameters, Chem. Rev. 91 (2) (1991) 165–195, https://doi.org/10.1021/cr00002a004.

[33] H.E. Kissinger, Reaction kinetics in differential thermal analysis, Anal. Chem. 29 (11) (1957) 1702–1706, https://doi.org/10.1021/ac60131a045.

[34] O. Takeo, A new method of analyzing thermogravimetric data, Bull. Chem. Soc. Jpn. 38 (11) (1965) 1881–1886, https://doi.org/10.1246/bcsj.38.1881.

[35] C. Zúñiga, M.S. Larrechi, G. Lligadas, J.C. Ronda, M. Galià, V. Cádiz,

Polybenzoxazines from renewable diphenolic acid, J. Polym. Sci., Part A: Polym. Chem. 49 (5) (2011) 1219–1227, https://doi.org/10.1002/pola.24541.

[36] P. Chutayothin, H. Ishida, Cationic ring-opening polymerization of 1,3-benzoxazines: mechanistic study using model compounds, Macromolecules 43 (10) (2010) 4562–4572, https://doi.org/10.1021/ma901743h.

[37] H. Ishida, Y. Rodriguez, Curing kinetics of a new benzoxazine-based phenolic resin by differential scanning calorimetry, Polymer 36 (16) (1995) 3151–3158, https://doi.org/10.1016/0032-3861(95)97878-J.

[38] Y. Lu, M. Li, Y. Zhang, D. Hu, L. Ke, W. Xu, Synthesis and curing kinetics of benzoxazine containing fluorene and furan groups, Thermochim Acta 515 (1) (2011) 32–37, https://doi.org/10.1016/j.tca.2010.12.014.

[39] K. Zhang, H. Ishida, Thermally stable polybenzoxazines via ortho-norbornene

functional benzoxazine monomers: Unique advantages in monomer synthesis, processing and polymer properties, Polymer 66 (2015) 240–248, https://doi.org/10.1016/j.polymer.2015.04.044.

[40] X. Lu, B. Jiang, Glass transition temperature and molecular parameters of polymer, Polymer 32 (3) (1991) 471–478, https://doi.org/10.1016/0032-3861(91)90451-N.

[41] Y.-L. Liu, C.-I. Chou, High performance benzoxazine monomers and polymers containing furan groups, J. Polym. Sci., Part A: Polym. Chem. 43 (21) (2005) 5267–5282, https://doi.org/10.1002/pola.21023.

[42] J. Joseph, E.D. Jemmis, Red-, blue-, or no-shift in hydrogen bonds: a unified explanation, J. Am. Chem. Soc. 129 (15) (2007) 4620–4632, https://doi.org/10.1021/ja067545z.

Chapter three: Sustainable Esterification of a Soda Lignin with Phloretic Acid

Understanding the structure of lignin biopolymer and the reactivity of lignin-like derivatives toward benzoxazine chemistry is essential to conceive lignin-derived benzoxazine. Interconnected phenolic units in lignin macromolecules are systematically *para*-substituted with non-reactive interunit linkages. The preliminary study disclosed in chapter two reveals the challenges to prepare a three-dimensional benzoxazine network from *ortho*-substituted phenols. Hence, research works focusing on the direct synthesis of lignin-derived benzoxazines are constrained due to the predominance of hindered phenolic units over unsubstituted counterparts in lignin macromolecules. This chapter reports a safe and sustainable process to improve the reactivity and processability of lignin macromolecules toward benzoxazine chemistry. In this study, technical soda lignin is esterified in solvent-free conditions with phloretic acid, a naturally occurring compound extracted from the leaves of apple trees. This sustainable synthetic route grants technical lignin with ester bonds and an affords an increase of the number of phenolic reactive sites.
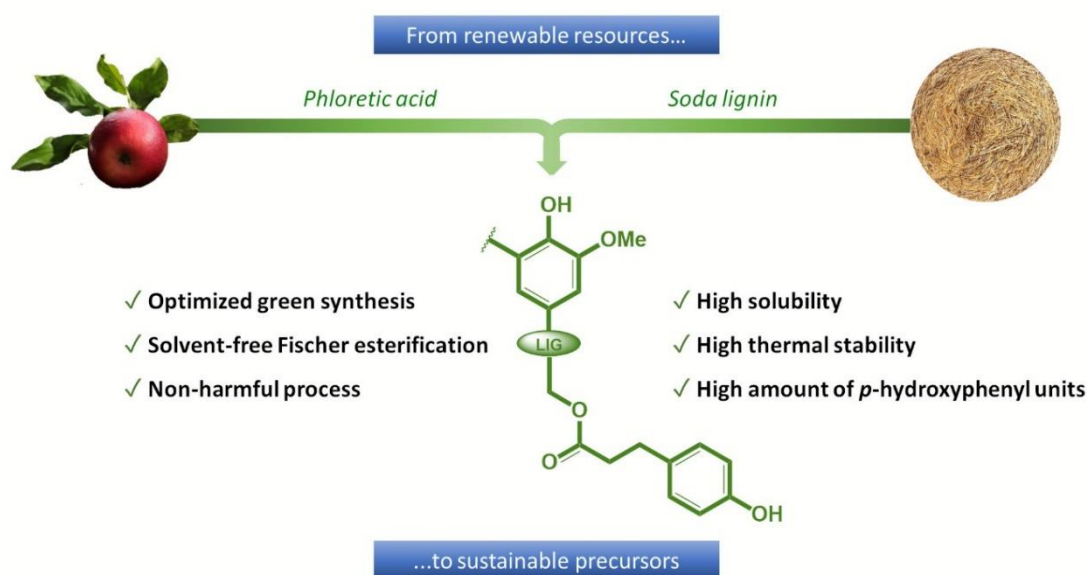
Contribution: I defined the strategy for the "design-of-experiment", made all experimental works, and interpretation of the data. I did all characterizations by my-self, with the help of Reiner Dieden for advanced discussion about NMR. I wrote the first draft of the publication, and did all the needed corrections, and revisions of the manuscript.

Sustainable Esterification of a Soda Lignin with Phloretic Acid

Antoine Adjaoud [1,2] , Reiner Dieden [1] and Pierre Verge [1,*]

1   Luxembourg Institute of Science and Technology, Materials Research and Technology Department,
    5 Avenue des Hauts-Fourneaux, L-4362 Esch-sur-Alzette, Luxembourg; antoine.adjaoud@list.lu (A.A.);
    reiner.dieden@list.lu (R.D.)
2   University of Luxembourg, 2, Avenue de l'Université, L-4365 Esch-sur-Alzette, Luxembourg
*   Correspondence: pierre.verge@list.lu

Abstract: In this work, a sustainable chemical process was developed through the Fischer esterification of Protobind® lignin, a wheat straw soda lignin, and phloretic acid, a naturally occurring phenolic acid. It aimed at increasing the reactivity of lignin by enhancing the number of unsubstituted phenolic groups via a green and solvent-free chemical pathway. The structural features of the technical and esterified lignins were characterized by complementary spectroscopic techniques, including ^{1}H, ^{13}C, ^{31}P, and two-dimensional analysis. A substantial increase in p-hydroxyphenyl units was measured (+64%, corresponding to an increase of +1.3 mmol g^{-1}). A full factorial design of the experiment was employed to quantify the impact of critical variables on the conversion yield. The subsequent statistical analysis suggested that the initial molar ratio between the two precursors was the factor predominating the yield of the reaction. Hansen solubility parameters of both the technical and esterified lignins were determined by solubility assays in multiple solvents, evidencing their high solubility in common organic solvents. The esterified lignin demonstrated a better thermal stability as the onset of thermal degradation shifted from 157 to 220 °C, concomitantly to the shift of the glass transition from 92 to 112 °C. In conclusion, the esterified lignin showed potential for being used as sustainable building blocks for composite and thermoset applications.

Keywords: lignin; sustainable; esterification; solubility

1. Introduction

A recent study from the Joint Research Center of the European Commission of Science revealed that bio-based chemicals represent only 3% of the global production in Europe [1]. It illustrates the strong dependence of the chemical industry on products derived from non-renewable feedstock. The necessity to reduce the dependence on limited petroleum resources has led to the emergence of bio-based alternatives. Lignin, a natural source of polyphenols, has been pointed out as a promising breeding ground of renewable carbon [2]. Every year, around 50 million tons of lignin are isolated as a by-product of the pulp and paper industries. Unmodified lignin meets few commercial applications due to the variation of its chemical and physical properties, closely related to the wood source and the isolation procedure [3]. However, promising recent applications have been reported [4–7]. The abundant aromatic and aliphatic hydroxyl functionalities contained in the structure of lignin affords a sustainable platform of chemical modification [8,9].

Phenolation is the most described approach among the numerous processes employed for the chemical modification of lignin [10–16]. Phenolation aims at improving lignin reactivity towards formaldehyde, and therefore at contributing to develop new prepolymers for the partial or the complete substitution of petroleum-based phenol in phenol–formaldehyde adhesives [13,14,17], phenolic foam [18] or polybenzoxazine thermoset resins [19]. Phenolation consists in a thermally induced condensation of phenols with the side-chain aliphatic hydroxyl groups of lignin, with the aim to increase the number of p-hydroxyphenyl units. Extreme reaction conditions and high amounts of acid catalysts are generally needed to

achieve the desired yield of modification. However, such drastic synthetic conditions lead to the fragmentation of lignin through the cleavage of a significant part of ether interunit linkages [10,11,15,16]. Moreover, even if substantial efforts have been done to employ synthons from renewable feedstocks [20–22], the synthesis pathway generally suffers from the use of petroleum-based harmful reactants.

Esterification is one of the oldest chemical reactions to functionalize lignin polyols [23]. Among the different esterification pathways, such as the condensation with acid anhydrides [24–27] or acyl chlorides [28–33], the Fischer esterification appeared as a straightforward strategy to produce esterified lignin [34–38], being more respectful toward the principles of green chemistry. For instance, dimer fatty acids from vegetable oils were successfully grafted onto lignin [34]. Sivasankarapillai et al. reported the synthesis of highly branched lignin-poly(ester-amine) or poly(ester-amine-amide) networks from the condensation of commercially available soda Protobind® lignin with branched carboxylic acid prepolymers [35,36]. More recently, Liu et al. proposed a sustainable strategy fitting most of the green chemistry principles for the esterification of a softwood kraft lignin and an organosolv hardwood lignin [37,38]. Several aliphatic organic acids of different chain lengths were concomitantly used as solvents and reagents. An innovative approach would be to find a sustainable synthetic pathway gathering both the phenolation and esterification of lignin.

In this study, a strategy was developed to esterify lignin with the aim to enhance the number of phenolic groups in a sustainable and environmentally friendly manner. Through a solvent-free Fischer esterification, Protobind® lignin was successfully reacted with phloretic acid, a bio-based phenolic acid originated from the leaves of apple trees [39]. Phloretic acid stands out due to its unique structure, a propionic acid terminated by a 4-hydroxyphenyl group, well-suited to the development of sustainable materials [40]. Advantageously, the oligomerization of phloretic acid is limited due the low reactivity of phenol under Fischer conditions. Protobind® lignin is a technical lignin extracted from wheat straw agro-based residues. A sulfur-free soda pulping process was employed to isolate lignin from crops [41,42]. The structure of the technical lignin differs from native lignin by the chemical modification of ether interunit linkages occurring during the delignification process. Only the aromatic repeating units and methoxyl groups remain similar throughout the isolation procedure. In addition to the high number of aliphatic hydroxyl (-OH) groups, this sulfur-free technical lignin contains carboxylic acid moieties formed during the pulping process and the three types of aromatic units, namely guaiacyl (G), syringyl (S), and *p*-hydroxyphenyl (H). A design of experiment (DOE) was drawn up to identify and quantify the dependence of pinpointed variables on the yield of conversion of the aliphatic -OH into aromatic -OH groups. The structural features of the esterified lignin were characterized by several spectroscopic techniques. 2D HSQC NMR was specifically performed to follow the structural modification of lignin substructures upon esterification. To the best of our knowledge, the enhancement of the number of phenolic groups of lignin by a solvent-free esterification with synthons from renewable resources has never been reported so far. The sustainable chemical pathway developed in this work aims to improve lignin reactivity to design alternatives to petroleum-based phenolic compounds.

2. Materials and Methods

2.1. Materials and Reagents

The different grades of the soda Protobind® lignin were purchased from the lignin company Tanovis AG (Switzerland, lignin > 90%, xylose < 4%). Prior to use, the lignin was dried overnight at T = 50 °C under reduced pressure (P = 10^{-2} mBar). All solvents and chemicals were purchased from Sigma–Aldrich (Overijse, Belgium) and used without further purification. The list of solvents is as follows: acetone (ACE), acetonitrile (ACN), butanone (MEK), chloroform (CHCl$_3$), dichloromethane (DCM), diethyl ether (DET), dioxane (DIOX), dimethylformamide (DMF), dimethylsulfoxide (DMSO), ethanol (EtOH), ethyl

acetate (ETAC), methanol (MeOH), pyridine (PYR), tetrahydrofuran (THF), toluene (TOL), water (H_2O), and basic water (NaOH, 1 M).

2.2. Esterification of Lignin

The scheme of the reaction is depicted on Scheme 1. In a 250 mL three-neck round bottom flask, dried lignin (brown powder, 2 g), phloretic acid (PA) and para-toluene sulfonic acid (*p*-TSA) were accurately weighed and mixed together by a motorized arm (200 rpm) at room temperature under a small flow of argon. Then, the temperature was gradually raised to T = 140 °C, above the melting temperature of phloretic acid (129 °C). The reaction was monitored under argon atmosphere. A water trap (calcium chloride, $CaCl_2$) was used to shift the reaction equilibrium towards the ester formation. At the end of the reaction, the temperature of the reaction medium was cooled down to room temperature. The resulting dark-brown residue was solubilized in 200 mL of acetone to collect the whole product. After the complete evaporation of acetone in open-air, the reaction crude was stirred overnight with 200 mL of diethylether to remove the excess of unreacted PA. Esterified lignin (light-brown powder) was collected after filtration, several washings with diethylether and a final drying step (T = 50 °C overnight under reduced pressure).
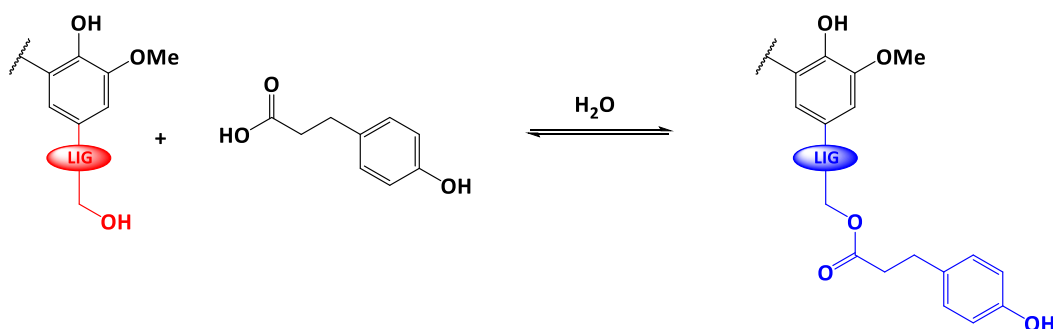
Scheme 1. Fischer esterification of Protobind® lignin with phloretic acid (LIG= -O-Ar, -O-Alk).

A DOE was carried out following a 2^3 full factorial design. An experimental matrix was employed to study the effect of critical variables on the reaction yield:

- the reaction time (**t**)
- the molar ratio between the carboxylic acid units from PA (n_{COOH_PA}) and the lignin aliphatic -OH groups determined by ^{31}P NMR (n_{OHali_P2400}) (**n**)
- the catalyst loading expressed as weight percentage (wt.%), relative to the initial amount of lignin (**c**)

The extreme levels of each critical variable were selected according to the common values reported in the literature and are tabulated in Table 1 (discrete values). The experimental matrix was generated randomly considering the extreme values of each variable and analyzed with Ellistat software (student license). All the experiments were run.

Table 1. Critical variables in the Fischer esterification of Protobind® lignin.

Reaction Parameters	Symbol	Level	
		−1	**+1**
Time (h)	t	12	48
Molar ratio ($n_{COOH\_PA}/n_{OHali\_P2400}$ [a])	n	1	5
Catalyst loading (wt.%)	c	0.5	2.5

[a] determined by ^{31}P NMR spectroscopy.

2.3. Equipments and Characterization

Nuclear magnetic resonance (NMR) spectroscopy was recorded using an AVANCE III HD spectrometer (Bruker, Fällanden, Switzerland) equipped with a 5 mm BBO-probe, operating at a proton frequency of 600 MHz. ^{31}P NMR analysis was performed following the common procedure reported by Granata and Argyropoulos [43]. 30 mg of dried lignin was accurately weighed in a 1 mL vial and afterwards dissolved in 500 μL of the solvent mixture (A) containing deuterated chloroform ($CDCl_3$) and anhydrous pyridine in a 1/1.6 (*v/v*) ratio. The mixture of solvents (A) was also used for the preparation of the relaxation agent and the internal standard solutions (respectively, B and C). Chromium (III) acetylacetonate (14 μmol mL^{-1}) and endo-N–hydroxy–5–norbornene–2,3–dicarboximide (108 μmol mL^{-1}) were selected as the relaxation reagent and the internal standard compounds, respectively [44]. Phosphitylation was performed by adding 50 μL of 2-chloro-4,4,5,5-tetramethyl-1,3,2-dioxaphospholane (TMDP) just after the addition of solutions A, B and C (respectively, V = 150, 100 and 100 μL). All ^{31}P NMR spectra were calibrated on the H_2O derivatized peak (sharp signal at δ = 132.2 ppm). The choice of the internal standard (IS), the assignment and the spectral integration limits of every peak was made according to the relevant suggestions reported by Balakshin et al. [45]. The ^{1}H NMR spectra of lignin samples (15 mg) were recorded in 0.6 mL of DMSO-d$_6$. The acquisition parameters were as follows: 25 °C, 12,019 Hz spectral width, 128 scans, 2.7 s acquisition time and 10 s relaxation delay (D1). All the chemical shifts were referenced to the DMSO-d$_6$ solvent peak ($δ_C$ = 39.5 ppm, energy from hydrogen bonds between molecules ($δ_H$) = 2.49 ppm). The ^{13}C NMR experiments were adapted from the procedure developed by Capanema et al. [46]. Typically, 16 mmol of Cr(acac)$_3$ and 200 mg of lignin were dissolved in 550 μL of DSMO-d$_6$. The acquisition parameters were as follows: 25 °C, 36,232 Hz spectral width, 20,000 scans, 1.4 s acquisition time, and 2.5 s relaxation delay. The ^{1}H-^{13}C 2D HSQC NMR experiment was adapted from the procedure reported by Tran et al. [47]. Typically, 200 mg of lignin were dissolved in 700 μL of DSMO-d$_6$. The 2D HSQC spectra were acquired using the standard Bruker pulse sequence "hsqcetgpsp.3". The acquisition parameters were as follows: 25 °C, 24 scans. F1 dimension: 25,641 Hz spectral width, 5.6 ms acquisition time. F2 dimension: 7212 Hz spectral width, 170 ms acquisition time. The ^{1}H -^{13}C 2D HMBC NMR experiment was adapted from the procedure reported by Huber et al. [48]. The 2D HMBC spectra were acquired using the standard Bruker pulse sequence "hmbcgplpndqf". The acquisition parameters were as follows: 25 °C, 16 scans. F1 dimension: 31,646 Hz spectral width, 32.4 ms acquisition time. F2 dimension: 6602 Hz spectral width, 310 ms acquisition time.

Elemental analysis (CHNS/O measurements) was performed on a Vario MACRO cube (Elementar France SARL, Lyon, France). Samples were put into an oxygen-enriched furnace at 1150 °C, where a combustion process converted carbon to carbon dioxide; hydrogen to water; nitrogen to nitrogen gas/oxides of nitrogen and sulfur to sulfur dioxide. The combustion products were heated separately to the corresponding desorption temperature ($T_{desorpt.}$) in order to release the components as follows: CO_2 ($T_{desorpt.}$ = 240 °C), H_2O ($T_{desorpt.}$ = 150 °C) and SO_2 ($T_{desorpt.}$ = 100 °C or 230 °C).

Fourier transform infrared spectroscopy (FTIR) was performed by using a TENSOR 27 (Bruker, Ettlingen, Germany) instrument in the attenuated total reflection (ATR) mode using a diamond crystal. All spectra were recorded at room temperature in a direct absorbance mode and a frequency range of 4000 to 400 cm^{-1} with 16 scans averaged at a 4 cm^{-1} resolution.

Solubility tests were performed similarly to the description by Sameni et al. with minor modifications [49]. 50 mg of dried lignin samples were mixed with 5 mL of organic solvent and subsequently sonicated for 15 min in a water bath sonicator. The insoluble fraction was filtered on 0.2 μm agilent syringe filters. The lignin samples were weighed before the mixing and after the evaporation of the solvent (one day under the fume hood and overnight under reduced pressure at T = 50 °C, if necessary). The temperature was

raised up to 80 °C when high-boiling-point solvents were employed. The soluble fraction was calculated as follows (1):

$$S \text{ (wt.\%)} = 100 \times [m_i - m_f]/m_f \tag{1}$$

where "m_i" corresponds to the initial mass of the lignin samples and "m_f" the mass of the soluble fraction. The lignin samples were subjected to an experimental estimation of Hansen solubility parameters (HSPs) [50]. The samples were graded as compatible with the solvent if S > 80 wt.% or incompatible with the solvent if S < 80 wt.%. With the help of the generated data set, the HSPs of each lignin samples were calculated using the HSPiP 5th edition, 5.0.13 software (Copyright © 2008–2015 Steven Abbott and Hiroshi Yamamoto).

Gel permeation chromatography (GPC) was performed on a 1260 Infinity II gel permeation chromatograph (Agilent technologies, Craven Arms, United Kingdom) to determine the molecular weight of the lignin samples. The chromatograph was equipped with an integrated IR detector, PLgel 5 mm MIXED-C, PLgel 5 mm MIXED-D columns and a PLgel guard column (Agilent Technologies, USA). THF was used as an eluent with a flow rate of 1.0 mL min^{-1} at 40 °C. Polystyrene standards (Agilent Technologies, $Mp = 162$–1500×10^3 g mol^{-1}) were used to perform the calibration of the system. The molecular weight is determined on the THF's soluble fraction part (4 mg mL^{-1}).

Differential scanning calorimetry (DSC) thermograms were recorded on the DSC 3+ device (Mettler Toledo, Greifensee, Switzerland) in standard pierced aluminum crucibles (40 μL). The sample was initially subjected to a first heating–cooling ramp from 25 to 150 °C to remove residual traces of moisture and clear the thermal history of the lignin samples (N$_2$ atmosphere, flow rate: 40 mL min^{-1}, heating rate: 10 °C min^{-1}, cooling rate: 20 °C min^{-1}). The sample was finally reheated from 25 to 225 °C (heating rate: 10 °C min^{-1}). The glass transition temperature (T_g) is defined as the midpoint temperature interval when the baseline shift upon heating (endothermic transition).

Thermogravimetric analysis (TGA) was performed on the TGA 2 device (Mettler Toledo, Greifensee, Switzerland) in a standard ceramic alumina pan from 25 to 800 °C (N$_2$ atmosphere, flow rate of 40 mL min^{-1}, heating rate: 10 °C min^{-1}). The onset of the degradation temperature and the major degradation temperatures were determined using the derivative of the TGA curves (DTG). The DTG curves were independently calculated considering the Equation (2):

$$\Delta m / \Delta T = [m_i - m_f] / [T_i - T_f] \tag{2}$$

where "m" stands for the relative mass (%) and "T" the temperature (°C).

3. Results

3.1. Structural Characterization of the Esterified Lignin

As phloretic acid melts above 129 °C, its mixture with lignin in the presence of *p*-TSA allows the reaction to be performed in melt at 140 °C, at the condition the lignin is thermally stable at this temperature. Among the different commercial grades proposed by Tanovis AG, Protobind® 2400 technical lignin (P2400) was selected based on this parameter (Table S1, Figure S1 in Supplementary Materials), as the onset of its thermal degradation is not reached before 157 °C. The structural features of the esterified lignin (P2400-PA) were characterized by ^{1}H, ^{13}C and HSQC NMR. Due to the complex structure of lignin, the three techniques were essential to accurately define the structure of P2400 and to determine the structural changes coming from the esterification. [31]P was also performed to quantify the rate of esterification. It is worthwhile to note that the esterification reaction was performed solventless. The ^{1}H NMR spectra of P2400 and P2400-PA are reported in Figure 1.
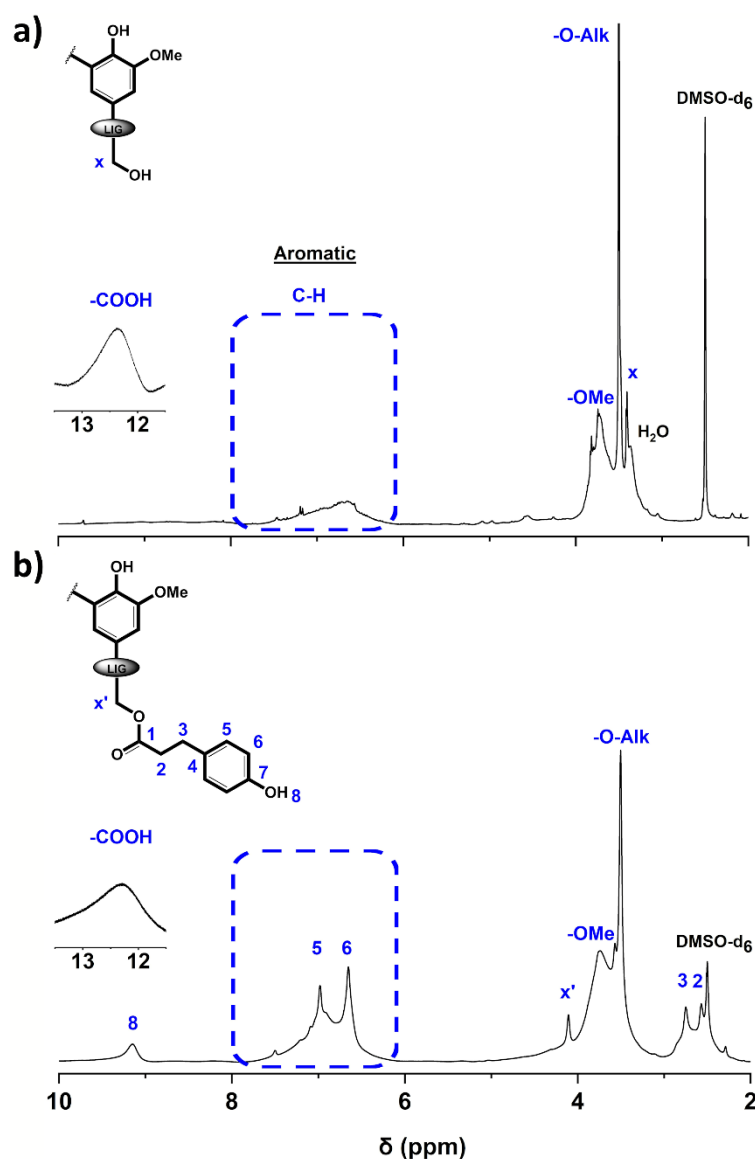
Figure 1. ^{1}H NMR spectra of (**a**) Protobind® 2400 technical lignin (P2400) and (**b**) esterified lignin (P2400-PA) (DMSO-d$_6$). A tenfold increase was performed in the carboxylic acid region (δ = 11.5–13.5 ppm).

For P2400, the peaks located at δ = 3.44, 3.52, 3.76 and 12.48 ppm correspond to the protons adjacent to an oxygen atom (α-protons adjacent to the aliphatic -OH groups and the etherified interunit linkages, H$_x$ and -O-Alk, respectively), the methoxyls (-OCH$_3$), and the carboxylic acid (-COOH) moieties, respectively (Figure 1a). The characteristic aromatic protons of the three phenylpropane units are attributed to the broad signal at δ = 6–7.5 ppm. The success of the esterification reaction was confirmed by the appearance of new peaks at δ = 2.57 and 2.75 ppm corresponding to the methylene protons (2, 3) of the bridge between the ester bond and the *p*-hydroxyphenyl group. In the aromatic area (δ = 6–8 ppm), the chemical modification was reflected by the appearance of two signals (5, 6) corresponding to the aromatic protons of the PA counterpart (δ = 6.69 and 7.02 ppm, respectively). The emergence of a strong peak at δ = 9.21 ppm is consistent with the introduction of phenolic groups (8). In addition to these new peaks, the characteristic α-protons adjacent to the aliphatic -OH groups shifted downfield due to the new chemical environment (H$_{x'}$, δ = 4.12 ppm).

Quantitative ^{13}C NMR was employed to provide more details about the structure by the identification of quaternary and oxygenated carbon over the spectral range $\delta = 20–180$ ppm (Figure 2).
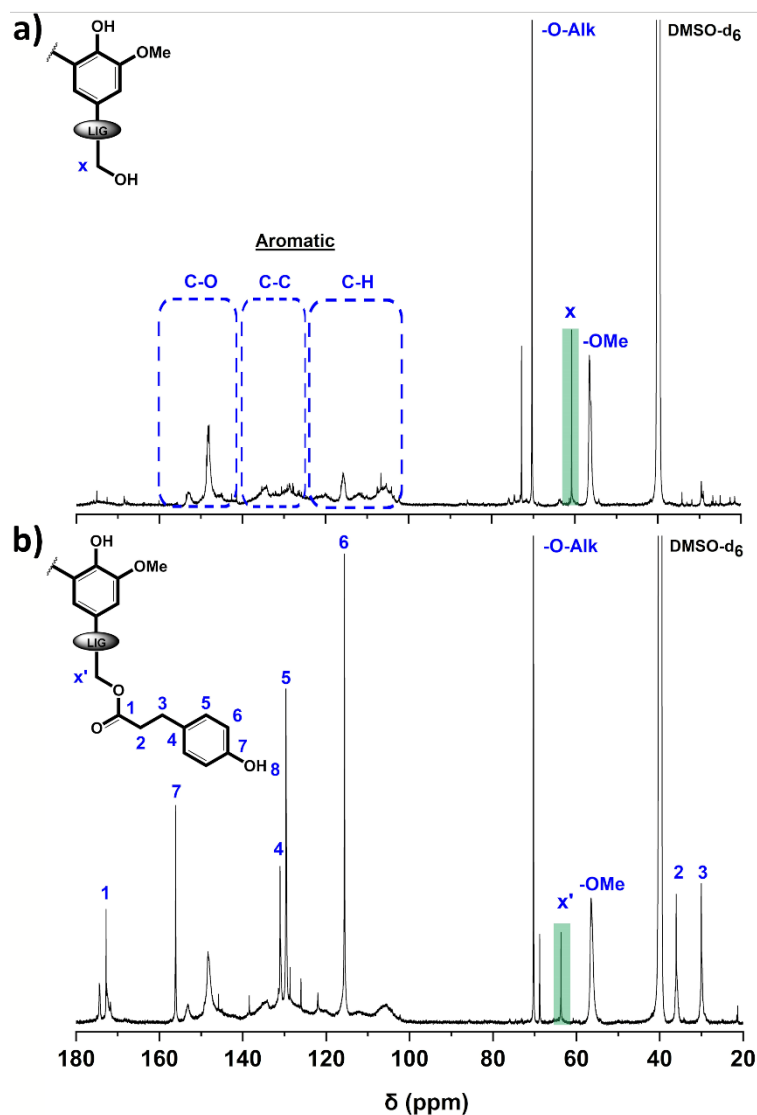
Figure 2. ^{13}C NMR spectra of (**a**) P2400 and (**b**) P2400-PA (DMSO-d_6).

The assignment of lignin's characteristic peaks was based on the comprehensive studies conducted by Capenama and coworkers [46,51]. Only peaks from the etherified interunit linkages and -OMe are clearly noticeable for the technical lignin (Figure 2a). The intense and sharp signals in the oxygenated aliphatic carbon range ($\delta = 58–90$ ppm) suggested that the interunit linkages and the aliphatic -OH groups of P2400 were chemically modified by the supplier during the isolation procedure [52]. The signal at $\delta = 56.5$ ppm is assigned to the characteristic methoxyl groups (-OMe). The methylene carbon in α-position of the aliphatic -OH groups (C_x) and etherified interunit linkage (-O-Alk) are observed at $\delta = 60.8$ and 70.3 ppm, respectively. The success of the reaction was confirmed by the shifting of the peaks associated to carbon in α-position of the aliphatic -OH groups, indicating a modification of the chemical environment ($C_{x'}$ at $\delta = 63.8$ ppm, Figure 2b). Aliphatic carbon atoms associated to the propionic chain of PA appeared at lower chemical shift (C_2 and C_3 at $\delta = 36.1$ and 30.0 ppm, respectively). The most significant evidence of the success of the esterification from ^{13}C NMR is the emergence of a peak in the aliphatic carboxyl range associated with the ester bond (C_1, $\delta = 172.8$ ppm). It is noteworthy that the absence

of conjugated ester peaks (δ = 166–168 ppm) originated from the esterification of phenol moieties, which underlines the selectivity of the Fisher esterification towards aliphatic -OH groups [46]. The aromatic region spans several spectral ranges according to the nature of the carbon, i.e., aromatic methine carbons (δ = 103–125 ppm), aromatic carbon–carbon moieties (non-oxygenated quaternary carbons, δ = 125–141 ppm), and aromatic oxygenated carbons (δ = 141–160 ppm) [53]. The number of methoxyls and aliphatic carboxyl functionalities per aromatic ring was calculated through a semi-quantitative interpretation of the ^{13}C NMR spectra. The number of carbons in the aromatic region (δ = 103–160 ppm) was normalized to 600 corresponding to 6 $\times$ 100 aromatic units (value expressed per 100 Ar) [51]. The methoxyl content (δ = 58–54 ppm) decreased from 132/100 Ar to 77/100 Ar for P2400 and P2400-PA, respectively. The amount of aliphatic carboxyl functionalities (δ = 168–175 ppm) shifted from 14/100 Ar for P2400 to 42/100 Ar for P2400-PA. The decrease in methoxyl groups through the increment of *p*-hydroxyphenyl units, together with the increase in carboxyl functionalities in the esterified lignin depicts the success of the reaction.

The HSQC spectra of P2400 and P2400-PA are reported in Figure 3 over two regions of interest: the aliphatic side chain (δ_C/δ_H: 25–80/2.4−4.4) and the aromatic (δ_C/δ_H: 100−155/6.0−8.0) regions. On the figures are also reported the structures and substructures identified in P2400 and P2400-PA. Cross peak signals listed in Table S2 were assigned with respect to comprehensive databases reported for wheat straw lignins [54–57]. In P2400, the most intense correlation was identified as methoxyl (-OMe) groups (δ_C/δ_H: 56.5/3.76, Figure 3a). Although the β-aryl ether (β-O-4′) stands for the most occurrent interunit linkages in wheat straw lignin [54], only the characteristic cross peak of the methylene in α-position of the lignin aliphatic -OH groups is observed (A_x, δ_C/δ_H: 60.8/3.52). This observation is in line with the chemical modification operated on interunit linkages during the extraction process (Figure 2a). Minor amounts of resinol (β-β') substructures were also detected (C_β and C_γ). Weak cross peak signals located at δ_C/δ_H = 73.1/3.13, 74.6/3.33, and 75.9/3.58 were assigned to the presence of xylan moieties (X_2, X_3 and X_4), as previously reported for soda lignin [54,56,57]. The aromatic region of P2400 highlighted the presence of the three types of phenylpropane units through syringyl (S_2 and S_6), guaiacyl (G_2, G_5 and G_6), and *p*-hydroxyphenyl ($H_{2,6}$ and $H_{3,5}$) cross peak signals (Figure 3c). Other minor substructures were distinguishable, including signals corresponding to α-oxidized esterified syringyl units ($S'_{2,6}$), ferulate (Fa) and *p*-coumarate (Pc) derivatives (Table S2 in Supplementary Materials) [54,55,57]. The success of the esterification was confirmed by signal modifications in the aliphatic side chain region of P2400-PA (Figure 3b). The signal corresponding to the α-methylene groups (A_x) was replaced by a new cross peak associated to the esterified substructures ($B_{x'}$, δ_C/δ_H: 63.8/4.12). The presence of this new peak confirms the involvement of the aliphatic -OH groups in the esterification to form the new structure noted B on Figure 3. Two new correlations appear between δ_H = 2–3 ppm, corresponding to the methylene bridge of PA counterparts (B_2 and B_3). Resinol (C) and xylan (X) substructures were not affected by the esterification process. In the aromatic region, only peaks originated from the esterification were identified (Figure 3d). The esterification of P2400 causes the appearance of aromatic correlations associated to the new phenolic units from PA counterparts ($B_{5,6}$). Signals of α-oxidized esterified syringyl units, ferulate and *p*-coumarate derivatives disappeared. Moreover, HMBC experiments were also performed on P2400-PA to substantiate the connectivity of ester moieties to the lignin backbone (Figure S2, Table S3 in Supplementary Materials) [48]. The spectral window region was chosen to show the correlations associated with the esterified substructure B (δ_C/δ_H: 125−180/2.4−4.4). The correlation of the carboxyl carbon (C_1, δ = 172.8 ppm) with the methylene bridge of PA (H_3 and H_2, δ = 2.75 and 2.57 ppm, respectively) and the α-methylene protons ($H_{x'}$, δ = 4.12 ppm) reflects the success of the esterification.
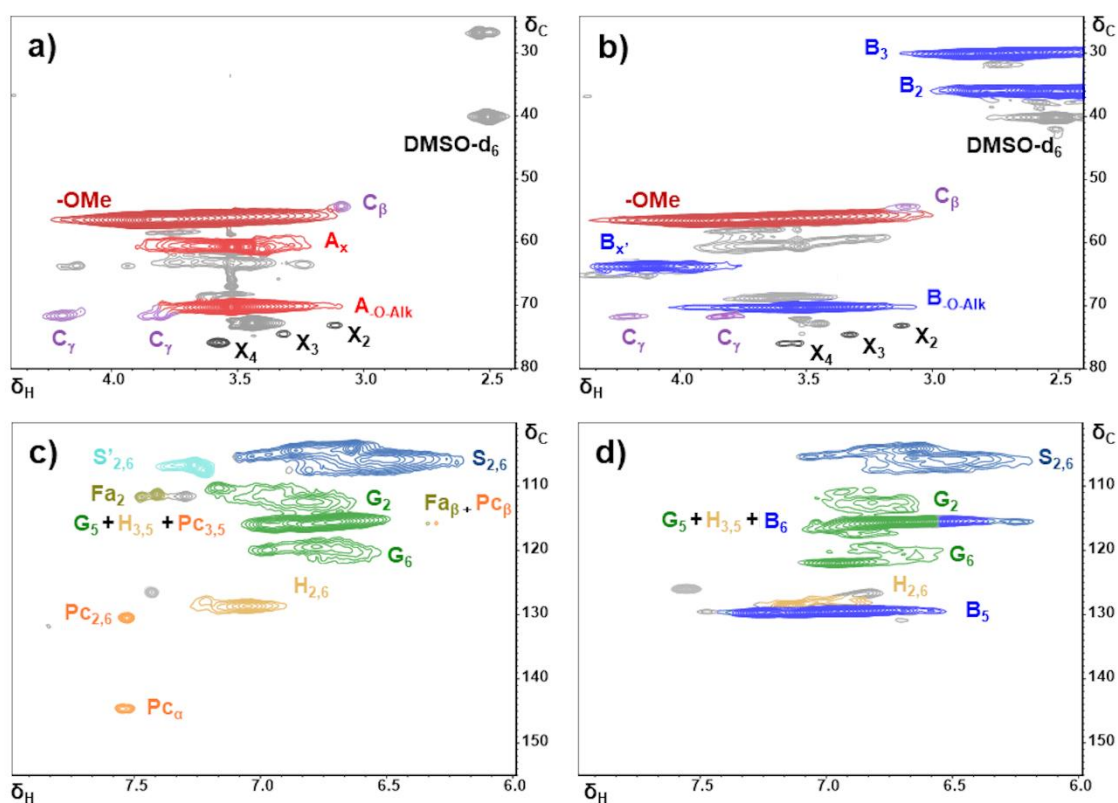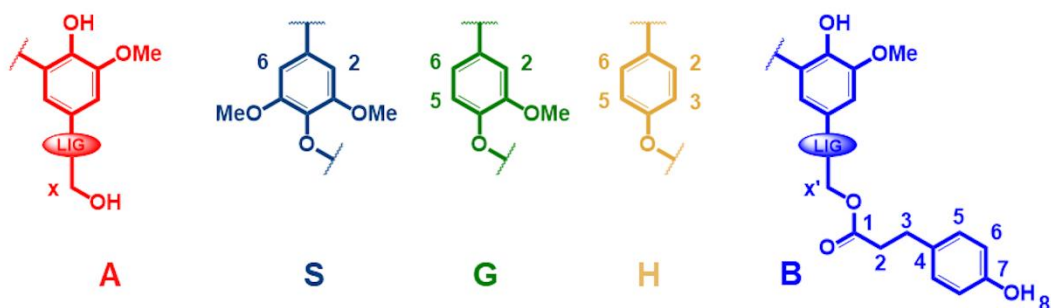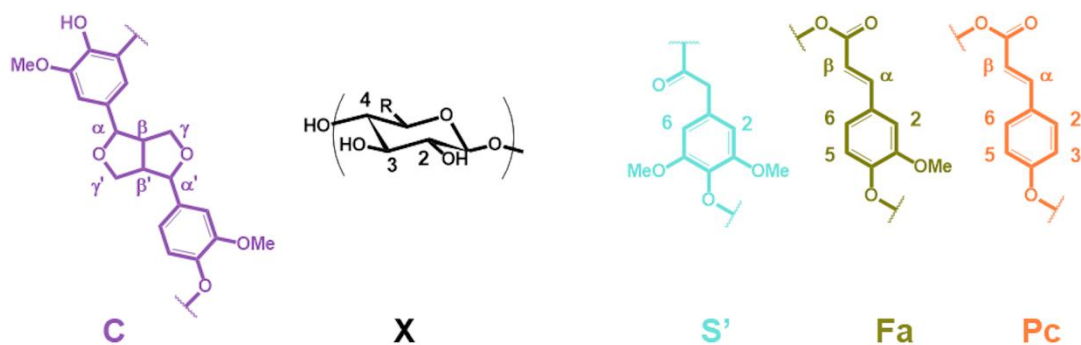
Figure 3. Aliphatic side chain (δ_C/δ_H: 25−80/2.4−4.4) and aromatic (δ_C/δ_H: 100−155/6.0−8.0) regions in the 2D HSQC NMR spectra of P2400 (**a,c**) and P2400-PA (**b,d**). Signal assignments are reported in Table S2. Major and minor lignin substructures were identified and shown below the HSQC NMR spectra.

Finally, the carboxylic, aromatic and aliphatic -OH groups of lignin were identified and quantified by ^{31}P NMR experiments [43]. The interval of the different types of lignin -OH groups were assigned as follows: aliphatic -OH (δ_{OHali} = 146–150 ppm), 5-substituted aromatic -OH (S and G condensed units, $\delta_{5-susbt.}$ = 141–144.5 ppm), G non-condensed aromatic -OH (δ_{Gnc} = 138.5–141 ppm), *p*-hydroxyphenyl aromatic -OH (δ_H = 137–138.5 ppm), and carboxyl groups (δ_{COOH} = 134–136 ppm) (Figure S3) [45]. A magnification of the ^{31}P NMR spectra of P2400 and P2400-PA between δ = 134–149 ppm is reported in Figure 4.
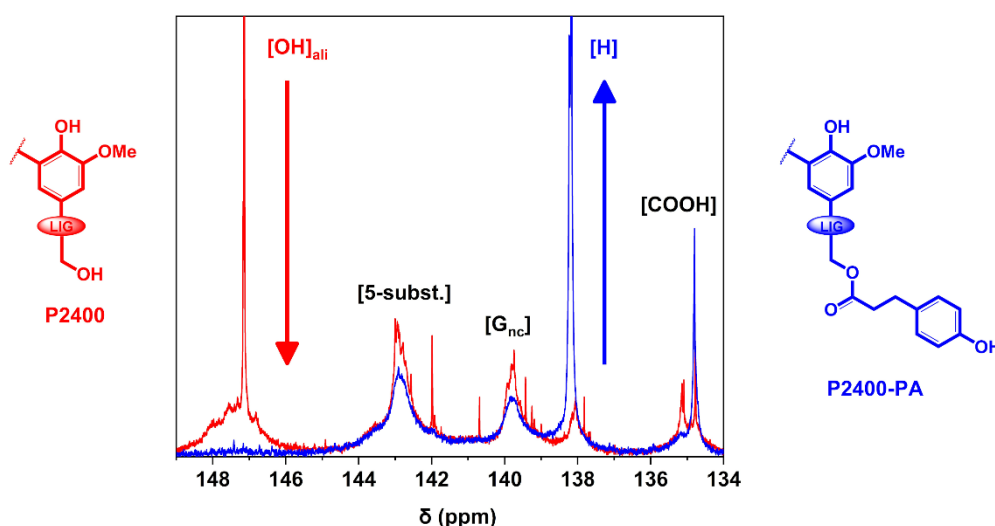
Figure 4. ^{31}P NMR spectra of P2400 and P2400-PA.

The unusual sharp signal observed in the aliphatic region of P2400 ([OH]$_{ali}$, δ = 147.1 ppm) tends to confirm the modification of the aliphatic -OH groups, as firstly reported by Azhavi et al. [52]. A significant drop of the aliphatic -OH groups concomitantly to the substantial increase in *p*-hydroxyphenyl units ([H], δ = 137.4 ppm) were observed by comparing both ^{31}P spectra. The results of the quantitative determination of lignin -OH groups through ^{31}P NMR analysis are gathered in Table 2. The amount of lignin functionalities are expressed in mmol of functional group per gram of lignin dry matter (mmol g^{-1}). The amount of [COOH] units for P2400-PA is nearly equivalent to the initial amount in P2400 (~0.80 mmol g^{-1}). As regards to the aromatic units, only the content in [H] units considerably increased for P2400-PA stemming from the chemical modification ([H] = 1.81 mmol g^{-1}). This sustainable esterification process led to an increase of 1.3 mmol g^{-1} in the amount of [H] units. For the sake of comparison, the phenolation pathway applied on a soda lignin contributes to an increase of 0.9 mmol g^{-1} for this type of unit [16]. The lower amount of [5-subst.] and [G$_{nc}$] tends to indicate that thermally induced side-reactions occurred during the esterification. The reaction also led to a significant decrease in the overall amount of lignin aliphatic -OH groups from 2.00 mmol g^{-1} for P2400 to 0.14 mmol g^{-1} for P2400-PA. However, the success of the reaction cannot just be followed by considering the decrease in the amount of aliphatic -OH groups ([OH]$_{ali}$). Indeed, the high temperature of the reaction is also suitable for lignin self-condensation, depolymerization and repolymerization, which could consume the amount of [OH]$_{ali}$ [58–60]. Consequently, the yield of the reaction must be determined by considering the increase in [OH]$_{aro}$, and more specifically the increase in [H] units (Table 2, column 5).

Table 2. Summary of the amount of functional groups in P2400 and P2400-PA quantified by ^{31}P NMR experiment (expressed in mmol per g of lignin dry matter, average of three measurements).

Sample	[COOH]	[5-subst.]	[G$_{nc}$]	[H]	[OH]$_{aro}$	[OH]$_{ali}$
P2400	0.78 ± 0.04	2.12 ± 0.23	1.29 ± 0.22	0.53 ± 0.07	3.94 ± 0.51	2.00 ± 0.23
P2400-PA	0.81 ± 0.03	1.79 ± 0.09	1.03 ± 0.07	1.81 ± 0.07	4.63 ± 0.22	0.14 ± 0.02

FTIR and elemental analysis provided complementary insights on the structural features of the esterified lignin. For the technical lignin, the weak absorption band at $\nu = 1705$ cm^{-1} corresponds to the conjugated carboxylic acid stretching of the ferulate and the *p*-coumarate derivatives (Figure S3) [61,62]. Although most of the absorption bands of P2400-PA overlapped with the pattern of P2400, a clear shift was observed in the carboxyl area corresponding to the ester stretching ($\nu = 1728$ cm^{-1}), confirming the success of the esterification. The elemental analysis (Table 3) indicated that a relatively low content of nitrogen and sulfur originated from the extraction process were measured (~0.6%) [63,64]. In P2400-PA, the carbon content increased at the expense of the oxygen content, in accordance with the chemical modification (67.20% and 25.89%, respectively).

Table 3. Elemental composition of P2400 and P2400-PA.

Sample	C (%)	H (%)	N (%)	S (%)	O (%)
P2400	64.44 ± 0.01	6.06 ± 0.14	0.56 ± 0.05	0.63 ± 0.03	28.31
P2400-PA	67.20 ± 0.04	5.68 ± 0.16	0.65 ± 0.03	0.58 ± 0.01	25.89

3.2. Optimization of the Fischer Esterification of Protobind® Lignin

A design of experiment methodology (DOE) was applied to identify and quantify the dependence of the reaction parameters on the solvent-free Fischer esterification of P2400 with PA. The temperature of the reaction was fixed at T = 140 °C, i.e., between the melting temperature of PA (T_m = 129 °C) and the onset temperature of thermal degradation of P2400 (T_{onset} = 157 °C). The reaction time (t), the initial molar reactant ratio (n) and the catalyst loading (c) were identified as the critical variables of the esterification (Table 1). A two-level three factors full factorial experiment (2^3) was built considering all the possible combinations of the extreme levels of the critical variables. Therefore, a series of eight experiments were completed (Table 4). Thus, the success of the esterification was defined by following the increase in the amount of [H] units. This designation encompasses the original *p*-hydroxyphenyl units of lignin and the 4-hydroxyphenyl groups from PA counterparts. It is worthwhile to indicate that unreacted PA was removed by washing several times with DET. The response associated to the DOE corresponds to the increase in the amount [H] units (determined by ^{31}P NMR spectroscopy) for the esterified lignin. The response was calculated according to Equation (3):

$$Y\ (\%) = 100 \times [X_{H\_P2400\text{-}PA} - X_{H\_P2400}]/X_{OHali\_P2400} \tag{3}$$

where "$X_{H\_P2400\text{-}PA}$" (mmol g^{-1}) stands for the amount of [H] units in the esterified lignin (EL), "X_{H_P2400}" (mmol g^{-1}) for the initial amount of [H] units in P2400 and "X_{OHali_P2400}" (mmol g^{-1}) for the initial amount of [OH]$_{ali}$ groups in P2400.

The conversion of the aliphatic -OH groups is relatively high for all esterified lignin ($\geq$70%). However, the evolution of the [H] units differs, since it is independent from lignin self-condensation, depolymerization and repolymerization. The following observations can be highlighted:

- when a stoichiometric amount of reactants is used (n = 1; Table 4, rows 1,2, 5 and 6), the increase in the amount of [H] units does not exceed 28%,
- when an excess of PA is used (n = 5; Table 3, rows 3, 4, 7, 8), higher conversion yields of aliphatic -OH groups (~90%) and amount of [H] units are reached (~50% and 65 % for t = 12 and 48 h, respectively),
- for n = 1, the amount of [H] units is equivalent to ~ 0.9 and ~1.1 mmol g^{-1} (c = 0.5 and 2.5 wt.%, respectively) independent of the reaction time,
- for an excess of PA (n = 5), this amount is equivalent to ~1.6 and 1.8 mmol g^{-1} (t = 12 and 48, respectively) regardless of the catalyst loading.

Table 4. Experimental matrix for the 2^3 full factorial DOE and corresponding values for the conversion of aliphatic -OH groups ([OH]$_{ali}$) and the increase in [H] units for the esterified lignin (EL).

Run	t (h)	n	c (wt.%)	[a] [OH]$_{ali}$ (mmol g^{-1})	[b] Conversion (%)	[a] [H] (mmol g^{-1})	[c] Response (%)
EL-1	12	1	0.5	0.61 ± 0.03	69.5	0.87 ± 0.02	17.0
EL-2	48	1	0.5	0.40 ± 0.06	80.0	0.96 ± 0.05	21.5
EL-3	12	5	0.5	0.33 ± 0.01	83.5	1.58 ± 0.08	52.5
EL-4	48	5	0.5	0.14 ± 0.02	93.0	1.78 ± 0.10	62.5
EL-5	12	1	2.5	0.51 ± 0.01	74.5	1.09 ± 0.17	28.0
EL-6	48	1	2.5	0.26 ± 0.08	87.0	1.04 ± 0.08	25.5
EL-7	12	5	2.5	0.19 ± 0.12	90.5	1.56 ± 0.12	51.5
EL-8	48	5	2.5	0.14 ± 0.02	93.0	1.81 ± 0.07	64.0

[a] determined by ^{31}P experiment, [b] relative conversion compared to the initial amount of [OH]$_{ali}$ in P2400, [c] calculated from the Equation (3).

Crosschecking these results indicates the amount of catalyst affects the increase in [H] units only when PA is introduced in stoichiometric proportion (n = 1). The highest increase in [H] units is obtained when an excess of PA is used for a longer reaction time (Table 4, rows 4 and 8). The catalyst loading does not significantly affect the increase in [H] units under these experimental conditions ([H] = 1.78 and 1.81 mmol g^{-1} for c = 0.5 and 2.5 wt.%, respectively). Under these optimal reaction conditions (n = 5, t = 48 h), most of the aliphatic -OH groups were converted into ester counterparts (93 %). In the context of this DOE, the initial molar ratio (n) appears as the main critical variables affecting the yield of the esterification. To confirm this result, the reaction time and the catalyst loading were both increased (from 12 to 48 h and from 0.5 to 2.5 wt.%, respectively). The results show it poorly enhanced the yield of the esterification.

A complete statistical analysis was carried out based on the experimental results using Ellistat software (95% confidence interval). The normalized impact of the individual critical variables (t, n and c) and the first order interaction effect of the temperature with the initial molar ratio (I_{tn}), the temperature with the catalyst loading (I_{tc}), and the initial molar ratio with the catalyst loading (I_{nc}), were evaluated in variance analysis using a Pareto chart (Figure 5).
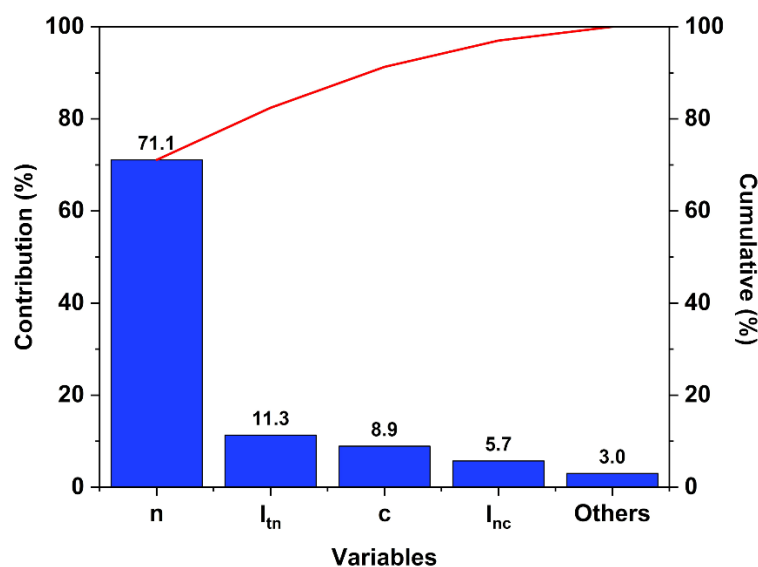
Figure 5. Pareto chart of the 2^3 DOE set up for the Fischer esterification of P2400. n: initial molar ratio; c: catalyst loading; I_{tn}: the first order interaction effect of the temperature with the initial molar ratio; I_{nc}: the first order interaction effect of the initial molar ratio with the catalyst loading.

The major contribution comes from the initial molar ratio factor (71.1%). Even if the time of the reaction stands for the less important factor (<2%), its interaction with the initial molar ratio contributes as much as the individual catalyst loading factor (~10%).

A linear predictive model was elaborated considering the most significative factors determined from the Pareto chart (contribution > 5%, Equation (4)):

$$Y = 7.36 + 8.18*n + 4.66*c + 0.06*I_{tn} + 0.91*I_{nc} \qquad (4)$$

where "Y" is the response (increase in [H] units), "n" the initial molar ratio, "c" the catalyst loading, "I_{tn}" the first order interaction effect of the temperature with the initial molar ratio and "I_{nc}" the first order interaction effect of the initial molar ratio with the catalyst loading. The predictive model enables one to predict with good accuracy the increase in [H] units in the experimental field (Figure S5 in Supplementary Materials, R^2 = 0.994). The results coming from the analysis of variance (ANOVA) reported in Table 5 indicate that most of the critical variables and their first order interaction effects considered for the elaboration of the predictive model were significant (degree of significance: $p < 0.05$, Table S4, raw 2). The initial molar ratio (n) was identified as the factor with the highest probability to influence the response (p = 0.002) (Table S4 in Supplementary Materials, column 4, row 2). Indeed, the weaker the p, the higher the probability that the factor affects the result. An additional experiment was carried out to assess the reliability of this predictive model by fixing the critical variables at the center of the DOE (t:n:c; 0:0:0) corresponding to a time of reaction of t = 30 h with an initial molar ratio of n = 3 and a catalyst loading of c = 1.5 wt.% (EL-9). This experiment confirmed the robustness of the model by a close agreement between the experimental and the model-predicted values (respectively, 43.5 and 48.5 %; details of the calculations reported in the Supplementary Materials file). In addition, to assess the pairwise effect of the critical variables, response surfaces (3D-visualization) stand for another efficient tool to estimate the response inside the experimental field (Figure S6). In conclusion, the experimental and statistical analysis shows that the initial molar ratio between the -COOH of phloretic acid and the lignin aliphatic -OH groups is the most significant critical variable affecting the yield of the esterification, as generally reported with Fischer-like esterifications [37,38]. It is worth indicating that an excess of PA helps the mixing of the reactants since the viscosity of the reaction medium is substantially decreased (melt-like condition). It explains, together with kinetic considerations, why the initial molar ratio is the most significant variable in the case of this synthesis. Finally, the DOE leads to the conclusion that the most suitable conditions are an excess of PA over P2400 (n = 5), an extended time of reaction (t = 48 h) and a higher catalyst loading (c = 2.5 wt.%).

Table 5. Hansen solubility parameters and molecular weight of P2400 and P2400-PA.

Sample	[a] δ_D (MPa$^{1/2}$)	[a] δ_P (MPa$^{1/2}$)	[a] δ_H (MPa$^{1/2}$)	[b] M_n (g mol^{-1})	[c] M_w (g mol^{-1})	[d] $Đ$
P2400	18.0	9.4	16.6	575	4323	7.5
P2400-PA	17.1	13.1	12.5	1570	8546	5.4

[a] estimation from HSPiP software, [b] Number average molecular weight, [c] Weight average molecular weight, [d] dispersity (M_w/ M_n). δ_D: energy from dispersion forces between molecules; δ_P: energy from the dipolar intermolecular forces between molecules; δ_H: energy from hydrogen bonds between molecules; M_n: number average molecular weight; M_w: weight average molecular weight.

3.3. Physicochemical Properties of Esterified Lignin

The solubilities of P2400 and P2400-PA were assessed in several organic solvents covering a wide range of polarity (Figure 6, Table S5) [49]. Lignin samples were subjected to an experimental estimation of Hansen solubility parameters (HSPs) [50]. To this aim, 50 mg of lignin were immersed in 50 mL of solvent. The percentage of solubility was determined by weighting the insoluble part after proper drying under reduced pressure and heating, if necessary, to remove the solvent. P2400 was highly soluble in most of the solvents. While less than 5 wt.% of P2400 was soluble in DET or TOL, the highest

solubilities were reached in ACE, MeOH, DMF, PYR, DMSO, THF and DIOX (S > 95 wt.%). The determination of the solubility of P2400 in the different solvents allows the estimation of its HSPs by using the Hansen solubility parameters in practice software (HSPiP). Estimated values of HSPs (δ_D = energy from dispersion forces between molecules, δ_P = energy from the dipolar intermolecular forces between molecules, δ_H = energy from hydrogen bonds between molecules) are reported in Table 5. A high value of δ_H seems to be the most important parameter to trigger the solubility of P2400 due to the high amount of –OH groups (Table 5). This solubility map comforts us in the solvent's choice for the purification (DET), NMR analysis (PYR for ^{31}P, DMSO for ^{1}H, ^{13}C and 2D spectra), and GPC analysis (THF). It also explains why the reaction depends so much on the initial molar ratio. Indeed, the similarity of the HSPs of PA ($\delta_D/\delta_P/\delta_H$ = 19.5/7.6/16.1 MPa$^{1/2}$, estimated from the software HSPiP) and P2400 (Table 5, columns 2, 3 and 4) emphasizes why the esterification reaction works in melt conditions, as molten PA could act as the "solvent" of the reaction. The overall solubility of P2400-PA was tightly like P2400. Esterified lignin was fully insoluble in water (neutral or acidic condition). The solubility of P2400-PA in alcohol solvents (EtOH and MeOH) considerably decreased as a result of the chemical modification of the aliphatic -OH groups (S = 91 and 96 wt.% for P2400, and S = 41 and 36 wt.% for P2400-PA, respectively). Inversely, the increase in the solubility in ester-containing solvents (ETAC and MEK) originates from the creation of ester bonds. The high solubility of the esterified lignin in a wide range of solvents is a key factor for subsequent engineering applications, for instance solution-state chemical modifications, composites processing, etc.
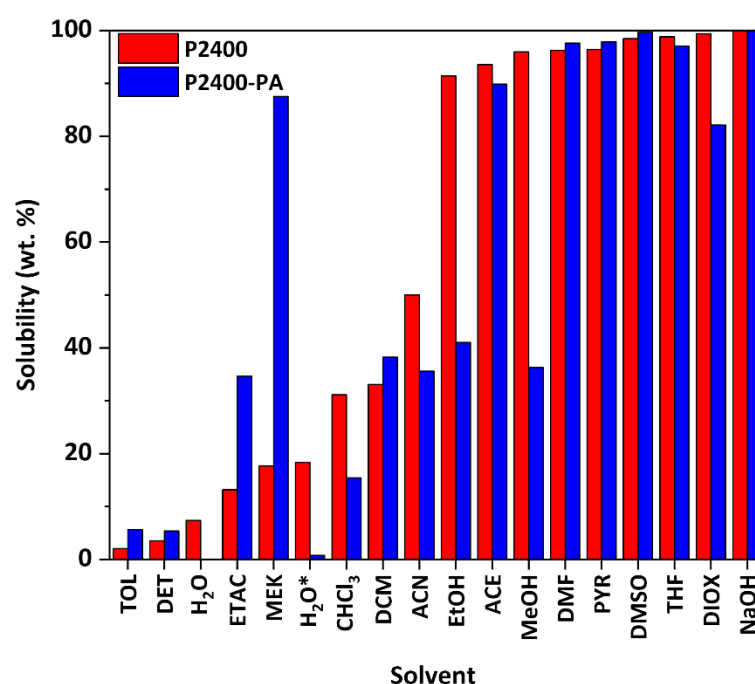
Figure 6. Solubility of P2400 and P2400-PA in several organic solvents.

The molecular weight of P2400 and P2400-PA was determined by GPC-SEC experiments (Figure S7 in Supplementary Materials). The number average molecular weight (M_n), the weight average molecular weight (M_w), and the dispersity ($Đ$) are reported in Table 5. The low molecular weight of P2400 is in the same range as the Protobind® lignin samples (M_n = 575 g mol^{-1}) [57,63]. The esterification of P2400 with PA is characterized by an increase of the molecular weight from 575 to 1570 g.mol^{-1}. The narrower dispersity of P2400-PA as compared to P2400 (5.4 and 7.5, respectively) could be explained by the extraction of low molecular weight compounds during the extraction process. The higher molecular weight of P2400-PA compared to P2400 is in good accordance with previous studies conducted on the esterification of lignin [32,33,37].

Finally, the thermal behaviors of P2400 and P2400-PA were investigated by thermogravimetric analysis (TGA) and differential scanning calorimetry (DSC). The TGA and first derivative (DTG) curves are displayed in Figure 7. Below 100 °C, a low weight loss was caused by the gradual evaporation of water (moisture content, <2%). The technical lignin follows a three-stage degradation pattern, starting from the dehydration of aliphatic -OH groups, followed by interunit linkages cleavage, and terminated with the decomposition of the polymer backbone (Table S1). In Table 6 the onset temperature of degradation (T_{onset}, determined from the first derivative), the maximum temperature of the main degradation stage (T_{max}), and the char residue of P2400 and P2400-PA are summarized. Lignin ester derivatives exhibited improved thermal stability as the T_{onset} shifted from 157 to 220 °C for P2400 and P2400-PA, respectively. For the esterified lignin, a two-stage degradation pattern was observed [32]. The T_{max} of the main degradation stage was also slightly higher for the P2400-PA than for P2400 (T_{max} = 367 and 359 °C, respectively). The higher value of residual char for P2400-PA (37.6%) was related to the higher carbon content (elemental analysis, Table 2), as well as to the increased number of phenolic rings. It also led to a small increase of the low oxygen index (LOI), from 31.1% to 32.5%, indicative of a slightly improved fire-retardant behavior [65]. The glass transition (T_g) of each material was measured on the second heating ramp from DSC measurement, evidencing the T_g of P2400 was increased from 92 to 112 °C after its esterification with PA (Table 6, column 6; Figure S8 in Supplementary Materials).
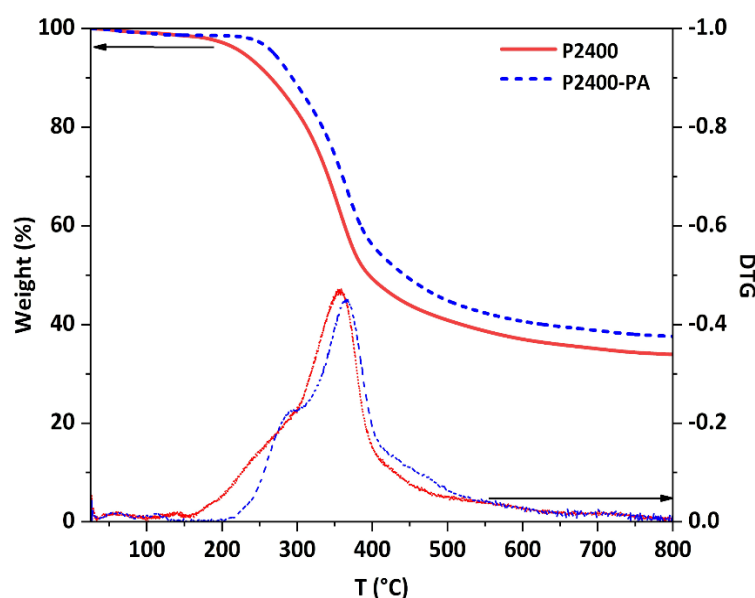
Figure 7. TGA curves of P2400 and P2400-PA (10 °C min^{-1}, N$_2$).

Table 6. Thermal properties of P2400 and P2400-PA.

Sample	[a] T_{onset} (°C)	[a,b] T_{max} (°C)	[c] Char (%)	[d] LOI (%)	[e] T_g (°C)
P2400	157	359	33.9	31.1	92
P2400-PA	220	367	37.6	32.5	112

[a] determined from the first derivative, [b] major degradation temperature (C, Figure S1, Table S1), [c] at 800 °C, [d] calculated according the equation of D.W. van Krevelen [65], [e] midpoint of the variation of the polymer heat capacity. T_{onset}: the onset temperature of degradation; T_{max}: the maximum temperature of the main degradation stage; LOI: low oxygen index; T_g: the glass transition temperature.

4. Conclusions

This work details how the reactivity of a soda Protobind® 2400 lignin can be enhanced by its solvent-free reaction with phloretic acid, fitting many of the green chemistry principles. A two-level full factorial DOE was carried out to spot the variables of interest,

and consequently to determine the optimal experimental conditions and to elaborate a reliable predictive model. The excess of phloretic acid appeared to be the most effective parameter monitoring the yield of the esterification. The esterification of Protobind® lignin with phloretic acid contributed to considerably increase the amount of *p*-hydroxyphenyl units (from 0.53 to 1.81 mmol g^{-1}). The structural features of the esterified lignin were substantiated by complementary NMR techniques (^{31}P, ^{1}H, ^{13}C, 2D HSQC and HMBC), FTIR and elemental analysis. Esterification stood for the main reaction occurring during the chemical process with a yield of reaction reaching 64 % (increase in [H] units). Minor side-reactions, such as self-condensation, were also detected. Solubility assays in various types of solvents were performed to determine the Hansen solubility parameters and to draw the solubility mapping of P2400 and its esterified form with phloretic acid. It highlighted a high solubility of both P2400 and P2400-PA in solvents of high δ_H, an important knowledge for practical applications and future research perspectives. Finally, the thermal properties of the esterified lignin were assessed by TGA and DSC. The onset of the thermal degradation shifted from 157 to 220 °C, concomitantly with the enhancement of the T_g from 92 to 112 °C, respectively, for P2400 and P2400-PA. To conclude, esterified lignin containing large amounts of phenolic units embodies a sustainable precursor to produce biobased and high-value-added materials of higher thermal stability. The promising chemical process developed in this work aims to magnify the reactivity of lignin towards a panel of industrial applications such as wood-based composites or thermoset.

Abbreviations: -OH: hydroxyl; DOE, design of experiment; HSQC, heteronuclear single quantum coherence; NMR, nuclear magnetic resonance; ACE, acetone; ACN, acetonitrile; MEK, butanone; CHCl$_3$, chloroform; DCM, dichloromethane; DET, diethyl ether; DIOX, dioxane; DMF, dimethylformamide; DMSO, dimethylsulfoxide; EtOH, ethanol; ETAC, ethyl acetate; MeOH, methanol; PYR, pyridine;

THF, tetrahydrofuran; TOL, toluene; H2O, water; PA, phloretic acid; *p*-TSA, para-toluene sulfonic acid; CaCl2, calcium chloride; LIG, lignin; -COOH, carboxylic acid; CDCl3, deuterated chloroform; TMDP, 2-chloro-4,4,5,5-tetramethyl-1,3,2-dioxaphospholane; DMSO-d_6, deuterated dimethylsulfoxide; HMBC, heteronuclear multiple bond correlation; FTIR, Fourier transform infrared spectroscopy; ATR, attenuated total reflection; HSPs, Hansen solubility parameters; GPC, gel permeation chromatography; DSC, differential scanning calorimetry; TGA, thermogravimetric analysis; DTG, first derivative of TGA curve; P2400, Protobind® 2400 technical lignin; P2400-PA, Esterified Protobind® 2400 lignin; -OCH3, methoxyl groups; EL, esterified lignin; ANOVA, analysis of variance; Đ, dispersity; T_{onset}, onset of thermal degradation; T_{max}, maximum of thermal degradation; LOI, low oxygen index; T_g, glass transition.

References

1. Spekreijse, J.; Lammens, T.; Parisi, C.; Ronzon, T.; Vis, M. *Insights into the European Market for Bio-Based Chemicals*; Publications office of the EU: Luxembourg, 2019.
2. Calvo-Flores, F.G.; Dobado, J.; Isac-García, J.; Martin-Martinez, F. *Lignin and Lignans as Renewable Raw Materials: Chemistry, Technology and Applications*; Wiley: Chichester, UK, 2015.
3. Strassberger, Z.; Tanase, S.; Rothenberg, G. The pros and cons of lignin valorisation in an integrated biorefinery. *RSC Adv.* **2014**, *4*, 25310–25318. [CrossRef]
4. Saratale, R.G.; Saratale, G.D.; Ghodake, G.; Cho, S.-K.; Kadam, A.; Kumar, G.; Jeon, B.-H.; Pant, D.; Bhatnagar, A.; Shin, H.S. Wheat straw extracted lignin in silver nanoparticles synthesis: Expanding its prophecy towards antineoplastic potency and hydrogen peroxide sensing ability. *Int. J. Biol. Macromol.* **2019**, *128*, 391–400. [CrossRef]
5. Ganesh Saratale, R.; Cho, S.-K.; Dattatraya Saratale, G.; Kadam, A.A.; Ghodake, G.S.; Kumar, M.; Naresh Bharagava, R.; Kumar, G.; Su Kim, D.; Mulla, S.I.; et al. A comprehensive overview and recent advances on polyhydroxyalkanoates (PHA) production using various organic waste streams. *Bioresour. Technol.* **2021**, *325*, 124685. [CrossRef]
6. Upton, B.M.; Kasko, A.M. Strategies for the Conversion of Lignin to High-Value Polymeric Materials: Review and Perspective. *Chem. Rev.* **2016**, *116*, 2275–2306. [CrossRef] [PubMed]
7. Wang, H.; Pu, Y.; Ragauskas, A.; Yang, B. From Lignin to Valuable Products–Strategies, Challenges, and Prospects. *Bioresour. Technol.* **2018**, *271*, 449–461. [CrossRef] [PubMed]
8. Laurichesse, S.; Avérous, L. Chemical modification of lignins: Towards biobased polymers. *Prog. Polym. Sci.* **2014**, *39*, 1266–1290. [CrossRef]
9. Kai, D.; Tan, M.J.; Chee, P.L.; Chua, Y.K.; Yap, Y.L.; Loh, X.J. Towards lignin-based functional materials in a sustainable world. *Green Chem.* **2016**, *18*, 1175–1200. [CrossRef]
10. Alonso, M.V.; Oliet, M.; Rodríguez, F.; García, J.; Gilarranz, M.A.; Rodríguez, J.J. Modification of ammonium lignosulfonate by phenolation for use in phenolic resins. *Bioresour. Technol.* **2005**, *96*, 1013–1018. [CrossRef]
11. Jiang, X.; Liu, J.; Du, X.; Hu, Z.; Chang, H.-m.; Jameel, H. Phenolation to Improve Lignin Reactivity toward Thermosets Application. *ACS Sustain. Chem. Eng.* **2018**, *6*, 5504–5512. [CrossRef]
12. Zhang, F.; Jiang, X.; Lin, J.; Zhao, G.; Chang, H.-m.; Jameel, H. Reactivity improvement by phenolation of wheat straw lignin isolated from a biorefinery process. *New J. Chem.* **2019**, *43*, 2238–2246. [CrossRef]
13. Yang, S.; Wen, J.-L.; Yuan, T.-Q.; Sun, R.-C. Characterization and phenolation of biorefinery technical lignins for lignin–phenol–formaldehyde resin adhesive synthesis. *RSC Adv.* **2014**, *4*, 57996–58004. [CrossRef]
14. Yang, S.; Zhang, Y.; Yuan, T.-Q.; Sun, R.-C. Lignin–phenol–formaldehyde resin adhesives prepared with biorefinery technical lignins. *J. Appl. Polym. Sci.* **2015**, *132*, 42493. [CrossRef]
15. Podschun, J.; Saake, B.; Lehnen, R. Reactivity enhancement of organosolv lignin by phenolation for improved bio-based thermosets. *Eur. Polym. J.* **2015**, *67*, 1–11. [CrossRef]
16. Podschun, J.; Stücker, A.; Saake, B.; Lehnen, R. Structure–Function Relationships in the Phenolation of Lignins from Different Sources. *ACS Sustain. Chem. Eng.* **2015**, *3*, 2526–2532. [CrossRef]
17. Çetin, N.S.; Özmen, N. Use of organosolv lignin in phenol–formaldehyde resins for particleboard production: I. Organosolv lignin modified resins. *Int. J. Adhes. Adhes.* **2002**, *22*, 477–480. [CrossRef]
18. Hu, L.; Zhou, Y.; Zhang, M.; Liu, R. Characterization and properties of a lignosulfonate-based phenolic foam. *Bioresources* **2011**, *7*, 554–564.
19. Abarro, G.J.; Podschun, J.; Diaz, L.J.; Ohashi, S.; Saake, B.; Lehnen, R.; Ishida, H. Benzoxazines with enhanced thermal stability from phenolated organosolv lignin. *RSC Adv.* **2016**, *6*, 107689–107698. [CrossRef]
20. Tan, T.T.M. Cardanol–lignin-based polyurethanes. *Polym. Int.* **1996**, *41*, 13–16. [CrossRef]
21. Zhao, B.Y.; Hu, K.A.; Wu, R.J. Primary study on the phenolic modification of sodium lignosulfonate. *Polym. Eng. Sci.* **2000**, *16*, 158–161.
22. Hoffmann, A.; Nong, J.P.; Porzel, A.; Bremer, M.; Fischer, S. Modification of Lignoboost Kraft Lignin from softwoods with dihydroxybenzenes. *React. Funct. Polym.* **2019**, *142*, 112–118. [CrossRef]
23. Lewis, H.F.; Brauns, F.E.; Buchanan, M.A.; Brookbank, E.B. Lignin Esters of Mono- and Dibasic Aliphatic Acids. *Ind. Eng. Chem. Res.* **1943**, *35*, 1113–1117. [CrossRef]

24. Xiao, B.; Sun, X.F.; Sun, R. The chemical modification of lignins with succinic anhydride in aqueous systems. *Polym. Degrad. Stab.* **2001**, *71*, 223–231. [CrossRef]

25. Fox, S.; McDonald, A. Chemical and Thermal Characterization of Three Industrial Lignins and Their Corresponding Lignin Esters. *BioResources* **2010**, *5*, 990–1009.

26. Sailaja, R.R.N.; Deepthi, M.V. Mechanical and thermal properties of compatibilized composites of polyethylene and esterified lignin. *Mater. Des.* **2010**, *31*, 4369–4379. [CrossRef]

27. Cachet, N.; Camy, S.; Benjelloun-Mlayah, B.; Condoret, J.-S.; Delmas, M. Esterification of organosolv lignin under supercritical conditions. *Indus. Crops Prod.* **2014**, *58*, 287–297. [CrossRef]

28. Thiebaud, S.; Borredon, M.E. Solvent-free wood esterification with fatty acid chlorides. *Bioresour. Technol.* **1995**, *52*, 169–173. [CrossRef]

29. Thiebaud, S.; Borredon, M.E.; Baziard, G.; Senocq, F. Properties of wood esterified by fatty-acid chlorides. *Bioresour. Technol.* **1997**, *59*, 103–107. [CrossRef]

30. Bonini, C.; D'Auria, M.; Emanuele, L.; Ferri, R.; Pucciariello, R.; Sabia, A. Polyurethanes and polyesters from lignin. *J. Appl. Polym. Sci.* **2005**, *98*, 1451–1456. [CrossRef]

31. Laurichesse, S.; Huillet, C.; Avérous, L. Original polyols based on organosolv lignin and fatty acids: New bio-based building blocks for segmented polyurethane synthesis. *Green Chem.* **2014**, *16*, 3958–3970. [CrossRef]

32. Gordobil, O.; Robles, E.; Egüés, I.; Labidi, J. Lignin-ester derivatives as novel thermoplastic materials. *RSC Adv.* **2016**, *6*, 86909–86917. [CrossRef]

33. Gordobil, O.; Herrera, R.; Llano-Ponte, R.; Labidi, J. Esterified organosolv lignin as hydrophobic agent for use on wood products. *Prog. Org. Coat.* **2017**, *103*, 143–151. [CrossRef]

34. Fang, R.; Cheng, X.S.; Lin, W.S. Preparation and application of dimer acid/lignin graft copolymer. *BioResources* **2011**, *6*, 2874–2884.

35. Sivasankarapillai, G.; McDonald, A.G. Synthesis and properties of lignin-highly branched poly (ester-amine) polymeric systems. *Biomass Bioenergy* **2011**, *35*, 919–931. [CrossRef]

36. Sivasankarapillai, G.; McDonald, A.; Li, H. Lignin valorization by forming toughened lignin-co-polymers: Development of hyperbranched prepolymers for cross-linking. *Biomass Bioenergy* **2012**, *47*, 99–108. [CrossRef]

37. Liu, L.-Y.; Hua, Q.; Renneckar, S. A simple route to synthesize esterified lignin derivatives. *Green Chem.* **2019**, *21*, 3682–3692. [CrossRef]

38. Liu, L.-Y.; Cho, M.; Sathitsuksanoh, N.; Chowdhury, S.; Renneckar, S. Uniform Chemical Functionality of Technical Lignin Using Ethylene Carbonate for Hydroxyethylation and Subsequent Greener Esterification. *ACS Sustain. Chem. Eng.* **2018**, *6*, 12251–12260. [CrossRef]

39. Picinelli, A.; Dapena, E.; Mangas, J.J. Polyphenolic Pattern in Apple Tree Leaves in Relation to Scab Resistance. A Preliminary Study. *J. Agric. Food. Chem.* **1995**, *43*, 2273–2278. [CrossRef]

40. Trejo-Machin, A.; Verge, P.; Puchot, L.; Quintana, R. Phloretic acid as an alternative to the phenolation of aliphatic hydroxyls for the elaboration of polybenzoxazine. *Green Chem.* **2017**, *19*, 5065–5073. [CrossRef]

41. Lora, J.H. Characteristics, Industrial Sources, and Utilization of Lignins from Non-Wood Plants. In *Chemical Modification, Properties, and Usage of Lignin*; Hu, T.Q., Ed.; Springer: Boston, MA, USA, 2002.

42. Lora, J.H.; Glasser, W.G. Recent Industrial Applications of Lignin: A Sustainable Alternative to Nonrenewable Materials. *J. Polym. Environ.* **2002**, *10*, 39–48. [CrossRef]

43. Granata, A.; Argyropoulos, D.S. 2-Chloro-4,4,5,5-tetramethyl-1,3,2-dioxaphospholane, a Reagent for the Accurate Determination of the Uncondensed and Condensed Phenolic Moieties in Lignins. *J. Agric. Food. Chem.* **1995**, *43*, 1538–1544. [CrossRef]

44. Zawadzki, M.; Ragauskas, A. N-Hydroxy Compounds as New Internal Standards for the 31P-NMR Determination of Lignin Hydroxy Functional Groups. *Holzforschung* **2001**, *55*, 283–285. [CrossRef]

45. Balakshin, M.; Capanema, E. On the Quantification of Lignin Hydroxyl Groups with 31P and 13C NMR Spectroscopy. *J. Wood Chem. Technol.* **2015**, *35*, 220–237. [CrossRef]

46. Capanema, E.; Balakshin, M.; Kadla, J. A Comprehensive Approach for Quantitative Lignin Characterization by NMR Spectroscopy. *J. Agric. Food. Chem.* **2004**, *52*, 1850–1860. [CrossRef]

47. Tran, F.; Lancefield, C.S.; Kamer, P.C.J.; Lebl, T.; Westwood, N.J. Selective modification of the β–β linkage in DDQ-treated Kraft lignin analysed by 2D NMR spectroscopy. *Green Chem.* **2015**, *17*, 244–249. [CrossRef]

48. McClelland, D.J.; Motagamwala, A.H.; Li, Y.; Rover, M.R.; Wittrig, A.M.; Wu, C.; Buchanan, J.S.; Brown, R.C.; Ralph, J.; Dumesic, J.A.; et al. Functionality and molecular weight distribution of red oak lignin before and after pyrolysis and hydrogenation. *Green Chem.* **2017**, *19*, 1378–1389. [CrossRef]

49. Sameni, J.; Krigstin, S.; Sain, M. Solubility of Lignin and Acetylated Lignin in Organic Solvents. *Bioresources* **2017**, *12*, 1548–1565. [CrossRef]

50. Hansen, C. *Hansen Solubility Parameters: A User's Handbook*; Taylor & Francis: New York, NY, USA, 2012.

51. Balakshin, M.; Capanema, E.; Santos, R.; Chang, H.-M.; Jameel, H. Structural analysis of hardwood native lignins by quantitative 13C NMR spectroscopy. *Holzforschung* **2015**, *70*, 95–108. [CrossRef]

52. Ahvazi, B.; Wojciechowicz, O.; Xu, P.; Ngo, T.; Hawari, J. Formation of Ligno-Polyols: Fact or Fiction. *Bioresources* **2017**, *12*, 6629–6655. [CrossRef]

53. Holtman, K.; Chang, H.-M.; Jameel, H.; Kadla, J. Quantitative 13 C NMR Characterization of Milled Wood Lignins Isolated by Different Milling Techniques. *J. Wood Chem. Technol.* **2006**, *26*, 21–34. [CrossRef]

54. Del Río, J.C.; Rencoret, J.; Prinsen, P.; Martínez, Á.T.; Ralph, J.; Gutiérrez, A. Structural Characterization of Wheat Straw Lignin as Revealed by Analytical Pyrolysis, 2D-NMR, and Reductive Cleavage Methods. *J. Agric. Food Chem.* **2012**, *60*, 5922–5935. [CrossRef]

55. Wen, J.-L.; Sun, S.-L.; Xue, B.-L.; Sun, R.-C. Recent Advances in Characterization of Lignin Polymer by Solution-State Nuclear Magnetic Resonance (NMR) Methodology. *Materials* **2013**, *6*, 359–391. [CrossRef]

56. Strassberger, Z.; Prinsen, P.; Klis, F.v.d.; van Es, D.S.; Tanase, S.; Rothenberg, G. Lignin solubilisation and gentle fractionation in liquid ammonia. *Green Chem.* **2015**, *17*, 325–334. [CrossRef]

57. Constant, S.; Wienk, H.L.J.; Frissen, A.E.; Peinder, P.d.; Boelens, R.; van Es, D.S.; Grisel, R.J.H.; Weckhuysen, B.M.; Huijgen, W.J.J.; Gosselink, R.J.A.; et al. New insights into the structure and composition of technical lignins: A comparative characterisation study. *Green Chem.* **2016**, *18*, 2651–2665. [CrossRef]

58. Funaoka, M.; Kako, T.; Abe, I. Condensation of lignin during heating of wood. *Wood Sci. Technol.* **1990**, *24*, 277–288. [CrossRef]

59. Demirbaş, A. Mechanisms of liquefaction and pyrolysis reactions of biomass. *Energy Convers. Manage.* **2000**, *41*, 633–646. [CrossRef]

60. Kim, J.-Y.; Hwang, H.; Oh, S.; Kim, Y.-S.; Kim, U.-J.; Choi, J.W. Investigation of structural modification and thermal characteristics of lignin after heat treatment. *Int. J. Biol. Macromol.* **2014**, *66*, 57–65. [CrossRef]

61. Ibrahim, M.; Iqbal, A.; Shen, C.; Bhawani, S.; Adam, F. Synthesis of lignin based composites of TiO2 for potential application as radical scavengers in sunscreen formulation. *BMC Chem.* **2019**, *13*, 17. [CrossRef] [PubMed]

62. Faix, O. Fourier Transform Infrared Spectroscopy. In *Methods in Lignin Chemistry*; Lin, S.Y., Dence, C.W., Eds.; Springer: Berlin/Heidelberg, Germany, 1992; pp. 233–241.

63. Schorr, D.; Diouf, P.N.; Stevanovic, T. Evaluation of industrial lignins for biocomposites production. *Indus. Crops Prod.* **2014**, *52*, 65–73. [CrossRef]

64. Sahoo, S.; Seydibeyoğlu, M.Ö.; Mohanty, A.K.; Misra, M. Characterization of industrial lignins for their utilization in future value added applications. *Biomass Bioenergy* **2011**, *35*, 4230–4237. [CrossRef]

65. Van Krevelen, D.W. Some basic aspects of flame resistance of polymeric materials. *Polymer* **1975**, *16*, 615–620. [CrossRef]

Research axis II

Synthesis of benzoxazine-based vitrimers

If thermosetting resins stand out from their unique mechanical and thermal properties, the permanent nature of the covalent cross-links making the three-dimensional network impedes their recyclability. This issue has triggered researchers to explore recycling strategies to enhance their end-of-life and avoid incineration, landfilling, or dispersion in the environment (Figure 1).
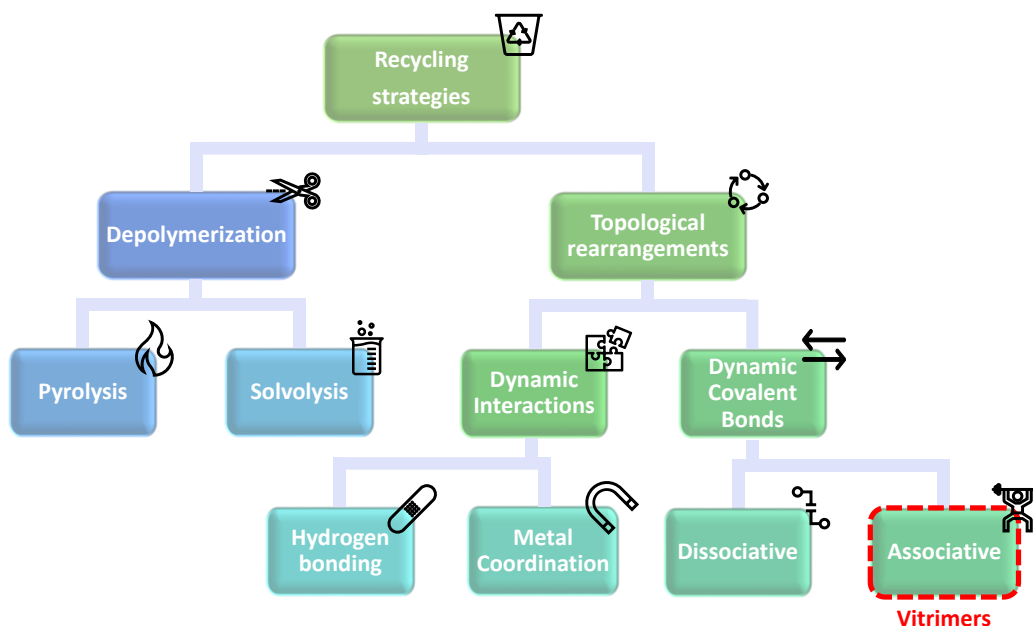
Figure 1 Overview of the strategies developed to recycle cross-linked materials.

Depolymerization pathways such as pyrolysis or solvolysis intend to dissociate polymeric chains into their parent monomers or polymerizable precursors. While the recycling of plastics involves high-temperature melt-processing techniques that are not compatible with infusible thermosets, their chemical resistance precludes solvent-assisted recycling. Moreover, the ring-opening of benzoxazine monomers is an irreversible process except in the specific case of the "*COLBERT*" reaction where the reversible formation of oxazine rings can be observed in the presence of thiol moieties.

The high design flexibility of polybenzoxazines makes them promising candidates for creating self-healable, recyclable, and degradable materials. For example, tuning the polymer structure with flexible segments can bring the required mobility to promote self-healing. Supramolecular interactions such as hydrogen bonds (afforded by the high number of phenolic moieties) and metal-ligand coordination present a clear advantage to prepare materials with self-healing and shape memory aptitudes. The versatile design of benzoxazine monomers can be also effective to introduce dynamic covalent bonds within the cross-linked network. The first example of dynamic bonds incorporated into benzoxazine focused on Diels-Alder (DA) chemistry. However, the kinetic of retro-DA reactions poses challenges in recycling these polymers on a reasonable time scale.

The following chapters introduce the foundation of benzoxazine-based vitrimers relying on fast dynamic transesterification exchanges. Significant attention has focused on highlighting the potential of benzoxazine matrix to develop recyclable materials with desirable properties under service conditions.

Chapter four: Polybenzoxazines a sustainable platform for the design of fast responsive and catalyst-free vitrimers based on transesterification exchanges

The following chapter describes the synthesis, characterization, and evaluation of the first polybenzoxazine vitrimer relying on reversible transesterification exchange. Polybenzoxazines benefit from a versatile design and can be conveniently functionalized with exchangeable bonds. Polyethylene glycol (PEG) of various chain lengths has been selected as green and biodegradable building-blocks for the two-step synthesis of quadri-telechelic benzoxazine monomers. The synthetic pathway comprises consecutive solvent-free Fischer esterification and Mannich-like ring-closure reactions, using diphenolic acid, PEG, paraformaldehyde, and ethanolamine as precursors. Once polymerized, the cross-linked network contains ester bonds and aliphatic hydroxyl groups that can undergo transesterification exchange at high temperatures. Interestingly, covalently bonded tertiary amines generated during the ROP act as internal catalyst toward dynamic exchanges, therefore preventing the introduction of external catalyst. The incorporation of dynamic covalent bonds in polybenzoxazines promotes topological rearrangements at the root of fast reshaping, self-healing, and reprocessing capabilities.

Contribution: I did all the experimental work, from the chemical synthesis of the molecules, to their polymerization. It also included all the characterizations (molecular, thermal, mechanical). I acquired all the data and handled their interpretation. I wrote the first draft of the publication and did all the needed corrections and revisions of the manuscript.

PAPER

Check for updates

Polybenzoxazines: a sustainable platform for the design of fast responsive and catalyst-free vitrimers based on trans-esterification exchanges†

Antoine Adjaoud, [a,b] Acerina Trejo-Machin, [a,b] Laura Puchot [a] and Pierre Verge [iD] *[a]

This work explores a new strategy, aiming for the synthesis of catalyst-free vitrimers by taking advantage of the abundant number of tertiary amines covalently bound into a polybenzoxazine network. A bio-based monomer was obtained by reacting 4,4-bis(4-hydroxyphenyl)valeric acid, polyethylene glycol, par-aformaldehyde and mono-ethanolamine, *via* consecutive solvent-free Fischer esterification and Mannich-like ring-closure. The two-step reaction led to the formation of quadri-telechelic benzoxazine-terminated polyethylene glycol monomers, containing ester bonds and aliphatic hydroxyl groups. The structural features of the resulting products were substantiated by ^{1}H NMR, ^{13}C NMR, elemental analysis, and FTIR. The occurrence of the thermally induced ring-opening polymerization was monitored by rheological measurements and DSC. At 140 °C, the monomers show a short gelation time (145 seconds). Once poly-merized, the polybenzoxazine exhibits a relatively high temperature of α mechanical relaxation (93 °C). Due to the ability of tertiary amines to catalyze transesterification reactions, and to the abundant number of hydroxyl groups, the material enables exchange reactions without the use of an external catalyst. It possesses all the typical characteristics of a vitrimer, such as recycling, reshaping, and self-healing. Short stress-relaxation times were measured (116 s at 170 °C). Finally, the effect of the structural features of the vitrimer was investigated by tuning the crosslinking density of the network and the number of hydroxyl groups, shedding more light on the mechanism of self-catalysis and the range of properties. Therefore, such a strategy constitutes an efficient and versatile route for an easy elaboration of mono-component, catalyst-free, and fast responsive vitrimers.

1. Introduction

Over the past few decades, the apogee of industrialization has led to a compelling increase in the consumption of thermosets worldwide, resulting in an abundant source of wastes which cannot be recycled or repaired.[1] To address this issue, revers-ible dissociative or associative bonds have been inserted within the chemical structure of thermosets to create covalent adaptable networks (CANs), enabling self-healability or recyclability.[2–4] In 2011, Leibler and co-workers successfully introduced dynamic covalent bonds (DCBs) in thermoset polymer networks and developed the first "vitrimer", combin-ing the antithetical properties of a thermoplastic and a ther-

moset.[5] At service temperatures, vitrimers behave like a tra-ditional thermoset with high mechanical properties, chemical resistance, and insolubility. At higher temperatures, they display the fluidity and the reprocessing ability of a thermoplastic.[5–7]

The different strategies and methodologies conceived to design performant vitrimers can be found in the excellent reviews published by Du Prez *et al.*,[8–11] and Hillmyer and Dichtel.[12] Among these strategies, the dynamic transesterifica-tion reaction (TER) occurring between ester bonds and hydroxyl (–OH) groups has been reported as the most represen-tative chemistry for driving vitrimer behaviors. In most cases, the TER requires the use of an external catalyst to trigger fast enough exchange reactions within a reasonable range of con-ditions. Numerous catalysts can be employed to control the transesterification reaction,[13] but solid or organic basic cata-lysts are preferred within a context of vitrimer material elabor-ation. Among them, zinc acetate (Zn(OAc)₂) is the most widely used, owing to its high efficiency.[5–7] Tertiary amine (NR₃) groups are also well-known sites of TER catalysis.[13–15] In one of their pioneering works, Leibler *et al.* evidenced that triazobi-

[a]Luxembourg Institute of Science and Technology, Materials Research and Technology Department, 5 Avenue des Hauts-Fourneaux, L-4362 Esch-sur-Alzette, Luxembourg. E-mail: pierre.verge@list.lu

[b]University of Luxembourg, 2, Avenue de l'Université, L-4365 Esch-sur-Alzette, Luxembourg

†Electronic supplementary information (ESI) available. See DOI: 10.1039/d1py00324k

cyclodecene (TBD), a bicyclic base containing a NR_3 group, gave similar results to $Zn(OAc)_2$.[5] Later, Williams et al.,[16] and more recently Zhang et al.,[17] have both demonstrated in elegant approaches that NR_3 covalently bound to the polymer network exert an internal catalysis on the transesterification reactions occurring in epoxy-acid systems. These studies join other recent research works dedicated to the development of internally catalyzed (or catalyst-free) vitrimers.[18–22] It is noteworthy that in the absence of a catalyst, the lifetime of a vitrimer relying on a transesterification mechanism could be greatly enhanced, particularly as the risk of ester hydrolysis would be reduced.[8] Thus, the elaboration of catalyst-free vitrimers appears of great importance, and the use of polymer structures containing tertiary amines seems to be a reasonable choice.

Polybenzoxazines (PBZs) are mono-component thermoset, polymers constituted of an abundant number of NR_3 coming from the auto-catalyzed ring-opening polymerization (ROP) of benzoxazines.[23] They are also a promising alternative to phenolic and epoxy resins thanks to their unique mechanical and thermal properties, such as a high glass transition temperature, near-zero shrinkage upon polymerization, and high char yield polymers.[24] Benzoxazine monomers are obtained from the condensation reaction of a phenolic compound, a primary amine and paraformaldehyde (PFA). For the past ten years, there has been an explosive growth of research works on polybenzoxazines, dedicated to the use of natural phenolic compounds and amines[25–43] as synthons of their monomers. As PFA can be synthesized from bio-ethanol or carbon dioxide, these precursors could be considered as 100% bio-based.[44] However, to solve the concern of its carcinogenetic, its substitution by more friendly aldehydes has been under the spotlight of very significant investigations.[45,46] It makes no doubts that polybenzoxazines with an excellent life cycle impact will emerge in the coming years.

As they are constituted from a permanent covalent network, PBZs suffer from similar drawbacks to traditional thermoset resins, and they cannot be recycled or reprocessed if they have not been specifically designed with this aim. Few works address this issue, mostly those written by Yagci and Kiskan.[47–49] Recently, Verge et al. developed the first vitrimer involving PBZs, showing recyclability, reshaping, and reversible adhesion properties.[50] The rearrangement of the permanent network was possible thanks to exchangeable disulfide bonds. However, to the best of our knowledge, none of the self-healable or reprocessable PBZs reported so far demonstrate vitrimer features from TER exchanges. Besides this, and more importantly, the NR_3 generated during the ROP of benzoxazines have never been considered as internal catalysts for TER exchanges.

Inspired by a bio-based PBZ we developed in the past,[51] and motivated by the outstanding achievements made on vitrimers over the past decade, this work attempts to illustrate how PBZs could be used to design catalyst-free vitrimers based on a transesterification mechanism. 4,4-Bis(4-hydroxyphenyl)valeric acid, more commonly known as diphenolic acid (DPA), is a

bio-based diphenol coming from levulinic acid, a chemical extracted from lignocellulosic biomass.[52] DPA was used to esterify the end-chains of polyethylene glycol (PEG) to form a quadri-telechelic phenol-terminated PEG (PEG-DPA) containing ester bonds. Thus, the hydroxyphenyl moieties were reacted via a Mannich-like condensation with mono-ethanolamine (mea), an amine derived from L-serine, sorbitol or glycolaldehyde.[53,54] This reaction led to the formation of PEG-DPA-mea, a quadri-telechelic benzoxazine-terminated polyethylene glycol monomer with pending aliphatic –OH groups connected to the nitrogen atom (in β-position). These –OH groups were expected to transesterify with the ester bonds. The following paragraphs describe the synthesis of a series of bio-based material and the evidence that their vitrimer behavior does not require the use of an external catalyst. These materials fit many of the Green Chemistry and Engineering principles, such as "Use of renewable feedstocks", "Safer solvents and auxiliaries", "Durability rather than immortality", "Renewable rather than depleting", and "Design for Commercial after-life", to cite but a few.

2. Experimental section

2.1 Materials and chemicals

4,4-Bis(4-hydroxyphenyl)valeric acid (95%, diphenolic acid, DPA), polyethylene glycol (average M_n = 200, 400 and 2000 g mol^{-1}; PEG_{200}, PEG_{400}, PEG_{2000}), mono-ethanolamine (≥98%, mea), furfurylamine (≥99%, fa) paraformaldehyde (95%, PFA), and para-toluene sulfonic acid monohydrate (≥98.5%, p-TSA) were purchased from Sigma-Aldrich. All chemicals were reagent grade and used as received without any further purification.

2.2 Equipment and characterizations

Nuclear Magnetic Resonance (NMR) spectroscopy was performed on an AVANCE III HD Bruker spectrometer equipped with a 5 mm BBO-probe operating at a proton frequency of 600 MHz. All chemical shifts are given as δ value (ppm) referenced to tetramethylsilane (TMS) as an internal standard. Assignments were performed using a combination of COSY, HSQC, and HMBC spectra. Methyl peak (–CH_3) in α-position of the aromatic ring was used as the reference for the integration of all other peaks (6.00H). Peak multiplicity was indicated as follows: singlet (s); doublet (d); triplet (t) or multiplet (m). The coupling constants (J) were reported in Hertz (Hz).

Fourier transform infrared spectroscopy (FTIR) was conducted on a Bruker TENSOR 27 instrument in the attenuated total reflection (ATR) mode using a diamond crystal. All spectra were recorded at room temperature in direct absorbance mode across 4000–400 cm^{-1} frequency range (32 scans, 4 cm^{-1} spectral resolution).

Elemental analysis (CHNS measurements) was performed on a Vario MACRO cube CHNS/O from Elementar France

SARL. Samples were put into an oxygen-enriched furnace at 1150 °C, where a combustion process converted carbon-to-carbon dioxide; hydrogen to water; nitrogen-to-nitrogen gas/oxides of nitrogen and sulfur-to-sulfur dioxide. The combustion products were swept out of the combustion chamber by an inert carrier gas (He, 600 mL min^{-1}) and passed over heated (850 °C) high purity copper. The separation of the measuring components took place as follows: nitrogen (N_2) was not adsorbed in the adsorption columns and was the first measuring component to enter the thermal conductivity detector directly. The other components were adsorbed in their respective adsorption column. Each of these columns was then heated separately to the corresponding desorption temperature ($T_{\text{desorpt.}}$) in order to release the components in the following order: CO_2 ($T_{\text{desorpt.}}$ = 240 °C), H_2O ($T_{\text{desorpt.}}$ = 150 °C) and SO_2 ($T_{\text{desorpt.}}$ = 100 °C or 230 °C). After desorption, each component was transported by the carrier gas flow into the measuring cell of a thermal conductivity detector (TCD).

Differential scanning calorimetry (DSC) thermograms were recorded on a Netzsch DSC 204 F1 Phoenix device in standard pierced aluminum crucibles (40 μL). A linear heating ramp from −25 to 300 °C at 10 °C min^{-1} rate was applied under inert atmosphere (N_2). The DSC thermogram of the PBZ material was recorded over two consecutive heating–cooling cycles from −25 to 250 °C (heating rate of 10 °C min^{-1} and cooling rate of 20 °C min^{-1}) to determine the glass transition (T_g) of the polymer and to ensure complete polymerization.

Thermogravimetric analysis (TGA) was completed on the Mettler Toledo TGA 2 device in standard ceramic alumina pan from 25 to 800 °C at 10 °C min^{-1} rate under air or inert atmosphere (N_2). The maximum of the degradation temperature was determined using the derivative of the TGA curve (DTG).

Rheological measurements were recorded using an Anton Paar Physica MCR 302 rheometer equipped with a CTD 450 temperature control device. Stress relaxation experiments were performed on disk-shaped solid geometry with a disposable aluminum plate–plate (ϕ = 25 mm). The relaxation modulus was followed as a function of time for 2000 s between 120 °C and 170 °C with a constant applied strain of 1% and normal force of 20 N. The original relaxation modulus (G_0) was extracted from the initial plateau of the stress relaxation curves (onset point of the second derivative curve). For the isothermal rheo-kinetic measurements, small quantities of the samples were loaded in a parallel plate-plate geometry (ϕ = 25 mm). The polymerization measurements were recorded in the oscillation mode at a frequency of 1 Hz and a controlled strain of 0.1%. Heating ramps of 20 °C min^{-1} were applied to reach a temperature of 140 °C. The sample deformation was ramped linearly from 1% to 0.2% to remain within the instrument's limitation and to maintain a linear viscoelastic behavior as the moduli (G' storage modulus, G'' loss modulus) increase by several orders of magnitude upon curing. The gap between the plates was maintained at 0.5 mm during all the experiments.

Rheology temperature sweep curves were performed on the bar-shaped solid in rectangular-torsion mode under constant deformation of 0.1% (1 Hz).

Dilatometry thermogram was recorded on the Netzsch DIL 402 C apparatus from 25 to 200 °C (2 °C min^{-1}) under an inert atmosphere (N_2) and a constant force to avoid buckling (30 cN). The material was introduced in a hollow cylinder capped at the extremities by two solid cylindrical end pieces to limit the side expansion.

Dynamic mechanical analysis (DMA) was used to evaluate the mechanical properties of the material after reprocessing. The cured and reprocessed materials were analyzed at room temperature (RT) in tension and in single cantilever mode (effective lengths of 10 and 5 mm, respectively, width 5 mm, thickness 1.25 mm). The measurements were performed at 1 Hz using a preload force of 0.05 N and a sinusoidal strain of 10 μm. The storage modulus (E') was recorded as a function of time. The reported values are an average of three values.

Optical microscopy was used to illustrate the self-healing performance of the PBZ vitrimer. The surface morphology of scratched samples was examined using the Nikon Universal Design Microscope UDM ECLIPSE LV100D-U (optics ×20, gain ×2.40, exposure 6 ms). The healing process was conducted at 150 °C in a convection oven. The width of the crack was measured before and after the healing process in a dynamic contrast mode at different time intervals.

Swelling experiments were conducted in acetone, chloroform and water by immersion at room temperature of 25 mg of the material in 2 mL of solvent at different time intervals for poly(PEG$_{400}$-DPA-mea). The crosslinking density was measured by swelling tests in water at different time intervals. The swelling ratio (W) is determined according to the eqn (1):

$$W = \frac{m_s - m_i}{m_i} \tag{1}$$

with m_i and m_s being the initial and the swollen mass, respectively. The molecular weight between the crosslinking nodes ($\overline{M_c}$) was calculated by applying the Flory Rehner equation (2):

$$\overline{M_c} = \frac{\rho \times V \times (0.5 \times \mu - \mu^{\frac{1}{3}})}{\ln(1 - \mu) + \mu + \chi_{\text{PEG/water}} \times \mu^2} \tag{2}$$

where ρ is the density of the polymer, V is the molar volume of water, μ is the polymer volume fraction in the equilibrium-swollen system and $\chi_{\text{PEG/water}}$ is the interaction parameter of PEG with water. We took the hypothesis that PEG moieties were driving the interaction of the network with water and $\chi_{\text{PEG/water}}$ approximated to 0.5.[55] μ is determined according to the eqn (3):

$$\mu = \left[1 + W \times \frac{d_{\text{polymer}}}{d_{\text{solvent}}}\right]^{-1} \tag{3}$$

where $d_{polymer}$ and $d_{solvent}$ are the density of the polybenzoxazine vitrimer and the water, respectively. The crosslinking density (ν_c) is calculated according the eqn (4):

$$\nu_c = \frac{d_{polymer}}{M_c} \qquad (4)$$

2.3 Synthetic procedure

2.3.1 Synthesis of PEG$_n$-DPA. Diphenol terminated polyethylene glycols (PEG$_n$-DPA) were synthesized *via* a Fischer esterification, from a previous work with minor modification.[51] Three PEG of different molecular weight (200, 400 or 2000 g mol^{-1}) were used for the synthesis. Typically, PEG$_n$ (1.0 eq.) was reacted with DPA (2.0 eq.) and *p*-TSA (0.5 wt%) in an open three-neck round bottom flask at 130 °C for 24 hours under mechanical stirring (Ministar 20 Digital, anchor stirrer, 200 rpm). The reaction crude was then solubilized in butanone and purified by three liquid–liquid extractions with distilled water to remove non-hydrolyzed *p*-TSA. The solvent was then evaporated under reduced pressure. Finally, the product was dried overnight under reduced pressure (<1 mBar) at T = 50 °C.

PEG$_{200}$-DPA (brown powder). ^{1}H NMR (DMSO-d$_6$, 600 MHz, 298°K): δ (ppm) = (assignment, multiplicity (coupling constant), [attribution], experimental integration, theoretical integration). δ = 1.46 (C–CH$_3$*, s, [c], exp 6.00H, th 6.00H); δ = 2.02 (CH$_2$–CH$_2$*–C=O, t (J = 6.91 Hz), [a], exp 3.98H, th 4.00H); δ = 2.24 (C–CH$_2$*–CH$_2$, t (J = 7.37 Hz), [b], exp 3.97H, th 4.00H); δ = 3.48 (O–CH$_2$*, t (J = 3.66 Hz), [3], exp 9.01H); δ = 3.55 (O=C–O–CH$_2$-βCH2*, m, [1], exp 4.04H, th 4.00H); δ = 4.06 (O=C-O-αCH$_2$*–CH$_2$, t, [2], exp 3.78H, th 4.00H); δ = 6.65 (C=CH*–CH, d (J = 8.56 Hz), [e], exp 8.00H, th 8.00H); δ = 6.93 (CH–CH*=C–O, d (J = 8.44 Hz), [d], exp 8.00H, th 8.00H); δ = 9.18 (Ar–OH*, s, [f], exp 3.99H, th 4.00H).

^{13}C NMR (DMSO-d$_6$, 600 MHz, 298°K): δ (ppm) = 27.7 [e]; 30.3 [b]; 36.7 [c]; 44.3 [d]; 63.6 [2]; 68.7 [1]; 70.2 [3]; 115.2 [h]; 128.2 [g]; 139.7 [f]; 155.5 [i]; 173.5 [a].

PEG$_{400}$-DPA (brown viscous substance). ^{1}H NMR (DMSO-d$_6$, 600 MHz, 298°K): δ (ppm) = (assignment, multiplicity (coupling constant), [attribution], experimental integration, theoretical integration). δ = 1.44 (C–CH$_3$*, s, [c], exp 6.00H, th 6.00H); δ = 2.03 (CH$_2$–CH$_2$*–C=O, t (J = 7.90 Hz), [a], exp 4.00H, th 4.00H); δ = 2.24 (C–CH$_2$*–CH$_2$, t (J = 7.93 Hz), [b], exp 3.99H, th 4.00H); δ = 3.48 (O–CH$_2$*, t (J = 2.78 Hz), [3], exp 30.3H); δ = 3.55 (O=C–O–CH$_2$-βCH2*, m, [1], exp 4.13H, th 4.00H); δ = 4.06 (O=C-O-αCH$_2$*–CH$_2$, t, [2], exp 3.98H, th 4.00H); δ = 6.65 (C=CH*–CH, d (J = 8.57 Hz), [e], exp 8.02H, th 8.00H); δ = 6.93 (CH–CH*=C–O, d (J = 8.53 Hz), [d], exp 7.98H, th 8.00H); δ = 9.19 (Ar–OH*, s, [f], exp 4.02H, th 4.00H).

^{13}C NMR (DMSO-d$_6$, 600 MHz, 298°K): δ (ppm) = 27.7 [e]; 30.3 [b]; 36.7 [c]; 44.3 [d]; 63.6 [2]; 68.7 [1]; 70.2 [3]; 115.1 [h]; 128.2 [g]; 139.6 [f]; 155.5 [i]; 173.5 [a].

FTIR (cm^{-1}); very strong (vs), strong (s), medium (m), weak (w), broad (br): 3339 (–OH stretching, br), 2869 (C–H stretching, vs), 1730 (C=O stretching from the ester, s), 1625–1475 (C=C stretching vibrations from the aromatic ring, m), 1175

(phenol C–O stretching and –OH in plane deformation, w), 1083 (C–O stretching from the ester, s).

PEG$_{2000}$-DPA (brown wax). ^{1}H NMR (DMSO-d$_6$, 600 MHz, 298°K): δ (ppm) = (assignment, multiplicity (coupling constant), [attribution], experimental integration, theoretical integration). δ = 1.46 (C–CH$_3$*, s, [c], exp 6.00H, th 6.00H); δ = 2.03 (CH$_2$–CH$_2$*–C=O, t (J = 8.04 Hz), [a], exp 4.11H, th 4.00H); δ = 2.24 (C–CH$_2$*–CH$_2$, t (J = 8.12 Hz), [b], exp 4.00H, th 4.00H); δ = 3.51 (O–CH$_2$*&O=C–O–CH$_2$-βCH2*, [3,1], exp 191.14H); δ = 4.06 (O=C-O-αCH$_2$*–CH$_2$, t, [2], exp 4.00H, th 4.00H); δ = 6.65 (C=CH*–CH, d (J = 8.61 Hz), [e], exp 7.95H, th 8.00H); δ = 6.93 (CH–CH*=C–O, d (J = 8.61 Hz), [d], exp 7.96H, th 8.00H); δ = 9.18 (Ar–OH*, s, [f], exp 4.07H, th 4.00H).

^{13}C NMR (DMSO-d$_6$, 600 MHz, 298°K): δ (ppm) = 27.7 [e]; 30.3 [b]; 36.7 [c]; 44.3 [d]; 63.6 [2]; 68.7 [1]; 70.2 [3]; 115.1 [h]; 128.2 [g]; 139.6 [f]; 155.5 [i]; 173.5 [a].

2.3.2 Synthesis of PEG$_n$-DPA-mea. Freshly prepared diphenol-terminated polyethylene glycol (PEG$_n$-DPA, 1.0 eq.) was reacted solventless with mea (4.0 eq.) and PFA (8.0 eq.) at 85 °C for 2.5 hours followed by 0.5 hours at 90 °C under mechanical stirring (Ministar 20 Digital, anchor stirrer, 200 rpm). PEG$_n$-DPA-mea benzoxazine monomers were all used without any purification.

PEG$_{200}$-DPA-mea (yellow powder). ^{1}H NMR (DMSO-d$_6$, 600 MHz, 298 K): δ (ppm) = (assignment, multiplicity (coupling constant), [attribution], experimental integration, theoretical integration). δ = 1.47 (C–CH$_3$*, s, [c], exp 6.00H, th 6.00H); δ = 2.03 (CH$_2$–CH$_2$*–C=O, m, [a], exp 3.97H, th 4.00H); δ = 2.25 (C–CH$_2$*–CH$_2$, m, [b], exp 3.87H, th 4.00H); δ = 2.71 (N–CH$_2$*–CH$_2$, m, [i], exp 6.06H, th 8.00H); δ = 3.48 (O–CH$_2$*, m, [3], exp 11.01H); δ = 3.55 (CH$_2$–CH$_2$*–OH & O=C–O–CH$_2$-βCH$_2$*, m, [1, j], exp 10.60H, th 12.00H); δ = 3.91 (Ar–CH$_2$*–N, s, [h], exp 5.30H, th 8.00H); δ = 4.05 (O=C-O-αCH$_2$*–CH$_2$, m, [2], exp 3.98H, th 4.00H); δ = 4.52 (CH$_2$–OH*, s, [k], exp 3.34H, th 4.00H); δ = 4.78 (O–CH$_2$*–N, s, [g], exp 5.62H, th 8.00H); δ = 6.82 (C=CH*–CH & C=CH*–C & CH–CH*=C–O, m, [d, f, e], exp 11.78, th 12.00H).

^{13}C NMR (DMSO-d$_6$, 600 MHz, 298 K): δ (ppm) = 27.5 [e]; 30.3 [b]; 36.5 [c]; 44.5 [d]; 50.6 [m]; 54.0 [n]; 60.0 [o]; 63.6 [2]; 68.7 [1]; 70.2 [3]; 83.1 [l]; 115.9 [i]; 120.3 [k]; 126.0 [g]; 126.6 [h]; 140.8 [f]; 152.3 [j]; 173.5 [a].

PEG$_{400}$-DPA-mea (orange viscous substance). ^{1}H NMR (DMSO-d$_6$, 600 MHz, 298 K): δ (ppm) = (assignment, multiplicity (coupling constant), [attribution], experimental integration, theoretical integration). δ = 1.45 (C–CH$_3$*, s, [c], exp 6.00H, th 6.00H); δ = 2.02 (CH$_2$–CH$_2$*–C=O, m, [a], exp 4.03H, th 4.00H); δ = 2.29 (C–CH$_2$*–CH$_2$, m, [b], exp 4.05H, th 4.00H); δ = 2.72 (N–CH$_2$*–CH$_2$, m, [i], exp 5.92H, th 8.00H); δ = 3.48 (O–CH$_2$*, m, [3], exp 30.68H); δ = 3.55 (CH$_2$–CH$_2$*–OH & O=C–O–CH$_2$-βCH$_2$*, m, [1, j], exp 10.20H, th 12.00H); δ = 3.88 (Ar–CH$_2$*–N, s, [h], exp 5.96H, th 8.00H); δ = 4.06 (O=C-O-αCH$_2$*–CH$_2$, m, [2], exp 3.99H, th 4.00H); δ = 4.51 (CH$_2$–OH*, s, [k], exp 3.88H, th 4.00H); δ = 4.80 (O–CH$_2$*–N, s, [g], exp 5.93H, th 8.00H); δ = 6.81 (C=CH*–CH & C=CH*–C & CH–CH*=C–O, m, [d, f, e], exp 12.07, th 12.00H).

^{13}C NMR (DMSO-d$_6$, 600 MHz, 298 K): δ (ppm) = 27.5 [e]; 30.3 [b]; 36.5 [c]; 44.5 [d]; 50.6 [m]; 54.0 [n]; 60.0 [o]; 63.7 [2];

68.7 [1]; 70.2 [3]; 83.1 [l]; 116.0 [i]; 120.3 [k]; 126.0 [g]; 126.6 [h]; 140.8 [f]; 152.3 [j]; 173.5 [a].

FTIR (cm^{-1}); very strong (vs), strong (s), medium (m), weak (w), broad (br): 3339 (–OH stretching, br), 2869 (C–H stretching, vs), 1730 (C=O stretching from the ester, s), 1625–1475 (C=C stretching vibrations from the aromatic ring, m), 1230 (C–O–C oxazine asymmetric stretching, m), 1083 (C–O stretching from the ester, s), 1030 (primary alcohol C–O stretching and –OH in plane deformation, w), 928 (C–H out-of-plane vibration in the trisubstituted benzene ring, m).

Elemental analysis (exp, th): C (67, 68), H (150, 98), N (4, 4), S (<0.05, 0).

PEG$_{2000}$-DPA-mea (yellowish wax). ^{1}H NMR (DMSO-d$_6$, 600 MHz, 298 K): δ (ppm) = (assignment, multiplicity (coupling constant), [attribution], experimental integration, theoretical integration). δ = 1.47 (C–CH$_3$*, s, [c], exp 6.00H, th 6.00H); δ = 2.04 (CH$_2$–CH$_2$*–C=O, m, [a], exp 3.81H, th 4.00H); δ = 2.26 (C–CH$_2$*–CH$_2$, m, [b], exp 4.00H, th 4.00H); δ = 2.72 (N–CH$_2$*–CH$_2$, m, [i], exp 5.44H, th 8.00H); δ = 3.51 (O–CH$_2$*& CH$_2$–CH$_2$*–OH & O=C–O–CH$_2$-βCH$_2$*, m, [3, 1, j], exp 197.19H); δ = 3.92 (Ar–CH$_2$*–N, s, [h], exp 5.61H, th 8.00H); δ = 4.07 (O=C–O-αCH$_2$*–CH$_2$, m, [2], exp 4.06H, th 4.00H); δ = 4.52 (CH$_2$–OH*, s, [k], exp 3.86H, th 4.00H); δ = 4.78 (O–CH$_2$*–N, s, [g], exp 5.41H, th 8.00H); δ = 6.83 (C=CH*–CH & C=CH*–C & CH–CH*=C–O, m, [d, f, e], exp 12.97, th 12.00H).

^{13}C NMR (DMSO-d$_6$, 600 MHz, 298 K): δ (ppm) = 27.6 [e]; 30.3 [b]; 36.6 [c]; 44.5 [d]; 50.6 [m]; 54.0 [n]; 60.0 [o]; 63.7 [2]; 68.7 [1]; 70.3 [3]; 83.1 [l]; 115.9 [i]; 120.3 [k]; 126.0 [g]; 126.6 [h]; 140.8 [f]; 152.3 [j]; 173.5 [a].

2.3.3 Synthesis of PEG$_{400}$-DPA-mea$_x$/fa$_{100-x}$. Typically, freshly prepared diphenol-terminated polyethylene glycol (PEG$_{400}$-DPA, 1.0 eq.) was reacted solventless with a mixture of mea (($(x/100) \times 4.0$ eq.) and fa ((($100 - x)/100) \times 4.0$ eq.), and PFA (8.0 eq.) at 70 °C for 36 hours under mechanical stirring (Ministar 20 Digital, anchor stirrer, 200 rpm). PEG$_{400}$-DPA-mea$_x$/fa$_{100-x}$ benzoxazine monomers were all used without any purification (orange viscous solid).

PEG$_{400}$-DPA-mea$_{75}$/fa$_{25}$. ^{1}H NMR (DMSO-d$_6$, 600 MHz, 298 K): δ (ppm) = (assignment, multiplicity (coupling constant), [attribution], experimental integration, theoretical integration). δ = 1.46 (C–CH$_3$*, s, [c], exp 6.00H, th 6.00H); δ = 2.04 (CH$_2$–CH$_2$*–C=O, m, [a], exp 3.89H, th 4.00H); δ = 2.26 (C–CH$_2$*–CH$_2$, m, [b], exp 3.99H, th 4.00H); δ = 2.72 (N–CH$_2$*–CH$_2$, m, [i], exp 4.73H, th 6.00H); δ = 3.49 (O–CH$_2$*, m, [3], exp 32.49H); δ = 3.55 (CH$_2$–CH$_2$*–OH & O=C–O–CH$_2$-βCH$_2$*, m, [1, j], exp 8.88H, th 10.00H); δ = 3.90 (fa-CH$_2$*–N & Ar–CH$_2$*–N, s, [l, h], exp 7.43H, th 10.00H); δ = 4.07 (O=C–O-αCH$_2$*-CH$_2$, m, [2], exp 4.01H, th 4.00H); δ = 4.51 (CH$_2$–OH*, s, [k], exp 2.75H, th 3.00H); δ = 4.78 (O–CH$_2$*–N, s, [g], exp 5.77H, th 8.00H); δ = 6.30 (fa-C=CH*–CH, s, [m], exp 0.91H, th 1.00H); δ = 6.41 (fa-CH–CH*=CH, s, [n], exp 0.92H, th 1.00H); δ = 6.82 (C=CH*–CH & C=CH*–C & CH–CH*=C–O, m, [d, f, e], exp 11.96, th 12.00H); δ = 7.60 (fa-CH=CH*–O, s, [o], exp 0.91H, th 1.00H).

^{13}C NMR (DMSO-d$_6$, 600 MHz, 298 K): δ (ppm) = 27.6 [e]; 30.3 [b]; 36.5 [c]; 44.5 [d]; 48.0 [p]; 49.6 [m$_{fa}$]; 50.6 [m$_{mea}$]; 54.0 [n]; 60.0 [o]; 63.7 [2]; 68.7 [1]; 70.3 [3]; 81.8 [l$_{fa}$]; 83.1 [l$_{mea}$];

109.1 [r]; 110.9 [s]; 115.9 [i]; 119.6 [k$_{fa}$]; 120.3 [k$_{mea}$]; 126.0 [g]; 126.6 [h]; 140.8 [f]; 143.1 [t]; 152.3 [j&q]; 173.5 [a].

PEG$_{400}$-DPA-mea$_{50}$/fa$_{50}$. ^{1}H NMR (DMSO-d$_6$, 600 MHz, 298 K): δ (ppm) = (assignment, multiplicity (coupling constant), [attribution], experimental integration, theoretical integration). δ = 1.48 (C–CH$_3$*, s, [c], exp 6.00H, th 6.00H); δ = 2.05 (CH$_2$–CH$_2$*–C=O, m, [a], exp 3.94H, th 4.00H); δ = 2.27 (C–CH$_2$*–CH$_2$, m, [b], exp 3.96H, th 4.00H); δ = 2.72 (N–CH$_2$*–CH$_2$, m, [i], exp 3.05H, th 4.00H); δ = 3.49 (O–CH$_2$*, m, [3], exp 31.12H); δ = 3.55 (CH$_2$–CH$_2$*–OH & O=C–O–CH$_2$-βCH$_2$*, m, [1, j], exp 7.32H, th 8.00H); δ = 3.90 (fa-CH$_2$*–N & Ar–CH$_2$*–N, s, [l, h], exp 9.58H, th 12.00H); δ = 4.07 (O=C–O-αCH$_2$*–CH$_2$, m, [2], exp 4.00H, th 4.00H); δ = 4.52 (CH$_2$–OH*, s, [k], exp 1.81H, th 2.00H); δ = 4.78 (O–CH$_2$*–N, s, [g], exp 6.10H, th 8.00H); δ = 6.29 (fa-C=CH*–CH, s, [m], exp 1.78H, th 2.00H); δ = 6.40 (fa-CH–CH*=CH, s, [n], exp 1.89H, th 2.00H); δ = 6.84 (C=CH*–CH & C=CH*–C & CH–CH*=C–O, m, [d, f, e], exp 11.91, th 12.00H); δ = 7.59 (fa-CH=CH*–O, s, [o], exp 1.87H, th 2.00H).

^{13}C NMR (DMSO-d$_6$, 600 MHz, 298 K): δ (ppm) = 27.5 [e]; 30.3 [b]; 36.5 [c]; 44.5 [d]; 48.0 [p]; 49.6 [m$_{fa}$]; 50.6 [m$_{mea}$]; 54.0 [n]; 60.0 [o]; 63.7 [2]; 68.7 [1]; 70.2 [3]; 81.8 [l$_{fa}$]; 83.1 [l$_{mea}$]; 109.1 [r]; 110.9 [s]; 115.9 [i]; 119.6 [k$_{fa}$]; 120.3 [k$_{mea}$]; 126.0 [g]; 126.6 [h]; 140.8 [f]; 143.1 [t]; 152.3 [j&q]; 173.5 [a].

PEG$_{400}$-DPA-mea$_{25}$/fa$_{75}$. ^{1}H NMR (DMSO-d$_6$, 600 MHz, 298 K): δ (ppm) = (assignment, multiplicity (coupling constant), [attribution], experimental integration, theoretical integration). δ = 1.48 (C–CH$_3$*, s, [c], exp 6.00H, th 6.00H); δ = 2.05 (CH$_2$–CH$_2$*–C=O, m, [a], exp 4.00H, th 4.00H); δ = 2.27 (C–CH$_2$*–CH$_2$, m, [b], exp 3.97H, th 4.00H); δ = 2.72 (N–CH$_2$*–CH$_2$, m, [i], exp 1.55H, th 2.00H); δ = 3.49 (O–CH$_2$*, m, [3], exp 31.38H); δ = 3.56 (CH$_2$–CH$_2$*–OH & O=C–O–CH$_2$-βCH$_2$*, m, [1, j], exp 6.09H, th 6.00H); δ = 3.89 (fa-CH$_2$*–N & Ar–CH$_2$*–N, s, [l, h], exp 10.79H, th 14.00H); δ = 4.07 (O=C–O-αCH$_2$*–CH$_2$, m, [2], exp 3.94H, th 4.00H); δ = 4.51 (CH$_2$–OH*, s, [k], exp 1.01H, th 1.00H); δ = 4.78 (O–CH$_2$*–N, s, [g], exp 5.82H, th 8.00H); δ = 6.29 (fa-C=CH*–CH, s, [m], exp 2.71H, th 3.00H); δ = 6.40 (fa-CH–CH*=CH, s, [n], exp 2.73H, th 3.00H); δ = 6.84 (C=CH*–CH & C=CH*–C & CH–CH*=C–O, m, [d, f, e], exp 11.99, th 12.00H); δ = 7.69 (fa-CH=CH*–O, s, [o], exp 2.80H, th 3.00H).

^{13}C NMR (DMSO-d$_6$, 600 MHz, 298 K): δ (ppm) = 27.5 [e]; 30.3 [b]; 36.5 [c]; 44.5 [d]; 48.0 [p]; 49.6 [m$_{fa}$]; 50.6 [m$_{mea}$]; 54.0 [n]; 60.0 [o]; 63.7 [2]; 68.7 [1]; 70.2 [3]; 81.8 [l$_{fa}$]; 83.1 [l$_{mea}$]; 109.1 [r]; 110.8 [s]; 116.0 [i]; 119.6 [k$_{fa}$]; 120.3 [k$_{mea}$]; 126.2 [g]; 126.8 [h]; 141.1 [f]; 143.1 [t]; 152.3 [j&q]; 173.5 [a].

2.3.3 Elaboration of the polybenzoxazine vitrimer: poly (PEG$_n$-DPA-mea$_x$/fa$_{100-x}$). The benzoxazine monomer was placed in a hollow Teflon® mold (70 × 20 × 0.3 mm). The mold was covered with a Kapton® polyimide film to ensure homogeneous and smooth surfaces. The mold was placed in a vacuum chamber and heated for one hour at 100 °C to remove traces of water (that could lead to bubbles inside the final material) and allow the monomer to flow in the mold. The mold was then transferred to an air-circulating oven at 150 °C for one hour for the curing step (speed fan of 30%). For poly (PEG$_{400}$-DPA-mea$_x$/fa$_{100-x}$), an additional post-curing step (170 °C for half an hour) was performed to ensure the com-

plete polymerization. The polymeric material was cooled to RT before testing. Starting from a disc or a bar-shaped mold, diverse material shapes, suitable for mechanical and vitrimer characterization, were achieved.

2.3.4 Reshaping and reprocessing of poly(PEG$_{400}$-DPA-mea). The original material was reshaped after heating above 100 °C for at least two minutes (heat gun). For the reprocessing, the cured material was firstly dipped in a liquid N$_2$ bath for a couple of minutes. The hardened polymeric material was ground to a fine powder using Retsch Ultra Centrifugal Mill ZM 200 apparatus (6000 rpm, ϕ < 40 μm). The powder was poured into a disc-shaped brass mold sandwiched between two steel plates covered by Teflon® and paper hot-pressed for one hour at 150 °C under low pressure (<10 Pa). The reprocessed PBZ was then removed from the mold and cooled to RT before testing.

3. Results and discussion

For the sake of clarity, the first part of the discussion is focusing on the synthesis and the characterization of PEG$_{400}$-DPA-mea. All the materials discussed later in this manuscript (subsection 3.2.2) have been prepared and characterized following the same procedures, detailed in the ESI.†

3.1 Synthesis and characterization of the vitrimer precursors

PEG$_{400}$-DPA-mea was synthesized solventless in two steps (Scheme 1), following a procedure previously reported by our group.[51] The phenolation of polyethylene glycol 400 (PEG$_{400}$) *via* a Fischer esterification was realized with diphenolic acid (DPA), with *p*-toluene sulfonic acid as the catalyst (*p*-TSA), and led to the formation of a quadri-telechelic phenol terminated PEG (PEG$_{400}$-DPA). It is noteworthy that PEG$_{400}$ was specifically considered for the synthesis of the benzoxazine monomers because its industrial production adheres to many of the principles of the Green Chemistry.[56] PEG$_{400}$-DPA was purified by liquid–liquid extractions to remove non-hydrolyzed *p*-TSA. PEG$_{400}$-DPA was then reacted with mono-ethanolamine (mea) and paraformaldehyde (PFA) *via* Mannich-like condensation followed by a ring-closure process. Mea was purposely used to cap the extremities of the monomer with pending –OH groups, which are able to react further by transesterification with the ester bonds of the PEG$_{400}$-DPA backbone. In fine, a quadri-telechelic benzoxazine-terminated PEG monomer was obtained (PEG$_{400}$-DPA-mea). It is noteworthy that this second step, *i.e.* Mannich-like condensation with an amino-alcohol, may compete with various detrimental side reactions when performed in a solvent, leading to the formation of hydroxybenzylaminoethanol, oxazolidine, triazacyclohexane, or diazaheptane derivatives (depending on the initial molar ratio).[57,58] To sidestep these competing reactions, the Mannich condensation was performed in various conditions (Table S1†). The highest conversion yields of phenolic counterparts into oxazine rings were obtained when the synthesis was performed in the absence of solvents and below 100 °C.

The structural features of PEG$_{400}$-DPA and PEG$_{400}$-DPA-mea were characterized by ^{1}H NMR, ^{13}C NMR, FTIR and elemental analysis (Fig. 1, Fig. S1–3†). The ^{1}H NMR spectrum of PEG$_{400}$-DPA (Fig. 1a) reveals peaks corresponding to methylene protons [1,2] adjacent to the carbonyl group in β- and α-position (δ = 3.55 and = 4.06 ppm respectively), attesting the successful esterification of PEG$_{400}$. Furthermore, the characteristic carbonyl peak [a] at δ = 173.5 ppm in ^{13}C NMR (Fig. S1†) and its correlation in 2D NMR with DPA characteristic methylene protons [1,2] confirm the formation of the ester bond. The absence of impurities or by-products peaks suggests that quantitative conversion was nearly reached. From the ^{1}H NMR spectrum of PEG$_{400}$-DPA-mea (Fig. 1b), the characteristic peaks corresponding to the formation of the benzoxazine rings are revealed at δ = 3.88 and δ = 4.80 ppm, which correspond to Ar–CH$_2$*–N [h] and O–CH$_2$*–N [g], respectively. The experimental integrations of the methylene protons of the oxazine rings are 5.81H and 5.95H, respectively, corresponding to roughly 75% of the closed benzoxazine rings (theoretical value of 8.00H each). The remaining 25% of end-capping is attributed to opened benzoxazine rings labelled with * in Fig. 1b. In such opened structures, the primary amine has reacted with the phenolic group, but the ring is not closed between the –OH and the nitrogen. The non-closed structures can still be involved in the crosslinking process and affect the rate of transesterification reactions similarly to closed structures. The disappearance of the peak at δ = 9.2 ppm suggests that 100% of the phenolic groups reacted, and this is confirmed by elemental analysis as the experimental ratio of carbon and nitrogen atoms C/N is equal to 67/4 (theoretical C/N = 68/4). The wide signal centered at δ = 4.51 ppm is attributed to the aliphatic hydroxyl groups –OH [k] (ex. 3.88H, th 4.00H). In the ^{13}C NMR spectrum (Fig. S2†), the characteristic oxazine ring carbons are found at δ = 50.6 and δ = 83.1 ppm (for Ar–*CH$_2$–N [m] and O–*CH$_2$–N [l], respectively). The formation of PEG$_{400}$-DPA-mea was also confirmed by FTIR analysis (Fig. S3†). The strong absorption peak at 1730 cm^{-1} is typical of the ester C=O stretching. The presence of the benzoxazine rings, confirmed by the characteristic bands at 1230 and 932 cm^{-1} (attributed to the C–O–C asymmetric stretching and the C–H out-of-plane vibration in the trisubstituted benzene ring, respectively), and by the decrease of the intensity of the –OH stretching vibration centered at 3339 cm^{-1}. Finally, the peak at 1030 cm^{-1} corresponds to the absorption of the primary alcohol C–O stretching and –OH in-plane deformation.

DSC measurements revealed that PEG$_{400}$-DPA and PEG$_{400}$-DPA-mea have a similar softening temperature (5.6 and 7.2 °C respectively, Fig. S4†). An exothermic peak ($T_{exo,1}$ = 110–220 °C) was observed only in the case of PEG$_{400}$-DPA-mea, attributed to the ring-opening polymerization (ROP) of benzoxazine moieties. It is worth indicating the benzoxazine ROP is triggered at a very low temperature compared to traditional benzoxazines, generally in the range of 150–200 °C.[59] The apparent low ROP temperature is related to the activating effect of alcohol functionality through hydrogen bonding, as
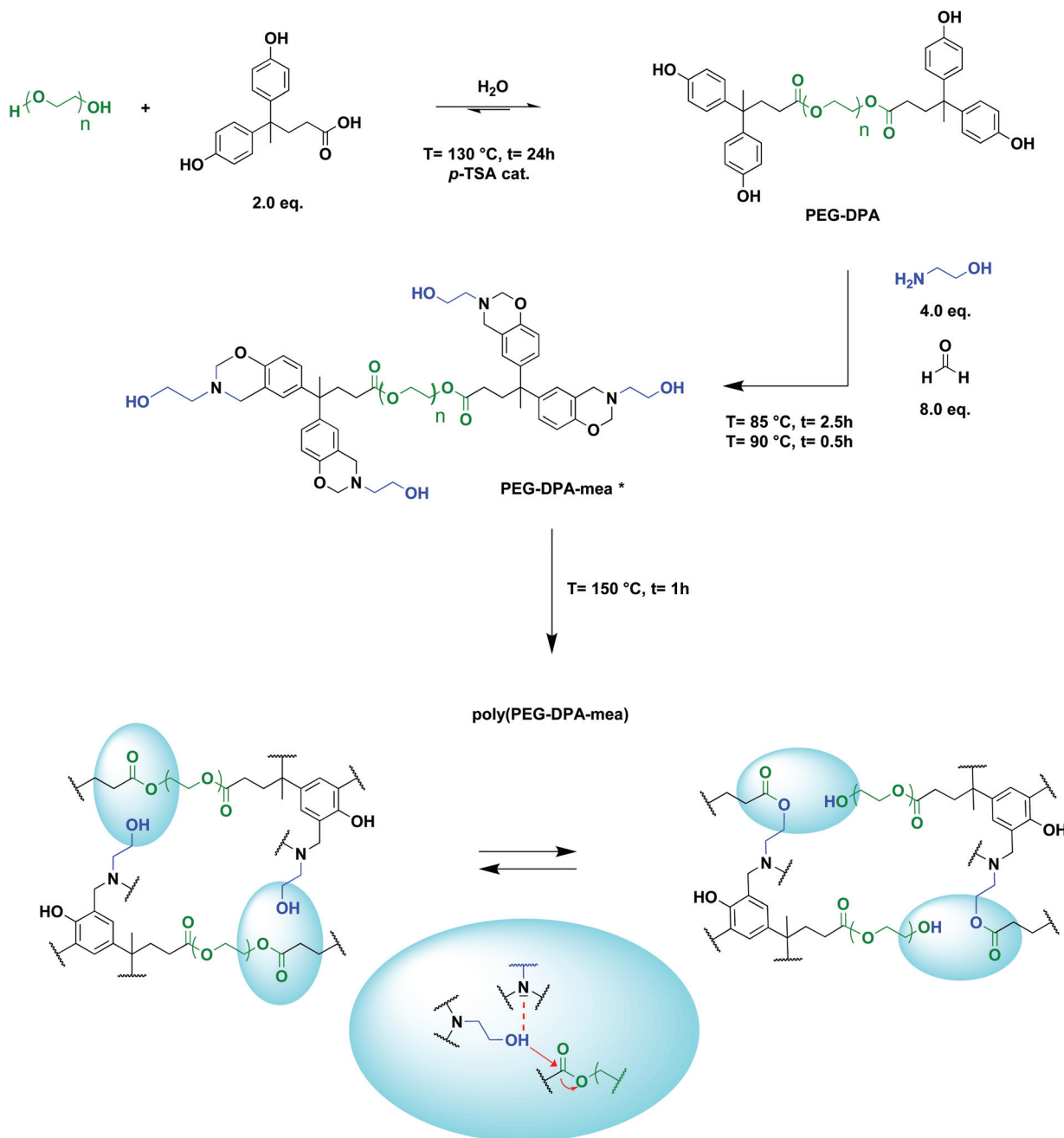
Scheme 1 Synthetic pathway to obtain poly(PEG–DPA–mea), and expected structure of the resulting vitrimer through topology rearrangement by transesterification reactions catalyzed by the *in situ* generated tertiary amines (*25% of unclosed benzoxazine rings).

previously reported in the literature.[60,61] A second exothermic peak centered around 250 °C ($T_{\mathrm{exo,2}}$) is attributed to a thermal degradation, also confirmed by TGA (Fig. S5†). PEG$_{400}$-DPA-mea was subjected to a curing treatment monitored by rheology at 140 °C (Fig. 2a). The recorded rheograms present the evolution of the storage modulus (G') and the loss modulus (G'') during the polymerization of the monomer. The behavior of PEG$_{400}$-DPA-mea when heated is typical to thermosets with a significant increase in both G' and G''. The approximate gelation (t_{gel}), defined as the crossover point of G' and G'', was

reached quickly after 145 s of isothermal curing. This high reactivity could be explained by the high functionality of the system. Rheological characterization of polymerized PEG$_{400}$-DPA-mea, so-called poly(PEG$_{400}$-DPA-mea), is reported in Fig. 2b. The measurement was done in torsion mode on a bar sample cured in a bar-shape mold as described in the Experimental section (one hour at $T = 150$ °C). The DSC thermogram of poly(PEG$_{400}$-DPA-mea) did not reveal an exothermic peak, indicating a complete polymerization (Fig. S6†). The moduli were measured to 0.6 GPa and 10 MPa in the glassy

Paper
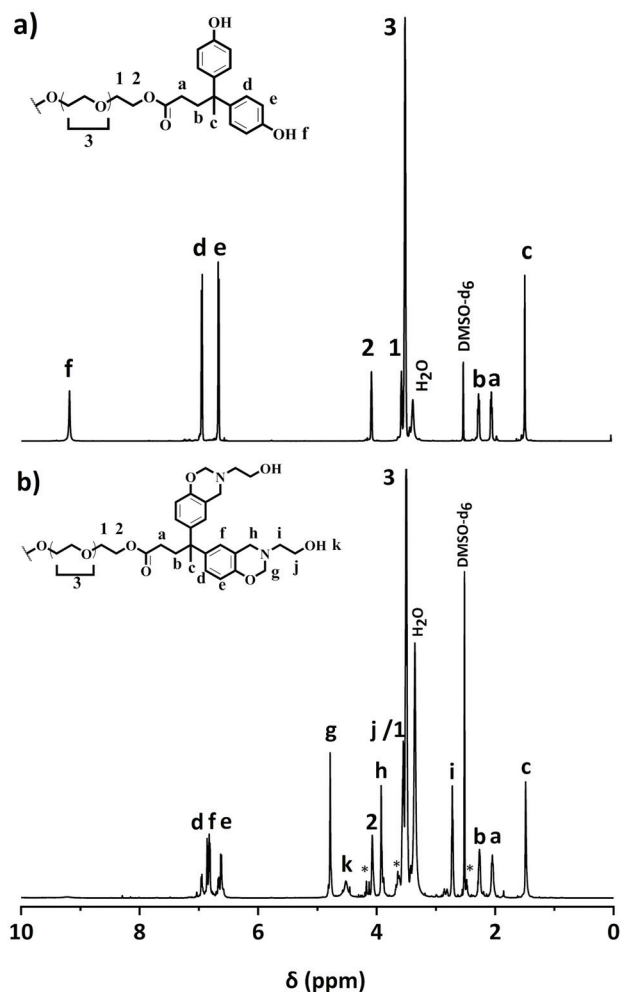
Fig. 1 ^{1}H NMR spectrum of (a) PEG$_{400}$-DPA and (b) PEG$_{400}$-DPA-mea (DMSO-d$_6$).

and rubbery states, respectively. The α mechanical relaxation (T_α) was measured at 93 °C according to the maximum of the tan δ. The significant broad tan delta is characteristic of networks constituted of a wide distribution of chemical structures, assigned to the transesterification reactions occurring during the curing. The T_g of poly(PEG$_{400}$-DPA-mea) was also measured by dilatometry (Fig. S7†). The transition was measured at the onset of the inflection (79 °C) and is more representative of the service temperature of the vitrimer than the T_α. It is worth indicating that the low thermal expansion associated to the T_g is consistent with the near-zero volumetric expansion characteristic of polybenzoxazines.[24]

3.2 Characterization of the polybenzoxazine vitrimer

3.2.1 Characterization of the vitrimer properties of poly (PEG$_{400}$-DPA-mea). The evolution of the relaxation modulus of poly(PEG400-DPA-mea) as a function of time and temperature (from 120 to 170 °C) shows a clear relaxation process of the modulus of poly(PEG$_{400}$-DPA-mea) (Fig. 3a). The relaxation time (τ^*), conventionally defined as the time for the vitrimer to relax to a value corresponding to 1/e (0.37) of its original modulus,[5] was measured to be 116 s at 170 °C. The temperature dependence of the relaxation time was plotted in Fig. 3b according to the Arrhenius law (5):

$$\ln\left(t^*\right)\frac{E_a}{R \times T} - \ln(A) \tag{5}$$

The linear fitting of ln (τ^*) *versus* 1/T plot (correlation coefficient of 0.991) suggests that the network follows an Arrhenius-like flow characteristic. The activation energy (E_a) of transesterification reactions was obtained from the slope of the Arrhenius equation and yielded 115 kJ mol^{-1} (Fig. S7;† the detail of the calculation is reported in the ESI†). The theoretical T_v was found at 88 °C for poly(PEG$_{400}$-DPA-mea), in the
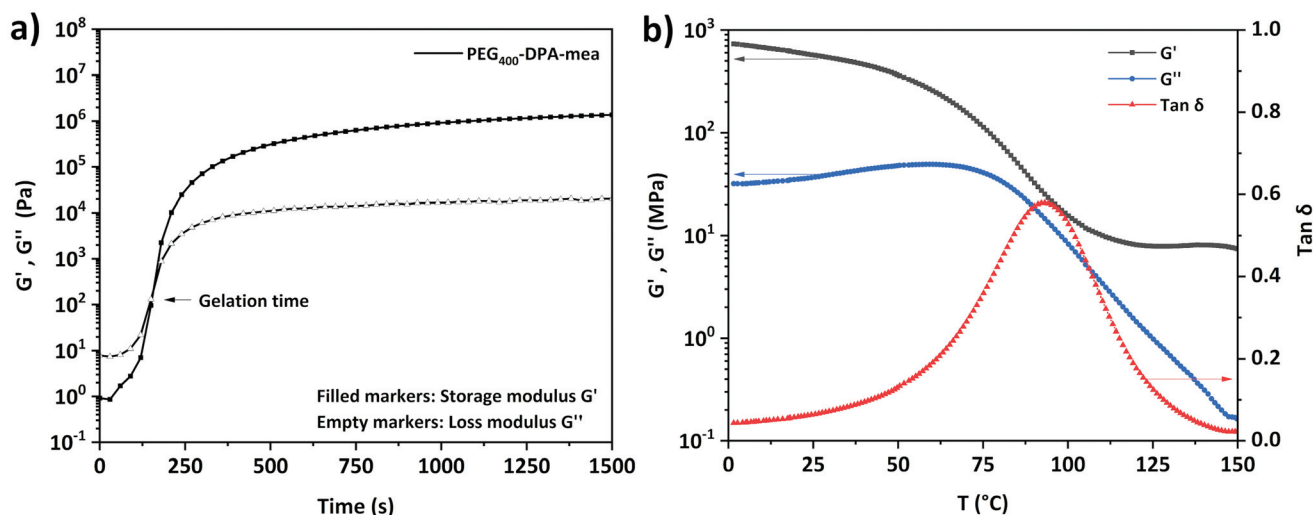
Fig. 2 (a) Isothermal rheology monitoring of PEG$_{400}$-DPA-mea at 140 °C (b) Rheology temperature sweep curves in torsion mode of poly(PEG$_{400}$-DPA-mea).
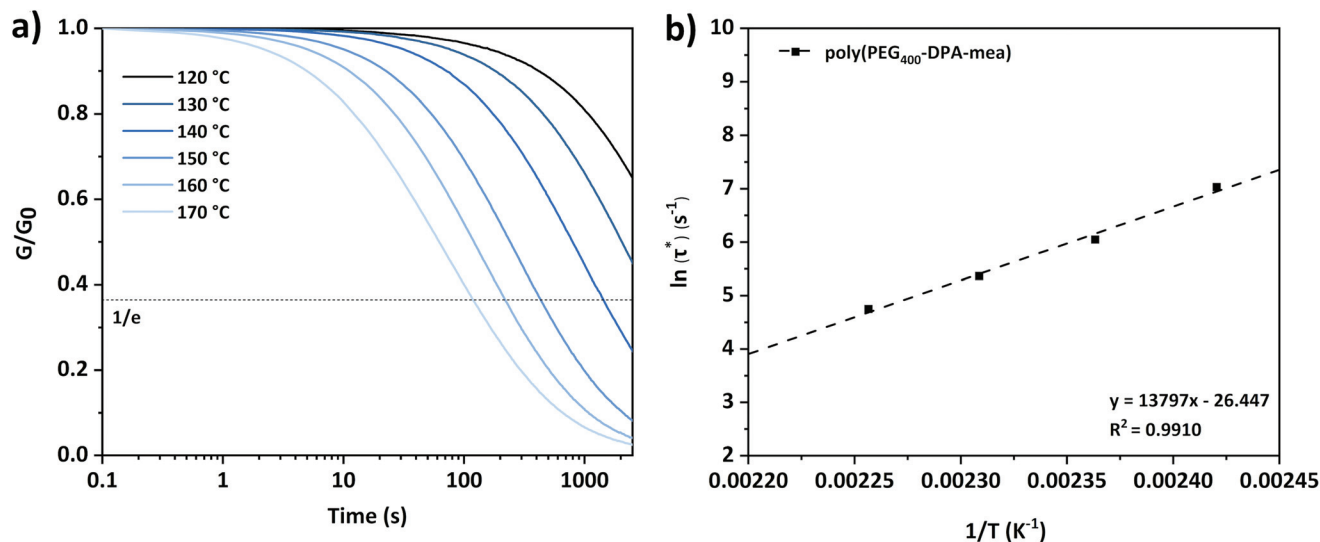
Fig. 3 (a) Stress relaxation curves of poly(PEG$_{400}$-DPA-mea) at different temperatures and (b) Arrhenius plot obtained from stress relaxation experiment of poly(PEG400-DPA-mea).

range of the vitrimers developed by Leibler *et al.* for epoxy/acid systems.[5,6] In the present work, the catalytic effect originates from the neighboring group participation (NGP) of the NR$_3$ groups in the mechanism of the TER (Scheme 1), in a similar fashion than described by Du Prez *et al.* in a recent review.[11] The activation of the –OH groups is promoted by intramolecular hydrogen bonding with the lone electron pair carried by the nitrogen atoms. While the energy of the H–O bonds decreased owing to the N–H interaction, the atom of oxygen became nucleophilic enough to attack the electrophilic center of the carbonyl bond, allowing the TER to occur.

3.2.2 Effect of the structural features on the vitrimer properties. It is generally admitted that the structural features of TER-based vitrimers are an important parameter driving their properties. The rate-enhancing effect in catalyst-free TER vitrimers is likely caused by tertiary amines and/or a high concentration of hydroxyl functions (Table 1, rows 1–7). An excess of –OH groups' was successfully used to activate ester functionalities with stress relaxation in the range of 104 s at 150 °C. (Table 1, rows 1, 3 and 4).[18–20] Later, the unique structural design of β-activated esters, more inclined to react reversibly with ester bonds due to proximity effects, was considered to elaborate vitrimers with fast stress relaxation (∼1000 s at 150 °C; Table 1, row 2).[21] More recently, studies on catalyst-free vitrimers were elegantly steered toward the covalent bonding of NR$_3$ groups. Although the number of amines per ester bonds was quite low in each case (between 0.027 and 0.5, Table 1, rows 5–7), the TER was greatly enhanced. The concentration of exchangeable groups and the crosslinking density of the vitrimers were also described to affect lavishly the dynamicity of the crosslinked network. Dichtel *et al.* prepared a series of crosslinked polyurethane (PHU) vitrimers (derived from bis (6-membered cyclic carbonate) covering different ranges of crosslinking density.[62] According to the stress-relaxation tests, the relaxation was faster for the sample with a lower cross-

linking density. They attributed this trend to the stiffness of the material and the highest chain mobility observed for the lowest crosslinking density. Abu-Omar *et al.* came to a similar conclusion for epoxy vitrimers.[63]

The effect of the structural features of the benzoxazine-based vitrimer was investigated by tuning the crosslinking density of the material and the number of –OH groups. The effect of the crosslinking density was assessed by preparing two materials with a PEG of molecular weight of either 200 or 2000 g mol^{-1}. In these materials, the ratio NR$_3$/ester/–OH groups (N/COO/OH) was similar (2/1/2), but the concentration of the dynamic exchangeable sites was decreasing along with the molecular weight of the PEG. Once polymerized, these materials were annotated as poly(PEG$_{200}$-DPA-mea) and poly (PEG$_{2000}$-DPA-mea) for the sake of clarity (Table 1, rows 8 and 13). The effect of the number of –OH groups was investigated by preparing three additional materials, where a part of monoethanolamine was substituted by furfurylamine (fa). They were called poly(PEG-DPA-mea$_{75}$/fa$_{25}$), poly(PEG-DPA-mea$_{50}$/fa$_{50}$), poly(PEG-DPA-mea$_{25}$/fa$_{75}$), corresponding to materials where 75%, 50% and 25% of mea was substituted by 75%, 50% and 25% of fa, respectively. NMR revealed that they correspond to materials containing a ratio of N/COO/OH equal to 2/1/1.38, 2/1/0.91 or 2/1/0.5, in respect to the order given in the sentence above (Table 1, rows 10–12). The details of the preparation and characterization of all the materials can be found in the ESI (Fig. S8–14 and S18–25†).

As expected, the crosslinking density was decreasing when the PEG molecular weight was increasing, reaching (81 ± 5) × 10^3 mol cm^{-3}, (24 ± 1) × 10^3 mol cm^{-3} and (1.5 ± 0.1) × 10^3 mol cm^{-3} for poly(PEG$_{200}$-DPA-mea), poly(PEG$_{400}$-DPA-mea) and poly(PEG$_{2000}$-DPA-mea) respectively. The crosslinking density of poly(PEG$_{400}$-DPA-mea$_x$/fa$_{100-x}$) were found to be similar to poly(PEG$_{200}$-DPA-mea), close to 100 × 10^3 mol cm^{-3}. They are higher than ν$_c$ of (polyPEG$_{400}$-DPA-mea) in reason of

Table 1 Summary of the crosslinking density, the ratio of functionalities in self-catalyzed TER vitrimers reported in the literature and comparison of their glass transitions, relaxation times and activation energies

Network	Type of internal catalysis	$10^3 \times \nu_c^a$ (mol cm)$^{-3}$	N/COO^b	OH/COO^d	T_g^e (°C)	T_α^g (°C)	E_a^h kJ mol^{-1}	τ^{*i} (S) [T]	Ref.
Epoxy resin	Excess of –COOH groups/β-hydroxy ester	—	—	1–2^c	—	8	104	~10^4 [150 °C]	18
Poly(hydroxyethylmethacrylate)	β-Keto ester	2.4 ± 0.3^c	—	1.5^c	—	130	111	~1000 [150 °C]	21
Epoxy resin	Excess of –OH groups	—	—	>8^c	63^f	70	63	~4500 [180 °C]	19
Epoxy resin	Excess of –OH groups	—	—	0.625^c	—	57	64	~5000 [180 °C]	20
Epoxy resin	Covalently bonded NR$_3$ groups	—	0.027^c	0.9^c	—	69	94	~1000 [160 °C]	16
Epoxy resin	Covalently bonded NR$_3$ groups/β-hydroxy ester	—	0.5^c	1^c	–1^f	22	—	>10^4 [170 °C]	17
Epoxy resin	Covalently bonded NR$_3$ groups/excess of –OH groups	—	<0.1^c	1^c	120^f	135	125	>10^4 [170 °C]	22
Polybenzoxazine	Poly(PEG$_{200}$-DPA-mea)	81 ± 5	2	1.67^c	125	—	106	814 [150 °C]	This work
	Poly(PEG$_{400}$-DPA-mea)	24 ± 1	2*	1.95*	125	93	115	422 [150 °C]	
	Poly(PEG$_{400}$-DPA-mea$_{75}$/fa$_{25}$)	69 ± 1	2	1.38*	113	—	126	2012 [150 °C]	
	Poly(PEG$_{400}$-DPA-mea$_{50}$/fa$_{50}$)	118 ± 17	2	0.91*	121	—	131	3172 [150 °C]	
	Poly(PEG$_{400}$-DPA-mea$_{25}$/fa$_{75}$)	117 ± 19	2	0.50*	125	—	136	3410 [150 °C]	
	Poly(PEG$_{2000}$-DPA-mea)	1.5 ± 0.1	2	1.93*	—	–34	154	36 [150 °C]	

^{a} Determined from the Flory Rehner equation (2). ^{b} Number of NR$_3$ functionalities per ester bonds (*confirmed by elemental analysis). ^{c} From the literature. ^{d} Number of –OH per ester bonds (* determined from ^{1}H NMR). ^{e} Determined by dilatometry experiment. ^{f} Determined by DSC experiment. ^{g} Measured from the maximum peak of tan δ curve. ^{h} Extrapolated from the Arrhenius equation. ^{i} Determined by stress relaxation experiment.

the involvement of the furan ring in the network formation.[30,41,59]

According to the stress relaxation curves, all these materials behaved like vitrimers (Tables S2–3, Fig. S15–17 and S26–29†). Their E_a and τ^* at 150 °C were determined from isothermal relaxation measurements (Table 1, column 8 and 9) and plotted in Fig. 4a and Fig. 4b as a function of their ν_c. A clear dependence of the E_a on the number of –OH groups is depicted on Fig. 4a (values encircled by a dashed line). Despite their similar crosslinking density, the E_a of poly(PEG-DPA-mea$_{75}$/fa$_{25}$), poly(PEG-DPA-mea$_{50}$/fa$_{50}$), and poly(PEG-DPA-mea$_{25}$/fa$_{75}$) are increasing while the amount of –OH groups is decreasing (E_a = 126, 131, 136 kJ mol^{-1} respectively). In the case of poly(PEG$_{2000}$-DPA-mea), which crosslinking density is the lowest, E_a reached the value of 156 kJ mol^{-1}. In the more crosslinked network (poly(PEG$_{200}$-DPA-mea)), E_a decreased to 106 kJ mol^{-1}. Lowering the concentration of –OH groups, either by decreasing the ν_c or the total amount of –OH groups leads to an increase of the E_a. These experiments confirm that the energy needed to activate the dynamic exchanges is clearly governed both by the excess of –OH groups and the concentration of dynamic sites in the network. It is worth indicating the E_a related to the relaxation of theses PBZs vitrimer are in the same range than other reported vitrimers catalyzed either by external or internal tertiary amine.[5,6,16,22] However it cannot be excluded that aromatic –OH groups may also be involved in the transesterification mechanism and contribute to the high value of E_a. Indeed, the transesterification with phenoxy is well documented.[64–66] Nevertheless, it is worthy to mention that even after a couple of hours at 170 °C, the relaxation of PEG$_{400}$-DPA-fa, *i.e.* in the absence of aliphatic –OH was not observed. The results do not exclude the possible involvement of the phenoxy groups in the exchanges, but it is not observed in the conditions of the experiments described here.

The evolution of τ^* follows another trend (Fig. 4b). A clear dependence exists with the concentration of –OH groups, as attested by the significant increase of τ^* when decreasing the amount of –OH groups for materials of similar ν_c (poly(PEG$_{400}$-DPA-mea$_x$/fa$_{100-x}$). τ^* remains reasonable (lower than 1 hour at 150 °C) even for the material displaying the lower amount of –OH groups (Table 1, row 12). However, despite their lowest concentration of dynamic sites, the fastest behaviors were reached for the materials with the lowest ν_c (Table 1, rows 9 and 13). This trend indicates that the speed of the dynamic exchange is also driven by the mobility of the chains.[62,63]

The very short τ^* compared to similar catalyst-free vitrimers can be explained by the abundant number of NR$_3$ groups (coming from the benzoxazine ROP). Indeed, the polymerization of PEG$_n$-DPA-mea$_x$/fa$_{100-x}$ follows a ROP, which leads to the formation of a network with an abundant number of tertiary amines, significantly higher in comparison to the previously reported catalyst-free vitrimers (Table 1, column 4). Therefore, the nucleophile substitution of the ester bonds by
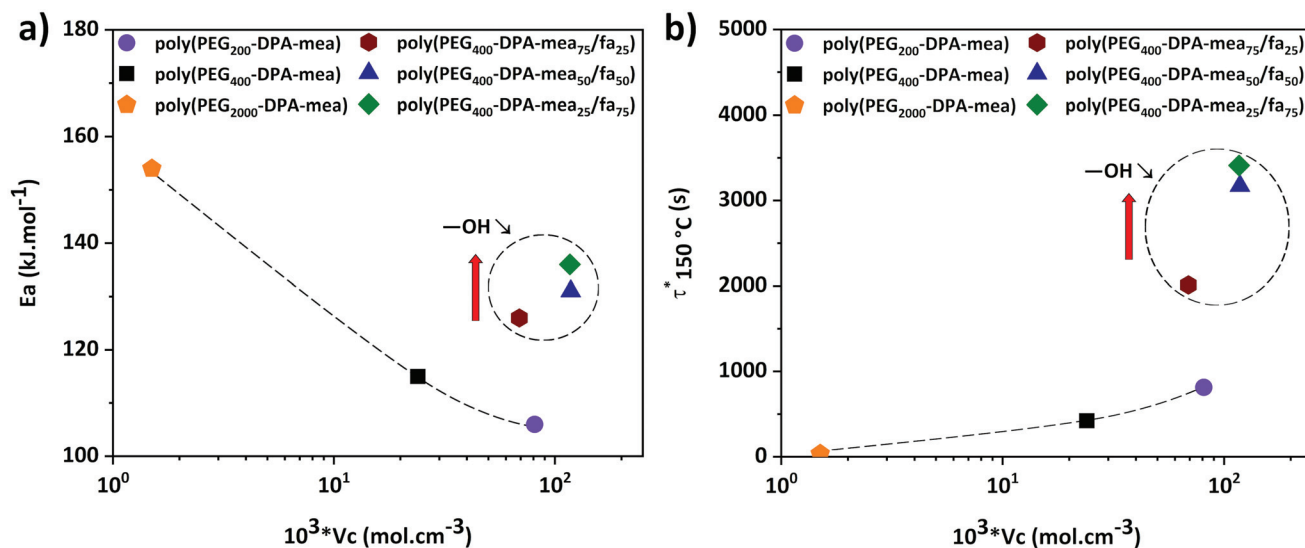
Fig. 4 Evolution of $\tau^*_{150°C}$ and E_a as a function of the crosslinking density of the different polybenzoxazine vitrimer.

the –OH groups is highly promoted. This behavior is in adequation with one of the first observations made by Leibler *et al.* about the relationship between the amount of catalyst and the short τ^* of vitrimers.[6] Moreover, the catalytic effect is more pronounced thanks to the close position of the NR_3 groups regarding the –OH groups, in agreement with the NGP

theory recently disclosed by Du Prez *et al.*[11] and illustrated in Scheme 1.

3.3 Self-healing, recycling, reprocessing and reshaping

Additional swelling experiments were performed in different solvents for poly(PEG$_{400}$-DPA-mea). The material is insoluble
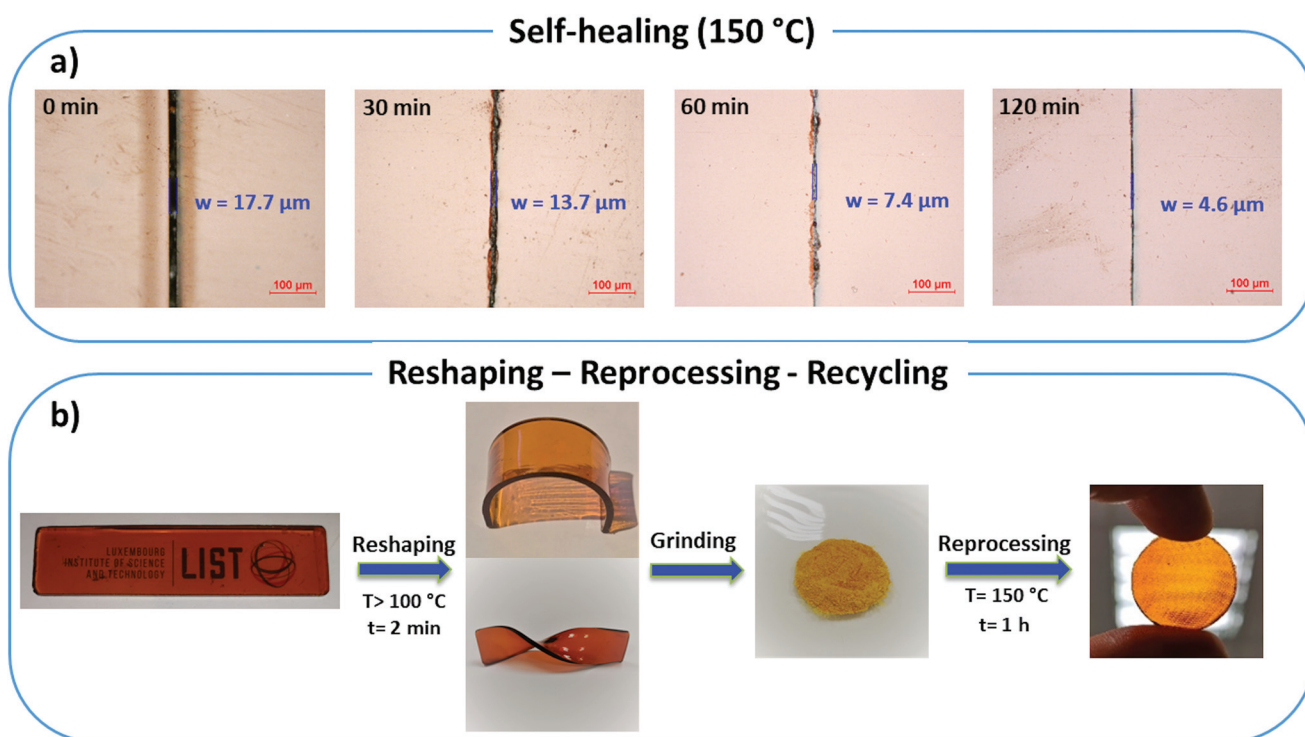
Fig. 5 (a) Self-healing behavior of poly(PEG$_{400}$-DPA-mea) (b) Life cycle of the bio-based polybenzoxazine vitrimer by reshaping, reprocessing and recycling.
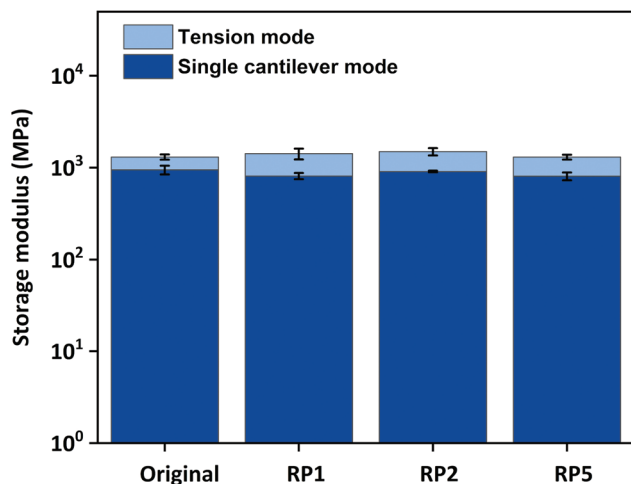
Fig. 6 Storage modulus of poly(PEG$_{400}$-DPA-mea) determined in tensile and single cantilever mode after successive recycling (one, two and five times respectively).

in acetone, water, and chloroform, in which it swells by 14%, 38%, and 103% respectively after 24 hours (Fig. S30†). Later, the samples were dried and weighted to determine the soluble part, measured to be lower than 5 wt%. The chemical recyclability of poly(PEG$_{400}$-DPA-mea) was illustrated by its chemical decomposition in acetic acid at RT (Fig. S31†). The self-healability of poly(PEG$_{400}$-DPA-mea) was demonstrated by surface morphology analysis recorded by optical microscopy (Fig. 5a). The cured material was notched with a scalpel blade, forming a scratch of 17.7 μm initial width. When exposed at 150 °C in pressure-free conditions, the width of the damaged area gradually decreased with time, reaching 4.6 μm (*i.e.* less than 25% of the initial scratch width) after 120 min. The reshaping, twisting and bending of materials made of poly(PEG$_{400}$-DPA-mea) were straightforward, thanks to the fast relaxation process (Fig. 5b). The reprocessability was investigated by grinding the material into a fine powder, after which it was compressed to the shape of either a disk or a bar. The reprocessed bar was then subjected to dynamic mechanical tests in tensile and single cantilever modes to determine the impact of the reprocessing on their mechanical properties (Fig. 6). The storage modulus (*E'*) of poly(PEG$_{400}$-DPA-mea) (1307 ± 86 MPa) was fully recovered even after being ground and reshaped five times (1306 ± 81 MPa). Besides storing the mechanical properties, the overlap of the FTIR spectra of both cured and reprocessed materials provides evidence that poly(PEG$_{400}$-DPA-mea) did not show any deterioration of its chemical structure after 5 recycling steps (Fig. S32†).

Conclusions

This study relates the synthesis and the properties of a catalyst-free and bio-based polybenzoxazine vitrimer. The synthesis

pathway consisted of a solventless two-step reaction, including the Fischer esterification of 4,4-bis(4-hydroxyphenyl) valeric acid and polyethylene glycol, which was then reacted with mono-ethanolamine and paraformaldehyde *via* a Mannich-like condensation. Quadri-telechelic benzoxazine-terminated polyethylene glycol monomers containing ester bonds and pendant aliphatic hydroxyl groups (PEG$_{400}$-DPA-mea) were obtained. The chemical structure of the monomers was confirmed by ^{1}H NMR, ^{13}C NMR, elemental analysis, and FTIR. The vitrimer (poly(PEG$_{400}$-DPA-mea)) was formed by triggering the ring-opening polymerization of the benzoxazine moieties at 150 °C for one hour, leading to a covalently bonded network with an abundant number of tertiary amines per ester bond. The mechanical properties of the resulting PBz were assessed by rheological characterization. The achievement of a cross-linked structure was attested by the ability of the material to swell in common organic solvents, with a soluble fraction lower than 5 wt%. Due to the ability of tertiary nitrogen groups to catalyze transesterification reactions, the material enabled fast exchange reactions without the use of an external catalyst, as attested by short stress-relaxation times (116 s at 170 °C). The activation energy of the ester bond exchange was found to be 115 kJ mol^{-1}, in the range of transesterification reactions catalyzed by tertiary amines. The effect of the structural features of the vitrimer was also investigated by tuning the cross-linking density of the network and the amount of –OH groups. It showed that the energy needed to activate the dynamic exchanges is clearly governed both by the excess of –OH groups and the concentration of dynamic sites in the network. The very short relaxation times were explained by the neighboring group participation theory, the abundant number of tertiary N groups and the flexibility of the network.

The self-healing, recycling, reshaping, and reprocessing of poly(PEG$_{400}$-DPA-mea) without any loss of properties were successfully demonstrated. Therefore, this research reflects the suitability of polybenzoxazines to design easily synthesizable mono-component, catalyst-free, and fast responsive vitrimers.

Abbreviations

CAN	Covalent adaptable network
DCB	Dynamic covalent bond
TER	Transesterification reaction
–OH	Aliphatic hydroxyl
Zn(OAc)$_2$	Zinc acetate
NR3	Tertiary amine
TBD	Triazobicyclodecene
PBZs	Polybenzoxazines
ROP	Ring-opening polymerization
PFA	Paraformaldehyde
DPA	Diphenolic acid
PEG	Polyethylene glycol
PEG-DPA	Quadri-telechelic phenol-terminated PEG
mea	Mono-ethanolamine

PEG-DPA-mea	Quadri-telechelic benzoxazine-terminated polyethylene glycol monomer
fa	Furfurylamine
p-TSA	*para*-Toluene sulfonic acid
NMR	Nuclear magnetic resonance
TMS	Tetramethylsilane
FTIR	Fourier transform infrared spectroscopy
ATR	Attenuated total reflection
N_2	Nitrogen
$T_{\text{desorpt.}}$	Desorption temperature
TCD	Thermal conductivity detector
DSC	Differential scanning calorimetry
T_g	Glass transition
TGA	Thermogravimetric analysis
DTG	Derivative tthermogravimetric Analysis
DMA	Dynamic mechanical analysis
RT	Room temperature
G_0	Original relaxation modulus
G'/E'	Storage modulus
G''	Loss modulus
W	Swelling ratio
$\overline{M_c}$	Molecular weight between crosslinks
ν_c	Crosslinking density
DMSO-d_6	Deuterated dimethylsulfoxide
Poly(PEG-DPA-mea)	Polymerized PEG-DPA-mea
PEG_n	Polyethylene glycol of molecular weight n (g mol^{-1})
Tan δ	Loss factor
τ^*	Relaxation time
E_a	Activation energy
NGP	Neighboring group participation

Author contributions

Antoine Adjaoud: validation, investigation, writing – original draft, writing – review and editing. Acerina Trejo-Machin: validation, investigation, writing – review and editing. Laura Puchot: validation, investigation, writing – original draft, writing – review and editing. Pierre Verge: conceptualization, validation, investigation, resources, writing – original draft, writing – review and editing, supervision, project administration.

Funding sources

Conflicts of interest

There are no conflicts of interest to declare.

Acknowledgements

Notes and references

1 K. L. Forsdyke and T. F. Starr, *Thermoset Resins*, iSmithers Rapra Publishing, 2002.
2 S. J. Rowan, S. J. Cantrill, G. R. L. Cousins, J. K. M. Sanders and J. F. Stoddart, *Angew. Chem., Int. Ed.*, 2002, **41**, 898–952.
3 S. D. Bergman and F. Wudl, *J. Mater. Chem.*, 2008, **18**, 41–62.
4 C. J. Kloxin, T. F. Scott, B. J. Adzima and C. N. Bowman, *Macromolecules*, 2010, **43**, 2643–2653.
5 D. Montarnal, M. Capelot, F. Tournilhac and L. Leibler, *Science*, 2011, **334**, 965–968.
6 M. Capelot, M. M. Unterlass, F. Tournilhac and L. Leibler, *ACS Macro Lett.*, 2012, **1**, 789–792.
7 M. Capelot, D. Montarnal, F. Tournilhac and L. Leibler, *J. Am. Chem. Soc.*, 2012, **134**, 7664–7667.
8 W. Denissen, J. Winne and F. Du Prez, *Chem. Sci.*, 2015, **7**, 30–38.
9 J. Winne, L. Leibler and F. Du Prez, *Polym. Chem.*, 2019, **10**, 6091–6108.
10 M. Guerre, C. Taplan, J. M. Winne and F. E. Du Prez, *Chem. Sci.*, 2020, **11**, 4855–4870.
11 F. Van Lijsebetten, J. O. Holloway, J. M. Winne and F. E. Du Prez, *Chem. Soc. Rev.*, 2020, **49**, 8425–8438.
12 D. J. Fortman, J. P. Brutman, G. X. De Hoe, R. L. Snyder, W. R. Dichtel and M. A. Hillmyer, *ACS Sustainable Chem. Eng.*, 2018, **6**, 11145–11159.
13 J. Otera, *Chem. Rev.*, 1993, **93**, 1449–1470.
14 U. Schuchardt, R. Sercheli and V. Matheus, *J. Braz. Chem. Soc.*, 1998, **9**, 199–210.
15 M. K. Kiesewetter, M. D. Scholten, N. Kirn, R. L. Weber, J. L. Hedrick and R. M. Waymouth, *J. Org. Chem.*, 2009, **74**, 9490–9496.
16 F. I. Altuna, C. E. Hoppe and R. J. J. Williams, *Eur. Polym. J.*, 2019, **113**, 297–304.
17 Y. Li, T. Liu, S. Zhang, L. Shao, M. Fei, H. Yu and J. Zhang, *Green Chem.*, 2020, **22**, 870–881.
18 F. I. Altuna, V. Pettarin and R. J. J. Williams, *Green Chem.*, 2013, **15**, 3360–3366.
19 J. Han, T. Liu, C. Hao, S. Zhang, B. Guo and J. Zhang, *Macromolecules*, 2018, **51**, 6789–6799.
20 T. Liu, S. Zhang, C. Hao, C. Verdi, W. Liu, H. Liu and J. Zhang, *Macromol. Rapid Commun.*, 2019, **40**, 1800889.
21 S. Debnath, S. Kaushal and U. Ojha, *ACS Appl. Polym. Mater.*, 2020, **2**, 1006–1013.

22 C. Hao, T. Liu, S. Zhang, W. Liu, Y. Shan and J. Zhang, *Macromolecules*, 2020, **53**, 3110–3118.

23 X. Ning and H. Ishida, *J. Polym. Sci., Part A: Polym. Chem.*, 1994, **32**, 1121–1129.

24 H. Ishida, in *Handbook of Benzoxazine Resins*, ed. H. Ishida and T. Agag, Elsevier, Amsterdam, 2011, pp. 3–81.

25 E. Calò, A. Maffezzoli, G. Mele, F. Martina, S. E. Mazzetto, A. Tarzia and C. Stifani, *Green Chem.*, 2007, **9**, 754–759.

26 N. N. Ghosh, B. Kiskan and Y. Yagci, *Prog. Polym. Sci.*, 2007, **32**, 1344–1391.

27 M. Comí, G. Lligadas, J. C. Ronda, M. Galià and V. Cádiz, *J. Polym. Sci., Part A: Polym. Chem.*, 2013, **51**, 4894–4903.

28 L. Dumas, L. Bonnaud, M. Olivier, M. Poorteman and P. Dubois, *J. Mater. Chem. A*, 2015, **3**, 6012–6018.

29 L. Puchot, P. Verge, T. Fouquet, C. Vancaeyzeele, F. Vidal and Y. Habibi, *Green Chem.*, 2016, **18**, 3346–3353.

30 C. Wang, J. Sun, X. Liu, A. Sudo and T. Endo, *Green Chem.*, 2012, **14**, 2799–2806.

31 N. K. Sini, J. Bijwe and I. K. Varma, *J. Polym. Sci., Part A: Polym. Chem.*, 2014, **52**, 7–11.

32 P. Thirukumaran, A. Shakila Parveen and M. Sarojadevi, *ACS Sustainable Chem. Eng.*, 2014, **2**, 2790–2801.

33 P. Froimowicz, C. R. Arza, L. Han and H. Ishida, *ChemSusChem*, 2016, **9**, 1921–1928.

34 L. Dumas, L. Bonnaud, M. Olivier, M. Poorteman and P. Dubois, *Green Chem.*, 2016, **18**, 4954–4960.

35 X. Liu, R. Zhang, T. Li, P. Zhu and Q. Zhuang, *ACS Sustainable Chem. Eng.*, 2017, **5**, 10682–10692.

36 B. Kiskan, *React. Funct. Polym.*, 2018, **129**, 76–88.

37 M. L. Salum, D. Iguchi, C. R. Arza, L. Han, H. Ishida and P. Froimowicz, *ACS Sustainable Chem. Eng.*, 2018, **6**, 13096–13106.

38 L. Bonnaud, B. Chollet, L. Dumas, A. A. M. Peru, A. L. Flourat, F. Allais and P. Dubois, *Macromol. Chem. Phys.*, 2019, **220**, 1800312.

39 N. Amarnath, S. Shukla and B. Lochab, *ACS Sustainable Chem. Eng.*, 2018, **6**, 15151–15161.

40 M. Monisha, N. Amarnath, S. Mukherjee and B. Lochab, *Macromol. Chem. Phys.*, 2019, **220**, 1970005.

41 S. Ren, X. Miao, W. Zhao, S. Zhang and W. Wang, *Mater. Today Commun.*, 2019, **20**, 100568.

42 Y. Lyu and H. Ishida, *Prog. Polym. Sci.*, 2019, **99**, 101168.

43 N. Amarnath, S. Shukla and B. Lochab, *ACS Sustainable Chem. Eng.*, 2019, **7**, 18700–18710.

44 L. E. Heim, H. Konnerth and M. H. G. Prechtl, *Green Chem.*, 2017, **19**, 2347–2355.

45 R. Tavernier, L. Granado, G. Foyer, G. David and S. Caillol, *Macromolecules*, 2020, **53**, 2557–2567.

46 R. Tavernier, L. Granado, G. Foyer, G. David and S. Caillol, *Polymer*, 2020, 123270.

47 O. S. Taskin, B. Kiskan and Y. Yagci, *Macromolecules*, 2013, **46**, 8773–8778.

48 M. Arslan, B. Kiskan and Y. Yagci, *Macromolecules*, 2015, **48**, 1329–1334.

49 M. Arslan, B. Kiskan and Y. Yagci, *Macromolecules*, 2018, **51**, 10095–10103.

50 A. Trejo-Machin, L. Puchot and P. Verge, *Polym. Chem.*, 2020, **11**, 7026–7034.

51 A. Trejo-Machin, P. Verge, L. Puchot and R. Quintana, *Green Chem.*, 2017, **19**, 5065–5073.

52 J. J. Bozell, L. Moens, D. C. Elliott, Y. Wang, G. G. Neuenscwander, S. W. Fitzpatrick, R. J. Bilski and J. L. Jarnefeld, *Resour., Conserv. Recycl.*, 2000, **28**, 227–239.

53 V. Froidevaux, C. Negrell, S. Caillol, J.-P. Pascault and B. Boutevin, *Chem. Rev.*, 2016, **116**, 14181–14224.

54 M. Pelckmans, T. Renders, S. Van de Vyver and B. F. Sels, *Green Chem.*, 2017, **19**, 5303–5331.

55 C. Özdemir and A. Güner, *J. Appl. Polym. Sci.*, 2006, **101**, 203–216.

56 J. Chen, S. K. Spear, J. G. Huddleston and R. D. Rogers, *Green Chem.*, 2005, **7**, 64–82.

57 H. A. Bruson, *J. Am. Chem. Soc.*, 1936, **58**, 1741–1744.

58 N. G. Kandile, T. M. A. Razek, A. M. Al-Sabagh and M. M. T. Khattab, *Egypt. J. Pet.*, 2014, **23**, 323–329.

59 A. Trejo-Machin, A. Adjaoud, L. Puchot, R. Dieden and P. Verge, *Eur. Polym. J.*, 2020, **124**, 109468.

60 B. Kiskan, B. Koz and Y. Yagci, *J. Polym. Sci., Part A: Polym. Chem.*, 2009, **47**, 6955–6961.

61 R. Kudoh, A. Sudo and T. Endo, *Macromolecules*, 2010, **43**, 1185–1187.

62 D. J. Fortman, J. P. Brutman, M. A. Hillmyer and W. R. Dichtel, *J. Appl. Polym. Sci.*, 2017, **134**, 44984.

63 S. Zhao and M. M. Abu-Omar, *Macromolecules*, 2019, **52**, 3646–3654.

64 R. S. Porter and L.-H. Wang, *Polymer*, 1992, **33**, 2019–2030.

65 Y. Yuan and E. Ruckenstein, *Polymer*, 1998, **39**, 1893–1897.

66 P. Baumhof, R. Mazitschek and A. Giannis, *Angew. Chem., Int. Ed.*, 2001, **40**, 3672–3674.

Chapter five: High-Tg and Degradable Isosorbide-Based Polybenzoxazine Vitrimer

The introduction of dynamic covalent bonds into polybenzoxazines significantly prolongs their lifetime while maintaining the inherent mechanical performance of thermosetting materials. In follow-up work, eco-friendly PEG was replaced by isosorbide, a sugar-based diol reputed to impart rigidity and thermal stability in a cross-linked network. Isosorbide was esterified solventless with a naturally occurring phenolic acid, namely phloretic acid, prior to condensation with a mixture of primary amine derivatives and paraformaldehyde to form a di-telechelic benzoxazine monomer. Mono-ethanolamine brings aliphatic hydroxyl groups reactive toward transesterification. Furfurylamine was used to control the stoichiometry of reactive functionalities and the cross-linking density of the resulting network. In addition to generating high-T_g materials, the following study explores a new facet of the sustainability of polybenzoxazine: "*design for degradation*". Ester labile bonds feature chemical recycling aptitude facilitating network degradation under mild conditions. A comparative study was conducted to determine the degradability of the isosorbide-based vitrimer in various solvent environments (basic, neutral, acid) at different times and temperatures. In the end, the ability of the polybenzoxazine vitrimer to be recycled mechanically and chemically was also demonstrated.
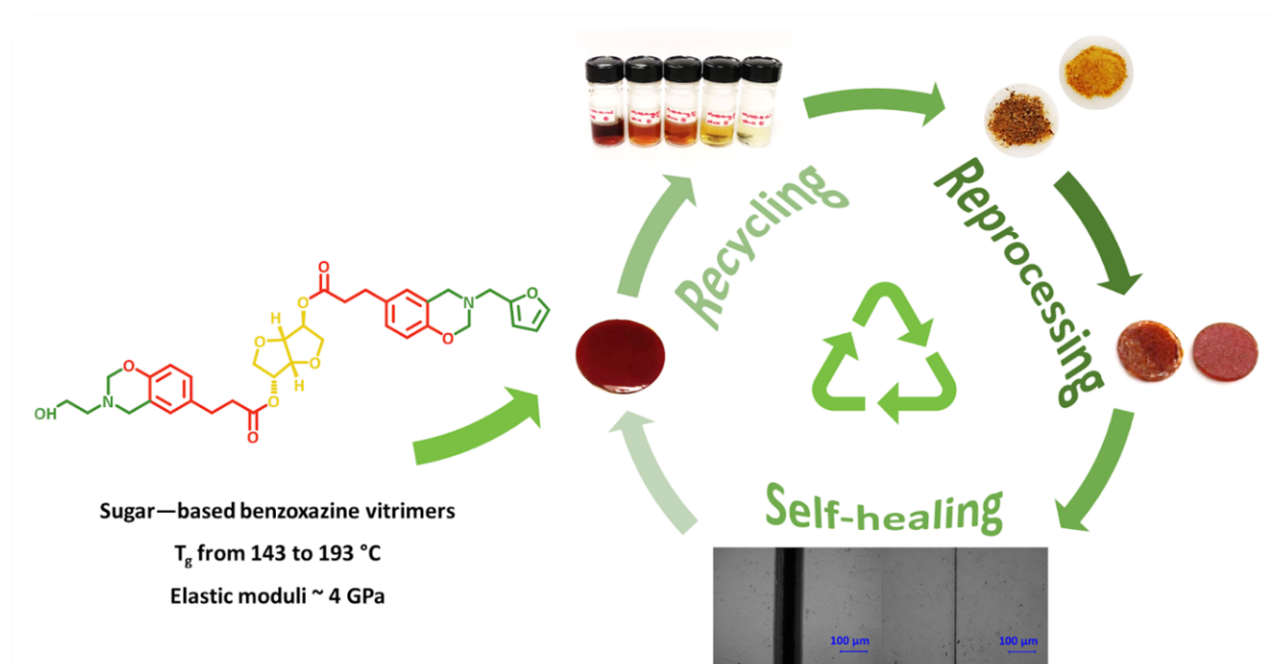
Sugar—based benzoxazine vitrimers

T_g from 143 to 193 °C

Elastic moduli ~ 4 GPa

Contribution: I did all the experimental work, from the chemical synthesis of the molecules to their polymerization. It also included all the characterizations (molecular, thermal, mechanical). I acquired all the data and handled their interpretation. I wrote the first draft of the publication and did all the needed corrections and revisions of the manuscript.

High-T_g and Degradable Isosorbide-Based Polybenzoxazine Vitrimer

Antoine Adjaoud, Laura Puchot, and Pierre Verge*

ACCESS | Metrics & More | Article Recommendations | Supporting Information

ABSTRACT: This work describes new fully bio-based vitrimers prepared from isosorbide, a renewable sugar-based chemical. Isosorbide was reacted with 4-hydroxypropionic acid, paraformaldehyde, mono-ethanolamine, and/or furfurylamine via consecutive solvent-free Fischer esterification and Mannich-like ring-closure reactions. The two-step synthesis led to the formation of a di-telechelic benzoxazine-terminated isosorbide monomer, containing ester bonds and aliphatic hydroxyl and/or furan groups. The atom economy factor yields 85%. The structural features of the resulting products were substantiated by spectroscopic techniques. The ring-opening polymerization was monitored by rheological and differential scanning calorimetry (DSC) measurements. Very high T_g values afforded by the isosorbide substructure were measured (from 143 to 193 °C), which increase with furan ring content. Internally catalyzed transesterification reactions conferred fast dynamic exchanges ($\tau^* = 300$ s at 180 °C). Self-healing and chemical and mechanical recycling were also demonstrated. Finally, the degradability of the sugar-based polybenzoxazine vitrimers was demonstrated as well. The materials were highly stable in pH-neutral water, even at 80 °C for 60 days, but owing to the isosorbide structure, pronounced degradation was observed under acidic or alkaline conditions. In summary, isosorbide is a suitable building block for the design of degradable and 100% recyclable high-T_g polybenzoxazine vitrimers.

KEYWORDS: polybenzoxazine, transesterification, catalyst-free, isosorbide, degradation
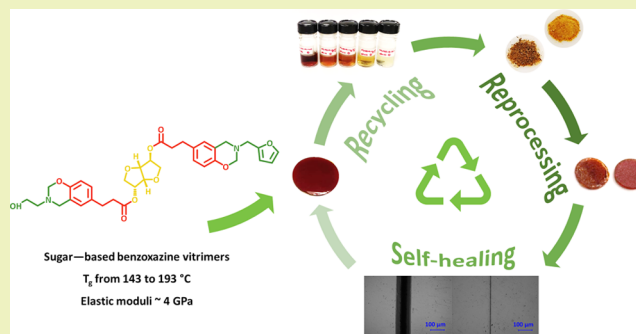
1. INTRODUCTION

Thermosets are chemically cross-linked polymers with a three-dimensional network, providing excellent mechanical strength, thermal stability, and solvent resistance. They find most of their applications as composite materials in the aerospace, building, and transportation sectors. Due to their permanent shape and cross-linked structure, end-of-life options are limited to incineration and landfilling, both having a negative impact on the environment.[1,2] To address this issue, reversible dissociative or associative bonds have been inserted within the chemical structure of thermosets to create covalent adaptable networks (CANs), conferring self-healing or recycling properties, for instance.[3−5] In this context, vitrimers are becoming more and more popular.[6−9] However, even for these materials, the question of the end of life when released into the environment, accidentally or not, is of concern. For these reasons, vitrimers able to degrade under mild conditions, but stable in service, are of significant interest.

The literature on degradable vitrimers has grown substantially of late. For instance, Athanassiou et al. have reported biodegradable epoxidized soybean oil acrylate vitrimers.[10] Degradable vitrimers prepared from poly(butylene succinate),[11] vanillin,[12] polycarbonate,[13] and glycyrrhizic acid[14] have also been reported, and the recent review of Shaver highlights the most recent achievements in this field.[15] However, the development of vitrimers with both a high glass-transition

temperature (T_g) and degradability under mild conditions is still a major challenge.

In this context, the recent development of polybenzoxazine vitrimers paves the way toward such materials.[16,17] Indeed, polybenzoxazine are thermosets with high mechanical and thermal properties.[18] Like traditional thermosets, they suffer from similar drawbacks, but the versatility of their chemical design offers opportunities to develop their self-healing,[16,17,19−22] recyclability,[16,17,23,24] and degradability,[25,26] among many other characteristics.[27−30] They are also known to be easily produced from natural resources.[31−33]

We report here the development of a degradable vitrimer prepared from D-isosorbide (DIS), a biodegradable sugar-based synthon produced at the industrial scale from renewable resources.[34] To this aim, isosorbide was esterified with phloretic acid (PA), a phenol found in the leaves of apple trees, and further reacted with mono-ethanolamine (mea) and/or furfurylamine (fa) and paraformaldehyde (PFA). The reaction led to the formation of DIS-PA-mea$_x$fa$_{100-x}$, a di-telechelic benzoxazine-

Scheme 1. Synthesis of DIS-PA-mea$_x$fa$_{100-x}$ Benzoxazine Precursors
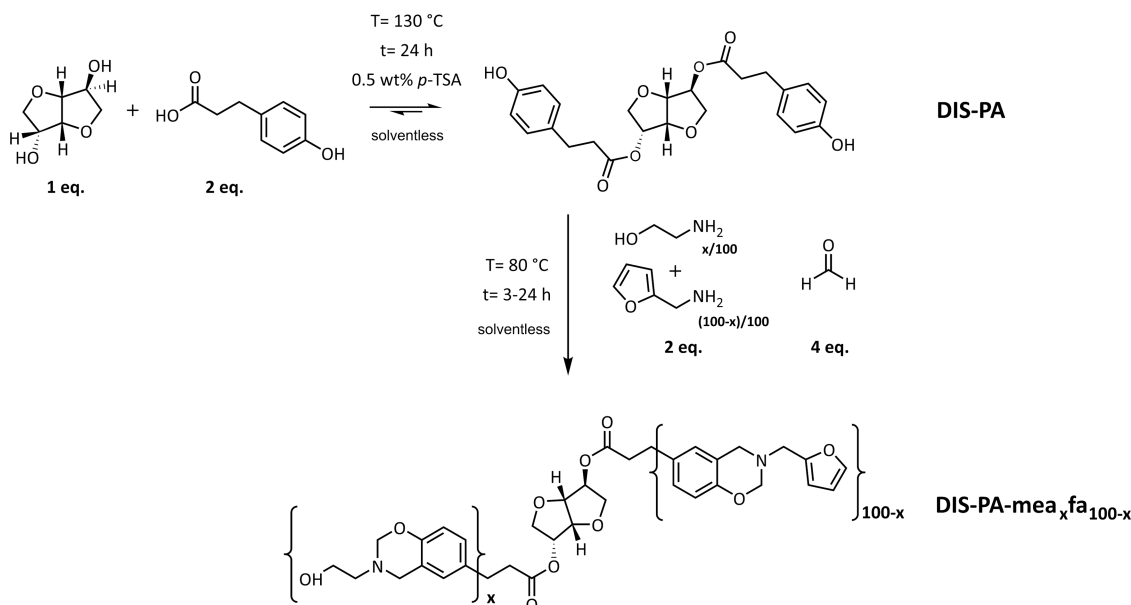
terminated isosorbide monomer with aliphatic hydroxyl (−OH) groups and/or furan rings connected to the nitrogen atom. The features of the materials are the results of the combination of each moiety:

- the tertiary amine from the benzoxazine ring-opening polymerization (ROP) catalyzes the transesterification reaction (TER), leading to fast dynamic exchanges.
- high T_g values are afforded by the isosorbide, the furan, and the benzoxazine moieties.
- the isosorbide moiety and the ester groups confer degradability under relatively mild conditions.

The following paragraphs describe the synthesis and properties of these materials, which fit many of the Green Chemistry and Engineering principles, such as "Use of renewable feedstocks", "Safer solvents and auxiliaries", "Durability rather than immortality", "Renewable rather than depleting", and "Design for Commercial after-life", to cite but a few.

2. EXPERIMENTAL SECTION

2.1. Materials and Chemicals. 1,4:3,6-Dianhydro-D-glucitol or D-isosorbide (98%, isosorbide, DIS), 3-(4-hydroxyphenyl) propionic acid (98%, phloretic acid, PA), p-toluene sulfonic acid monohydrate (≥98.5%, p-TSA), mono-ethanolamine (>98%, mea), furfurylamine (≥99%, fa), and paraformaldehyde (95%, PFA) were purchased from Sigma-Aldrich Chemicals. Carbonate buffer (pH = 10.0 ± 0.02), phosphate buffer (pH = 7.0 ± 0.02), and citrate buffer (pH = 4.0 ± 0.02) solutions were purchased from Acros Organics. All chemicals were used as received without any purification.

2.2. Synthetic Procedure. The precursors were obtained following a two-step procedure. First, diphenol-terminated isosorbide (DIS-PA) was synthesized by Fischer esterification via the synthesis protocol from previous works with minor modifications.[17,35,36] DIS (1.0 equiv) was reacted with PA (2.0 equiv) and p-TSA (0.5 wt %) in an open three-neck round-bottom flask at 130 °C for 24 h under mechanical stirring (Ministar 20 Digital, anchor stirrer, 250 rpm). After 24 h, the reaction crude was solubilized in butanone and purified by three liquid−liquid extractions with 5% NaHCO$_3$ to remove non-hydrolyzed p-TSA, followed by three liquid−liquid extractions with distilled water. The organic layer was dried over magnesium sulfate (MgSO$_4$) and evaporated under reduced pressure. Finally, the product was dried overnight under reduced pressure (<1 mBar) at T = 50 °C.

For the second step, DIS-PA (1.0 equiv) was reacted solventless with a mixture of mea ((x/100) × 2.0 equiv), fa ((($(100-x)$)/100) × 2.0 equiv), and PFA (4.0 equiv) at 80 °C for 3−24 h under mechanical stirring (Ministar 20 Digital, anchor stirrer, 250 rpm). For instance, for DIS-PA-mea$_{25}$/fa$_{75}$, 1.0 equiv of DIS-PA was reacted solventless with 4.0 equiv of PFA, 0.5 equiv of mea, and 1.5 equiv of fa. The details for each precursor are given in Table S1 in the Supporting Information (SI). DIS-PA-mea$_x$fa$_{100-x}$ benzoxazine monomers were all used without any purification (orange/yellow viscous solid).

2.3. Formation of the Polybenzoxazine Vitrimer Poly(DIS-PA-mea$_x$fa$_{100-x}$). The benzoxazine precursors DIS-PA-mea$_x$fa$_{100-x}$ were polymerized in open molds in an air-circulating oven at 150 °C (1 h), 170 °C (1 h) plus an additional post-curing step at 190 °C ($^1/_2$ h) for the furan-group-containing monomers.

2.4. Swelling Tests and Calculation of the Cross-Linking Density. Swelling experiments were conducted in water by immersion at room temperature of 200 mg of the cured material in 10 mL of solvent at different time intervals.

2.5. Degradability Assays. The degradability of the different polybenzoxazine samples was investigated by immersing, at 25 or 80 °C, 200 mg of disk-shaped materials with a diameter of 12.5 mm and 1 mm thick in 10 mL of acetic acid (AA), sodium hydroxide (NaOH 1 M), distilled water (DW), or phosphate-buffered saline (PBS). The extent of degradation (D) was monitored over time according to eq 1

$$D = \frac{m_i - m_s}{m_i} \tag{1}$$

with m_i and m_s the initial mass and the sample mass over degradation time, respectively. A value of $D < 0$ is associated with a swelling behavior, while a value of $D > 0$ is associated with degradation. $D = 1$ corresponds to complete degradation of the material. A similar study was conducted at 80 °C over 20 days, considering carbonate buffer (pH = 10.0), phosphate buffer (pH = 7.0), and citrate buffer (pH = 4.0) solutions. Each test was done in triplicate.

2.6. Self-Healing. The self-healing ability of all vitrimer samples was demonstrated by surface morphology analysis recorded by optical microscopy. The cured material was notched with a scalpel blade, forming a scratch, and then exposed at 200 °C under pressure-free conditions. The width of the scratch was measured after 2 h of thermal treatment.

2.7. Recycling. *2.7.1. Mechanical Grinding.* The material was ground to a fine powder using Retsch Ultra Centrifugal Mill ZM 200 apparatus (8000 rpm, ring sieve with trapezoid holes 0.50 mm).

2.7.2. Chemical Degradation. Materials degraded in acetic acid were recovered by evaporation of the acid under reduced pressure.

2.7.3. Reprocessing. The resulting powders (produced either chemically or mechanically as indicated above) were dried overnight under reduced pressure (<1 mbar) at $T = 50$ °C, poured into a disk-shaped brass mold (diameter = 12.5 mm, thickness = 1 mm), sandwiched between two plates, and hot-pressed for 1 h at 175 °C under low pressure (<10 Pa). The retention of mechanical properties was calculated according to eq 2

$$\text{retention} = \frac{E'_0 - E'_{Rn}}{E'_0} \quad (2)$$

where E'_0 stands for the storage modulus of the original vitrimer sample and E'_{Rn} stands for the storage modulus of the vitrimer sample reprocessed "n" times.

3. RESULTS AND DISCUSSION

3.1. Synthesis and Characterization of the Vitrimer Precursors. The precursors DIS-PA-mea$_x$fa$_{100-x}$ were synthesized solventless in a two-step reaction (Scheme 1), following a procedure reported by our group.[17,35,36] The esterification of DIS with PA was catalyzed by *p*-TSA to produce DIS-PA (Figures S1−S5). The clear disappearance of the peaks associated with the aliphatic hydroxyl groups of isosorbide (δ = 4.72 and 5.12 ppm) on the ^{1}H spectrum of DIS-PA (Figure S2) highlights their similar reactivity, not governed by endo/exo isomeric effects. After purification by liquid−liquid extractions, DIS-PA was reacted with mono-ethanolamine (mea) and/or furfurylamine (fa) and paraformaldehyde (PFA) via a Mannich-like condensation to form the benzoxazine rings. In the end, a di-telechelic benzoxazine monomer was prepared (DIS-PA-mea$_x$fa$_{100-x}$). The atom economy factor (E)[37] yields a high value of 85% as only water is released during the synthesis. The bio-based content can be estimated to 100%: Isosorbide and furfurylamine are bio-based (agricultural wastes) and produced regionally; phloretic acid is a lignin derivative found in apple tree leaves; paraformaldehyde can be obtained from bio-methanol; and mono-ethanolamine is from bio-based ammonia.

The structural features of DIS-PA-mea$_x$fa$_{100-x}$ were substantiated by ^{1}H NMR, ^{13}C NMR, Fourier transform infrared (FTIR) spectroscopy, and elemental analysis (Supporting Information Figures S6−S11). The characteristic peaks of the benzoxazine rings are observed on the ^{1}H NMR spectrum of DIS-PA-mea$_x$fa$_{100-x}$ (Figure 1). For instance, for DIS-PA-mea, the peaks at δ = 3.93 and 4.78 ppm corresponding to N-CH$_2$*-Ar [12] and N-CH$_2$*-O [13] can be observed. The experimental integrations of the methylene protons count for 3.07H and 3.07H, respectively (4.00H theoretical). It is worth noting that 100% of the phenolic groups have reacted with mono-ethanolamine (two nitrogen atoms per molecule were measured by elemental analysis). The calculation of the integrations indicates that 77% of the oxazine rings are closed, the remaining 23% being opened as reported elsewhere.[17,35] The wide signal centered at 4.52 ppm is attributed to the aliphatic hydroxyl groups. The ^{13}C NMR and FTIR spectra reported in the SI confirm the structure of the precursors by the emergence of characteristic benzoxazine peaks.

Differential scanning calorimetry (DSC) measurements of the precursors are reported in Figure 2a. A softening is observed for each monomer in the range of 20−25 °C, independently of the mea/fa ratio. A first exothermic peak ($T_{exo,1}$ = 130−255 °C) was observed corresponding to the ring opening of the benzoxazine, in the same range as benzoxazine vitrimers with a similar structure.[17] A second exothermic peak centered around 250 °C
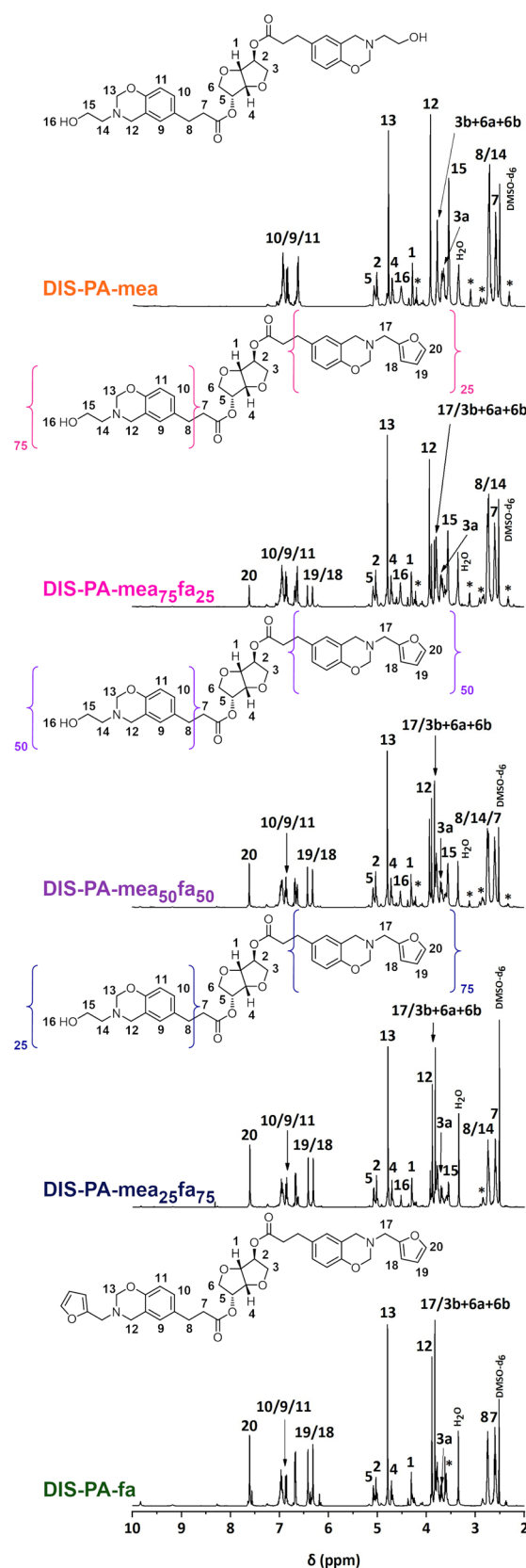
Figure 1. ^{1}H NMR spectra of the isosorbide-based benzoxazine precursors.

($T_{exo,2}$) is attributed to thermal degradation, confirmed by thermogravimetric analysis (TGA) (Figure S21).
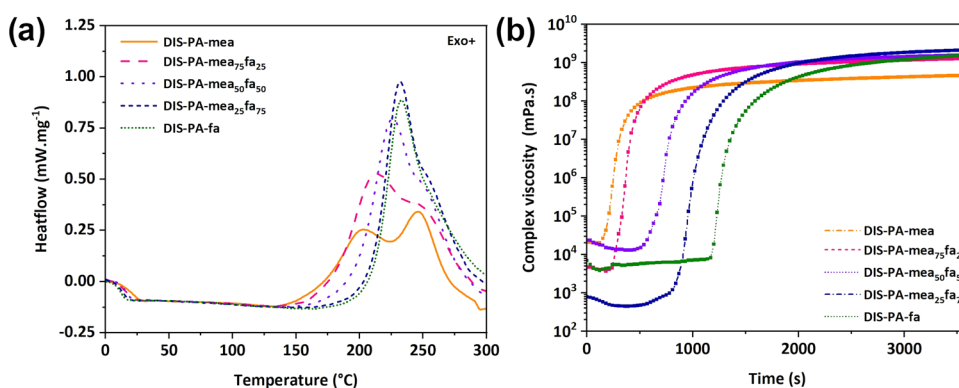
Figure 2. (a) DSC curves and (b) rheokinetic isothermal curing (170 °C) of DIS-PA-mea$_x$fa$_{100-x}$.

DIS-PA-mea$_x$fa$_{100-x}$ was subjected to isothermal curing by rheology. The recorded data at 170 °C depict the evolution of the complex viscosity of each precursor (Figure 2b). Presumably as a result of the catalytic effect of the −OH groups,[38,39] the gelations are reached faster when the number of −OH groups is higher, from 122 to 1170 s for DIS-PA-mea and DIS-PA-fa, respectively.

3.2. Characterization of the Sugar-Based Vitrimers. Benzoxazine precursors DIS-PA-mea$_x$fa$_{100-x}$ were cured in an oven at 150 °C (1 h) then at 170 °C (1 h) followed by a post-cure step at 190 °C ($^1/_2$ h) for furan-containing monomers. DSC and FTIR measurements were done on each polymerized precursor, so-called poly(DIS-PA-mea$_x$fa$_{100-x}$), to confirm the complete curing of the materials (Figures S12 and S13). Dynamic mechanical analyses (DMA) in the three-point bending mode were performed to assess the mechanical glass-transition temperature (T_g) (Figures S14−S19). The T_g values were derived from the maximum of the tan δ curve. The cross-linking density of each polymerized material was determined by swelling experiments in water, according to eqs 1−4 in the SI (Figure S20). Figure 3 depicts the evolution of T_g and the cross-linking density as a function of the mea/fa ratio. The T_g value increases with the amount of fa, as expected since fa is known to be involved in the cross-linking process of benzoxazine.[40,41] However, the strong jump of the T_g from 143 to 160 °C for polymerized materials when only 25% of mea are substituted by fa (Table 1, rows 2 and 3) cannot only be explained by the

involvement of fa in the cross-linking density. Indeed, the v_c values of poly(DIS-PA-mea) and poly(DIS-PA-mea$_{75}$fa$_{25}$) are similar (0.7 and 0.9 mol cm^{-3}, respectively; Table 1 column 3).

This significant T_g increase may presumably be due to a reduction of the segmental mobility and/or to interactions between the cyclic and bicyclic five-atom rings of fa and isosorbide, in a similar manner to that reported for copolymers of isosorbide and furfuryl alcohol,[47−49] and in the range of T_g of benzoxazines prepared from isosorbide and furfurylamine.[40] It is worth noting that the T_g reached by these materials is among the highest reported in the literature (Table 1, rows 7−11). Finally, the thermal behavior of each vitrimer sample was investigated by thermogravimetric analysis (TGA, Figure S21). The thermal stability of the materials ranges from T_d = 244 °C for poly(DIS-PA-mea) to T_d = 304 °C for poly(DIS-PA-fa) (Table 1, column 4). Here also, a substantial effect of fa is observed, still emphasizing a possible synergy between the structures of furfurylamine and isosorbide.

3.3. Degradability in Aqueous Environment. Hydrolytic degradation experiments were performed by immersing poly-(DIS-PA-mea) in various aqueous media such as phosphate-buffered solution (pH = 7.4), distilled water (pH = 7.1), 1 M NaOH solution, and glacial acetic acid. The mass loss method was employed to assess ester-bond cleavage in an aqueous environment.[50] These conditions were selected as they are representative of both *in vivo* degradation and industrial composting systems. The degradation experiments were monitored at 25 and 80 °C. This last temperature was selected to observe the completion of the degradation in an accessible time frame (Figure S22). In acetic acid and 1 M NaOH, poly(DIS-PA-mea) is fully degraded in less than 5 days, due to acid hydrolysis and saponification reactions, respectively (Figure 4a). The degradation, both in alkaline and acid solutions, follows the surface erosion model, consistent with the behavior of polyesters under similar conditions.[51] The degradation products were analyzed by ¹H NMR (Figure S23). Fragments of polybenzoxazine were detected (C-alkyl methylene) and C-aromatic protons). Isosorbide moieties were also detected, attesting the cleavage of the ester bonds. Interestingly, traces of single-ring opened isosorbide and D-sorbitol were also identified, as previously reported.[52] No toxic compounds were identified from the analysis of the degradation products (e.g., free formaldehyde). Nonetheless, it is a rough assessment and additional analyses are needed to fully determine the nature of the chemicals released from these degradation processes.

In phosphate-buffered saline (PBS), the degradation followed the bulk erosion model. The polymer samples became opaque
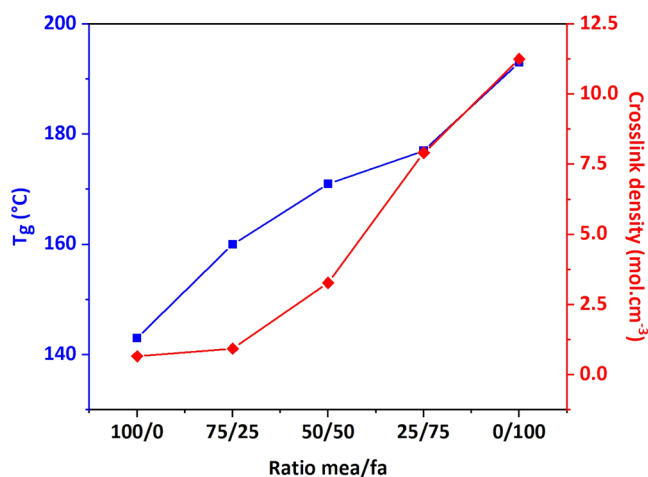
Figure 3. Evolution of the T_g and cross-linking density of each poly(DIS-PA-mea$_x$fa$_{100-x}$) as a function of the mea/fa ratio.

Table 1. Summary of the Thermal and Mechanical Properties of Isosorbide-Based and High-T_g Vitrimers Reported in This Work and in the Literature

network	dynamic exchange	$^a T_g$ (°C)	$^b E$ (GPa)	$^c \nu_c$ (mol cm^{-3})	$^d T_d$ (°C)	^{e}char (%)	refs
poly(DIS-PA-mea)	internally catalyzed transesterification reactions (TER)	143	4.0	0.7	244	31.0	this work
poly(DIS-PA-mea$_{75}$fa$_{25}$)		160	3.8	0.9	261	37.6	
poly(DIS-PA-mea$_{50}$fa$_{50}$)		171	4.1	3.3	268	44.6	
poly(DIS-PA-mea$_{25}$fa$_{75}$)		177	3.4	7.9	280	46.7	
poly(DIS-PA-fa)		193	3.5	11.3	304	47.3	
isosorbide-based polyurethane	urethane exchange	−29	14.10^{-3}	n.a.	≈260	0	42
isosorbide-based epoxy-amine	disulfide	41	2.0	n.a.	269	n.a.	43
epoxy-anhydride	internally catalyzed TER	135	1.8	n.a.	216	n.a.	44
epoxy-anhydride	Zn-catalyzed TER	187	2.0	n.a.	302	n.a.	45
poly(thiourethane)	thiourethane exchange	129	5.1	n.a.	255	n.a.	46

^{a}determined from the maximum of tan δ curve in DMA three-point bending mode, ^{b}Elastic modulus at 25 °C determined from the storage modulus (E'), ^{c}determined according to eq 4 in the SI, ^{d}onset of thermal degradation determined by TGA experiment, and ^{e}residual carbon at 800 °C.
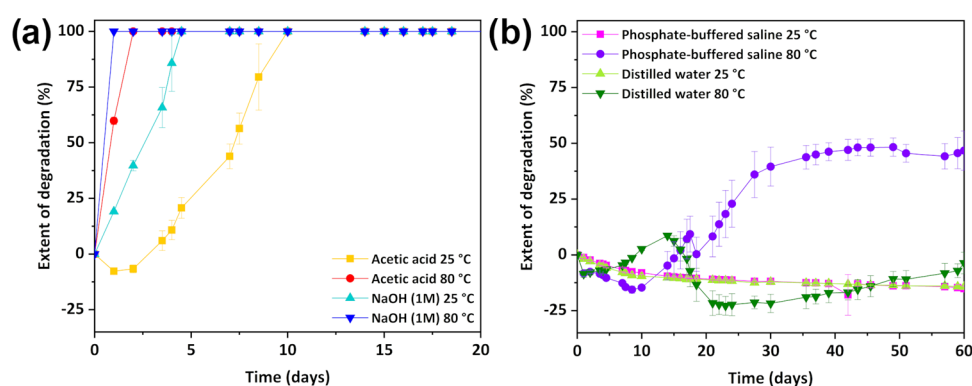
Figure 4. Evolution of the extent of degradation of poly(DIS-PA-mea) over time in (a) alkaline and acidic media and (b) in neutral-pH environment.
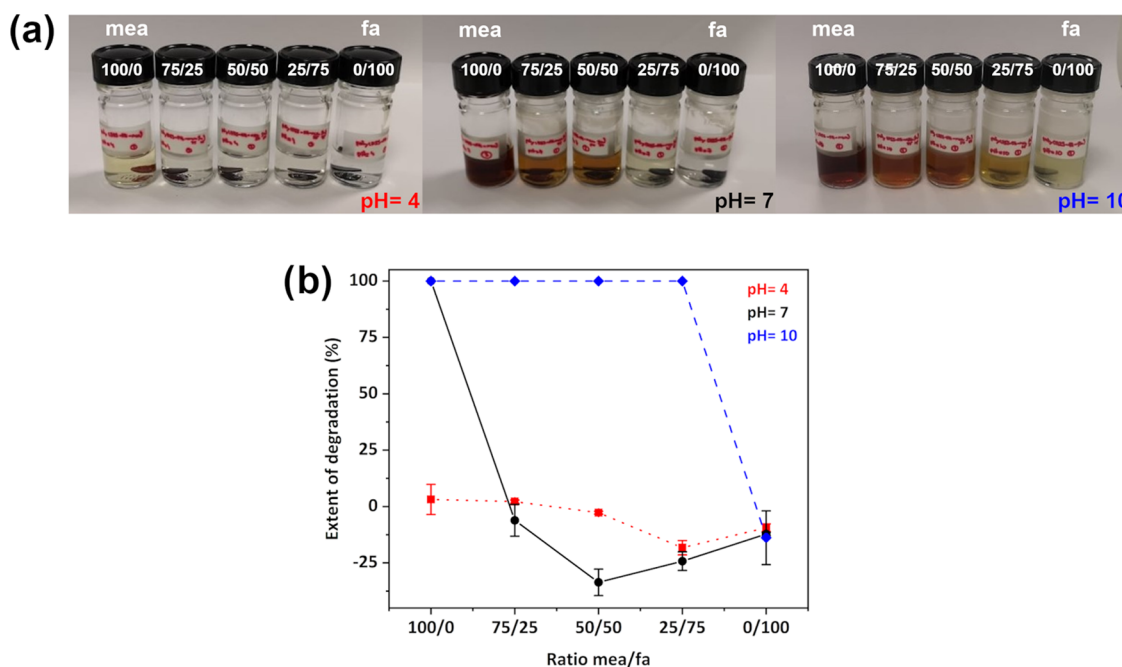
Figure 5. (a) Photographs of immersed poly(DIS-PA-mea$_x$fa$_{100-x}$) samples at pH = 4.0, 7.0, and 10.0 buffer solutions after 10 days of immersion. (b) Extent of degradation after 20 days of immersion at different pH and as a function of the mea/fa ratio.

and swelled during the induction period with weight loss following. Nonetheless, stability was significant, up to 20 days at 80 °C, and no degradation at all was detected at 25 °C (Figure

4b) during the time of the observation (60 days). Finally, at 25 °C in distilled water, the material did not degrade. At 80 °C, some degradation occurred, following the bulk erosion model
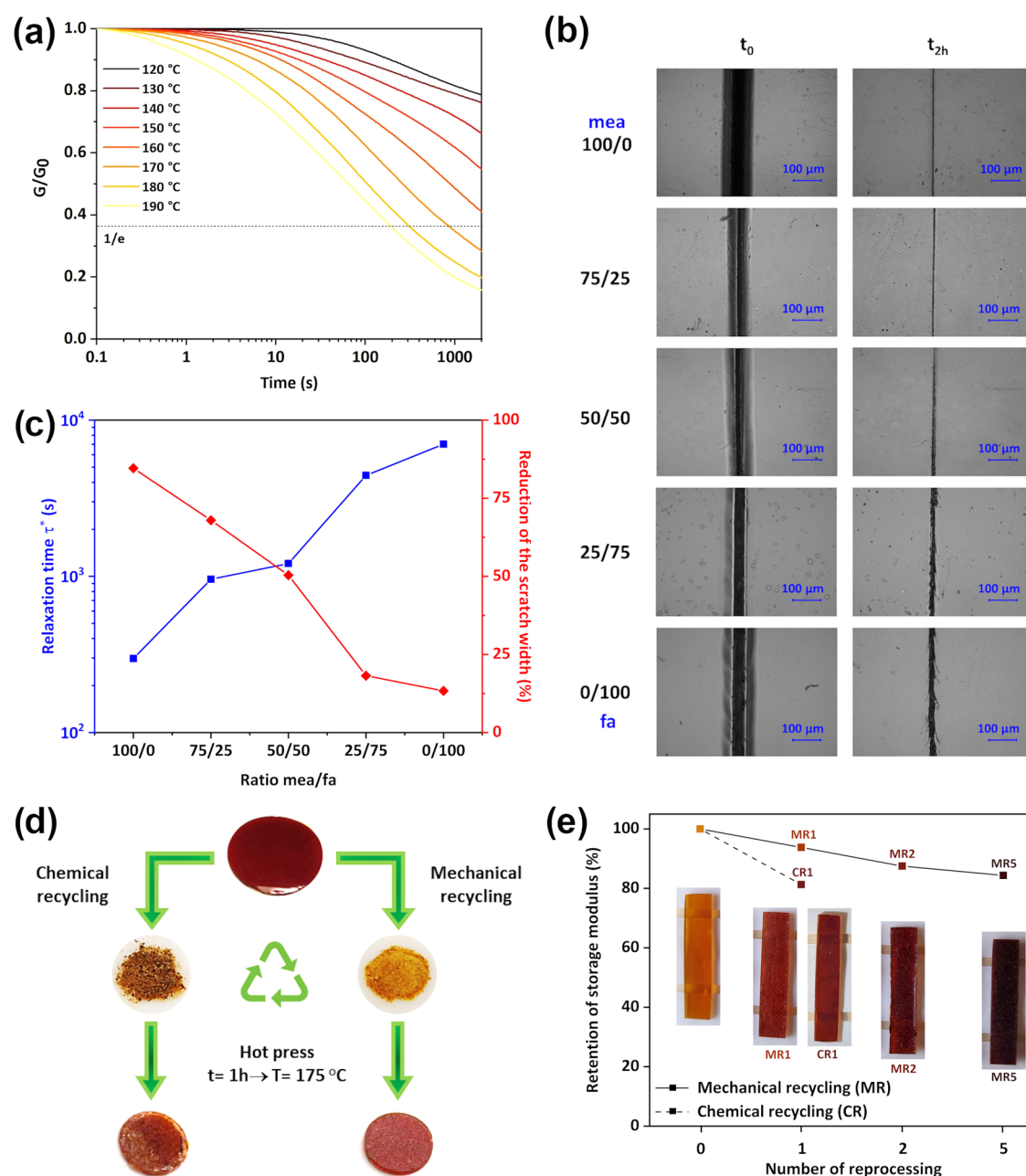
Figure 6. (a) Stress relaxation curves of poly(DIS-PA-mea). (b) Micrographs self-healing of poly(DIS-PA-mea$_x$fa$_{100-x}$) showing the scratch width before (t_0) and after (t_{2h}) thermal treatment at T = 200 °C. (c) Evolution of relaxation time (τ^*) at 180 °C and the reduction of the scratch width as a function of mea/fa ratio. (d) Photographs of the mechanical and chemical recycling of poly(DIS-PA-mea). (e) Retention of the storage modulus of poly(DIS-PA-mea) as a function of the number of reprocessing cycles.

(material swelling followed by a weight loss), but to a very limited extent. It is posited that this behavior, likely due to partial hydrolysis of the pendant aliphatic −OH groups during the first days of immersion, could be suppressed by adjusting the number of hydroxyl groups.

The ability to adjust vitrimer properties was demonstrated via variations in the mea/fa ratio. Photographic images of each material immersed for 10 days at 80 °C in buffer solutions of pH = 4.0, 7.0, and 10.0, respectively, are reported in Figure 5a. Figure 5b depicts the extent of degradation at 80 °C and different pHs as a function of the mea/fa ratio. For the duration of the experiment, hydrolysis conditions in the buffer solution of pH = 4 were insufficient to induce significant degradation in contrast to the test in acetic acid reported above. At pH = 7.0,

only the vitrimer composed of 100% mea is degraded. At pH = 10.0, the degradation of each material is total and follows the bulk erosion model (Figures S24−S26), except for the polymer composed only of fa. The poor hydrolytic degradability of poly(DIS-PA-fa) tends to confirm the involvement of primary alcohols in the hydrolysis of ester bonds[53] and emphasizes the ease with which the stability of these vitrimers may be adjusted through changes in their chemical structure.

3.4. Relaxation, Self-Healing, and Mechanical and Chemical Recycling. Transesterification reactions are the dynamic exchanges occurring in poly(DIS-PA-mea$_x$fa$_{100-x}$) affording for the vitrimeric behavior. The evolution of the relaxation modulus of poly(DIS-PA-mea) as a function of time and temperature was recorded by rheological measurement

(Figure 6a). The evolution of the relaxation time (τ^*), corresponding to the time needed for the vitrimer to relax to a value corresponding to 1/e (0.37) of its original modulus, was measured and is plotted in Figure 6c as a function of the mea/fa ratio. At 180 °C, the relaxation time of poly(DIS-PA-mea) is 300 s. The activation energy (E_a) of poly(DIS-PA-mea) as determined from the Arrhenius equation is 126 kJ mol^{-1}, in the range of other transesterification-based vitrimers internally catalyzed by a tertiary amine group (Figure S31).[17,54,55] Each poly(DIS-PA-mea$_x$fa$_{100-x}$) relaxes, with a kinetic decreasing with the mea/fa ratio, from 100% mea to 100% fa (Figures S27−S30).

The self-healing of each material was demonstrated at 200 °C and is illustrated in Figure 6b. The reduction of the scratch width (Figure 6b,c) is correlated to the mea/fa ratio (Figures S33−S34), from 84.6% for poly(DIS-PA-mea) to 13.4% for poly(DIS-PA-fa). Surprisingly, poly(DIS-PA-fa) has very slight vitrimeric behavior in spite of the absence of aliphatic −OH groups. This could be explained by the involvement of the aromatic −OH or to aliphatic −OH groups originating from a possible opening of the isosorbide cycles during the curing.

Finally, the ability of the isosorbide-based vitrimers to be recycled is illustrated in Figure 6d,e. The mechanical recycling was performed after grinding the material in particles of average size 100 μm. The chemical recycling was performed on a sample degraded in glacial acetic acid (AA). AA was evaporated under reduced pressure to yield a yellow powder. Each powder (either from the chemical or mechanical degradation) was then compressed under low pressure (<10 Pa) at 175 °C, to yield self-supporting materials in both cases, implying complete (100%) recyclability.[37] After the first mechanical recycling, the storage modulus of the vitrimer is like the original material, as attested by a retention rate of the storage modulus of 93.6%. After five mechanical recycling, the retention rate decreases to 84.4%, still indicative of the very good recyclability of the vitrimer. The chemical recycling disturbs more the properties of the materials, as the retention rate of the storage modulus after the first reprocessing reaches 81.3%. All of these data are good metrics to illustrate the significant recyclability of these isosorbide-based benzoxazine vitrimers.

4. CONCLUSIONS

This study relates the synthesis and the properties of a fully bio-based high-performance and degradable polybenzoxazine vitrimer prepared from isosorbide. The synthesis pathway consisted of a solventless two-step reaction, including the Fischer esterification of phloretic acid and isosorbide, which was then reacted with mono-ethanolamine and/or furfurylamine and paraformaldehyde via a Mannich-like condensation. The sugar-based vitrimer was formed by heating the precursors, yielding materials with high T_g values, from 143 to 193 °C depending on the ratio between mea and fa. Each isosorbide-based vitrimer is strongly stable in water and PBS at 25 °C. The degradation process is significantly accelerated in alkaline environment and at 80 °C in acidic environment as well.

Finally, these degradable high-T_g sugar-based materials enabled fast exchange reactions without the use of an external catalyst, providing self-healing capabilities and 100% recyclability via both mechanical and chemical routes.

■ ASSOCIATED CONTENT

Ⓢ Supporting Information

The Supporting Information is available free of charge at https://pubs.acs.org/doi/10.1021/acssuschemeng.1c07093.

Equipment and characterizations; swelling tests and calculation of the cross-linking density; structural characterization of precursors; committed reagents for the synthesis of DIS-PA-mea$_x$fa$_{100-x}$ benzoxazine precursors (Table S1); ^{1}H NMR spectrum of DIS (Figure S1); ^{13}C NMR spectrum of DIS (Figure S2); ^{1}H NMR spectrum of DIS-PA (Figure S3); ^{13}C NMR spectrum of DIS-PA (Figure S4); effect of the temperature on the conversion of PA followed by ^{1}H NMR (Figure S5); ^{13}C NMR spectrum of DIS-PA-mea (Figure S6); ^{13}C NMR spectrum of DIS-PA-mea$_{75}$fa$_{25}$ (Figure S7); ^{13}C NMR spectrum of DIS-PA-mea$_{50}$fa$_{50}$ (Figure S8); ^{13}C NMR spectrum of DIS-PA-mea$_{25}$fa$_{75}$ (Figure S9); ^{13}C NMR spectrum of DIS-PA-fa (Figure S10); FTIR spectra of the benzoxazine precursors DIS-PA-mea$_x$fa$_{100-x}$ (Figure S11); DSC curves of the polybenzoxazine vitrimers poly(DIS-PA-mea$_x$fa$_{100-x}$) (Figure S12); FTIR spectra of the polybenzoxazine vitrimers poly(DIS-PA-mea$_x$fa$_{100-x}$) and photographs of the materials (Figure S13); evolution of the storage and loss moduli and tan delta of poly(DIS-PA-mea) as a function of the temperature measured by DMA (Figure S14); evolution of the storage and loss moduli and tan delta of poly(DIS-PA-mea$_{75}$fa$_{25}$) as a function of the temperature measured by DMA (Figure S15); evolution of the storage and loss moduli and tan delta of poly(DIS-PA-mea$_{50}$fa$_{50}$) as a function of the temperature measured by DMA (Figure S16); evolution of the storage and loss moduli and tan delta of poly(DIS-PA-mea$_{25}$fa$_{75}$) as a function of the temperature measured by DMA (Figure S17); evolution of the storage and loss moduli and tan delta of poly(DIS-PA-fa) as a function of the temperature measured by DMA (Figure S18); evolution of tan δ of poly(DIS-PA-mea$_x$fa$_{100-x}$) as a function of the temperature measured by DMA (Figure S19); evolution of the swelling equilibrium of poly(DIS-PA-mea$_x$fa$_{100-x}$) in water at room temperature (Figure S20); evolution of the weight loss of poly(DIS-PA-mea$_x$fa$_{100-x}$) as a function of the temperature (inert atmosphere) (Figure S21); photographs of poly(DIS-PA-mea) after 60 days of immersion in acetic acid, distilled water, phosphate-buffered solution, and NaOH (1 M) solutions at 25 and 80 °C (Figure S22); ^{1}H NMR spectrum of the degradation products of poly(DIS-PA-mea) after 60 days of immersion in glacial acetic acid (Figure S23); evolution of the extent of degradation of poly(DIS-PA-mea$_x$fa$_{100-x}$) over time at pH = 4 (Figure S24); evolution of the extent of degradation of poly(DIS-PA-mea$_x$fa$_{100-x}$) over time at pH = 7 (Figure S25); evolution of the extent of degradation of poly(DIS-PA-mea$_x$fa$_{100-x}$) over time at pH = 10 (Figure S26); stress relaxation curves of poly(DIS-PA-mea$_{75}$fa$_{25}$) at 160, 170, and 180 °C (Figure S27); stress relaxation curves of poly(DIS-PA-mea$_{50}$fa$_{50}$) at 160, 170, and 180 °C (Figure S28); stress relaxation curves of poly(DIS-PA-mea$_{25}$fa$_{75}$) at 160, 170, and 180 °C (Figure S29); stress relaxation curves of poly(DIS-PA-fa) at 160, 170, and 180 °C (Figure S30); Arrhenius plot of poly(DIS-PA-mea) (Figure S31); and storage modulus values of vitrimer materials recycled either by mechanical or chemical reprocessing (Table S2) (PDF)

■ AUTHOR INFORMATION

Corresponding Author

Pierre Verge − *Materials Research and Technology Department, Luxembourg Institute of Science and Technology, L-4362 Esch-sur-Alzette, Luxembourg;* ⓞ orcid.org/0000-0001-9844-0394; Email: pierre.verge@list.lu

Authors

Antoine Adjaoud − *Materials Research and Technology Department, Luxembourg Institute of Science and Technology, L-4362 Esch-sur-Alzette, Luxembourg; University of Luxembourg, L-4365 Esch-sur-Alzette, Luxembourg*

Laura Puchot − *Materials Research and Technology Department, Luxembourg Institute of Science and Technology, L-4362 Esch-sur-Alzette, Luxembourg*

Complete contact information is available at:
https://pubs.acs.org/10.1021/acssuschemeng.1c07093

Notes

The authors declare no competing financial interest.

■ ABBREVIATIONS

CAN:covalent adaptable network; T_g:glass transition; DIS:D-isosorbide; PA:phloretic acid; mea:mono-ethanolamine; fa:furfurylamine; PFA:paraformaldehyde; DIS-PA-mea$_x$fa$_{100-x}$:benzoxazine precursors; −OH:hydroxyl; ROP:ring-opening polymerization; p-TSA:*para*-toluene sulfonic acid; NMR:nuclear magnetic resonance; TMS:tetramethylsilane; FTIR:Fourier transform infrared; ATR:attenuated total reflection; DSC:differential scanning calorimetry; N_2:nitrogen; TGA:thermogravimetric analysis; G_0:original relaxation modulus; G':storage modulus; G'':loss modulus; DIS-PA:diphenol-terminated isosorbide; $MgSO_4$:magnesium sulfate; poly(DIS-PA-mea$_x$fa$_{100-x}$):polymerized DIS-PA-mea$_x$fa$_{100-x}$; W:swelling ratio; $\overline{Mc}$:molecular weight between cross-links; ν_c:cross-linking density; AA:acetic acid; NaOH:sodium hydroxide; DW:distilled water; PBS:phosphate-buffered saline; D:extent of degradation; tan δ:loss factor; T_d:onset of thermal degradation; τ^*:relaxation time; E_a:activation energy

■ REFERENCES

(1) Witik, R. A.; Teuscher, R.; Michaud, V.; Ludwig, C.; Månson, J.-A. E. Carbon fibre reinforced composite waste: An environmental assessment of recycling, energy recovery and landfilling. *Composites, Part A* **2013**, *49*, 89−99.

(2) Vajdová, I.; Jenčová, E.; Szabo, S.; Melníková, L.; Galanda, J.; Dobrowolska, M.; Ploch, J. Environmental Impact of Burning Composite Materials Used in Aircraft Construction on the Air. *Int. J. Environ. Res. Public Health* **2019**, *16*, No. 4008.

(3) Denissen, W.; Winne, J.; Du Prez, F. Vitrimers: Permanent Organic Networks with Glass-Like Fluidity. *Chem. Sci.* **2016**, *7*, 30−38.

(4) Fortman, D. J.; Brutman, J. P.; De Hoe, G. X.; Snyder, R. L.; Dichtel, W. R.; Hillmyer, M. A. Approaches to Sustainable and Continually Recyclable Cross-Linked Polymers. *ACS Sustainable Chem. Eng.* **2018**, *6*, 11145−11159.

(5) Zheng, N.; Xu, Y.; Zhao, Q.; Xie, T. Dynamic Covalent Polymer Networks: A Molecular Platform for Designing Functions beyond Chemical Recycling and Self-Healing. *Chem. Rev.* **2021**, *121*, 1716−1745.

(6) Montarnal, D.; Capelot, M.; Tournilhac, F.; Leibler, L. Silica-Like Malleable Materials from Permanent Organic Networks. *Science* **2011**, *334*, 965−968.

(7) Capelot, M.; Unterlass, M. M.; Tournilhac, F.; Leibler, L. Catalytic Control of the Vitrimer Glass Transition. *ACS Macro Lett.* **2012**, *1*, 789−792.

(8) Liu, T.; Zhao, B.; Zhang, J. Recent development of repairable, malleable and recyclable thermosetting polymers through dynamic transesterification. *Polymer* **2020**, *194*, No. 122392.

(9) Taplan, C.; Guerre, M.; Du Prez, F. E. Covalent Adaptable Networks Using β-Amino Esters as Thermally Reversible Building Blocks. *J. Am. Chem. Soc.* **2021**, *143*, 9140−9150.

(10) Zych, A.; Tellers, J.; Bertolacci, L.; Ceseracciu, L.; Marini, L.; Mancini, G.; Athanassiou, A. Biobased, Biodegradable, Self-Healing Boronic Ester Vitrimers from Epoxidized Soybean Oil Acrylate. *ACS Appl. Polym. Mater.* **2021**, *3*, 1135−1144.

(11) Yin, Y.; Yang, J.; Meng, L. Preparation of poly(butylene succinate) vitrimer with thermal shape stability via transesterification reaction. *J. Appl. Polym. Sci.* **2021**, *138*, No. 51010.

(12) Yu, Q.; Peng, X.; Wang, Y.; Geng, H.; Xu, A.; Zhang, X.; Xu, W.; Ye, D. Vanillin-based degradable epoxy vitrimers: Reprocessability and mechanical properties study. *Eur. Polym. J.* **2019**, *117*, 55−63.

(13) Snyder, R. L.; Fortman, D. J.; De Hoe, G. X.; Hillmyer, M. A.; Dichtel, W. R. Reprocessable Acid-Degradable Polycarbonate Vitrimers. *Macromolecules* **2018**, *51*, 389−397.

(14) Wu, J.; Yu, X.; Zhang, H.; Guo, J.; Hu, J.; Li, M.-H. Fully Biobased Vitrimers from Glycyrrhizic Acid and Soybean Oil for Self-Healing, Shape Memory, Weldable, and Recyclable Materials. *ACS Sustainable Chem. Eng.* **2020**, *8*, 6479−6487.

(15) Şucu, T.; Shaver, M. P. Inherently degradable cross-linked polyesters and polycarbonates: resins to be cheerful. *Polym. Chem.* **2020**, *11*, 6397−6412.

(16) Trejo-Machin, A.; Puchot, L.; Verge, P. A cardanol-based polybenzoxazine vitrimer: recycling, reshaping and reversible adhesion. *Polym. Chem.* **2020**, *11*, 7026−7034.

(17) Adjaoud, A.; Trejo-Machin, A.; Puchot, L.; Verge, P. Polybenzoxazines: a sustainable platform for the design of fast responsive and catalyst-free vitrimers based on trans-esterification exchanges. *Polym. Chem.* **2021**, *12*, 3276−3289.

(18) Ishida, H. *Handbook of Benzoxazine Resins*; Elsevier: Amsterdam, 2011; p 688.

(19) Taskin, O. S.; Kiskan, B.; Yagci, Y. Polybenzoxazine Precursors As Self-Healing Agents for Polysulfones. *Macromolecules* **2013**, *46*, 8773−8778.

(20) Arslan, M.; Motallebzadeh, A.; Kiskan, B.; Demirel, A. L.; Kumbaraci, I. V.; Yagci, Y. Combining benzoxazine and ketene chemistries for self-healing of high performance thermoset surfaces. *Polym. Chem.* **2018**, *9*, 2031−2039.

(21) Fu, F.; Huang, M.; Zhang, W.; Zhao, Y.; Liu, X. Thermally assisted self-healing behavior of anhydride modified polybenzoxazines based on transesterification. *Sci. Rep.* **2018**, *8*, No. 10325.

(22) Zhang, L.; Zhao, Z.; Dai, Z.; Xu, L.; Fu, F.; Endo, T.; Liu, X. Unexpected Healability of an ortho-Blocked Polybenzoxazine Resin. *ACS Macro Lett.* **2019**, *8*, 506−511.

(23) Arslan, M.; Kiskan, B.; Yagci, Y. Recycling and Self-Healing of Polybenzoxazines with Dynamic Sulfide Linkages. *Sci. Rep.* **2017**, *7*, No. 5207.

(24) He, Y.; Gao, S.; Jubsilp, C.; Rimdusit, S.; Lu, Z. Reprocessable polybenzoxazine thermosets crosslinked by mussel-inspired catechol-Fe3+ coordination bonds. *Polymer* **2020**, *192*, No. 122307.

(25) Gao, S.; Liu, Y.; Feng, S.; Lu, Z. Reprocessable and Degradable Thermoset with High Tg Cross-linked via Si-O-Ph Bonds. *J. Mater. Chem. A* **2019**, *7*, 17498−17504.

(26) Wang, P.; Zhang, S.; Xu, W.; Xiao, T.; Ran, Q. High Heat-Resistant and Degradable Polybenzoxazines with a Diacetal Structure. *ACS Sustainable Chem. Eng.* **2021**, *9*, 7913−7921.

(27) Mohamed, M. G.; Kuo, S.-W. Crown Ether-Functionalized Polybenzoxazine for Metal Ion Adsorption. *Macromolecules* **2020**, *53*, 2420−2429.

(28) Samy, M. M.; Mohamed, M. G.; Kuo, S.-W. Pyrene-functionalized tetraphenylethylene polybenzoxazine for dispersing single-walled carbon nanotubes and energy storage. *Compos. Sci. Technol.* **2020**, *199*, No. 108360.

(29) Samy, M. M.; Mohamed, M. G.; Kuo, S.-W. Directly synthesized nitrogen-and-oxygen−doped microporous carbons derived from a bio-derived polybenzoxazine exhibiting high-performance supercapacitance and CO2 uptake. *Eur. Polym. J.* **2020**, *138*, No. 109954.

(30) Mohamed, M. G.; Chen, T.-C.; Kuo, S.-W. Solid-State Chemical Transformations to Enhance Gas Capture in Benzoxazine-Linked Conjugated Microporous Polymers. *Macromolecules* **2021**, *54*, 5866−5877.

(31) Lyu, Y.; Ishida, H. Natural-sourced benzoxazine resins, homopolymers, blends and composites: A review of their synthesis, manufacturing and applications. *Prog. Polym. Sci.* **2019**, *99*, No. 101168.

(32) Hao, B.; Han, L.; Liu, Y.; Zhang, K. An apigenin-based bio-benzoxazine with three polymerizable functionalities: sustainable synthesis, thermal latent polymerization, and excellent thermal properties of its thermosets. *Polym. Chem.* **2020**, *11*, 5800−5809.

(33) Machado, I.; Hsieh, I.; Rachita, E.; Salum, M. L.; Iguchi, D.; Pogharian, N.; Pellot, A.; Froimowicz, P.; Calado, V.; Ishida, H. A truly bio-based benzoxazine derived from three natural reactants obtained under environmentally friendly conditions and its polymer properties. *Green Chem.* **2021**, *23*, 4051−4064.

(34) Dussenne, C.; Delaunay, T.; Wiatz, V.; Wyart, H.; Suisse, I.; Sauthier, M. Synthesis of isosorbide: an overview of challenging reactions. *Green Chem.* **2017**, *19*, 5332−5344.

(35) Trejo-Machin, A.; Verge, P.; Puchot, L.; Quintana, R. Phloretic acid as an alternative to the phenolation of aliphatic hydroxyls for the elaboration of polybenzoxazine. *Green Chem.* **2017**, *19*, 5065−5073.

(36) Adjaoud, A.; Dieden, R.; Verge, P. Sustainable Esterification of a Soda Lignin with Phloretic Acid. *Polymers* **2021**, *13*, No. 637.

(37) Tabone, M. D.; Cregg, J. J.; Beckman, E. J.; Landis, A. E. Sustainability Metrics: Life Cycle Assessment and Green Design in Polymers. *Environ. Sci. Technol.* **2010**, *44*, 8264−8269.

(38) Kiskan, B.; Koz, B.; Yagci, Y. Synthesis and characterization of fluid 1,3-benzoxazine monomers and their thermally activated curing. *J. Polym. Sci., Part A: Polym. Chem.* **2009**, *47*, 6955−6961.

(39) Kudoh, R.; Sudo, A.; Endo, T. A Highly Reactive Benzoxazine Monomer, 1-(2-Hydroxyethyl)-1,3-Benzoxazine: Activation of Benzoxazine by Neighboring Group Participation of Hydroxyl Group. *Macromolecules* **2010**, *43*, 1185−1187.

(40) Wang, C.; Sun, J.; Liu, X.; Sudo, A.; Endo, T. Synthesis and copolymerization of fully bio-based benzoxazines from guaiacol, furfurylamine and stearylamine. *Green Chem.* **2012**, *14*, 2799−2806.

(41) Trejo-Machin, A.; Adjaoud, A.; Puchot, L.; Dieden, R.; Verge, P. Elucidating the thermal and polymerization behaviours of benzoxazines from lignin derivatives. *Eur. Polym. J.* **2020**, *124*, No. 109468.

(42) Kim, H.-N.; Lee, D.-W.; Ryu, H.; Song, G.-S.; Lee, D.-S. Preparation and Characterization of Isosorbide-Based Self-Healable Polyurethane Elastomers with Thermally Reversible Bonds. *Molecules* **2019**, *24*, No. 1061.

(43) Ma, Z.; Wang, Y.; Zhu, J.; Yu, J.; Hu, Z. Bio-based epoxy vitrimers: Reprocessibility, controllable shape memory, and degradability. *J. Polym. Sci., Part A: Polym. Chem.* **2017**, *55*, 1790−1799.

(44) Hao, C.; Liu, T.; Zhang, S.; Liu, W.; Shan, Y.; Zhang, J. Triethanolamine-Mediated Covalent Adaptable Epoxy Network: Excellent Mechanical Properties, Fast Repairing, and Easy Recycling. *Macromolecules* **2020**, *53*, 3110−3118.

(45) Liu, T.; Hao, C.; Zhang, S.; Yang, X.; Wang, L.; Han, J.; Li, Y.; Xin, J.; Zhang, J. A Self-Healable High Glass Transition Temperature Bioepoxy Material Based on Vitrimer Chemistry. *Macromolecules* **2018**, *51*, 5577−5585.

(46) Gamardella, F.; De la Flor, S.; Ramis, X.; Serra, A. Recyclable poly(thiourethane) vitrimers with high Tg. Influence of the isocyanate structure. *React. Funct. Polym.* **2020**, *151*, No. 104574.

(47) Kasmi, N.; Ainali, N. M.; Agapiou, E.; Papadopoulos, L.; Papageorgiou, G. Z.; Bikiaris, D. N. Novel high Tg fully biobased poly(hexamethylene-co-isosorbide-2,5-furan dicarboxylate) copolyesters: Synergistic effect of isosorbide insertion on thermal performance enhancement. *Polym. Degrad. Stab.* **2019**, *169*, No. 108983.

(48) Terzopoulou, Z.; Papadopoulos, L.; Zamboulis, A.; Papageorgiou, D. G.; Papageorgiou, G. Z.; Bikiaris, D. N. Tuning the Properties of Furandicarboxylic Acid-Based Polyesters with Copolymerization: A Review. *Polymers* **2020**, *12*, No. 1209.

(49) Bonnaud, L.; Chollet, B.; Dumas, L.; Peru, A. A. M.; Flourat, A. L.; Allais, F.; Dubois, P. High-Performance Bio-Based Benzoxazines from Enzymatic Synthesis of Diphenols. *Macromol. Chem. Phys.* **2019**, *220*, No. 1800312.

(50) Chamas, A.; Moon, H.; Zheng, J.; Qiu, Y.; Tabassum, T.; Jang, J. H.; Abu-Omar, M.; Scott, S. L.; Suh, S. Degradation Rates of Plastics in the Environment. *ACS Sustainable Chem. Eng.* **2020**, *8*, 3494−3511.

(51) Woodard, L. N.; Grunlan, M. A. Hydrolytic Degradation and Erosion of Polyester Biomaterials. *ACS Macro Lett.* **2018**, *7*, 976−982.

(52) Koo, J. M.; Kim, S. H.; Im, S. S. Structural deformation phenomenon of synthesized poly(isosorbide-1,4-cyclohexanedicarboxylate) in hot water. *RSC Adv.* **2017**, *7*, 6315−6322.

(53) Zhang, H.; Grinstaff, M. W. Synthesis of Atactic and Isotactic Poly(1,2-glycerol carbonate)s: Degradable Polymers for Biomedical and Pharmaceutical Applications. *J. Am. Chem. Soc.* **2013**, *135*, 6806−6809.

(54) Altuna, F. I.; Pettarin, V.; Williams, R. J. J. Self-healable polymer networks based on the cross-linking of epoxidised soybean oil by an aqueous citric acid solution. *Green Chem.* **2013**, *15*, 3360−3366.

(55) Debnath, S.; Kaushal, S.; Ojha, U. Catalyst-Free Partially Bio-Based Polyester Vitrimers. *ACS Appl. Polym. Mater.* **2020**, *2*, 1006−1013.

Research axis I+II

Design and synthesis of new lignin-based benzoxazine vitrimers

Chapter six: Lignin-based benzoxazines A tunable key-precursor for the design of hydrophobic coatings, fire resistant materials and catalyst-free vitrimers

The low reactivity of technical lignins toward Mannich condensation is one of the main challenges impeding the development of lignin-derived benzoxazines. The enriched platform of *ortho*-free phenolic rings described in chapter two addresses this issue. In chapter six , the esterified lignin was combined with bio-based amine derivatives to produce a series of lignin-derived benzoxazine monomers with a processing window suitable for thermosets elaboration. The resultant self-supported resins exhibit a structure-to-property relationship that correlates to the functionality of the amine side group. Long-alkyl chain amine confers increased solubility and hydrophobicity well-suited for coating application. Furan-based precursor provides mechanically robust materials with flame retardancy aptitude. Amino-alcohol derivative grants recyclability to the cross-linked lignin-benzoxazine network allowed by topological rearrangements. Made from renewable feedstocks and featuring closed-loop recyclability, the lignin-derived benzoxazine vitrimer reported in this study embraces the pillars of the circular polymer economy.
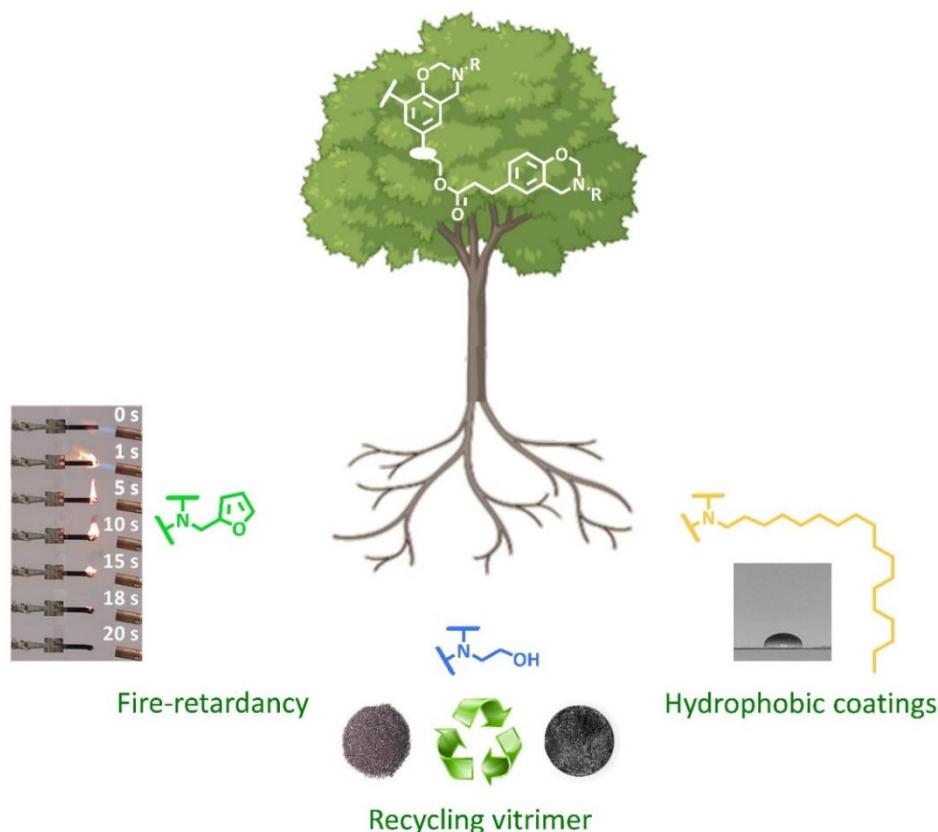
Fire-retardancy

Recycling vitrimer

Hydrophobic coatings

Contribution: I did all the experimental work, from the chemical synthesis of the molecules to their polymerization. It also included all the characterizations (molecular, thermal, mechanical), excepting AFM characterization done by Rohan Das and the micro-tomography performed by Carlos Eloy Federico. I acquired all the data and handled their interpretation. I wrote the first draft of the publication and did all the needed corrections and revisions of the manuscript.

Lignin-based benzoxazines: A tunable key-precursor for the design of hydrophobic coatings, fire resistant materials and catalyst-free vitrimers

Antoine Adjaoud [a,b], Laura Puchot [a], Carlos Eloy Federico [a], Rohan Das [a,b], Pierre Verge [a,*]

[a] *Luxembourg Institute of Science and Technology, Materials Research and Technology Department, 5 Avenue des Hauts-Fourneaux, L-4362 Esch-sur-Alzette, Luxembourg*
[b] *University of Luxembourg, 2, Avenue de l'Université, L-4365 Esch-sur-Alzette, Luxembourg*

ARTICLE INFO

ABSTRACT

The meaningful concept of circular economy has prompted the scientific community to re-think the design of materials. In this work, lignin-based benzoxazines (LBZs) thermosets with tuneable properties were synthesized in agreement with the principles of Green Chemistry, following a straightforward two-step synthetic route. The reactivity of a soda lignin was enhanced by its esterification with phloretic acid, a naturally occurring phenolic acid. Thereafter, the resulting structure enriched in phenolic rings with no ortho substituents, was used to prepare LBZs precursors with a bio-based primary amine via a Mannich-like ring-closure reaction. The structure and properties of each LBZ precursor were confirmed by multiple NMR techniques, Fourier transform infrared spectroscopy, elemental analysis, gel permeation chromatography, differential scanning calorimetry, rheology, and solubility assays. Lignin-based polybenzoxazine with high lignin mass fraction (between 46 and 66 wt.%) were obtained following curing via a vacuum compression molding manufacture process. Lignin-based thermosets exhibit a single-phase confirmed by X-ray computed tomography analysis, a T_g ranging from 136 to 197 °C, and storage moduli from 0.5 to 3.1 GPa. The features of each lignin-based precursor were tuned depending on the structure of the bio-based primary amine used to close the oxazine ring. Stearylamine confers good processability and yields hydrophobic coatings with a water contact angle reaching 91°. Furfurylamine-based LBZs generate high-T_g (197 °C) and fire-resistant materials with a peak of heat release rate of no>47 W.g^{-1}. Finally, ethanolamine produces lignin-based thermosets capable of internally catalysed bond exchange via transesterification, providing vitrimeric properties such as fast stress relaxation ($\tau^*_{200 \, °C}$ = 233 s) and a complete circularity.

1. Introduction

Lignin represents the primary source of phenolic compounds used in the conception of bio-derived materials [1]. Lignin is traditionally produced during the pulp and paper refining and used as low-value fuel. Notwithstanding, the rise of biorefineries provides a new source of lignin production [2,3], and its increasing availability and the substantial efforts focusing on its valorization pave the way toward more economically viable technologies.

A common approach to valorize lignin is its use as a filler [4]. Lignin can be incorporated into plastics to improve mechanical properties [5], antioxidant activity [6], and UV-shielding performance [7]. However, this approach is constrained by the highly-branched architecture of technical lignins which limits compatibility with most of the polymers [8]. Lignin fractionation [9] and depolymerization into high value-added chemicals such as vanillin [10], syringaldehyde [11], and ferulic acid [12] broadens the range of well-defined chemicals that may be produced from lignin. Chemical modifications are also a way to retain

---

Table 1
Reaction conditions for the synthesis of *eLig-Bz* through Mannich-like condensation.

| Reagents | | | | Reaction conditions | | | Material | |
Type	m (g)	n (mmol)	N (eq.)	Solvent	T (°C)	t (h)	Sample	m_f (g)
eLig	5.00	15.25 [a]	1.0	THF	70	3	*e*Lig-mea	5.23
PFA	0.92	30.50	2.0					
mea	0.93	15.25	1.0					
eLig	5.00	15.25 [a]	1.0	THF	70	24	*e*Lig-fa	5.64
PFA	0.92	30.50	2.0					
fa	1.48	15.25	1.0					
eLig	5.00	15.25 [a]	1.0	DIOX	80	24	*e*Lig-ste	6.69
PFA	0.92	30.50	2.0					
ste	4.11	15.25	1.0					

[a] Number of reactive phenolic units determined by quantitative ^{31}P NMR experiment ([H] + [G_{nc}] = 3.05 mmol.g^{-1}).

the stiffness and the aromaticity of lignin which are two assets for the development of thermosets [13,14]. The abundance of reactive functional groups in lignin has inspired researchers to identify new synthetic pathways for the elaboration of bio-based polymers [15] including polyurethanes [16,17], polyesters [18–20], epoxides [21–23], and phenol–formaldehyde resins [24,25].

Polybenzoxazines (PBZs) are also a potential and suitable class of polymers that could be used to valorize lignin. Polybenzoxazines stand out thanks to their superior mechanical properties and thermal stability, and are excellent candidates for applications requiring fire retardancy [26]. Applications of PBZs cover numerous fields [27], i.e. aerospace [28], solid state batteries [29], hydrophobic coatings [30], and biomedical applications [31], to cite but a few. A clear asset of PBZs comes from the versatility of their chemical design, which can confer a wide range of properties. PBZs are prepared from the Mannich-like condensation of a phenol, an amine, and a methylene donor (generally paraformaldehyde) [32]. In addition to the substituent groups on the aromatic ring [33,34], the functionality of the amine side-chain confers specific features to the final benzoxazine material. Substantial efforts have been made to synthesize benzoxazines from lignin-like derivatives [35,36] such as guaiacol [37,38], vanillin [39,40], and eugenol [41,42].

There are very few research works treating of lignin-derived benzoxazine. In [43,44], the authors used lignin to catalyze the ring opening polymerization of a commercial benzoxazine. Ishida and Saake are the only one who reported a chemical modification of lignin to make a benzoxazine precursor [45]. The challenge to the use of lignin as a building block to prepare benzoxazine is the low number of suitable reactive sites. Indeed, benzoxazine synthesis and polymerization require phenolic moieties with unsubstituted ortho position, i.e [G_{nc}] and [H], otherwise the benzoxazine ring closure and polymerization cannot proceed. However, commercial lignins are mainly constituted of *ortho*-substituted phenolic units, milled wood lignin as well. [46] Ishida and Saake tackled this drawback by phenolating lignin to increase the number of unsubstituted phenolic groups. However, the lack of mechanical data is suggesting that the authors suffered from difficulties to produce their materials, presumably because the number of benzoxazine rings was not yet high enough.

The novelty of this work is the new sustainable chemical approach

developed to increase the number of phenolic moieties with no ortho substituents of lignin, allowing for the first time the elaboration of self-supporting lignin-based benzoxazine materials. To the best of our knowledge, it is the first reported approach that yields lignin-based benzoxazine specimens which thermal and mechanical properties can be fully characterized. In addition, the approach is versatile enough to use different types of amines to close the benzoxazine rings and to bring additional functionalities. Here, the amines used to close the oxazine rings were carefully selected based on two criteria: (a) their origin from renewable resources and (b) their functionality related to specific applications.

- Stearylamine is a fatty amine derived from stearic acid, a natural fatty acid found in various plant oils. Stemming from the long alkyl side-chain, benzoxazine precursors made of this amine benefit from enhanced hydrophobicity and the ability to coat a surface [47].
- Furfurylamine is derived from furfural, a natural dehydration product of xylose that is produced industrially from seasonal crops. The furan ring is known to be involved in the polymerization of benzoxazines through chemical crosslinking. Its use leads to a significant enhancement of the thermal properties of the resulting thermosets. The glass transition temperature (T_g) is significantly affected as well as the fire properties [48].
- Mono-ethanolamine can be produced from renewable feedstocks via the decarboxylation of L-serine through metabolic engineering [49]. Benzoxazine precursors containing both ester and free –OH groups (provided by an amino-alcohol intermediate) undergo significant dynamic exchanges conferring vitrimeric properties to the resulting polybenzoxazine [50,51].

The first part of this report will focus on the synthesis, and molecular and thermal assessments of the lignin-based materials. The second part will be dedicated to the characterization of their applications oriented properties as a function of the amine used to close the oxazine ring.

2. Experimental section

2.1. Materials and chemicals

Protobind 2400 (Lig) wheat straw soda lignin was supplied in 2020 by Tanovis AG (Table S1). 3-(4-hydroxyphenyl) propionic acid (98 %, phloretic acid, PA), *para*-toluene sulfonic acid monohydrate (≥98.5 %, p-TSA), mono-ethanolamine (>98 %, mea), furfurylamine (≥99 %, fa), stearylamine (≥99 %, ste), and paraformaldehyde (95 %, PFA) were purchased from Sigma-Aldrich Chemicals. All solvents and chemicals were used as received without any purification. The list of solvents is as follows: acetone (ACE), acetonitrile (ACN), butanone (MEK), chloroform (CHCl$_3$), dichloromethane (DCM), diethyl ether (DET), dioxane (DIOX), dimethylformamide (DMF), dimethylsulfoxide (DMSO), ethanol (EtOH), ethyl acetate (ETAC), hexane (HEX), isopropanol (IPA), methanol (MeOH), pyridine (PYR), tetrahydrofuran (THF), toluene (TOL), and water (H$_2$O, Merck Millipore Milli-Q™ Reference Ultrapure Water Purification System). The list of equipments and methods utilized is given in the ESI.

2.2. Synthetic procedure of lignin-based benzoxazine precursors: eLig-Bz

The general procedure for the synthesis of lignin-based benzoxazine precursors (*eLig-Bz*) via an esterification-based reactivity enhancement step is described below. Details of the synthesis of lignin-based benzoxazine precursors (Lig-Bz) produced via direct Mannich condensation of the technical lignin are reported in the ESI (Table S2).

Fischer esterification: Protobind 2400 (Lig) was esterified according to our previous work [52]. A typical procedure is as follows: dried lignin powder (5 g, 2.41 mmol.g^{-1} of aliphatic –OH measured by ^{31}P NMR, Table S3), phloretic acid (10.01 g, 60.3 mmol), and *para*-toluene sulfonic acid (25 mg, 0.15 mmol) were reacted at 140 °C (48 h) under argon atmosphere and mechanical stirring (250 rpm). After several washings with diethylether to remove unreacted phloretic acid, traces of solvent were removed under vacuum to yield an enhanced lignin (*eLig*) as homogeneous brown powder. *eLig* was determined to contain 3.05 mmol. g^{-1} of phenolic units able to further react through Mannich condensation ([H] and [G$_{nc}$] units, 1.98 and 1.07 mmol.g^{-1} measured by quantitative ^{31}P NMR, respectively). m_f = 5.12 g.

Mannich-like condensation: The reaction was carried out dissolving 5 g of freshly prepared *eLig* (1 eq.), the amine precursor (1 eq.), and paraformaldehyde (2 eq., 0.92 g) in a minimum amount of solvent (20 mL, THF for mea and fa, DIOX for ste) in a 100 mL round bottom flask sealed with a rubber septum. Specific amount of amine precursors and selection of reaction solvent are reported in Table 1 (columns 1–4). The mixture was magnetically stirred at room temperature for 1 h under a nitrogen atmosphere. The temperature was raised to 70 or 80 °C and kept for 3 or 24 h (Table 1, columns 5–7). After cooling to room temperature, the crude product was concentrated under reduced pressure using rotary evaporator. Then, the extract was redissolved in 200 mL of diethylether, filtered in a Büchner funnel, and washed thoroughly with excess water and diethylether. After a final drying step (T = 50 °C overnight under reduced pressure), isolated *eLig-Bz* were recovered as fine dark-brown powder (Table 1, columns 8–9).

2.3. Solubility tests

Solubility tests were performed according to the method of Sameni *et al.* with minor modifications [53]. 50 mg samples of dried lignin were each mixed with 5 mL of organic solvent and subsequently sonicated for 15 min in a water bath sonicator. The insoluble fraction was removed with a 0.2 μm Agilent syringe filters. The lignin samples were weighed before the mixing and after the evaporation of the solvent (one day under the fume hood and overnight under reduced pressure at T = 50 °C, if necessary). The temperature was raised to 80 °C when high-boiling-point solvents were employed. The soluble fraction (S) was calculated according equation (1):

$$S\,(\text{wt.\%}) \,=\, 100 * \frac{m_i\text{-}m_f}{m_f} \tag{1}$$

where "m_i" corresponds to the initial mass of lignin sample and "m_f" corresponds to the mass of the soluble fraction. The Hansen solubility parameters (HSPs) of the LBZ precursors were experimentally estimated [54]. With the help of the generated data set, the HSPs of each sample were calculated using the HSPiP, 5.0.13 software package (Copyright © 2008–2015 Steven Abbott and Hiroshi Yamamoto).

2.4. Preparation of the lignin-based polybenzoxazine thermosets: p(eLig-Bz)

Lignin-based benzoxazine precursors (*eLig-Bz*) were polymerized in a MeltPrep® vacuum compression moulding unit (VCM, Ø= 25 mm disc tool). The VCM tool was filled with dried lignin-based benzoxazine powder (0.8 g), which was then compacted at 100 °C for 1 h prior polymerization. The curing was performed at 150 °C (1 h), 170 °C (1 h) plus an additional post-curing step at 190 °C ($^1/_2$ h) for monomers containing furan groups. Finally, the VCM tool was placed on a separate cooling unit ($^1/_2$ h) before retrieving the material. Densities were estimated by weighing the disk-shaped cured thermoset samples and dividing by the calculated sample volume (Ø= 25 mm, thickness = 1.2 mm).

2.5. Swelling and gel content

Swelling experiments were conducted at room temperature by immersion of 200 mg of samples lignin-based thermosets in 10 mL of solvent (chloroform, dioxane, toluene, or water). The swelling ratio (W) is calculated according equation (2):

$$W\,(\text{wt.\%}) \,=\, 100 * \frac{m_w\text{-}m_i}{m_i} \tag{2}$$

with m_i and m_w being the initial and the swollen mass, respectively. The reported values are an average of three measurements. Gel content (GC) values of the lignin-based thermosets were determined in the above-mentioned series of solvents as well. After one week of immersion, the insoluble fraction was removed and then dried under vacuum at 50 °C until a constant weight was reached. The gel content was calculated by the equation (3):

$$GC\,(\text{wt.\%}) \,=\, 100 * \frac{m_f}{m_i} \tag{3}$$

with m_i and m_f being the mass before and after the extraction, respectively. The reported values are an average of three measurements.

2.6. Surface wettability test

Preparation of lignin-based benzoxazine coatings: Dried lignin samples were dissolved in anhydrous dimethyl formamide (*eLig-mea* and *eLig-fa*) or tetrahydrofuran (*eLig-ste*) at different weight concentrations (2, 5, 10, and 20 g.mL^{-1}). Coatings were prepared on clean glass substrate (1.5 × 1.5 cm^2 surfaces delimited by hydrophobic adhesive band) by the dropcasting method at different surface concentration (50, 75 and 100 μL. cm^{-2}). The solvent was evaporated under a fume hood at 50 °C (1 h), followed by a drying step at 100 °C (1 h) in a vacuum bell (dynamic vacuum, P = 10^{-2} mBar). Films were then systematically cured in convection oven by applying the stepwise cured schedule described in section 2.4 to obtain lignin-based polybenzoxazine p(*eLig-Bz*) coatings. The thickness of the resulting coatings was determined by a KLA Tencor® P-17 profilometer.

Contact angle measurement: Ultrapure water droplets (5 μL) were dispensed onto the surface of each p(*eLig-Bz*) coatings. Images were captured using a digital camera (40x magnification, eight light emitting
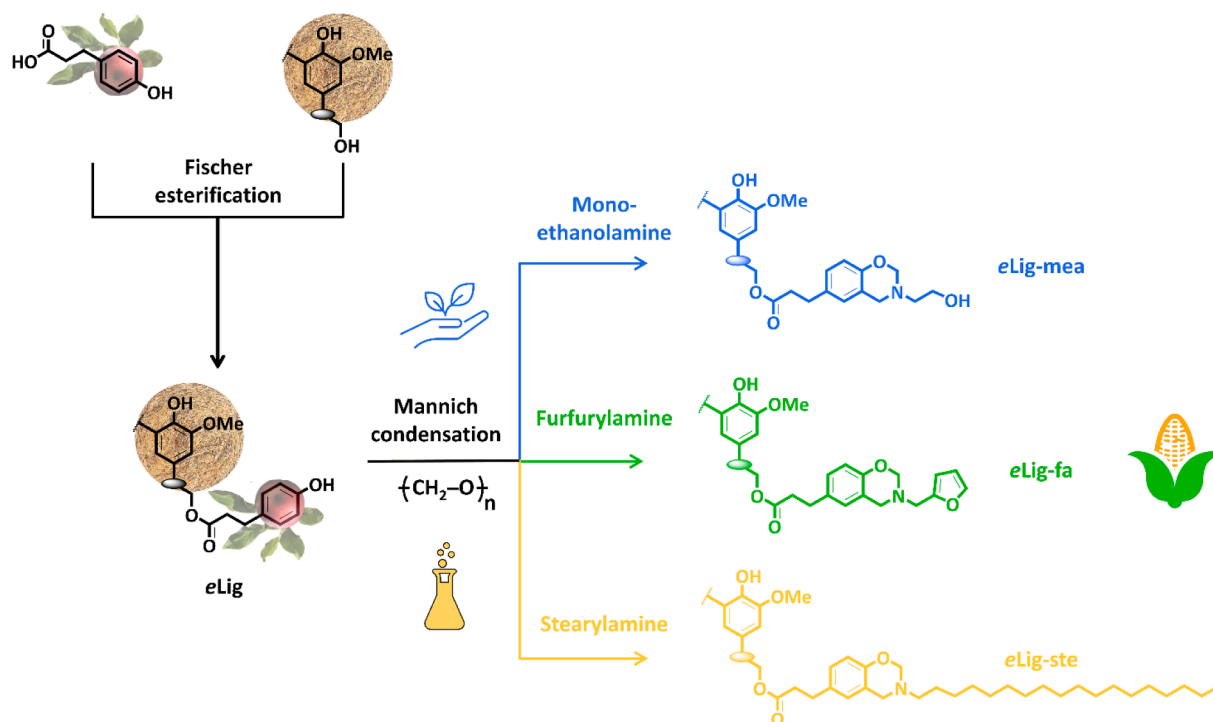
Fig. 1. Schematic synthetic route of lignin-based benzoxazine precursors.

diodes for illumination). The initial contact angle was measured by ImageJ 1.53 k software package.

2.7. Flammability tests

A horizontal burn test was performed to study the flame retardancy of p(*e*Lig-Bz) materials. For the purpose of this experiment, *e*Lig-Bz was cured in a hot press following the procedure described in the previous section (length:width:thickness = 75:10:1.25 mm). A butane flame was applied to the extremity of the clamped material for 3 s (free length = 55 mm, distance from the flame: 3.5 cm). The initial time of combustion (t_0) was defined as the moment of the application of the flame (video provided in the ESI).

2.8. Reprocessing and degradability tests

Reprocessing: The material was ground to a fine powder using a Retsch ZM-200 Ultra Centrifugal Mill (6000 rpm, Ø <40 μm). The resulting powder was poured into a disk-shaped brass mold (Ø= 25 mm), sandwiched between two plates, and hot-pressed for 1 h at 175 °C under low pressure (<10 Pa).

Degradability: 0.5 g of p(*e*Lig-Bz) thermoset was immersed at 25 °C in 25 mL of sodium hydroxide solution (NaOH 1 M).

3. Results and discussion

3.1. Synthesis and characterization of the lignin-based benzoxazine precursors

Extracted from wheat straw, Protobind 2400 (Lig) soda lignin was selected specifically to design lignin-based benzoxazine precursors via the two-step synthetic route shown in Fig. 1. Among the different processes used to obtain lignin, the sulfur-free soda process of seasonal crops residues (wheat straw, sugarcane bagasse, flax) has the advantage to lead to a high-purity lignin with a structure similar to the parent biopolymer. The high purity and the absence of sulfur species are both essential for efficient chemical modifications, including benzoxazine
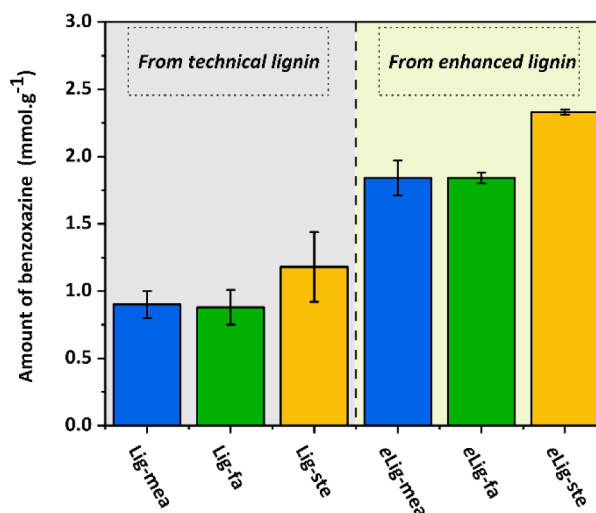
Fig. 2. Amount of benzoxazine units of each precursor synthesized from the technical lignin (Lig-Bz) and the enhanced lignin (*e*Lig-Bz).

chemistry. This process also leads to a high-volume production and soda lignin is commercially available (Protobind®). Among the three types of phenolic units contained in herbaceous plant lignin, only non-condensed guaiacyl [G_{nc}] and *para*-hydroxyphenyl [H] units can react through Mannich-like condensation to form benzoxazine rings. The enhancement of technical lignin reactivity was achieved by esterification with phloretic acid, a naturally occurring phenolic acid, following our optimized procedure [52]. The resulting enhanced lignin (*e*Lig) had an increased number of [H] units (+1.44 mmol.g^{-1}, 60 % increase), bringing the number of [G_{nc}] and [H] lignin reactive phenolic units to 3.05 mmol.g^{-1} ([G_{nc}] + [H] = 1.99 mmol.g^{-1} for Lig, Table S3). It is noteworthy that this approach would be also of interest with milled wood lignin, which 1-aliphatic –OH is of 4.00 mmol.g^{-1}. [46] *e*Lig was further reacted with PFA and one of the three bio-based amines:
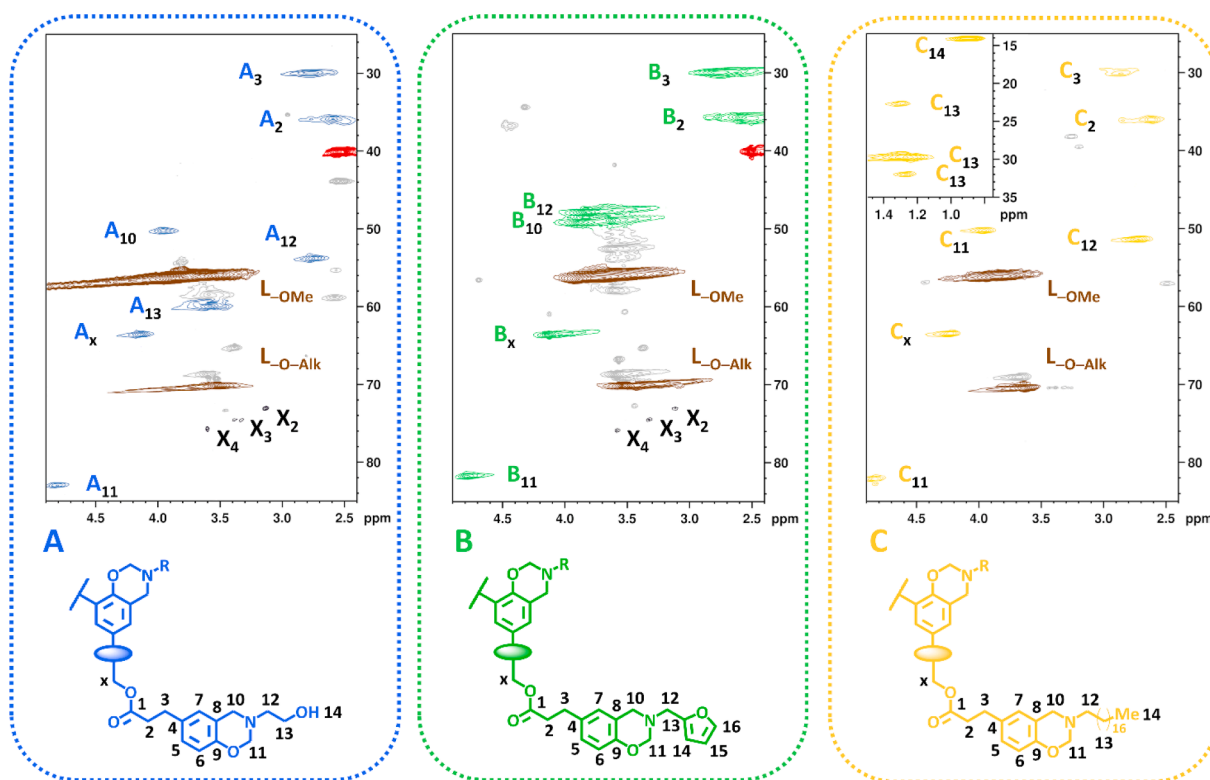
Fig. 3. ^1H–^{13}C HSQC NMR spectra of a) *e*Lig-mea, b) *e*Lig-fa, and c) *e*Lig-ste over the aliphatic region (δ_C/δ_H: 25–85 ppm /2.4–4.9 ppm).

Table 2
Physicochemical properties of *e*Lig-Bz.

Lignin Sample	Molecular weight			Thermal properties			
	[a] M_n (g.mol^{-1})	[b] M_w (g.mol^{-1})	[c] Đ	[d] T_g (°C)	[e] T_{onset} (°C)	[f] T_{max} (°C)	[g] t_{gel} (s)
*e*Lig	1971	9272	4.7	114	n.a.	n.a.	n.a.
*e*Lig-mea	2995	32,994	11.0	105	125	188	462
*e*Lig-fa	2960	16,454	5.6	100	141	200	1042
*e*Lig-ste	4506	19,623	4.3	105	155	219	1274

[a] number average molecular weight, [b] weight average molecular weight, [c] dispersity (M_w/M_n), [d] glass transition (midpoint DSC), [e] onset of thermal polymerization (DSC), [f] maximum temperature of the exothermic peak (DSC), and [g] gelation time at 150 °C, obtained from the crossover between the storage and the loss moduli (rheology).

furfurylamine (fa), mono-ethanolamine (mea), or stearylamine (ste), leading to lignin-based benzoxazine precursors (*e*Lig-Bz). For the sake of comparison, Lig was also reacted with each type of amine without any reactivity enhancement step. These materials are simply called Lig-Bz (ESI). The characteristic oxazine O-CH$_2$*-N methylene resonance (δ = 4.7–4.8 ppm) is prominent in the ^1H NMR spectrum of each *e*Lig-Bz, indicating the presence of benzoxazine units (Fig. S1). Furthermore, the resonance signal at δ = 9.2 ppm in the ^1H spectrum of *e*Lig which corresponds to the phenolic [H] units introduced during the esterification step have completely vanished after the Mannich-like condensation step (Fig. S1.b). The number of benzoxazine units decorating the lignin structure was calculated by quantitative ^{31}P NMR analytical method (Table S4-S5). The decrease of lignin reactive phenolic units ([G_{nc}] and [H]) was credited to benzoxazine functionalization (Fig. 2). As expected, *e*Lig-Bz has a higher number of benzoxazine units than Lig-Bz with at least 1.85 mmol.g^{-1} of lignin reactive phenolic units converted into benzoxazine rings. Finally, the lignin mass fraction of each monomer was calculated and the precursors contain 66, 63 and 46 wt.% of lignin for *e*Lig-mea, *e*Lig-fa and *e*Lig-ste, respectively.

The structural features of *e*Lig-Bz were also substantiated by ^{13}C NMR, ^1H–^{13}C HSQC NMR, FTIR, and CHNS/O elemental analysis (ESI,

Table S5, Figs. S2-S9). HSQC spectra of the aliphatic (δ_C/δ_H: 25–85 ppm /2.4–4.9 ppm) and aromatic regions (δ_C/δ_H: 100–160 ppm /6.0–8.5 ppm) are displayed in Fig. 3 and Fig. S8, respectively. Typical cross-peak signals from the core-lignin matrix were detected, including methoxy groups (-OMe, δ_C/δ_H: 56.5 /3.76 ppm), etherified interunit linkages (-O-Alk, 70.3 /3.50 ppm) groups, and xylan moieties (X$_2$, X$_3$, X$_4$) [55–57]. The emergence of new cross-peak signals assigned to the oxazine Ar-CH$_2$*-N (δ_C/δ_H: 49–51 /3.8–3.9 ppm) and O-CH$_2$*-N (δ_C/δ_H: 81–83 /4.7–4.8 ppm) methylene resonances reflect the formation of benzoxazine rings in *e*Lig-Bz. All structural features of the amine side chains can be detected and are detailed in the ESI. In the aromatic region, only peaks originating from the Mannich-like condensation and the aromatic protons from the three types of phenolic units are identified (Fig. S8). The successful chemical modification is also confirmed by elemental analysis (ESI) and FTIR experiments (Fig. S9). The elemental composition reveals an increase in nitrogen content, from < 0.5 % for *e*Lig to 3.7, 3.2, and 2.7 % for *e*Lig-mea, *e*Lig-fa, and *e*Lig-ste, respectively.

The molecular weight of the *e*Lig-Bz compounds was determined by size exclusion chromatography (*SEC*, Fig. S10, Table 2 columns 2–4) confirming an increase from M_n = 1971 g.mol^{-1} for *e*Lig to M_n = 2995, 2960, and 4506 g.mol^{-1} for *e*Lig-mea, *e*Lig-fa, and *e*Lig-ste, respectively.
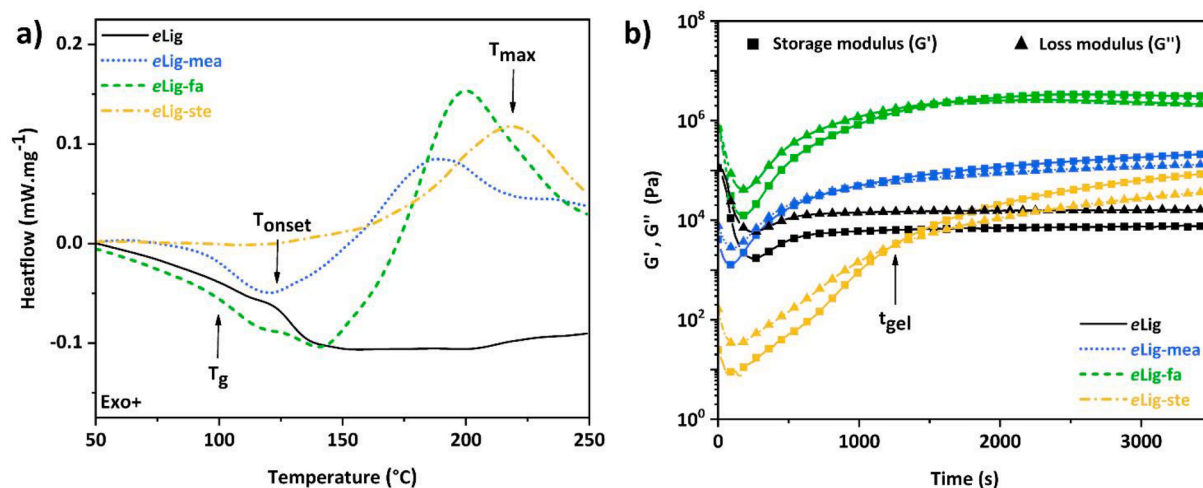
Fig. 4. (a) DSC curves (10 °C.min^{-1}, N$_2$) and (b) rheokinetic isothermal curing (150 °C) of eLig and eLig-Bz.

The broad molecular weight distributions of *e*Lig-mea (Đ= 11.0) is presumably due to dynamic ester exchanges, as discussed later in this manuscript (lignin-based vitrimers). The thermal properties of each *e*Lig-Bz were evaluated by differential scanning calorimetry (DSC) (Fig. 4.a). The endothermic transition around 100 °C is associated with the glass transition (T$_g$) of *e*Lig (Table 2, column 5) [52]. The DSC profile of each *e*Lig-Bz compound has an exothermic peak characteristic of the benzoxazine ring opening-polymerization (ROP). The low polymerization temperature (T$_{onset}$ = 141 and 155 °C for *e*Lig-fa and *e*Lig-ste, respectively) is assumed to be due to a catalytic effect of the functional groups of lignin [45,58]. In the case of *e*Lig-mea (T$_{onset}$ = 125 °C), this effect is even further enhanced presumably due to the aliphatic –OH groups of mea, as reported elsewhere [50,59]. The maximum temperature of the exothermic peak of each *e*Lig-Bz is reached around 200 °C (Table 2, column 7). The curing kinetics were characterized by isothermal cure rheology as reported in Fig. 4.b. During this isothermal test, the storage modulus of *e*Lig remains constant, highlighting the absence of growing of a polymeric network. On the contrary, for each *e*Lig-Bz compound, a characteristic crossover of the loss and storage moduli indicates the formation of a crosslinked network. For *e*Lig-mea, the gelation is reached in 8 min at 150 °C. The gelation times of *e*Lig-fa and *e*Lig-ste are similar (t$_{gel}$≈ 17 and 20 min, respectively). The evolution of the complex viscosity follows the same trend, increasing from 10^5 to 10^9 mPa.s for *e*Lig-ste and *e*Lig-fa, respectively (Fig. S11).

3.2. Manufacture and characterization of lignin-based benzoxazine thermosets

Monocomponent lignin-based thermosets were prepared by the curing of their respective precursor. For the sake of clarity, each *e*Lig-Bz is referred to as p(*e*Lig-Bz) once polymerized. Complete curing was confirmed by the disappearance of the exothermic peak associated with the ROP of the benzoxazine (T = 125–200 °C) in the DSC thermogram (Fig. S12). When cured, each material produces self-supporting and homogeneous specimens (Fig. 5.a). The internal structure of these specimens was investigated by micro-computed X-ray tomography analysis (Fig. 5.b). The uniform mass densities observed for p(*e*Lig-fa) and p(*e*Lig-ste) demonstrate the homogeneity of the cured resins at the micron scale, which is noteworthy for a lignin-based material. The segregated regions surrounded by porous structures of p(*e*Lig-mea) may originate from heterogeneousity of the precursor as revealed by *SEC* (ESI, Fig. S13). The porous structure originates from the high hygroscopy of *e*Lig-mea. During the curing, the materials release water, even if the monomers are dried under reduced pressure (0.1 mBar) at 50 °C overnight and processed immediately once removed from the drying

bell. It is then essential to consider a process with a way to evacuate water, and vacuum compressive molding (MeltPrep®) appeared to be the most efficient. To illustrate the significant differences between materials obtained by MeltPrep® and hot press molding, X-ray tomograms were recorded, and the voids volume fraction was calculated (Table S6). When samples are prepared by hot pressing, the voids volume fraction is of 14.1 %, while of 2.6 % for specimens prepared by Meltprep® (fig. S14). Lignin-based polybenzoxazine thermosets exhibit a density around 1.0 g.cm^{-3} (Table 3, column 2). The thermo-mechanical properties of each p(*e*Lig-Bz) were investigated by torsional rheology (Fig. 5.c) and displayed a decrease of the storage and loss moduli upon heating that is characteristic of crosslinked thermoset materials. The sharp α-transition peak is assigned to the broad distribution of lignin complex macromolecular structure (Fig. 5.d) [19,23,60]. The maximum of the tan δ curve was attributed to the T$_g$ of p(*e*Lig-Bz) (Table 3, column 3). Even if the T$_g$ is strongly affected by the rigidity of the aromatic lignin backbone, the functionality of the benzoxazine amine group governs the mechanical properties (T$_g$ = 136, 182, and 197 °C for p(*e*Lig-ste), p(*e*Lig-mea), and p(*e*Lig-fa), respectively). The evolution of mechanical properties (Table 3, column 4) is consistent with the crosslink densities determined by swelling experiments (Table 3, columns 6–9, Figs. S15-S17). For instance, p(*e*Lig-fa) is a highly crosslinked network (W < 2 wt.% in all solvents tested) with a modulus of 3.1 GPa. The higher swelling ratio of p(*e*Lig-ste) (W > 100 wt.%, except in water) is explained by its lower crosslinking density due to the long alkyl chain of stearylamine. This later dilutes the number of reactive sites and crosslinking nodes in the material. Indeed, the theoretical concentrations of reactive sites in *e*Lig-ste is 2.33 mmol.g^{-1}, compared to 1.85 mmol.g^{-1} for *e*Lig-fa or *e*Lig-mea. Shear stress–strain measurements were done to characterize the mechanical properties of the lignin-based polybenzoxazines [61,62]. The shear stress–strain curves reported in Fig. S18 shows that p(*e*Lig-fa) and p(*e*Lig-mea) have the typical behaviour of thermoset. The ultimate shear strength reaches 12.2 and 37.1 MPa, and the shear strains at break 1.6 and 2.7 % for p(*e*Lig-mea) and p(*e*Lig-fa), respectively. P(*e*Lig-ste) has a ductile behavior. The shear strain at break reaches 9.5 %, and the shear stress at break 5.1 MPa. The mechanical differences between p(*e*Lig-ste), and p(*e*Lig-fa) and p(*e*Lig-mea) can also be explained by the alkyl chain of stearylamine, which plasticizes the material.

The thermal stability of the lignin-based thermosets were investigated by thermogravimetric analysis (TGA) and values are reported in Table 3 (columns 11–13). Each resin degrades following a two step process (Figs. S19-S20), with the lowest initial degradation temperature (T$_{d5\%}$) observed for p(*e*Lig-ste) (243 °C) and the highest value observed for p(*e*Lig-fa) (275 °C). For p(*e*Lig-fa), a char yield CR$_{800}$ = 45.8 % is reached as the furan ring is involved in the network formation.
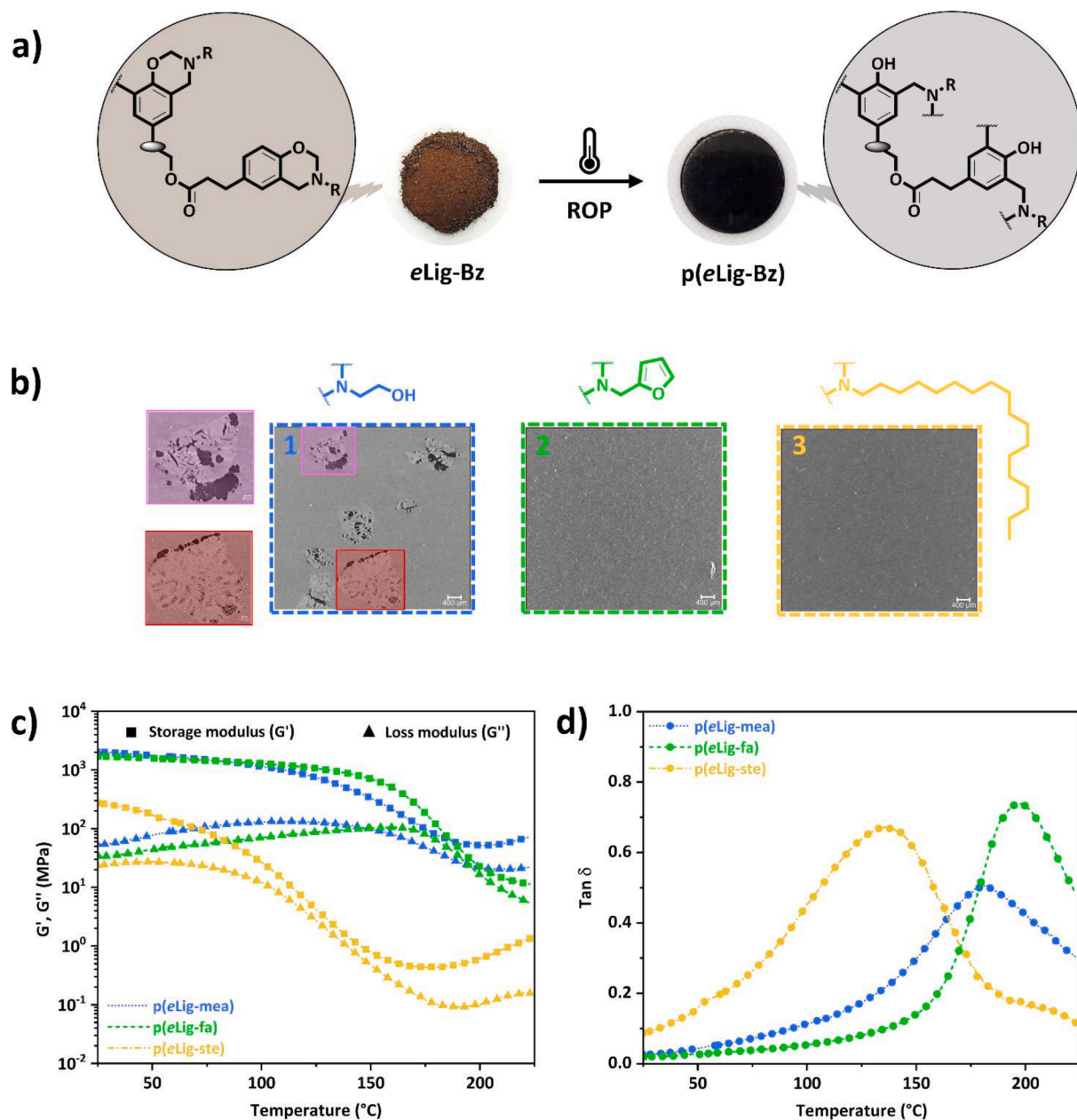
Fig. 5. (a) Schematic representation of p(*e*Lig-Bz) manufactured by vacuum compression moulding, (b) representative 2D orthoslices of p(*e*Lig-Bz) parallel to the rotation axis of the tomogram, (c) storage and loss moduli, and (d) loss factor curves of p(*e*Lig-Bz) determined by torsional rheology.

Table 3
Thermo-mechanical properties of p(eLig-Bz).

Network	Mechanical properties					[e] Swelling (wt.%)				Thermal properties		
	[a] ρ (g.cm^{-3})	[b] T_α (°C)	[c] E' (GPa)	[d] Shear strain at break (%)	[d] Shear stress at break (MPa)	W (TOL)	W (CHCl3)	W (DIOX)	W (H2O)	[f] $T_{d5\%}$ (°C)	[g] T_{max} (°C)	[h] CR$_{800}$ (%)
p(*e*Lig-mea)	1.0	182	1.7	1.6	12.2	2 ± 2	8 ± 7	8 ± 7	16 ± 4	266	369	42.6
p(*e*Lig-fa)	1.1	197	3.1	2.7	31.7	0 ± 0	2 ± 2	0 ± 0	0 ± 0	275	380	45.8
p(*e*Lig-ste)	1.1	136	0.5	9.5	5.1	111 ± 53	196 ± 27	118 ± 14	3 ± 4	243	383	28.4

[a] density determined on an average on three measurements, [b] α-relaxation temperature determined from the maximum of the loss factor curve (torsional rheology), [c] storage modulus at room temperature (DMA, three-point bending mode), [d] determined at room temperature (rheology, torsion mode), [e] determined after a week of immersion according eq. (2), [f] 5 % weight loss temperature, [g] maximum rate of weight loss, and [h] char residue at 800 °C (N$_2$, 10 °C.min^{-1}).
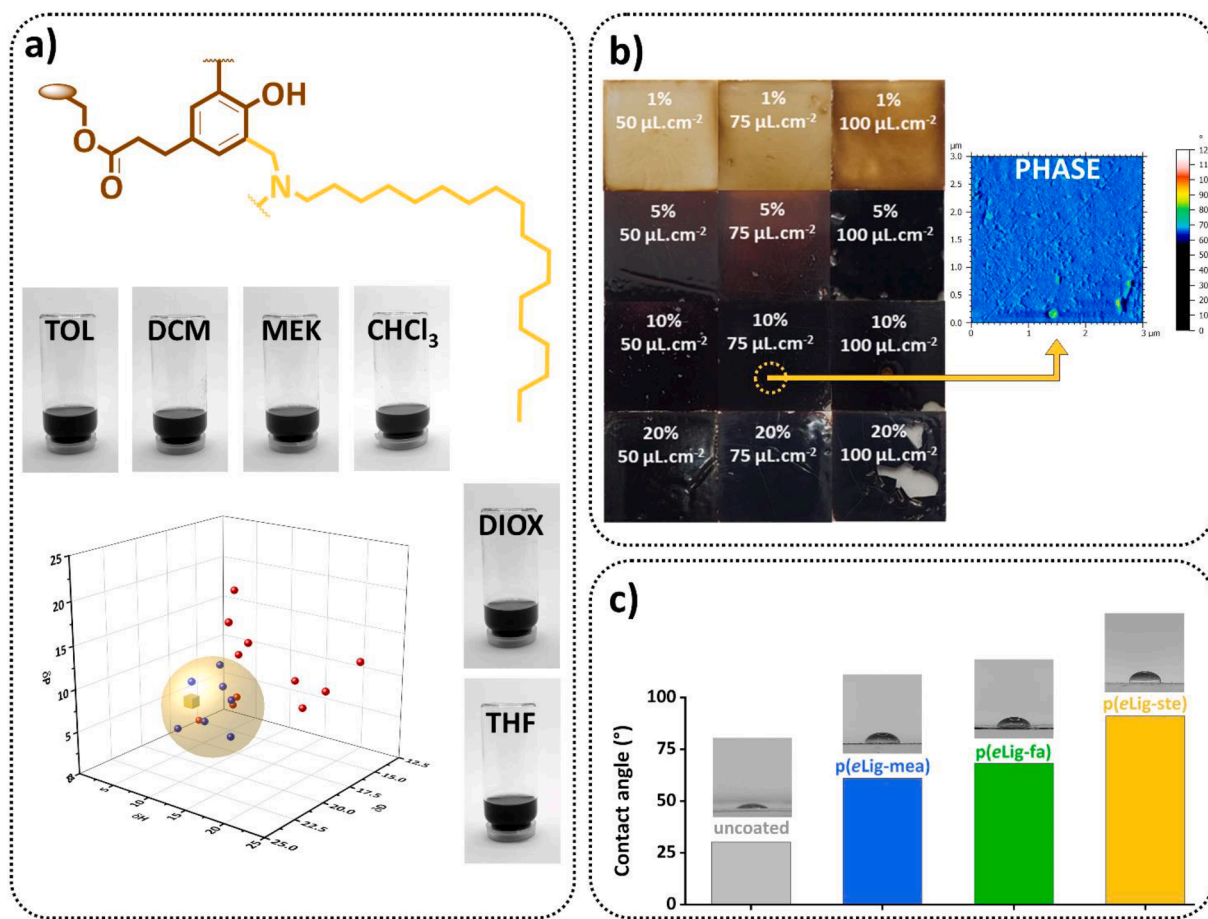
Fig. 6. a) Solubility of *e*Lig-ste in common organic solvents and HSP solubility sphere, b) optimization of the casting procedure and AFM phase image of p(*e*Lig-ste) (10 wt.%, 75 μL. cm^{-2}) and c) contact angles of p(*e*Lig-Bz) coated onto a glass substrate (10 wt.%, 75 μL. cm^{-2}).

3.3. Directed design of lignin-based benzoxazine

The structural design of each lignin-based benzoxazine precursor was intentionally conceived with a specific application in mind. While lignin is the same common building block, the amine used to close the oxazine ring was expected to drive the final properties and applications of each material. The following amines were used:

- Stearylamine: Benzoxazine precursors made of this amine would benefit from an enhanced hydrophobicity and ability to coat a surface.
- Furfurylamine: The furan ring is known to be involved in the polymerization of benzoxazines and enhances the thermal properties of the thermosets, the T_g, and the fire properties.
- Mono-ethanolamine: Benzoxazine precursors composed of ester and mono-ethanolamine undergo significant dynamic exchanges conferring vitrimeric properties to the resulting polybenzoxazine.

In the following section the range of possible applications afforded by suitable selection of the amine is illustrated.

3.3.1. Easy-to-apply and hydrophobic lignin-based coatings

The development of coatings from lignin is a growing field of investigation relying on the main asset that lignin is hydrophobic by nature. Such coatings find no>15 applications as reported in the recent review of Sadanandan *et al.,* such as antibacterial or anticorrosive coatings, to cite but a few [63]. The development of such material is generally impeded by the low solubility of lignin in solvents.

The solubility of lignin is the critical point to address when attempting to form coatings through dip-, drop-, spray-, or spin-coating casting techniques. Although the isolation procedure seems to govern the overall solubility of lignin, chemical modifications also help to enhance this parameter for the preparation of homogeneous and functional coatings [53]. Therefore, the solubility (S) determined for each *e*Lig-Bz was explored over a series of 19 organic solvents covering a wide range of polarity (ESI, Fig. S21). The Hansen solubility parameters of each precursor are reported in the supporting information (Table S7). *e*Lig-ste is readily soluble in many solvents (S > 80 wt.%), including chlorinated, non-polar and polar aprotic solvents. (Fig. 6.a). The long alkyl substituents (C$_{18}$) constrain the lignin chains in extended conformation regardless of the polarity of the solvent [64].

To demonstrate the utility of this feature, *e*Lig-ste was casted from THF onto a glass substrate and a homogeneous coating was obtained (Fig. 6.b) with an optimized weight and surface concentration of 75 μL. cm^{-2} and 10 wt.% respectively (thickness = 31.4 μm). The surface and thickness of the other p(*e*Lig-Bz)-coatings are reported in the ESI (Fig. S22, Table S8). The topography image of p(*e*Lig-ste) obtained by atomic force microscopy (AFM) shows a smooth surface (Fig. 6.b), consisting of a uniform single phase matrix (~59° ± 7) with a modulus of E = 500 ± 129 MPa (Fig. S23, ESI). The water contact angles of p(*e*Lig-Bz) specimens are reported in Fig. 6.c, revealing that p(*e*Lig-mea) and p(*e*Lig-fa) are quite hydrophilic (63.3° and 71.0° respectively). In contrast, the long alkyl side chain of stearylamine affords p(*e*Lig-ste) a more hydrophobic character, as illustrated by the water contact angle of 91.1° (Fig. S24). The latter is in the same range as that of the hydrophobic lignin-based polyester [18] and polyurethane [65,66] coatings reported in the literature to date. In summary, stearylamine is a suitable amine for easy-to-cast hydrophobic lignin-based benzoxazine coatings.
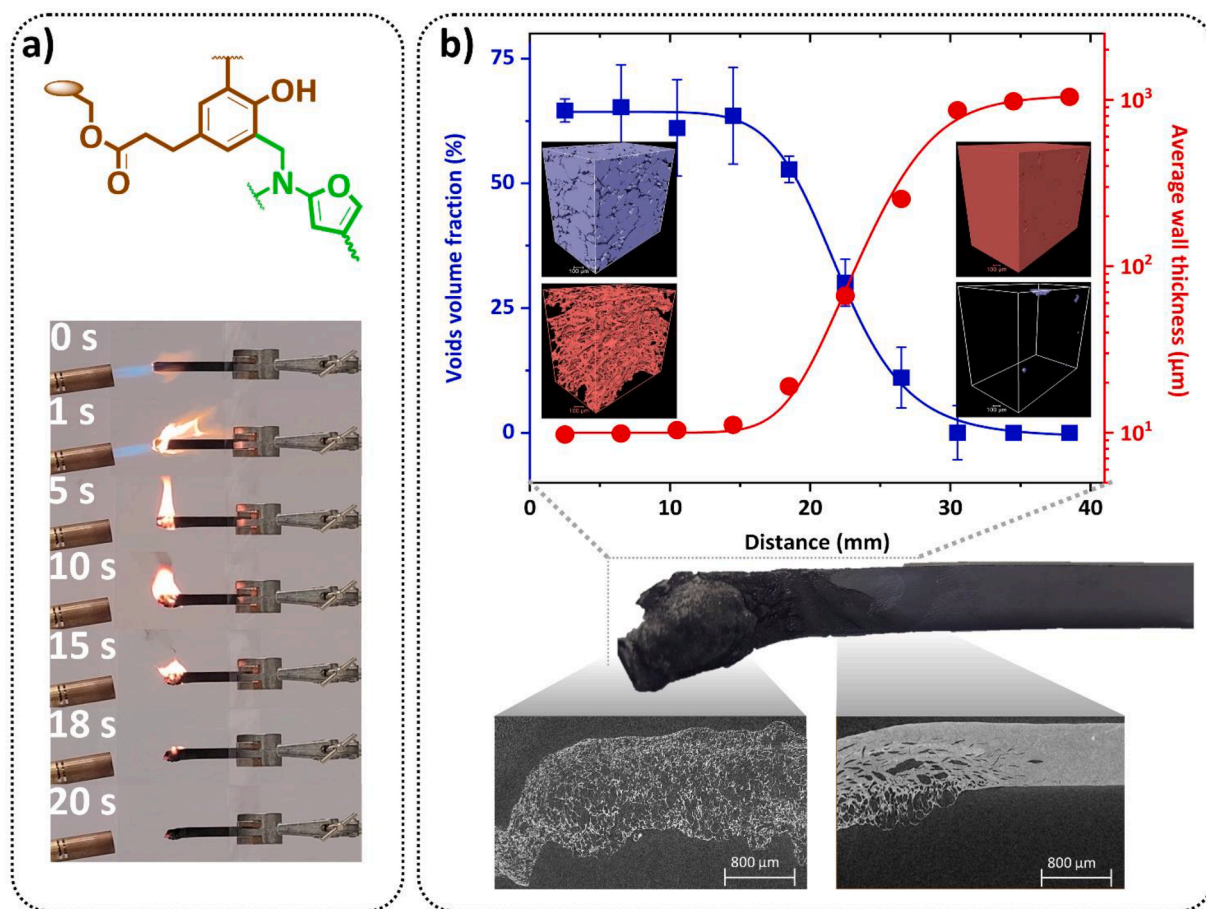
Fig. 7. (a) Digital photographs of the horizontal burning test of p(*e*Lig-fa). (b) Representative 2D orthoslices of residues and experimental fitting of voids volume fraction and average walls thickness across burn residue.

3.3.2. Flame retardant lignin-based benzoxazine

Stemming from its unique aromatic structure, lignin generates a high char yield upon combustion, logically driving research works towards the exploitation of this feature [67–70]. In this study, p(*e*Lig-fa) has a high thermal stability (Table 3) afforded both by the lignin and the furan ring structure. The high char yield (CR$_{800}$ = 45.8 °C) resulting from the thermal degradation of p(*e*Lig-fa) reveals that it has a high limiting oxygen index value (LOI = 35.8 %) that is beneficial to fire resistance. The flammability of p(*e*Lig-fa) was tested through a horizontal burning test (video 1 provided in the ESI). After exposure to flame, the sample self-extinguished in<20 s, and no burning drips were observed (Fig. 7.a).

The flame was not able to spread across the whole sample and 84 % of the material remained unburned. Interestingly, it was observed that the flame propagation on p(*e*Lig-fa) was also impeded by the formation of an intumescent phase (Fig. 7.b). The morphology of the burned residues of p(*e*Lig-fa) is typical of intumescent char, and is attributed to the foamed cellular structure generated in the condensed phase. In contrast, the unburned fraction is uniform. The cross-section of the material exposed to the flame was investigated from the burned extremity (0 mm, zone 1) to the unburned part (40 mm, zone 6) by X-ray micro-computed tomography (Fig. S25). Fig. 7.b shows the experimental distribution of voids and condensed phases across the burned residue of p(*e*Lig-fa).

Table 4
Summary of lignin-based intumescent flame retardant (IFR) reported in the literature and comparison of their nitrogen and phosphorous content, limiting oxygen index, and statistic heat-resistant index.

Network	Composition	[a] N (%)	P (%)	[b] CR$_{800}$ (%)	[c] LOI (%)	Ref.
Lignin-based benzoxazine	Esterified soda lignin-based furfurylamine-based benzoxazine (p(*e*Lig-fa)	3.2	0	45.8	35.8	This work
Lignin-based DOPO and piperazine	Phenolated enzymatic hydrolysis lignin- derived piperazine and 9,10-dihydro-9-oxa-10-phosphaphenanthrene-10-oxide (DOPO) (Lig-M)	5.4	3.7	41.6	34.1	[68]
Lignin-based phosphate and melamine	Liquified enzymatic lignin- derived polyphosphoric acid and melamine (LPMC)	16.8	13.1	53.3	38.8	[69]
Lignin-based phosphate and amino-triazole	Kraft lignin- derived 3-amino-1,2,4-triazole, phosphoryl chloride and 1,10-decandiol (D-36)	3.0	7.0	55.0	39.5	[70]

[a] nitrogen content determined by elemental analysis, [b] char residue at 800 °C, and [c] limiting oxygen index determined according eq. S1.
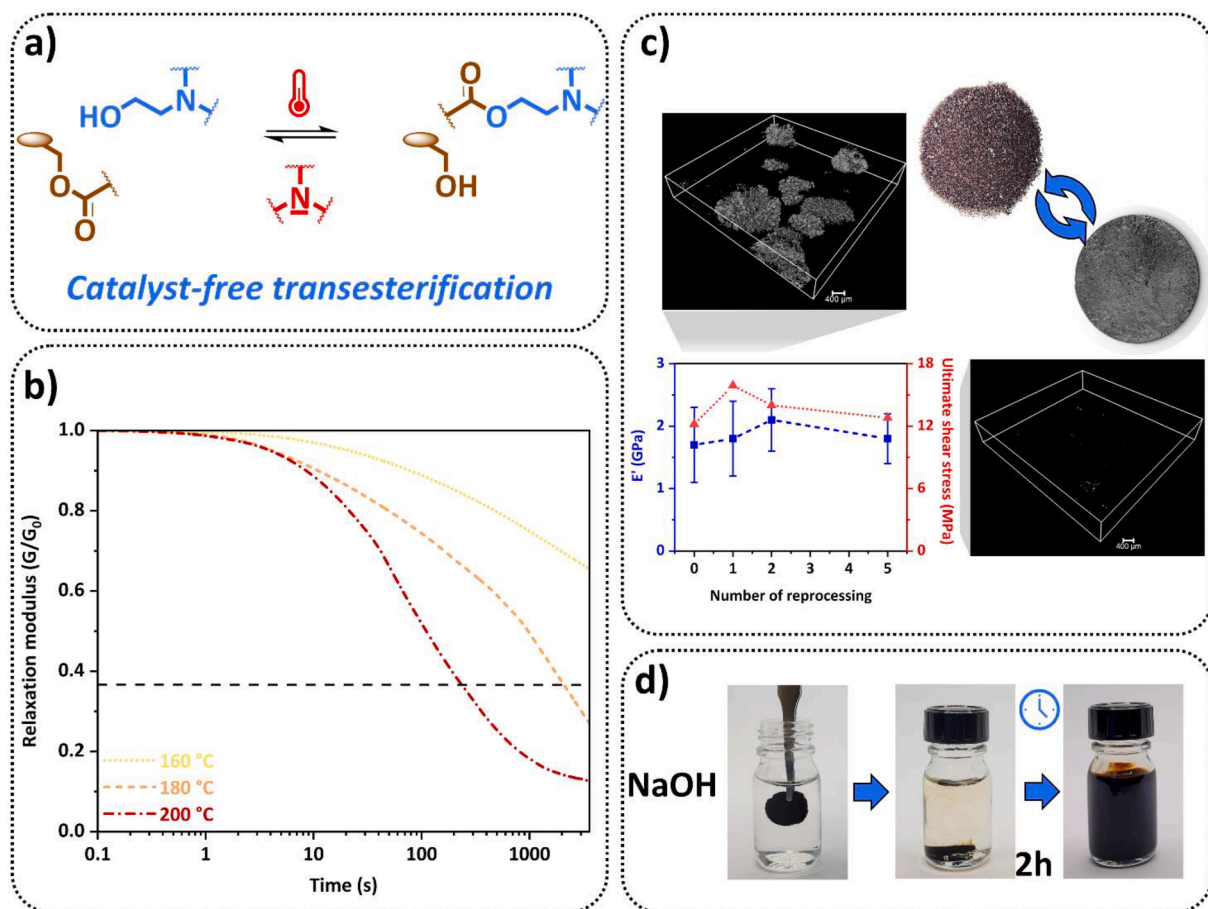
Fig. 8. (a) Pattern of internally catalyzed transesterification exchanges b) stress-relaxation curves of p(*e*Lig-mea) as function of temperature, (c) photographs of the mechanical recycling, retention of mechanical properties (blue curve: elastic modulus, red curve: ultimate shear strength), representative 3D rendering of voids in recycled p(*e*Lig-mea), and (d) chemical degradability of p(*e*Lig-mea) in NaOH (1 M).

Before combustion, the sample is homogeneous and free of observable voids. After combustion, the voids fraction increases when moving from the unburned to the burned part. A logistic function was applied to estimate the voids volume fraction and the wall thickness of the observed cells in the foamed part along the length of the specimen ($R^2 = 0.99$, equation S2, Table S9, ESI). The aromatic lignin framework is reinforced with the addition of the phenolic moieties from the esterification and the furanic groups in the polymerized structure. The presence of nitrogen element promoted the release of non-combustible gases during combustion, diluting the concentration of flammable volatiles in the gas phase. Entrapped gas in the condensed phase was responsible for the swelling of the carbon layer [67,68]. The resulting porous structures act as a thermally insulating layer, thus slowing down the burning process and improving the flame-retardant properties. The maximum rate of heat release of p(*e*Lig-fa) was also investigated by pyrolysis-combustion flow calorimetry (PCFC) [71,72]. The heat release curves of the technical lignin (Lig), the enhanced lignin (*e*Lig) and the lignin-based flame-retardant p(*e*Lig-fa) are reported in Fig. S26 and in Table S11. HRR curve of p(*e*Lig-fa) shows a major decomposition peak at TpHRR = 377 °C followed by a shoulder characteristic of a multi-step decomposition. As compared to Lig, the pHRR of p(*e*Lig-fa) significantly decreased from 87 to 47 W.g^{-1}, proving the decreased flammability afforded by the highly crosslinked PBZ network. Overall, it is noteworthy that the rate of heating release of poly(*e*Lig-fa) is very low, even lower than resins specifically designed for high flame retardancy [73–75]. Finally, this approach leads to an effective phosphorus-free fire retardant as compared to other lignin-based intumescent flame retardant reported in Table 4.

3.3.3. Lignin-based benzoxazine vitrimers

In 2011, Leibler *et al.* introduced dynamic covalent exchanges in cross-linked materials, paving the way toward recyclable thermosets, to make the first "vitrimers" [76]. Among the different chemistries enabling exchanges in covalent adaptable networks (CANs), thermally activated transesterification reactions (TERs) aroused considerable interest stemming from their easy implementation in conventional polymer systems. In a similar manner to the recently disclosed polybenzoxazine vitrimers relying on TERs [50,51], mono-ethanolamine has been employed as a bio-based synthon to close the oxazine ring with a primary amine bearing an aliphatic –OH group. It was expected that these hydroxyl groups and the ester bonds contained in the precursor would participate into dynamic TER exchanges (Fig. 8. a), resulting in a vitrimeric behaviour [77]. An advantage in designing vitrimers from benzoxazine is the presence of the tertiary amine (NR₃) generated from benzoxazine ROP, which in turn catalyses the TER. Ester-containing vitrimers such as p(*e*Lig-mea) do not require the addition of a separate catalyst as a result. p(*e*Lig-mea) is a fully cross-linked material, as illustrated by its insolubility and swelling in various solvents (Table 3, columns 6–9; Table S6, Fig. S15). Fast dynamic exchanges are illustrated by the evolution of the relaxation modulus reported on Fig. 8.b. The relaxation time (τ^*, time to relax to 1/e of the initial modulus) measured at 200 °C ($\tau^* < 4$ min) is in the same range than previously reported lignin-based vitrimer (Table 6, column 5). The activation energy (E_a) was calculated as 181 kJ.mol^{-1}, higher than that of other tertiary amine catalyzed TER-based vitrimers [50,51,78–81] (details of the calculations are reported in the ESI, Fig. S27). This value was ascribed to the relatively low number of exchangeable functions in

Table 5

Summary of lignin-vitrimers based on TERs reported in the literature and comparison of their glass transitions, relaxation times and activation energies.

Network	Composition	Type of catalyst	[a] T_α (°C)	[b] τ^* (s)[T]	[c] Ea (kJ/mol)	Ref.
Lignin-based benzoxazine	Esterified soda lignin-based mono-ethanolamine-based benzoxazine (monocomponent) p(eLig-mea)	Internally catalyzed by NR₃ groups	182	233 [200]	181	This work
Lignin-based epoxy vitrimer	Ozonated lignin (Oz-L)/ sebacic acid-derived epoxy (Se-EP) (Oz-L/ Se-EP = 1:1.5)	Externally catalyzed by Zn(acac)₂	133	80 [200]	n.a.	[82]
Lignin-based epoxy vitrimer	Etherified enzymatic hydrolysis lignin (GEL)/ diglycidyl ether bisphenol A (DGEBA) (GEL/ DGEBA = 1:4)	Externally catalyzed by Zn(acac)₂	41	1570 [160]	n.a.	[83]
Lignin-based epoxy vitrimer	Kraft lignin-based polycarboxylic acid (L-COOH) / poly (ethylene glycol) diglycidyl ether (PEG-epoxy) (L-COOH/ PEG-epoxy = 1:1)	Externally catalyzed by Zn(acac)₂	37	720 [200]	54	[84]
Lignin-based epoxy vitrimer	Enzymatic lignin-based epoxy (EP-EL) and carboxyl (CA-EL) crosslinked with polyethylene glycol 400 (PEG₄₀₀) (EP-EL:CA-EL:PEG₄₀₀ = 4:4:4)	Excess of –OH groups	n.a.	~ 2400 [200]	18	[85]

[a] α-relaxation temperature determined from the maximum of the loss factor curve, [b] relaxation time, and [c] activation energy determined from the Arrhenius law according to eq. S3.

the modified lignin precursor. At this step, it is important to note that none of Lig, eLig, p(eLig-fa) and p(eLig-ste) have any vitrimeric behavior, as (in comparison to p(eLig-mea)) they do not simultaneously contain –OH groups, esters and tertiary amines groups. The ability of the lignin-based vitrimer to be recycled is illustrated in Fig. 8.c. p(eLig-mea) was ground into a fine powder which was then hot-pressed to yield self-supporting parts. The effects of reprocessing on the morphology of the thermoset revealed an improved mass distribution and the elimination of voids (Fig. S28). Scanning electron microscopy (SEM) also confirms the X-ray tomograms (Fig. S29). The initially measured elastic modulus of 1.8 GPa was maintained even after the material was recycled 5 times. The shear strain–stress curves of the recycled vitrimer also evidenced the retention of the mechanical properties (Fig. S30). Additionally, no structural changes were observed via FTIR analysis following recycling (Fig. S31). Finally, the degradability of p(eLig-mea) was also assessed in Fig. 8.d. The vitrimer sample was fully degraded after immersion in 1 M NaOH for several hours due to the saponification of the ester bonds and the high solubility of soda lignin in basic media. For the sake of comparison, the properties of other lignin-based vitrimers based on TERs reported to date are gathered in Table 5, highlighting p(eLig-mea) as the first internally catalyzed and high-T_g lignin-based vitrimer. This lignin-based polybenzoxazine vitrimer helps to close the loop on the circular economy of polymers, from an eco-friendly design to a sustainable end-of-life by recyclability and degradability.

4. Conclusions

This works demonstrates that the reactivity enhancement of a soda lignin with a bio-based phenolic compound affords the development of a wide range of benzoxazine precursors. The resulting lignin-based benzoxazines thermosets were prepared through a chemical pathway that agrees with most of the principles of Green Chemistry. Water is the only waste generated from the straightforward synthesis. The synthesis yields materials with a high lignin mass fraction, between 46 and −66 wt.%. Thanks to the structure of lignin and the characteristics of benzoxazine, these materials exhibit attractive mechanical and thermal properties. The glass transition temperatures range from 136 to 197 °C and the storage moduli range from 0.5 to 3.1 GPa. The most appealing aspect of this work is the demonstration that the features of these precursors can be tuned depending on the nature of the amine used to close the oxazine ring:

- Stearylamine was used to prepare easy-to-cast hydrophobic coatings,
- Thermal properties and burning tests demonstrated that a furan-containing lignin-based benzoxazine is fire resistant and self-extinguishing,
- Finally, an –OH terminated amine was used to develop a catalyst-free lignin-based vitrimer. The aliphatic –OH groups and ester bonds underwent topological rearrangements through internally catalysed transesterification reactions, rendering the resultant lignin-based thermoset both reprocessable and degradable.

In a close future, other lignin-derivatives could be developed by varying the amine used, and their potential could be analysed as anti-oxidant additives or anti-corrosive coatings for instance. Most of all, the combination of different amines could also be engineered with the perspective to develop high-T_g bio-based vitrimers with low fire-smoke and toxicity properties, paving the way toward truly circular composites.

Declaration of Competing Interest

The authors declare that they have no known competing financial interests or personal relationships that could have appeared to influence the work reported in this paper.

Data availability

Data will be made available on request.

Vancaeyzeele for the tensile tests. The author would also like to thank Farida Baraka for her helpful advice on the conceptual design of figures.

Appendix A. Supplementary data

Supplementary data to this article can be found online at https://doi.org/10.1016/j.cej.2022.139895.

References

[1] D.S. Bajwa, G. Pourhashem, A.H. Ullah, S.G. Bajwa, A concise review of current lignin production, applications, products and their environmental impact, Ind. Crops Prod. 139 (2019), 111526, https://doi.org/10.1016/j.indcrop.2019.111526.

[2] E. Paone, T. Tabanelli, F. Mauriello, The rise of lignin biorefinery, Current Opinion in Green and Sustainable, Chemistry 24 (2020) 1–6, https://doi.org/10.1016/j.cogsc.2019.11.004.

[3] Y. Cao, S.S. Chen, S. Zhang, Y.S. Ok, B.M. Matsagar, K.C.W. Wu, D.C.W. Tsang, Advances in lignin valorization towards bio-based chemicals and fuels: Lignin biorefinery, Bioresour. Technol. 291 (2019), 121878, https://doi.org/10.1016/j.biortech.2019.121878.

[4] M. Mariana, T. Alfatah, A.K. H.p.s., E.B. Yahya, N.G. Olaiya, A. Nuryawan, E. M. Mistar, C.K. Abdullah, S.N. Abdulmadjid, H. Ismail, A current advancement on the role of lignin as sustainable reinforcement material in biopolymeric blends, J. Mater. Res. Technol. 15 (2021) 2287–2316.

[5] O. Gordobil, R. Delucis, I. Egüés, J. Labidi, Kraft lignin as filler in PLA to improve ductility and thermal properties, Ind. Crops Prod. 72 (2015) 46–53, https://doi.org/10.1016/j.indcrop.2015.01.055.

[6] A. Gregorová, B. Košíková, R. Moravčík, Stabilization effect of lignin in natural rubber, Polym. Degrad. Stab. 91 (2006) 229–233, https://doi.org/10.1016/j.polymdegradstab.2005.05.009.

[7] H. Sadeghifar, A. Ragauskas, Lignin as a UV Light Blocker—A Review, Polymers 12 (5) (2020) 1134, https://doi.org/10.3390/polym12051134.

[8] C. Pouteau, S. Baumberger, B. Cathala, P. Dole, Lignin–polymer blends: evaluation of compatibility by image analysis, C.R. Biol. 327 (9) (2004) 935–943, https://doi.org/10.1016/j.crvi.2004.08.008.

[9] H. Sadeghifar, A. Ragauskas, Perspective on Technical Lignin Fractionation, ACS Sustainable Chem. Eng. 8 (22) (2020) 8086–8101, https://doi.org/10.1021/acssuschemeng.0c01348.

[10] M. Fache, B. Boutevin, S. Caillol, Vanillin, a key-intermediate of biobased polymers, Eur. Polym. J. 68 (2015) 488–502, https://doi.org/10.1016/j.eurpolymj.2015.03.050.

[11] M. Ibrahim, R.B. Sriprasanthi, S. Shamsudeen, F. Adam, S. Bhawani, A concise review of the natural existence, synthesis, properties, and applications of syringaldehyde, Bioresources 7 (3) (2012) 4377–4399.

[12] N. Kumar, V. Pruthi, Potential applications of ferulic acid from natural sources, Biotechnol. Rep, 4 (2014) 86–93, https://doi.org/10.1016/j.btre.2014.09.002.

[13] B.M. Upton, A.M. Kasko, Strategies for the Conversion of Lignin to High-Value Polymeric materials: Review and Perspective, Chem. Rev. 116 (4) (2016) 2275–2306, https://doi.org/10.1021/acs.chemrev.5b00345.

[14] A. Eraghi Kazzaz, Z. Hosseinpour Feizi, P. Fatehi, Grafting strategies for hydroxy groups of lignin for producing materials, Green Chem. 21 (21) (2019) 5714–5752, https://doi.org/10.1039/C9GC02598G.

[15] S. Laurichesse, L. Avérous, Chemical modification of lignins: Towards biobased polymers, Prog. Polym. Sci. 39 (7) (2014) 1266–1290, https://doi.org/10.1016/j.progpolymsci.2013.11.004.

[16] Y. Cao, Z. Liu, B. Zheng, R. Ou, Q. Fan, L. Li, C. Guo, T. Liu, Q. Wang, Synthesis of lignin-based polyols via thiol-ene chemistry for high-performance polyurethane anticorrosive coating, Compos. B Eng. 200 (2020), 108295, https://doi.org/10.1016/j.compositesb.2020.108295.

[17] X. Zhang, Y. Kim, I. Elsayed, M. Taylor, T.L. Eberhardt, E.I.B. Hassan, R. Shmulsky, Rigid polyurethane foams containing lignin oxyalkylated with ethylene carbonate and polyethylene glycol, Ind. Crops Prod. 141 (2019), 111797, https://doi.org/10.1016/j.indcrop.2019.111797.

[18] C. Scarica, R. Suriano, M. Levi, S. Turri, G. Griffini, Lignin Functionalized with Succinic Anhydride as Building Block for Biobased Thermosetting Polyester Coatings, ACS Sustainable Chem. Eng. 6 (3) (2018) 3392–3401, https://doi.org/10.1021/acssuschemeng.7b03583.

[19] Y. Xu, K. Odelius, M. Hakkarainen, One-Pot Synthesis of Lignin Thermosets Exhibiting Widely Tunable Mechanical Properties and Shape Memory Behavior, ACS Sustainable Chem. Eng. 7 (15) (2019) 13456–13463, https://doi.org/10.1021/acssuschemeng.9b02921.

[20] W. Wang, F. Wang, C. Zhang, J. Tang, X. Zeng, X. Wan, Versatile value-added application of hyperbranched lignin derivatives: Water-resistance adhesive, UV protection coating, self-healing and skin-adhesive sensing, Chem. Eng. J. 404 (2021), 126358, https://doi.org/10.1016/j.cej.2020.126358.

[21] C. Gioia, G. Lo Re, M. Lawoko, L. Berglund, Tunable Thermosetting Epoxies Based on Fractionated and Well-Characterized Lignins, J. Am. Chem. Soc. 140 (11) (2018) 4054–4061, https://doi.org/10.1021/jacs.7b13620.

[22] C. Gioia, M. Colonna, A. Tagami, L. Medina, O. Sevastyanova, L.A. Berglund, M. Lawoko, Lignin-Based Epoxy Resins: Unravelling the Relationship between Structure and Material Properties, Biomacromolecules 21 (5) (2020) 1920–1928, https://doi.org/10.1021/acs.biomac.0c00057.

[23] E. Feghali, D.J. van de Pas, K.M. Torr, Toward Bio-Based Epoxy Thermoset Polymers from Depolymerized Native Lignins Produced at the Pilot Scale, Biomacromolecules 21 (4) (2020) 1548–1559, https://doi.org/10.1021/acs.biomac.0c00108.

[24] T.V. Lourençon, S. Alakurtti, T. Virtanen, A.-S. Jääskeläinen, T. Liitiä, M. Hughes, W.L.E. Magalhães, G.I.B. Muniz, T. Tamminen, Phenol-formaldehyde resins with suitable bonding strength synthesized from "less-reactive" hardwood lignin fractions, Holzforschung, 74 (2), 2020, 175-183. doi: doi:10.1515/hf-2018-0203.

[25] L. Wang, L. Lagerquist, Y. Zhang, R. Koppolu, T. Tirri, I. Sulaeva, S.V. Schoultz, L. Vähäsalo, A. Pranovich, T. Rosenau, P.C. Eklund, S. Willför, C. Xu, X. Wang, Tailored Thermosetting Wood Adhesive Based on Well-Defined Hardwood Lignin Fractions, ACS Sustainable Chem. Eng. 8 (35) (2020) 13517–13526.

[26] I. Machado, C. Shaer, K. Hurdle, V. Calado, H. Ishida, Towards the Development of Green Flame Retardancy by Polybenzoxazines, Prog. Polym. Sci. 121 (2021), 101435, https://doi.org/10.1016/j.progpolymsci.2021.101435.

[27] B. Kiskan, Adapting benzoxazine chemistry for unconventional applications, React. Funct. Polym. 129 (2018) 76–88, https://doi.org/10.1016/j.reactfunctpolym.2017.06.009.

[28] D. Iguchi, S. Ohashi, G.J.E. Abarro, X. Yin, S. Winroth, C. Scott, M. Gleydura, L. Jin, N. Kanagasegar, C. Lo, C.R. Arza, P. Froimowicz, H. Ishida, Development of Hydrogen-Rich Benzoxazine Resins with Low Polymerization Temperature for Space Radiation Shielding, ACS Omega 3 (9) (2018) 11569–11581, https://doi.org/10.1021/acsomega.8b01297.

[29] S. Shukla, A. Ghosh, U.K. Sen, P.K. Roy, S. Mitra, B. Lochab, Cardanol benzoxazine-Sulfur Copolymers for Li-S batteries: Symbiosis of Sustainability and Performance, ChemistrySelect 1 (3) (2016) 594–600, https://doi.org/10.1002/slct.201600050.

[30] C. Zhou, X. Lu, Z. Xin, J. Liu, Y. Zhang, Hydrophobic benzoxazine-cured epoxy coatings for corrosion protection, Prog. Org. Coat. 76 (9) (2013) 1178–1183, https://doi.org/10.1016/j.porgcoat.2013.03.013.

[31] S. Konda, S. Raparthi, K. Bhaskar, R.K. Munaganti, V. Guguloth, L. Nagarapu, D. M. Akkewar, Synthesis and antimicrobial activity of novel benzoxazine sulfonamide derivatives, Bioorg. Med. Chem. Lett. 25 (7) (2015) 1643–1646, https://doi.org/10.1016/j.bmcl.2015.01.026.

[32] N.N. Ghosh, B. Kiskan, Y. Yagci, Polybenzoxazines—New high performance thermosetting resins: Synthesis and properties, Prog. Polym. Sci. 32 (11) (2007) 1344–1391, https://doi.org/10.1016/j.progpolymsci.2007.07.002.

[33] N. Amarnath, S. Mukherjee, B. Lochab, Understanding the Stereochemical Effect on the Properties of Emerging Thermosets: Sustainable Polybenzoxazines, ACS Sustainable Chem. Eng. 9 (22) (2021) 7550–7560, https://doi.org/10.1021/acssuschemeng.1c01266.

[34] A. Trejo-Machin, A. Adjaoud, L. Puchot, R. Dieden, P. Verge, Elucidating the thermal and polymerization behaviours of benzoxazines from lignin derivatives, Eur. Polym. J. 124 (2020), 109468, https://doi.org/10.1016/j.eurpolymj.2019.109468.

[35] M. Comí, G. Lligadas, J.C. Ronda, M. Galià, V. Cádiz, Renewable benzoxazine monomers from "lignin-like" naturally occurring phenolic derivatives, J. Polym. Sci., Part A: Polym. Chem. 51 (22) (2013) 4894–4903, https://doi.org/10.1002/pola.26918.

[36] Y. Lyu, H. Ishida, Natural-sourced benzoxazine resins, homopolymers, blends and composites: A review of their synthesis, manufacturing and applications, Prog. Polym. Sci. 99 (2019), 101168, https://doi.org/10.1016/j.progpolymsci.2019.101168.

[37] C. Wang, J. Sun, X. Liu, A. Sudo, T. Endo, Synthesis and copolymerization of fully bio-based benzoxazines from guaiacol, furfurylamine and stearylamine, Green Chem. 14 (10) (2012) 2799–2806, https://doi.org/10.1039/C2GC35796H.

[38] G.A. Phalak, D.M. Patil, S.T. Mhaske, Synthesis and characterization of thermally curable guaiacol based poly(benzoxazine-urethane) coating for corrosion protection on mild steel, Eur. Polym. J. 88 (2017) 93–108, https://doi.org/10.1016/j.eurpolymj.2016.12.030.

[39] L. Puchot, P. Verge, T. Fouquet, C. Vancaeyzeele, F. Vidal, Y. Habibi, Breaking the symmetry of dibenzoxazines: a paradigm to tailor the design of bio-based thermosets, Green Chem. 18 (11) (2016) 3346–3353, https://doi.org/10.1039/C5GC03102H.

[40] N.K. Sini, J. Bijwe, I.K. Varma, Renewable benzoxazine monomer from Vanillin: Synthesis, characterization, and studies on curing behavior, J. Polym. Sci., Part A: Polym. Chem. 52 (1) (2014) 7–11, https://doi.org/10.1002/pola.26981.

[41] P. Thirukumaran, A. Shakila Parveen, M. Sarojadevi, Synthesis and Copolymerization of Fully Biobased Benzoxazines from Renewable Resources, ACS Sustainable Chem. Eng. 2 (12) (2014) 2790–2801, https://doi.org/10.1021/sc500548c.

[42] L. Dumas, L. Bonnaud, M. Olivier, M. Poorteman, P. Dubois, Eugenol-based benzoxazine: from straight synthesis to taming of the network properties, J. Mater. Chem. A 3 (11) (2015) 6012–6018, https://doi.org/10.1039/C4TA06636G.

[43] E.M. Nour-Eddine, Q. Yuan, F. Huang, Investigation of curing and thermal behavior of benzoxazine and lignin mixtures, J. Appl. Polym. Sci. 125 (3) (2012) 1773–1781, https://doi.org/10.1002/app.36262.

[44] H.M.E. Haque, Z. Islam, T. Kawauchi, T. Takeichi, Preparation and Properties of Polybenzoxazine/Lignin Alloy, Applied Mechanics and Materials 217–219 (2012) 571–577, https://doi.org/10.4028/www.scientific.net/AMM.217-219.571.

[45] G.J. Abarro, J. Podschun, L.J. Diaz, S. Ohashi, B. Saake, R. Lehnen, H. Ishida, Benzoxazines with enhanced thermal stability from phenolated organosolv lignin, RSC Adv. 6 (109) (2016) 107689–107698, https://doi.org/10.1039/C6RA22334F.

[46] R. El Hage, N. Brosse, L. Chrusciel, C. Sanchez, P. Sannigrahi, A. Ragauskas, Characterization of milled wood lignin and ethanol organosolv lignin from miscanthus, Polym. Degrad. Stab. 94 (10) (2009) 1632–1638, https://doi.org/10.1016/j.polymdegradstab.2009.07.007.

[47] Y. Lu, K. Zhang, Synthesis and properties of biobased mono-benzoxazine resins from natural renewable pterostilbene, Eur. Polym. J. 156 (2021), 110607, https://doi.org/10.1016/j.eurpolymj.2021.110607.

[48] Y.-L. Liu, C.-I. Chou, High performance benzoxazine monomers and polymers containing furan groups, J. Polym. Sci., Part A: Polym. Chem. 43 (21) (2005) 5267–5282, https://doi.org/10.1002/pola.21023.

[49] M. Foti, R. Médici, H.J. Ruijssenaars, Biological production of monoethanolamine by engineered Pseudomonas putida S12, J. Biotechnol. 167 (3) (2013) 344–349, https://doi.org/10.1016/j.jbiotec.2013.07.013.

[50] A. Adjaoud, A. Trejo-Machin, L. Puchot, P. Verge, Polybenzoxazines: a sustainable platform for the design of fast responsive and catalyst-free vitrimers based on trans-esterification exchanges, Polym. Chem. 12 (22) (2021) 3276–3289, https://doi.org/10.1039/D1PY00324K.

[51] A. Adjaoud, L. Puchot, P. Verge, High-Tg and Degradable Isosorbide-Based Polybenzoxazine Vitrimer, ACS Sustainable Chem. Eng. 10 (1) (2022) 594–602, https://doi.org/10.1021/acssuschemeng.1c07093.

[52] A. Adjaoud, R. Dieden, P. Verge, Sustainable Esterification of a Soda Lignin with Phloretic Acid, Polymers 13 (4) (2021) 637, https://doi.org/10.3390/polym13040637.

[53] J. Sameni, S. Krigstin, M. Sain, Solubility of Lignin and Acetylated Lignin in Organic Solvents, Bioresources 12 (2017) 1548–1565. doi: 10.15376/biores.12.1.1548-1565.

[54] C. Hansen, Hansen Solubility Parameters: A User's Handbook, Second Edition (2012), https://doi.org/10.1201/9781420006834.

[55] J.C. del Río, J. Rencoret, P. Prinsen, Á.T. Martínez, J. Ralph, A. Gutiérrez, Structural Characterization of Wheat Straw Lignin as Revealed by Analytical Pyrolysis, 2D-NMR, and Reductive Cleavage Methods, J. Agric. Food. Chem. 60 (23) (2012) 5922–5935, https://doi.org/10.1021/jf301002n.

[56] J.-L. Wen, S.-L. Sun, B.-L. Xue, R.-C. Sun, Recent Advances in Characterization of Lignin Polymer by Solution-State Nuclear Magnetic Resonance (NMR) Methodology, Materials 6 (2013) 359–391, https://doi.org/10.3390/ma6010359.

[57] Z. Strassberger, P. Prinsen, F.V.D. Klis, D.S.V. Es, S. Tanase, G. Rothenberg, Lignin solubilisation and gentle fractionation in liquid ammonia, Green Chem. 17 (1) (2015) 325–334.

[58] B. Lochab, M. Monisha, N. Amarnath, P. Sharma, S. Mukherjee, H. Ishida, Review on the Accelerated and Low-Temperature Polymerization of Benzoxazine Resins: Addition Polymerizable Sustainable Polymers, Polymers 13 (8) (2021) 1260, https://doi.org/10.3390/polym13081260.

[59] B. Kiskan, B. Koz, Y. Yagci, Synthesis and characterization of fluid 1,3-benzoxazine monomers and their thermally activated curing, J. Polym. Sci., Part A: Polym. Chem. 47 (24) (2009) 6955–6961, https://doi.org/10.1002/pola.23735.

[60] M.E. Jawerth, C.J. Brett, C. Terrier, P.T. Larsson, M. Lawoko, S.V. Roth, S. Lundmark, M. Johansson, Mechanical and Morphological Properties of Lignin-Based Thermosets, ACS Appl. Polym. Mater. 2 (2) (2020) 668–676, https://doi.org/10.1021/acsapm.9b01007.

[61] K. Giannadakis, J. Varna, Analysis of nonlinear shear stress–strain response of unidirectional GF/EP composite, Compos. A Appl. Sci. Manuf. 62 (2014) 67–76, https://doi.org/10.1016/j.compositesa.2014.03.009.

[62] B. Ahmad, X. Fang, Modeling Shear Behavior of Woven Fabric Thermoplastic Composites for Crash Simulations, Appl. Compos. Mater. 27 (6) (2020) 739–765, https://doi.org/10.1007/s10443-020-09844-0.

[63] M.M. Sreejaya, R. Jeevan Sankar, R. K, N.P. Pillai, K. Ramkumar, P. Anuvinda, V.S. Meenakshi, S. Sadanandan, Lignin-based organic coatings and their applications: A review, Mater. Today:. Proc. 60 (2022) 494–501.

[64] J.V. Vermaas, M.F. Crowley, G.T. Beckham, Molecular Lignin Solubility and Structure in Organic Solvents, ACS Sustainable Chem. Eng. 8 (48) (2020) 17839–17850, https://doi.org/10.1021/acssuschemeng.0c07156.

[65] J.C. de Haro, C. Allegretti, A.T. Smit, S. Turri, P. D'Arrigo, G. Griffini, Biobased Polyurethane Coatings with High Biomass Content: Tailored Properties by Lignin Selection, ACS Sustainable Chem. Eng. 7 (13) (2019) 11700–11711, https://doi.org/10.1021/acssuschemeng.9b01873.

[66] G. Griffini, V. Passoni, R. Suriano, M. Levi, S. Turri, Polyurethane Coatings Based on Chemically Unmodified Fractionated Lignin, ACS Sustainable Chem. Eng. 3 (6) (2015) 1145–1154, https://doi.org/10.1021/acssuschemeng.5b00073.

[67] H. Yang, B. Yu, X. Xu, S. Bourbigot, H. Wang, P. Song, Lignin-derived bio-based flame retardants toward high-performance sustainable polymeric materials, Green Chem. 22 (7) (2020) 2129–2161, https://doi.org/10.1039/D0GC00449A.

[68] P. Dai, M. Liang, X. Ma, Y. Luo, M. He, X. Gu, Q. Gu, I. Hussain, Z. Luo, Highly Efficient, Environmentally Friendly Lignin-Based Flame Retardant Used in Epoxy Resin, ACS Omega 5 (49) (2020) 32084–32093, https://doi.org/10.1021/acsomega.0c05146.

[69] H. Zhu, Z. Peng, Y. Chen, G. Li, L. Wang, Y. Tang, R. Pang, Z.U.H. Khan, P. Wan, Preparation and characterization of flame retardant polyurethane foams containing phosphorus–nitrogen-functionalized lignin, RSC Adv. 4 (98) (2014) 55271–55279, https://doi.org/10.1039/C4RA08429B.

[70] Y. Matsushita, D. Hirano, D. Aoki, S. Yagami, Y. Takagi, K. Fukushima, A Biobased Flame-Retardant Resin Based on Lignin, Adv. Sustain. Syst. 1 (10) (2017) 1700073, https://doi.org/10.1002/adsu.201700073.

[71] R.E. Lyon, R.N. Walters, Pyrolysis combustion flow calorimetry, J. Anal. Appl. Pyrol. 71 (1) (2004) 27–46, https://doi.org/10.1016/S0165-2370(03)00096-2.

[72] R. Sonnier, H. Vahabi, L. Ferry, J.M. Lopez-Cuesta, Pyrolysis-Combustion Flow Calorimetry: A Powerful Tool To Evaluate the Flame Retardancy of Polymers, Fire and Polymers VI: New Advances in Flame Retardant Chemistry and Science, American Chemical Society (2012) 361–390. 10.1021/bk-2012-1118.ch024.

[73] S. Tretsiakova-McNally, P. Joseph, Thermal and Calorimetric Evaluations of Polyacrylonitrile Containing Covalently-Bound Phosphonate Groups, Polymers 10 (2) (2018) 131.

[74] Q. Luo, Y. Sun, B. Yu, C. Li, J. Song, D. Tan, J. Zhao, Synthesis of a novel DPPA-containing benzoxazine to flame-retard epoxy resin with maintained thermal properties, Polym. Adv. Technol. 30 (8) (2019) 1989–1995, https://doi.org/10.1002/pat.4631.

[75] A. Bifulco, D. Parida, K.A. Salmeia, R. Nazir, S. Lehner, R. Stämpfli, H. Markus, G. Malucelli, F. Branda, S. Gaan, Fire and mechanical properties of DGEBA-based epoxy resin cured with a cycloaliphatic hardener: Combined action of silica, melamine and DOPO-derivative, Mater. Des. 193 (2020), 108862, https://doi.org/10.1016/j.matdes.2020.108862.

[76] D. Montarnal, M. Capelot, F. Tournilhac, L. Leibler, Silica-Like Malleable Materials from Permanent Organic Networks, Science 334 (6058) (2011) 965–968.

[77] F. Van Lijsebetten, J.O. Holloway, J.M. Winne, F.E. Du Prez, Internal catalysis for dynamic covalent chemistry applications and polymer science, Chem. Soc. Rev. 49 (23) (2020) 8425–8438, https://doi.org/10.1039/D0CS00452A.

[78] Y. Li, T. Liu, S. Zhang, L. Shao, M. Fei, H. Yu, J. Zhang, Catalyst-free vitrimer elastomers based on a dimer acid: robust mechanical performance, adaptability and hydrothermal recyclability, Green Chem. 22 (3) (2020) 870–881, https://doi.org/10.1039/C9GC04080C.

[79] F.I. Altuna, C.E. Hoppe, R.J.J. Williams, Epoxy vitrimers with a covalently bonded tertiary amine as catalyst of the transesterification reaction, Eur. Polym. J. 113 (2019) 297–304, https://doi.org/10.1016/j.eurpolymj.2019.01.045.

[80] C. Hao, T. Liu, S. Zhang, W. Liu, Y. Shan, J. Zhang, Triethanolamine-Mediated Covalent Adaptable Epoxy Network: Excellent Mechanical Properties, Fast Repairing, and Easy Recycling, Macromolecules 53 (8) (2020) 3110–3118, https://doi.org/10.1021/acs.macromol.9b02243.

[81] T. Liu, S. Zhang, C. Hao, C. Verdi, W. Liu, H. Liu, J. Zhang, Glycerol Induced Catalyst-Free Curing of Epoxy and Vitrimer Preparation, Macromol. Rapid Commun. 40 (7) (2019) 1800889, https://doi.org/10.1002/marc.201800889.

[82] S. Zhang, T. Liu, C. Hao, L. Wang, J. Han, H. Liu, J. Zhang, Preparation of a lignin-based vitrimer material and its potential use for recoverable adhesives, Green Chem. 20 (13) (2018) 2995–3000, https://doi.org/10.1039/C8GC01299G.

[83] B. Xue, R. Tang, D. Xue, Y. Guan, Y. Sun, W. Zhao, J. Tan, X. Li, Sustainable alternative for bisphenol A epoxy resin high-performance and recyclable lignin-based epoxy vitrimers, Ind. Crops Prod. 168 (2021), 113583, https://doi.org/10.1016/j.indcrop.2021.113583.

[84] C. Hao, T. Liu, S. Zhang, L. Brown, R. Li, J. Xin, T. Zhong, L. Jiang, J. Zhang, A. High-Lignin-Content, Removable, and Glycol-Assisted Repairable Coating Based on Dynamic Covalent Bonds, ChemSusChem 12 (5) (2019) 1049–1058, https://doi.org/10.1002/cssc.201802615.

[85] L. Du, X. Jin, G. Qian, W. Yang, L. Su, Y. Ma, S. Ren, S. Li, Lignin-based vitrimer for circulation in plastics, coatings, and adhesives with tough mechanical properties, catalyst-free and good chemical solvent resistance, Ind. Crops Prod. 187 (2022), 115439, https://doi.org/10.1016/j.indcrop.2022.115439.

GENERAL CONCLUSION

The remarkable advancements made in enhancing the sustainability of polymeric materials have offered highly promising solutions to address both environmental and human health concerns. Renewability and recyclability have become worth concepts that rule the development of the next generation of polymeric materials, by considering a sustainable-by-design approach. The aim of this thesis was to investigate if these two concepts could be combined to develop new vitrimeric materials from lignin relying on the chemistry of benzoxazines. To reach this objective, this research works needed to address two main research axes: the development of lignin-based benzoxazine, and the development of benzoxazine-based vitrimers. The ultimate goal was in the end to develop a new approach for lignin-based vitrimers.

The first research axis centered on investigating the following research question: Can lignin macromonomers be chemically modified to create benzoxazine thermosets? The research work presented in the second chapter focuses on the development and characterization of benzoxazine precursors prepared from model molecules derived from lignin. The study leads to the conclusion that it would be needed to increase the amount of unsubstituted phenol in lignin biopolymer to produce lignin-derived benzoxazine. Therefore, a sustainable pathway was identified in chapter three to incorporate *ortho*-free phenols into lignin to increase the reactivity of lignin toward the chemistry of benzoxazine. The final chapter confirms that the reactivity of lignin for benzoxazine chemistry has been improved compared to the unmodified starting material, finally addressing the research question of this axis of investigation.

The investigations dedicated to the second research axis explored the possibility to design benzoxazine-based vitrimers. Benzoxazine is a type of phenolic resin that can be easily produced by sustainable and green chemistry synthetic pathways, and have also a chemical structure well suited for the design of catalyst-free vitrimers relying on transesterification exchanges. The initial hypothesis that benzoxazine can be used to develop vitrimers was first validated on a system composed of PEG_{400}, esterified with valeric acid, and condensed *via* a Mannich reaction with ethanolamine. The resulting structures were composed of the essential features for a vitrimer: ester bonds, aliphatic –OH groups, and tertiary amines, these later being involved in a neighbouring group participation promoting transesterification exchanges. The resulting vitrimers have a high T_g in the range of 120 °C, high mechanical properties, and can be recycled, reshaped, and able to self-heal efficiently in a short time. The investigation also focused on fine-tuning their thermomechanical and dynamic properties by varying their degree of functionality and crosslinking density. The fifth chapter describes how this approach can be extended to other building blocks, in this case isosorbide, thereby significantly broadening the scope of possibilities for this newly developed chemistry. The study also demonstrates the long-term stability of

the sugar-based vitrimer in various aqueous environments and proposes a mild chemical recycling route comparable to mechanical reprocessing.

The final chapter describes how the scientific knowledge generated from the two mentioned research axes can be used to achieve the development of lignin-derived benzoxazine materials, including vitrimers relying on transesterification exchanges. It concludes this research work by providing evidence that the chemistry of benzoxazine is suitable to design lignin-derived materials and vitrimers.

Given the wide number of available precursors and their possible combinations, the new synthetic route detailed in this manuscript opens up to an infinite range of opportunities to design benzoxazine-based vitrimers. However, many research questions still need to be addressed:

➢ An investigation that is still in progress concerns a concerted mechanism occurring between the transesterification and the ring-opening polymerization of benzoxazines. Indeed, the ROP of benzoxazine is generally triggered at a temperature above 190 °C for long duration. The crosslinking of benzoxazine-based vitrimers occurs at 140 °C and takes a couple of minutes. To shed more light on this phenomenon, a series of model benzoxazine molecules composed of permanent and dynamic bonds has been developed and the products of the internally catalyzed transesterification reactions have been analysed by spectroscopic and coupled thermogravimetric analysis. The study is still in progress but reveals that synergistic effects of catalyst-free exchange and benzoxazine ring-opening polymerization occurs. A publication is planned to be submitted in the coming months.

➢ Another anomaly also detected in benzoxazine-based vitrimers concerns a non-linear relationship between the rate of conversion of polybenzoxazine and their viscoelastic properties like the stress relaxation. Indeed, many experiments tends to conclude that the response is parabolic, with relaxation times surprisingly long around a conversion rate of 50%, and much shorter for lower and higher conversion rate. This topic deserves more investigations.

➢ The recycling performance of benzoxazine-based vitrimers, effective at the macroscopic level, is based on topological rearrangements and the occurrence of reversible exchanges in the dynamic network. The optimization and understanding of the process still needs significant investigations. While the successful demonstration of resin recycling is commendable, it is crucial to shift the focus to the manufacturing level and explore efficient ways of utilizing recycled materials. How can recycling be effectively integrated into the manufacturing process is still a research question to address.

- The manufacturing of composites made of these vitrimers is still a field of investigation. Even if significant progresses have been done in projects started in parallel of this thesis at LIST, many developments are still needed to compete with the manufacturing of composites with conventional resins.

- The introduction of exchangeable bonds in cross-linked networks must equal and ideally improve the mechanical, dimensional, and thermal properties of thermosets. The resistance to creep of the materials has also to be investigated and demonstrated, as long-term stability is crucial for final parts, regardless of the service conditions.

- One limitation of the materials developed in this thesis is their susceptibility to water-induced plasticization, owing to the presence of polar groups such as ester bonds and hydroxyl groups, which restricts their potential applications. Results on lignin-based vitrimers offers a promising opportunity to enhance this property, but further research is required to fully address this challenge.

- This study presents a methodology for converting a specific type of lignin into a benzoxazine vitrimer. However, there are many other types of lignin, depending on their source or method of extraction. Additional investigations would be needed to explore the extension of this method to these lignins.

- Finally, the societal and environmental impact of the polymeric materials produced in this thesis should be assessed though a life cycle analysis (LCA) methodology. Alongside the environmental burdens associated with their production, the dynamic covalent bonds should be compatible with different classes of polymers and economically accessible for industrial processes.

In summary, this thesis has examined the potential of vitrimers derived from lignin as a promising avenue for the development of sustainable materials. It was successfully demonstrated that lignin can be converted into benzoxazine-based vitrimers, with remarkable thermal, mechanical, and vitrimer properties. These findings emphasize the significance of lignin as a valuable precursor for the creation of environmentally friendly materials with enhanced performances. However, further investigations are required to optimize synthesis processes, explore alternative sources of lignin, and evaluate the scalability of lignin-based vitrimers for industrial applications. This thesis provides a foundation for future advancements in lignin-based vitrimer research, contributing to the progress of sustainable materials and supporting the realization of a more environmentally respectful future.

Annexes

Annex I: Elucidating the thermal and polymerization behaviours of benzoxazines from lignin derivatives

Elucidating the thermal and polymerization behaviours of benzoxazines from lignin derivatives

Antoine Adjaoud[a, b], Acerina Trejo-Machin[a,b], Laura Puchot[a], Reiner Dieden[a] and Pierre Verge[*a]

a. Luxembourg Institute of Science and Technology, Materials Research and Technology Department, 5 Avenue des Hauts Fourneaux, L-4362 Esch-sur-Alzette (Luxembourg)

b. University of Luxembourg, 2, Avenue de l'Université, L-4365 Esch-sur-Alzette (Luxembourg)

Correspondence to: *Pierre Verge (pierre.verge@list.lu)*

SUPPORTING INFORMATION CONTENT

Figure S1. *^{1}H NMR (in DMSO-d6(*)) of G-fa Bz. (**water)*

Figure S2. *^{1}H NMR (in DMSO-d6(*)) of V-fa Bz. (**water)*

	Assignment	Chemical shift [ppm]	Theoretical integration	Experimental integration
G-fa	N-CH$_2$-Ar [2]	3.82	2.00 H	1.99 H
	N-CH$_2$-O [1]	4.82	2.00 H	1.98 H
	-OCH$_3$ [5]	3.73	3.00 H	3.03 H
	-NCH$_2$ [6]	3.82	2.00 H	2.00 H
	*H-Ar [4,10]	6.80	2.00 H	1.98 H
Cr-fa	N-CH$_2$-Ar [2]	3.84	2.00 H	2.01 H
	N-CH$_2$-O [1]	4.77	2.00 H	2.00 H
	-OCH$_3$ [5]	3.72	3.00 H	3.02 H
	-NCH$_2$ [6]	3.81	2.00 H	2.00 H
	*Ar-CH$_3$ [10]	2.19	3.00 H	3.02 H
V-fa	N-CH$_2$-Ar [2]	4.01	2.00 H	1.98 H
	N-CH$_2$-O [1]	4.98	2.00 H	1.98 H
	-OCH$_3$ [5]	3.83	3.00 H	2.98 H
	-NCH$_2$ [6]	3.84	2.00 H	2.00 H
	*(-(C=O)-H [10]	9.79	1.00 H	0.98 H
MV-fa	N-CH$_2$-Ar [2]	3.97	2.00 H	2.00 H
	N-CH$_2$-O [1]	4.94	2.00 H	2.00 H
	-OCH$_3$ [5,10]	3.81	6.00 H	5.96 H
	-NCH$_2$ [6]	3.82	2.00 H	2.00 H
	*-(C=O)-O-CH$_3$ [5,10]	3.81	6.00 H	5.96 H
VA-fa	N-CH$_2$-Ar [2]	3.97	2.00 H	1.99 H
	N-CH$_2$-O [1]	4.92	2.00 H	1.98 H
	-OCH$_3$ [5]	3.80	3.00 H	3.04 H
	-NCH$_2$ [6]	3.82	2.00 H	2.00 H
	*-(C=O)-OH [10] (From solid ^{1}H NMR)	13-16	-	-

Table S1. *NMR data corresponding to the –CH$_2$ resonance signals of the oxazine rings of the pure BZ monomers: G-fa, Cr-fa, V-fa, MV-fa, VA-fa.*
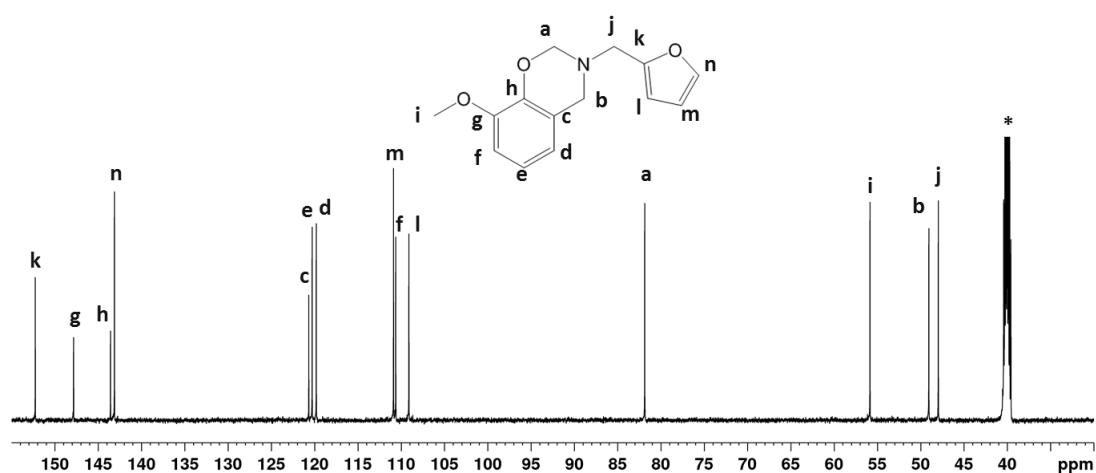
Figure S3. ^{13}C NMR (in DMSO-d6(*)) of G-fa Bz.
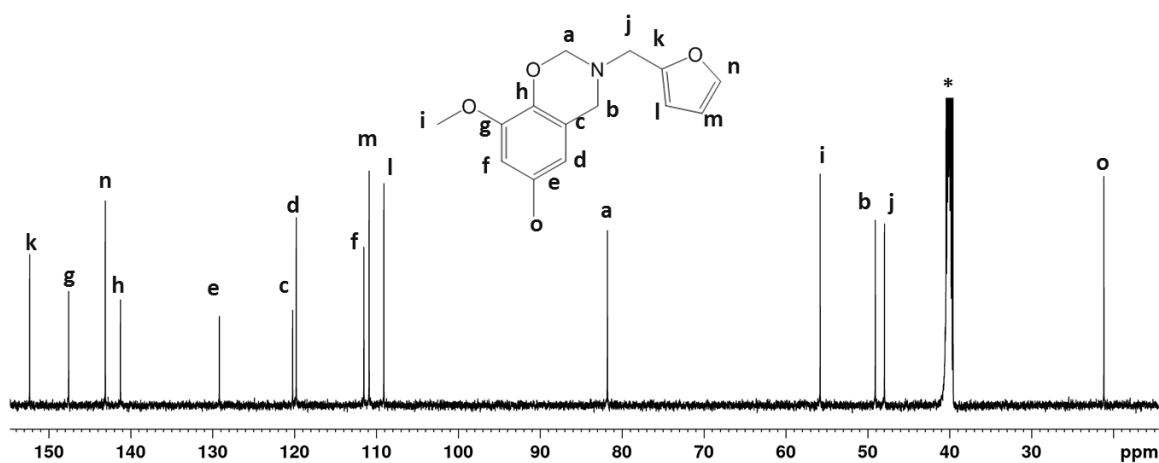
Figure S4. ^{13}C NMR (in DMSO-d6(*)) of Cr-fa Bz.
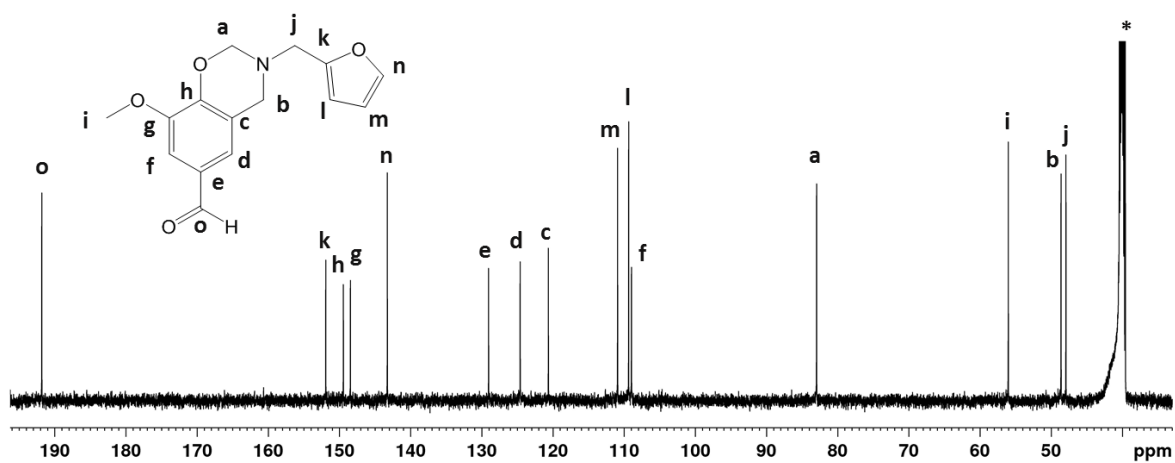
Figure S5. ^{13}C NMR (in DMSO-d6(*)) of V-fa Bz.
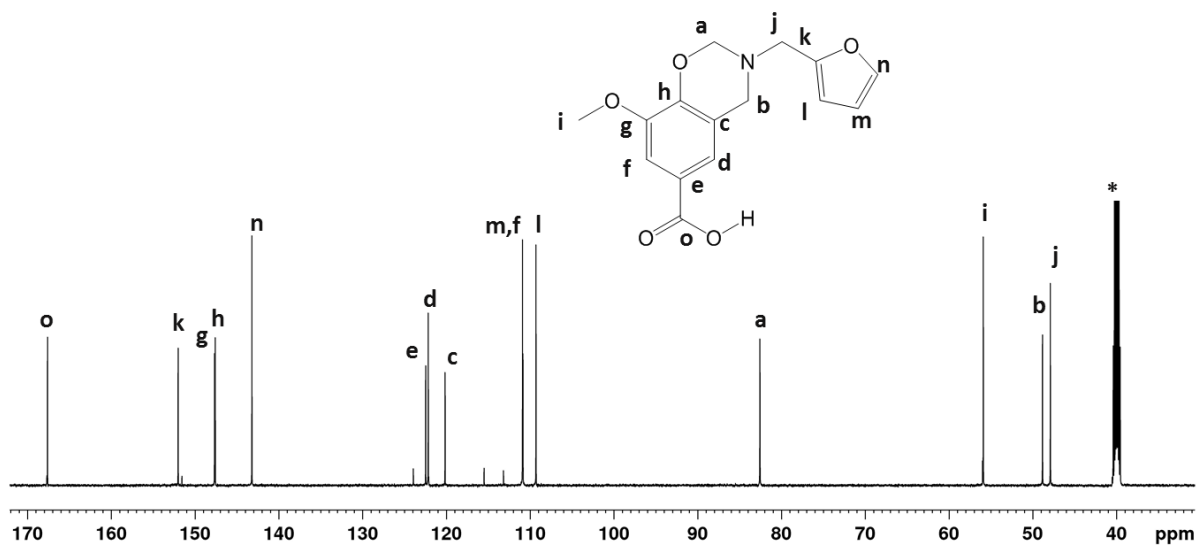
Figure S6. ^{13}C NMR (in DMSO-d6(*)) of VA-fa Bz.
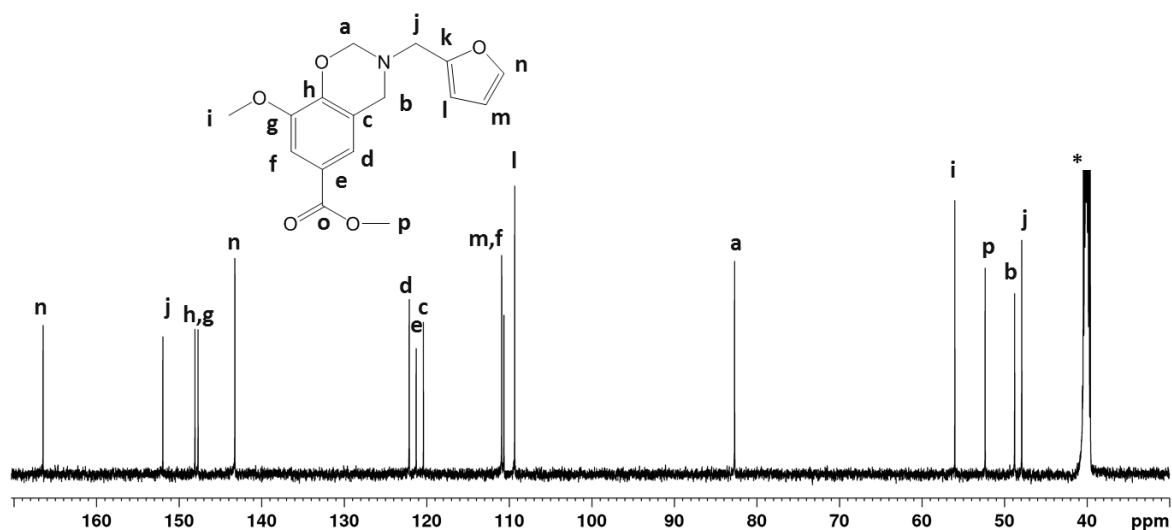
Figure S7. ^{13}C NMR (in DMSO-d6(*)) of MV-fa Bz.
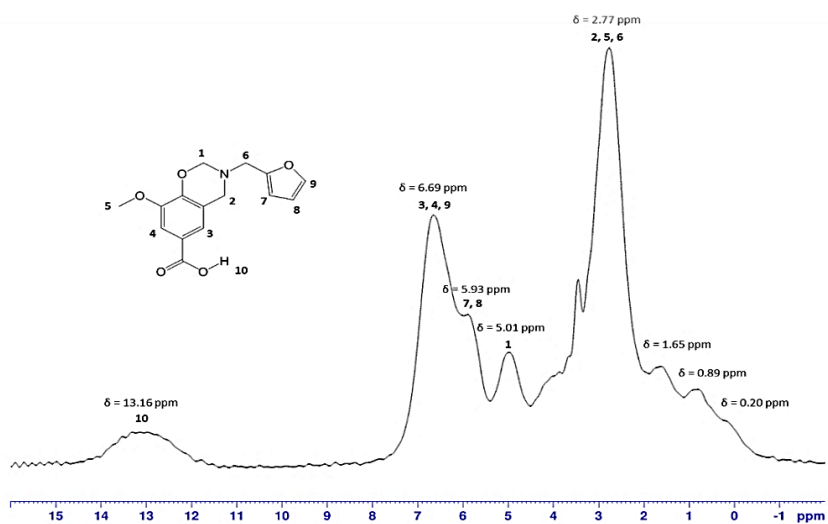
Figure S8. Solid state ^1H NMR of VA-fa monomer acquired using CRAMPS.
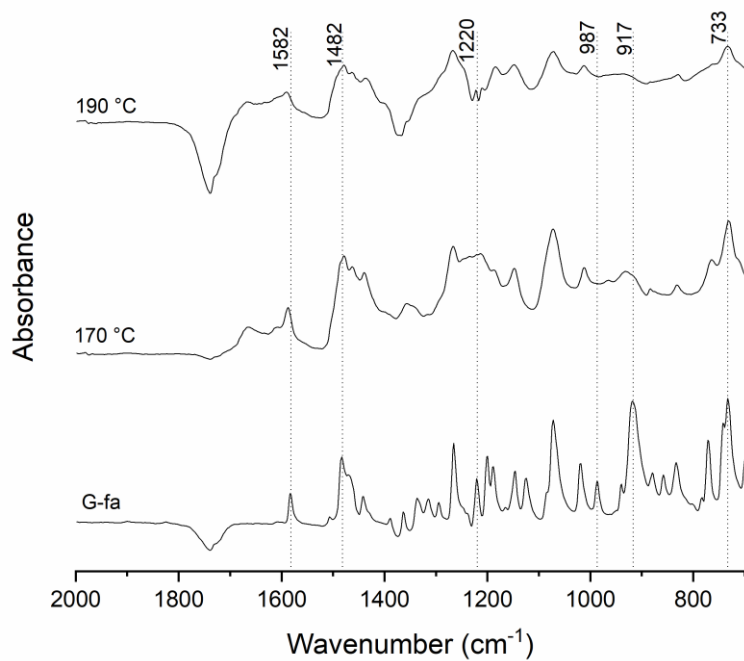
Figure S9. FTIR spectrum of G-fa Bz monomer, after 1 h at 170 °C and 30 min at 190 °C.
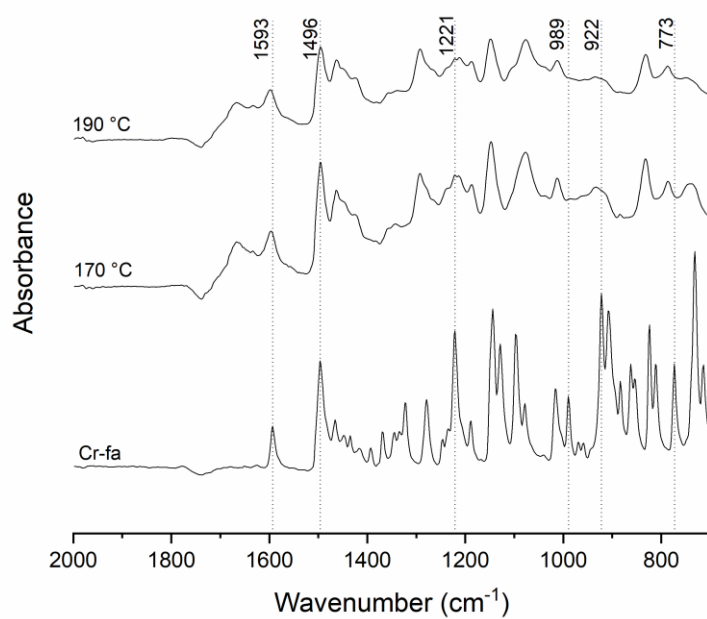
Figure S10. FTIR spectrum of Cr-fa Bz monomer, after 1 h at 170 °C and 30 min at 190 °C.
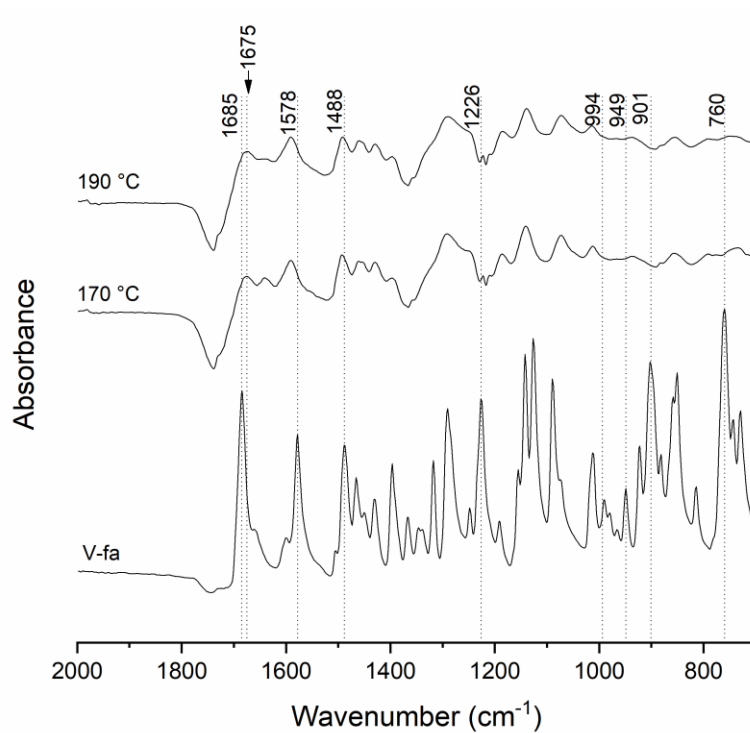
Figure S11. FTIR spectrum of V-fa Bz monomer, after 1 h at 170 °C and 30 min at 190 °C.
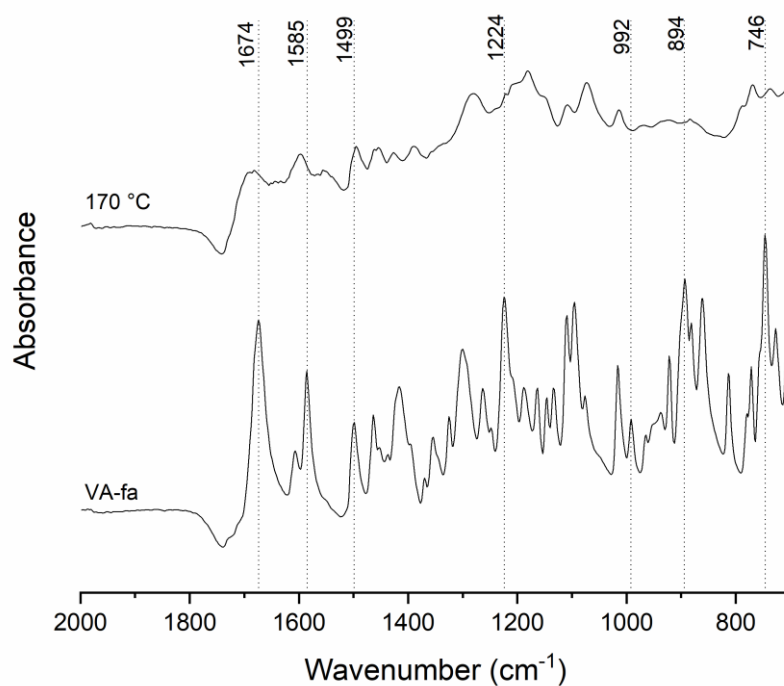
Figure S12. FTIR spectrum of VA-fa Bz monomer, after 1 h at 170 °C and 30 min at 190 °C.
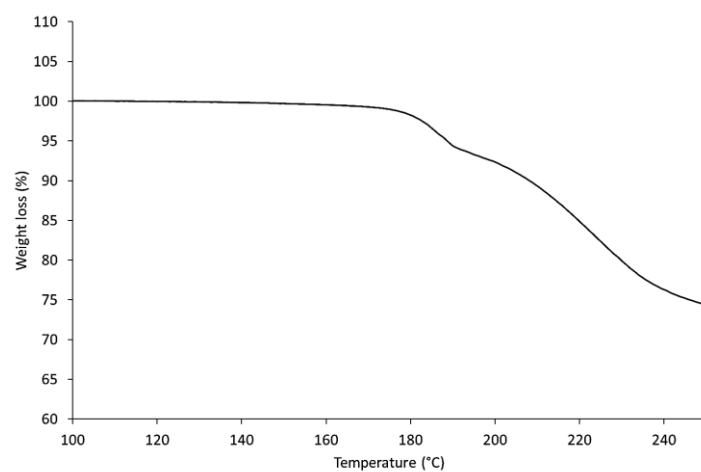
Figure S13. *TGA thermogram of VA-fa monomer under N_2 atmosphere.*
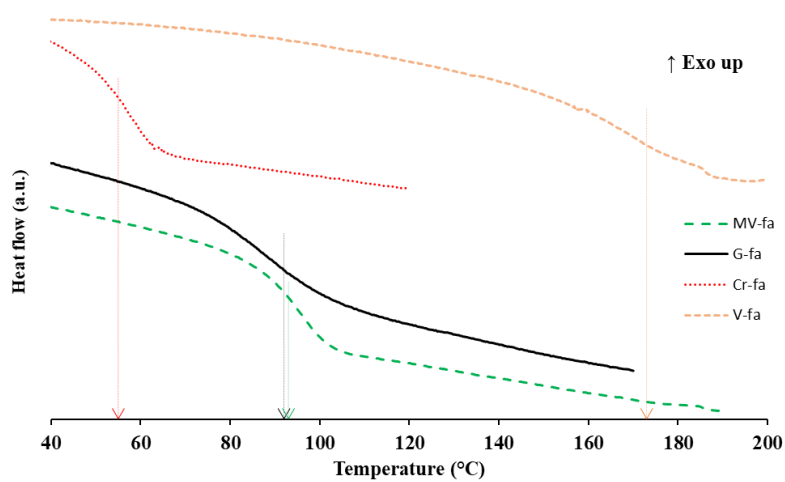
Figure S14. *DSC thermograms of poly(MV-fa), poly(G-fa), poly(Cr-fa) and poly(V-fa) (N_2, 10 °C·min^{-1})*
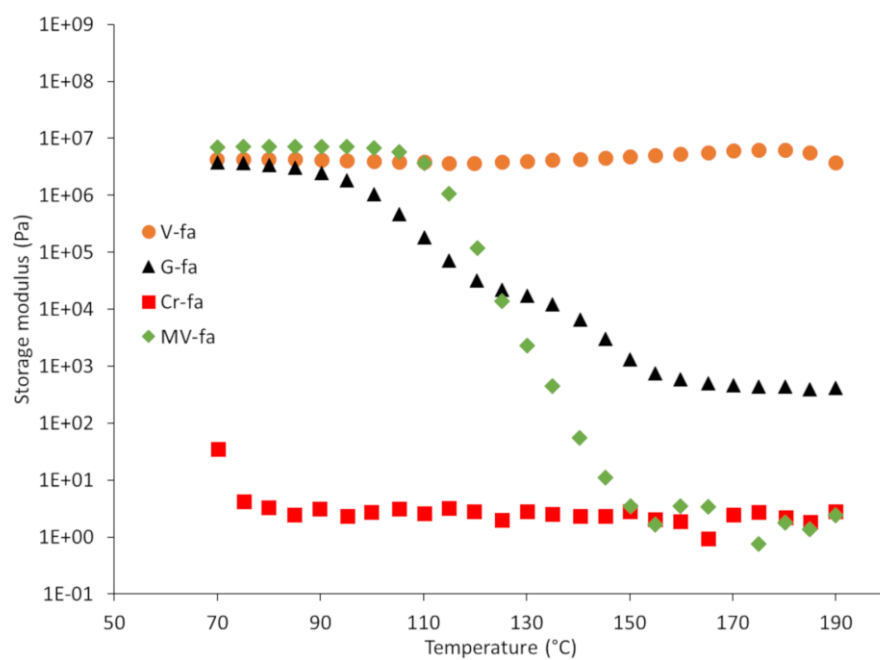
Figure S15. *Evolution of the storage modulus of poly(MV-fa), poly(G-fa), poly(Cr-fa) and poly(V-fa) as a function of the temperature.*
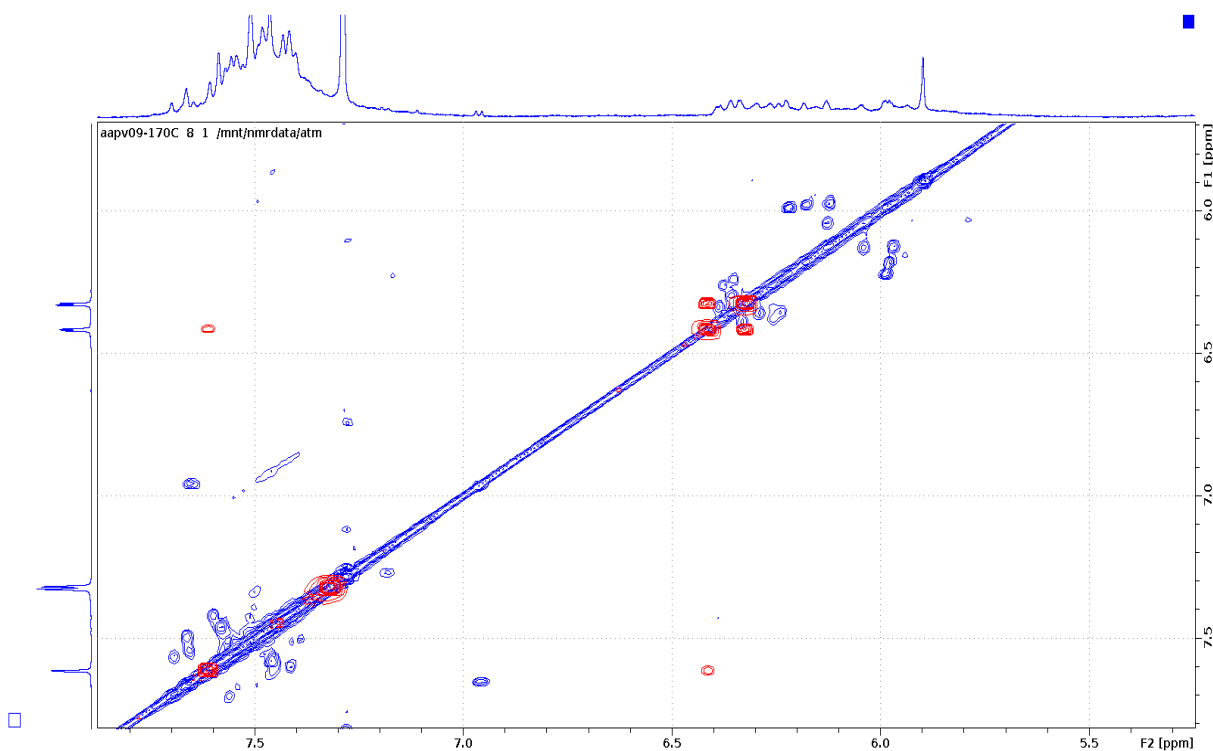
Figure S16. *Comparison of the COSY spectra of MV-fa (red, left projection) and polymerized poly(MV-fa) (blue, top projection).*

Annex II: Sustainable Esterification of a Soda Lignin with Phloretic Acid

Sustainable Esterification of a Soda Lignin with Phloretic Acid

Antoine Adjaoud [1,2], Reiner Dieden [1], Pierre Verge [1,*]

[1] Luxembourg Institute of Science and Technology, Materials Research and Technology Department, 5 Avenue des Hauts-Fourneaux, L-4362 Esch-sur-Alzette, Luxembourg; antoine.adjaoud@list.lu (A.A.); reiner.dieden@list.lu (R.D.)

[2] University of Luxembourg, 2, Avenue de l'Université, L-4365 Esch-sur-Alzette, Luxembourg

* Correspondence: pierre.verge@list.lu (P.V.)

Table of figures

➤ **Thermogravimetric analysis of Protobind® grades**

Figure S1 TGA and DTG curves of Protobind® lignin

TGA curves of the different grades of the Protobind® lignin are reported in Figure S1. The moisture content, the onset of thermal degradation (T_{onset}), the major degradation temperatures (A, B, C), and the char residue at 800 °C are gathered in Table S1. The DTG curves of the different grades of Protobind® lignin exhibited roughly similar decomposition pattern that can be sundered in three degradation ranges: A around 180°C, B around 300°C and the major degradation D around 350°C. The onset of the degradation temperature depends on the Protobind® grade. Although the highest T_{onset} is observed for the grade P2400 (157 °C), this grade exhibits the lowest char yield (33.9 %). The other grades of Protobind® lignin displayed a char yield around 37-38 %, with the highest obtained for the grade P4000 (39.4 %).

Table S1 Thermogravimetric analysis of the various grades of Protobind® lignin (10 °C.min^{-1}, N$_2$)

Protobind® grades	[a] T_{onset} (°C)	[a] Major degradation temperature (°C)			[b] Char (%)
		A	B	C	
P1000	130	-	259	369	37.6
P2000	124	-	247	361	36.7
P2400	157	-	299	359	33.9
P4000	121	207	302	342	39.4
P6000	115	169	283	348	38.5

[a] determined from the first derivative, [b] at 800 °C.

➢ **Structural characterization of the esterified lignin**

Table S2 Assignments of the lignin $^{13}C-^1H$ correlation peaks in the 2D HSQC spectra of P2400 and P2400-PA

Label	δ_C/δ_H (ppm)	Assignments	P2400	P2400-PA
B_3	30.0/2.75	C_3-H_3 in substructure **B**		x
B_2	36.1/2.57	C_2-H_2 in substructure **B**		x
C_β	54.2/3.09	$C_\beta-H_\beta$ in resinol β- β′ substructure **C**	x	x
$-OCH_3$	56.5/3.76	$C-H$ in methoxyl **–OMe**	x	x
A_x	60.8/3.52	C_x-H_x in substructure **A**	x	
$B_{x'}$	63.8/4.12	$C_{x'}-H_{x'}$ in substructure **B**		x
A_{-O-Alk}	70.3/3.52	$C_{-O-Alk}-H_{-O-Alk}$ in substructure **A**	x	
B_{-O-Alk}	70.3/3.52	$C_{-O-Alk}-H_{-O-Alk}$ in substructure **B**		x
C_γ	71.6/4.20;3.82	$C_\gamma-H_\gamma$ in resinol β- β′ substructure **C**	x	x
X_2	73.1/3.13	C_2-H_2 in xylan substructure **X**	x	x
X_3	74.6/3.33	C_3-H_3 in xylan substructure **X**	x	x
X_4	75.9/3.58	C_4-H_4 in xylan substructure **X**	x	x
$S_{2,6}$	104.2/6.71	$C_{2,6}-H_{2,6}$ in syringyl units **S**	x	x
$S'_{2,6}$	106.8/7.27	$C_{2,6}-H_{2,6}$ in α-oxidized syringyl units **S′**	x	
Fa_2	111.2/7.41	C_2-H_2 in ferulate **Fa**	x	
G_2	112.6/6.83	C_2-H_2 in guaiacyl units **G**	x	x
B_6	115.6/6.69	C_6-H_6 in substructure **B**		x
G_5	115.6/6.70	C_5-H_5 in guaiacyl units **G**	x	x
Pc_β	115.8/6.32	$C_\beta-H_\beta$ in *p*-coumarate **Pc**	x	
Fa_β	116.1/6.40	$C_\beta-H_\beta$ in ferulate **Fa**	x	
G_6	119.3/6.78	C_6-H_6 in guaiacyl units **G**	x	x
$H_{2,6}$	128.8/7.06	$C_{2,6}-H_{2,6}$ in *p*-hydroxyphenyl units **H**	x	x
B_5	129.7/7.02	C_5-H_5 in substructure **B**		x
$Pc_{2,6}$	130.6/7.53	$C_{2,6}-H_{2,6}$ in *p*-coumarate **Pc**	x	
Pc_α	144.7/7.55	$C_\alpha-H_\alpha$ in *p*-coumarate **Pc**	x	
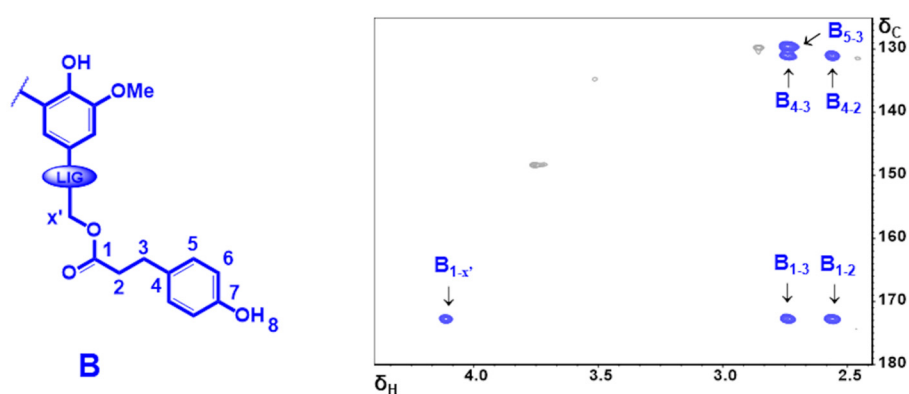
Figure S2 Aromatic region in the 2D HMBC NMR spectra of P2400-PA (δ_C/δ_H: 125−180/2.4−4.4). Signal assignments are reported in Table S3.

Table S3 Assignments of the lignin $^{13}C-^1H$ correlation peaks in the 2D HMBC spectra of P2400-PA

Label	δ_C/δ_H (ppm)	Assignments
B_{5-3}	129.7/2.75	$C_5–H_3$ in substructure **B**
B_{4-2}	131.0/2.57	$C_4–H_2$ in substructure **B**
B_{4-3}	131.0/2.75	$C_4–H_3$ in substructure **B**
B_{1-2}	172.8/2.57	$C_1–H_2$ in substructure **B**
B_{1-3}	172.8/2.75	$C_1–H_3$ in substructure **B**
$B_{1-x'}$	172.8/4.12	$C_1–H_{x'}$ in substructure **B**
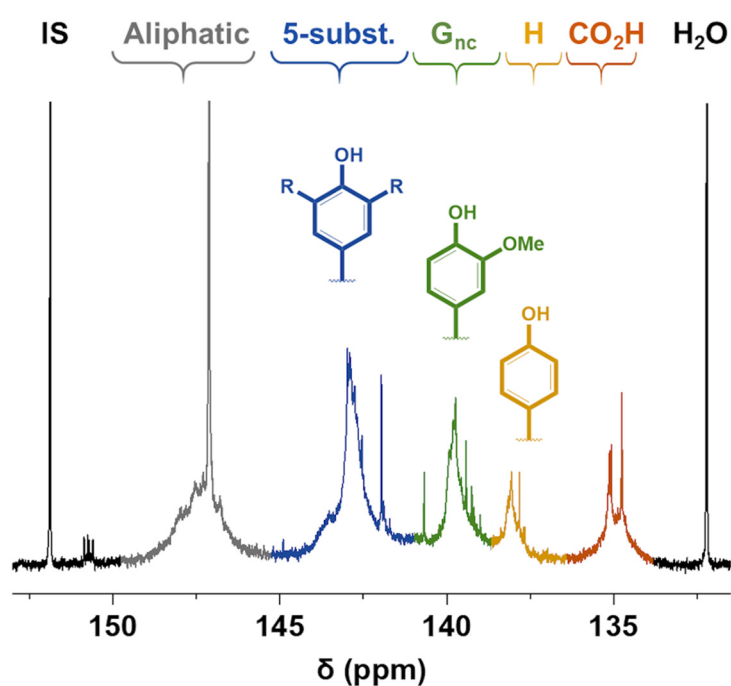
Figure S3 ^{31}P NMR spectra of P2400 (R= -OMe, -O-lignin, lignin)
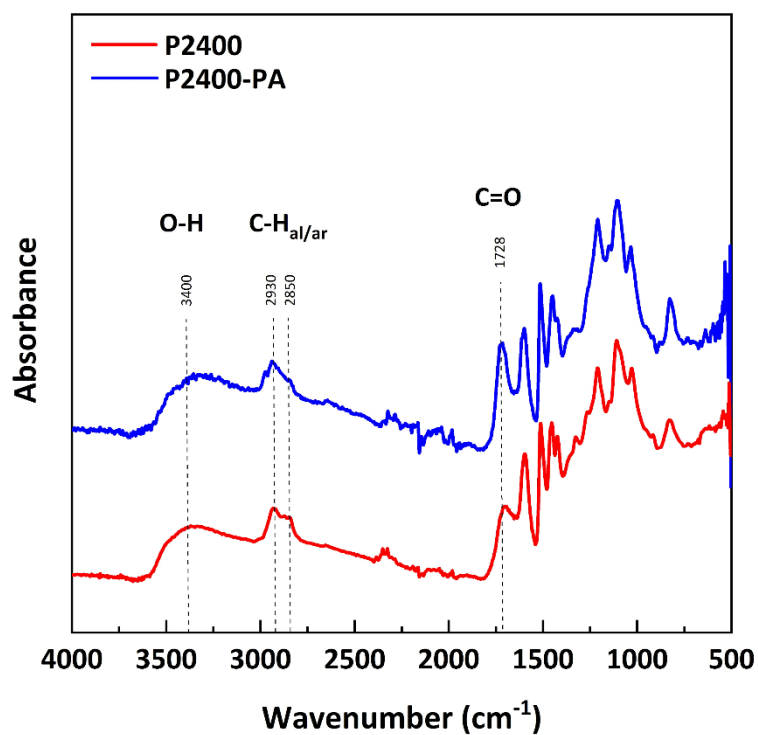
Figure S4 FTIR spectra of P2400 and P2400-PA

➤ **Design of Experiment methodology**

$Y = 7.36 + 8.18 \cdot n + 4.66 \cdot c + 0.06 \cdot I_{tn} + 0.91 \cdot I_{nc}$

$R^2 = 0.994$
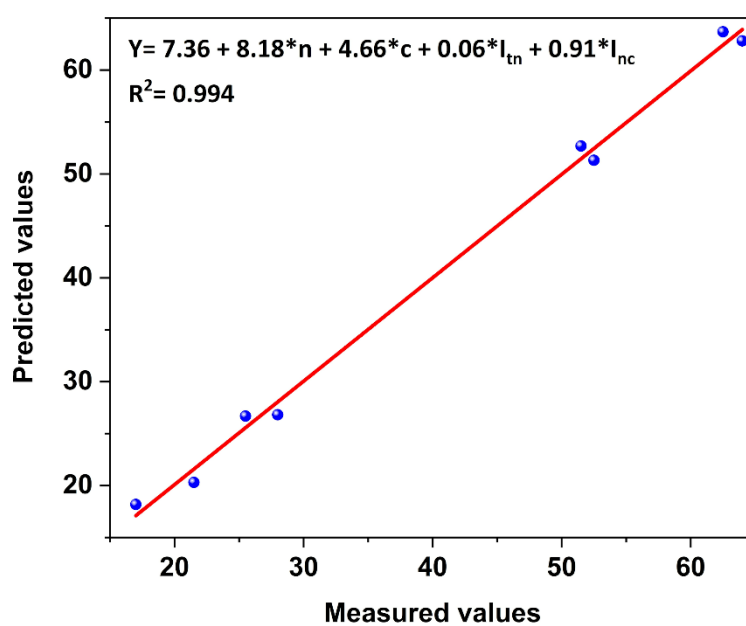
Figure S5 Linear predictive model, equation **(4)**

Evaluation of the predictive model (EL-9): $Y = 7.36 + 8.18 \cdot 3 + 4.66 \cdot 1.5 + 0.06 \cdot 30 \cdot 3 + 0.91 \cdot 3 \cdot 1.5 = 48.5$ %

Table S4 Effect and p-values of the individual variables and their first order interaction effects for the esterification of P2400 with PA

Model	Factor	t	n	c	I_{tn}	I_{tc}	I_{nc}
Linear predictive model **(4)**	Effect	Ø	10.1019	3.2330	4.9669	Ø	-2.2669
	p	Ø	0.002	0.048	0.016	Ø	0.108
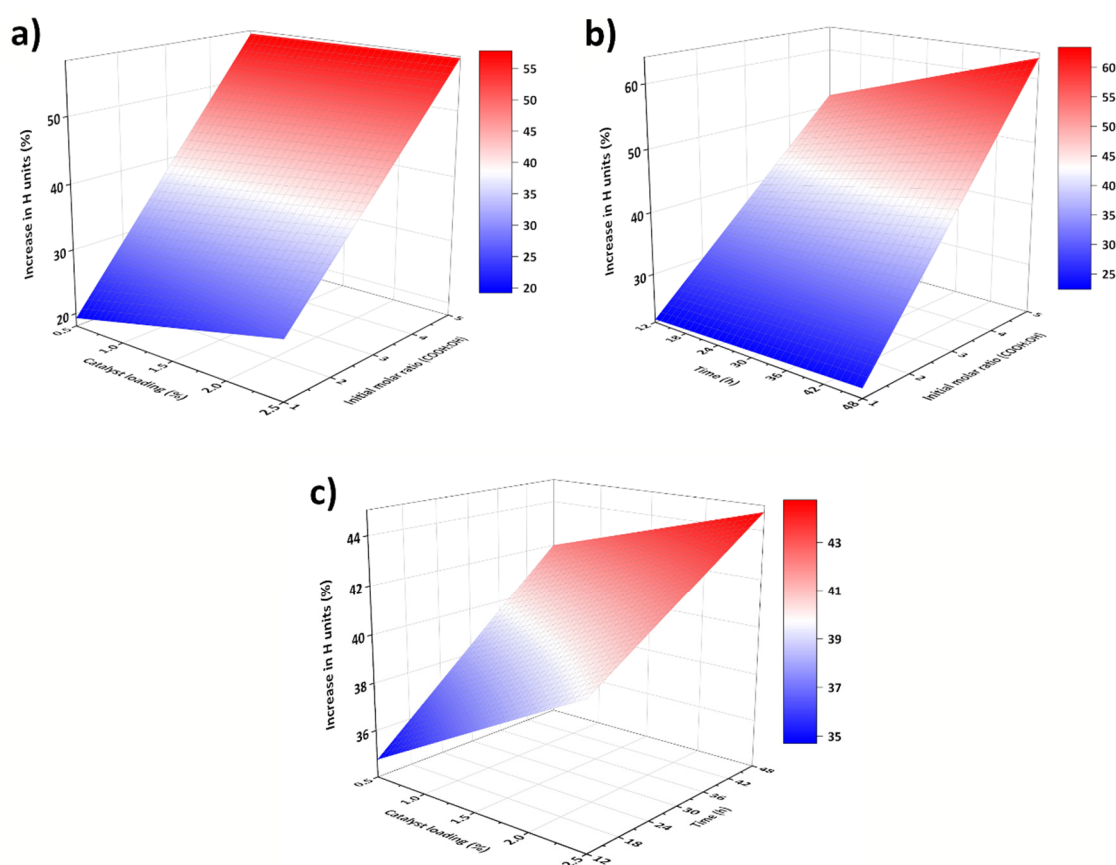
Figure S6 Surface response associated to a) c/n, b) t/ n and c) c/t critical variables

➢ **Physicochemical properties of the esterified lignin**

Table S5 Hansen partial solubility parameters of the solvent used for the solubility assays

Solvent	δ_D (MPa$^{1/2}$)	δ_P (MPa$^{1/2}$)	δ_H (MPa$^{1/2}$)
Acetone (ACE)	15.5	10.4	7.0
Acetonitrile (ACN)	15.3	18.0	6.1
Chloroform (CHCl$_3$)	17.8	3.1	5.7
Dichloromethane (DCM)	17.0	7.3	7.1
Diethyl ether (DET)	14.5	2.9	4.6
Dimethyl formamide (DMF)	17.4	13.7	11.3
Dimethyl sulfoxide (DMSO)	18.4	16.4	10.2
Dioxane (DIOX)	17.5	1.8	9.0
Ethanol (EtOH)	15.8	8.8	19.4
Ethyl acetate (ETAC)	15.8	5.3	7.2
Methanol (MeOH)	14.7	12.3	22.3
Methyl ketone (MEK)	16.0	9.0	5.1
Pyridine (PYR)	19.0	8.8	5.9
Tetrahydrofuran (THF)	16.8	5.7	8.0
Toluene (TOL)	18.0	1.4	2.0
Water (H$_2$O)	15.5	16	42.3
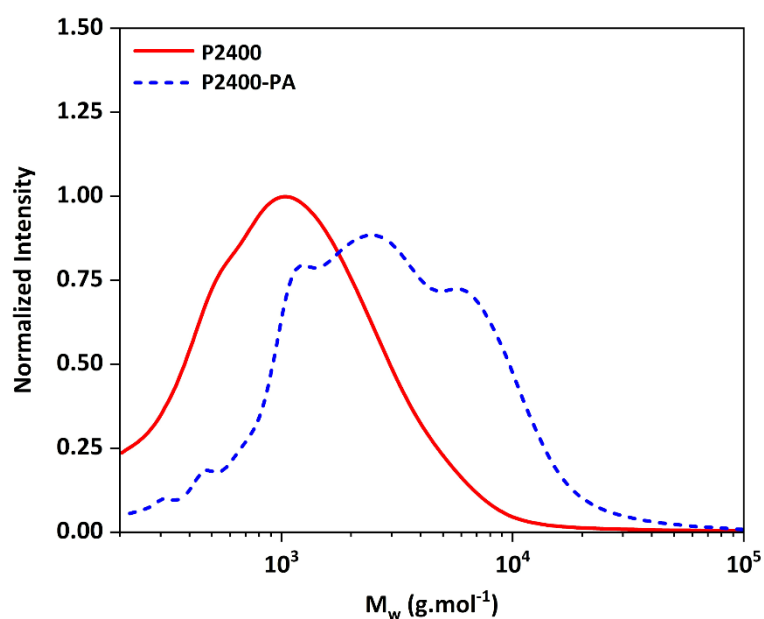
Figure S7 Weight average molecular weight of P2400 and P400-PA (4 mg.ml^{-1} in THF)
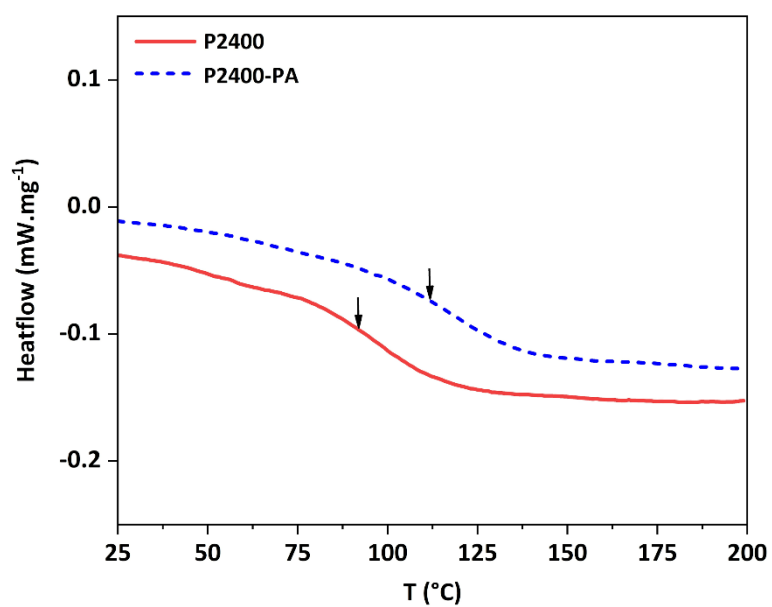
Figure S8 DSC thermogram of P2400 and P400-PA (10 °C.min^{-1}, N$_2$)

Annex III: Polybenzoxazines a sustainable platform for the design of fast responsive and catalyst-free vitrimers based on transesterification exchanges

Polymer Chemistry

ELECTRONIC SUPPORTING INFORMATION

Polybenzoxazines: a sustainable platform for the design of fast responsive and catalyst-free vitrimers based on trans-esterification exchanges

Antoine Adjaoud[a,b], Acerina Trejo-Machin[a,b], Laura Puchot[a] and Pierre Verge[*a]

[a] Luxembourg Institute of Science and Technology, Materials Research and Technology Department, 5 Avenue des Hauts-Fourneaux, L-4362 Esch-sur-Alzette (Luxembourg)

[b] University of Luxembourg, 2, Avenue de l'Université, L-4365 Esch-sur-Alzette (Luxembourg)

*To whom correspondence should be addressed.
E-mail: pierre.verge@list.lu

Table of figures

Table S1. Optimization of the conditions of reaction

Reaction step	Solvent	Time (h)	Temperature (°C)	Yield (%)
1. Fischer esterification	Ø	24	110	86
	Ø	24	130	97
2. Mannich condensation	Ø	3	70	70
	Ø	3	85	69
	Ø	3	100	Ø*
	Ø	12	70	66
	Ø	12	85	Ø*
	Ø	2.5 (+0.5)	85 (+90)	75
	Butanone	2.5 (+0.5)	85 (+90)	Ø**

* cross-linked, ** Viscous reddish material corresponding to hydroxybenzylaminoethanol
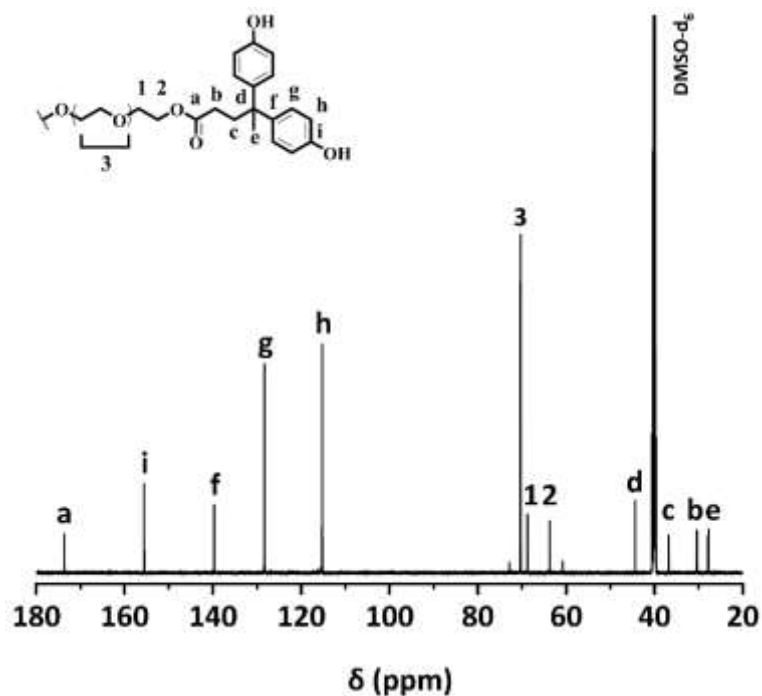
Figure S1 ^{13}C NMR spectra of PEG$_{400}$-DPA in DMSO-d$_6$
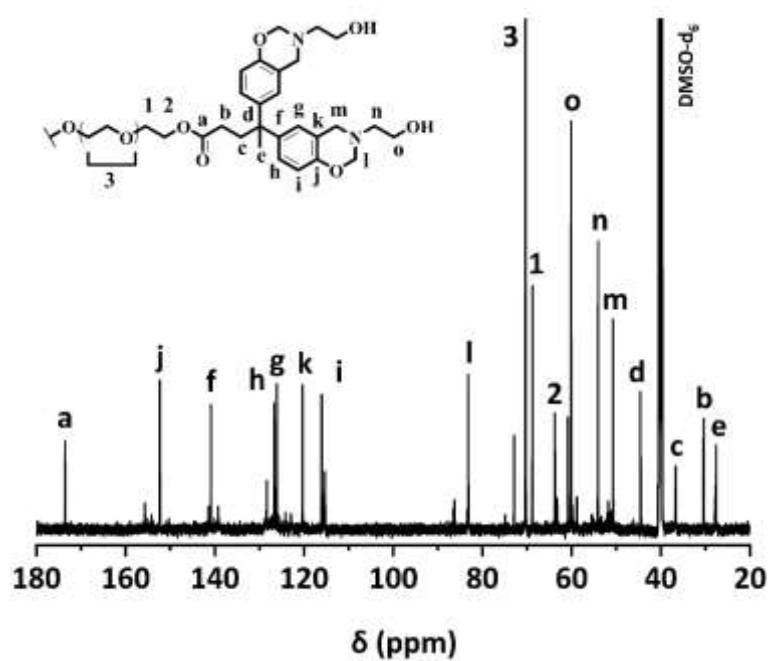
Figure S2 ^{13}C NMR spectra of PEG$_{400}$-DPA–mea in DMSO-d$_6$
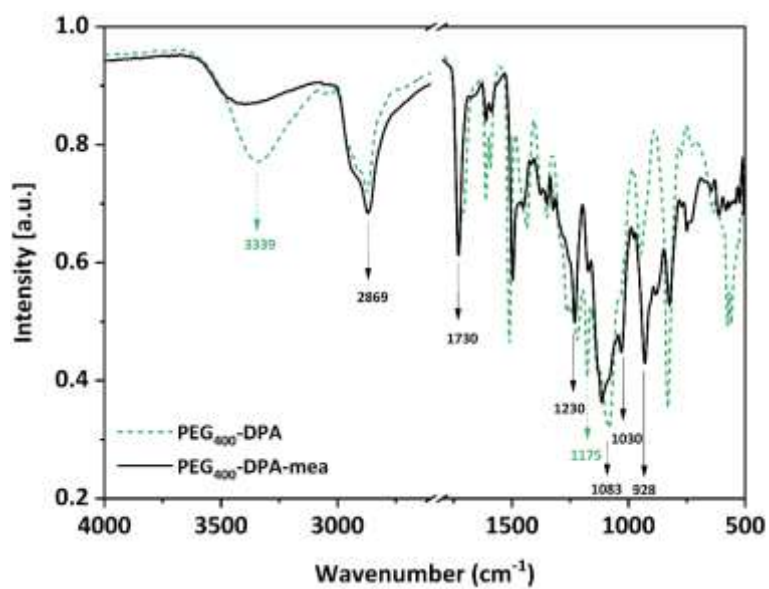
Figure S3 FTIR spectra of PEG$_{400}$-DPA (green) and PEG$_{400}$-DPA-mea (black)
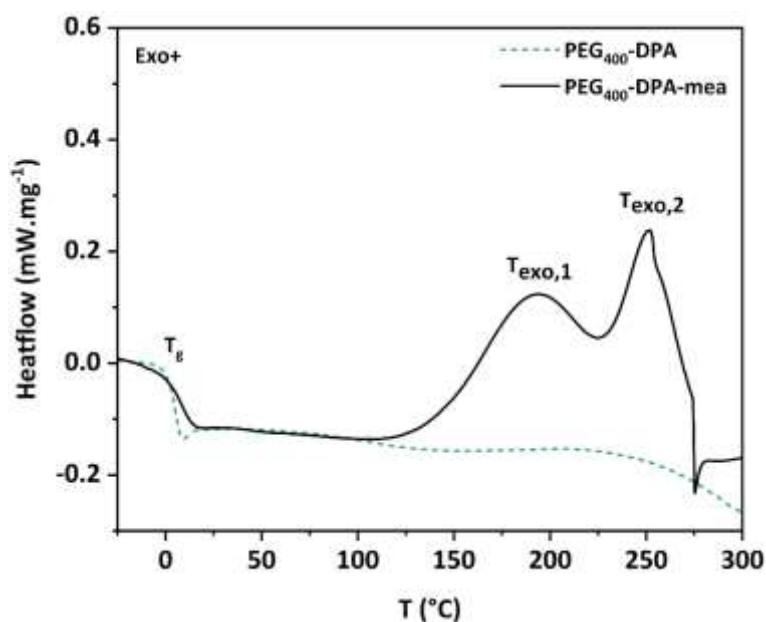
Figure S4 DSC thermogram of PEG_{400}-DPA (green) and PEG_{400}-DPA-mea (black) (10 °C.min^{-1}, N_2 atmosphere)
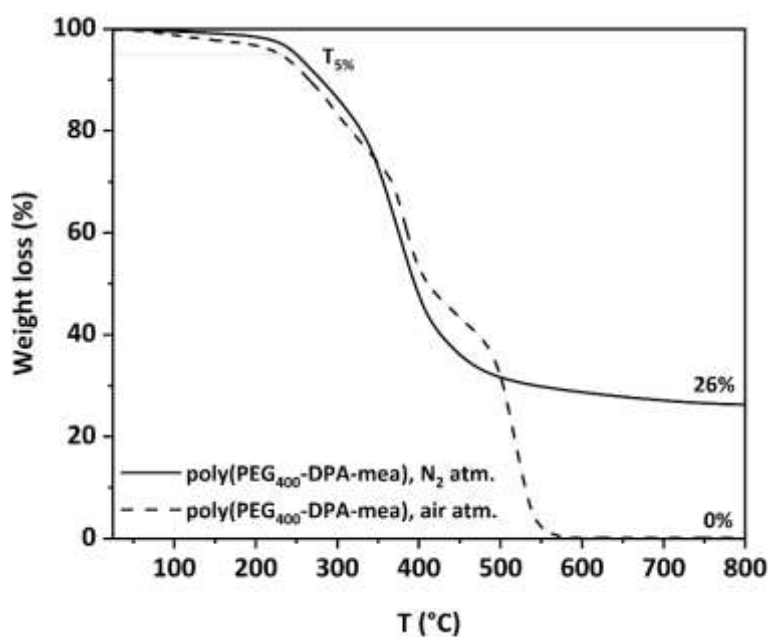
Figure S5 TGA thermogram of poly(PEG_{400}-DPA-mea) (10 °C.min^{-1}, N_2 and air atmosphere)

The thermal stability of poly(PEG_{400}-DPA-mea), monitored by TGA (N_2, 10 °C·min^{-1}), was represented by a two-step degradation process. The first degradation step, starting at $T_{5\%}$= 248 °C, may correspond to the thermal decomposition of the aliphatic ester[49] and is consistent with the DSC measurements. The second thermal degradation stage (starting around T≈ 380 °C) was assigned to the degradation of the polymer backbone, terminating with the formation of a char at 800 °C (char yield = 26%).
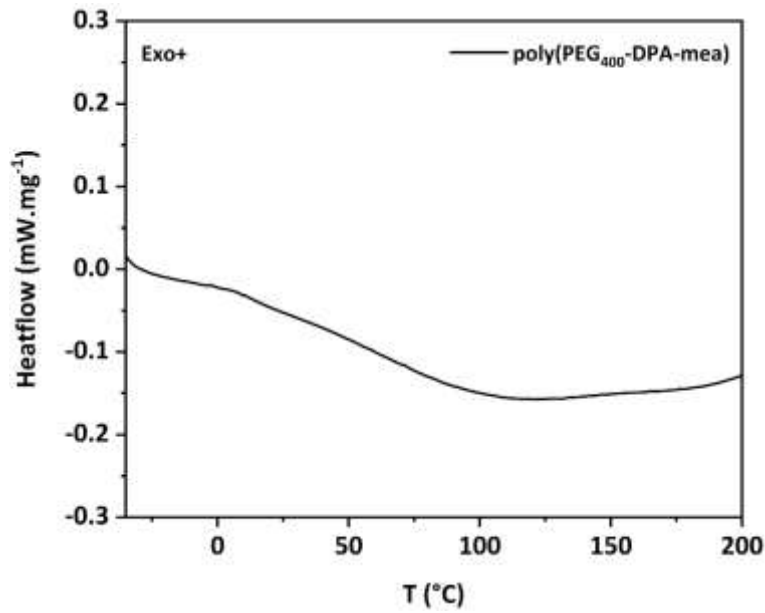
Figure S6 DSC thermogram of poly(PEG$_{400}$-DPA-mea) (10 °C.min^{-1}, N$_2$ atmosphere)
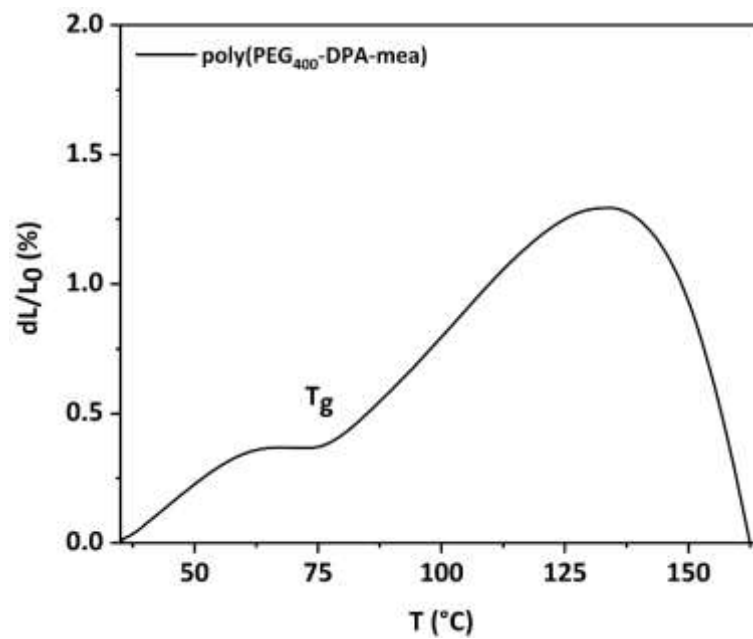
Figure S7 Dilatometry thermogram of poly(PEG$_{400}$-DPA-mea) (2 °C·min^{-1})

> ### *Determination of the activation energy (Ea) from the stress relaxation experiment*

Arrhenius model: $\tau^* = \tau_0 \cdot e^{\wedge}(Ea/R \cdot T) \leftrightarrow \ln(\tau^*) = Ea/(R \cdot T) + \ln(\tau_0) \Rightarrow$ Arrhenius plot: $\ln(\tau^*) = f(1/T)$.

Equation extracted from the experimental Arrhenius plot $\Rightarrow$ y = 13797x − 26.447 (R^2 = 0.9910) By identification to the experimental equation: 13797= Ea/R $\leftrightarrow$ Ea = 13797*R with R= 8.314 J.K^{-1}.mol^{-1}

$\Rightarrow$ Ea = 13797*1000*8.314 = **115 kJ.mol^{-1}** (and -26.447= ln (τ$_0$) $\leftrightarrow$ τ$_0$ = e^(-26.447) = 3.27*10^{-12} s)

6

> ## Determination of the topology freezing temperature (T_v) from the Maxwell equation

The average plateau modulus was extracted from the rheology temperature sweep curves (Figure 2.b) using the following equation: $G^2 = G'^2 + G''^2$. The average plateau modulus of the material was approximately 7.9 MPa and η = 1012 Pa.s at the liquid-to-glass transition temperature (T_v for vitrimers).

$\Rightarrow$ Maxwell model: $\tau^* = η/G \leftrightarrow \tau^* = 1.27 \times 105$ s

$\Rightarrow T_v = [13797/(\ln(1.27 \times 105) + 26.447)] - 273.15 = $ **88 °C**

> ## Investigation on the effect of the crosslinking density onto the relaxation of poly(PEG_n-DPA-mea)

Synthesis of PEG_{200}-DPA-mea

Diphenol terminated polyethylene glycol (PEG_{200}-DPA) was synthesized via a Fischer esterification. PEG_{200} (5 g, 25 mmol, 1.0 eq.) was reacted with DPA (14.32 g, 50 mmol, 2.0 eq.) and *p*-TSA (25 mg, 0.15 mmol, 0.5% wt) in an open three-neck round bottom flask at 130 °C for 24 hours under mechanical stirring (Ministar 20 Digital, anchor stirrer, 200 rpm). The reaction crude was then solubilized in butanone and purified by three liquid-liquid extractions with distilled water to remove non-hydrolyzed *p*-TSA. The solvent was then evaporated under reduced pressure. The product was dried overnight under reduced pressure (<1 mBar) at T= 50 °C. Then diphenol-terminated polyethylene glycol (PEG_{200}-DPA, 10 g, 13.6 mmol, 1.0 eq.) was reacted solventless with mono-ethanolamine (3.32 g, 54.3 mmol, 4.0 eq.), and PFA (3.26 g, 108.6 mmol, 8.0 eq.) at 85 °C for 2.5 hours followed by 0.5 hour at 90 °C under mechanical stirring (Ministar 20 Digital, anchor stirrer, 200 rpm).
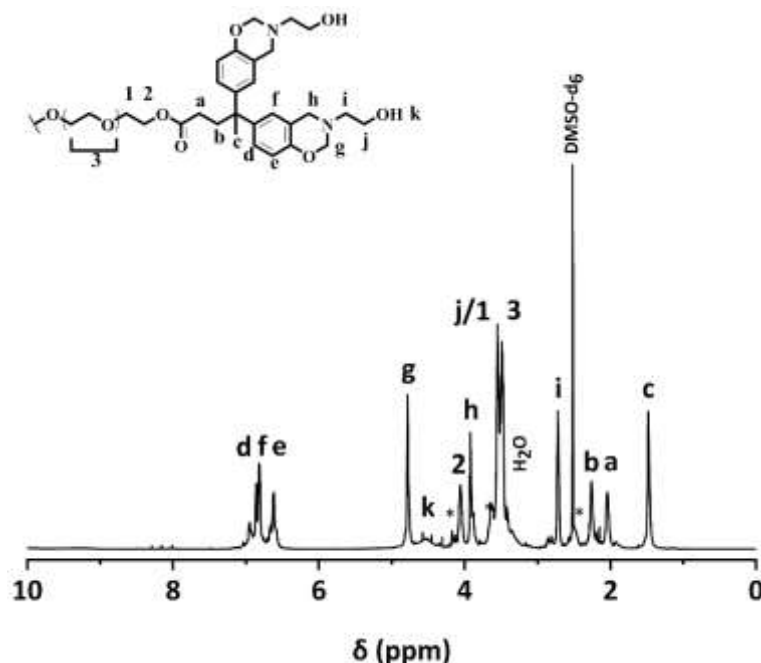
Figure S8 ^{1}H NMR spectrum of PEG_{200}-DPA-mea (DMSO-d$_6$)
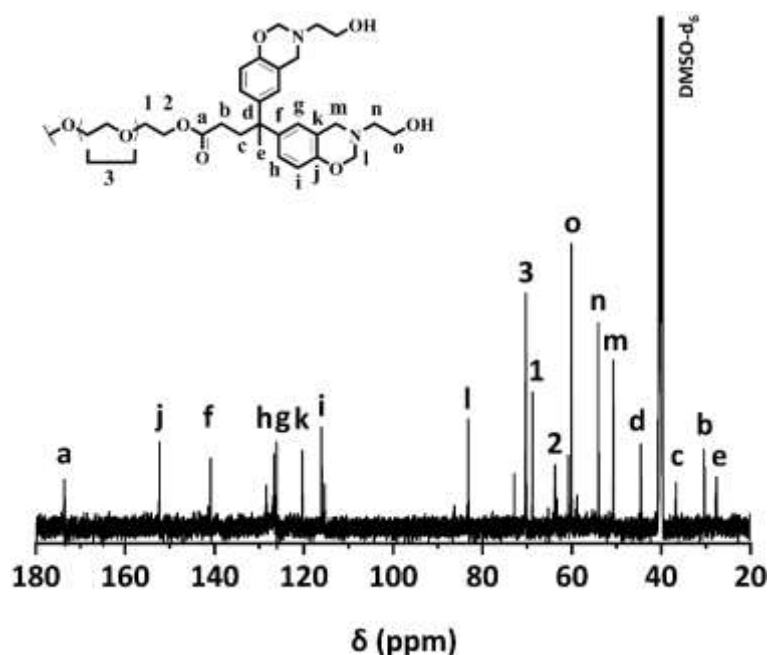
Figure S9 ^{13}C NMR spectrum of PEG$_{200}$-DPA-mea (DMSO-d$_6$)

Synthesis of PEG$_{2000}$-DPA-mea

Diphenol terminated polyethylene glycol (PEG$_{2000}$-DPA) was synthesized via a Fischer esterification. PEG$_{2000}$ (5 g, 2.5 mmol, 1.0 eq.) was reacted with DPA (1.43 g, 5 mmol, 2.0 eq.) and *p*-TSA (25 mg, 0.15 mmol, 0.5% wt) in an open three-neck round bottom flask at 130 °C for 24 hours under mechanical stirring (Ministar 20 Digital, anchor stirrer, 200 rpm). The reaction crude was then solubilized in butanone and purified by three liquid-liquid extractions with distilled water to remove non-hydrolyzed *p*-TSA. The solvent was then evaporated under reduced pressure. The product was dried overnight under reduced pressure (<1 mBar) at T= 50 °C. Then diphenol-terminated polyethylene glycol (PEG$_{2000}$-DPA, 5 g, 2.0 mmol, 1.0 eq.) was reacted solventless with mono-ethanolamine (0.48 g, 7.9 mmol, 4.0 eq.), and PFA (0.47 g, 15.8 mmol, 8.0 eq.) at 85 °C for 2.5 hours followed by 0.5 hour at 90 °C under mechanical stirring (Ministar 20 Digital, anchor stirrer, 200 rpm).
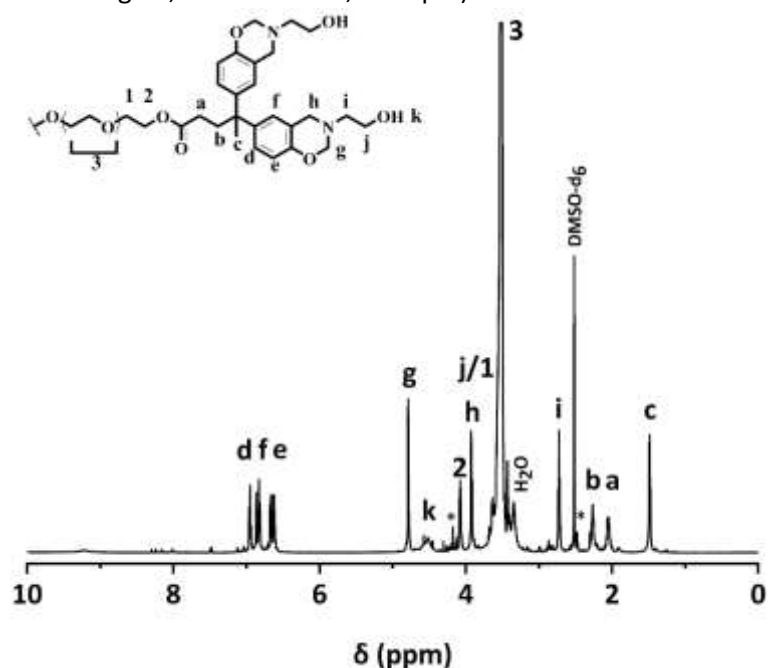
Figure S10 ^{1}H NMR spectrum of PEG$_{2000}$-DPA-mea (DMSO-d$_6$)

8
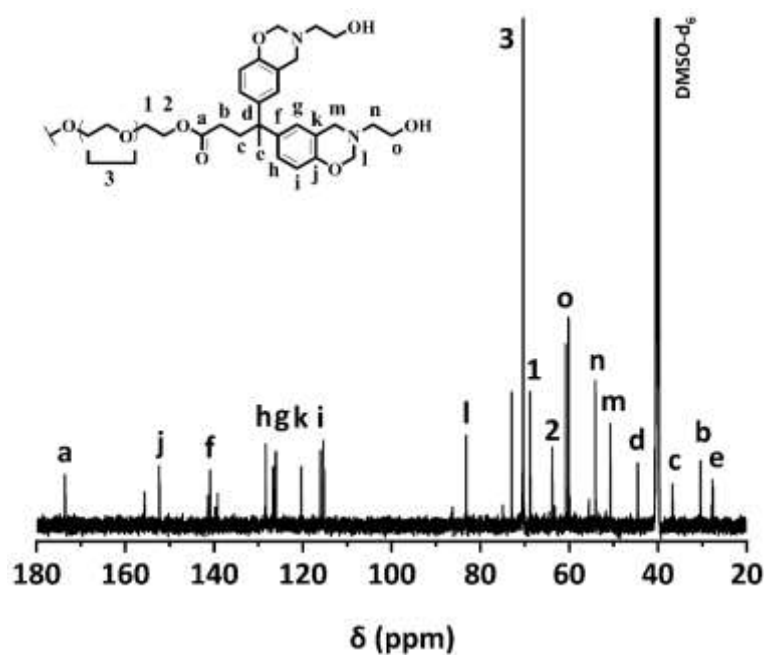
Figure S11 ^{13}C NMR spectrum of PEG$_{2000}$-DPA-mea (DMSO-d$_6$)

Thermal properties of PEG$_n$-DPA-mea
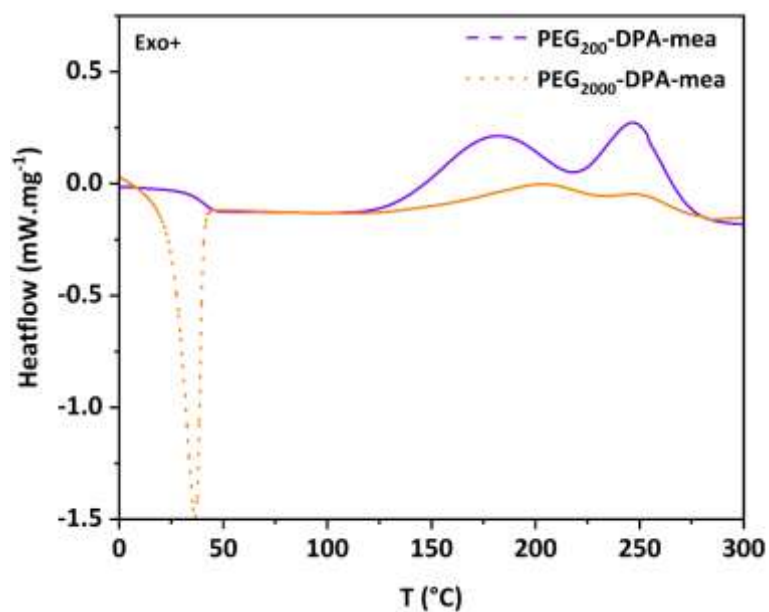
Figure S12 DSC thermogram of PEG$_{200}$-DPA-mea and PEG$_{2000}$-DPA-mea
(10 °C.min^{-1}, N$_2$ atmosphere)

9
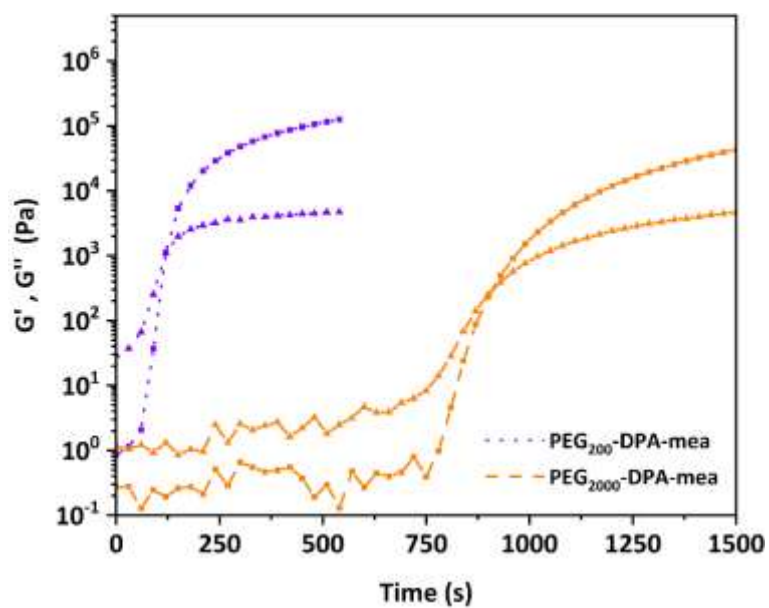
Figure S13 Isothermal rheology monitoring at 140 °C of PEG$_{200}$-DPA-mea and PEG$_{2000}$-DPA-mea

Polymerization and Determination of Ea and T$_v$
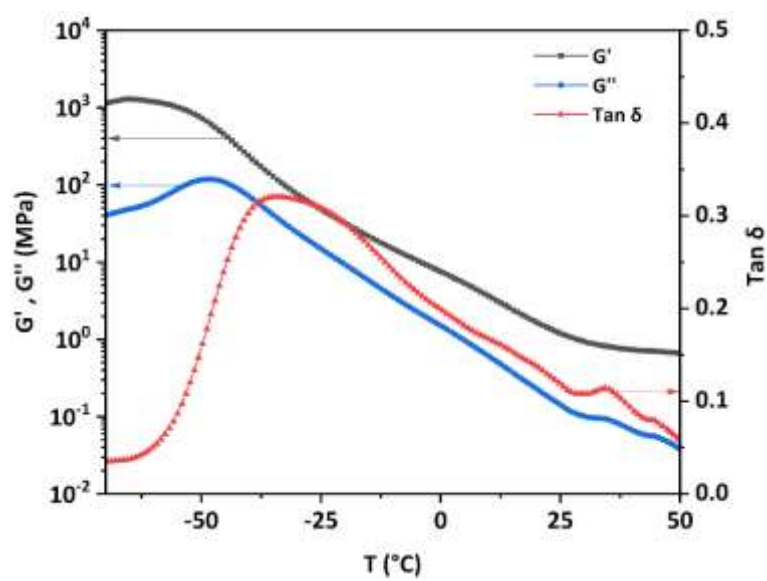
Figure S14 Rheology temperature sweep curves in torsion mode of poly(PEG$_{2000}$-DPA-mea)

10
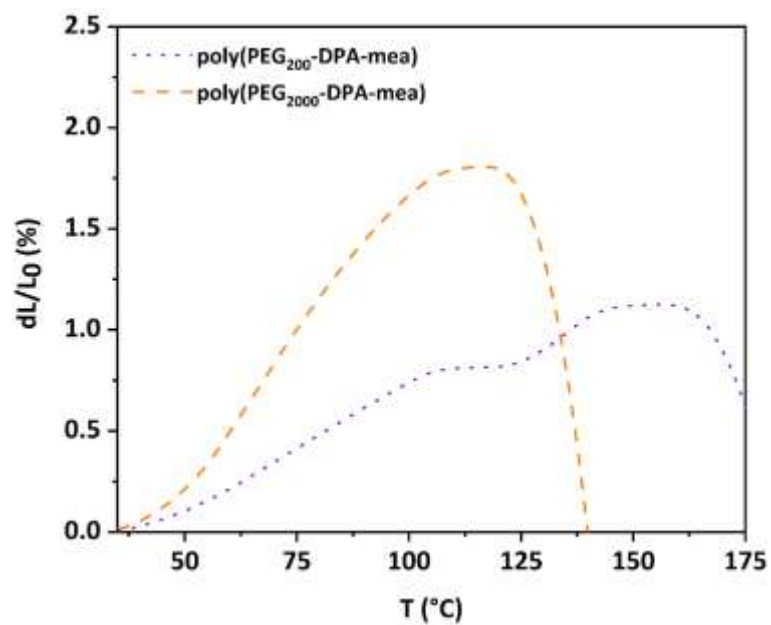
Figure S15 Dilatometry thermogram of poly(PEG$_{200}$-DPA-mea) and poly(PEG$_{2000}$-DPA-mea)
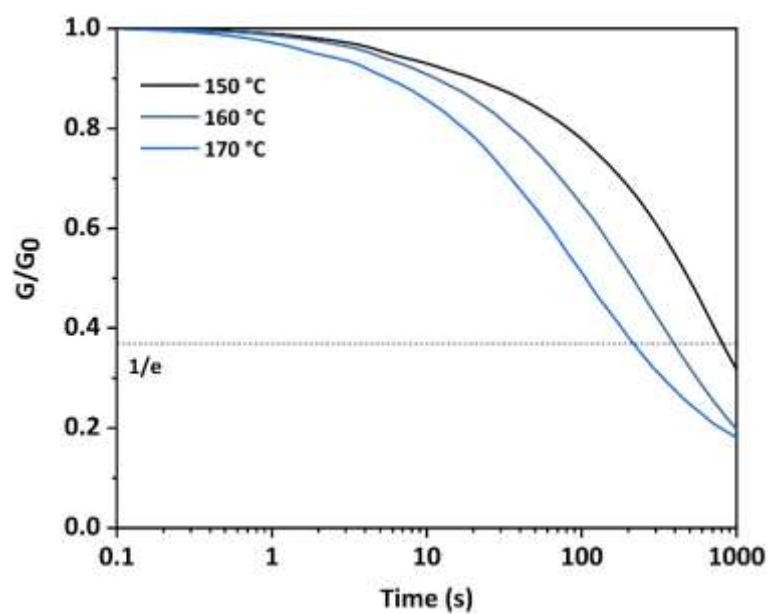
Figure S16 Stress relaxation curves of poly(PEG$_{200}$-DPA-mea) at different temperatures
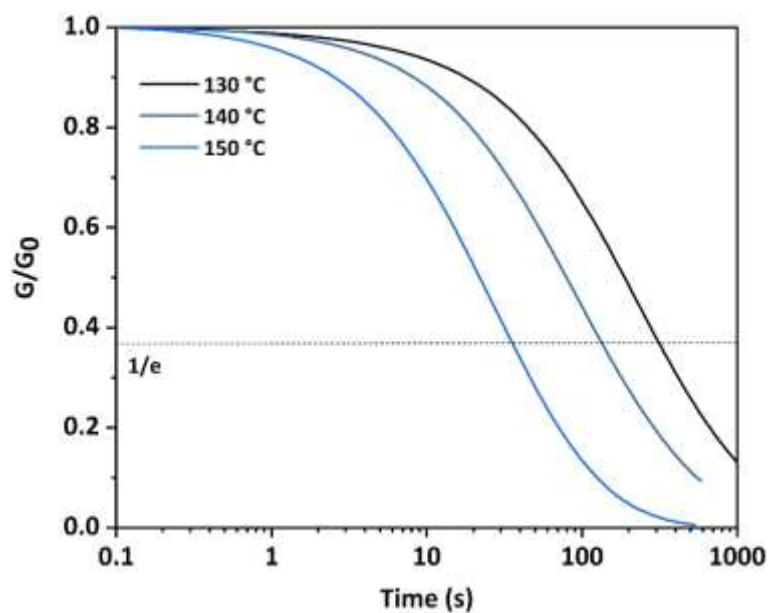
Figure S17 Stress relaxation curves of poly(PEG$_{2000}$-DPA-mea) at different temperatures

Table S2 Summary of the thermal properties of each PEG$_n$-DPA-mea and determination of the $\overline{Mc}$ of poly(PEG$_n$-DPA-mea)

Network	[a] t_{gel} (s)	[b] $T_{exo,1}$ (°C)	[b] $T_{max\_exo,2}$ (°C)	[c] W (%)	[d] ρ (kg.m^{-3})	[e] $\overline{Mc}$ (g.mol^{-1})
poly(PEG$_{200}$-DPA-mea)	116	105-220	248	13 ± 1	1202	15 ± 1
poly(PEG$_{400}$-DPA-mea)	145	110-220	250	38 ± 1	1193	49 ± 2
poly(PEG$_{2000}$-DPA-mea)	864	120-235	246	211 ± 7	1012	673 ± 48

[a] defined as the crossover point of G' and G'' by isothermal rheology monitoring at 140 °C (before curing); [b] determined by DSC experiment (10 °C.min^{-1}, N$_2$, before curing); [c] determined from the swelling ratio equation **(1)**; [d] calculated by measuring values of mass and volume; [e] determined from the Flory Rehner equation **(2)**

> ## *Effect of hydroxyl group content onto the relaxation of poly(PEG$_{400}$-DPA-mea$_x$/fa$_{100-x}$)*

Synthesis of PEG$_{400}$-DPA-mea$_{75}$/fa$_{25}$

Diphenol-terminated polyethylene glycol (PEG$_{400}$-DPA, 10 g, 10.7 mmol, 1.0 eq.) was reacted solventless with mono-ethanolamine (1.96 g, 32.0 mmol, 3.0 eq.), furfurylamine (1.04 g, 10.7 mmol, 1.0 eq.), and PFA (2.56 g, 85.4 mmol, 8.0 eq.) at 70 °C for 36 hours under mechanical stirring (Ministar 20 Digital, anchor stirrer, 200 rpm). PEG-DPA-mea$_{75}$/fa$_{25}$ benzoxazine monomer is a viscous solid substance, used without any purification (N/COO/OH = 2/1/1.5).
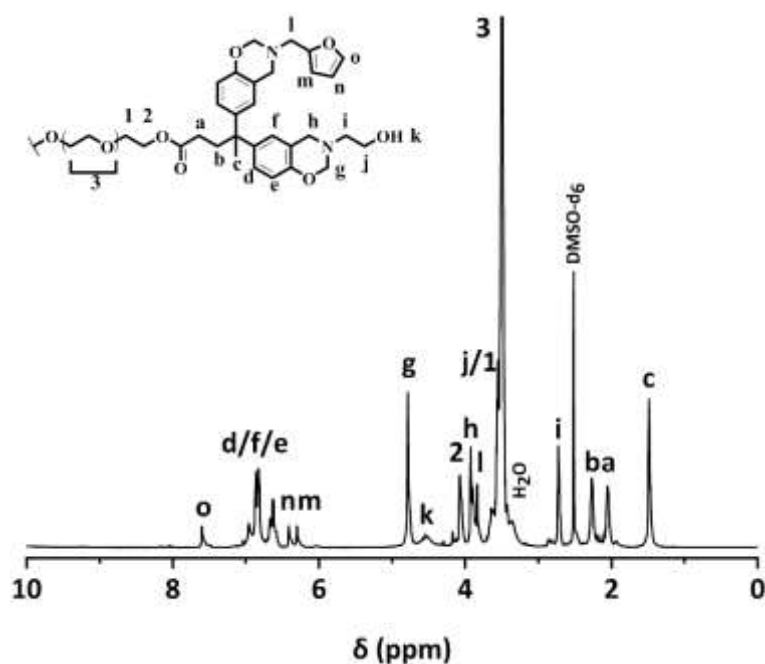
Figure S18 ^{1}H NMR spectrum of PEG$_{400}$-DPA-mea$_{75}$/fa$_{25}$ (DMSO-d$_6$)
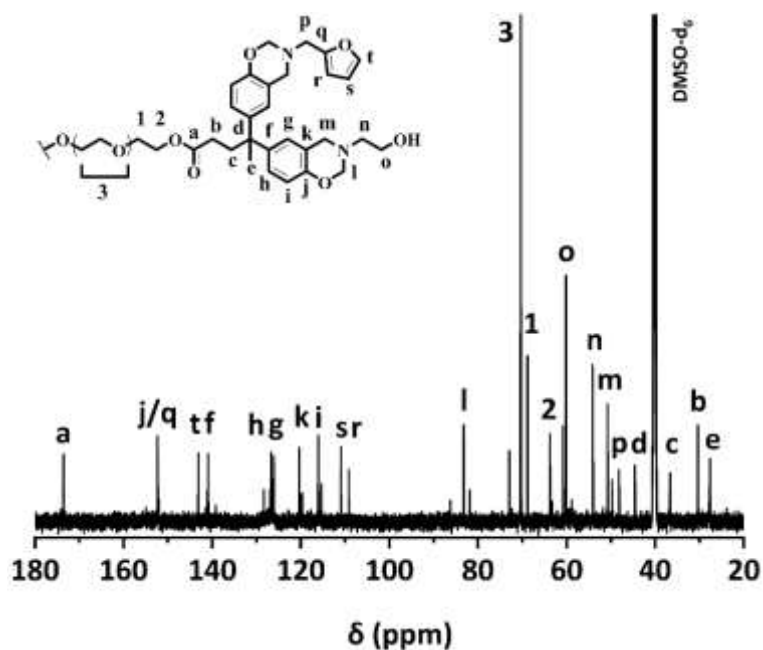
Figure S19 ^{13}C NMR spectrum of PEG$_{400}$-DPA-mea$_{75}$/fa$_{25}$ (DMSO-d$_6$)

13

Synthesis of PEG$_{400}$-DPA-mea$_{50}$/fa$_{50}$

Diphenol-terminated polyethylene glycol (PEG$_{400}$-DPA, 10 g, 10.7 mmol, 1.0 eq.) was reacted solventless with mono-ethanolamine (1.30 g, 21.4 mmol, 2.0 eq.), furfurylamine (2.07 g, 21.4 mmol, 2.0 eq.), and PFA (2.56 g, 85.4 mmol, 8.0 eq.) at 70 °C for 36 hours under mechanical stirring (Ministar 20 Digital, anchor stirrer, 200 rpm). PEG-DPA-mea$_{50}$/fa$_{50}$ benzoxazine monomer is a viscous solid substance, used without any purification (N/COO/OH = 2/1/1).
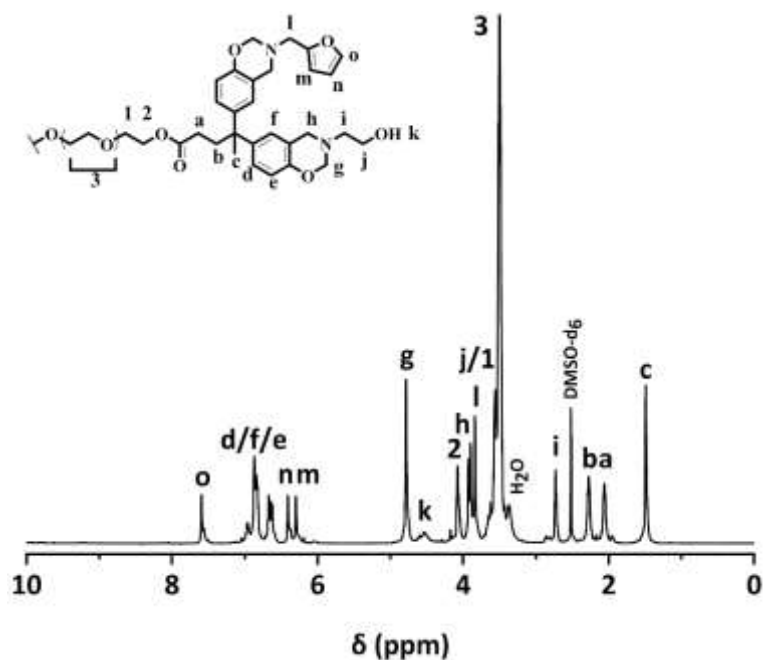
Figure S20 ^{1}H NMR spectrum of PEG$_{400}$-DPA-mea$_{50}$/fa$_{50}$ (DMSO-d$_6$)
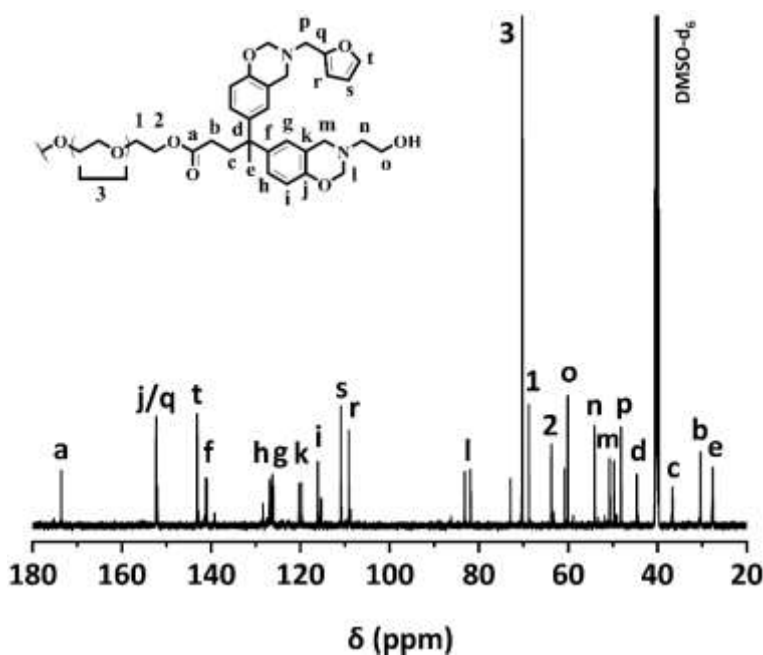
Figure S21 ^{13}C NMR spectrum of PEG$_{400}$-DPA-mea$_{50}$/fa$_{50}$ (DMSO-d$_6$)

14

Synthesis of PEG$_{400}$-DPA-mea$_{25}$/fa$_{75}$

Diphenol-terminated polyethylene glycol (PEG$_{400}$-DPA, 10 g, 10.7 mmol, 1.0 eq.) was reacted solventless with mono-ethanolamine (0.65 g, 10.7 mmol, 1.0 eq.), furfurylamine (3.11 g, 32.0 mmol, 3.0 eq.), and PFA (2.56 g, 85.4 mmol, 8.0 eq.) at 70 °C for 36 hours under mechanical stirring (Ministar 20 Digital, anchor stirrer, 200 rpm). PEG-DPA-mea$_{25}$/fa$_{75}$ benzoxazine monomer is a viscous solid substance, used without any purification (N/COO/OH = 2/1/0.5).
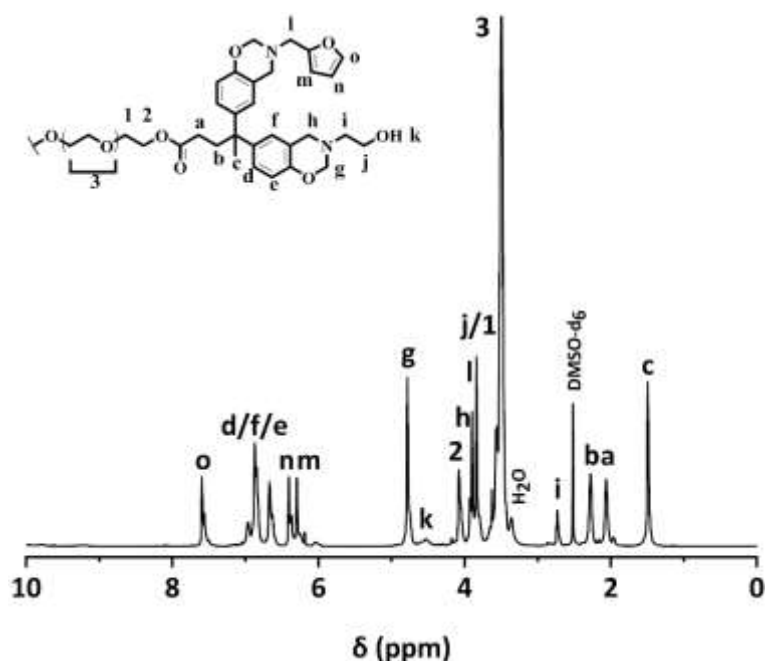
Figure S22 ^{1}H NMR spectrum of PEG$_{400}$-DPA-mea$_{25}$/fa$_{75}$ (DMSO-d$_6$)
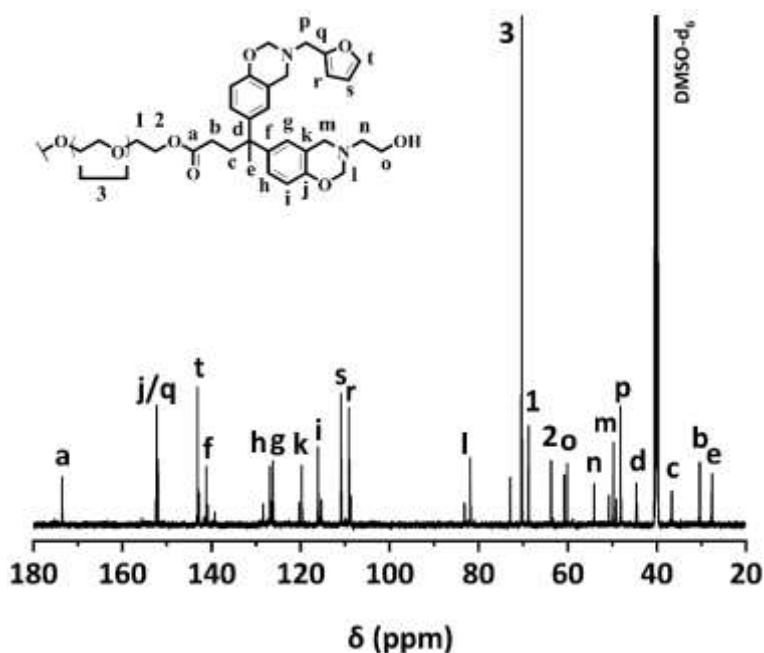
Figure S23 ^{13}C NMR spectrum of PEG$_{400}$-DPA-mea$_{25}$/fa$_{75}$ (DMSO-d$_6$)

15

Thermal properties of PEG$_{400}$-DPA-mea$_x$/fa$_{100-x}$
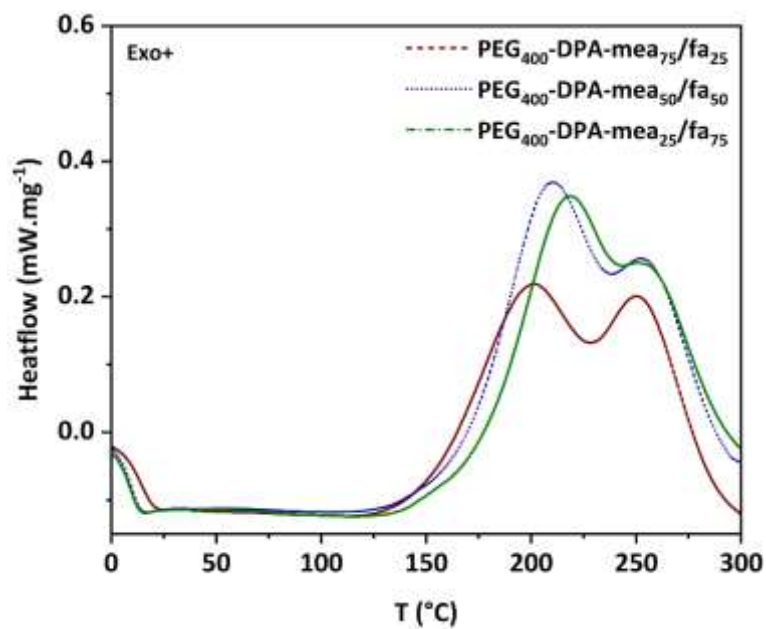
Figure S24 DSC thermogram of PEG$_{400}$-DPA-mea$_{75}$/fa$_{25}$, PEG$_{400}$-DPA-mea$_{50}$/fa$_{50}$ and PEG$_{400}$-DPA-mea$_{25}$/fa$_{75}$ (10 °C.min^{-1}, N$_2$ atmosphere)
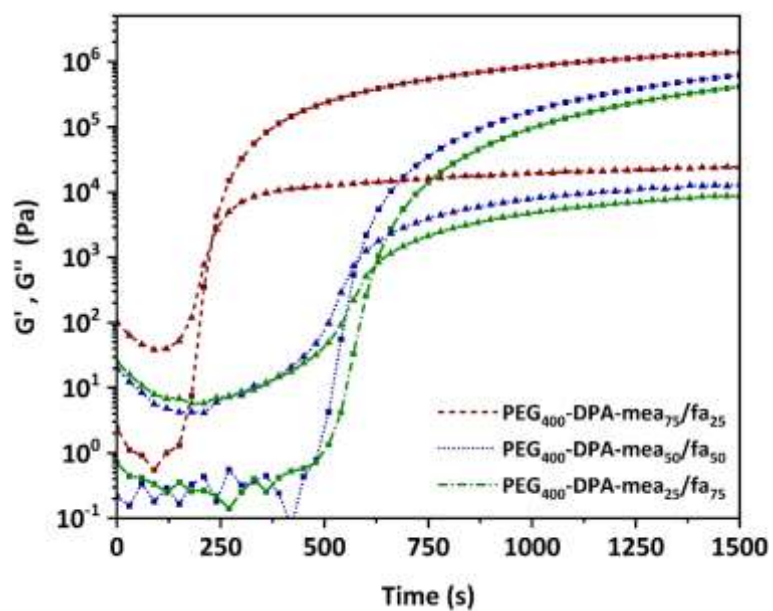
Figure S25 Isothermal rheology monitoring at 140 °C of PEG$_{400}$-DPA-mea$_{75}$/fa$_{25}$, PEG$_{400}$-DPA-mea$_{50}$/fa$_{50}$ and PEG$_{400}$-DPA-mea$_{25}$/fa$_{75}$

Polymerization and Determination of Ea and T$_v$
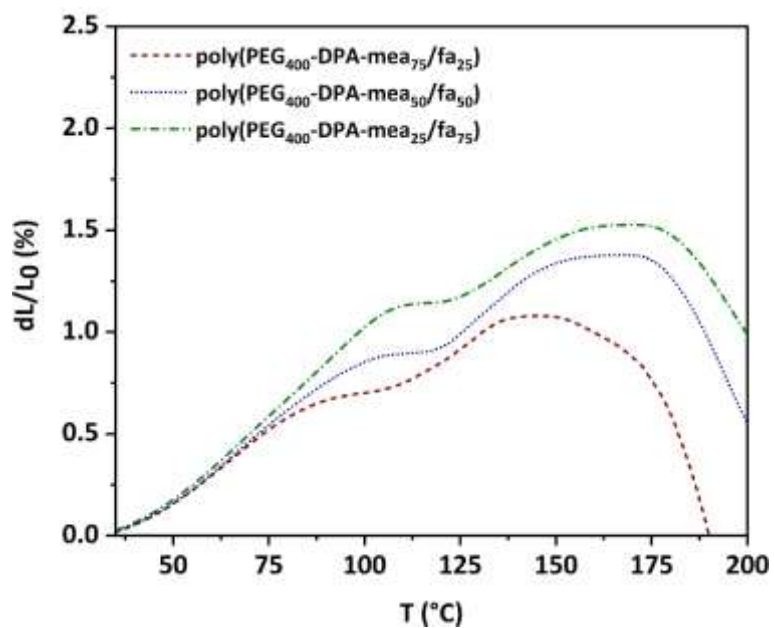
Figure S26 Dilatometry thermogram of poly(PEG$_{400}$-DPA-mea$_{75}$/fa$_{25}$), poly(PEG$_{400}$-DPA-mea$_{50}$/fa$_{50}$) and poly(PEG$_{400}$-DPA-mea$_{25}$/fa$_{75}$)
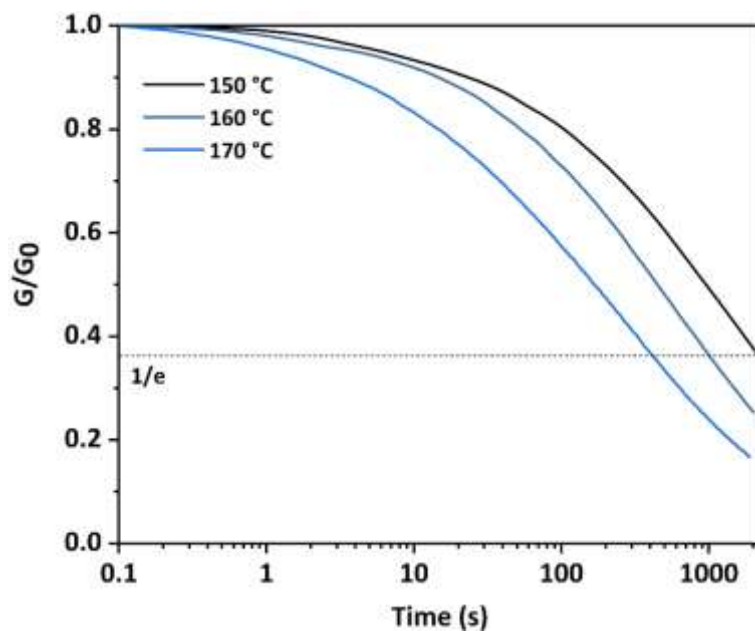
Figure S27 Stress relaxation curves of poly(PEG$_{400}$-DPA-mea$_{75}$/fa$_{25}$) at different temperatures
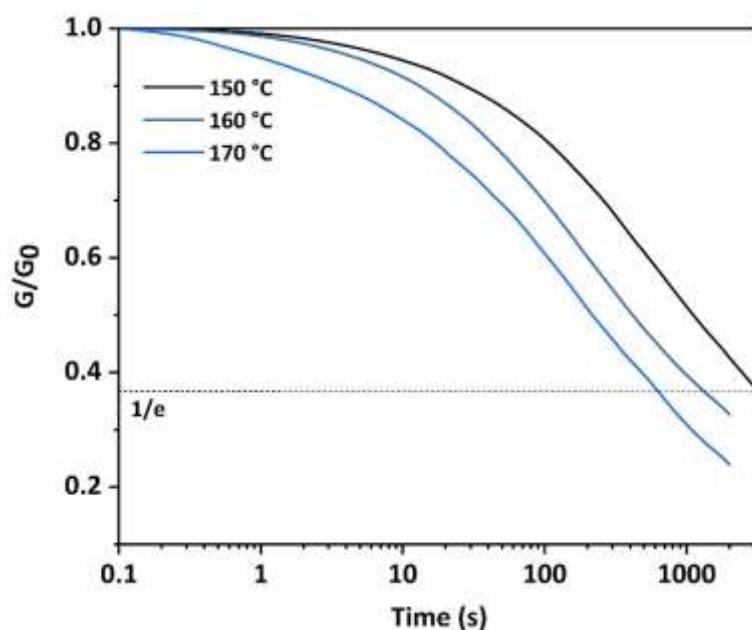
Figure S28 Stress relaxation curves of poly(PEG$_{400}$-DPA-mea$_{50}$/fa$_{50}$) at different temperatures
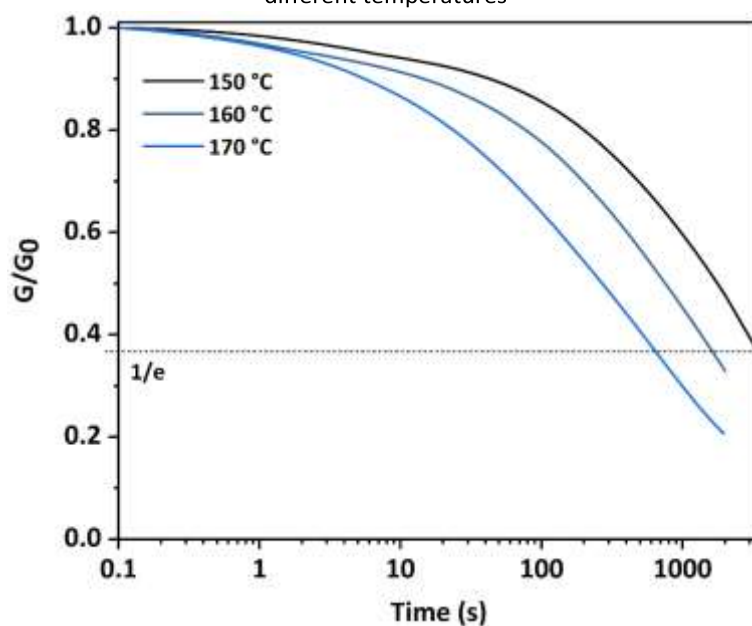
Figure S29 Stress relaxation curves of poly(PEG$_{400}$-DPA-mea$_{25}$/fa$_{75}$) at different temperatures

Table S3 Summary of the thermal properties of PEG$_{400}$-DPA-mea$_x$/fa$_{100-x}$ and determination of the $\overline{Mc}$ of poly(PEG$_{400}$-DPA-mea$_x$/fa$_{100-x}$)

Network	[a] t_{gel} (s)	[b] $T_{exo,1}$ (°C)	[b] $T_{max\_exo,2}$ (°C)	[c] W (%)	[d] ρ (kg.m^{-3})	[e] $\overline{Mc}$ (g.mol^{-1})
poly(PEG$_{400}$-DPA-mea$_{75}$/fa$_{25}$)	221	123-229	250	16 ± 1	1164	17 ± 1
poly(PEG$_{400}$-DPA-mea$_{50}$/fa$_{50}$)	579	127-238	253	9 ± 2	1104	10 ± 1
poly(PEG$_{400}$-DPA-mea$_{25}$/fa$_{75}$)	623	135-243	252	9 ± 2	1162	10 ± 2

[a] defined as the crossover point of G' and G'' by isothermal rheology monitoring at 140 °C (before curing); [b] determined by DSC experiment (10 °C.min^{-1}, N$_2$, before curing); [c] determined from the swelling ratio equation **(1)**; [d] calculated by measuring values of mass and volume; [e] determined from the Flory Rehner equation **(2)**

18
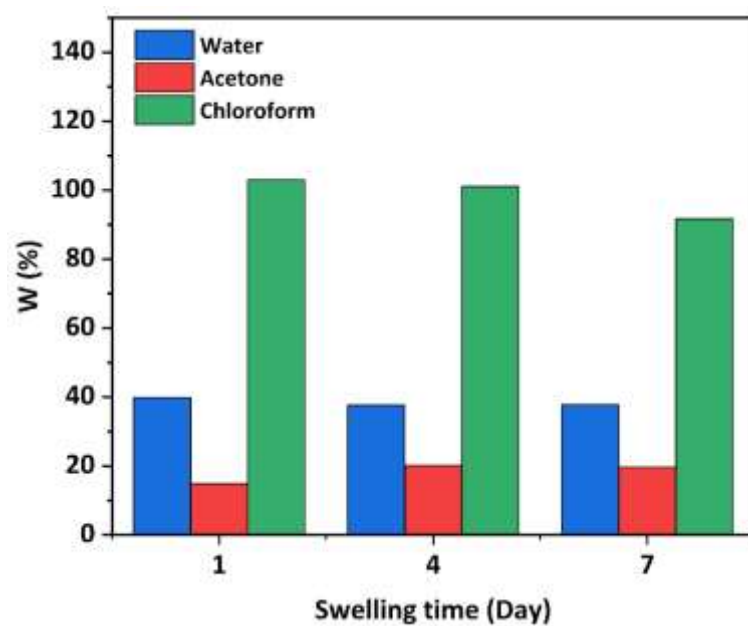
Figure S30 Swelling test of poly(PEG$_{400}$-DPA-mea)

Figure S31 Chemical recycling of poly(PEG$_{400}$-DPA-mea) in acetic acid
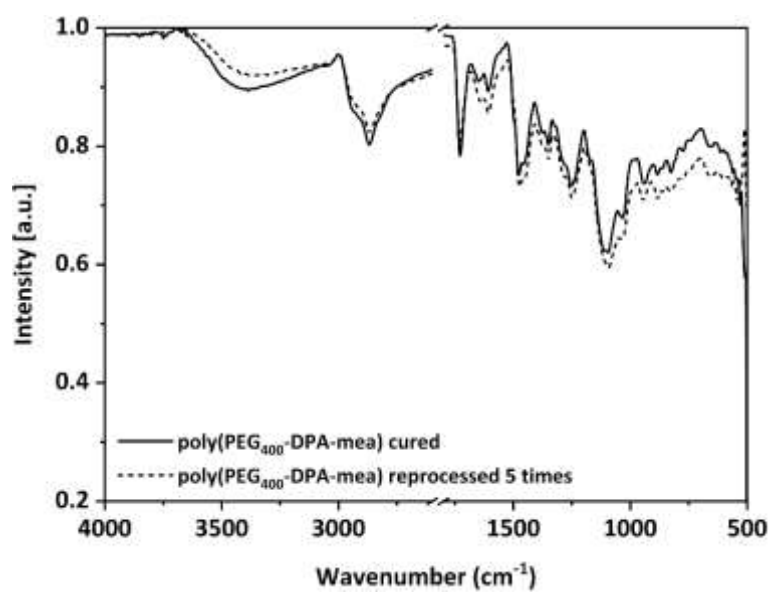
Figure S32 FTIR spectra of poly(PEG$_{400}$-DPA-mea) cured (solid) and reprocessed five times (dash)

19

Annex IV: High-Tg and Degradable Isosorbide-Based Polybenzoxazine Vitrimer

SUPPORTING INFORMATION

High T$_g$ and degradable isosorbide-based

polybenzoxazine vitrimer

Antoine Adjaoud [†, ‡], Laura Puchot [†] and Pierre Verge [†,]*

[†] Luxembourg Institute of Science and Technology, Materials Research and Technology

Department, 5 Avenue des Hauts-Fourneaux, L-4362 Esch-sur-Alzette (Luxembourg)

[‡] University of Luxembourg, 2, Avenue de l'Université, L-4365 Esch-sur-Alzette (Luxembourg)

* Corresponding author: pierre.verge@list.lu

Number of pages: 28

Number of figures: 31

Number of tables: 2

1. Equipment and characterizations

Nuclear Magnetic Resonance (NMR) spectroscopy was performed on an AVANCE III HD Bruker spectrometer equipped with a 5 mm BBO-probe operating at a proton frequency of 600 MHz. All chemical shifts are given as δ value (ppm) referenced to tetramethylsilane (TMS) as an internal standard. Assignments were performed using a combination of COSY, HSQC, and HMBC spectra. Peak multiplicity was indicated as follows: singlet (s); doublet (d); triplet (t) or multiplet (m). The coupling constants (J) were reported in Hertz (Hz).

Fourier transform infrared spectroscopy (FTIR) was conducted on a Bruker TENSOR 27 instrument in the attenuated total reflection (ATR) mode using a diamond crystal. All spectra were recorded at room temperature in direct absorbance mode across 4000-400 cm^{-1} frequency range (32 scans, 4 cm^{-1} spectral resolution).

Elemental analysis (CHNS measurements) was performed on a Vario MACRO cube CHNS/O from Elementar France SARL.

Differential scanning calorimetry (DSC) thermograms were recorded on a Netzsch DSC 204 F1 Phoenix device in standard pierced aluminum crucibles (40 μL). A linear heating ramp from 0 to 300 °C at 10 °C·min^{-1} rate was applied under inert atmosphere (N_2). The DSC thermogram of the vitrimer samples was recorded over two consecutive heating-cooling cycles from 25 to 250 °C (heating rate of 10 °C·min^{-1} and cooling rate of 20 °C·min^{-1}) to determine the glass transition (T_g) of the polymer and to ensure complete polymerization.

Thermogravimetric analysis (TGA) was completed on the Mettler Toledo TGA 2 device in ceramic alumina pan from 25 to 800 °C at 10 °C·min^{-1} rate under inert atmosphere (N_2).

Rheological measurements were recorded using an Anton Paar Physica MCR 302 rheometer equipped with a CTD 450 temperature control device. Stress relaxation experiments

were performed on disk-shaped solid geometry with a disposable aluminum plate-plate (Ø= 25 mm). The relaxation modulus was followed as a function of time for 2500 s between 120 and 190 °C with a constant applied strain of 1% and normal force of 10 N. The original relaxation modulus (G_0) was extracted from the initial plateau of the stress relaxation curves (onset point of the second derivative curve). For the isothermal rheo-kinetic measurements, small quantities of the samples were loaded in a parallel plate-plate geometry (Ø= 25 mm, gap 0.5 mm). The polymerization measurements were recorded in the oscillation mode at a controlled strain of 0.1% (1 Hz). Heating ramps of 20 °C·min^{-1} were applied to reach a temperature of 170 °C. The sample deformation was ramped linearly from 1% to 0.2% to remain within the instrument's limitation and to maintain a linear viscoelastic behavior as the moduli (G' storage modulus, G'' loss modulus) increase by several orders of magnitude upon curing.

Dynamic mechanical analysis (DMA) was used to evaluate the mechanical properties of vitrimer samples (length:width:thickness = 60mm:12mm:2mm) in the three-point bending mode (1 Hz) recorded on DMA 242 C dynamic mechanical analyzer. The samples were prepared by the curing of DIS-PA-mea$_x$fa$_{100-x}$ monomers in open molds in an air-circulating oven at 150 °C (1h), 170 °C (1h) plus an additional post-curing step at 190 °C (1/2 h) for the furan-groups containing monomers. The storage modulus (E'), the loss modulus (E") and the loss factor (tan δ) was recorded from 25 to 200 °C (2 °C.min^{-1}). The mechanical properties of reprocessed vitrimer materials (length:width:thickness = 30mm:5mm:1mm) was recorded at room temperature on Netzsch DMA GABO EPLEXOR apparatus in dynamic tensile mode (static strain: 1 %, dynamic strain: 0.25 %, contact force: 0.80 N, frequency: 1 Hz).

Optical microscopy was used to illustrate the self-healing performance of the isosorbide-based vitrimer. The surface morphology of scratched samples was examined using the Nikon

Universal Design Microscope UDM ECLIPSE LV100D-U (optics x20, gain x2.40, exposure 6 ms). The healing process was conducted at 200 °C in a convection oven. The width of the crack was measured before and after the healing process in a dynamic contrast mode.

2. Swelling tests and calculation of the crosslinking density

The swelling ratio (W) is determined according to the equation **(1)**:

$$W = \frac{m_s - m_i}{m_i} \quad \textbf{(1)}$$

with m_i and m_s being the initial and the swollen mass, respectively. The molecular weight between the crosslinking nodes ($\overline{Mc}$) was calculated by applying the Flory Rehner equation **(2)**:

$$\overline{Mc} = \frac{\rho * V * (0.5 * \mu - \mu^{\frac{1}{3}})}{\ln(1-\mu) + \mu + \chi_{isosorbide/water} * \mu^2} \quad \textbf{(2)}$$

where ρ is the density of the polymer, V is the molar volume of water, μ is the polymer volume fraction in the equilibrium-swollen system and $\chi_{Isosorbide/water}$ is the interaction parameter of isosorbide with water. We took the hypothesis that PEG moieties were driving the interaction of the network with water and $\chi_{Isosorbide/water}$ approximated to 0.5. μ is determined according to the equation **(3)**:

$$\mu = [1 + W * \frac{d_{polymer}}{d_{solvent}}]^{-1} \quad \textbf{(3)}$$

where $d_{polymer}$ and $d_{solvent}$ are the density of the polybenzoxazine vitrimer and the water, respectively. The crosslinking density (ν_c) is calculated according the equation **(4)**:

$$\nu_c = \frac{d_{polymer}}{\overline{Mc}} \textbf{(4)}$$

3. Structural characterization of precursors

> *Isosorbide (DIS)*

^{1}H NMR (DMSO-d$_6$, 600 MHz, 298 °K): δ (ppm) = (assignment, multiplicity (coupling constant), [attribution], experimental integration, theoretical integration). δ= 3.25 (O-CH$_2$*-CH(OH), t (J = 8.19 Hz), [3a], exp 1.00H, th 1.00H); δ= 3.69 (O-CH$_2$*-CH(OH), m, [7b&3b], exp 1.90H, th 2.00H); δ= 3.73 (O-CH$_2$*-CH(OH), dd (J = 3.53&9.52 Hz), [7a], exp 0.99H, th 1.00H); δ= 4.04 (CH$_2$-CH*(OH)-CH, t (J = 3.37 Hz), [6], exp 0.98H, th 1.00H); δ= 4.09 (CH$_2$-CH*(OH)-CH, m, [2], exp 1.02H, th 1.00H); δ= 4.23 (CH(OH)-CH*-O, d (J = 4.18 Hz), [4], exp 1.00H, th 1.00H); δ= 4.36 (CH(OH)-CH*-O, t (J = 4.45 Hz), [8], exp 1.01H, th 1.00H); δ= 4.72 (CH-OH*, d (J = 6.68 Hz), [1], exp 1.01H, th 1.00H); δ= 5.12 (CH-OH*, d (J = 3.77 Hz), [5], exp 0.99H, th 1.00H).

^{13}C NMR (DMSO-d$_6$, 600 MHz, 298 °K): δ (ppm) = 29.9 [9a]; 30.0 [9b]; 35.7 [8a]; 35.9 [8b]; 70.6 [2]; 72.8 [5]; 74.1 [4]; 77.9 [1]; 80.8 [3]; 85.9 [6]; 115.5 [12a]; 115.6 [12b]; 129.6 [11a]; 129.7 [11b]; 130.8 [10a]; 130.9 [10b]; 156.0 [13a]; 156.1 [13b]; 172.1 [7a], 172.2 [7b].

> *Isosorbide terminated phloretic acid (DIS-PA)*

^{1}H NMR (DMSO-d$_6$, 600 MHz, 298 °K): δ (ppm) = (assignment, multiplicity (coupling constant), [attribution], experimental integration, theoretical integration). δ= 2.57 (CH$_2$-CH$_2$*-CO), m, [7a&7b], exp 4.00H, th 4.00H); δ= 2.73 (Ar-CH$_2$*-CH$_2$), m, [8a&8b], exp 4.00H, th 4.00H); δ= 3.68 (O-CH$_2$*-CH(OC), dd (J = 4.24 & 9.98 Hz), [3a], exp 1.04H, th 1.00H); δ= 3.79 (O-CH$_2$*-CH(OC), m, [3b&6a&6b], exp 3.01H, th 3.00H); δ= 4.29 (CH(OH)-CH*-O, d (J = 4.87 Hz), [1], exp 1.02H, th 1.00H); δ= 4.71 (CH(OH)-CH*-O, t (J = 5.31 Hz), [4], exp 1.01H, th 1.00H); δ= 5.02 (CH$_2$-CH*(OC)-CH, m, [2], exp 1.02H, th 1.00H); δ= 5.06 (CH$_2$-CH*(OC)-CH, q (J = 4.46 Hz), [5], exp 0.98H, th 1.00H); δ= 6.67 (CH=CH*-C-OH, m, [10a&10b], exp 4.02H, th 4.00H); δ= 7.01 (C-C-CH*=CH, m, [9a&9b], exp 4.01H, th 4.00H); δ= 9.17-9.18 (Ar-OH*, m, [11a&11b], exp 2.00H, th 2.00H).

^{13}C NMR (DMSO-d$_6$, 600 MHz, 298 °K): δ (ppm) = 29.9 [9a]; 30.0 [9b]; 35.7 [8a]; 35.9 [8b]; 70.6 [2]; 72.8 [5]; 74.1 [4]; 77.9 [1]; 80.8 [3]; 85.9 [6]; 115.5 [12a]; 115.6 [12b]; 129.6 [11a]; 129.7 [11b]; 130.8 [10a]; 130.9 [10b]; 156.0 [13a]; 156.1 [13b]; 172.1 [7a], 172.2 [7b].

> *Benzoxazine monomer DIS-PA-mea*

^{1}H NMR (DMSO-d$_6$, 600 MHz, 298 °K): δ (ppm) = (assignment, multiplicity (coupling constant), [attribution], experimental integration, theoretical integration). δ= 2.59 (CH$_2$-CH$_2$*-CO), t (J= 7.26 Hz), [7], exp 4.00H, th 4.00H; δ= 2.73 (Ar-CH$_2$*-CH$_2$ & N-CH$_2$*-CH$_2$), m, [8&14], exp 7.32H, th 8.00H; δ= 3.55 (HO-CH$_2$*-CH$_2$), t (J= 5.90 Hz), [15], exp 3.88H, th 4.00H; δ= 3.70 (O-CH$_2$*-CH(OC)), m, [3a], exp 1.17H, th 1.00H; δ= 3.79 (O-CH$_2$*-CH(OC)), m, [3b&6a&6b], exp 2.94H, th 3.00H; δ= 3.93 (N-CH$_2$*-Ar, s, [12], exp 3.07H, th 4.00H; δ= 4.29 (CH(OH)-CH*-O, m, [1], exp 1.02H, th 1.00H; δ= 4.52 (CH$_2$-OH*, s, [16], exp 1.80H, th 2.00H; δ= 4.70 (CH(OH)-CH*-O, m, [4], exp 1.03H, th 1.00H; δ= 4.78 (N-CH$_2$*-O, s, [13], exp 3.07H, th 4.00H; δ= 5.02 (CH$_2$-CH*(OC)-CH, m, [2], exp 1.02H, th 1.00H; δ= 5.07 (CH$_2$-CH*(OC)-CH, m, [5], exp 0.96H, th 1.00H; δ= 6.63 (CH*=CH-C-O, m, [10], exp 1.94H, th 2.00H; δ= 6.84-6.95 (C-CH*=C & CH=CH*-C-O, m, [9&11], exp 4.11H, th 4.00H).

^{13}C NMR (DMSO-d$_6$, 600 MHz, 298 °K): δ (ppm) = 29.9 [9]; 35.7-35.9 [8]; 50.3 [16]; 53.8 [18]; 60.0 [19]; 70.6 [2]; 72.8 [5]; 74.1 [4]; 77.9 [1]; 80.8 [3]; 83.1 [17]; 85.9 [6]; 116.1-116.2 [13]; 120.8 [15]; 127.6 [12]; 127.7 [11]; 132.2-132.3 [10]; 152.7-152.8 [14]; 172.0-172.1 [7].

Elemental analysis (experimental, theoretical): C (29.9; 30), H (31.2; 40), N (1.8; 2), S (0; 0), O (10.8; 10).

FTIR (cm^{-1}); very strong (vs), strong (s), medium (m), weak (w), broad (br): 3650-3200 (–OH stretching, br), 2932 (C–H aromatic stretch, m), 2874 (C–H alkyl stretch, m), 1732 (C=O α-β unsaturated ester stretch, vs), 1499 (C= C trisubstituted benzene ring stretch,

s), 1230 (C–O–C oxazine asymmetric stretch, m), 1153 (C-O stretch ester, s), 1015 (C–O–C oxazine symmetric stretch, m w), 935 (C–H trisubstituted benzene ring stretch, m).

> *Benzoxazine monomer DIS-PA-mea$_{75}$fa$_{25}$*

^{1}H NMR (DMSO-d$_6$, 600 MHz, 298 °K): δ (ppm) = (assignment, multiplicity (coupling constant), [attribution], experimental integration, theoretical integration). δ= 2.59 (CH$_2$-CH$_2$*-CO), t (J= 7.28 Hz), [7], exp 4.00H, th 4.00H); δ= 2.73 (Ar-CH$_2$*-CH$_2$ & N-CH$_2$*-CH$_2$), m, [8&14], exp 6.45H, th 7.00H); δ= 3.55 (HO-CH$_2$*-CH$_2$), m, [15], exp 2.72H, th 3.00H); δ= 3.68 (O-CH$_2$*-CH(OC), m, [3a], exp 0.93H, th 1.00H); δ= 3.77-3.82 (O-CH$_2$*-CH(OC) & *fa*-CH$_2$*-Ar), m, [3b&6a&6b&17], exp 3.52H, th 4.00H); δ= 3.88-3.93 (*fa*-N-CH$_2$*-Ar & *mea*-N-CH$_2$*-Ar, s, [12], exp 3.17H, th 4.00H); δ= 4.30 (CH(OH)-CH*-O, m, [1], exp 1.02H, th 1.00H); δ= 4.52 (CH$_2$*-OH, s, [16], exp 1.43H, th 1.50H); δ= 4.70 (CH(OH)-CH*-O, m, [4], exp 1.06H, th 1.00H); δ= 4.78 (N-CH$_2$*-O, s, [13], exp 3.02H, th 4.00H); δ= 5.02 (CH$_2$-CH*(OC)-CH, m, [2], exp 1.09H, th 1.00H); δ= 5.08 (CH$_2$-CH*(OC)-CH, m, [5], exp 0.93H, th 1.00H); δ= 6.31 (*fa*-CH*=CH-CH, d (J= 2.76 Hz), [18], exp 0.48H, th 0.50H); δ= 6.42 (*fa*-CH=CH*-CH, t (J= 2.26 Hz), [19], exp 0.46H, th 0.50H); δ= 6.65 (CH*=CH-C-O, m, [10], exp 2.03H, th 2.00H); δ= 6.82-6.99 (C-CH*=C & CH=CH*-C-O, m, [9&11], exp 4.05H, th 4.00H); δ= 7.61 (*fa*-CH*=CH-O, m, [20], exp 0.40H, th 0.50H).

^{13}C NMR (DMSO-d$_6$, 600 MHz, 298 °K): δ (ppm) = 29.9 [9]; 35.4-35.6 [8]; 48.0 [20]; 49.2-50.3 [16]; 53.8 [18]; 60.0 [19]; 70.6 [2]; 72.9 [5]; 74.1 [4]; 77.9 [1]; 80.8 [3]; 81.9-83.1 [17]; 85.9 [6]; 109.1 [22]; 110.8 [23]; 116.1 [13]; 120.8 [15]; 127.7 [12]; 127.8 [11]; 132.2-132.4 [10]; 143.1 [24]; 152.5 [21]; 152.8 [14]; 172.0-172.1 [7].

Elemental analysis (experimental, theoretical): C (28.8; 31.0), H (37.2; 40.0), N (1.8; 2.0), S (0; 0), O (12.0; 10.0).

FTIR (cm^{-1}); very strong (vs), strong (s), medium (m), weak (w), broad (br): 3650-3200 (–OH stretching, br), 2932 (C–H aromatic stretch, m), 2874 (C–H alkyl stretch, m), 1732 (C=O α-β unsaturated ester stretch, vs), 1499 (C= C trisubstituted benzene ring stretch,

s), 1230 (C–O–C oxazine asymmetric stretch, m), 1153 (C-O stretch ester, s), 1015 (C–O–C oxazine symmetric stretch, m w), 935 (C–H trisubstituted benzene ring stretch, m).

> ➤ *Benzoxazine monomer DIS-PA-mea$_{50}$fa$_{50}$*

^{1}H NMR (DMSO-d$_6$, 600 MHz, 298 °K): δ (ppm) = (assignment, multiplicity (coupling constant), [attribution], experimental integration, theoretical integration). δ= 2.59 (CH$_2$-CH$_2$*-CO), m, [7], exp 4.00H, th 4.00H); δ= 2.73 (Ar-CH$_2$*-CH$_2$ & N-CH$_2$*-CH$_2$), m, [8&14], exp 5.64H, th 6.00H); δ= 3.55 (HO-CH$_2$*-CH$_2$), m, [15], exp 1.85H, th 2.00H); δ= 3.69 (O-CH$_2$*-CH(OC), m, [3a], exp 1.15H, th 1.00H); δ= 3.78-3.82 (O-CH$_2$*-CH(OC) & *fa*-CH$_2$*-Ar), m, [3b&6a&6b&17], exp 4.85H, th 5.00H); δ= 3.88-3.92 (*fa*-N-CH$_2$*-Ar & *mea*-N-CH$_2$*-Ar, s, [12], exp 3.35H, th 4.00H); δ= 4.30 (CH(OH)-CH*-O, m, [1], exp 0.99H, th 1.00H); δ= 4.52 (CH$_2$*-OH, s, [16], exp 0.96H, th 1.00H); δ= 4.71 (CH(OH)-CH*-O, m, [4], exp 1.12H, th 1.00H); δ= 4.79 (N-CH$_2$*-O, s, [13], exp 3.25H, th 4.00H); δ= 5.02 (CH$_2$-CH*(OC)-CH, m, [2], exp 1.09H, th 1.00H); δ= 5.08 (CH$_2$-CH*(OC)-CH, m, [5], exp 0.89H, th 1.00H); δ= 6.31 (*fa*-CH*=CH-CH, d (J= 2.53 Hz), [18], exp 0.96H, th 1.00H); δ= 6.42 (*fa*-CH=CH*-CH, t (J= 2.53 Hz), [19], exp 0.96H, th 1.00H); δ= 6.65 (CH*=CH-C-O, m, [10], exp 1.93H, th 2.00H); δ= 6.84-6.98 (C-CH*=C & CH=CH*-C-O, m, [9&11], exp 4.03H, th 4.00H); δ= 7.61 (*fa*-CH*=CH-O, m, [20], exp 0.88H, th 1.00H).

^{13}C NMR (DMSO-d$_6$, 600 MHz, 298 °K): δ (ppm) = 29.9 [9]; 35.4-35.6 [8]; 48.0 [20]; 49.2-50.3 [16]; 53.8 [18]; 60.0 [19]; 70.6 [2]; 72.9 [5]; 74.1 [4]; 77.9 [1]; 80.8 [3]; 81.9-83.1 [17]; 85.9 [6]; 109.1 [22]; 110.9 [23]; 116.1-116.3 [13]; 120.1-120.8 [15]; 127.7 [12]; 127.8 [11]; 132.2-132.4 [10]; 143.1 [24]; 152.5 [21]; 152.8 [14]; 172.0-172.1 [7].

Elemental analysis (experimental, theoretical): C (32.0; 32.0), H (39.8; 40.0), N (1.7; 2.0), S (0; 0), O (10.3; 10.0).

FTIR (cm^{-1}); very strong (vs), strong (s), medium (m), weak (w), broad (br): 3650-3200 (–OH stretching, br), 2932 (C–H aromatic stretch, m), 2874 (C–H alkyl stretch, m), 1732 (C=O α-β unsaturated ester stretch, vs), 1499 (C= C trisubstituted benzene ring stretch,

s), 1230 (C–O–C oxazine asymmetric stretch, m), 1153 (C-O stretch ester, s), 1015 (C–O–C oxazine symmetric stretch, m w), 935 (C–H trisubstituted benzene ring stretch, m).

> *Benzoxazine monomer DIS-PA-mea$_{25}$fa$_{75}$*

^{1}H NMR (DMSO-d$_6$, 600 MHz, 298 °K): δ (ppm) = (assignment, multiplicity (coupling constant), [attribution], experimental integration, theoretical integration). δ= 2.59 (CH$_2$-CH$_2$*-CO), m, [7], exp 4.00H, th 4.00H); δ= 2.74 (Ar-CH$_2$*-CH$_2$ & N-CH$_2$*-CH$_2$), m, [8&14], exp 5.08H, th 5.00H); δ= 3.55 (HO-CH$_2$*-CH$_2$), m, [15], exp 1.12H, th 1.00H); δ= 3.70 (O-CH$_2$*-CH(OC), m, [3a], exp 1.02H, th 1.00H); δ= 3.78-3.82 (O-CH$_2$*-CH(OC) & *fa*-CH$_2$*-Ar), m, [3b&6a&6b&17], exp 5.46H, th 6.00H); δ= 3.88-3.92 (*fa*-N-CH$_2$*-Ar & *mea*-N-CH$_2$*-Ar, s, [12], exp 3.41H, th 4.00H); δ= 4.30 (CH(OH)-CH*-O, m, [1], exp 1.04H, th 1.00H); δ= 4.52 (CH$_2$*-OH, s, [16], exp 0.41H, th 0.50H); δ= 4.71 (CH(OH)-CH*-O, m, [4], exp 1.02H, th 1.00H); δ= 4.79 (N-CH$_2$*-O, s, [13], exp 3.28H, th 4.00H); δ= 5.02 (CH$_2$-CH*(OC)-CH, m, [2], exp 1.06H, th 1.00H); δ= 5.07 (CH$_2$-CH*(OC)-CH, m, [5], exp 0.87H, th 1.00H); δ= 6.31 (*fa*-CH*=CH-CH, d (J= 2.98 Hz), [18], exp 1.45H, th 1.50H); δ= 6.42 (*fa*-CH=CH*-CH, t (J= 2.61 Hz), [19], exp 1.45H, th 1.50H); δ= 6.67 (CH*=CH-C-O, m, [10], exp 1.87H, th 2.00H); δ= 6.85-6.97 (C-CH*=C & CH=CH*-C-O, m, [9&11], exp 4.05H, th 4.00H); δ= 7.61 (*fa*-CH*=CH-O, m, [20], exp 1.38H, th 1.50H).

^{13}C NMR (DMSO-d$_6$, 600 MHz, 298 °K): δ (ppm) = 29.9 [9]; 35.4-35.6 [8]; 48.0 [20]; 49.2-50.3 [16]; 53.8 [18]; 60.0 [19]; 70.6 [2]; 72.9 [5]; 74.1 [4]; 77.9 [1]; 80.8 [3]; 81.9-83.1 [17]; 85.9 [6]; 109.1 [22]; 110.9 [23]; 116.2-116.3 [13]; 120.1-120.8 [15]; 127.7 [12]; 127.8 [11]; 132.2-132.4 [10]; 143.1 [24]; 152.3 [21]; 152.6 [14]; 172.0-172.1 [7].

Elemental analysis (experimental, theoretical): C (32.9; 33.0), H (38.7; 40.0), N (1.7; 2.0), S (0; 0), O (10.4; 10.0).

FTIR (cm^{-1}); very strong (vs), strong (s), medium (m), weak (w), broad (br): 3650-3200 (–OH stretching, br), 2932 (C–H aromatic stretch, m), 2874 (C–H alkyl stretch, m), 1732 (C=O α-β unsaturated ester stretch, vs), 1499 (C= C trisubstituted benzene ring stretch,

s), 1230 (C–O–C oxazine asymmetric stretch, m), 1153 (C-O stretch ester, s), 1015 (C–O–C oxazine symmetric stretch, m w), 935 (C–H trisubstituted benzene ring stretch, m).

> *Benzoxazine monomer DIS-PA-fa*

^{1}H NMR (DMSO-d$_6$, 600 MHz, 298 °K): δ (ppm) = (assignment, multiplicity (coupling constant), [attribution], experimental integration, theoretical integration). δ= 2.59 (CH$_2$-CH$_2$*-CO), t (J= 7.48 Hz), [7], exp 4.00H, th 4.00H); δ= 2.74 (Ar-CH$_2$*-CH$_2$), t (J= 7.18 Hz), [8], exp 4.03H, th 4.00H); δ= 3.68 (O-CH$_2$*-CH(OC), m, [3a], exp 1.00H, th 1.00H); δ= 3.77 (O-CH$_2$*-CH(OC), m, [3b&6a&6b], exp 3.04H, th 3.00H); δ= 3.82 (*fa*-CH$_2$*-Ar, s, [17], exp 2.90H, th 4.00H); δ= 3.88 (N-CH$_2$*-Ar, s, [12], exp 3.00H, th 4.00H); δ= 4.30 (CH(OH)-CH*-O, m, [1], exp 0.99H, th 1.00H); δ= 4.70 (CH(OH)-CH*-O, m, [4], exp 1.02H, th 1.00H); δ= 4.79 (N-CH$_2$*-O, s, [13], exp 2.90H, th 4.00H); δ= 5.02 (CH$_2$-CH*(OC)-CH, m, [2], exp 1.15H, th 1.00H); δ= 5.08 (CH$_2$-CH*(OC)-CH, m, [5], exp 0.85H, th 1.00H); δ= 6.31 (*fa*-CH*=CH-CH, m, [18], exp 1.72H, th 2.00H); δ= 6.42 (*fa*-CH=CH*-CH, m, [19], exp 1.94H, th 2.00H); δ= 6.68 (CH*=CH-C-O, m, [10], exp 1.95H, th 2.00H); δ= 6.85-6.98 (C-CH*=C & CH=CH*-C-O, m, [9&11], exp 3.98H, th 4.00H); δ= 7.60 (*fa*-CH*=CH-O, m, [20], exp 1.88H, th 2.00H).

^{13}C NMR (DMSO-d$_6$, 600 MHz, 298 °K): δ (ppm) = 29.9 [9]; 35.4-35.6 [8]; 48.0 [16]; 49.2 [20]; 70.6 [2]; 72.9 [5]; 74.1 [4]; 77.9 [1]; 80.8 [3]; 81.9 [17]; 85.9 [6]; 109.1 [22]; 110.9 [23]; 116.3 [13]; 120.1 [15]; 127.8 [12]; 127.9 [11]; 132.6-132.7 [10]; 143.1 [24]; 152.2 [14]; 152.5 [21]; 172.0-172.1 [7].

Elemental analysis (experimental, theoretical): C (33.9; 34.0), H (48.3; 40.0), N (1.9; 2.0), S (0; 0), O (9.7; 10.0).

FTIR (cm^{-1}); very strong (vs), strong (s), medium (m), weak (w), broad (br): 3650-3200 (–OH stretching, br), 2932 (C–H aromatic stretch, m), 2874 (C–H alkyl stretch, m), 1732 (C=O α-β unsaturated ester stretch, vs), 1499 (C= C trisubstituted benzene ring stretch, s), 1230 (C–O–C oxazine asymmetric stretch, m), 1153 (C-O stretch ester, s), 1015 (C–O–C oxazine symmetric stretch, m w), 935 (C–H trisubstituted benzene ring stretch, m).

4. Supplementary Figures and Tables

Table S1 Table of committed reagents for the synthesis of DIS-PA-mea$_x$fa$_{100-x}$ benzoxazine precursors

	Reagents	M (g.mol^{-1})	m (g)	n (mmol)	N (eq.)
DIS-PA-mea	Isosorbide ester (DIS-PA)	442.5	7.50	16.9	1.0
	Ethanolamine (mea)	61.1	2.07	33.9	2.0
	Paraformaldehyde (PFA)	30.0	2.03	67.8	4.0
DIS-PA-mea$_{75}$fa$_{25}$	Isosorbide ester (DIS-PA)	442.5	7.50	16.9	1.0
	Ethanolamine (mea)	61.1	1.55	25.4	1.5
	Furfurylamine (fa)	97.1	0.82	8.5	0.5
	Paraformaldehyde (PFA)	30.0	2.03	67.8	4.0
DIS-PA-mea$_{50}$fa$_{50}$	Isosorbide ester (DIS-PA)	442.5	7.50	16.9	1.0
	Ethanolamine (mea)	61.1	1.04	16.9	1.0
	Furfurylamine (fa)	97.1	1.65	16.9	1.0
	Paraformaldehyde (PFA)	30.0	2.03	67.8	4.0
DIS-PA-mea$_{25}$fa$_{75}$	Isosorbide ester (DIS-PA)	442.5	7.50	16.9	1.0
	Ethanolamine (mea)	61.1	0.42	8.5	0.5
	Furfurylamine (fa)	97.1	2.47	25.4	1.5
	Paraformaldehyde (PFA)	30.0	2.03	67.8	4.0
DIS-PA-fa	Isosorbide ester (DIS-PA)	442.5	7.50	16.9	1.0
	Furfurylamine (fa)	97.1	3.29	33.9	2.0
	Paraformaldehyde (PFA)	30.0	2.03	67.8	4.0
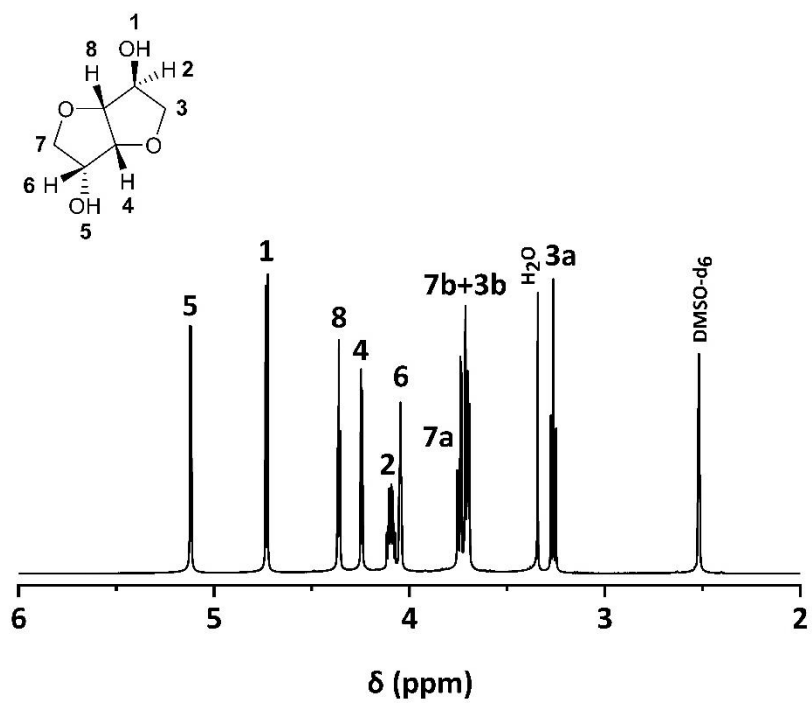
Figure S1. ^{1}H NMR spectrum of DIS
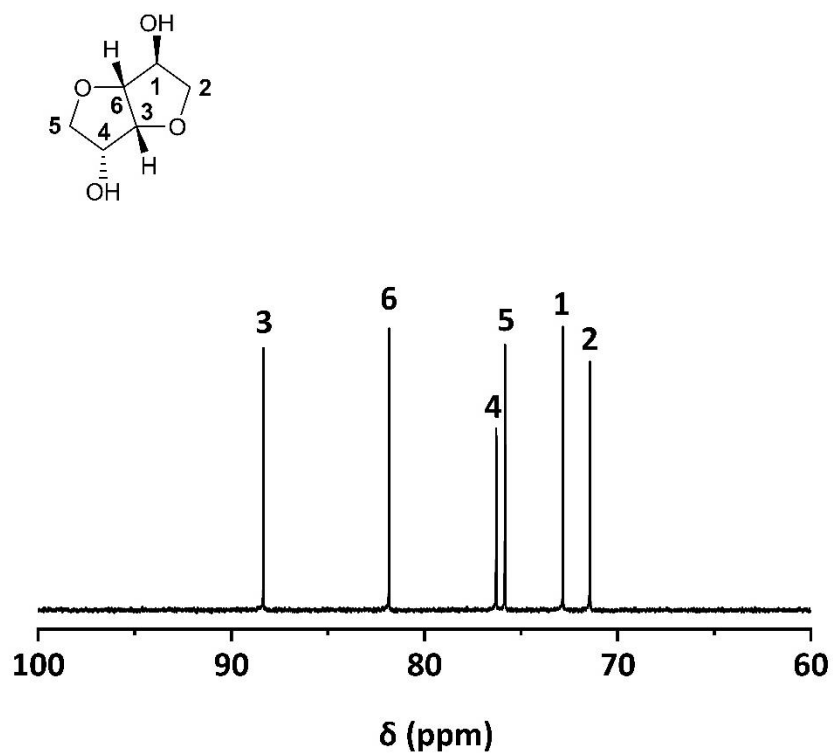
Figure S2. ^{13}C NMR spectrum of DIS
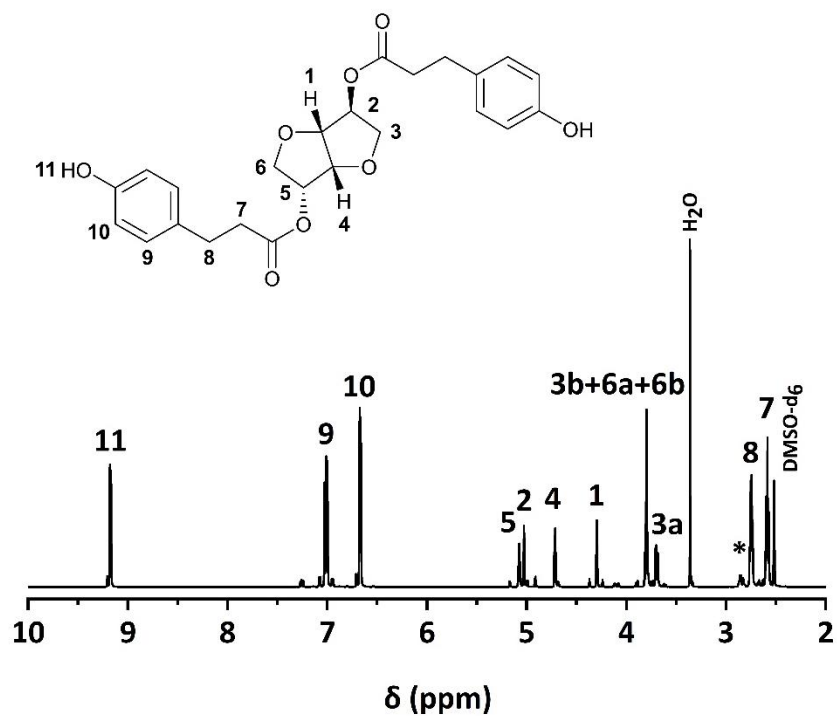
Figure S3. ^{1}H NMR spectrum of DIS-PA
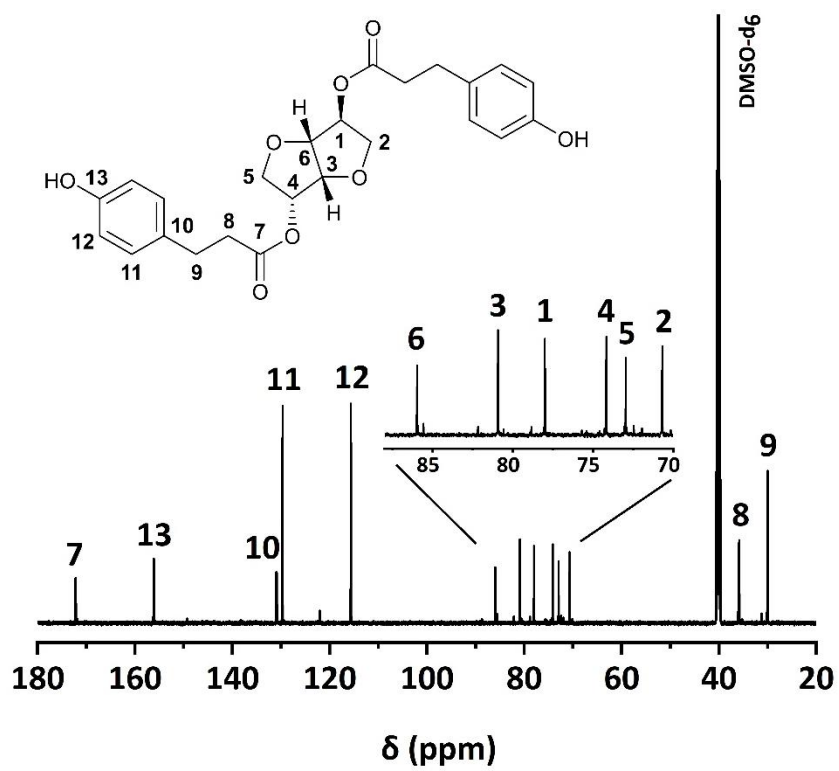
Figure S4. ^{13}C NMR spectrum of DIS-PA

The effect of the temperature on the conversion of PA was monitored by ^{1}H NMR experiment and plotted in Figure S5 as function of time. After a day of a reaction, higher esterification's temperature contributes to reach higher conversion of PA's COOH groups (90 % at 130 °C).
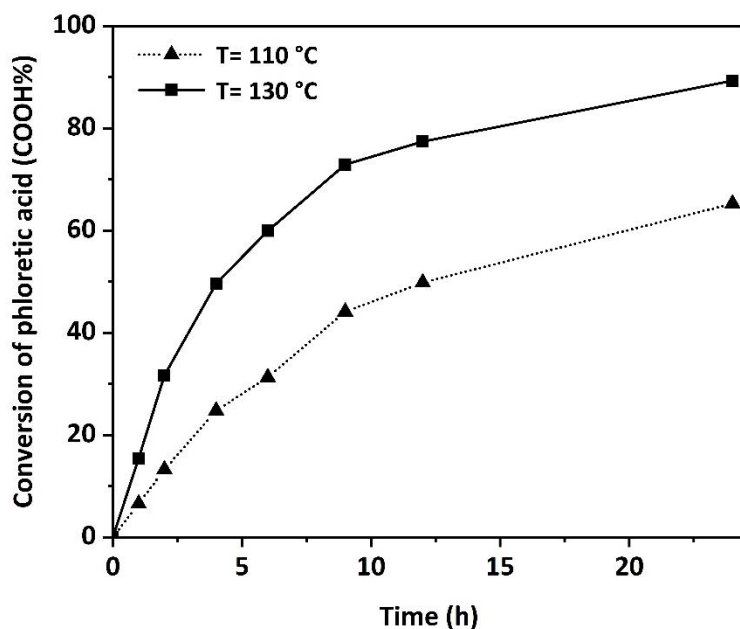
Figure S5. Effect of the temperature on the conversion of PA followed by ^{1}H NMR
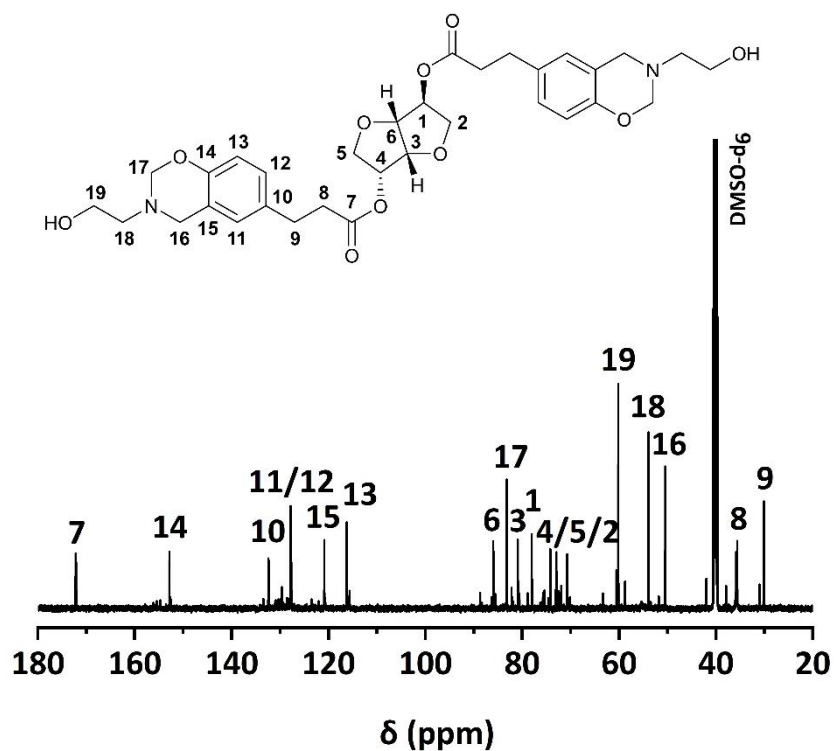
Figure S6. ^{13}C NMR spectrum of DIS-PA-mea
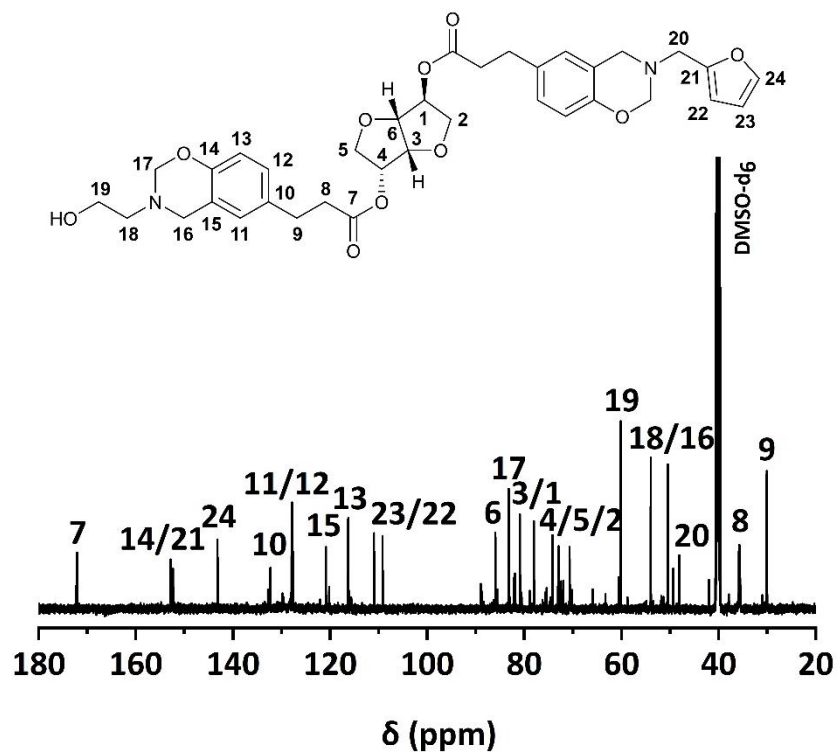
Figure S7. ^{13}C NMR spectrum of DIS-PA-mea$_{75}$fa$_{25}$
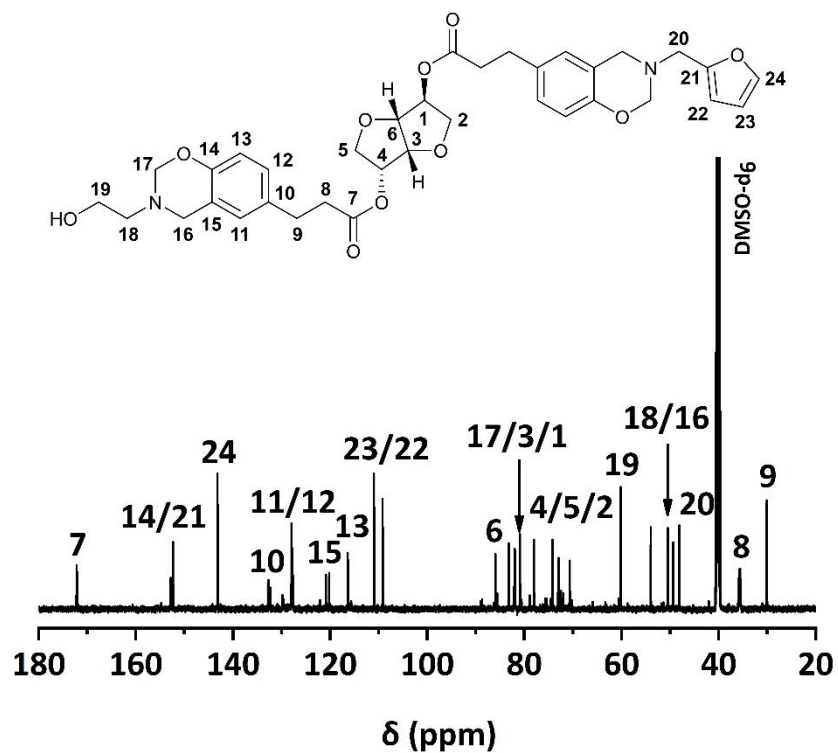
Figure S8. ^{13}C NMR spectrum of DIS-PA-mea$_{50}$fa$_{50}$
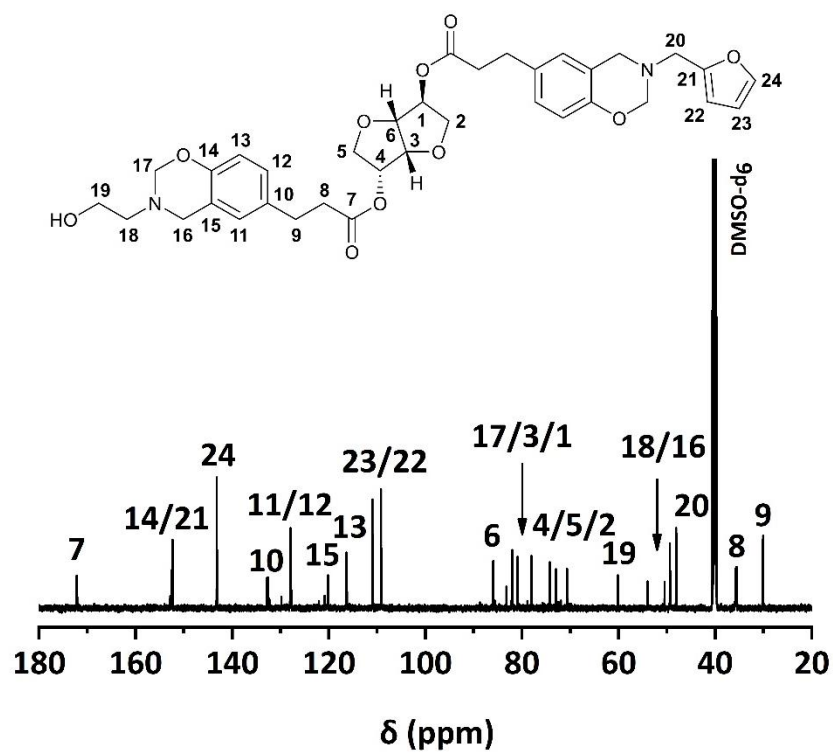
Figure S9. ^{13}C NMR spectrum of DIS-PA-mea$_{25}$fa$_{75}$
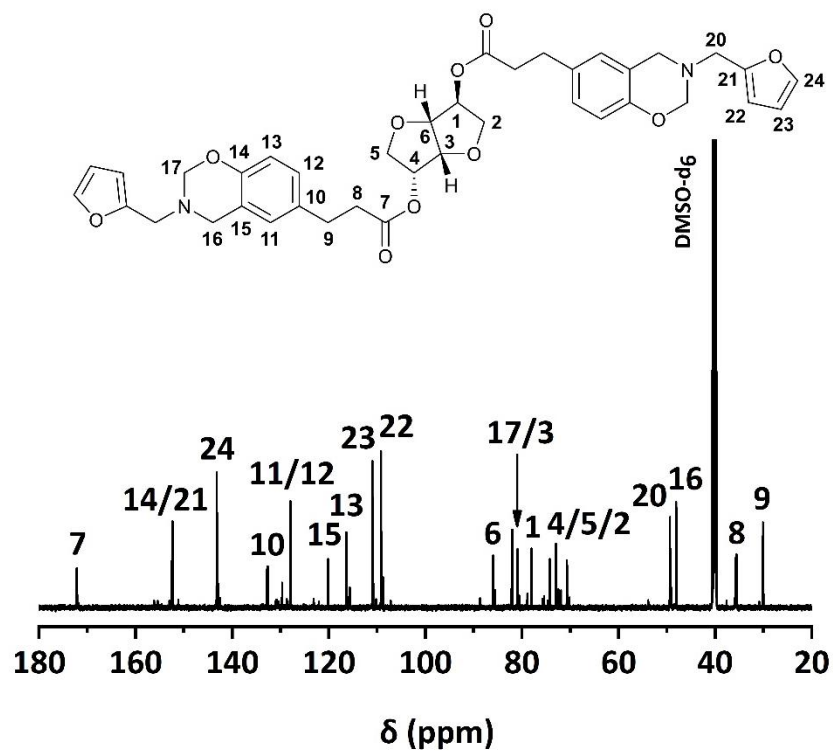
Figure S10. ^{13}C NMR spectrum of DIS-PA-fa
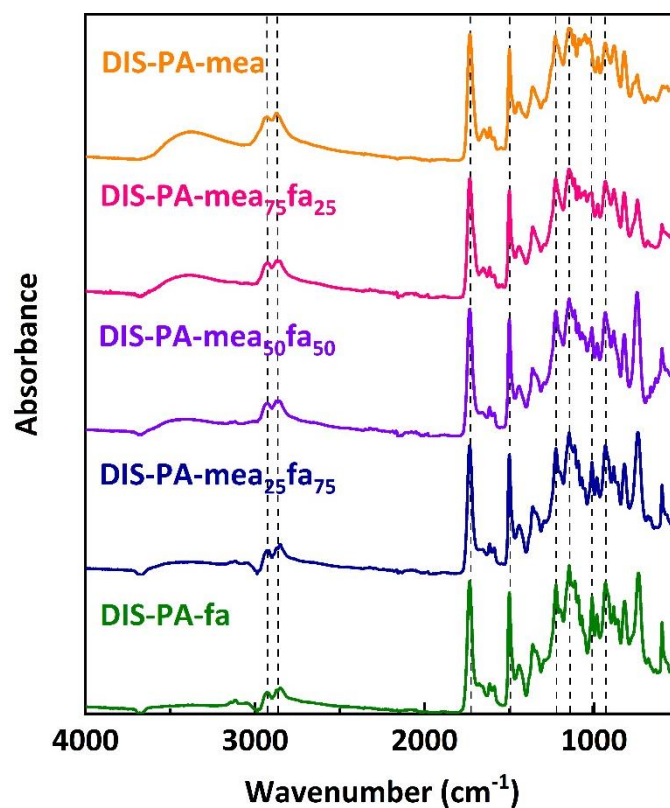
Figure S11. FTIR spectra of the benzoxazine precursors DIS-PA-mea$_x$fa$_{100-x}$
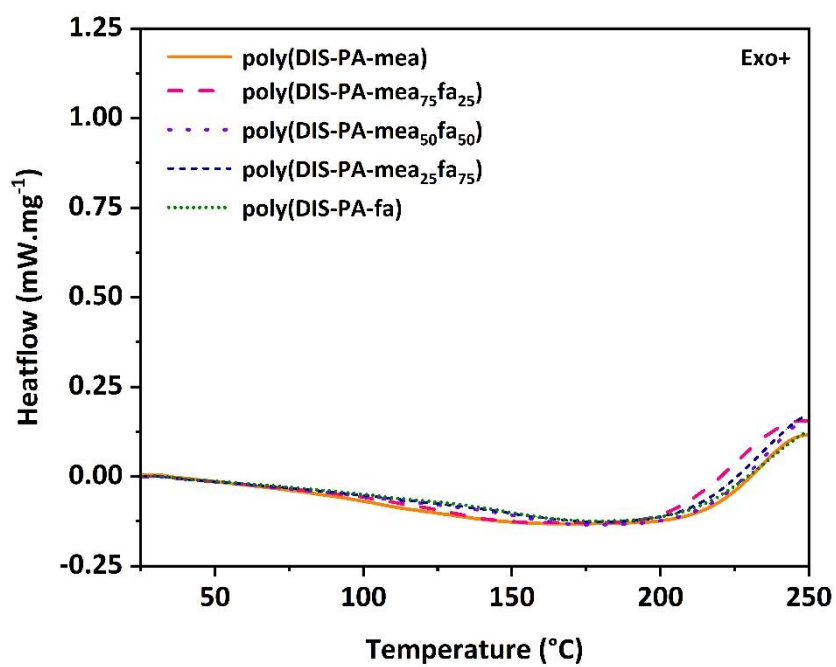
Figure S12. DSC curves of the polybenzoxazine vitrimers poly(DIS-PA-mea$_x$fa$_{100-x}$)
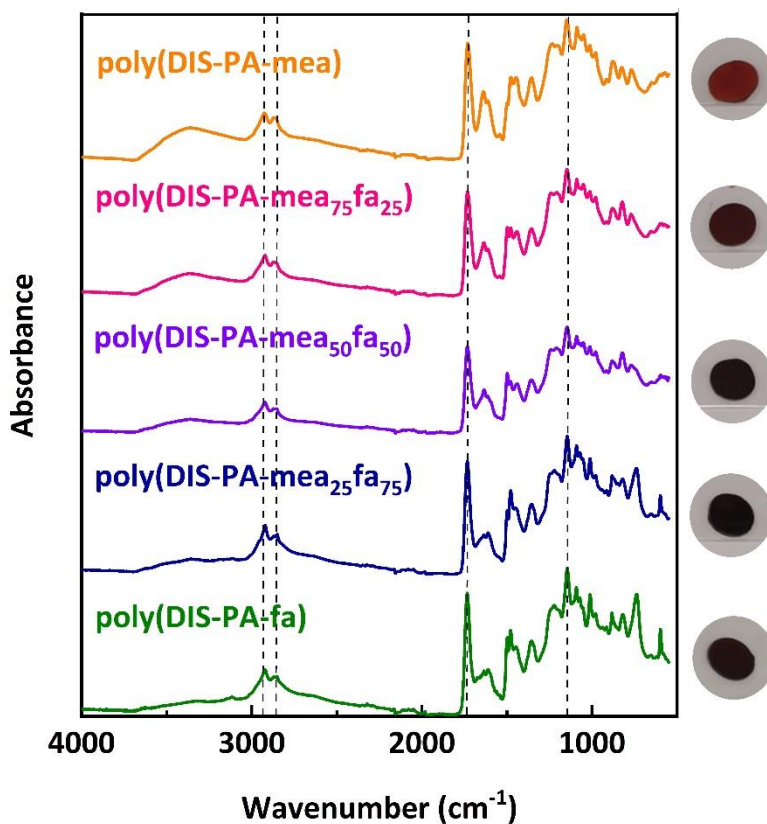
Figure S13. (left) FTIR spectra of the polybenzoxazine vitrimers poly(DIS-PA-mea$_x$fa$_{100-x}$) and (right) photographs of the materials

FTIR (cm^{-1}): 3650-3200 (–OH stretching, br), 2932 (C–H aromatic stretch, m), 2874 (C–H alkyl stretch, m), 1732 (C=O α-β unsaturated ester stretch, vs), 1230 (C–O–C oxazine asymmetric stretch, m), 1153 (C-O stretch ester, s).

Figure S14. Evolution of the storage and loss moduli and tan delta of
poly(DIS-PA-mea) as a function of the temperature measured by
DMA

Figure S15. Evolution of the storage and loss moduli and tan delta of
poly(DIS-PA-mea$_{75}$fa$_{25}$) as a function of the temperature measured by DMA
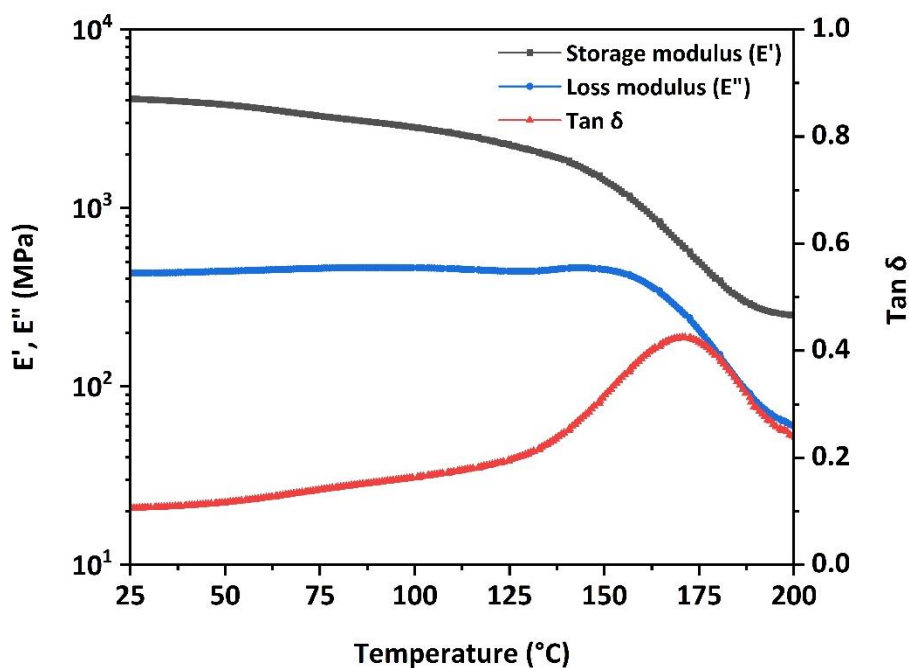
Figure S16. Evolution of the storage and loss moduli and tan delta of poly(DIS-PA-mea$_{50}$fa$_{50}$) as a function of the temperature measured by DMA

Figure S17. Evolution of the storage and loss moduli and tan delta of poly(DIS-PA-mea$_{25}$fa$_{75}$) as a function of the temperature measured by DMA
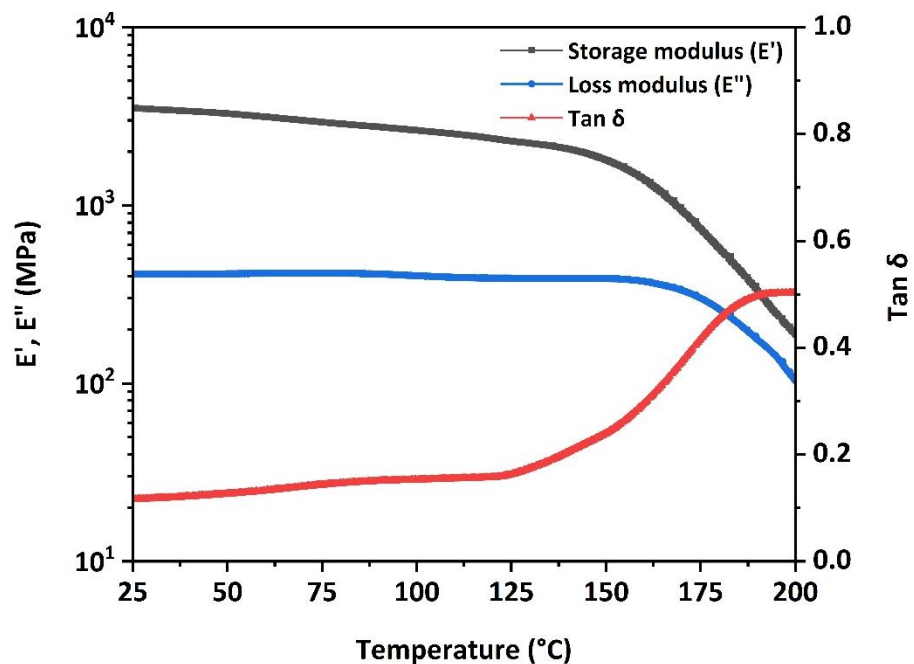
Figure S18. Evolution of the storage and loss moduli and tan delta of poly(DIS-PA-fa) as a function of the temperature measured by DMA

Figure S19. Evolution of tan δ of poly(DIS-PA-mea$_x$fa$_{100-x}$) as a function of the temperature measured by DMA

Figure S20. Evolution of the swelling equilibrium of poly(DIS-PA-mea$_x$fa$_{100-x}$) in water at room temperature
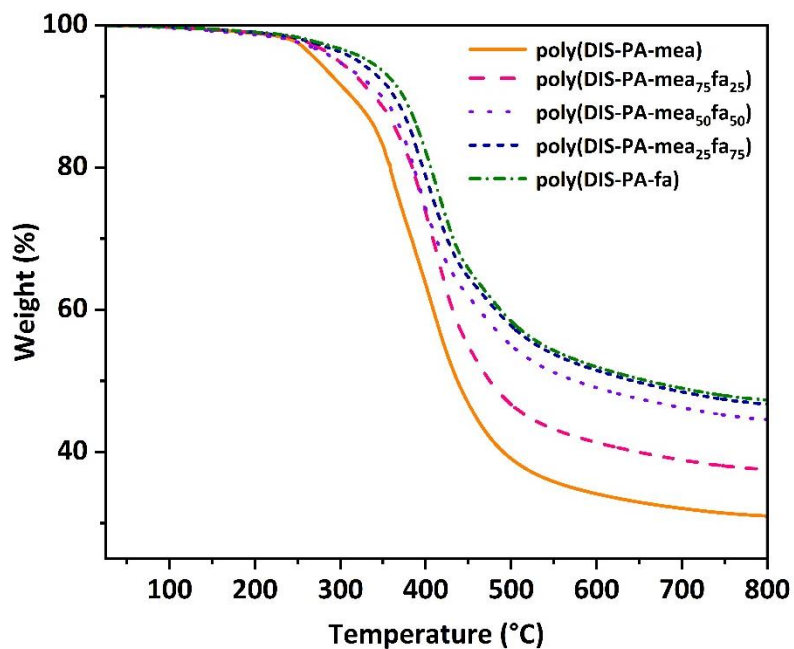
Figure S21. Evolution of the weight loss of poly(DIS-PA-mea$_x$fa$_{100-x}$) as a function of the temperature (inert atmosphere)
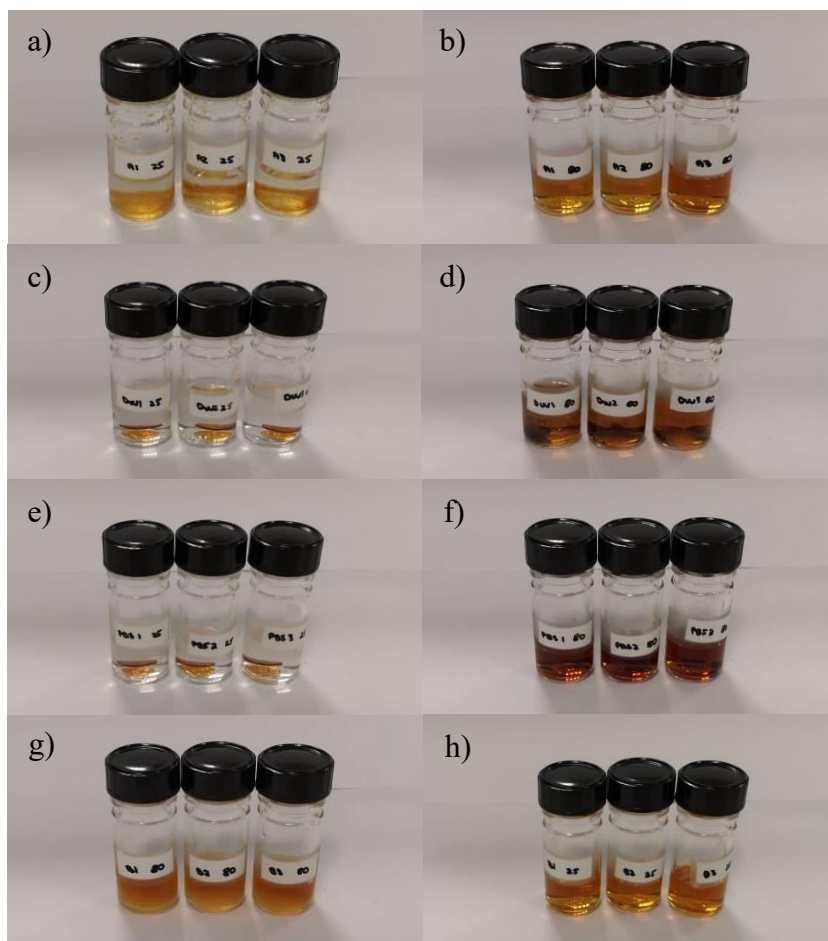
Figure S22. Photographs of poly(DIS-PA-mea) after 60 days of immersion in a/b) acetic acid, c/d) distilled water, e/f phosphate buffered solution and g/h) NaOH (1m) solutions at 25 °C (a/c/e/g) and 80 °C (b/d/f/h)
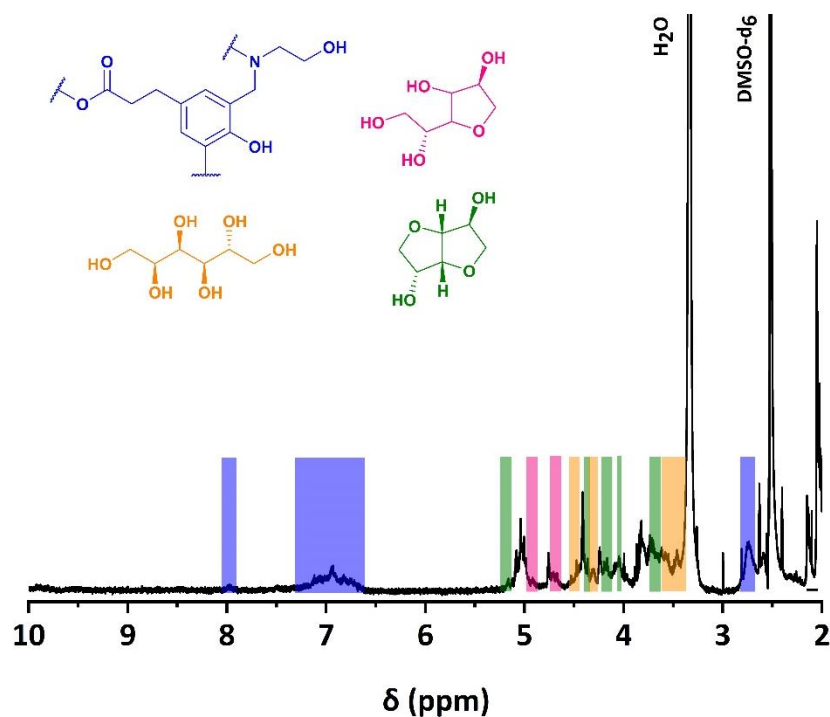
Figure S23. ^{1}H NMR spectrum of the degradation products of poly(DIS-PA-mea) after 60 days of immersion in glacial acetic acid
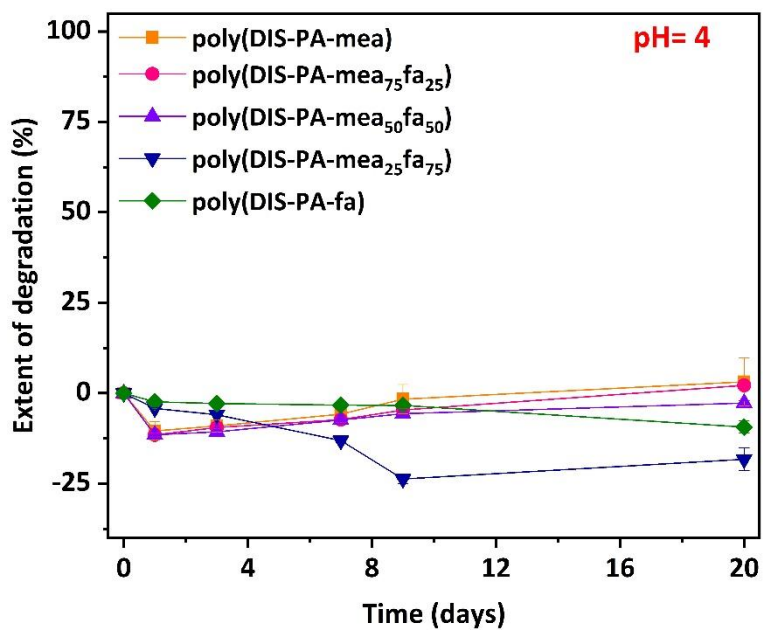
Figure S24. Evolution of the extent of degradation of poly(DIS-PA-mea$_x$fa$_{100-x}$) over time at pH= 4
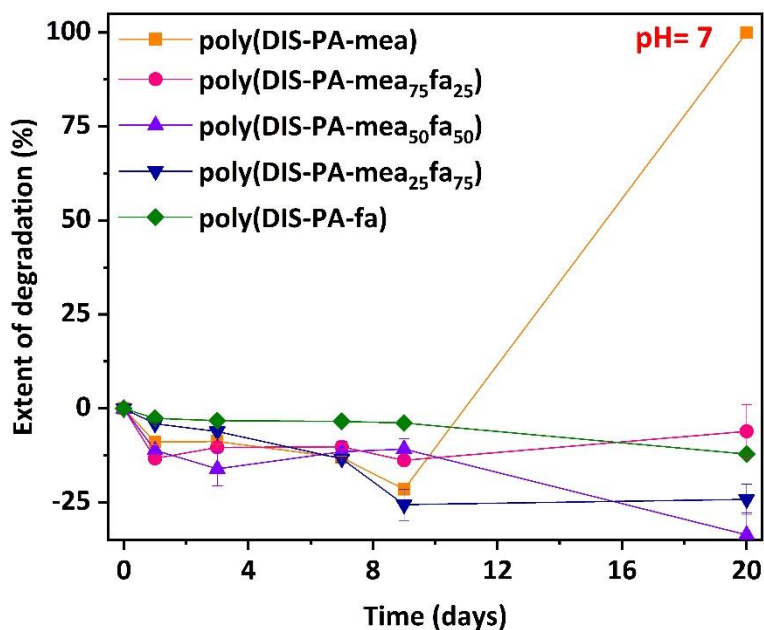
Figure S25. Evolution of the extent of degradation of poly(DIS-PA-mea$_x$fa$_{100-x}$) over time at pH= 7
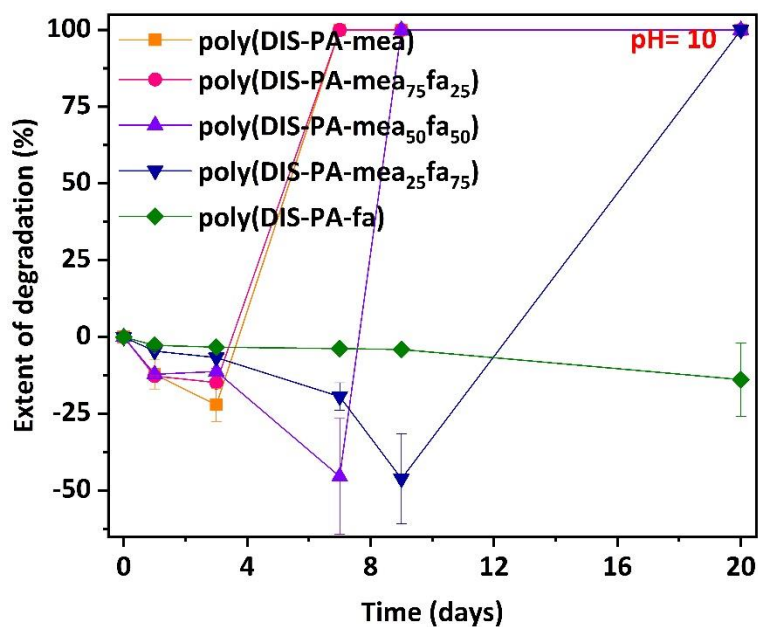
Figure S26. Evolution of the extent of degradation of poly(DIS-PA-mea$_x$fa$_{100-x}$) over time at pH= 10
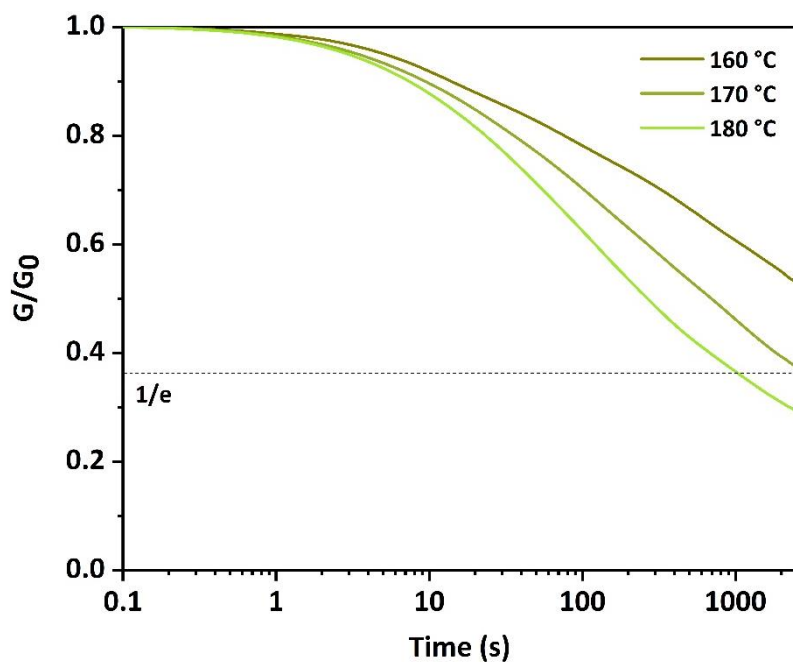
Figure S27. Stress relaxation curves of poly(DIS-PA-mea$_{75}$fa$_{25}$) at 160 °C, 170 °C and 180 °C.
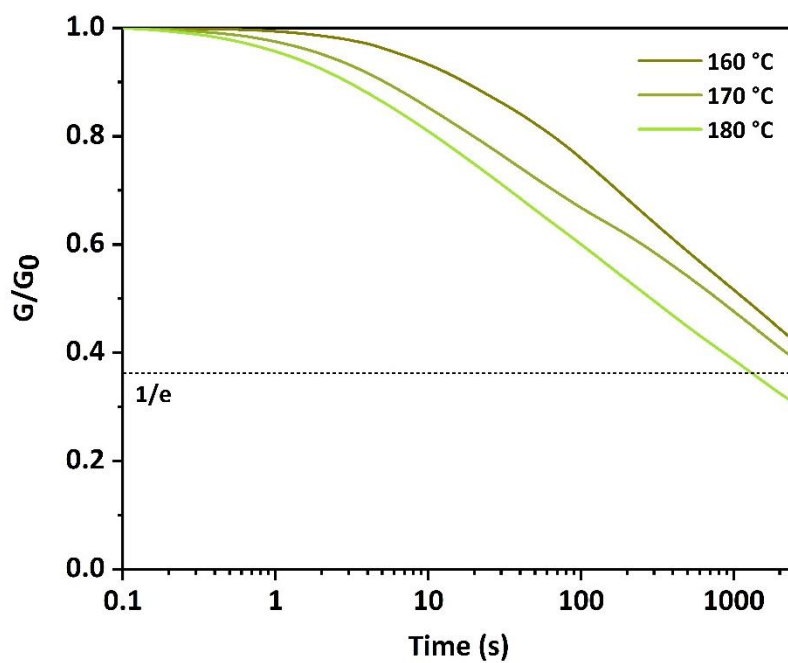
Figure S28. Stress relaxation curves of poly(DIS-PA-mea$_{50}$fa$_{50}$) at 160 °C, 170 °C and 180 °C.
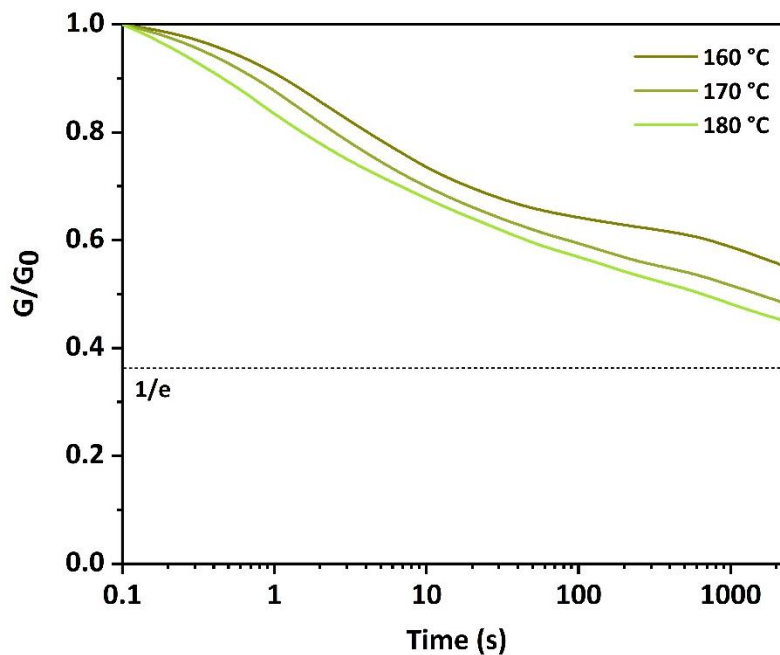
Figure S29. Stress relaxation curves of poly(DIS-PA-mea$_{25}$fa$_{75}$) at 160 °C, 170 °C and 180 °C.
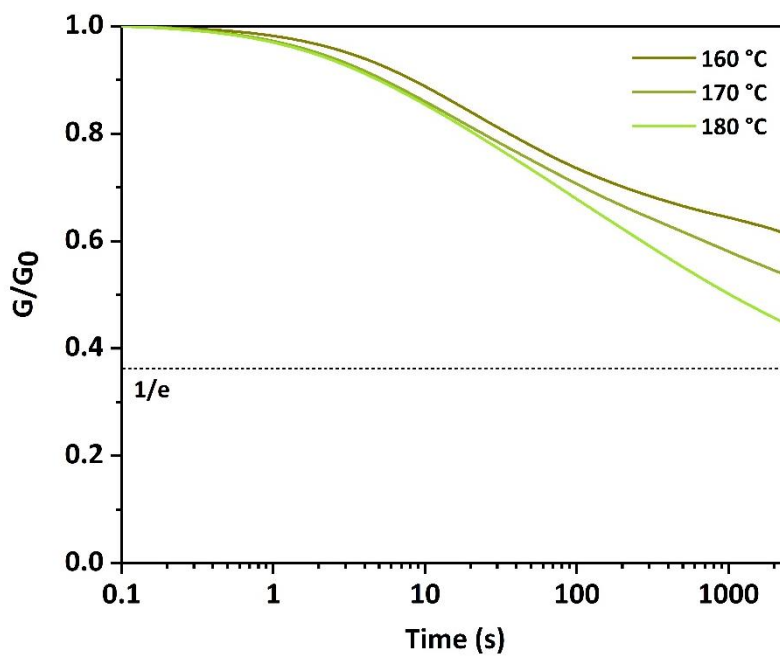
Figure S30. Stress relaxation curves of poly(DIS-PA-fa) at 160 °C, 170 °C and 180 °C.
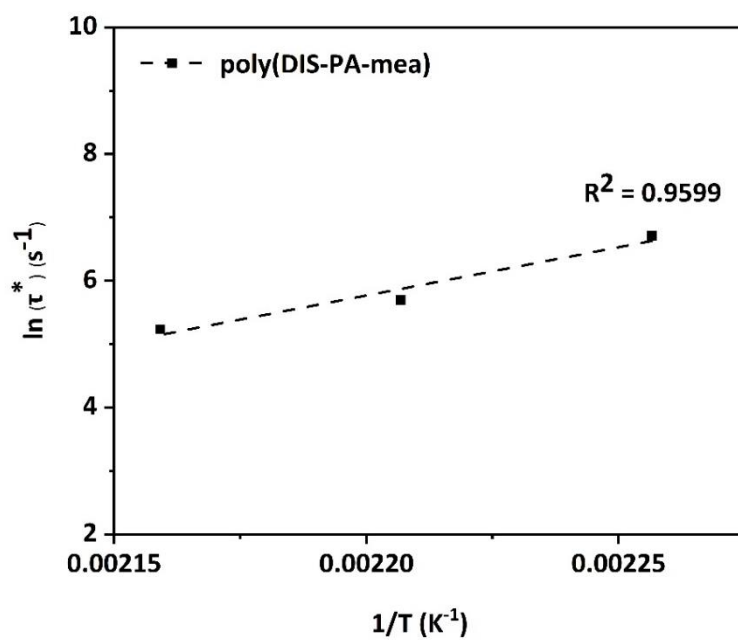
Figure S31. Arrhenius plot of poly(DIS-PA-mea)

Table S2. Storage modulus of poly(DIS-PA-mea) measured by DMA after each mechanical or chemical recycling

	Number of reprocessing	0	1	2	5
E' (GPa)	Mechanical recycling		3.0	2.8	2.7
		3.2			
	Chemical recycling		2.6	n.a.	n.a.

Annex V: Lignin-based benzoxazines A tunable key-precursor for the design of hydrophobic coatings, fire resistant materials and catalyst-free vitrimers

Lignin-based benzoxazines: a tuneable key-precursor to design fire resistant materials, hydrophobic coatings and catalyst-free vitrimers

Antoine Adjaoud [†, ‡], Laura Puchot [†], Carlos Eloy Federico [†], Rohan Das [†, ‡], and Pierre Verge [†],*

† Luxembourg Institute of Science and Technology, Materials Research and Technology Department, 5 Avenue des Hauts-Fourneaux, L-4362 Esch-sur-Alzette (Luxembourg)

‡ University of Luxembourg, 2, Avenue de l'Université, L-4365 Esch-sur-Alzette (Luxembourg)

* Corresponding author: pierre.verge@list.lu

Number of pages: 35

Number of figures: 31

Number of tables: 11

SUPPORTING INFORMATION

SUPPORTING INFORMATION

SUPPORTING INFORMATION

SUPPORTING INFORMATION

1. Equipments and characterizations

Nuclear Magnetic Resonance (NMR) spectroscopy was performed on an AVANCE III HD Bruker spectrometer equipped with a 5 mm BBO-probe operating at a proton frequency of 600 MHz. ^{31}P NMR analysis was performed following the procedure reported by Granata and Argyropoulos [1]. Chromium (III) acetylacetonate and endo-N–hydroxy–5–norbornene–2,3–dicarboximide were selected as the relaxation reagent and the internal standard compounds, respectively [2]. All ^{31}P NMR spectra were calibrated on the H_2O derivatized peak (δ = 132.2 ppm). The ^{1}H NMR spectra of lignin samples (15 mg) were recorded in 0.6 mL of deuterated dimethyl sulfoxide (DMSO-d6), except for *e*Lig-ste which is fully soluble in deuterated chloroform (CDCl$_3$). The acquisition parameters were as follows: 25 °C, 12.019 Hz spectral width, 128 scans, 2.7 s acquisition time and 10 s relaxation delay (D$_1$). The ^{13}C NMR experiments were recorded following the procedure developed by Capanema *et al.* [3]. The acquisition parameters were as follows: 25 °C, 36.232 Hz spectral width, 20,000 scans, 1.4 s acquisition time, and 2.5 s relaxation delay. The ^{1}H-^{13}C 2D HSQC NMR experiment was adapted from the procedure reported by McClelland *et al.* [4]. The 2D HSQC spectra were acquired using the standard Bruker pulse sequence "hsqcedetgpsisp2.2". The acquisition parameters were as follows: 25 °C, 20 scans. F1 dimension: 33113 Hz spectral width, 9 ms acquisition time. F2 dimension: 7212 Hz spectral width, 233 ms acquisition time.

Fourier transform infrared spectroscopy (FTIR) was conducted on a Bruker INVENIO® instrument in the attenuated total reflection (ATR) mode using a diamond crystal. All spectra were recorded at room temperature in direct absorbance mode across 4000-400 cm^{-1} frequency range (32 scans, 4 cm^{-1} spectral resolution).

Elemental analysis (CHNS measurements) was performed on a Vario MACRO cube CHNS/O from Elementar France SARL.

Size-exclusion chromatography (SEC) was performed on a 1200 Infinity II gel permeation chromatograph to determine the molecular weight of the lignin samples (Agilent technologies). The chromatograph was equipped with an integrated IR detector, a PL PolarGel-M column, and a PL PolarGel-

M guard column (Agilent technologies). 0.1 M solution of $Li(CF_3SO_2)_2N$ (LiTFSI) in DMF was used as an eluent with a flow rate of 1.0 mL.min^{-1} at 50 °C. Polystyrene standards (Agilent Technologies, Mp = 162–1500*10^3 g.mol^{-1}) were used to perform the calibration of the system. The molecular weight is determined on the eluent's soluble fraction part (4 mg.mL^{-1}).

Differential scanning calorimetry (DSC) thermograms were recorded on a Netzsch DSC 204 F1 Phoenix device in standard pierced aluminum crucibles (40 µL). Lignin-based benzoxazine precursors were initially subjected to a first heating–cooling ramp from 25 to 125 °C to clear the thermal history and to remove residual traces of moisture (heating rate: 10 °C.min^{-1}, cooling rate: 20 °C.min^{-1}, N_2 atmosphere). The sample was finally reheated from 25 to 250 °C at a heating rate of 10 °C.min^{-1} under N_2 atmosphere . The DSC thermogram of the cured materials was recorded over two consecutive heating-cooling cycles from 25 to 200 °C (heating rate: 10 °C.min^{-1}, cooling rate: 20 °C.min^{-1}, N_2 atmosphere).

Rheological measurements were recorded using an Anton Paar Physica MCR 302 rheometer equipped with a CTD 450 temperature control device. Isothermal rheo-kinetic measurements were performed with a disposable aluminum parallel plate-plate geometry (Ø= 25 mm, gap 0.5 mm). The polymerization measurements were recorded in the oscillation mode at a controlled 0.1% strain amplitude (1 Hz). Heating ramps of 20 °C.min^{-1} were applied to reach the isothermal curing temperature. The sample deformation was ramped linearly from 1 to 0.2 % to remain within the instrument's limitation and the linear viscoelastic regime. Rheology temperature sweep curves were performed in rectangular-torsion mode from 25 to 225 °C (heating rate: 2 °C.min^{-1}) on bar-shaped material under constant deformation of 0.1% at a frequency of 0.5 Hz (sample size: length:width:thickness = 25mm:5mm:1.25mm). Stress relaxation experiments were performed on disk-shaped solid geometry with a disposable aluminum plate-plate (Ø= 25 mm). The relaxation modulus was followed as a function of time for 1 hour between 160 and 200 °C with a constant applied strain of 5 % and normal force of 10 N. The original relaxation modulus (G_0) was extracted from the initial plateau of the stress relaxation curves (onset point of the second derivative curve).

SUPPORTING INFORMATION

The shear stress-strain curves were measured on rectangular-shaped bars a shear rate of 0.5 %.min^{-1} until the material breaks (sample size: length:width:thickness = 25mm:5mm:1.25mm).

Micro-computed x-ray tomography (μCT) was performed on a laboratory x-ray cone-beam CT system EasyTom 160 produced by RX Solutions. The acquired projections were used as an input for the 3D volume reconstruction by using the software Xact64. Geometrical corrections and ring artefacts attenuation were previously applied. Finally, the volume reconstruction was carried out by means of the filtered back-projection algorithm implemented in the software Xact64. 3D image analysis of μCT results was carried out with the commercial software Avizo. The different phases in the material were segmented by thresholding the greyscale intensity histogram. Finally, the images were statistically studied through different morphological parameters.

Dynamic mechanical analysis (DMA) was used to evaluate the mechanical properties of the cured materials and vitrimer samples after reprocessing (sample size: length:width:thickness = 25mm:5mm:1.25mm). The storage modulus (E") was recorded as a at room temperature as function of time in the tension mode (f= 1 Hz, preload force= 0.05 N, sinusoidal strain= 10 μm).

Thermogravimetric analysis (TGA) was completed on the Mettler Toledo TGA 2 device in ceramic alumina pan from 25 to 800 °C at 10 °C.min^{-1} rate under inert atmosphere (N_2). Limiting oxygen index (LOI) was calculated by the equation S1 [5]:

$$LOI\ (\%) = 17.5 + 0.4 * CR_{800}\ (S1)$$

where CR_{800} corresponds to the char residue at 800 °C.

Calorimetric measurements were carried out at C2MA-IMT Mines Alès, in France. Pyrolysis-Combustion Flow Calorimetry (PCFC) was carried out under anaerobic pyrolysis with heating rate of 1 °K.s^{-1} up to 750 °C.

The thickness of the different coatings was determined on KLA Tencor P-17 profilometer from the average step height measured between the glass substrate and the coating (scan speed: 100 μm.s^{-1}, scan rate of 200 Hz, applied force: 2 mg).

Atomic force microscopy (AFM) analysis was performed in amplitude modulation-frequency modulation (AM-FM) mode to determine the surface morphology of lignin-based coatings using cantilever Tap 190DLC (BudgetSensors) which has a resonance frequency of 190 kHz and a spring constant of 48 N.m^{-1}. The resulting nanographs were processed in the topography, phase, and frequency channels.

Scanning electron microscopy (SEM) was used to analyze the morphology of the lignin-based vitrimer. Micrographs were captured at different magnifications using Helios 650 Nanolab SEM instrument through the Lens Secondary Electron Detector operating at 2-5 kV voltage and 100 pA-0.2 nA current."

2. Characterisation of the raw material

Table S1 *Physicochemical properties of the technical lignin*

Lig	[a] ^{31}P NMR			[b] ^{13}C NMR	GPC		
	[OH]$_{aliphatic}$	[OH]$_{phenolic}$	[OH]$_{carboxylic}$	MeO / Ar	[c] M_n (g.mol^{-1})	[d] M_w (g.mol^{-1})	[e] Đ
P2400	2.41 ± 0.12	4.51 ± 0.28	0.70 ± 0.11	1.28	688	3341	4.9

[a] expressed in mmol per g of lignin dry matter (standard error of three samples), [b] aromatic region of ^{13}C NMR (δ= 100-160 ppm) normalized to one aromatic ring (6C) [c] number average molecular weight, [d] weight average molecular weight, and [e] dispersity (M_w/ M_n).

3. Synthetic procedure of lignin-benzoxazine precursors: Lig-Bz

P2400 (Lig) was determined to contain 1.99 mmol.g^{-1} of phenolic units liable to react through Mannich condensation ([H] and [G$_{nc}$] units, 0.54 and 1.45 mmol.g^{-1} measured by quantitative ^{31}P NMR, respectively). The reaction was carried out dissolving 5 g of technical lignin P2400 (1 eq.), the amine precursor (1 eq.), and paraformaldehyde (2 eq., 0.63 g) in a minimum amount of solvent (20 mL, THF for mea and fa, DIOX for ste) in a 100 mL round bottom flask sealed with a rubber septum. Specific amount of amine precursors and selection of reaction solvent are reported in Table S2 (column 1-4). The mixture was magnetically stirred at room temperature for 1 h under nitrogen atmosphere. The temperature was raised to 70 or 80 °C and kept for 3 or 24 h (Table S2, column 5-7). After cooling to room temperature, the crude product was concentrated under reduced pressure using rotary evaporator. Then, the extract was redissolved in 200 mL of diethylether, filtered on Büchner funnel, and washed thoroughly with excess water and diethylether. After a final drying step (T= 50 ºC overnight under reduced pressure), isolated Lig-Bz were recovered as dark-brown fine powder (Table S2, column 8-9).

Table S2 Reaction conditions for the synthesis of Lig-Bz through Mannich-like condensation.

Reagents				Reaction conditions			Material	
Type	m (g)	n (mmol)	N (eq.)	Solvent	T (°C)	t (h)	Sample	m$_f$ (g)
Lig	5.00	9.95 *	1.0	THF	70	3	Lig-mea	5.28
PFA	0.63	20.90	2.0					
mea	0.61	9.95	1.0					
Lig	5.00	9.95 *	1.0	THF	70	24	Lig-fa	5.37
PFA	0.63	20.90	2.0					
fa	0.97	9.95	1.0					
Lig	5.00	9.95 *	1.0	DIOX	80	24	Lig-ste	6.85
PFA	0.63	20.90	2.0					
ste	2.68	9.95	1.0					

[a] amount of reactive phenolic units determined by quantitative ^{31}P NMR experiment ([H] + [G$_{nc}$] = 1.99 mmol.g^{-1})

4. Structural features of lignin-benzoxazine precursors: *e*Lig-Bz

3.1 eLig-mea

^{1}H NMR (DMSO-d$_6$, 600 MHz, 298 ºK): δ (ppm) = 2.56 [2]; 2.72 [3]; 2.84 [12]; 3.50 [-O-Alk]; 3.57 [13]; 3.76 [-OMe]; 3.92 [10]; 4.11 [x]; 4.56 [14]; 4.78 [11]; 6.62-7.01 [6&7&5].

^{13}C NMR (DMSO-d$_6$, 600 MHz, 298 ºK): δ (ppm) = 30.1 [3]; 35.9 [2]; 50.4 [10]; 53.9 [12]; 56.5 [-OMe]; 60.1 [13]; 63.7 [x]; 70.3 [-O-Alk]; 83.1 [11]; 116.2 [6]; 120.8 [8]; 127.7-129.6 [5/7]; 132.5 [4]; 152.7 [9]; 172.8 [1].

Elemental analysis (%): C (63.6), H (6.2), N (3.7), S (0.6), O (25.9)

3.2 eLig-fa

^{1}H NMR (DMSO-d$_6$, 600 MHz, 298 ºK): δ (ppm) = 2.56 [2]; 2.73 [3]; 3.50 [-O-Alk]; 3.75 [-OMe]; 3.82 [12]; 3.88 [10]; 4.11 [x]; 4.78 [11]; 6.31 [14]; 6.39 [15]; 6.60-7.01 [6&7&5]; 7.56 [16].

^{13}C NMR (DMSO-d$_6$, 600 MHz, 298 ºK): δ (ppm) = 30.0 [3]; 35.9 [2]; 48.0 [12]; 49.3 [10]; 56.5 [-OMe]; 63.7 [x]; 70.3 [-O-Alk]; 81.9 [11]; 109.1 [14]; 110.9 [15]; 116.3 [6]; 120.1 [8]; 127.9 [5]; 128.6 [7]; 131.0 [4]; 143.1 [16]; 152.3 [9/13]; 172.8 [1].

Elemental analysis (%): C (65.5), H (6.2), N (3.2), S (0.6), O (24.6)

3.3 eLig-ste

^{1}H NMR (CDCl$_3$, 600 MHz, 298 ºK): δ (ppm) = 0.81 [14]; 1.18 [13]; 2.54 [2]; 2.71 [3]; 2.78 [12]; 3.57 [-O-Alk]; 3.80 [10]; 3.88 [-OMe]; 4.15 [x]; 4.76 [11]; 6.50-6.87 [6&7&5].

^{13}C NMR (CDCl$_3$, 600 MHz, 298 ºK): δ (ppm) = <14.1 [14]; 22.7 [13]; 29.7 [3/13]; 31.9 [13]; 36.0 [2]; 50.3 [10]; 51.4 [12]; 56.3 [-OMe]; 63.6 [x]; 70.6 [-O-Alk]; 82.3 [11]; 116.3 [6]; 120.1 [8]; 127.2-127.5 [5/7]; 132.4 [4]; 152.6 [9]; 172.9 [1].

Elemental analysis (%): C (73.7), H (9.5), N (2.7), S (0.5), O (12.6)

5. Supplementary Figures and Tables

Table S3 *Determination of hydroxyls content in P2400 and eLig quantified by ^{31}P NMR (expressed in mmol per g of lignin dry matter, standard error of three samples).*

Hydroxyls content		P2400 (Lig)	*e*Lig
Aliphatic –OH (mmol.g^{-1})		2.41 ± 0.12	0.25 ± 0.00
Phenolic –OH	[5-subst.] (mmol.g^{-1})	2.52 ± 0.12	1.92 ± 0.15
	[G$_{nc}$] (mmol.g^{-1})	1.45 ± 0.11	1.07 ± 0.05
	[H] (mmol.g^{-1})	0.54 ± 0.04	1.98 ± 0.09
Carboxylic–OH (mmol.g^{-1})		0.70 ± 0.11	0.77 ± 0.06
Total –OH (mmol.g^{-1})		7.61 ± 0.48	5.98 ± 0.25

Table S4 *Determination of hydroxyls content in lignin-benzoxazine synthesized from technical lignin quantified by ^{31}P NMR (expressed in mmol per g of lignin dry matter, standard error of three samples).*

Hydroxyls content		Lig-mea	Lig-fa	Lig-ste
Aliphatic –OH (mmol.g^{-1})		2.35 ± 0.19	1.58 ± 0.12	1.37 ± 0.25
Phenolic –OH	[5-subst.] (mmol.g^{-1})	2.52 ± 0.15	2.50 ± 0.11	2.05 ± 0.54
	[G$_{nc}$] (mmol.g^{-1})	0.81 ± 0.04	0.87 ± 0.09	0.58 ± 0.17
	[H] (mmol.g^{-1})	0.28 ± 0.06	0.24 ± 0.04	0.24 ± 0.11
Carboxylic–OH (mmol.g^{-1})		0.47 ± 0.02	0.58 ± 0.04	0.47 ± 0.03
Total –OH (mmol.g^{-1})		6.43 ± 0.35	5.77 ± 0.21	4.70 ± 1.06

Table S5 *Determination of hydroxyls content in lignin-benzoxazine synthesized from esterified lignin quantified by ^{31}P NMR (expressed in mmol per g of lignin dry matter, standard error of three samples).*

Hydroxyls content		*e*Lig-mea	*e*Lig-fa	*e*Lig-ste
Aliphatic –OH (mmol.g^{-1})		1.45 ± 0.17	0.18 ± 0.02	0.10 ± 0.01
Phenolic –OH	[5-subst.] (mmol.g^{-1})	1.44 ± 0.15	1.40 ± 0.05	0.89 ± 0.05
	[G$_{nc}$] (mmol.g^{-1})	0.65 ± 0.06	0.44 ± 0.01	0.35 ± 0.01
	[H] (mmol.g^{-1})	0.56 ± 0.07	0.77 ± 0.03	0.37 ± 0.01
Carboxylic–OH (mmol.g^{-1})		0.47 ± 0.03	0.42 ± 0.02	0.28 ± 0.01
Total –OH (mmol.g^{-1})		4.56 ± 0.53	3.10 ± 0.08	2.00 ± 0.07

Comment: The amount of aliphatic –OH groups increased solely for *e*Lig-mea, the precursor synthesized from an amino-alcohol derivative ([OH]$_{ali}$= 1.4 mmol.g^{-1}). *e*Lig-ste exhibits the lowest amount of total –OH groups ([OH]$_t$= 2.00 mmol.g^{-1}) due to the diluting effect of the long alkyl side-chain.
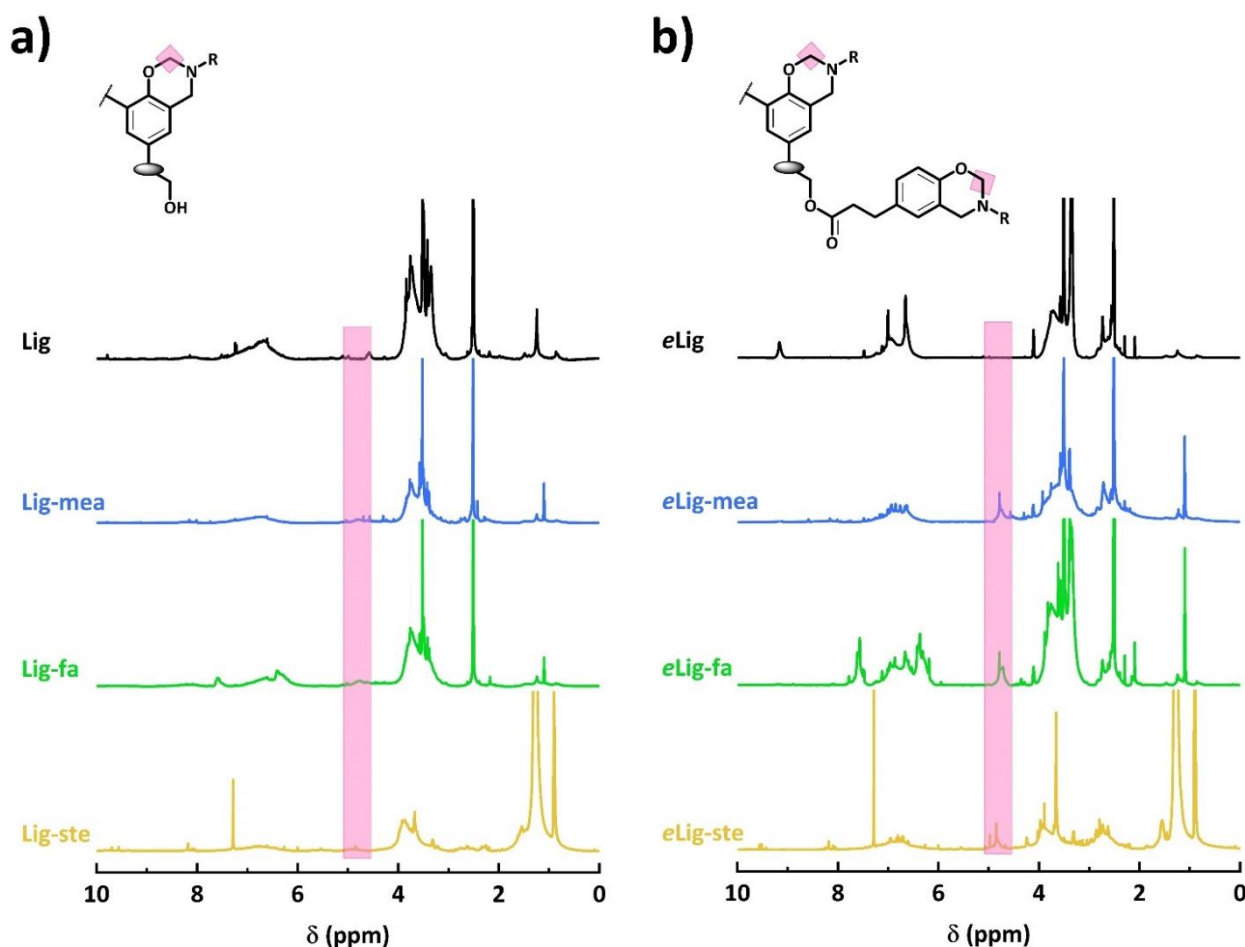
Figure S1 ^1H NMR spectra of (a) Lig-Bz and (b) eLig-Bz: identification of the oxazine methylene peak (O-CH$_2$*-N).
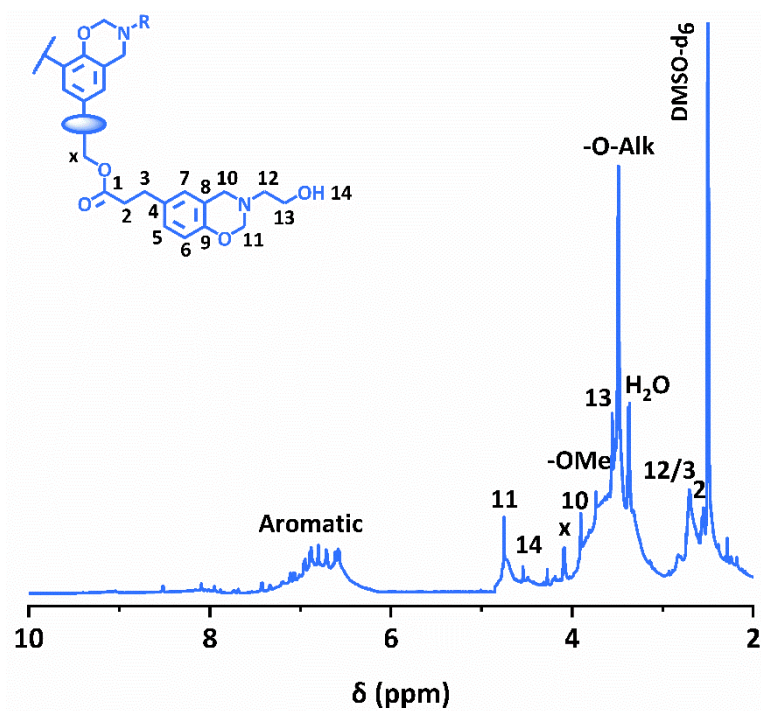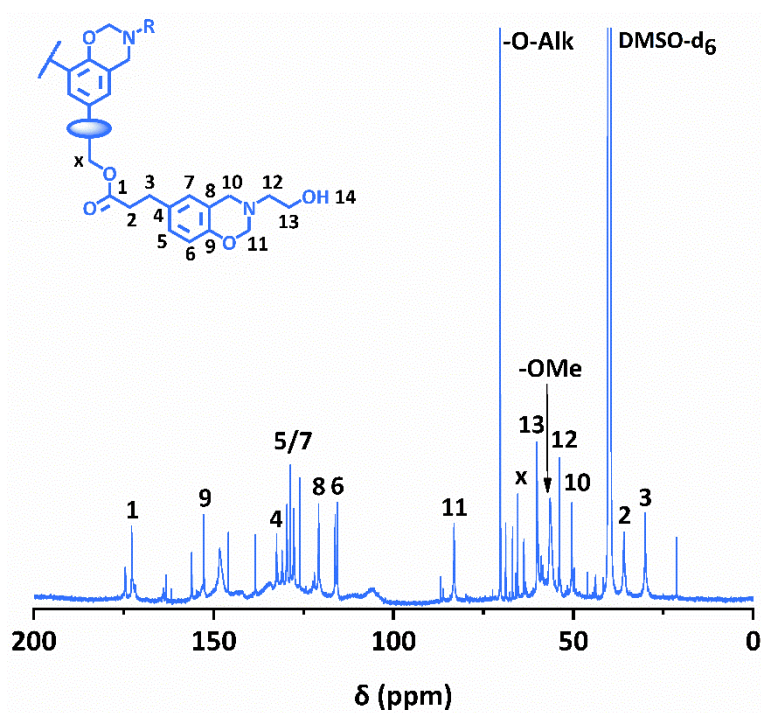
Figure S2 ^1H *NMR spectra of eLig-mea.*

Figure S3 ^{13}C *NMR spectra of eLig-mea.*

Figure S4 ^1H *NMR spectra of eLig-fa.*

Figure S5 ^{13}C *NMR spectra of eLig-fa.*

Figure S6 ^{1}*H NMR spectra of eLig-ste.*

Figure S7 ^{13}*C NMR spectra of eLig-ste.*
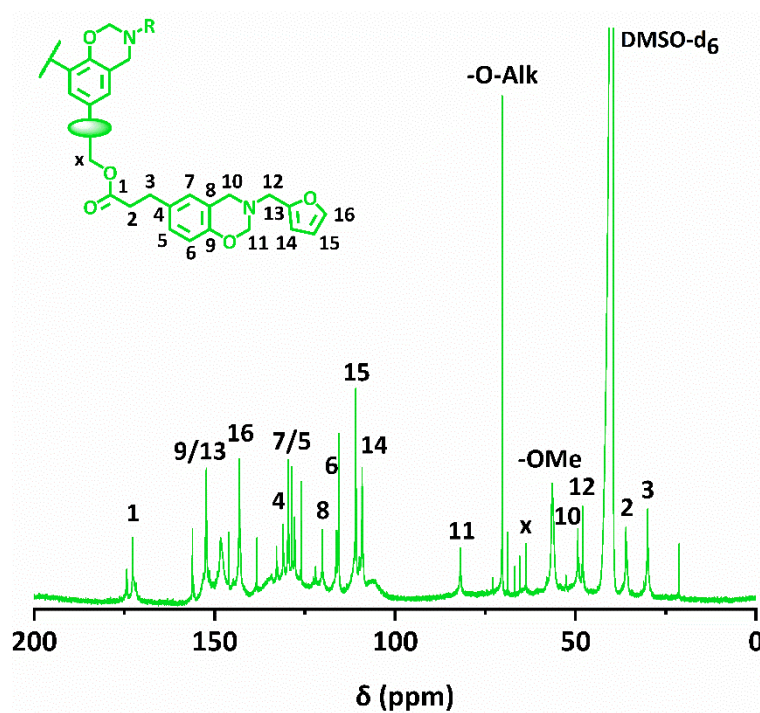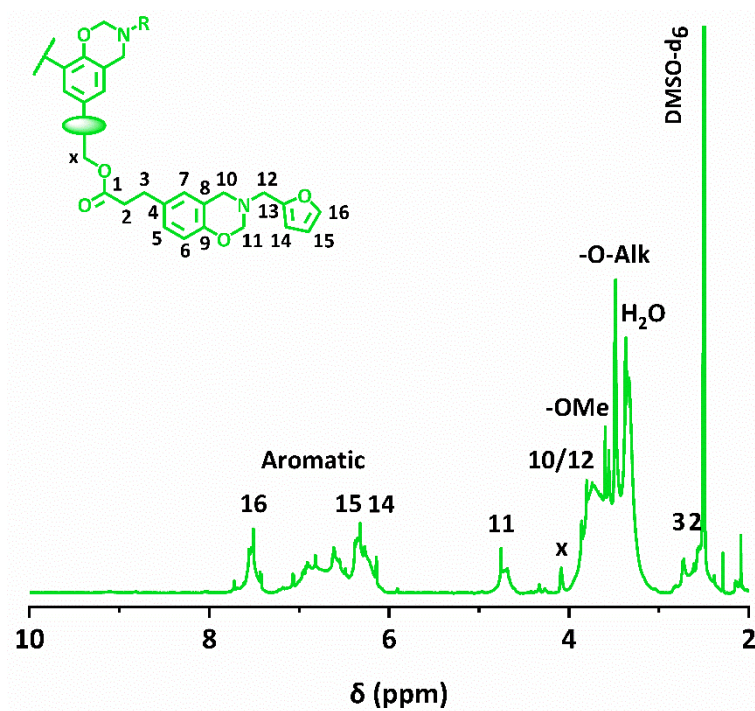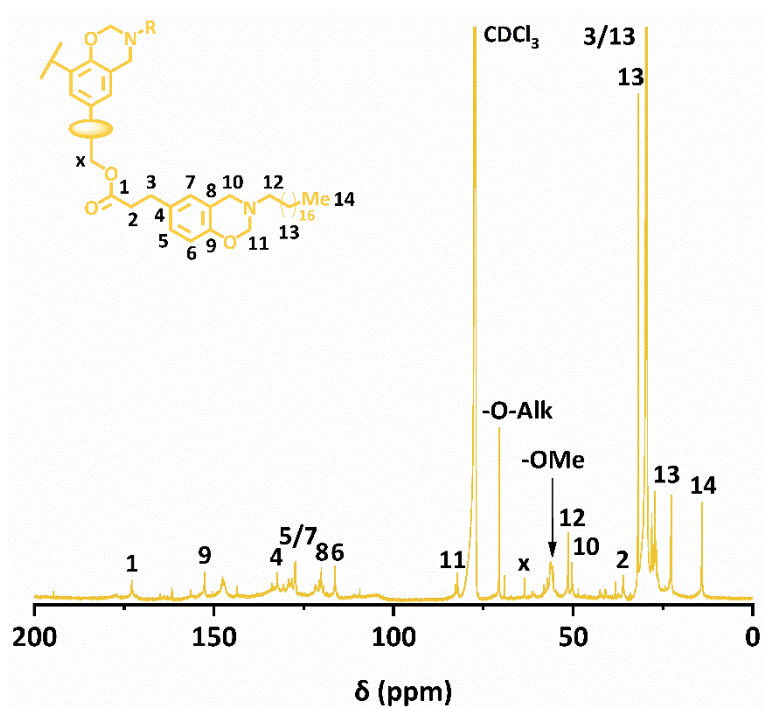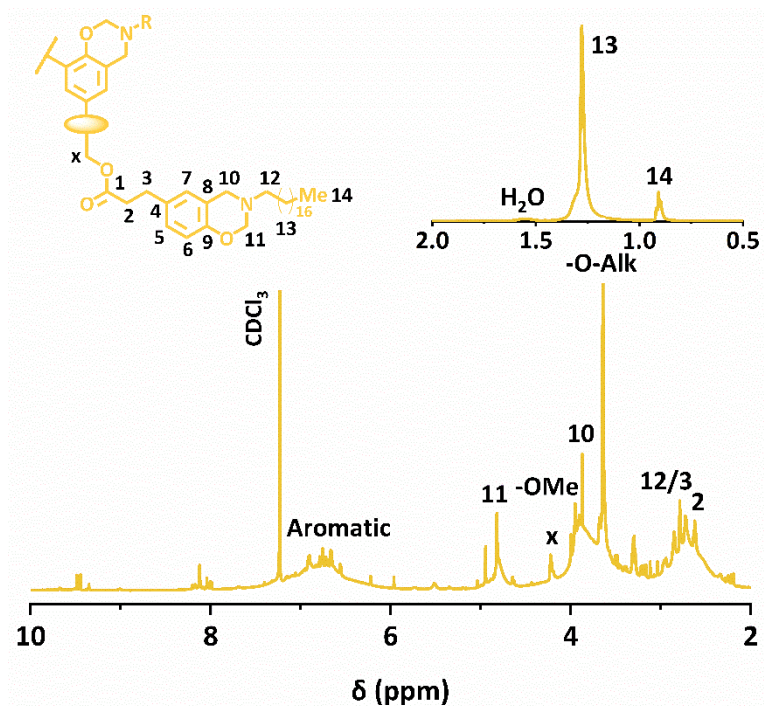
Comment: The β– and α-alcohol methylene protons are observed in the aliphatic region of *e*Lig-mea at δ_C/δ_H: 53.9 /2.89 ppm (A_{12}) and δ_C/δ_H: 60.1 /3.57 ppm (A_{13}), respectively. The increase of the number of aliphatic –OH groups measured by ^{31}P NMR (Table S5) and the appearance of the signal in ^{1}H NMR at δ= 4.56 ppm correspond to the added aliphatic –OH groups (Figure S2). In addition to the aliphatic side-chain cross-peak signal B_{12} (δ_C/δ_H: 48.0 /3.82 ppm), new cross-peak signals are identified in the aromatic region of *e*Lig-fa attributed to the protons from the furan ring (B_{14}, B_{15}, and B_{16} in Figure S8.b). The chemical shifts in the range of δ_C/δ_H: 10-35 /0.8-1.4 ppm in *e*Lig-ste is attributed to the methyl (C_{14}) and methylene groups (C_{13}) from the long alkyl chain.
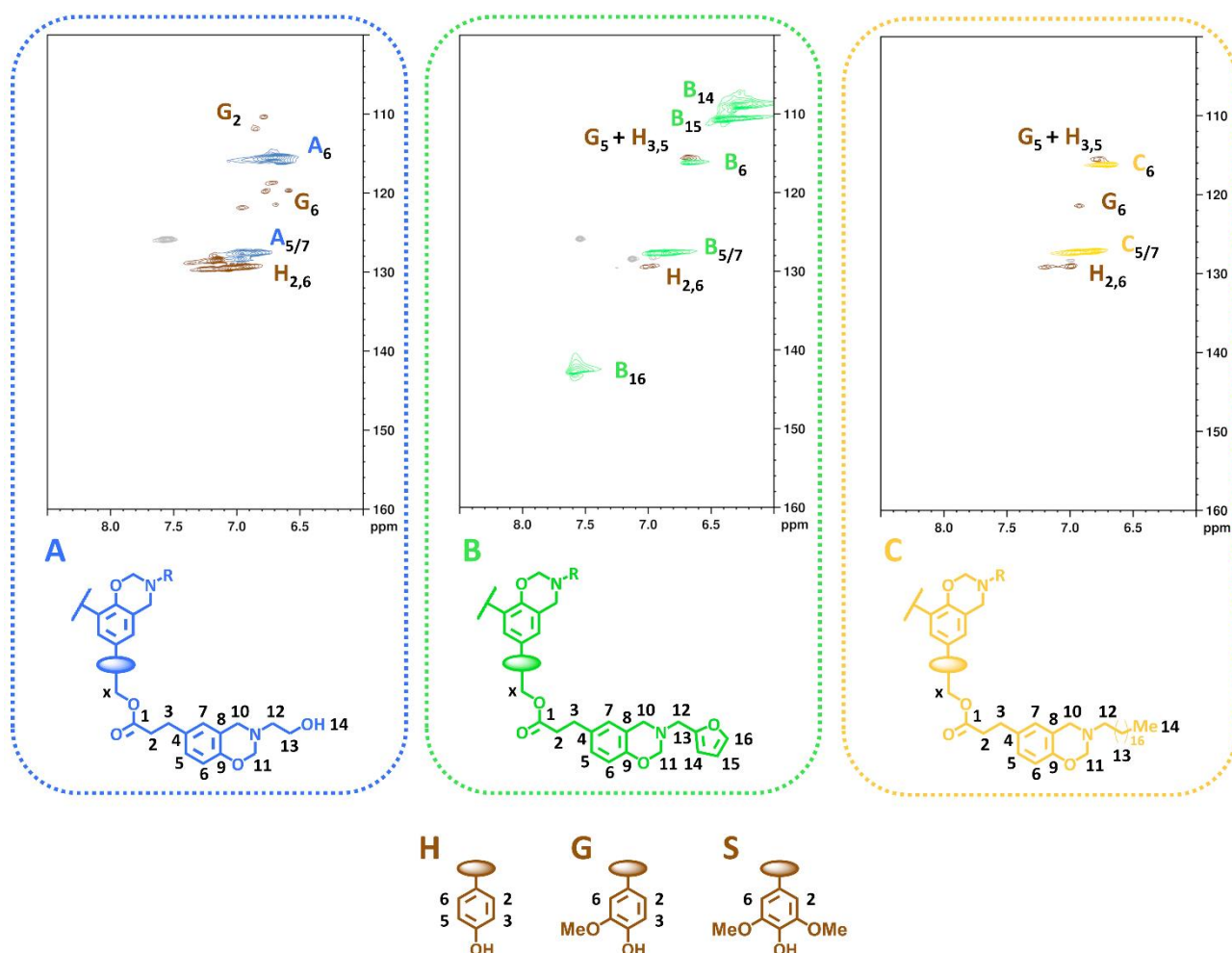
Figure S8 *^{1}H-^{13}C HSQC NMR spectra of a) eLig-mea, b) eLig-fa, and c) eLig-ste over the aromatic region*
(δ_C/δ_H: 100-160 ppm / 6.0-8.5 ppm).
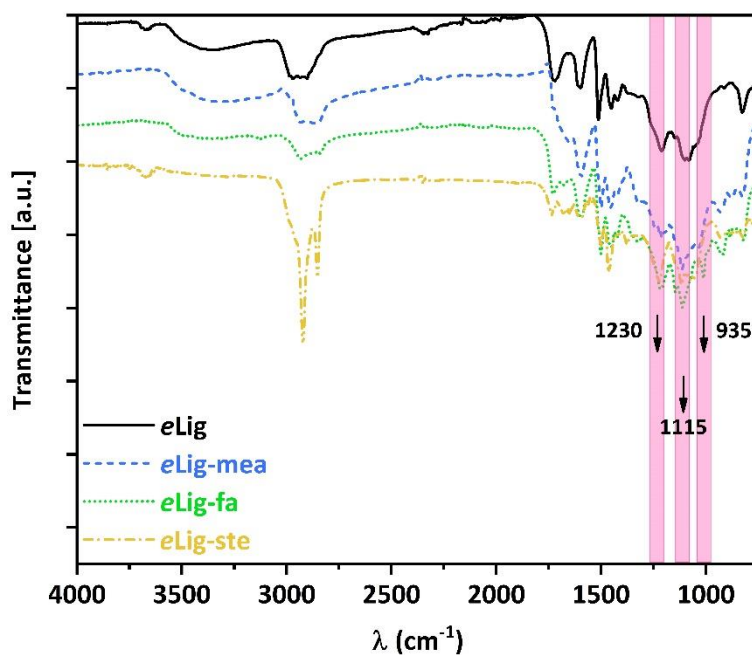
Figure S9 *FTIR spectra of eLig and eLig-Bz.*

Comment: The appearance of characteristic absorption peaks at υ= 1230, 1115, and 932 cm^{-1} (C-O-C asymmetric stretching, the primarily antisymmetric C-N-C stretching and the C–H out-of-plane vibration in the trisubstituted benzene ring, respectively) is assigned to the formation of benzoxazine rings.
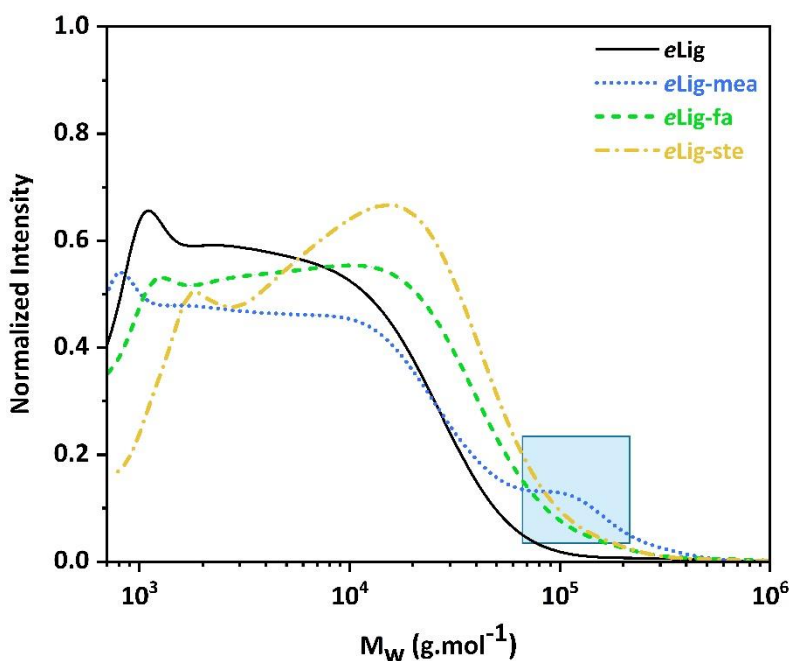
Figure S10 *Average molecular weight of eLig and eLig-Bz (4 mg.ml^{-1} in 0.1 M LiTFSI in DMF).*
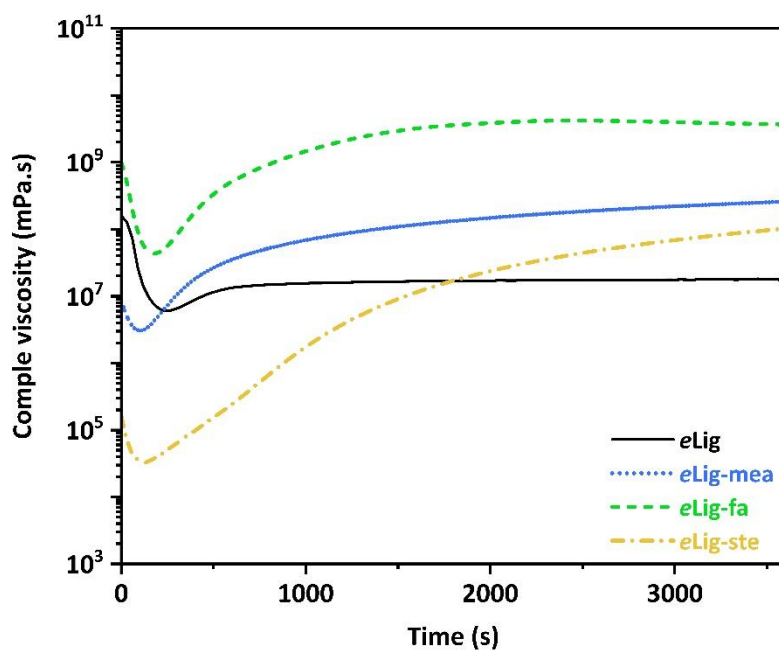
Figure S11 *Complex viscosity curves of eLig and eLig-Bz recorded by isothermal curing by rheology (150 °C).*
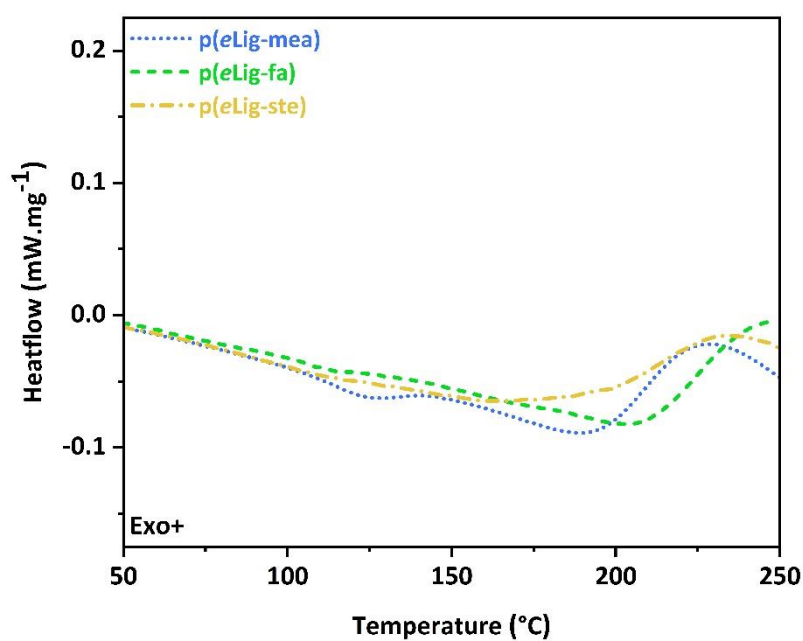
Figure S12 *DSC curves of p(eLig-Bz) (10 °C.min^{-1}, N$_2$).*
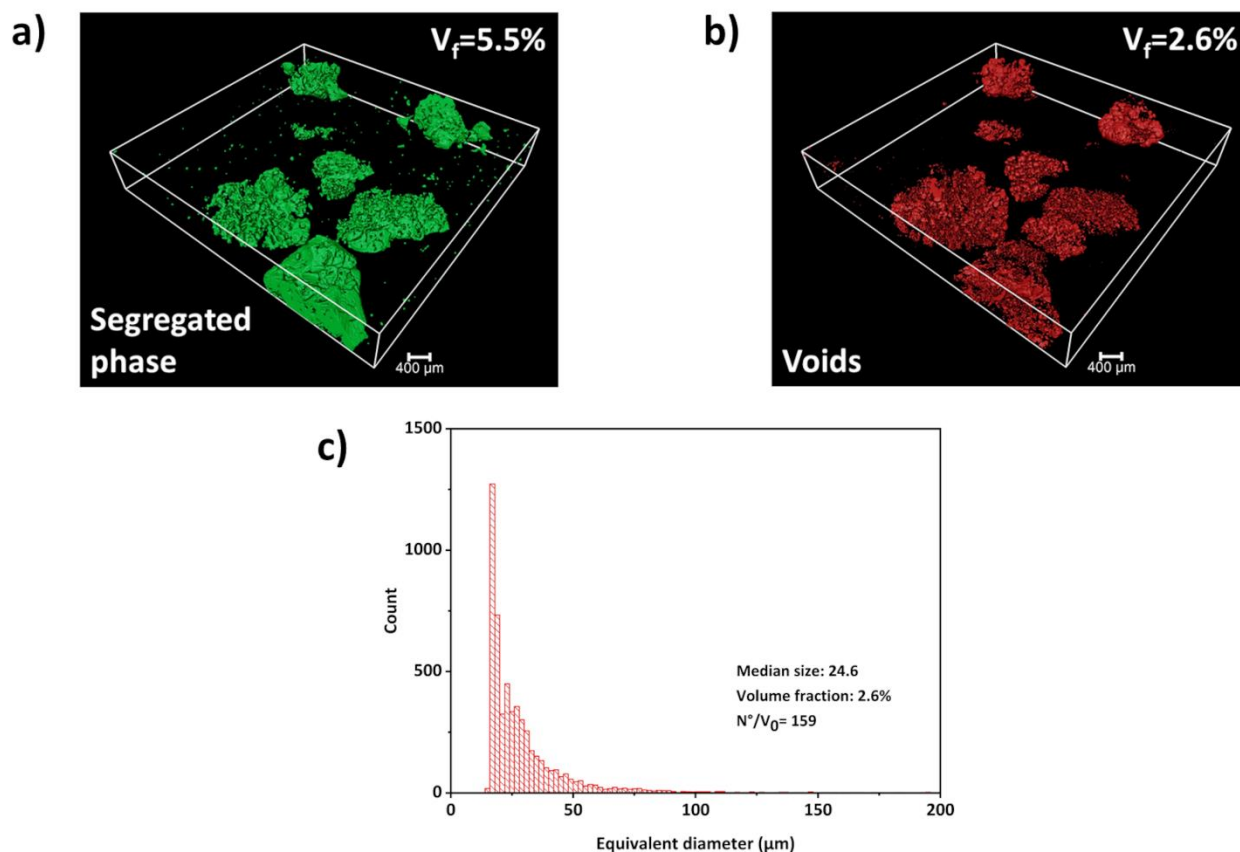
Figure S13 Cured p(eLig-mea) manufactured by vacuum compression molding: 3D rendering of (a) segregated phase and (b) voids fraction. c) Equivalent diameter histogram of voids.

Comment: Thermally activated transesterification reactions give rise to longer polymer chains within the thermoset network attested by the larger molecular weight distributions of *e*Lig-mea (Figure S10). Therefore, these dynamic exchanges may cause lignin oligomers to coalesce into regions of higher density. Submicron-sized high-density nodules may correspond to ultrastructural regions assigned to topological defects such as polymer chain entanglements. The volume fraction of these segregated phases yields $V_f=$ 5.5% (Figure S13.a). The observed holes surrounding these regions of higher density are originating from moisture evaporation during the curing process. The abundant number of aliphatic −OH groups determined *e*Lig-mea (Table S4), contributes to form more hydrogen bonds, and consequently lead to higher moisture sorption. The moisture content of each eLig-Bz determined by TGA experiment revealed that *e*Lig-mea contains the higher amount of water (1 wt.%) as compared to other precursors (0.2 wt.%). The evaporation of water results in the creation of voids during curing processes representing a volume fraction of $V_f=$ 2.6 % (Figure 13.b). An estimation of the equivalent diameter over the porous fragments (N= 159) revealed a median pore size of Ø= 24.6 μm (Figure S13.c).
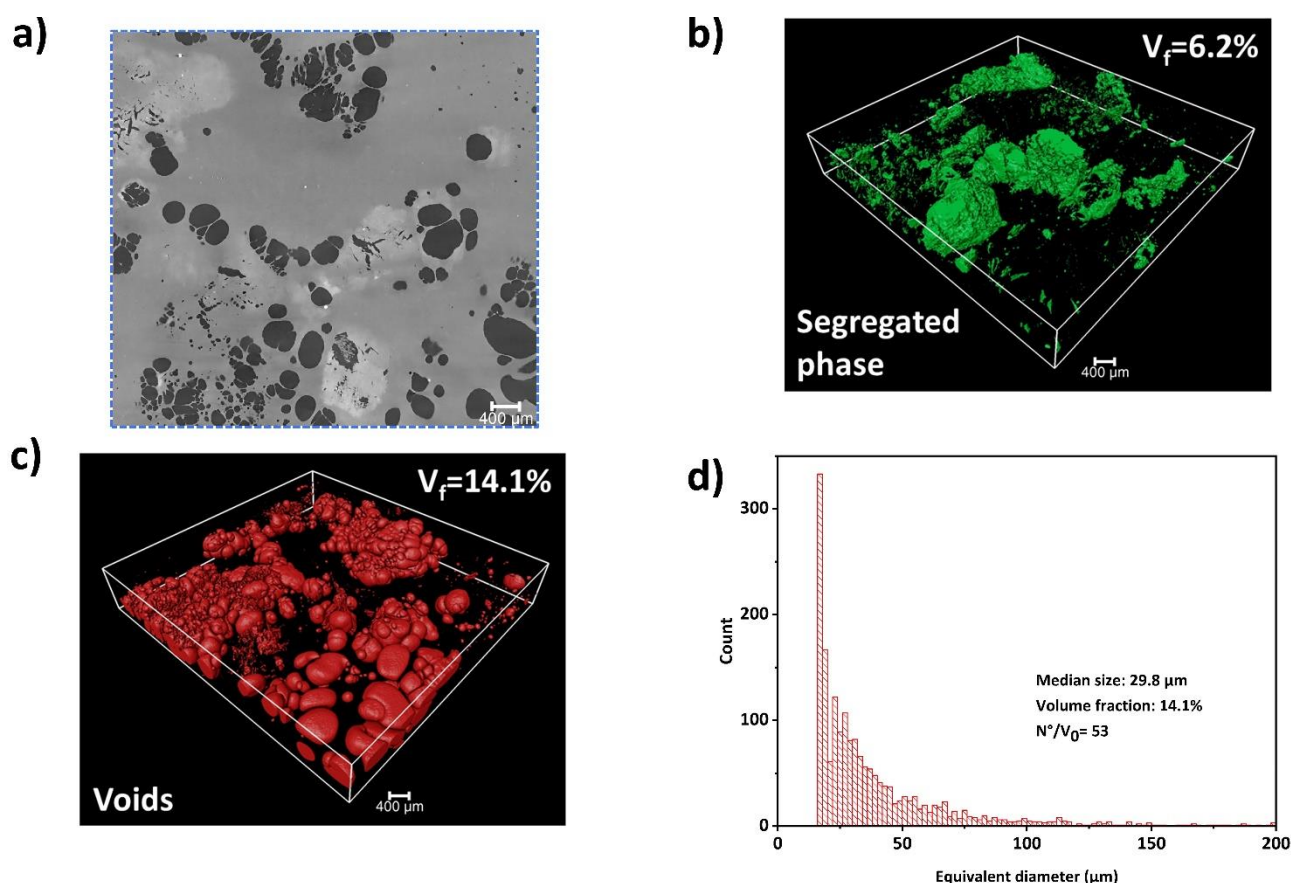
Figure S14 Cured p(eLig-mea) manufactured by hot-press treatment: (a) representative 2D orthoslices parallel to the rotation axis of the tomogram. 3D rendering of (b) segregated phase and (c) voids fraction.(d) Equivalent diameter histogram of voids.

Table S6 3D rendering results of p(eLig-mea) manufactured either by vacuum molding compression or by hot-press treatment

| Sample	Segregated phase (%)	Voids volume fraction (%)	Median size pore (μm)
p(eLig-mea) **MELTPREP**	5.5	2.6	24.6
p(eLig-mea) **HOT-PRESS**	6.2	**14.1**	29.8
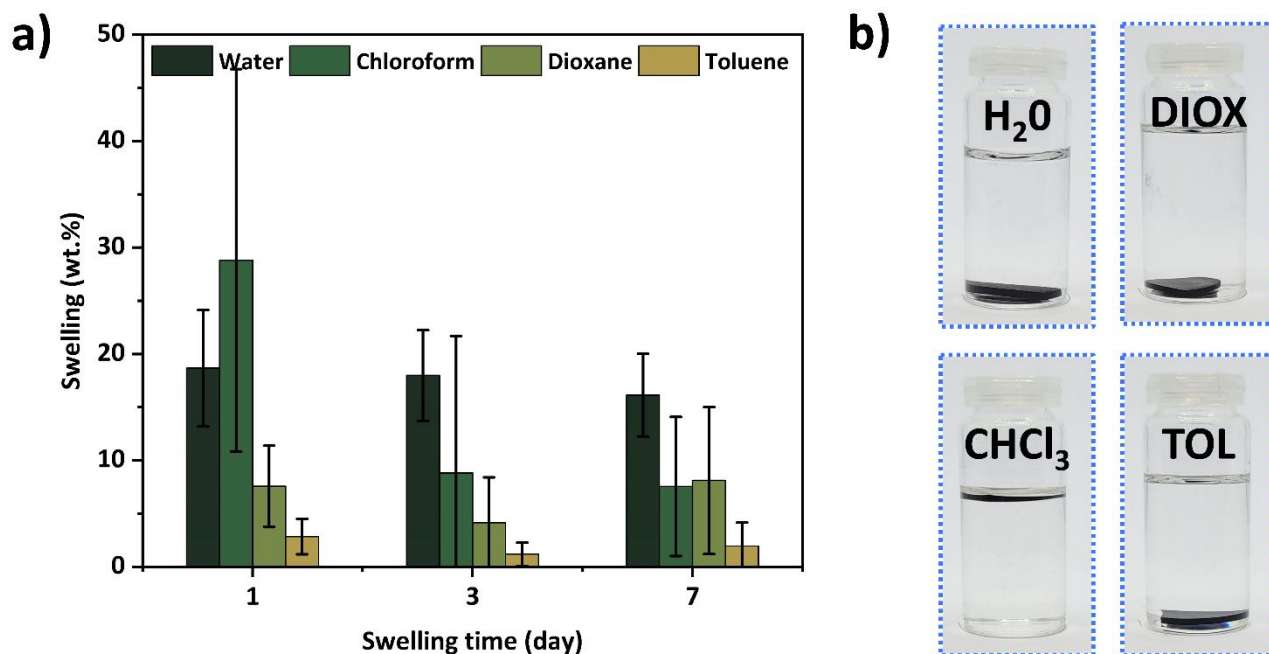
Figure S15 *(a) Swelling of p(eLig-mea) in various solvents and (b) digital photographs of the cured material after a week of immersion in organic solvent (standard error of three samples).*
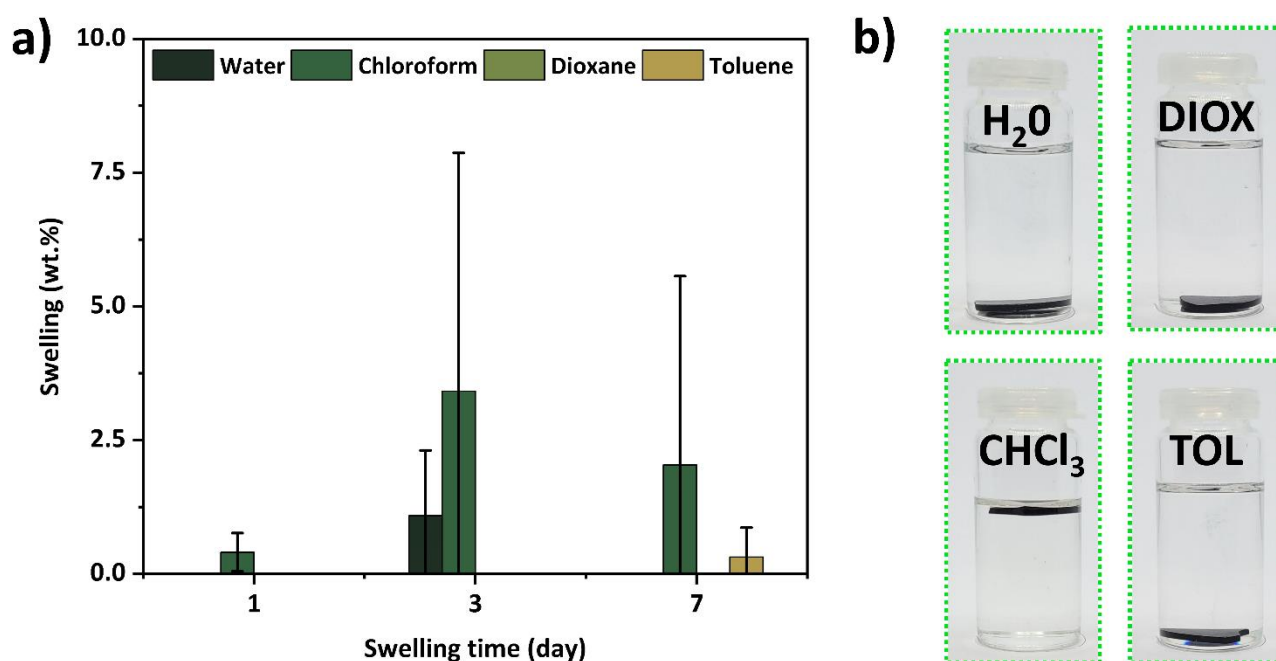
Figure S16 *(a) Swelling of p(eLig-fa) in various solvents and (b) digital photographs of the cured material after a week of immersion in organic solvent (standard error of three samples).*

a)

b)
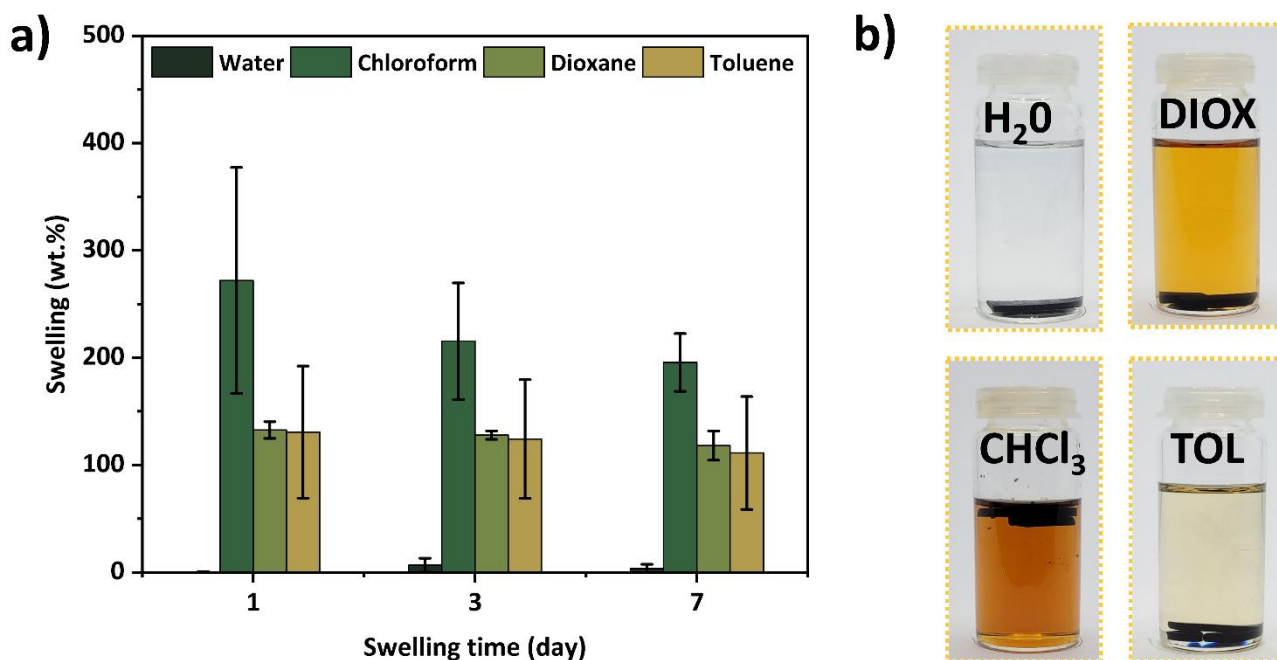
Figure S17 (a) Swelling of p(eLig-ste) in various solvents and (b) digital photographs of the cured material after a week of immersion in organic solvent (standard error of three samples).

Table S7 Gel content of p(eLig-Bz) in various solvent.

Network	[a] Gel content (wt.%)			
	CHCl$_3$	DIOX	TOL	H$_2$0
p(*e*Lig-mea)	100 ± 0	99 ± 1	100 ± 0	97 ± 3
p(*e*Lig-fa)	100 ± 0	100 ± 0	100 ± 0	100 ± 0
p(*e*Lig-ste)	62 ± 24	76 ± 6	78 ± 9	100 ± 0

[a] determined after a week of immersion according eq. (3).

Comment: The swelling ratio (W) of p(*e*Lig-Bz) in toluene (TOL), chloroform (CHCl$_3$), dioxane (DIOX), and water (H$_2$0) are reported in Table 3 (columns 7-10). Water appears as the optimal solvent to swell alcohol-terminated p(*e*Lig-mea) (W= 16 wt.%). p(*e*Lig-ste) swells by more than 100 wt.% in chloroform (CHCl$_3$), toluene (TOL), and dioxane (DIOX). Furthermore, although lignin is well known for its intrinsic heterogeneity, the high a gel content (GC) value revealed the robustness of the network (Table S7). Only p(*e*Lig-ste) shows a lower GC ($\approx$ 80%) stemming from longer dangling chain ends preventing cross-linking.
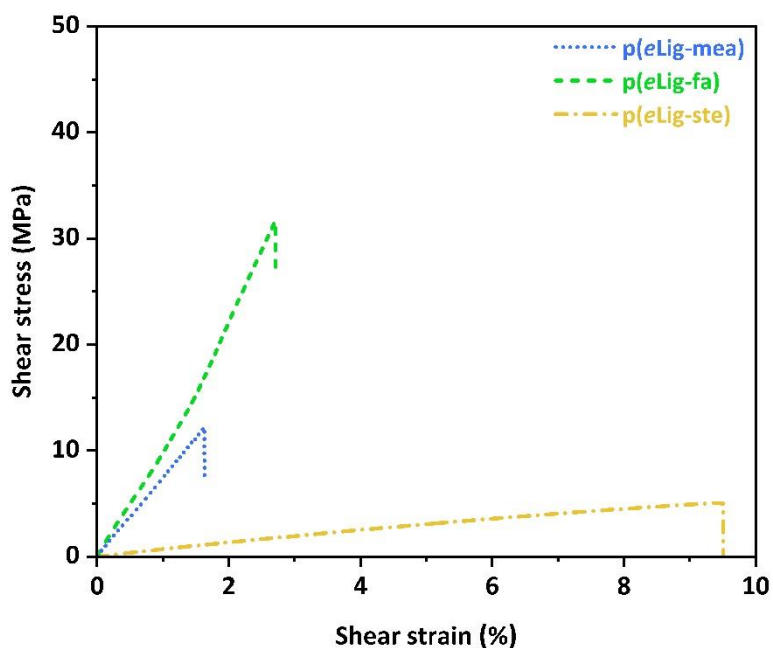
Figure S18 *Shear strain- stress curves of p(eLig-Bz)*
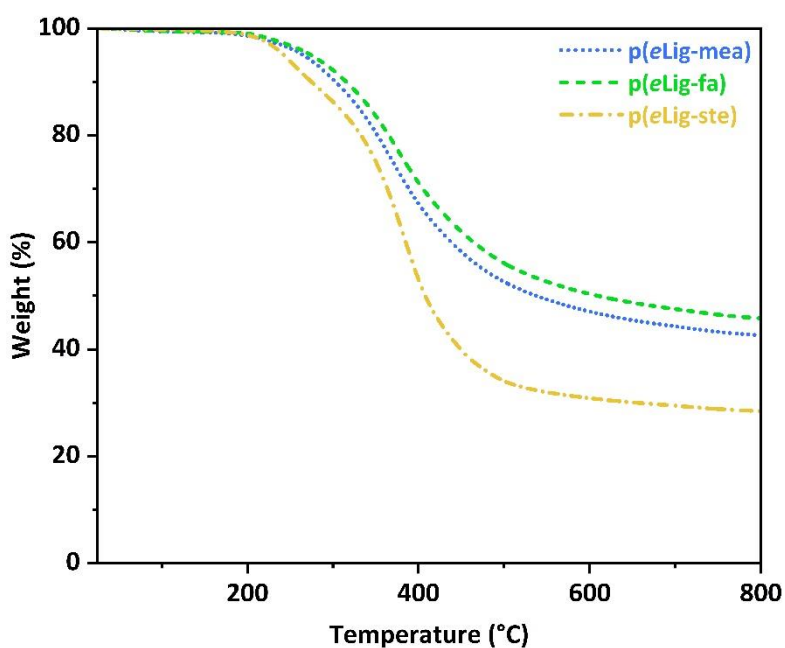

Figure S19 *TGA curves of p(eLig-Bz) (10 °C.min^{-1}, N$_2$).*

Comment: In agreement with DSC curves of p(*e*Lig-Bz) (Figure S12), the first degradation stage between 200 and 300 °C is mainly related to the breaking of the aliphatic ester and side-chain interunit linkages. The second degradation stage corresponds to the thermal decomposition of the crosslinked network (T$_{max}$≈ 380 °C).
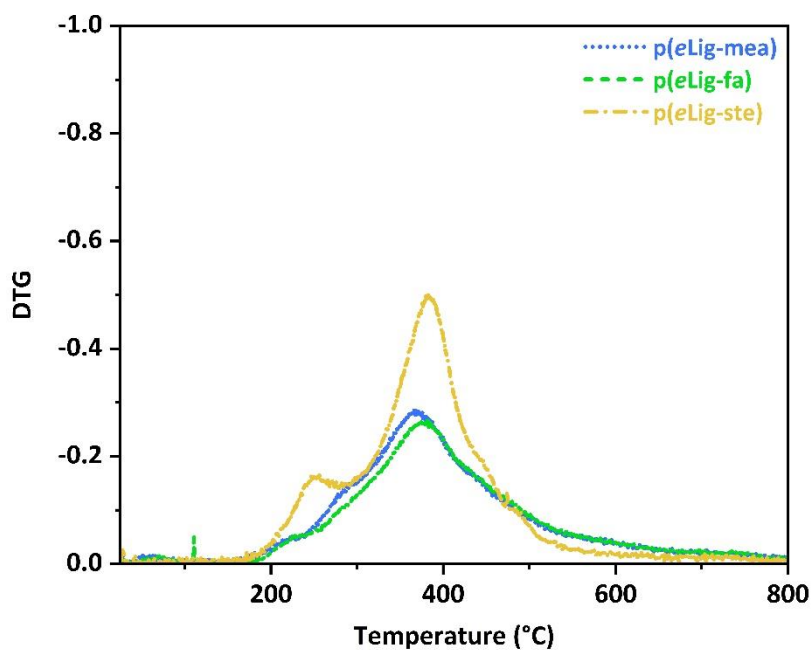
Figure S20 DTG curves of p(eLig-Bz) (10 °C.min⁻¹, N₂).
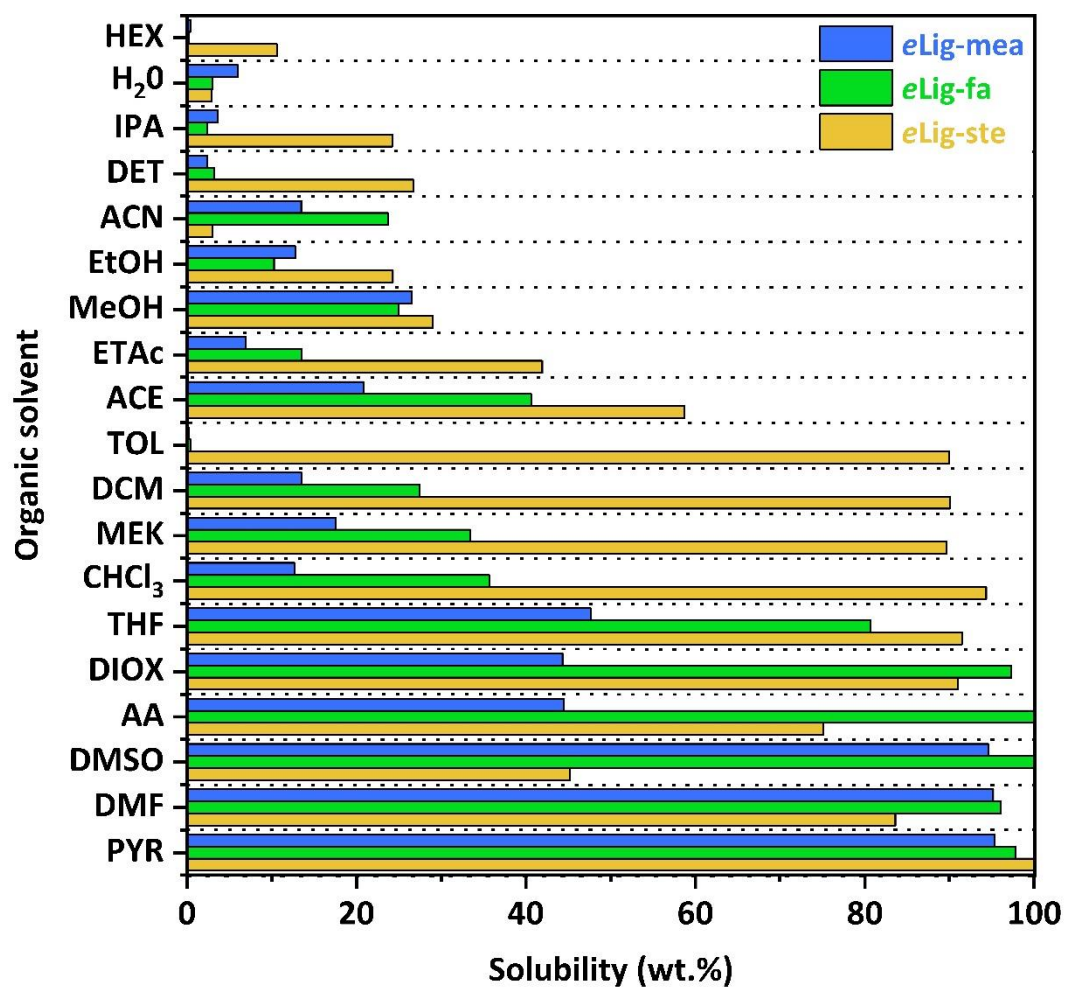
Figure S21 Solubility map of eLig-Bz in common organic solvent.

Comment: All lignin samples were almost fully insoluble in water (H_2O) and hexane (HEX) stemming from the compacted conformation of lignin in solvents of extreme polarity [6]. The relatively low solubility (S < 40 wt.%) of aliphatic –OH terminated *e*Lig-mea in alcohol solvents tends to indicate that lignin solubility is not solely driven by the intermolecular hydrogen bonding. The profuse number of chemical functionalities (alcohol, phenol, (m)ethoxy, ester, amine) promotes local intramolecular hydrogen bonds at the expense of intermolecular ones in a protic solvent. The greatest solubility was reached in dimethylformamide (DMF) and pyridine (PYR).

***Table S8** Hansen solubility parameters of eLig-Bz.*

Sample	[a] δ_D (MPa$^{1/2}$)	[b] δ_P (MPa$^{1/2}$)	[c] δ_H (MPa$^{1/2}$)	[d] δ_T (MPa$^{1/2}$)	[e] R	Fit
*e*Lig-mea	18.56	12.54	7.79	23.8	4.5	1.000
*e*Lig-fa	19.90	8.71	14.06	25.9	9.2	0.766
*e*Lig-ste	18.76	6.24	5.53	20.5	6.2	1.000

Estimation from HSPiP software: [a] δ_D: energy from dispersion forces between molecules; [b] δ_P: energy from the dipolar intermolecular forces between molecules; [c] δ_H : energy from hydrogen bonds between molecules; [d] δ_T total solubility (Hildebrand) parameters; and [e] radius of the sphere

Comment: Estimated HSP values were calculated from the experimental dataset according to the sphere method and the classic Hansen fitting algorithm [7]. The score of the solvent ranging from 1 to 6 is defined as follows: 1 ($100 \leq S \leq 90$), 2 ($90 < S \leq 80$), 3 ($80 < S \leq 60$), 4 ($60 < S \leq 40$), 5 ($40 < S \leq 20$), 6 ($20 < S \leq 0$). The fitting score demonstrates the capabilities and the limitations of the model.
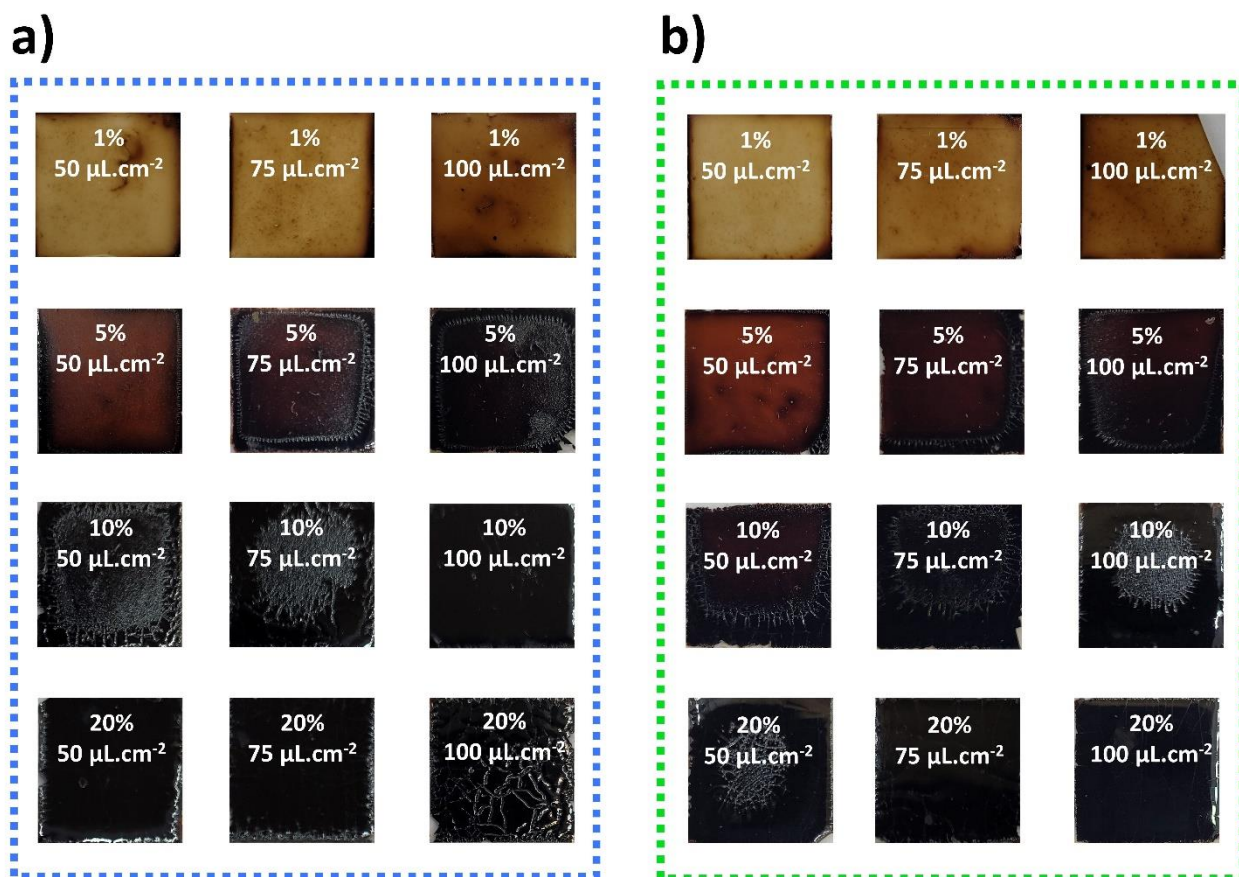
a)

b)

Figure S22 *Digital photographs of biobased coatings at different weight and surface concentrations: (a) p(eLig-mea) and (b) p(eLig-fa).*

Comment: Several parameters may be responsible on the different apparent states the lignin-based coatings including the mechanical properties of the lignin-based thermoset (low modulus results in brittle coatings at high lignin concentration), the ability to laminate (i.e. p(eLig-ste) lead to smooth coating), but also the appearance of the lignin-based benzoxazine precursor that depends on the lignin's mass fraction and the functionality of the amine side-chain (Table 1, column 8).

Table S9 *Thickness of the p(eLig-Bz)-coatings*

Concentration	1 wt.%	5 wt.%	10 wt.%	20 wt.%
50 µL.cm^{-2}	1.1 0.9 1.8	12.1 9.6 11.7	22.7 21.6 18.9	> 50
75 µL.cm^{-2}	1.6 1.1 1.8	14.1 14.3 15.0	35.5 31.4 36.6	> 50
100 µL.cm^{-2}	2.4 1.9 2.2	15.4 18.4 17.9	42.0 33.1 42.7	> 50

* p(eLig-mea), p(eLig-fa), and p(eLig-ste).

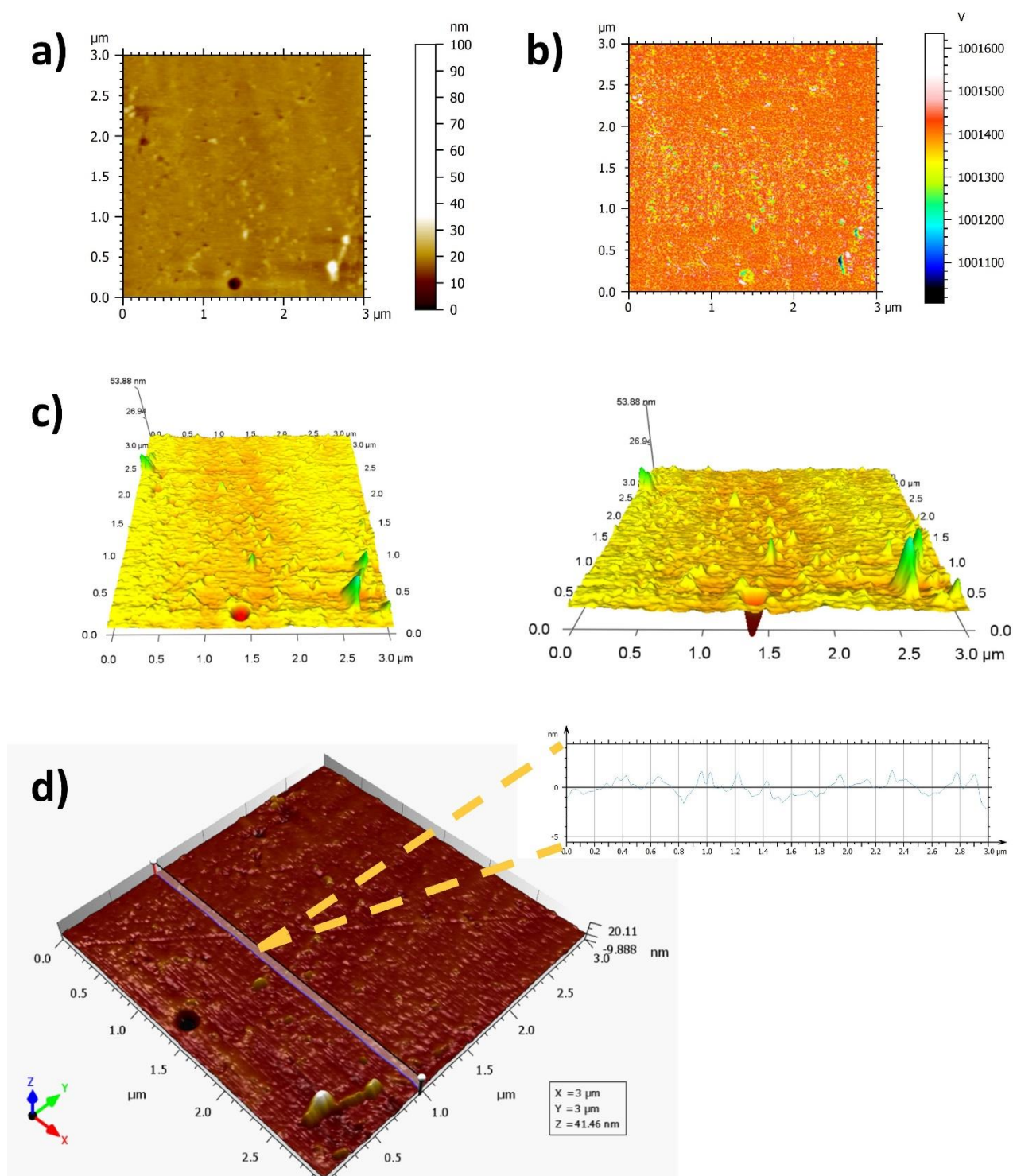*Figure S23* a) Topography, b) Frequency, c) 3D topography images, and d) line profile of p(eLig-ste) coating (10 wt.%, 75 µL.cm^{-2}) recorded by AFM.
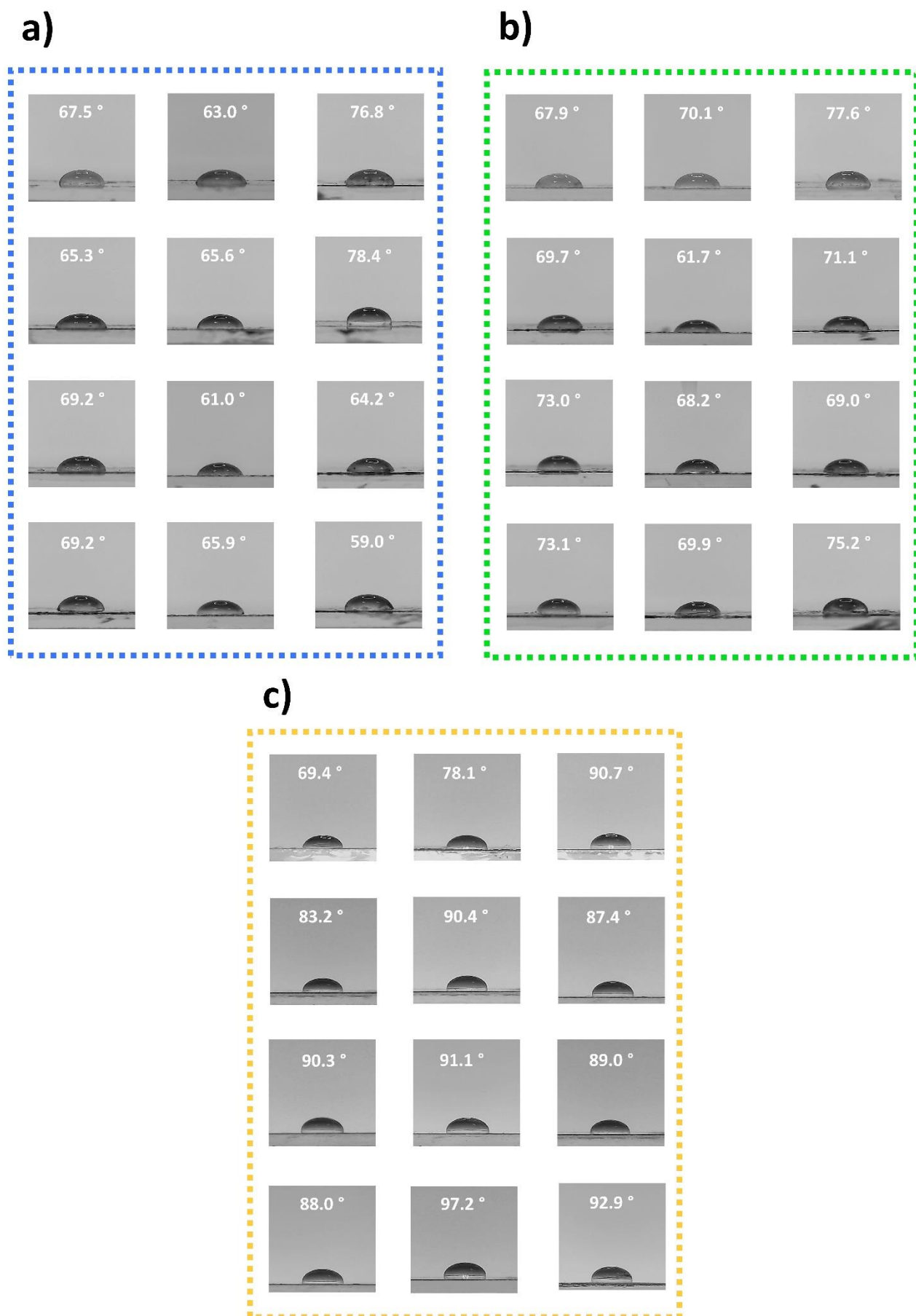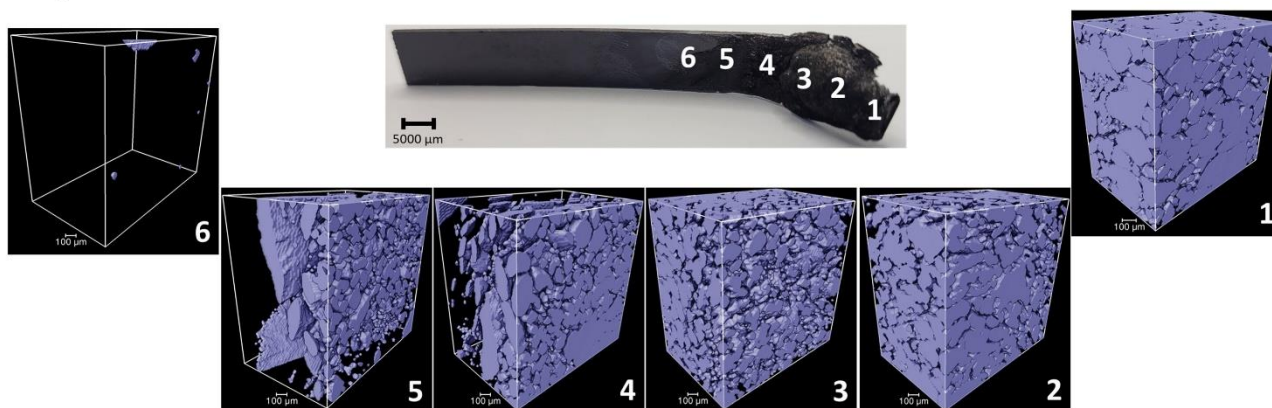
Figure S24 *Contact angle measurements of biobased coatings at different weight and surface concentrations: (a) p(eLig-mea), (b) p(eLig-fa), and (c) p(eLig-ste).*
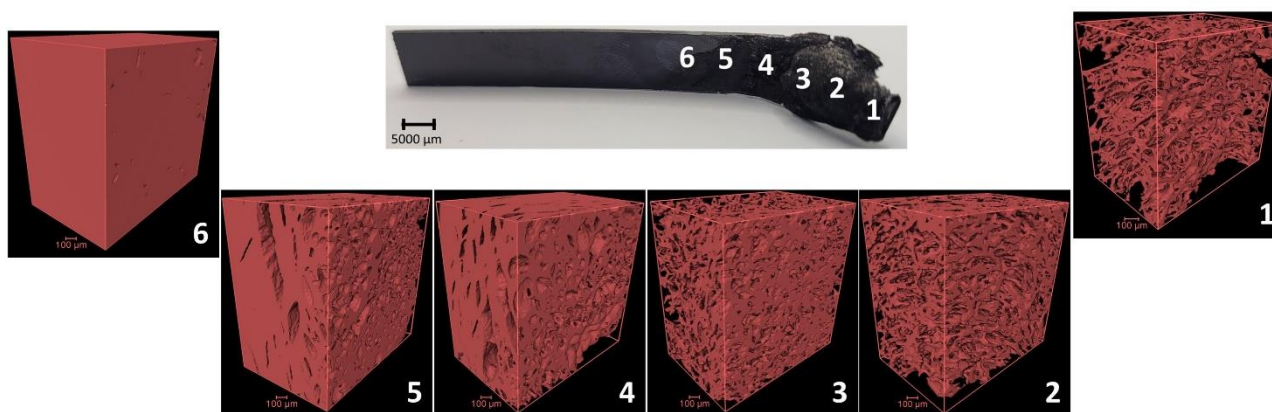
a)

b)

Figure S25 *(a) 3D rendering of gaz phase evolution from the burning zone, (b) 3D rendering of the condensed phase evolution from the burning zone of p(eLig-fa).*

Comment: The thickness distribution of the condensed phase was determined by a three-step process on the binarized images, consisting in: i) calculation of Euclidian distance mapping of the condensed phase, ii) skeletonization and iii) extraction of the maximum intensity of the skeletonized images [8, 9].

The parameters for the experimental fitting are gathered in Table S10 and calculated using equation S2:

$$Y = A_2 * \frac{A_1 - A_2}{1 + (x/x_0)^P} \quad (S2)$$

with x corresponding to the distance of the examined fraction as function of the total length of the material.

Table S10 *Parameters for the experimental fit of the gaz and condensed phase of the p(eLig-fa) residues after burning test (eq. S2).*

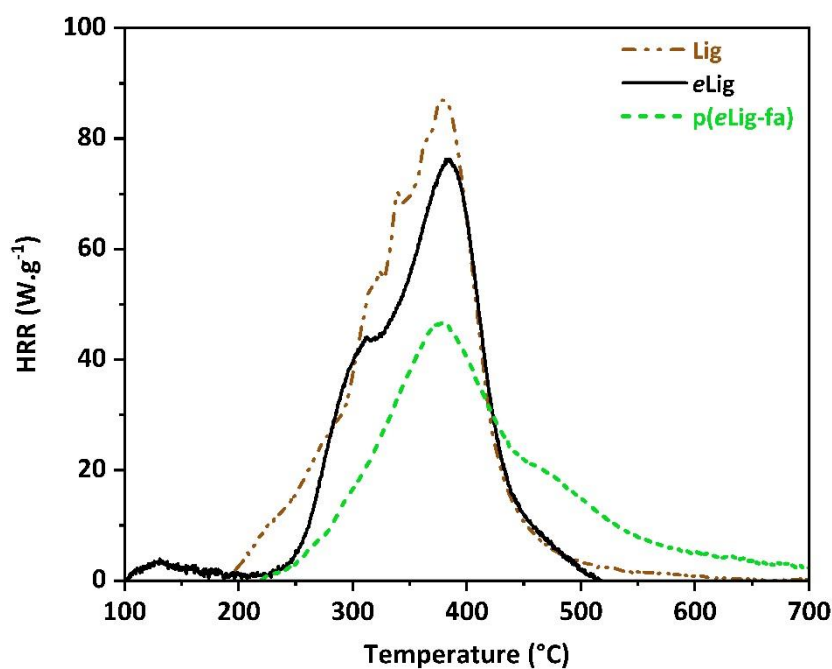| Parameters	A_1	A_2	x_0	P	R^2
Gas phase	64.33	-0.82	22.08	8.97	0.99
Condensed phase	9.99	1067.61	28.31	12.13	0.99

Figure S26 *Heat release rate curve of the technical lignin, the enhanced lignin, and the flame-retardant lignin-based polybenzoxazine determined by pyrolysis-combustion flow calorimetry*

Table S11 *Flammability characteristic of the technical, the enhanced, and the flame-retardant lignin-based polybenzoxazine determined by microscale combustion calorimetry*

Sample	pHRR (W.g^{-1})	TpHRR (°C)
Lig	87	380
eLig	76	385
p(eLig-fa)	47	377

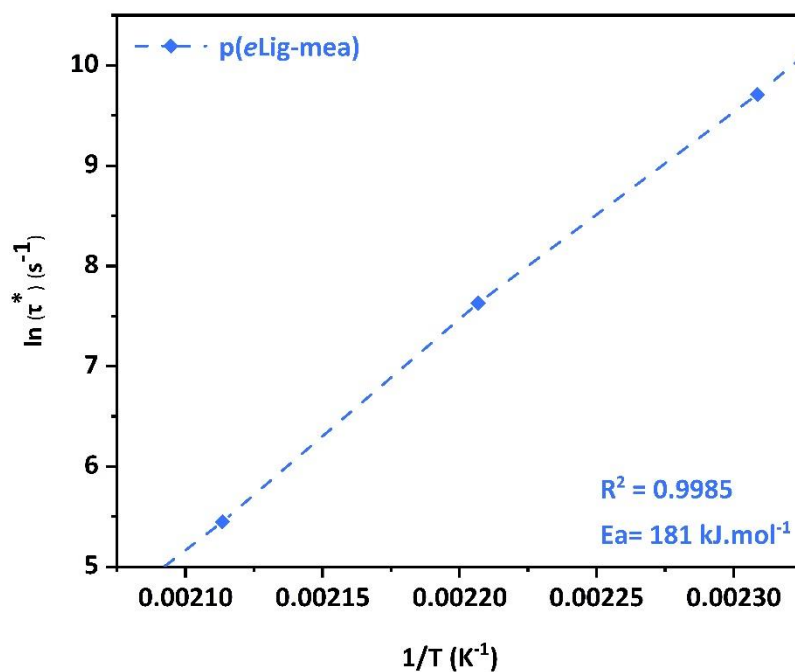**Figure S27** *Arrhenius plot of p(eLig-mea).*

Comment: The activation energy (Ea) was calculated according the Arrhenius equation S3:

$$\tau^* = A_0 * e^\wedge(\frac{E_a}{R*T}) \qquad (S3)$$

with τ^* the experimental relaxation time (s), E_a the activation energy (kJ.mol^{-1}), R the universal gas molar constant (R= 8.314 J.K^{-1}.mol^{-1}), and T the temperature (°K).

Equation: $\ln(\tau^*)= f(T^{-1}) \rightarrow$ slope= 21805, intercept= -40.584
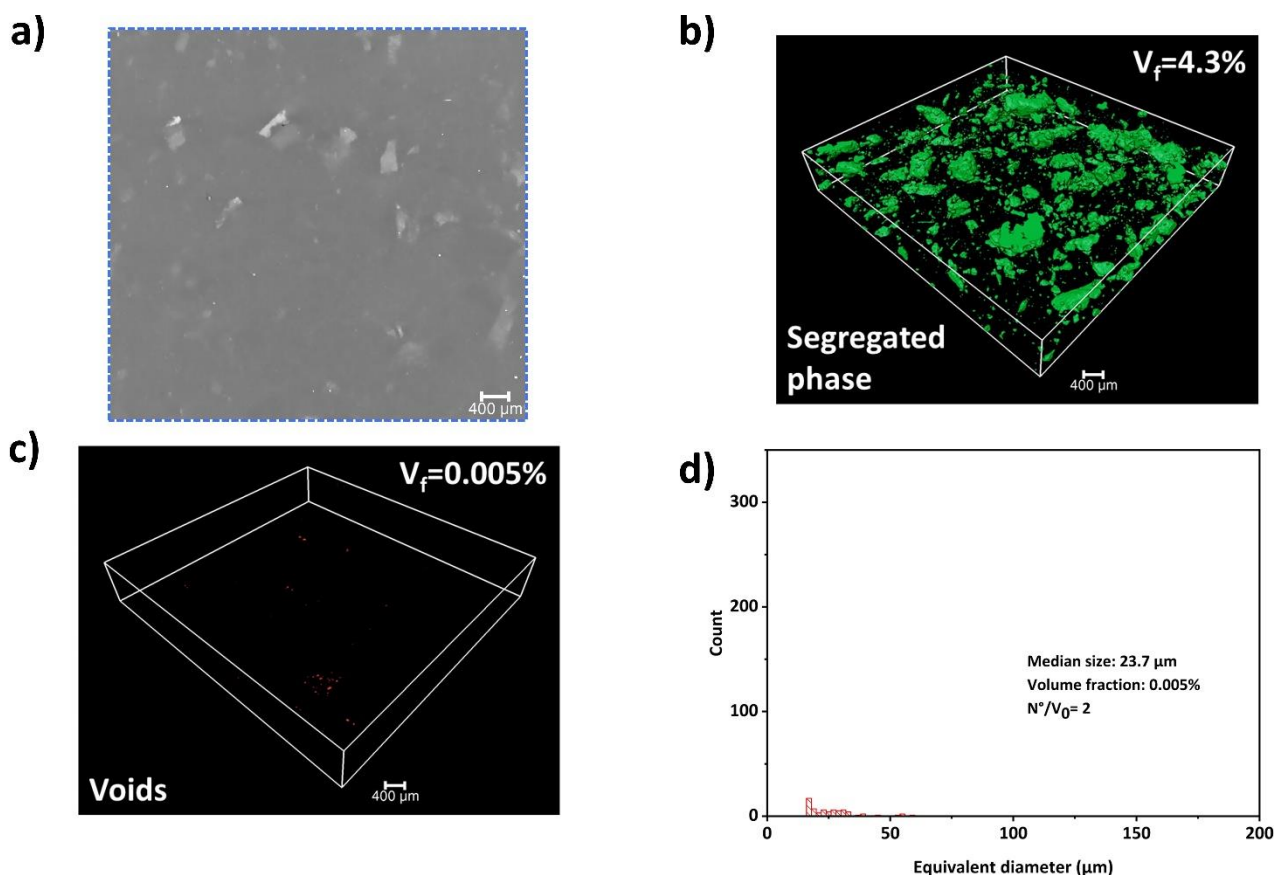
Figure S28 *Recycled p(eLig-mea): (a) representative 2D orthoslices parallel to the rotation axis of the tomogram. 3D rendering of (b) segregated phase and (c) voids fraction.(d) Equivalent diameter histogram of voids.*

Comment: The morphology of the recycled sample shown in Figure S28.a reveals a better mass distribution in comparison with the cured material (Figure 5.b). Segregated phases are more dispersed across the material (V_f= 4.3 %, Figure S28.b). Voids inside the material almost totally vanished (V_f= 0.005 %, Figure S28.c). The estimation of the pore size over the porous fragments (N= 2) displayed a similar a median pore size of Ø= 23.7 μm (Figure S28.d). The difference in morphology might be explained by the difference in the manufacture method, suggesting that hot-press treatment could lead to uniform material.
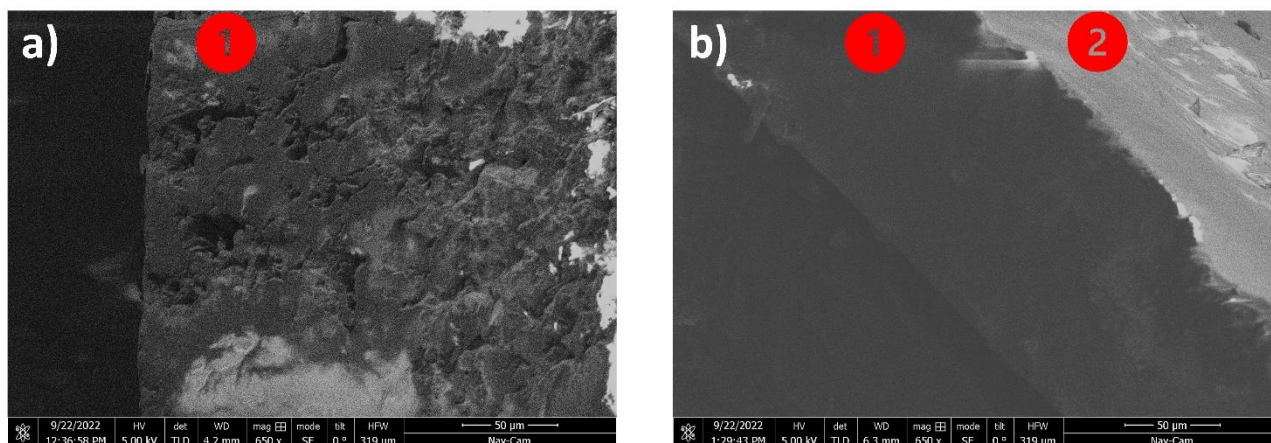

Figure S29 *SEM images of p(eLig-mea) a) original material prepared by MeltPrep manufacture process and b) reprocessed vitrimer obtained by hot-press treatment (1: cross-section, 2: surface)*

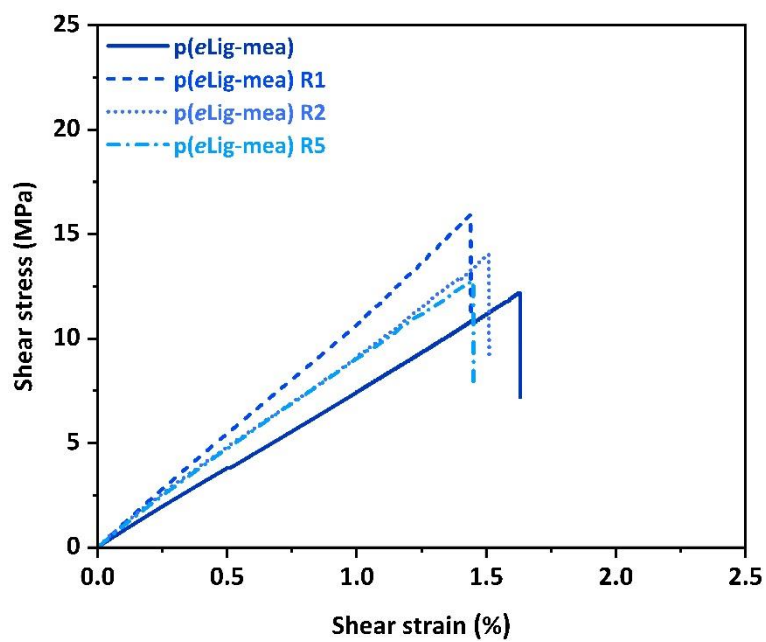***Figure S30*** *Strain-stress curves of reprocessed p(eLig-mea)*

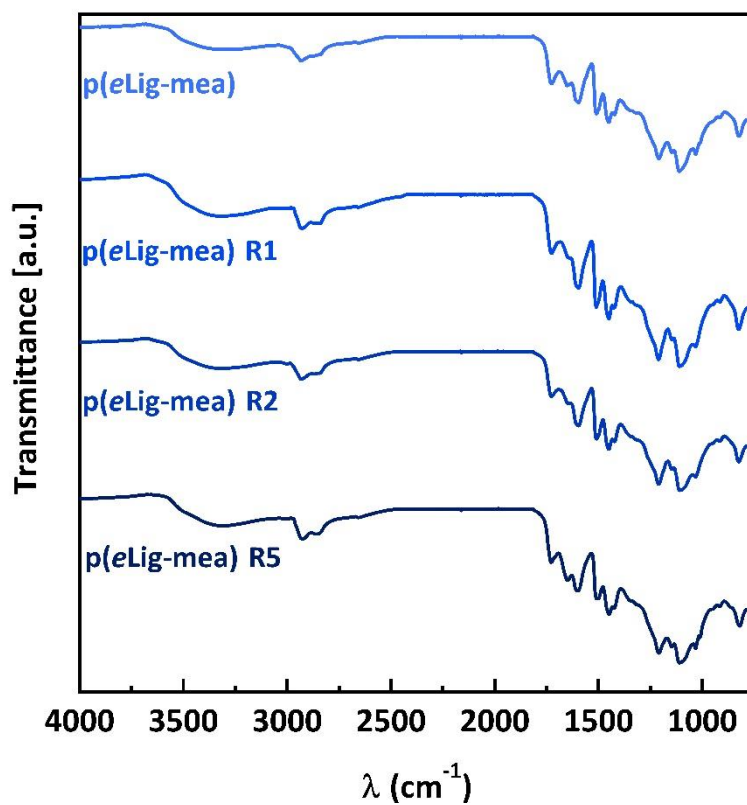***Figure S31*** *FTIR spectra of cured and reprocessed p(eLig-mea) vitrimer.*

6. References

[1] A. Granata, D.S. Argyropoulos, 2-Chloro-4,4,5,5-tetramethyl-1,3,2-dioxapholane, a Reagent for the Accurate Determination of the Uncondensed and Condensed Phenolic Moieties in Lignins, Journal of Agricultural and Food Chemistry, 43 (6), **1995**, 1538-1544. https://doi.org/10.1021/jf00054a023.

[2] M. Zawadzki, A. Ragauskas, N-Hydroxy Compounds as New Internal Standards for the 31P-NMR Determination of Lignin Hydroxy Functional Groups, Holzforschung, 55, **2001**, 283-285. https://doi.org/10.1515/HF.2001.047.

[3] E.A. Capanema, M.Y. Balakshin, J.F. Kadla, A Comprehensive Approach for Quantitative Lignin Characterization by NMR Spectroscopy, Journal of Agricultural and Food Chemistry, 52 (7), **2004**, 1850-1860. https://doi.org/10.1021/jf035282b.

[4] D.J. McClelland, A.H. Motagamwala, Y. Li, M.R. Rover, A.M. Wittrig, C. Wu, J.S. Buchanan, R.C. Brown, J. Ralph, J.A. Dumesic, G.W. Huber, Functionality and molecular weight distribution of red oak lignin before and after pyrolysis and hydrogenation, Green Chemistry, 19 (5), **2017**, 1378-1389. https://doi.org/10.1039/C6GC03515A.

[5] D.W. van Krevelen, Some basic aspects of flame resistance of polymeric materials, Polymer, 16 (8), **1975**, 615-620. https://doi.org/https://doi.org/10.1016/0032-3861(75)90157-3.

[6] J.V. Vermaas, M.F. Crowley, G.T. Beckham, Molecular Lignin Solubility and Structure in Organic Solvents, ACS Sustainable Chemistry & Engineering, 8 (48), **2020**, 17839-17850. https://doi.org/10.1021/acssuschemeng.0c07156.

[7] C. Hansen, Hansen Solubility Parameters: A User's Handbook, Second Edition, 2012. https://doi.org/10.1201/9781420006834.

[8] T. Hildebrand, P. Rüegsegger, A new method for the model-independent assessment of thickness in three-dimensional images, Journal of Microscopy, 185 (1), **1997**, 67-75. https://doi.org/https://doi.org/10.1046/j.1365-2818.1997.1340694.x.

[9] S. Pérez-Tamarit, E. Solórzano, A. Hilger, I. Manke, M.A. Rodríguez-Pérez, Multi-scale tomographic analysis of polymeric foams: A detailed study of the cellular structure, European Polymer Journal, 109, **2018**, 169-178. https://doi.org/https://doi.org/10.1016/j.eurpolymj.2018.09.047.

Annex VI: Patents

(19) ⬛ LE GOUVERNEMENT
DU GRAND-DUCHÉ DE LUXEMBOURG
Ministère de l'Économie

(11) N° de publication : **LU101846**

(12) **BREVET D'INVENTION** **B1**

(21) N° de dépôt: LU101846

(22) Date de dépôt: 10/06/2020

(51) Int. Cl.:
C07D 265/16, C08G 65/48, C08G 73/02

(30) Priorité:

(43) Date de mise à disposition du public: 10/12/2021

(47) Date de délivrance: 10/12/2021

(73) Titulaire(s):
LUXEMBOURG INSTITUTE OF SCIENCE AND
TECHNOLOGY (LIST) – 4362 ESCH-SUR-
ALZETTE (Luxembourg)

(72) Inventeur(s):
ADJAOUD Antoine – Luxembourg, PUCHOT Laura –
Luxembourg, TREJO MACHIN Acerina – Luxembourg,
VERGE Pierre – Luxembourg

(74) Mandataire(s):
Lecomte & Partners Sàrl – L-
2146 Luxembourg (Luxembourg)

(54) **BENZOXAZINE DERIVATIVES VITRIMERS.**

(57) The invention concerns an ester containing benzoxazine monomer and to a process for synthesizing said monomer and to vitrimers obtained through the polymerization of the ester containing benzoxazine monomer. The invention also relates to an use of the vitrimer as a reversible adhesive, sealant, coating or encapsulating systems for substrates selected from the group consisting of a metal, polymer, glass and ceramic material

�54 **BENZOXAZINE DERIVATIVES VITRIMERS.**

�57 The invention relates to a process for synthesizing an ester-containing benzoxazine monomer comprising the following steps consisting of: reacting a phenolic acid derivative with a polyfunctional molecule or oligomer at a temperature of from 25°C to 200°C, during 1h-72h, in the presence of a catalyst of Bronsted acid type, resulting in a phenol terminated oligomer or molecule, and reacting said phenol terminated oligomer or molecule with a mixture of: - an amino-alcohol, - a primary amine derivative, and - paraformaldehyde at a temperature range of from 80°C to 100°C, from 1h to 10h, under stirring, for obtaining the ester-containing benzoxazine monomer.

(54) **CATALYSTS FOR BENZOXAZINE.**

(57) The invention relates to a proces for producing of a benzoxazine containing free aliphatic hydroxyl groups and monoester comprising the following steps of: reaction of a phenolic acid derivative with a monofonctional oligomer or molecule R- OH, at a temperature of from 80°C to 200°C, during 12h-48h, in a presence of a Bronsted type acid catalyst, resulting in a monophenol terminated oligomer or molecule, and reaction of said monophenol terminated oligomer or molecule with a mixture of - an amino-alcohol, - a primary amine derivative, and - paraformaldehyde, at a temperature range of from 80°C to 100°C, from 1h to 48h, under stirring for obtaining said benzoxazine containing free aliphatic hydroxyl groups and monoester.

Figure à publier avec l'abrégé

(54) **HIGH-PERFORMANCE BENZOXAZINE DERIVATIVES VITRIMERS.**

(57) The invention also relates to a process for synthesizing an ester-containing benzoxazine monomer comprising the following steps consisting of reacting a phenolic acid derivative with a polyfunctional molecule or oligomer at a temperature of from 25°C to 200°C, during 1h-72h, in the presence of a catalyst of Bronsted acid type, resulting in a phenol terminated oligomer or molecule and reacting said phenol terminated oligomer or molecule with a mixture of an amino-alcohol, a primary amine derivative and paraformaldehyde at a temperature range of from 80°C to 100°C, from 1h to 10h, under stirring. The invention also relates to an ester-containing benzoxazine monomer and to a process for preparing a polybenzoxazine derivative vitrimer comprising the step of polymerization of an ester-containing benzoxazine monomer at temperatures within the range of from 100°C to 250°C for 1h to 24h.
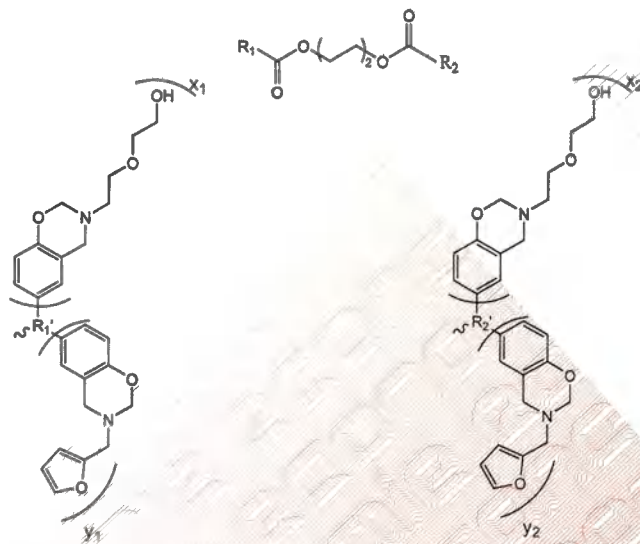
Par courrier électronique

LUXEMBOURG INSTITUTE OF
SCIENCE AND TECHNOLOGY (LIST)
Michel CANCELLIER
5, avenue des Hauts-Fourneaux
L - 4362 ESCH-SUR-ALZETTE

Votre réf.: P-2022-22-VERGE-Dual curable benzoxazine vitrimer (MRT)	Notre réf.: PT08435LU-A	Date: 27 décembre 2022

Concerne: Nouvelle demande de brevet au Luxembourg (No 503197)

Déposant/Titulaire(s):   LUXEMBOURG INSTITUTE OF SCIENCE AND TECHNOLOGY (LIST)

Inventeur(s):   Pierre VERGE, Ambre MEYER, Antoine ADJAOUD, Laura PUCHOT, Alexander SHAPLOV, Joamin GONZALEZ GUTIERREZ

Titre: DUAL CURABLE BENZOXAZINE VITRIMER

Cher Michel,

Faisant suite à vos instructions du 15 décembre 2022 nous avons le plaisir de vous informer qu'une demande de brevet a été déposée au Luxembourg correspondant aux données ci-dessus. Nous avons payé les taxes officielles afférentes à ce dépôt et les particularités de la demande sont reprises ci-dessous.

Veuillez noter que compte tenu que la demande de brevet a été rédigée en langue anglaise, nous avons conformément aux exigences de l'Office des brevets au Luxembourg, préparé et déposé une traduction des revendications dans une des langues officielles du pays, en l'occurrence en français.

L'Office Européen des Brevets (OEB), dans sa qualité d'autorité de recherche pour le Luxembourg, va nous faire parvenir un rapport de recherche et une première prise de position concernant la brevetabilité de votre invention. Ce rapport nous parvient en général dans les prochains 4 à 9 mois.

Le contenu de votre demande va rester confidentiel pendant 18 mois. Après ce délai, l'Office va procéder à sa publication.

Nous vous prions de noter la date du **16 décembre 2023**. Jusqu'à cette date vous aurez la possibilité de déposer une demande pour la même invention dans des pays autres que le Luxembourg, en revendiquant la priorité de votre demande de brevet en rubrique. Nous allons bien évidemment revenir vers vous à ce sujet en temps utile.

LECOMTE & PARTNERS Sàrl
76-78, rue de Merl, L-2146 Luxembourg
VAT-No : LU 22115175 - RCS LUX: B 132841

info@ip-lecomte.com
www.ip-lecomte.com

tel.   +352 248394-1
fax   +352 248394-2

Par courrier électronique

LUXEMBOURG INSTITUTE OF
SCIENCE AND TECHNOLOGY (LIST)
Michel CANCELLIER
5, avenue des Hauts-Fourneaux
L - 4362 ESCH-SUR-ALZETTE

Votre réf.: P-2022-22-VERGE-Dual curable benzoxazine vitrimer (MRT)   Notre réf.: PT08435LU-B   Date: 27 décembre 2022

Concerne: Nouvelle demande de brevet au Luxembourg (No 503198)
         Déposant/Titulaire(s):   LUXEMBOURG INSTITUTE OF SCIENCE AND TECHNOLOGY (LIST)
         Inventeur(s):   Pierre VERGE, Ambre MEYER, Antoine ADJAOUD, Alexander SHAPLOV, Laura PUCHOT, Joamin GONZALEZ GUTIERREZ
         Titre: DUAL CURABLE BENZOXAZINE VITRIMER

Cher Michel,

Faisant suite à vos instructions du 15 décembre 2022 nous avons le plaisir de vous informer qu'une demande de brevet a été déposée au Luxembourg correspondant aux données ci-dessus. Nous avons payé les taxes officielles afférentes à ce dépôt et les particularités de la demande sont reprises ci-dessous.

Veuillez noter que compte tenu que la demande de brevet a été rédigée en langue anglaise, nous avons conformément aux exigences de l'Office des brevets au Luxembourg, préparé et déposé une traduction des revendications dans une des langues officielles du pays, en l'occurrence en français.

L'Office Européen des Brevets (OEB), dans sa qualité d'autorité de recherche pour le Luxembourg, va nous faire parvenir un rapport de recherche et une première prise de position concernant la brevetabilité de votre invention. Ce rapport nous parvient en général dans les prochains 4 à 9 mois.

Le contenu de votre demande va rester confidentiel pendant 18 mois. Après ce délai, l'Office va procéder à sa publication.

Nous vous prions de noter la date du **16 décembre 2023**. Jusqu'à cette date vous aurez la possibilité de déposer une demande pour la même invention dans des pays autres que le Luxembourg, en revendiquant la priorité de votre demande de brevet en rubrique. Nous allons bien évidemment revenir vers vous à ce sujet en temps utile.

Par courrier électronique

LUXEMBOURG INSTITUTE OF
SCIENCE AND TECHNOLOGY (LIST)
Michel CANCELLIER
5, avenue des Hauts-Fourneaux
L - 4362 ESCH-SUR-ALZETTE

Votre réf.: P-2022-23-VERGE-Vitrimers with wide processing window (MRT)	Notre réf.: PT08436LU	Date: 23 décembre 2022

Concerne: Nouvelle demande de brevet au Luxembourg (No 503199)
.
Déposant/Titulaire(s):   LUXEMBOURG INSTITUTE OF SCIENCE AND TECHNOLOGY (LIST)
Inventeur(s):   Pierre VERGE (adresse privée), Antoine ADJAOUD, Laura PUCHOT (adresse privée)
Titre: VITRIMERS WITH WIDE PROCESSING WINDOW

Cher Michel,

Faisant suite à vos instructions du 15 décembre 2022 nous avons le plaisir de vous informer qu'une demande de brevet a été déposée au Luxembourg correspondant aux données ci-dessus. Nous avons payé les taxes officielles afférentes à ce dépôt et les particularités de la demande sont reprises ci-dessous.

Veuillez noter que compte tenu que la demande de brevet a été rédigée en langue anglaise, nous avons conformément aux exigences de l'Office des brevets au Luxembourg, préparé et déposé une traduction des revendications dans une des langues officielles du pays, en l'occurrence en français.

L'Office Européen des Brevets (OEB), dans sa qualité d'autorité de recherche pour le Luxembourg, va nous faire parvenir un rapport de recherche et une première prise de position concernant la brevetabilité de votre invention. Ce rapport nous parvient en général dans les prochains 4 à 9 mois.

Le contenu de votre demande va rester confidentiel pendant 18 mois. Après ce délai, l'Office va procéder à sa publication.

Nous vous prions de noter la date du **16 décembre 2023**. Jusqu'à cette date vous aurez la possibilité de déposer une demande pour la même invention dans des pays autres que le Luxembourg, en revendiquant la priorité de votre demande de brevet en rubrique. Nous allons bien évidemment revenir vers vous à ce sujet en temps utile.

LECOMTE & PARTNERS Sàrl
76-78, rue de Merl, L-2146 Luxembourg
VAT-No : LU 22115175 - RCS LUX: B 132841

info@ip-lecomte.com
www.ip-lecomte.com

tel. +352 248394-1
fax +352 248394-2

Annex VII: Poster

Lignin-based benzoxazines:
a tunable key-precursor for various applications

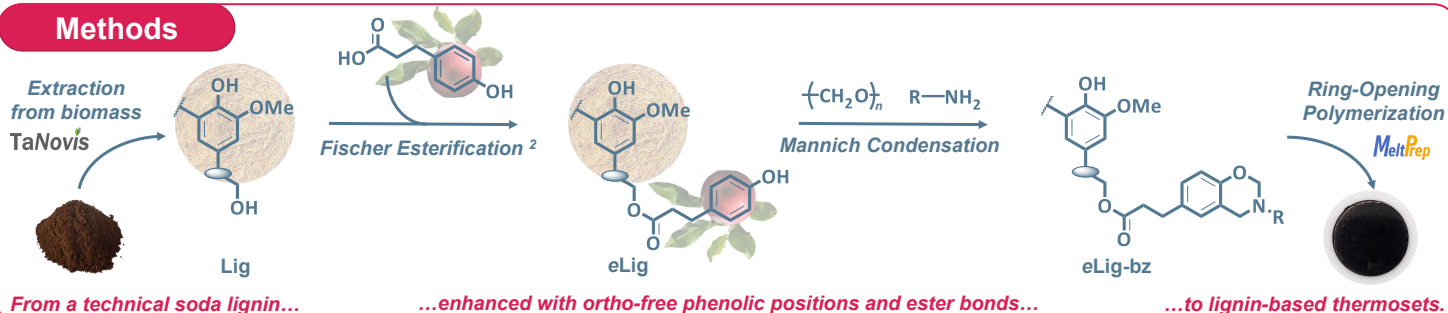*Antoine Adjaoud* [1,2], Laura Puchot [1], Carlos Eloy Federico [1], Rohan Das [1,2], and Pierre Verge [1,*]

[1] Luxembourg Institute of Science and Technology, Materials Research and Technology Department, 5 Avenue des Hauts-Fourneaux, L-4362 Esch-sur-Alzette (Luxembourg)
[2] University of Luxembourg, 2, Avenue de l'Université, L-4365 Esch-sur-Alzette (Luxembourg)
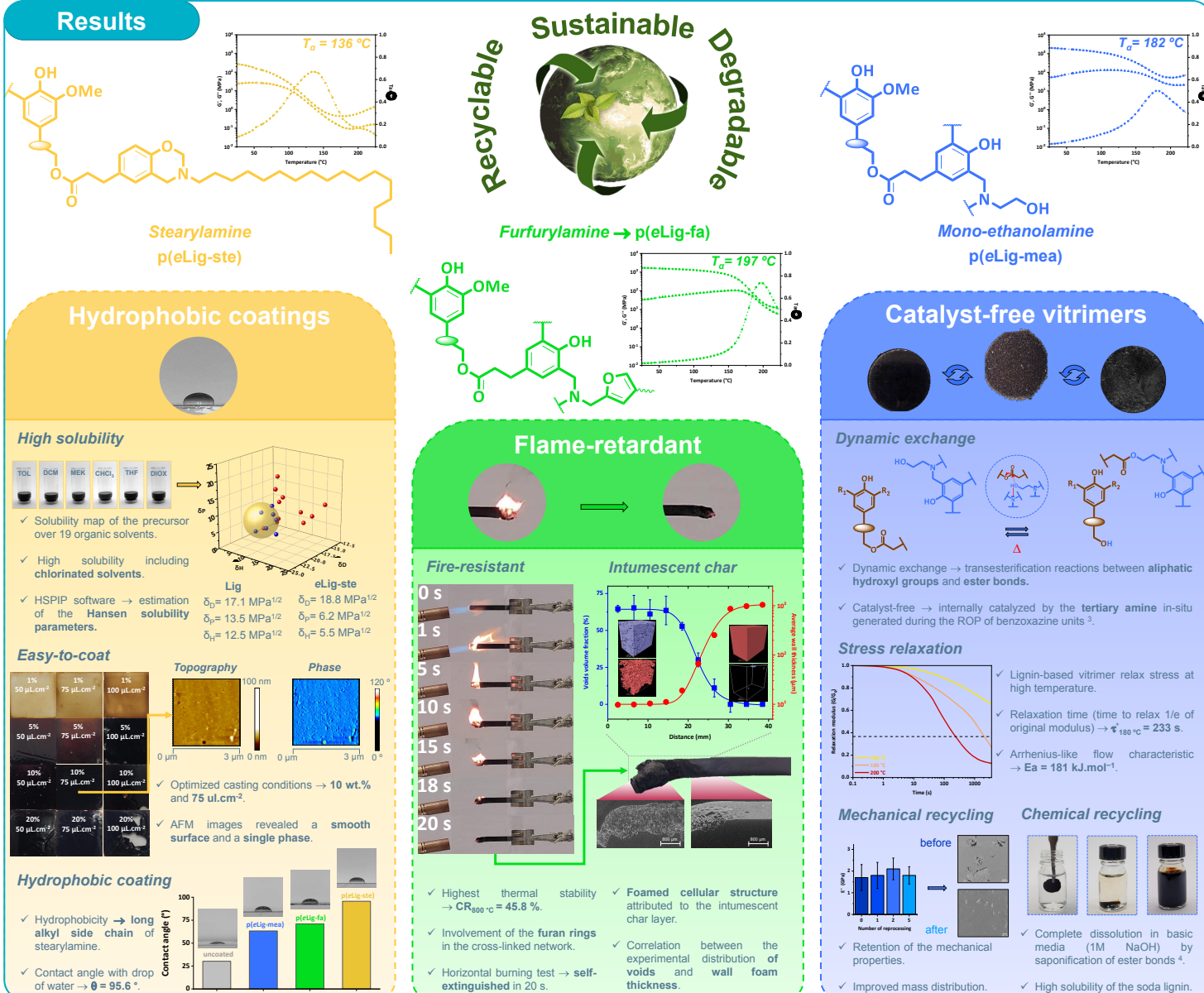
Motivation

The meaningful concept of circular economy has prompted the scientific community to transform the polymer industry toward sustainable materials. Lignin, an earthbound polymer, epitomized the main source of phenolic compounds for the conception of bio-derived materials. In this study, a series of lignin-based benzoxazine thermosets (LBZs) with tuneable applications were prepared [1]. Bio-based amines synthons such as long-alkyl chain stearylamine confers hydrophobicity to LBZs coatings, while furfurylamine-based LBZs generate high-T_g materials well adapted for fire-retardancy applications. Amino-alcohol grants recyclability to cross-linked lignin-vitrimers thanks to catalyst-free dynamic transesterification exchanges.

Methods

Extraction from biomass TaNovis

From a technical soda lignin…

Fischer Esterification [2]

Lig

Mannich Condensation $(CH_2O)_n$ $R—NH_2$

…enhanced with ortho-free phenolic positions and ester bonds…

eLig

Ring-Opening Polymerization MeltPrep

eLig-bz

…to lignin-based thermosets.

Results

$T_\alpha = 136\ °C$

Stearylamine p(eLig-ste)

Sustainable · Recyclable · Degradable

$T_\alpha = 182\ °C$

Mono-ethanolamine p(eLig-mea)

Furfurylamine → p(eLig-fa)

$T_\alpha = 197\ °C$

Hydrophobic coatings

High solubility

TOL DCM MEK CHCl₃ THF DIOX

✓ Solubility map of the precursor over 19 organic solvents.

✓ High solubility including **chlorinated solvents**.

✓ HSPIP software → estimation of the **Hansen solubility parameters**.

	Lig	eLig-ste
δ_D	17.1 MPa$^{1/2}$	18.8 MPa$^{1/2}$
δ_P	13.5 MPa$^{1/2}$	6.2 MPa$^{1/2}$
δ_H	12.5 MPa$^{1/2}$	5.5 MPa$^{1/2}$

Easy-to-coat

Topography / Phase

✓ Optimized casting conditions → **10 wt.%** and **75 ul.cm^{-2}**.

✓ AFM images revealed a **smooth surface** and a **single phase**.

Hydrophobic coating

✓ Hydrophobicity → **long alkyl side chain** of stearylamine.

✓ Contact angle with drop of water → θ = 95.6 °.

Flame-retardant

Fire-resistant

0 s, 1 s, 5 s, 10 s, 15 s, 18 s, 20 s

Intumescent char

✓ Highest thermal stability → **CR$_{800\ °C}$ = 45.8 %**.

✓ Involvement of the **furan rings** in the cross-linked network.

✓ Horizontal burning test → **self-extinguished** in 20 s.

✓ **Foamed cellular structure** attributed to the intumescent char layer.

✓ Correlation between the experimental distribution **of voids** and **wall foam thickness**.

Catalyst-free vitrimers

Dynamic exchange

✓ Dynamic exchange → transesterification reactions between **aliphatic hydroxyl groups** and **ester bonds**.

✓ Catalyst-free → internally catalyzed by the **tertiary amine** in-situ generated during the ROP of benzoxazine units [3].

Stress relaxation

✓ Lignin-based vitrimer relax stress at high temperature.

✓ Relaxation time (time to relax 1/e of original modulus) → $\tau^*_{180\ °C}$ = 233 s.

✓ Arrhenius-like flow characteristic → Ea = 181 kJ.mol^{-1}.

Mechanical recycling

before / after

✓ Retention of the mechanical properties.

✓ Improved mass distribution.

Chemical recycling

✓ Complete dissolution in basic media (1M NaOH) by saponification of ester bonds [4].

✓ High solubility of the soda lignin.

Conclusions

This study envisions the possibility to produce tuneable substitute for petroleum-based materials considering lignin as an independent polymeric phase. Afforded by the benzoxazine features, these bio-derived materials close the loop of the circular polymer economy, from the sustainable design to the sustainable end-of-life.

References

[1] A. Adjaoud, L. Puchot, C. E. Federico, R. Das, P. Verge; *Chem. Eng. J.*, 2023, 453 (2), 139895.
[2] A. Adjaoud, R. Dieden, P. Verge; *Polymers.*, 2021, **13** (4), 637.
[3] A. Adjaoud, A. Trejo-Machin, L. Puchot, P. Verge; *Polym. Chem.*, 2021, **12**, 3276-3289.
[4] A. Adjaoud, L. Puchot, P. Verge; *ACS Sust. Chem. Eng.*, 2022, **10** (1), 594-602.

Contacts

Antoine Adjaoud – antoine.adjaoud@list.lu
Luxembourg Institute of Science and Technology
5, avenue des Hauts-Fourneaux
L-4362 Esch/Alzette

"N'est stupide que la stupidité"

Forrest Gump